THE RESERVOIR GEOCHEMISTRY OF ARA CARBONATES IN THE GREATER BIRBA AREA IN THE SOUTH OMAN SALT BASIN IN SOUTH OF SULTANATE OF OMAN

Mohammed Rashid Khalfan Al-Ghammari

A thesis submitted to Newcastle University in partial fulfilment of the requirements for the degree of Doctor of philosophy in the faculty of Science, Agriculture and Engineering

School of Civil Engineering and Geosciences
Newcastle University, Newcastle upon Tyne
UK

November, 2006

Declaration

I hereby certify that the content of this thesis is the original work of the author, except where otherwise acknowledged, and has not been submitted previously for a degree at this, or any other, university.

Mohammed R. K. S. Al-Ghammari

Abstract

This thesis describes a detailed geochemical evaluation of the petroleum fluids in the Greater Birba Area in the South Oman Salt Basin located in South of Sultanate Oman. These crude oils were found in the Infracambrian (Precambrian-Cambrian) Ara group carbonates (Upper Huqf supergroup), which are sealed by anhydrites. The reservoirs are heavily shattered due to halokinetic movement and so the migration of oil to these sealed carbonate slabs was probably vertical through these halokinetic faults.

The Greater Birba area oils are characterized by large variations in some of the important properties. API gravity ranges from 23.70 to 51.00. Dead oil and live oil viscosities vary a lot from a minimum of 1.50 cp and 0.92 cp to a maximum of 188 cp and 41.03 cp respectively. The acidity of the oil (TAN) varies from a low TAN of 0.11 mgKOH/g oil to a high TAN value of 1.24 mgKOH/g oil. Most of the oils show high TAN values (>0.50) and only few oils show low TAN values. Sulphur content also varies a lot and ranges from 0.78 wt% in a black oil to 4.7 wt% in a gas condensates and generally negatively correlated with API gravity. Therefore, an important aim of this study was to improve the understanding of the underlying controls on these properties using both geochemistry and PVT modelling.

A comprehensive study was undertaken on these oils using twenty two oil samples, twenty reservoir core samples, five gas samples and data from eleven PVT reports. Hydrocarbons molecular geochemistry, gasoline range hydrocarbon data, bulk composition and isotopic data as well as PVT modelling were employed in this study to evaluate and characterize crude oils and attempt to identify the controls on observed fluid properties variations in the Greater Birba area.

Most of the crude oils in the Greater Birba area show typical characteristics of oils sourced from evaporite-carbonate source facies deposited in hypersaline and highly reducing environment, except for two oil samples, one from BBN1 (from A3C reservoir unit), which might be contaminated and the other is from Kaukab1 (from A1C reservoir unit). Some of these characteristics are high sulphur content, low asphaltene contents, high relative abundance of Pregnanes, gammacerane, and C_{35} homohopanes as well as other geochemical features. Various maturity parameters (e.g. MPI and C_{29} (S+R) αββ/ (ααα+αββ) in C_{15+} Saturated and aromatic hydrocarbons

suggested that these oils were generated from a source rock in the middle of oil window (0.8-0.9%R).

No evidence was found for water washing and biodegradation effects in the studied oils. There was no evidence to prove or deny thermochemical or bacterial sulphate reduction, although general observations suggest that this is less likely to occur in the Greater Birba area.

Number of facies sensitive parameters and maturity sensitive parameters as well as isotopic data show that these oils are genetically related and only minor variations exist between them, largely due to minor facies variations. These small variations can not account for the large variations observed in bulk properties. Two samples were exceptional from the above statement O5 from BBN1 (reservoir A3C), which is probably a contaminated sample with most likely younger oil and O15 from Kaukab1 (reservoir A1C) and this is different because it is from A1C reservoir unit which is in contact with middle Huqf source rocks.

PVT modelling, gasoline range hydrocarbons data and absolute concentrations of biomarkers suggest that the main control behind the variations observed in the petroleum fluids in the Greater Birba area were mixing of oil and gas condensate with a dry gas probably derived from highly mature pre-salt source rocks. This oil-condensate-gas mixing increased the bubble point pressure above reservoir pressure in some of the oil accumulation in the studied area (e.g. main Birba Field), which resulted in the formation of two phases in these accumulations. Sulphur content was probably controlled by both oil-condensate mixing and the minor facies variations between the original oils. The variations in the absolute concentrations of biomarkers in the oils were mainly controlled by dilution effects caused by mixing of oils with alkane rich condensate charge. The formation of a gas phase and related Phase fractionation effects might be responsible for the significant variations in acidity, API gravity and the distribution of alkylphenols. Birba oils (A4C oils of well BB1, and BB2) were suggested to have migrated longer distance than the other oils on the basis of alkylcarbazoles isomer distribution.

Acknowledgments

I would like to express my delightful thanks to PDO, for funding the whole of this project and providing me the samples and analysis I needed. Many thanks also go Shell for their quick delivery for the samples and data needed for this study. I would like to thank Dr. Jan Schooners and Dr. Alan from PDO for their support during this research. I would especially like to expresses my delightful thanks to Dr. Qassim Al-Riyami (PDO) for his infinite help throughout the PVT modelling work. I don't want to forget to thanks Abdullah Al-Riyami and Salim Al-Buwaiqi from PDO for their help during data collection.

My project was carried out under supervision of Prof. Steve Larter and I would like to thank him for being patient and his enthusiastic support. Although he was away from me in the last two years, I learnt from him so many things that enable me to conduct this research. I am also grateful for the help I received from Paul Taylor from PDO, he was a fantastic leader and I am happy to work under his supervision in the future. I would like also to thank Dr. Martin Jones (Newcastle) for his support during the third year. My special thanks go to Paul Farrimond, who has been patient and helpful especially in biomarkers side of this project during the second year. I would like to thank Bernie Bowler for the valuable discussion of the contents of this research as well as his technical support. Many thanks for Prof. David Manning, Prof. Andy Aplin and Dr Richard Tyson for their help and discussion in some of the contents of this work.

I would like to thank Ian Harrison for his assistance with the GC analysis and Phil Green for his provision of lab needs. I would like to thank Paul Donohoe for his enthusiastic assistance with the GC-MS. Yvonne Hall, this lady should receive special and big thank you for her charming and pleasant help and support throughout the four years.

Last and certainly not least, I would like to express my special thanks and gratitude to Family for their encouragement and patience throughout my study in UK.

Contents

Chapter 1 Introduction

1.1 Background

The study area for this project is the Greater Birba Area, which is located in the South Oman Salt Basin in South of sultanate of Oman (Figure 1-1). The focus is on the Birba field but some of the immediately surrounding wells have also been included because they share the same reservoir units. The Birba Field is located 20km northwest of the Marmul field. Thirteen wells are included in the study; six wells are in the Birba field, two wells are in the Birba North Block, and the others are well Omraan1, well Durra1, well Kaukab1, well Nassir1, and well Shamah1.

The development of the Greater Birba area is summarised in (Al-Riyami, 2005; Green & Graham, 1983; Protoy *et al.*, 1995; Riemens, 1988), from which a concise summary will be presented here. Oil was first discovered in the Greater Birba area by well Nassir-1, which was drilled in 1976 to test an interpreted pre-salt carbonate build up in the Buah (middle Huqf source rock of Precambrian age). This subsequently proved to be a 74m thick dolomite stringer, which, on testing, produced 960 m^3/d of 23 API gravity oil. Based on seismic interpretation, several stringers were recognised over an area in excess of 300 km^2 in the Nassir area. In 1978, well BB-1 was proposed to test a closed structure 7km to the north and down dip of the Nassir accumulation. Three dolomite stringers were discovered by well BB1 well near the base of the Ara Salt. The top stringer (so-called A4C) produced 1440 m^3/d of oil with an API gravity of 28. After this success, twelve wells were drilled in and around the Birba field itself, of which three wells have been potential producers. Disappointing results were obtained from wells BB-4, BB-5 (core samples available from these two), and BB-6, as they were dry holes. In mid 1986, the field was closed in, awaiting a decision to carry out a gas injection project or to deplete the reservoir. Limited oil production took place between 1988 and 1990. Shamah-1 was drilled in 1990 to test the carbonate stringers in a large anticlinal structure. The first stringer encountered was water bearing whereas the deeper stringer, the basal Birba Carbonate and the Buah were very tight. It was decided to develop the field using a gas injection strategy. In 1991, the field was shut-in for the construction of the gas injection facilities. In preparation for gas injection, injector BBS-1 was sidetracked in 1991 and BB-2 and BB-3 were worked over in 1992. Birba was back on stream mid 1993 with gas

injection in BBS-1. 3D seismic was acquired in 1991 over the Greater Birba area. A cross section resulting from this 3D seismic survey is shown in Figure 1-2.

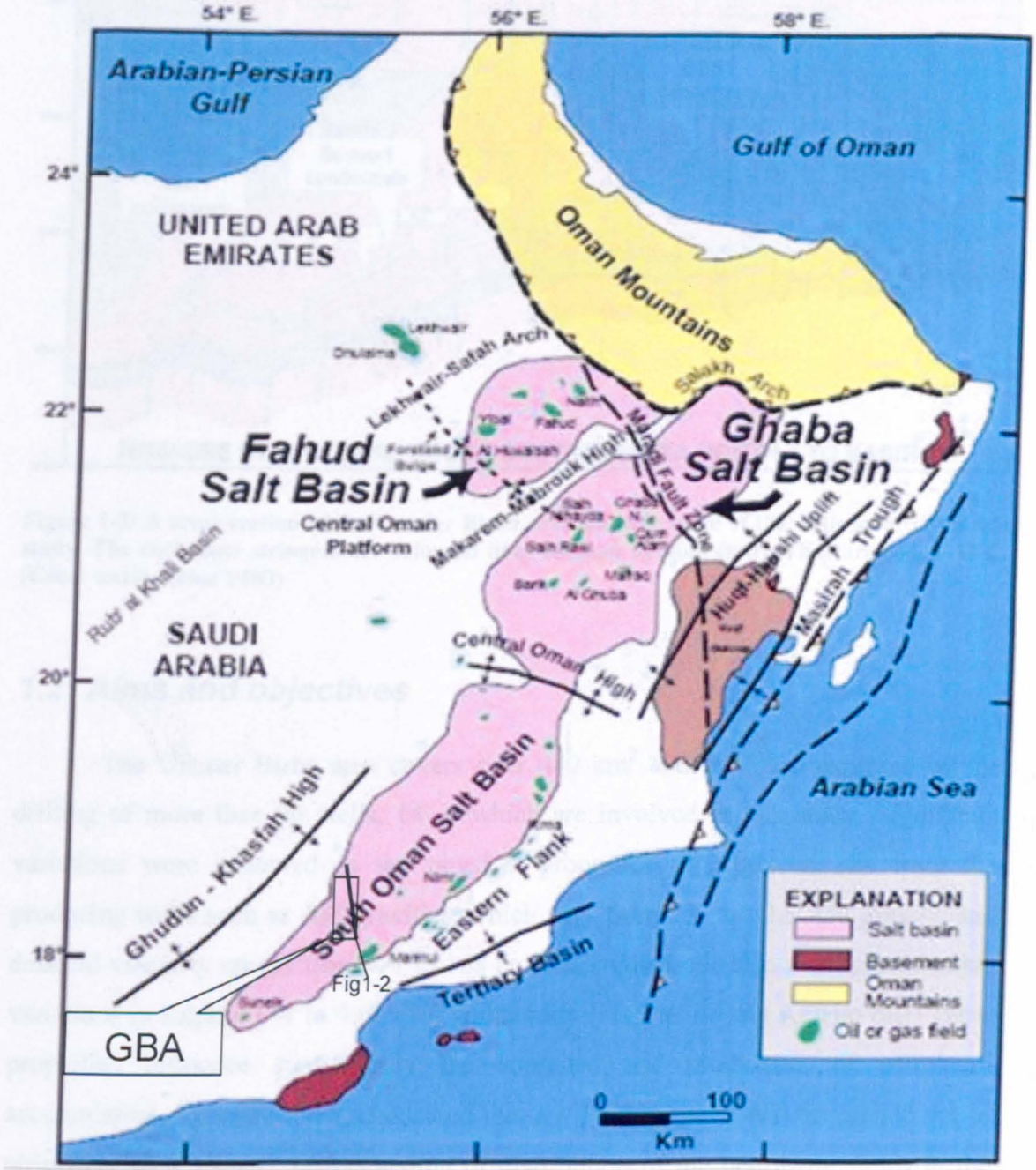

Figure 1-1: The study area: the greater Birba area in the South Oman Salt Basin. Modified after Loosveld & Terken, (1996).

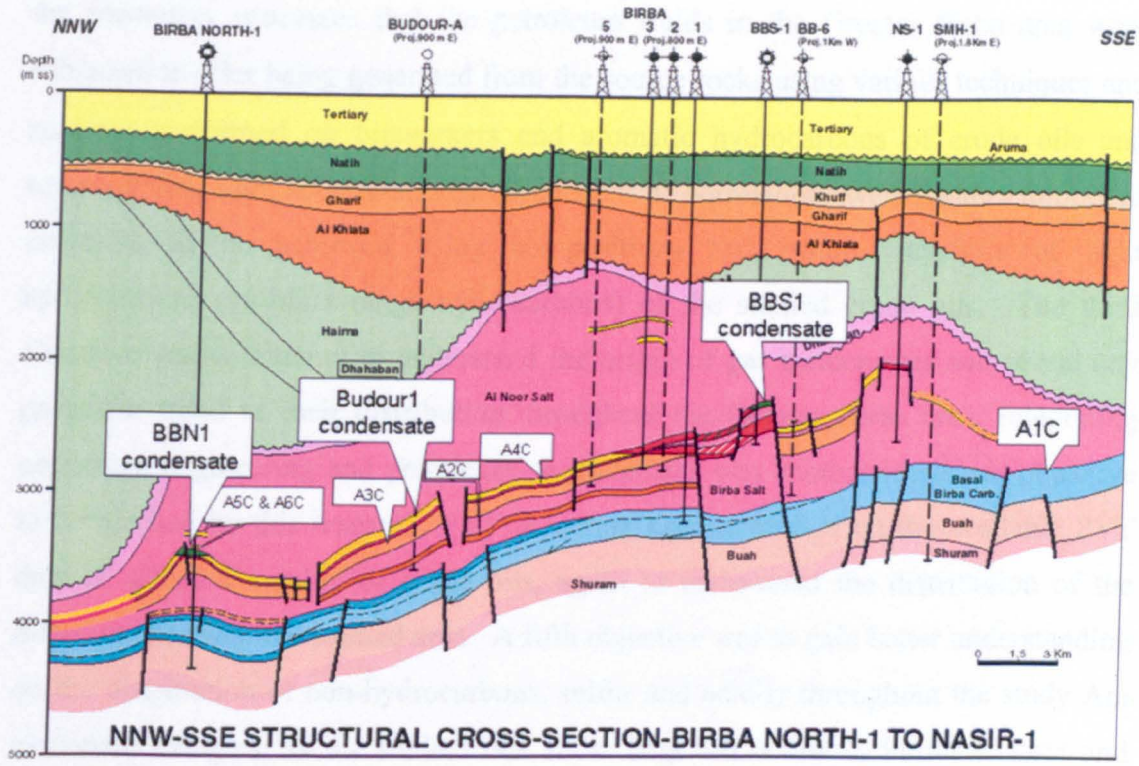

Figure 1-2: A cross-section of the Greater Birba area showing some of the wells involved in this study. The carbonate stringers are coloured lines encased by pink (salt). They are coded AXC. (Cross section from PDO)

1.2 Aims and objectives

The Greater Birba area covers over 480 km^2 and has been explored by the drilling of more than 20 wells, 14 of which are involved in this study. Significant variations were observed in the physical properties of produced oils from the producing wells such as API gravities, which vary from 23° to 50.5°API gravity, and dead oil viscosity ranges from < 1 to 188 cp. The studied oils also show considerable variations in sulphur (<1 to 4.6wt %) and acidity (<0.5 to 1.4 mg KOH/g oil). These properties influence significantly the appraisal and production of petroleum accumulation. Therefore, it was decided that my PhD research will be carried out to ultimately gain a better understanding of distribution of the petroleum fluids in the Greater Birba area and attempt to attribute the variations in some of the important bulk properties to specific controls where possible.

By heading towards the main aim, various objectives related to this aim were achieved throughout this research. The first objective was to obtain a geochemical characterization of the petroleum fluids from the Greater Birba area and identifying

the secondary processes that the petroleum fluids in the Greater Birba area were subjected to after being generated from the source rocks using various techniques and analysis performed on biomarkers and aromatic hydrocarbons of crude oils and reservoir core samples. Oil-oil and oil-condensate correlations were another important objective to be achieved using compositions and isotopic analysis of light hydrocarbons (gasoline range hydrocarbons) of the studied crude oils. The third objective was to attempt to understand the origin of gas condensates and reveal any particular trend of their distribution throughout the Greater Birba area. Integrating petroleum engineering and petroleum geochemistry was another important objective to be reached by this research; PVT modeling was performed on the available PVT data of selected number of crude oils, again to understand the distribution of the different phases in the studied area. A fifth objective was to gain better understanding on the distribution of non-hydrocarbons, sulfur and acidity throughout the study Ara carbonate stringers, as the studied oils show large variations in Sulfur content and Total acid numbers (TAN). This also will include the alkylphenols, and alkylcarbazoles in the study oils.

The importance of this research is also realised from the age of the reservoired oils and the types of reservoir system. Literature indicates that the studied carbonate stringers started filling in Cambrian (>400Ma) according to Basin modelling studies in the South Oman Salt Basin, and the source rocks spans the Precambrian to early Cambrian age (Grantham *et al.*, 1990). The age and the type of the reservoir system (carbonate stringer completely enveloped by salt) have probably had a great influence on the physical and chemical properties of the petroleum fluids. This issue was not considered in this research project, but we invite future work to explore this issue due to its high importance.

1.3 Thesis outline

The PhD thesis consists of four chapters in addition to the introduction (chapter 1), the geological setting (chapter 2), the experimental (chapter 3), and the conclusions and future work (chapter 8) chapters.

Chapter 2 provides a detailed review of geological setting of the Greater Birba area in South Oman Salt Basin. This chapter reviews the tectonic evolution of South Oman Salt Basin including salt tectonics. It also provides a detailed summary of the general stratigraphy of lithological units in this basin as well as a detailed description of internal stratigraphy and depositional setting of the Ara group which consists of the reservoir units. The chapter also includes a summary of diagenetic history and reservoir quality of the reservoir rocks. There is also a detailed review of the petroleum geochemistry literature have been done on South Oman Salt Basin.

Chapter 3 presents a detailed description of the methods and techniques used in this study. All various types of data incorporated in the study are described and attributed to their sources (e.g. isotopic data from Shell). This chapter also descries the statistical data analysis performed on the studied samples such as principal component analysis

Chapter 4 provide a characterization of the studied petroleum using biomarkers and aromatic hydrocarbons and statistical evaluations of these data as well as gas analysis.

Chapter 5 presents a characterization of the light hydrocarbons of the studied petroleum and provide an understanding of the distribution of petroleum fluids in the Greater Birba area.

Chapter 6 presents polar fraction analysis (carbazoles and phenols), acid analysis and sulphur analysis. It also provides an appreciation of the variations observed in API gravities and viscosities.

Chapter 7 gives a detailed description of the PVT modelling done on the studied oils and an integration of this work with reservoir geochemistry

1.4 Biomarkers and aromatic hydrocarbons used in this study

This section is dedicated to introduce the reader to the different biomarkers used in this study as well as the aromatic hydrocarbons. Biomarkers or biological markers or molecular fossils are organic compounds found in geological samples, whose carbon skeletons are formed by living organisms and preserved in recognisable form throughout diagenesis and much of catagenesis (functional groups (e.g. O=) may be lost but the carbons skeleton stay intact) (Killops & Killops, 1993).

The stereochemistry (i.e. 3-D structure) is of prime importance to the understanding of the structures of biomarkers and their applications to geochemical studies (Peters *et al.*, 2005). A saturated carbon atom has four bonds radiating outwards toward the corners of an imaginary tetrahedron. If all four substituents are different (e.g. Cl, C, H, F), then the centre carbon atom of the tetrahedron is referred to as "chiral centre". The molecule with a chiral centre will exists in two forms, which are mirror image to each other (if one is represented by right hand, the other is represented by the left hand), or they are called enantiomers (Peters *et al.*, 2005). If the chiral centre is part of a ring system, the two forms or stereoisomers are described as α or β; while if the chiral centre is in non-ring system, it is more convenient to be described as S or R. when the molecule is drawn on a plane, if the defined bond points into the page, it is described as α configuration, while if it points out of the page, it is described as β configuration. R and S configurations refers to a chiral centre where, if the substituent of lowest propriety is lined up away from the viewer, the remaining three groups have a decreasing mass in a clockwise (R) or anticlockwise (S) directions respectively.

The main biomarkers incorporated in this study are tricyclic terpanes, pentacyclic terpanes (hopanes), steranes, monoaromatic steroid hydrocarbons, and triaromatic steroid hydrocarbons. In addition to these biomarkers, several polyaromatic hydrocarbons are also involved in the study. I will provide an outline about each of these hydrocarbon classes with their molecular structures. Full names of these biomarkers were listed in this section in Table 1-1.

1.4.1 Tricyclic and tetracyclic terpanes

Many terpanes in petroleum are derived from bacterial membrane lipids (Peters *et al.*, 2005). They include several homologs series, including acyclic, bicyclic, tricyclic, tetracyclic and pentacyclic terpanes (Peters *et al.*, 2005). Only the tricyclic (3 six membered-rings), tetracyclic (4 six membered-rings) and pentacyclic (4 six membered and 1 five membred-rings) terpanes have been included in this study (see Figure 1-4 and Figure 1-3 for structures). C_{19}-C_{30} tricyclic terpanes are found in most petroleum (Aquino Neto *et al.*, 1983). The tricyclic terpanes less than C_{30} are thought to be generated from tricyclohexaprenol, a constituent of prokaryotic cell membranes (Aquino Neto *et al.*, 1983). Tasmanite has been suggested as a possible source for these compounds because of their high abundance reported in Tasmanite rock extracts (Peters *et al.*, 2005). Abundant tricyclic terpanes of carbon range C_{19}-C_{40} was reported in lacustrine black shales as well as the absence of hopanes (Kruge *et al.*, 1990). These were attributed to unusual prokaryotes, or to maturity or fractionation effects related to oil expulsion from the shales (Kruge *et al.*, 1990). C_{19} to C_{45} tricyclic terpanes were identified in crude oils and attributed to unsaturated isoprenoid solanesol, which occurs in plants (Moldowan *et al.*, 1983). Mass spectra of tricyclic terpanes contain a base peak at m/z 191 and thus this ion is used to monitor these compounds.

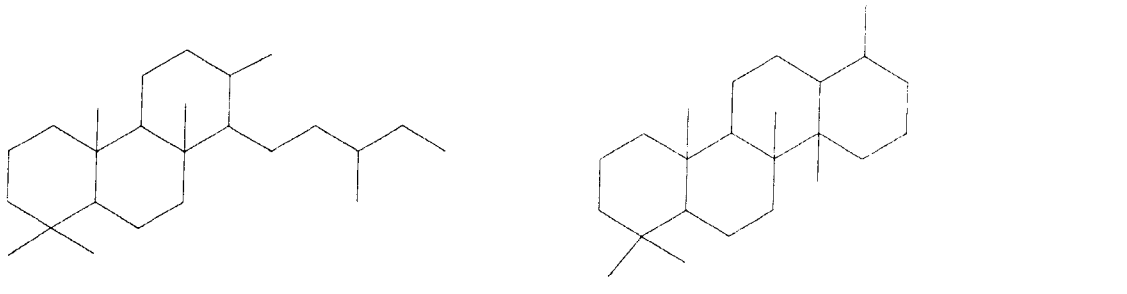

C25 Tricyclic terpanes (C25 extended ent-isocopalane)

C_{24} Tetracyclic terpane (Des-E-hopane: a C_{24} 17,21-secohopane)

Figure 1-3: Molecular structures of a tricyclic terpane and a tetracyclic terpane.

C_{24}Tetra/C_{23}βαTri ratio is important to distinguish different groups of oils sourced from carbonate and evaporate facies (Aquino Neto *et al.*, 1983). Tetracyclic compounds are thought to originate by thermal or microbial fragmentation of E-ring in hopanes or may be from bacteria through biosynthetic route or from terrigenous precursors (Peters *et al.*, 2005). C_{24} Tetracyclics are more abundant in oils sourced from carbonate and evaporate source rocks or from terrigenous organic matter as discussed before. C_{26}(S+R) Tri/C_{25}(S+R) Tri is another important ratio is very useful parameter to distinguish between lacustrine from marine oils (Peters *et al.*, 2005). The tricyclics/hopanes ratio has been reported to increase with thermal stress due to the higher stability of tricyclics (van Graas, 1990).

1.4.2 Pentacyclic triterpanes (hopanes)

The distribution of hopanes is monitored by m/z 191. The C_{30} homologue usually shows the highest peak since this compound fragments to produce two m/z191 fragments in the source of mass spectrometer. However, petroleum sourced from carbonate evaporitic source rocks usually show enhanced abundances of the C_{29} hopane relative to the C_{30} hopane (molecular structure is drawn in Figure 1-4) (Clark & Philp, 1989; Connan *et al.*, 1986; Zumberge, 1984); this was also observed in petroleum derived from terrestrial source rocks (Brooks, 1986).

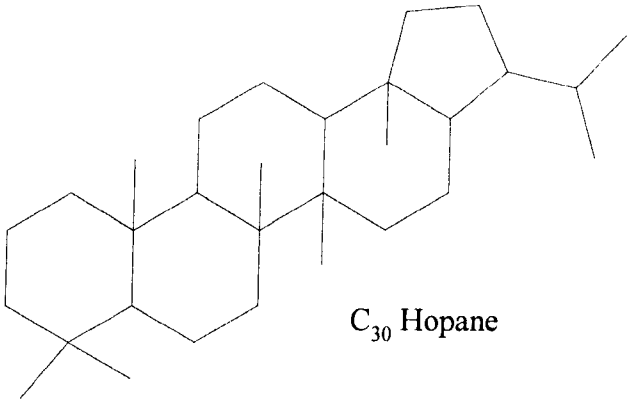

Figure 1-4: Molecular structure of C_{30} hopane.

The distribution of homohopanes carbon numbers (C_{31}-C_{35}) was suggested and used to unravel different types of sources (Peters & Moldowan, 1991). Homohopane Index is the ratio of C_{35} hopanes to the sum of C_{31}-C_{35} hopanes was also used for this purpose (Peters & Moldowan, 1991). High values of the homohopane index indicate marine, sulfur rich reducing depositional environment because of the preservation of bacteriohopanetetrol skeleton by incorporation of sulfur into the side chain. This skeleton appears to be not preserved under anoxic freshwater conditions, possibly due to non-operative sulfur incorporation under these conditions (Peters & Moldowan, 1991).

28,30-bisnorhopane (BNH) is another source indicative parameter. Curiale *et al.* (1985) found that this compound abundance was correlated well with benzothiophene and pristane/phytane ratio. It was also found a good correlation of BNH with the levels of organic sulfur compounds extractable by organic solvents (Grantham *et al.*, 1981). Therefore, it was suggested as a good indicator of highly reducing depositional environment (Curiale *et al.*, 1985). This compound was also found in high abundance in highly anoxic sediments and subsequently suggested as a good indicator of anoxia depositional conditions in thermally immature sediments (Katz & Elrod, 1983). Katz & Elrod, 1983 proposed a source for BNH from sulfur reducing bacteria, while Williams, 1984 suggested bacteria *Beggiatoaceae* to be the source of BNH; these bacteria oxidize H_2S using molecular oxygen, and live in the transition between anoxic sediments and oxic water column. BNH possibly exists as a free lipid and not attached to the kerogen (Peters *et al.*, 2005). BNH/$C_{30}\alpha\beta$ hopane is a common source parameter but readily affected by thermal maturity and so it is only useful for oils with similar thermal stress (Curiale *et al.*, 1985).

1.4.3 Steroid Hydrocarbons

1.4.3.1 Steranes:

C_{27}-C_{29} steranes are very common in petroleum and believed to be derived from sterols in the cell walls of Eukaryotes, which possibly perform a similar role to bacteriohopanetetrol in Prokaryotes. Therefore, the ratio of steranes to hopanes in petroleum may be useful to indicate the relative contribution of Eukaryotic and prokaryotic organisms to the source organic matter (Mackenzie *et al.*, 1982; Peters *et al.*, 2005; Volkman, 1986).

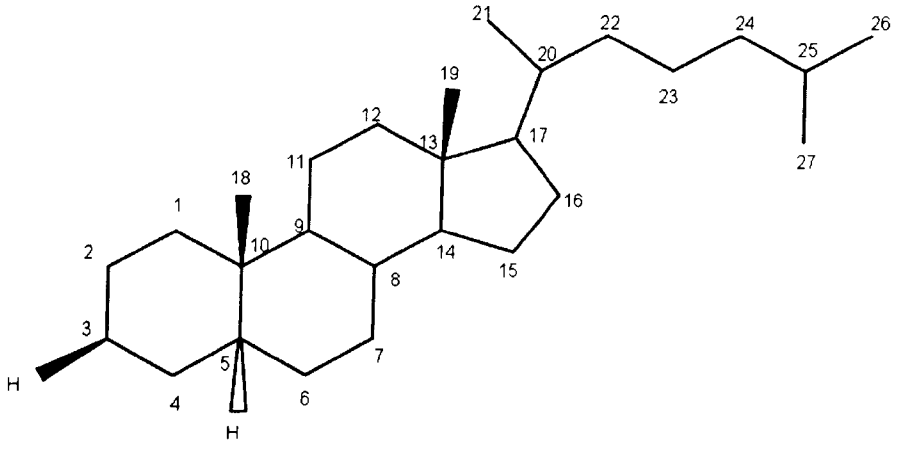

Figure 1-5: molecular structure of C_{27} sterane.

The precursor sterols have 8β(H) 9α(H) 10β(H) 13β(CH_3) 14α(H) 17α(H) 20R stereochemistry. Stereochemical changes only occur to asymmetric carbons at C-14 C-17 and C-20 during burial diagenesis and catagenesis (Mackenzie, 1984). Steranes are generated by the reduction of sterols and sterenes via hydrogenation of the double bonds at C-5 in sterols during diagenesis (Mackenzie *et al.*, 1982). 5α(H) epimer is more stable than 5β(H) epimer and so the later is rarely found in petroleum and the high abundance of 5β(H) suggests low thermal maturity (Peters & Moldowan, 1993). Steranes in immature sediments and petroleum keep the same molecular flatness as the precursor sterols by having 5α(H) 14α(H) 21α(H) 20R (oraaa) stereochemistry. With increasing burial and thermal maturity, the C-20 stereochemistry changes from R to S and 14α(H) 21α(H) is lost to 14β (H) 21β (H) (i.e. flatness lost) (Mackenzie, 1984).

Steranes have mass spectra with a base peak of m/z 217, and so they are monitored using this ion. The distribution of steranes carbon number (preferably ααα R, less affected by maturity) has been identified as powerful correlation tool for oils and source rocks. A ternary plot of these sterane carbon numbers is a widely used graphic representation for this purpose. The plot was proposed to differentiate different depositional environments (Moldowan *et al.*, 1985) but mainly to differentiate groups of oils from different organic facies of the same source rock (e.g. Grantham *et al.*, 1988). C_{27} and C_{28} steranes have been reported to indicate different algae and C_{29} steranes has been reported to indicate land plants input (Peters & Moldowan, 1993) but may also be derived from algae (Volkman, 1986). The predominance of C_{29} steranes usually indicates a terrestrial source for the organic matter. However, as land plants didn't evolve before the Devonian, the dominating C_{29} in the pre-Devonian oils has been attributed to an algal origin (Volkman *et al.*, 1986). Other studies have indicated that C_{29} sterols can be derived from brown and green algae (Moldowan *et al.*, 1985 and references therein) and diatom cultures (Volkman *et al.*, 1981) as well as cyanobacteria (Fowler & Douglas, 1984). Moldowan *et al.*, 1985 interpreted this absence in petroleum older than 500 Ma due to a lag in the evolution of marine organisms that had C30 sterols. However, C_{30} steranes were later detected e.g. in bitumen extracts from Precambrian Chuar rock in Arizona (J) (Peters & Moldowan, 1993) and 2700 Ma old extracts from the Pilbara Craton, Australia (Brocks *et al.*, 1999). C_{27}/C_{29} and C_{28}/C_{29} steranes ratios have been used as source parameters. However, the principal use of the C_{28}/C_{29} sterane ratio is to infer the age of the oils and source rocks. Moldowan *et al.* (1985) reported a general decrease in C_{29} steranes and relative increase in C_{28} steranes through geologic history. The C_{28} sterane increase is thought to be due to increased diversification of phytoplankton assemblages such as diatoms (Moldowan *et al.*, 1985). A C_{28}/C_{29} sterane ratio less than 0.5 was observed for lower Palaeozoic oils and older, while a ratio greater than 0.7 is for Upper Jurassic to Miocene (Grantham & Wakefield, 1988). Pregnanes and homopregnanes were reported in evaporitic source rocks deposited in hypersaline environment (ten Haven *et al.*, 1985); however, Wingert & Pomerantz, (1986) proposed a thermal origin from steranes. They showed that 5α(H), 14α(H), 17β(H) pregnanes and homopregnanes isomers coelute with the thermodynamically

less stable 5α(H)), 14α(H), 17α(H) compounds and so they concluded that αββ pregnanes and homopregnanes are predominant in highly mature oil samples. The hopanes/steranes ratio has been reported to increase with maturation (Peters & Moldowan, 1993), but it has also been reported to decrease with maturity (Norgate *et al.*, 1999).

1.4.3.2 Diasteranes

The rearranged steranes (or diasteranes) are also common in petroleum. Diasteranes have the C-18 and C-19 methyl groups attached to the sterane skeleton at the C-5 and C-14 positions. The rearrangement process of steranes to diasteranes in source rocks during thermal stress is believed to be catalysed by the acidic sites on clays (Rubintsein *et al.*, 1975; Sieskind *et al.*, 1979). However, other studies have shown that the primary control on the abundance of diasteranes in oils is the clay rich minerals (Moldowan *et al.*, 1992; Palacas *et al.*, 1984). Therefore, low content of diasteranes in an oil was regarded to be indicative of a non-clastic or carbonate source for the petroleum and Moldowan *et al.*, 1986 suggested that diasterane abundance in oils was controlled by the redox conditions during the deposition of organic matter. The major fragment in the mass spectrum of diasteranes is m/z 259 and thus it is used to monitor them, but they also give m/z 217 ion.

Table 1-1: the full compound names of the biomarkers used in the study

Name used in the study	Compound name	Molecular formula	m/z
Steranes			
C_{21} pregnane	5α sterane	$C_{21}H_{36}$	217
C_{22} pregnane	5α sterane	$C_{22}H_{38}$	217
C_{27} ααα S sterane	5α(H), 14α(H), 17α(H), 20(S)-Cholestane	$C_{27}H_{48}$	217
C_{27} αββ R sterane	5α(H), 14β (H), 17β (H), 20(R)-Cholestane	$C_{27}H_{48}$	217
C_{27} αββ S sterane	5α(H), 14β (H), 17β (H), 20(S)-Cholestane	$C_{27}H_{48}$	217
C_{27} ααα R sterane	5α(H), 14α(H), 17α(H), 20(R)-Cholestane	$C_{27}H_{48}$	217
C_{28} ααα S sterane	24-methyl-5α(H), 14α(H), 17α(H), 20(S)-Cholestane	$C_{28}H_{50}$	217
C_{28} αββ R sterane	24-methyl-5α(H), 14 β (H), 17 β (H), 20(R)-Cholestane	$C_{28}H_{50}$	217
C_{28} αββ S sterane	24-methyl-5α(H), 14 β (H), 17 β (H), 20(S)-Cholestane	$C_{28}H_{50}$	217
C_{28} ααα R sterane	24-methyl-5α(H), 14α(H), 17α(H), 20(R)-Cholestane	$C_{28}H_{50}$	217
C_{29} ααα S sterane	24-ethyl-5α(H), 14α(H), 17α(H), 20(S)-Cholestane	$C_{29}H_{52}$	217
C_{29} αββ R sterane	24-ethyl-5α(H), 14 β (H), 17 β (H), 20(R)-Cholestane	$C_{29}H_{52}$	217
C_{29} αββ S sterane	24-ethyl-5α(H), 14 β (H), 17 β (H), 20(S)-Cholestane	$C_{29}H_{52}$	217
C_{29} ααα R sterane	24-ethyl-5α(H), 14α(H), 17α(H), 20(R)-Cholestane	$C_{29}H_{52}$	217
Isoprenoids			
Pristane	2,6,10,14-Tetramethylpentadecane	$C_{19}H_{40}$	GC
Phytane	2,6,10,14-Tetramethylhexadecane	$C_{20}H_{42}$	GC
Triterpanes			
C_{20} βα Tricyclic terpane	13β (H), 14α (H)-C_{20} Tricyclic terpane	$C_{20}H_{36}$	191
C_{21} βα Tricyclic terpane	13β (H), 14α (H)-C_{21} Tricyclic terpane	$C_{21}H_{38}$	191
C_{22} βα Tricyclic terpane	13β (H), 14α (H)-C_{22} Tricyclic terpane	$C_{22}H_{40}$	191
C_{22} αα Tricyclic terpane	13α (H), 14α (H)-C_{22} Tricyclic terpane	$C_{22}H_{40}$	191
C_{23} βα Tricyclic terpane	13β (H), 14α (H)-C_{23} Tricyclic terpane	$C_{23}H_{42}$	191
C_{24} βα Tricyclic terpane	13β (H), 14α (H)-C_{24} Tricyclic terpane	$C_{24}H_{44}$	191
C_{25} βα Tricyclic terpane	13β (H), 14α (H)-C_{25} Tricyclic terpane	$C_{25}H_{46}$	191
C_{24} Tetracyclic terpane	C_{24} Tetracyclic terpane	$C_{24}H_{42}$	191
C_{26} βα Tricyclic terpane	13β (H), 14α (H)-C_{26} (24S)Tricyclic terpane	$C_{26}H_{48}$	191
C_{26} βα Tricyclic terpane	13β (H), 14α (H)-C_{26} (24R) Tricyclic terpane	$C_{26}H_{48}$	191
C_{28} βα Tricyclic terpane	13β (H), 14α (H)-C_{28} (24S) Tricyclic terpane	$C_{28}H_{52}$	191
C_{28} βα Tricyclic terpane	13β (H), 14α (H)-C_{28} (24R) Tricyclic terpane	$C_{28}H_{52}$	191
C_{29} βα Tricyclic terpane	13β (H), 14α (H)-C_{29} (24S) Tricyclic terpane	$C_{29}H_{54}$	191
C_{29} βα Tricyclic terpane	13β (H), 14α (H)-C_{29} (24R) Tricyclic terpane	$C_{29}H_{54}$	191
C_{30} βα Tricyclic terpane	13β (H), 14α (H)-C_{30} (24S) Tricyclic terpane	$C_{30}H_{54}$	191
C_{30} βα Tricyclic terpane	13β (H), 14α (H)-C_{30} (24R) Tricyclic terpane	$C_{30}H_{54}$	191
Ts	18α(H)-22,29,30-trisnorneohopane	$C_{27}H_{46}$	191
Tm	17α(H)-22,29,30-trisnorhopane	$C_{27}H_{46}$	191
C_{28} BNH	17α(H), 18α (H), 21β (H)-28,30-Bisnorhopane	$C_{28}H_{48}$	191
C_{29}αβ hopane	17α(H), 21β (H)-norhopane	$C_{29}H_{50}$	191
C_{30}αβ hopane	17α(H), 21β (H)-hopane	$C_{30}H_{52}$	191
C_{31}αβ hopane	17α(H), 21β (H), 22(S)-homohopane	$C_{31}H_{54}$	191
C_{31}αβ hopane	17α(H), 21β (H), 22(R)-homohopane	$C_{31}H_{54}$	191
C_{32}αβ hopane	17α(H), 21β (H), 22(S)-Bishomohopane	$C_{32}H_{56}$	191
C_{32}αβ hopane	17α(H), 21β (H), 22(R)-Bishomohopane	$C_{32}H_{56}$	191
C_{33}αβ hopane	17α(H), 21β (H), 22(S)-Trishomohopane	$C_{33}H_{58}$	191
C_{33}αβ hopane	17α(H), 21β (H), 22(R)-Trishomohopane	$C_{33}H_{58}$	191
C_{34}αβ hopane	17α(H), 21β (H), 22(S)-Tetrakishomohopane	$C_{34}H_{60}$	191
C_{34}αβ hopane	17α(H), 21β (H), 22(R)-Tetrakishomohopane	$C_{34}H_{60}$	191
C_{35}αβ hopane	17α(H), 21β (H), 22(S)-Pentakishomohopane	$C_{35}H_{62}$	191
C_{35}αβ hopane	17α(H), 21β (H), 22(R)-Pentakishomohopane	$C_{35}H_{62}$	191

1.4.3.3 Aromatic steroids hydrocarbons

Aromatic biomarkers and hydrocarbon ratios are often useful in determining the thermal maturity of organic matter (Hase & Hites, 1976; Johns, 1986; Radke, 1987) but they can also provide valuable information on source organic matter. Ring A monoaromatic steroids (MAS) are possibly formed from sterol precursors. The aromatization of ring A is accompanied by shift of methyl group at C-19 of the sterol from position C-10 to position C-1 or position C-4 and this was thought to be due to a combination of acid catalysis and microbial activity, (Hussler *et al.*, 1981). Ring C-MAS occur in immature sediments and predominate over ring- A steroids in oils and bitumen (Seifert *et al.*, 1983). Ring C-MAS are suggested to form by rearrangement of stera-3,5-dienes (Mackenzie *et al.*, 1982). Rearranged ring-C aromatic steroids have also been reported in petroleum; those steroids have the methyl group of the A/B ring is attached at C-5 instead of C-10, (Riolo *et al.*, 1986). Triaromatic steroids may originate from monoaromatic steroids via aromatization and loss of a methyl group but this is not the only mechanism and there must be other precursors as there is no correlation between C_{27}/C_{29} monoaromatic steroids and C_{26}/C_{27} triaromatic steroids (Peters *et al.*, 2005). The aromatization involves the loss of the C-19 methyl group at the A/B ring junction to form BC ring diaromatic steroids and may be rapidly followed by the aromatization of the ring-A to form ABC triaromatic steroids.

MAS and TAS are monitored using m/z 253 and m/z 231 respectively. Ternary plots of the C_{27}-C_{28}-C_{29} MAS were used as source correlation, similar but believed to be more powerful than in steranes (Moldowan *et al.*, 1985). A dominance of C_{29} MAS has been attributed to marine carbonate sourced oils (Peters *et al.*, 2005).

Table 1-2: Full names of monoaromatic steroid hydrocarbons and triaromatic steroid hydrocarbons.

Name used in the study	Compound name	m/z
C-ring Monoaromatic steroids		
C_{21} Monoaromatic steroid	C_{21} Monoaromatic steroid	253
C_{22} Monoaromatic steroid	C_{22} Monoaromatic steroid	253
$C_{27}\beta S$ Monoaromatic steroid	5β(H), 20(S)-C_{27} Monoaromatic steroid	253
$C_{27}\beta R$ Monoaromatic steroid	5β(H), 20(R)-C_{27} Monoaromatic steroid	253
$C_{28}\beta S$ Monoaromatic steroid	5β(H), 20(S)-C_{28} Monoaromatic steroid	253
$C_{28}\alpha S$ Monoaromatic steroid	5α(H), 20(S)-C_{28} Monoaromatic steroid	253
$C_{28}\alpha R$ Monoaromatic steroid	5α(H), 20(R)-C_{28} Monoaromatic steroid	253
$C_{29}\beta S$ Monoaromatic steroid	5β(H), 20(S)-C_{29} Monoaromatic steroid	253
$C_{29}\alpha S$ Monoaromatic steroid	5α(H), 20(S)-C_{29} Monoaromatic steroid	253
$C_{29}\beta R$ Monoaromatic steroid	5β(H), 20(R)-C_{29} Monoaromatic steroid	253
$C_{29}\alpha R$ Monoaromatic steroid	5α(H), 20(R)-C_{29} Monoaromatic steroid	253
ABC-ring Triaromatic steroids		
C_{20} Triaromatic steroid	C_{20} Triaromatic steroid	231
C_{21} Triaromatic steroid	C_{21} Triaromatic steroid	231
$C_{26}S$ Triaromatic steroid	20(S)-C_{26} Triaromatic steroid	231
$C_{26}R$ Triaromatic steroid	20(R)-C_{26} Triaromatic steroid	231
$C_{27}S$ Triaromatic steroid	20(S)-C_{27} Triaromatic steroid	231
$C_{27}R$ Triaromatic steroid	20(R)-C_{27} Triaromatic steroid	231
$C_{28}S$ Triaromatic steroid	20(S)-C_{28} Triaromatic steroid	231
$C_{28}R$ Triaromatic steroid	20(R)-C_{28} Triaromatic steroid	231

1.4.4 Aromatic hydrocarbons

Aromatic compounds are major constituent of petroleum and the organic source facies. They are also present in recent sediments. The term aromatic is used to characterize highly unsaturated and stable compounds, the stability means both thermodynamically (relative to the imaginary olefinic equivalents) and reactively (i.e. small tendency to addition reactions) (Radke, 1987). Aromatic hydrocarbons are those with one or more rings with delocalized π bonds and generally obey the formula C_nH_{2n-6y}, where y is the number of the aromatic rings. The number of the rings classifies the aromatic hydrocarbons in to different groups: monoaromatic (1 ring), diaromatic (2 rings), triaromatic (3 rings) and tetraromatic (4 rings) HC. Those aromatic HC with 2 or more aromatic rings are grouped together as Polynuclear Aromatic Hydrocarbons (PAH). Here below examples of those PAHs, those are included in this study.

Monoaromatics

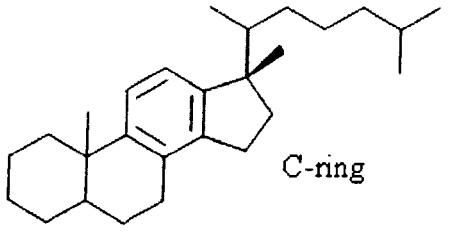

Monoaromatic steroids

$C_{27}H_{42}$

Diaromatics

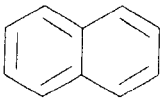

Naphthalene

$C_{10}H_8$

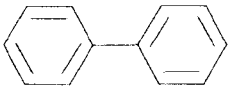

Biphenyl

$C_{12}H_{10}$

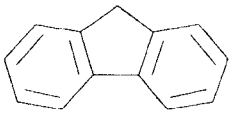

Fluorene

Triaromatics

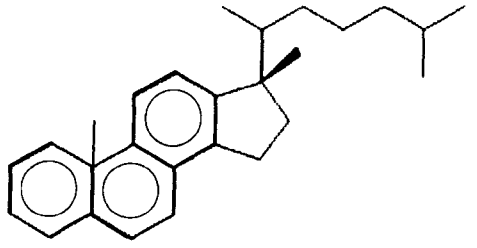

Triaromatic steroids

$C_{26}H_{32}$

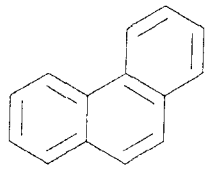

Phenanthrene

$C_{14}H_{10}$

Sulfur compounds:

Benzothiophene

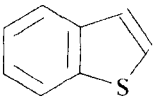

Dibenzothiophene

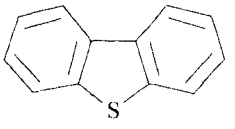

Aromatic hydrocarbons are present in living organisms, and found in recent sediments as well as ancient sediment (Radke, 1987); the later is of prime importance to the study. Only small amounts of naphthalenes, methyl- and dimethylnaphthalene isomers have been found to occur in land plants (Radke, 1987). The most widely accepted model for lignin structure is that it consists of phenyl propane building blocks, with a hydroxyl and different types of linkages (e.g. C-O, C-C) interlink a methoxy group in each phenyl ring and the rings. When two benzene rings are linked with C-C bond, this forms biphenyl group. Significant amount of lignin units with biphenyl type linkages was found in milled spruce lignin and found to be preferentially incorporated by mechanical stress into the structure of compression wood lignin. These biphenyls were also reported to occur in coal tar (Radke, 1987). Biphenyls may also be formed by condensation reactions at higher temperatures (Radke, 1987), complicating the use of biphenyls as source parameter. Changes of abundance of steroids and triterpenoid biomarker molecules in petroleum and coal through geologic history have been attributed to evolution of living organism (Radke, 1987).

Insignificant amount of low molecular weight aromatic hydrocarbon were found in recent sediments, which suggests that those hydrocarbons were not generated during early diagenetic stages. Whereas PAH are widespread and common in both recent and ancient sediments (Radke, 1987). The recent sediments are found to have high abundance of unsubstituted PAH, while the petroleum and ancient sediments have higher concentrations of the alkyl-substituted PAH compounds (Radke, 1987). The alkyl-PAH found in recent sediments were found to show little variations, suggesting common origin for all PAH regardless the type of the sediments (Radke, 1987). The natural fires were proposed to be the major source for those PAH (Radke, 1987). There are controversial discussions on the effect of leaching in the distribution of PAH; whether the non-alkylated PAH can be easily removed by water than other PAH or not (Radke, 1987). Sorption and desorption partitioning of individual PAH that occur between the sediments and water, has not been believed to be a controlling factor in geochemical distribution of these compounds (Radke, 1987). Microbial interaction is another factor that affect the PAH distributions (Radke, 1987). Erosion, successive resedimentation and anthropogenic pollution obscure the possibility to

detect the primary sources of PAH compounds (Radke, 1987). Saturated and partially unsaturated six membered rings in steroids and polycyclic terpenoids undergo stepwise aromatization during diagenesis and catagenesis; for example triaromatic steroid hydrocarbons are consequence of aromatization of steranes (Radke, 1987). Therefore, some aromatic hydrocarbons can be related to their biogenic source (Radke, 1987). Genetic relationships between C_{13}-C_{15} alkyl benzene and terpenoids have been suggested and proved (Radke, 1987). The aromatic hydrocarbons are mainly useful for maturity evaluation. There are other applications such as correlation and biodegradation. The abundance of alkylbenzothiophene was reported to decrease relative to alkylbenzenes under increasing thermal stress; this may not be conversion, but kinetic stability of those two different compounds (Radke, 1987). BDR is the ratio between the amount of sulfur in benzothiophene and its alkyl homologs to the total amount of sulfur in dibenzothiophene and its alkyl homologs (Radke, 1987). This is found to decrease with maturity from 1.6 for immature to 0.4 for mature petroleum and those oils which are altered have a value of about 0.7 (Radke, 1987). However, this is easily affected by evaporative losses leading to erroneously low BDR values (Radke, 1987). Most of the above statements are summerised after Radke (1987), and the original references are cited in his paper.

Chapter 2 Geological Setting

2.1 Overview of geography and geology of sultanate of Oman

The sultanate of Oman lies in the Southeastern Arabia with an area of about 300, 000 km^2 (Figure 1-1). High Mountains are a striking feature in Oman, which are made up of obducted ophiolites, thrust sheets, and associated ocean-floor and sedimentary rocks. The dominant structural trend is NE-SW, along which the sub basins formed (Figure 1-1). This is partly due to the uplift of the eastern margin of the Arabian plate during the late Palaeozoic, Mesozoic, and Tertiary. In northern Oman, the Hawasina and Semail Thrust complex were emplaced during the Late Cretaceous. Another important geological feature is the Maradi Fault Zone (Figure 1-1), which is wrench fault lineament with sinistral movement initiated in the late Cretaceous. (Alsharhan & Nairn, 1997)

The area exploited for petroleum exploration has an area of about 170,600 km^2 (Alsharhan & Nairn, 1997). The Oman basin started to form in the Infracambrian, and the southern part of the basin were subjected to a complicated depositional and structural history during the Palaeozoic (Visser, 1991). The Palaeozoic strata were deformed by folding and faulting, mainly due to salt withdrawal on the southern flank of the south Oman subbasin and salt piercement elsewhere prior to the deposition of the Mesozoic beds (Millson *et al.*, 1996). During Mesozoic and later, the basin was part of the Arabian basin (Alsharhan & Nairn, 1997). The Oman Mountains and the area of the Gulf of Oman were part of the Oman-Zagros-Taurus Trough, which was affected by upper Cretaceous and Tertiary orogenic events (Alsharhan & Nairn, 1997). The Oman Basin comprises seven sub basins: The Huqf Subbasin, Oman interior subbasin, the Oman Foreland subbasin, the offshore Musandam basin, the Gulf of Oman subbasin, the Masirah subbasin and the west Oman subbasin.

The Infracambrian salt deposits of southern and central Oman characterize the northeast-southwest trend Oman Interior Sedimentary Basin. The basin consists of three subbasins, Fahud, Ghaba and south Oman Salt Basins (Figure 1-1). The major oil discoveries in Oman have been found in these subbasins. These basins are characterized by major deformation at the margins and mild deformation in the middle, (Visser, 1991). The Birba field is located in the southern part of the South Oman Salt Basin.

2.2 Structural setting and tectonic evolution of the South Oman Salt Basin

The South Oman Salt Basin is a half graben structure with a NE-SW axis, similar structure style to most of the basins in the interior and south of Oman, (Loosveld *et al.*, 1996) (Figure 1-1). The South Oman Salt Basin is bound by the Huqf-Haushi axis from the east and the Ghudun Khasfah High from the west and the Qara Arch from the south. The basin is separated from the Ghaba Basin by a basement high (the Oman central High). The eastern and the southern margins of the basin are exposed along the Huqf-Haushi axis and the Qara Arch respectively (Figure 1-1) (Visser, 1991)). Variable tectonic histories between the northern and the southern basins of the Oman interior sedimentary Basin led to different burial histories (Visser, 1991). The northern basins are buried deeper and the depth may reach up to 10 Km while the South Oman Salt Basin (SOSB) attained a maximum burial of approximately 8 km (Béchennec *et al.*, 1994)

Extension and rifting during the Pan African Orogeny (the last phase of the collision of western Arabia and North Africa); were believed to be the main mechanisms of the formation and early evolution of the Interior Oman Sedimentary Basin (Husseini, 1988; Loosveld *et al.*, 1996). An N-S trending suture was produced, followed by subsequent wrench tectonics including up to 300 km of sinistral displacement along the NW-SE trending Najd Fault System. Pull-apart basins formed along this NW-SE trending Najd Fault, of these are Oman Interior sub basins. However, Mattes and Morris (1991) suggested that this extension that led to the formation of the Oman Interior Basin was caused by intra plate tensional stresses and crustal thinning directly related to the final pulse of the Pan African Orogeny, as the

Najd Fault related extension may have post-dated the formation of the Salt Basins in Oman inertia. This is believed to be supported by the presence of the NE-SW trending system of the Infracambrian Ghudun-Khasfah faults of Southern Oman and Dibba fault system of the Gulf States (Mattes & Conway Morris, 1990). Immerz *et al.*, (2000) proposed an alternative model for the formation of the Interior Oman sedimentary Basin, based on seismic interpretations. They interpreted the Western Deformation Front as a stack of Neoproterozoic III -Early Cambrian thrust sheets. The Huqf Supergroup would have been deposited in strike-slip basins in intracratonic setting in the distal foreland of the Pan African orogenic belt (Immerz *et al.*, 2000).

The tectono-stratigraphy of the South Oman Salt Basin is summarised and illustrated in Figure 2-1. Two major rift sequences were recognised, the lower to middle Huqf supergroup (Abu Mahara and Nafun Group respectively) and Upper Huqf supergroup (the Ara group carbonate-evaporite cycles) (Loosveld *et al.*, 1996). The clastics, which mainly dominate the western margin stratigraphy, were probably shed from the structural highs (Loosveld *et al.*, 1996).

The Abu Mahara group (lower Huqf supergroup) and the Nafun Group (middle Huqf supergroup) were deposited in a period of no tectonics evidenced by the absence of volcanics and coarse grained clastics (Gorin *et al.*, 1982). The deposition of this group was thought to be controlled by the vertical movements of earth crust and eustatic level following the rifting event and/or the onset of the second rifting event (Loosveld *et al.*, 1996). This is followed by E-W compression that resulted in the formation of basement arches between subbasins e.g. the Ghudun-Khasfah arch. Deposition of the Ara Group (contains the study petroleum reservoirs) occurred in

restricted and generally sediment-starved sag depressions between these arches. Loosveld *et al.* (1996) suggested that the Upper Huqf (i.e. Ara group) in Oman was probably deposited under rapid subsidence and reactivated tectonics; probably related to Najd Fault reactivation (Husseini, 1991). The clastics found near Ghudun high and in the Oman Mountains and thick Ara salt potentially support this model (Loosveld *et al.*, 1996; Mattes & Conway Morris, 1990). No matter what caused these arches, they caused the restricted conditions that lead to the formations of the Ara cycles, (Mattes & Conway Morris, 1990). (Figure 2-3)

The Arabian plate was situated on the northern Gondwana continental passive margin on the southern side of the Palaeotethyan oceanic domain during most of the early Palaeozoic (Husseini, 1991). The beginning of Palaeozoic assemblage was marked by the final stage of uplift and erosion of the Huqf group strata that was associated with Late Proterozoic suturing of Arabia and adjacent plates (Millson *et al.*, 1996). During Haima group deposition, the eastern flank of the Interior Oman Sedimentary Basin was uplifted and Ara salt was dissolved, causing progressive retreat of the salt to its present-day edge (Heward, 1990; Loosveld *et al.*, 1996). Significant erosion of Devonian sediments was caused by Hercynian movements that started in the Middle Devonian (Husseini, 1991). The distribution of Haushi Group sediments was controlled by supply from the structural highs along the present-day coastline of Oman. These highs represented thermally uplifted domes preceding Gondwana break-up (Loosveld *et al.*, 1996). The subsequent relatively continuous sedimentary succession deposited up to late Cretaceous was indications of the relative stable conditions on passive continental margin, (Loosveld *et al.*, 1996).

The Ophiolites in Oman were emplaced during late Cretaceous as a result of the closure of the Neo-Tethys (Loosveld *et al.*, 1996). The obduction caused significant downwarping in the northern Interior Oman Sedimentary Basin (Béchennec, 1994). With the development of a new subduction zone offshore Iran, the deformation in Oman stopped abruptly and was followed by relatively quiet tectonic conditions leading to passive margin sedimentation in the Tertiary (Loosveld *et al.*, 1996). Continental collision along the Zagros suture caused uplift of the Oman Mountains during the Oligocene and Pliocene (Loosveld *et al.*, 1996).

Halokinesis (salt movement) and the emplacement of the ophiolite were the main mechanisms that shape the present day structure of the northern Interior Oman sedimentary Basin , while the structural evolution in the South Oman Salt Basin was mainly controlled by salt removal on the Eastern Flank and halokinesis (section 2.2.1) in the central basin (Heward, 1990; Loosveld *et al.*, 1996)

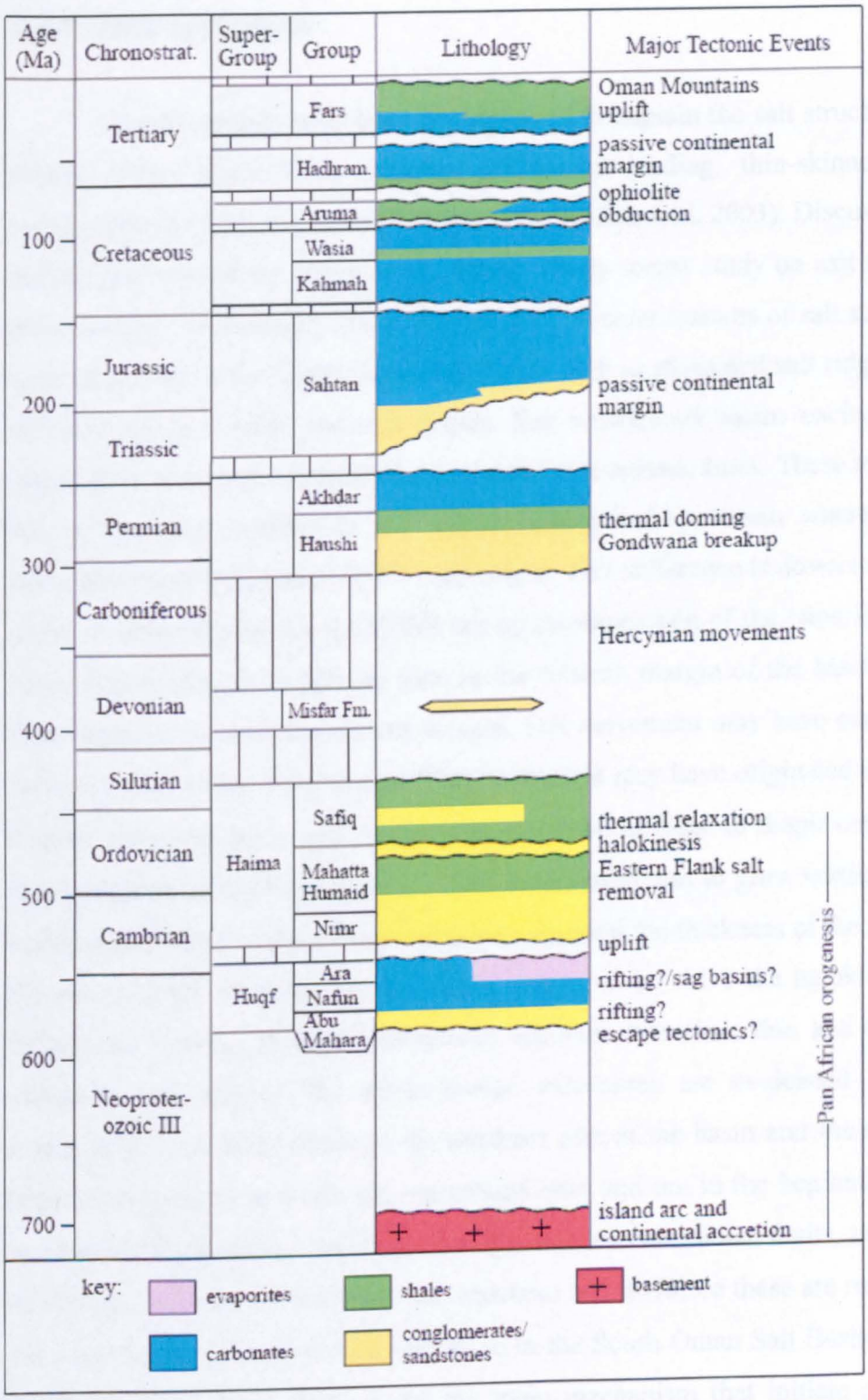

Figure 2-1: : Tectono-stratigraphy of Oman including South Oman Salt Basin, after Loosveld *et al.* (1996).

2.2.1 Salt Tectonics

Several models have been hypothesised to explain the salt structures found in Oman. These were down building differential loading, thin-skinned extension, compressional diapirism, and salt dissolution (Al-Barwani, 2003). Discussion all these models are beyond the scope of this study. Fairly recent study on salt tectonics was presented by Al-Barwani, 2003 (Figure 2-2). Several features of salt structures have been identified in the South Oman Salt Basin such as elongated salt ridges, elongated salt pillows, salt walls, and salt diapirs. Salt withdrawal basins encircled with salt ridges have also been identified in the basin from seismic lines. These minibasins are sub circular and smaller in the western margin of the basin whereas elongated minibasins with elongated NE-SW salt ridges. This difference is down to the different styles of sedimentation in the SOSB during the deposition of the Nimr Group and the Amin Formations, with alluvial fans in the western margin of the basin and braided river deposits towards the eastern margin. Salt movement may have occurred during the deposition of the Nimr Group. This movement may have originated in the form of diapirs, which began as salt ridges. The transition of ridge to diapir occurred during the deposition of the Haima group. . The diapir continues to grow vertically by down building as thermal sag and sedimentation increased the thickness of the post-salt load. Several different mechanisms may have triggered and drive the halokinesis such as differential loading, thermal convection, regional extension, thin and thick-skinned extension and others. The thick-skinned extensions are evidenced by basement extensional reactivated faults in the northern part of the basin and the central Oman High. However, these faults are reactivated later and not in the beginning of the salt movement. No evidence was found for thin-skinned extensional faults, salt dissolution minibasins, or even contractional salt tectonics and therefore these are ruled out as the main mechanism for minibasin formation in the South Oman Salt Basin. Differential loading may be more likely to be the main mechanism that initiate and drive the diapirism. This probably occurred at the early stages during the deposition of the the Nimr Group and the lower Haima group. Sediment progradation from the west and southwest was probably the main driving force of salt movement. Thick-skinned faults or basement faults may have been important in determining the direction of salt migration.

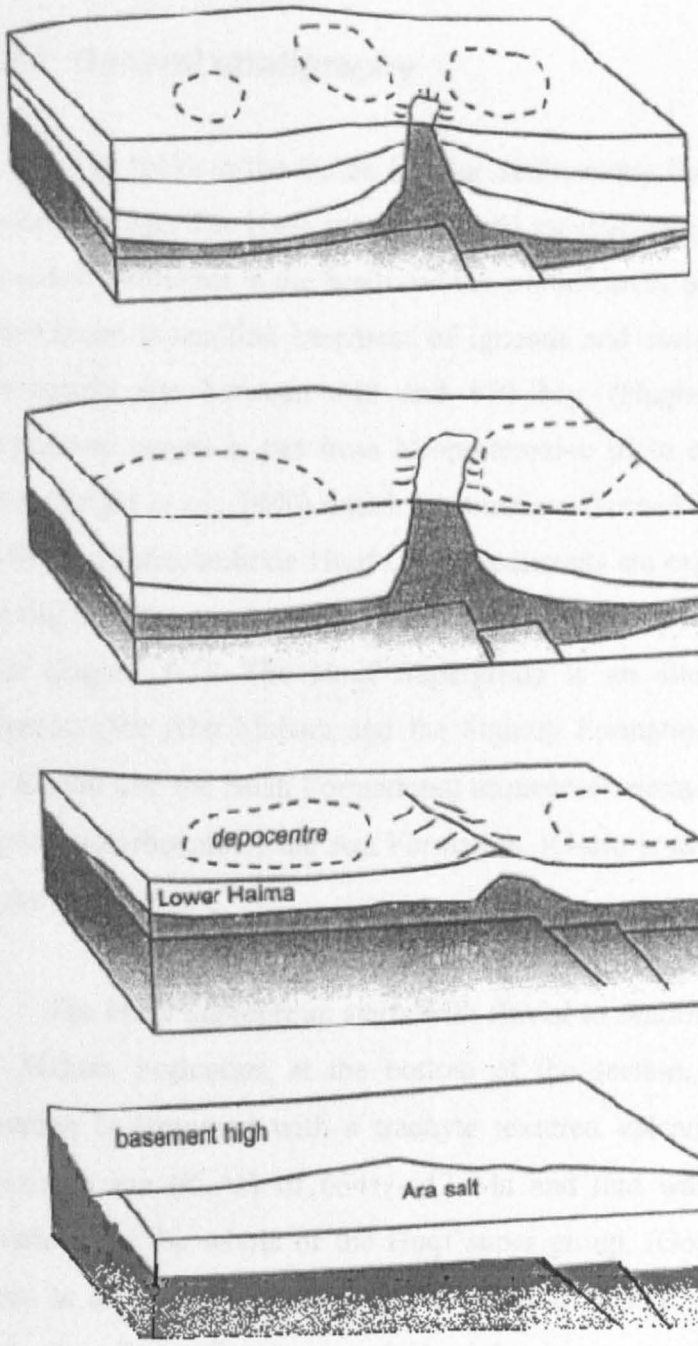

Figure 2-2: Halokinetic movements model for Ara group in South Oman Salt Basin, (Al-Barwani, 2003).

2.3 Stratigraphy and depositional environment

2.3.1 General stratigraphy

The rocks in the Oman Interior Sedimentary Basin span from Precambrian to Quaternary age. The Huqf supergroup of Late Precambrian to middle Cambrian age is the oldest sediments in the basin and the whole Oman, and it is directly situated on the Pan-African crystalline basement of igneous and metamorphic rocks, which has a radiometric age between 740 and 870 Ma, (Hughes-Clarke, 1988). The Huqf Supergroup ranges in age from Neoproterozioc III to early Cambrian, (Gorin *et al.*, 1982; Wright *et al.*, 1990) which is sometimes termed Infracambrian, (Wright *et al.*, 1990). The Infracambrian Huqf Group sediments are exposed along the Huqf-Dhofar axis highs in the southern and east central Oman and in the Oman mountains in the north (Figure 1-1). The Huqf Supergroup is an alternating sequence of clastic sediments (the Abu Mahara and the Shuram Formations) and carbonate sediments (the Khufai and the Buah Formations) sequences overlain by alternating sequence of evaporates-carbonate of the Ara Formation, (Gorin *et al.*, 1982; Wright *et al.*, 1990) (Figure 2-1).

The Huqf Supergroup starts with fluvial to shallow marine siliciclastics of the Abu Mahara Formation at the bottom of the section, (Gorin *et al.*, 1982). This Formation is bottomed with a trachyte textured volcanic sediments which give a radiometric age (K-Ar) of 654+/- 12 Ma and that was taken as the base of the Formation and the whole of the Huqf super group, (Gorin *et al.*, 1982). The Abu Mahara is divided in to two units, the Ghadir Mankil Formation and the younger Masira Bay Formation separated by dolomitic unit of approximately 10m thick (Droste, 1997). The Abu Mahara group was probably deposited in braided stream to tidal flat regime (Gorin *et al.*, 1982) or as synrift non-marine to intertidal glacially deposits within Najd rift basin (Loosveld *et al.*, 1996).

The Nafun Group (middle Huqf) was deposited between 600 and 550 Ma (Al-Barwani, 2003) with a thickness of 1700m (Gorin *et al.*, 1982). This group is divided into three formations: the Khufai, the Shuram, and the Buah Formations (Figure 2-3). The Khofai Formation conformably overlies Abu Mahara and varies in thickness from

240-340m. The Khufai Formation consists of shallow subtidal, intertidal and supratidal (Ṣabkha) carbonates. The basin appeared to be suffering from starvation of clastics and Oxygen as indicated by relatively high organic content in Khufai Formation. This is probably because some pre-Khufai arches caused some restriction in water flow. (Gorin *et al.*, 1982; Wright *et al.*, 1990)

Influx of clastics marked a change in the weather to probably wet climate and marked the beginning of second carbonate-clastic cycle (Buah-Shuram Formations). These clastics are fine grained heavily reworked, (Gorin *et al.*, 1982) which indicates a rapid sea level rise occurred due to change in climate, (Schrooder, 2000). These deep-water fine clastics comprise the Shuram Formation, which pass upwards in to the Buah Formation Carbonates. The Buah Formation was probably deposited in shallow subtidal and intertidal environment. Wright *et al.*, (1990) argued that the basal part of the Buah and the Khufai Formations were not deposited in lagoonal setting as interpreted by Gorin *et al.*, 1982 but rather deposited in marine setting below storm wave base. The Shuram formation has a thickness of 600m while the thinner Buah Formation has a thickness of 250-340m. Deposition of the Huqf group ended with the evaporate-carbonate cycles of the Ara Group that record an important phase of basin restriction, (Mattes & Conway Morris, 1990). These will be explained in details in a separate section (2.3.2).

The Haima supergroup is subdivided in to three groups: the Nimr sequence (lower Haima), the Mahatta Humaid sequence and the Safiq sequence (Upper Haima). The Lower Haima group (Nimr sequence) consists of very fine grained sandstone passing to a shale interval interbedded with silts and sandstone and the whole sequence varies in thickness from 400 to 800m in the South Oman Salt Basin (Droste, 1997). This sequence was classified to be the upper part of the second rift sequence (Loosveld *et al.*, 1996) and interpreted to be braided river channel and sheet flood deposits in a prograding alluvial apron (Droste, 1997; Heward, 1990).

The Nimer sequence or the Ara Group in some parts of the basin (where Nimer is not present or eroded) is roofed with an angular unconformity (the Angudan Unconformity) as a result of Cambrian uplift (Hughes-Clarke, 1988). This marks a shift in deposition from restricted marine to continental which predominate the

Cambrian to Silurian Haima supergroup (Hughes-Clarke, 1988; Millson *et al.*, 1996).The Mahatta Humaid sequence is a composite clastic rock unit of Cambrian to Lower Ordovician in age. This sequence is divided in to three formations: the Amin Formation, the Mahwis Formation, and the Ghudun Formation (Figure 2-3). The Amin Formation overlies the unconformity and consists of sandstones interbedded with conglomerates of variable thickness (30-400m). This formation was believed to be deposited as proximal alluvial fan deposits sourced from the uplifted basin margins highs (Droste, 1997). The Amin Formation is overlain by the shaley sandy Mahwis Formation (Hughes-Clarke, 1988). The Mahawis Formation consists of an overall fining upwards sequence of 200-800m of micaceous shaley sandstone interbedded with conglomerated grading vertically and laterally into fine grained micaceous sandstone and siltstone (Hughes-Clarke, 1988). This formation is divided in to two members: a lower sandstone/conglomerate member (the Miqrat) and an upper sandstone/siltstone member (the Andam) (Figure 2-3). The Mahawis Formation was interpreted to be as a proximal part of semi-arid alluvial fans system that laterally graded into alluvial plains with sheet flood deposits and ephemeral lakes/sabkhas (Heward, 1990). The Ghudun Formation is the most widespread and the thickest unit of the Haima supergroup (Hughes-Clarke, 1988). This formation thins towards the southeast and it is missing on the eastern flank and the Central Oman High of the South Oman Salt Basin (Hughes-Clarke, 1988). The formation consists of sandstones and siltstones with very low clay contents and abundant sedimentary structures such as cross-bedding, parallel laminations and current ripples. It is believed to be deposited as fluvial channels and sheet flood deposits (Droste, 1997). The Ghudun Formation is conformably overlain by generally clay rich beds of the lower Safiq (Hughes-Clarke, 1988). However, the Safiq Formation has not been found in the South Oman Salt Basin and only restricted to the western part of the Interior Basin (the Fahud subbasin) (Hughes-Clarke, 1988).

The Ghudun Formation is very often overlain unconformably by the Haushi group in the South Oman Salt Basin (Hughes-Clarke, 1988). The absence of upper Silurian to Middle carboniferous sediments in the South Oman Salt Basin records the influence of Hercynian orogeny on the eastern Arabian plate, (Husseini, 1991; Loosveld *et al.*, 1996). The Lower Devonian Misfar Formation is the only unit that escapes this tectonics and is locally preserved (Loosveld *et al.*, 1996). The Haushi

group is divided into two formations: the continental deposited Alkhalta (100-240m thick) and the fluvio-marine Gharif formations (150-200m thick)\(Hughes-Clarke, 1988). The glaciogenic Al-Khalta Formation forms the basal unit of Haushi Group, overlain by fluvial to shallow marine siliciclastics of the Gharif Formation, (Hughes-Clarke, 1988) the Permo-Carboniferous Haushi Group is unconformably overlying mainly the Silurian Haima shallow marine sediments and this unconformity possibly represents the Upper Carboniferous Gondwana deglaciation and related transgression, (Schrooder, 2000).

The break up of the Pangaea, started in Triassic led to form a passive continental margin in Oman. Large carbonate platforms were established along the southern margin of Tethys, of which Oman was part (Loosveld *et al.*, 1996). This platform consists of dominantly shallow marine carbonates represented by the Akhdar and the Sahtan groups, (Loosveld *et al.*, 1996). Progressive rise of sea level throughout Jurassic lead the platform to be drowned and deep water sediments deposited of the lower Kahmah group, (Loosveld *et al.*, 1996). Shallow water carbonate platform restored again in Middle Cretaceous, which consist of the upper Kahmah and the Wasia Groups, (Hughes-Clarke, 1988).

The ophiolite complex were obducted during Upper Cretaceous as well as the Hawasina and the Semail Nappes as a result of Tethys closure between Eurasia and Arabian plate during the formation of South Atlantic ocean (Loosveld *et al.*, 1996). The Aruma Group were deposited in the foreland of advancing thrust sheets. Deep water sediments dominate the northern settings of the basin and pass southward into carbonate platform, (Hughes-Clarke, 1988). After ophiolite emplacement, deposition on a stable passive margin was restored (Loosveld *et al.*, 1996). The Tertiary Hadhramaut and the Fars Groups record deposition of slope, to shallow marine and reefal, to lagoonal carbonates interbedded with evaporites and continental clastics (Figure 2-1; Hughes Clarke 1988). Quaternary deposits in the Interior Oman Sedimentary Basin are characterized by alluvial, fluvial, lacustrine and aeolian conditions (Hughes-Clarke, 1988).

2.3.2 Ara group

2.3.2.1 Internal Stratigraphy

The Infracambrian Ara group is the youngest unit in the Huqf supergroup and consists of carbonate/evaporate cyclic sequences with thick salt intervals. The Ara group consists of 6 or 7 3rd order eustatic evaporite-carbonate cycles (A1-A6 (Schrooder, 2000) or A0-A6 (Amthor *et al.*, 2005)) capped by siliciclastic dominated sediments derived from structural highs at the end of the Ara group deposition (Mattes & Conway Morris, 1990). Syn- and Post depositional salt movements affect largely the distribution of the carbonate bodies with respect to the salt. Most of the carbonate bodies are dissected, non-continuous, and floating on salt. The carbonate bodies are termed "**Carbonate Stringers**" by PDO geologists.

Each Ara cycle (Figure 2-3) is termed (AX (E/C)); where A stand for Ara, X for the cycle number and E/C for Evaporite/Carbonate respectively (Amthor *et al.*, 2005; Schrooder, 2000); i.e. A2C is 2nd cycle of Ara carbonates. Cycles A1 to A3 is grouped as Birba Formation and A5 and A6 is grouped as Al-Noor Formation. The Carbonate Stringer in the middle cycle (A4) is anomalously rich in Uranium and therefore it is called U Formation, (Schrooder, 2000). U formation has a distinctive negative carbon isotope signature (-2 to -4‰ $\delta^{13}C$) (Schrooder, 2000). The first four (A1-A4) or five (0-A4) cycles were probably deposited during periods of high and relatively continuous subsidence (Mattes & Conway Morris, 1990). The Al-Noor Formation consists of much thicker evaporates with only thin and discontinuous Carbonate layers (Schrooder, 2000).

The Ara cycles are mainly controlled by both tectonics and eustatic sea level. The deposition of these cycles was probably related to a pulse of increased subsidence in the basin to allow for the deposition of the thick salt bodies (Mattes & Conway Morris, 1990). The beginning of this subsidence is believed to occur simultaneously with the start of Ara sedimentation. This is evidenced by the presence of both shallow shelf and deeper basin facies in the basal Ara carbonate separated by fault controlled shelf edge (Amthor *et al.*, 2005; Mattes & Conway Morris, 1990). The thick salt accumulation might have compensated the difference in relief between the platform

and the basin, however, this was probably not perfect because all carbonate stringers in Ara formation contain faulted shelf margin separating the shallow and deeper marine facies (Schrooder, 2000). The deposition of salt and carbonate is mainly controlled by eustatic sea level; the carbonates intervals were deposited during high sea level when the basin is connected to an open ocean (Mattes & Conway Morris, 1990). While the evaporites precipitated during low sea level with the water flow being restricted, and the net evaporation resulted in the formation of large saline lakes surrounded by sandy desert with playas and sabkhas (Mattes & Conway Morris, 1990). Sharp breaks characterize the boundaries between the carbonate bodies and salt bodies (Mattes & Conway Morris, 1990).

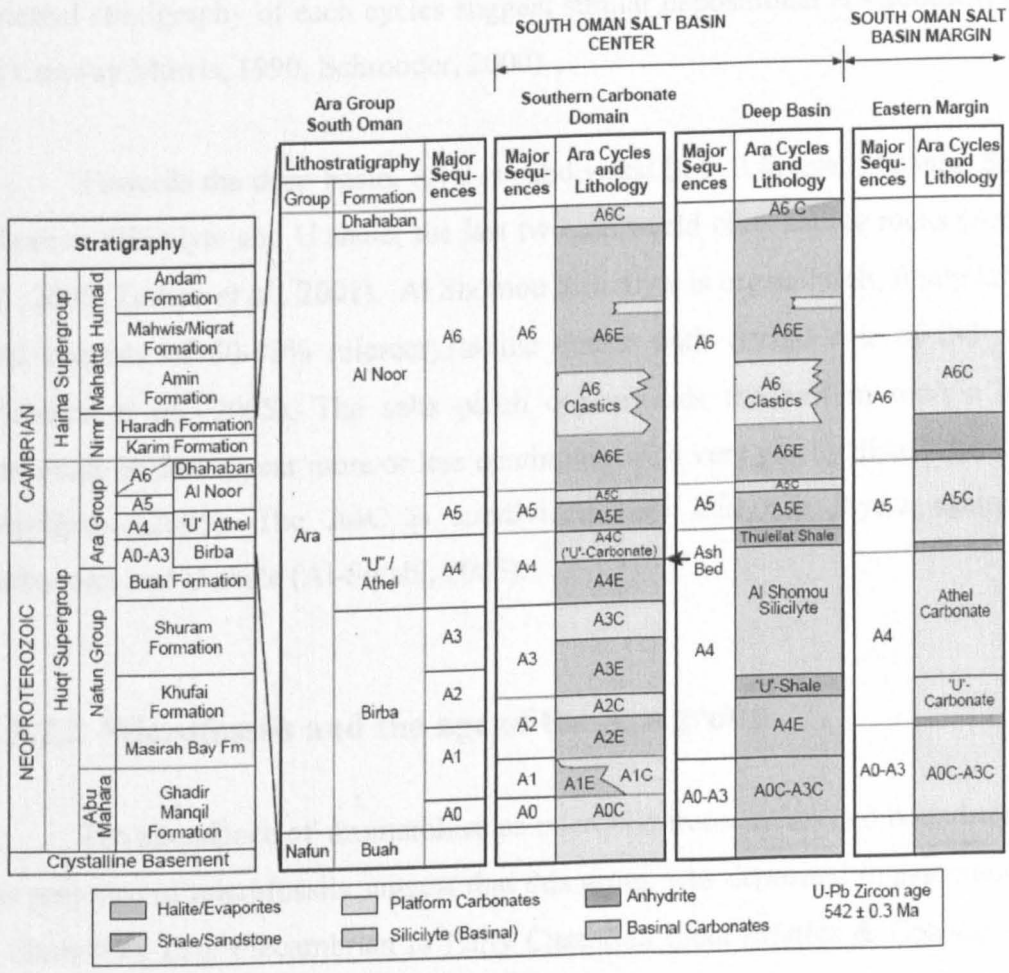

Figure 2-3: Generalized stratigraphy of the Huqf Supergroup in the South Oman Salt in the first column on the left and subdivisions of Ara group in the centre of the basin in the second and third columns to the right, and their equivalence in the eastern margin (eastern flank). After Al-Siyabi (2005).

The stratigraphy of individual cycles is very similar (Mattes & Conway Morris, 1990; Schrooder, 2000). The Evaporites consist of anhydrite, halite and minor amounts of other salts. Anhydrite forms largely by diagenetic conversion of primary Gypsum and form the only sulphate present in Ara sediments, (Mattes & Conway Morris, 1990). The carbonate stringers at present are completely dolomitized and form a major hydrocarbon exploration target in Oman (Al-Siyabi, 2005). Each carbonate stringer varies in thickness from few metres to 200m, and the associated sulphate beds are generally less than 20m thick (Mattes & Conway Morris, 1990). Enormous variations of thickness in salt are down to salt movement and salt removal (Heward, 1990) as well as sediment loadings (Mattes & Conway Morris, 1990). The internal stratigraphy of each cycles suggest similar depositional environment (Mattes & Conway Morris, 1990; Schrooder, 2000).

Towards the deep basin, A4C is subdivided in to 3 layers, Thuleilat Shale, Al Shomou Sillicilyte and U shale; the last two are world class source rocks (Amthor *et al.*, 2005; Terken *et al.*, 2001). Al Shomou Sillicilyte is organic rich, finely laminated and consists of 80-90% microcrystalline quartz with crystal size of 2-3 microns (Amthor *et al.*, 2005). The salts pinch out towards the eastern margin and the carbonate bodies appear more or less continuous with very patchy distribution of salts (Al-Siyabi, 2005). The A4C is subdivided here into two layers again, Athel carbonates and U shale (Al-Siyabi, 2005).

2.3.2.2 Microfossils and the age of the Ara group

The abundance of stromatolites as microbial framestones and boundstones and the presence of microfossils suggest that this group was deposited in association with a flourishing Late Precambrian to Early Cambrian biota (Mattes & Conway Morris, 1990). Well-defined remains of fossil cyanobacteria were recorded in shallow and deep-water sedimentary facies of Ara Formation. Other fossils found in Ara sediments are unornamented calcareous dolomitic and siliceous cyst-like spheres deposited in settings ranging from platform shoal to deeper basin. These were suggested to be attributed to cyanobacterial origin (Mattes & Conway Morris, 1990). Other spherical nannofossils of uncertain affinity were also found in a number of Ara cores. They are

associated with the shallow water framestones and nodular thrombolitic structures. These nannofossils were thought to be of cyanobacterial origin again, (Mattes & Conway Morris, 1990). Other microfossils found in Ara sediments are Micritic bush like masses and Tabular shelly fossils with compound walls associated with framestones and boundstones. The former shows close affinity to the cyanobacterial genus *Angulocellularia* Vologdin, which occur commonly in shallow water facies of the Ara carbonates. (Mattes & Conway Morris, 1990). The later is probably related to *Cloudina* Germs found in Nama Group in Namibia which has been attributed to the Latest Precambrian suggesting this microffosil to be the oldest metazoan with hard parts in the fossil record (Amthor *et al.*, 2003).

The facies association and the microfossil content both suggest that Ara group was deposited in the Precambrian-Cambrian boundary (Infracambrian) and possibly can be dated at 570Ma by comparison with the Nemakit/Daldyn River Basin in Siberia (Amthor *et al.*, 2003; Mattes & Conway Morris, 1990). A volcanic ash horizon has been found at the base of the A4C and was dated at 542.8 ± 0.8 Ma (Schrooder, 2000). The strong negative carbon isotope anomaly in A4C cycle was correlated with the excursion observed globally near the Neoproterozoic III-Cambrian boundary (Mattes & Conway Morris, 1990). This has been confirmed by carbon isotopic and chronometric studies, which dated the A4C isotope anomaly at 542.8 ± 0.8 Ma old (Schrooder, 2000) and 542.0±0.3 (Amthor *et al.*, 2003) based on U-Pb age on Zircon.

2.3.2.3 Depositional model

A number of depositional models, published and unpublished, were proposed for the deposition of the Ara cycles. However, all models agree that Ara group was deposited in the form of a silled basin that provided the necessary restriction for the formation of carbonate-evaporite cycles. Only two models have been published and those were proposed by Mattes & Conway Morris, (1990) and Schrooder (2000). The two models were very similar; therefore, the summary will be based on both of them.

Carbonate and evaporite were deposited in response to changes in sea level and restriction of water flow from the ocean. During relatively high sea level, shallow water sediments were deposited on the basin margins and on active tectonic highs, whereas deep water-carbonates and black shales were deposited in deeper parts of the basin. Each Ara carbonates unit progrades from shallow shelf or ramp, towards the troughs of the basin. This carbonate sequence consists of six types of carbonate facies. The basinal sediments are organic rich, finely laminated dolomite mudstone and calcareous shale. They are deposited in quiet environment well above the wave base. These are overlain by rhythmically laminated mudstones characterized by small kinks and overturned folds and small-scale normal faults suggesting slope type of facies. Stromatolites, packstones, and wackstones facies assemblage overlay these facies. These are thought to be deposited in well-oxygenated shallower open marine platform or ramp setting. Bioherms and grainstones overly these facies assemblages and believed to be typical platform barrier deposits. These facies separate the open platform facies from the carbonate sediments deposited in restricted platform. These include mainly very finely laminated muddy stromatolites, dolomitic mudstones, and cross-laminated silty dolomites. These are capped by dolomites associated with nodular and massive anhydrite as well as storm deposited carbonate silts and conglomerates. These are thought to represent coastal plain or shallow platform deposits. (See Figure 2-4)

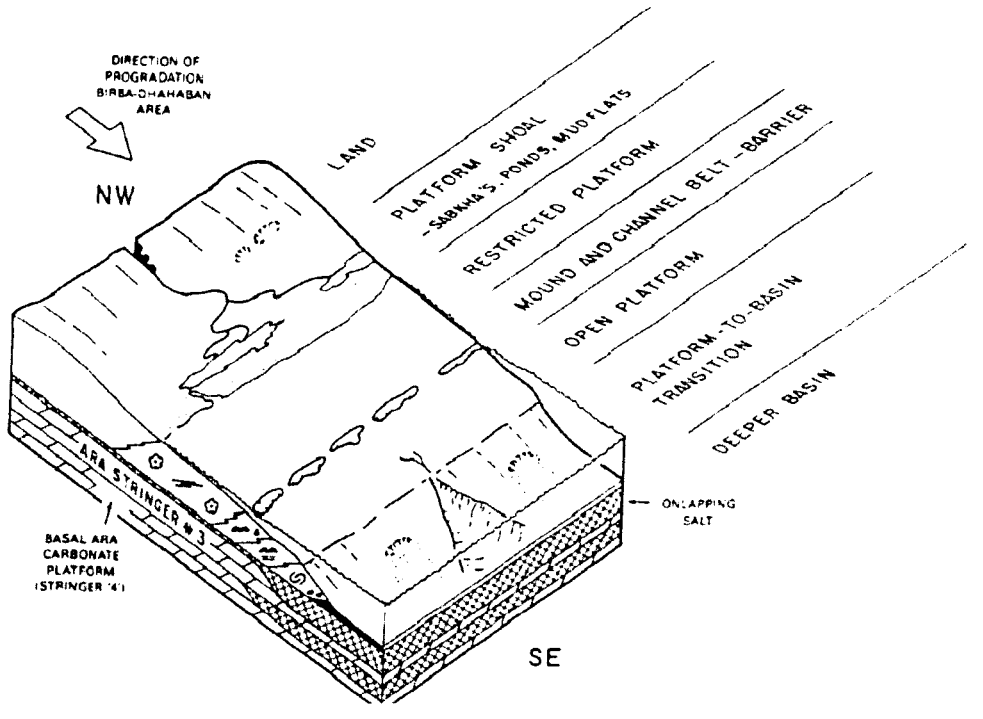

Figure 2-4: Schematic diagram illustrating the depositional environment at which the carbonate stringers were deposited (Mattes & Conway Morris, 1990).

The evaporites were deposited when the sea level dropped to a level where the net evaporation is higher than the fresh water flux received from the ocean. Repeated connection to the ocean was probably necessary to accumulate thick salts (Mattes & Conway Morris, 1990). However, sea level cannot be alone responsible of producing such thick salt bodies; subsidence also played an important role to provide accommodation (Schrooder, 2000) (Figure 2-5). Each carbonate unit is sandwiched by floor anhydrite in the bottom and roof anhydrite in the top of the unit with sharp contacts (Mattes & Conway Morris, 1990) but Schrooder, (2000) observed gradual change from carbonate to roof anhydrite over a metre or so in prograding sequence in A4C core. These anhydrites were deposited at elevated salinity level caused by the evaporation of the restricted water body in the basin shelf. The increase of salinity to 35% or greater results in precipitation of halite and potassium salts deposits. The retrograding succession from halite to floor anhydrite to carbonate was not incorporated in Mattes & Conway Morris, (1990)'s model, although it can be inferred. This sequence is characterized by sharp contacts at the top and the bottom of floor anhydrite that are probably related to flooding events (Schrooder, 2000).

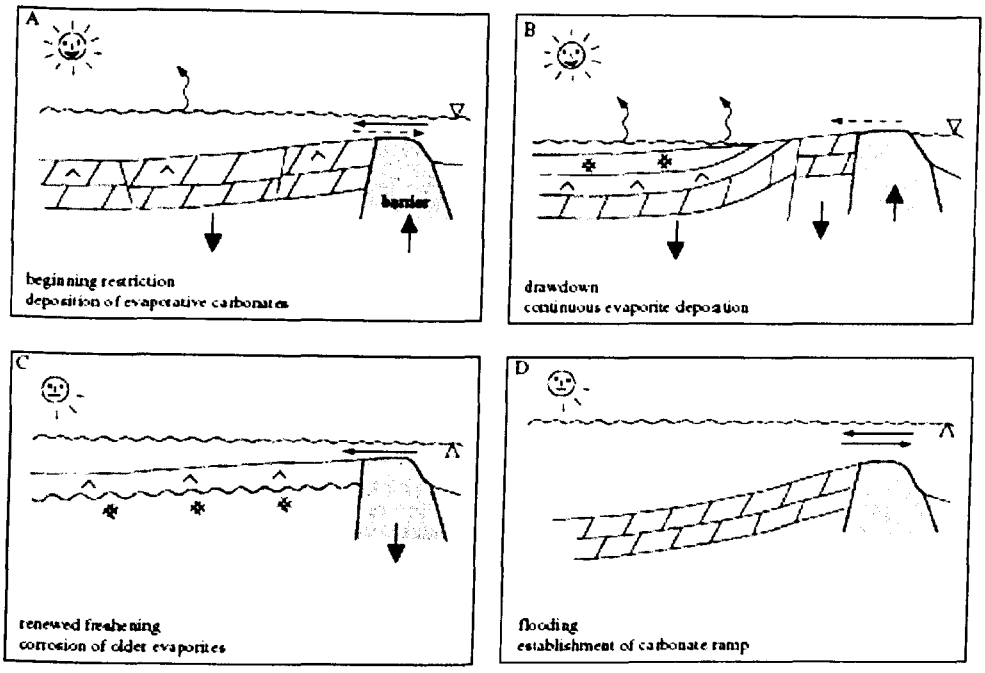

Figure 2-5: a schematic model of the silled basin and depositional setting that lead to the formation Ara salts and carbonates (Schrooder, 2000).

2.4 Diagenetic history

The early and late diagenesis of Ara carbonate stringers were described by Schrooder, 2000 as well as few notes by Mattes & Conway Morris, (1990) and Hollis *et al.*, (2002). Therefore, a summary of their observations will be presented in this section (see Figure 2-6).

- Early diagenetic processes: Generally, early diagenesis is rarely preserved. Some of these preserved processes:
  - Micritization of grains (syndepositional)
  - The precipitation of botryoidal aragonite cements in framework pore of thromobolites (syndepositional)
  - Early leaching (only observed locally). This resulted in destruction of porosity.
- Dolomitization. This major diagenesis process led to creation and preservation of porosity and permeability. This was widespread and occurred at various phases of diagenesis. The dolomotization in A4C unit was observed to be complete and fabric sensitive. This process occurred probably by organogenesis and reflux dolomitization in open

systems. When the carbonate became sealed by evaporites, the carbonate diagenesis was slowed down and was mainly dolomite neomorphism that led to relatively homogenous geochemical composition. Very often, the early dolomite fabrics were overprinted by coarser dolomites occurred as a later phase, probably by enhanced fluid flow in high porosity and permeability mediums and by pressure solution.

- Late diagenetic processes:
  - Anhydrite replaced carbonate, plugged the pores, and destroyed the porosity. This phase overlaps most other phases.
    - Anhydrite nodules in carbonates often predate compaction.
    - Replacive anhydrite and anhydrite cements post-dated late dolomite.
  - Halite cementation (late phase).
- Other diagenetic processes:
  - Dedolomite: the break down of dolomite in to basic components calcite and magnesium carbonate under high thermal stress.
  - Replacive silica
  - Silica cement
  - Precipitation of exsudatinite
  - Pyrites occur randomly.
  - Fracturing and leaching (localized and minor): these are related to salt movement. Although they enhance the permeability, they encouraged salt plugging resulting in space and mobility destruction. (Mattes & Conway Morris, 1990)

Most of the above are porosity destructive, except for dolomotization and early leaching. Dolomotization can enhance both permeability and porosity of the host facies that have high initial porosity, but it is limited to one phase of early recrystallisation and does not transform poor quality reservoir rocks to high quality reservoir rocks (Hollis *et al.*, 2002). The sucrosic dolomite mosaics resulted from

dolomotization are characterized by good permeability even in mudstones. It is worth to note that hydrocarbon staining and the exsudatinite were regarded as important evidence of that an expulsion of hydrocarbons occurred under thermal stress from the organic rich beds of carbonate (Mattes & Conway Morris, 1990). Crinky laminate with good vuggy porosity found at the base of A4C indicates that this part was away from evaporite cementation. It was suggested that early expelled charge of hydrocarbons probably slowed or stopped diagenesis and preserved the present day good vuggy porosity in this bed (Schrooder, 2000). The coarser facies like grainstones and stromatolites preserved the depositional fabric suggesting that early recrystallisation and cementation helped to preserve high porosity and permeability (Mattes & Conway Morris, 1990).

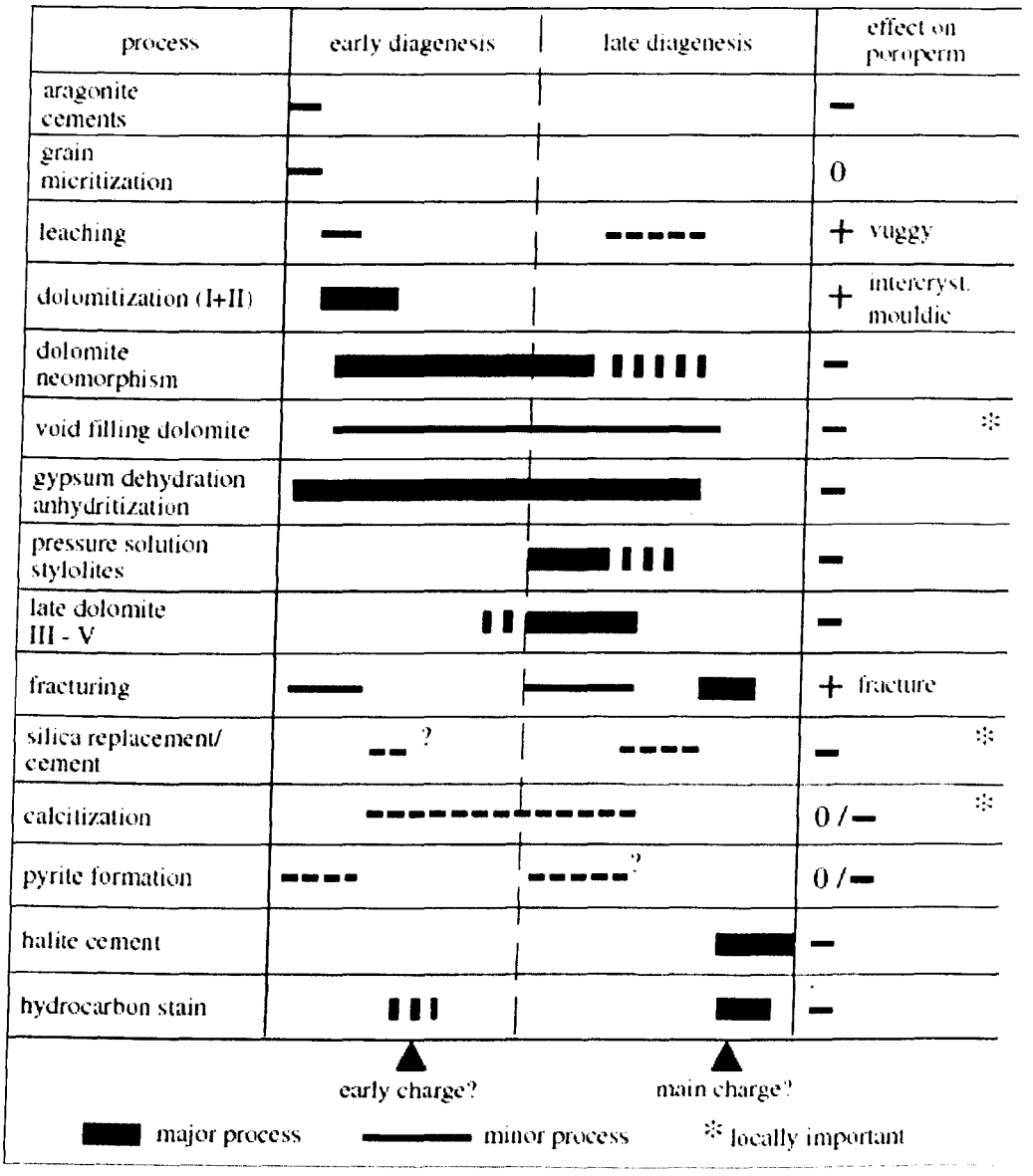

Figure 2-6: Diagenetic history of carbonate stringers of Ara group, (Schrooder, 2000).

2.5 Reservoir quality

Dolomitisation of Ara carbonates provides an important exploration target (Al-Siyabi, 2005). The carbonate stringers are completely encased in evaporites and are thus perfectly sealed and over pressured as clear in Figure 1-2. Diagenesis in the evaporitic setting was apparently very complex and commonly masked depositional fabrics, (Mattes & Conway Morris, 1990). The lack of outcrop equivalents has hampered full understanding of the depositional and diagenetic system (Schrooder, 2000). The Ara carbonates contain facies with high initial porosity, for example grainstones/ packstones, stromatolites and thrombolites, which are potentially good reservoirs (Mattes & Conway Morris, 1990). Dolomitic and evaporitic cements may plug the pores in these types of facies (Mattes & Conway Morris, 1990; Schrooder, 2000) as clear from Figure 2-7. The salts plugs affect mostly those with high initial porosity and permeability. There are intervals with moderate primary porosity and permeability that are not affected by dolomitisation and well preserved, for example crinky laminated beds at the base of A4C section (Schrooder, 2000).

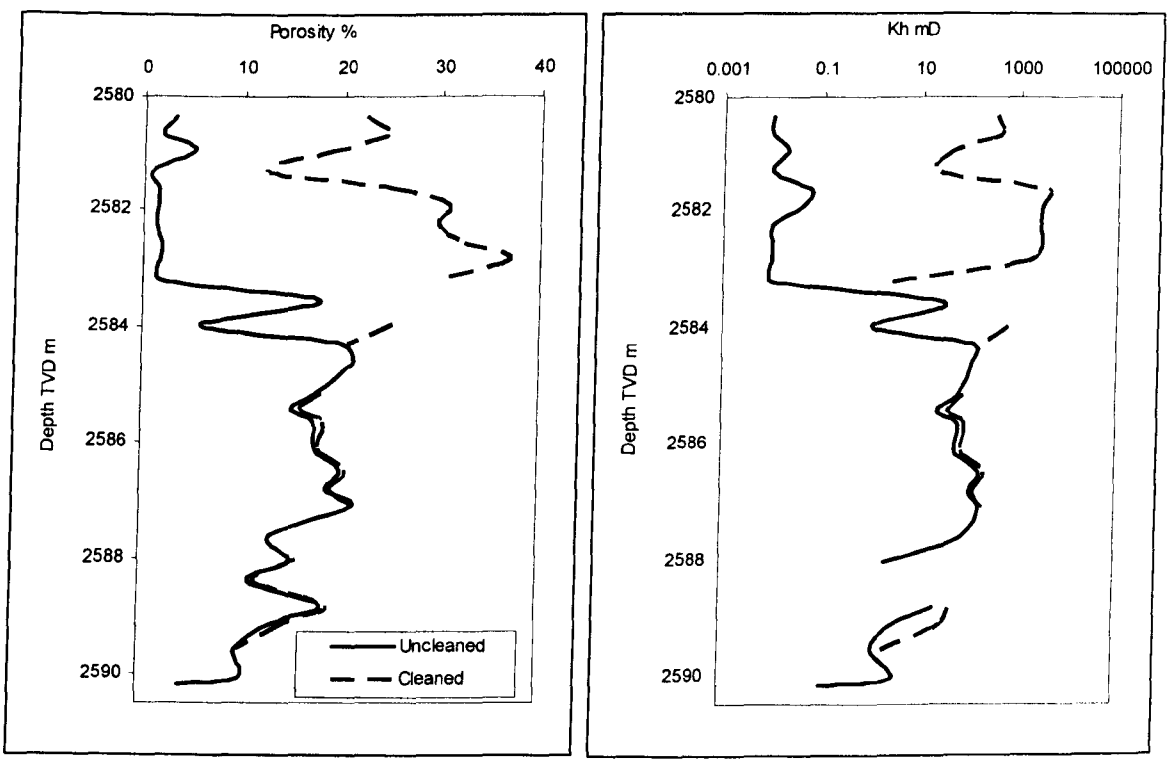

Figure 2-7: The variation of porosity and horizontal permeability with depth through A4C stringer in well BB2 in the Greater Birba area. The solid line is for the measured porosity and permeability without cleaning salts, and the broken line shows the porosity and permeability after cleaning the salts from the pores.

Shallow water packstones/grainstones and stromatolites at present show only low to moderate porosity and permeability due to burial diagenesis (Figure 2-8). Whereas, the crinky laminated facies in the lower part of the carbonate unit show moderate to good porosity and permeability. Porosities observed in A4C column are mostly around 10% and permeability commonly higher than 10mD. These facies when well preserved are characterized by organic rich laminae with intercrystalline and vuggy porosity (Schrooder, 2000). The recrystallisation digenetic process degraded the reservoir quality by pressure solution accompanying this process (Al-Siyabi, 2005; Schrooder, 2000). This resulted in reducing porosity and permeability by isolating the vugs and filling the pores. Thrombolites reefs are characterized by low porosity and permeability in the A4C section studied (Schrooder, 2000). This is due to the complex cementation and significant halite plugging as well as dolomite recrystallisation. (Schrooder, 2000). Table 2-1 shows the average porosities and permeabilities, and water saturation of different stringers from different wells incorporated in the study.

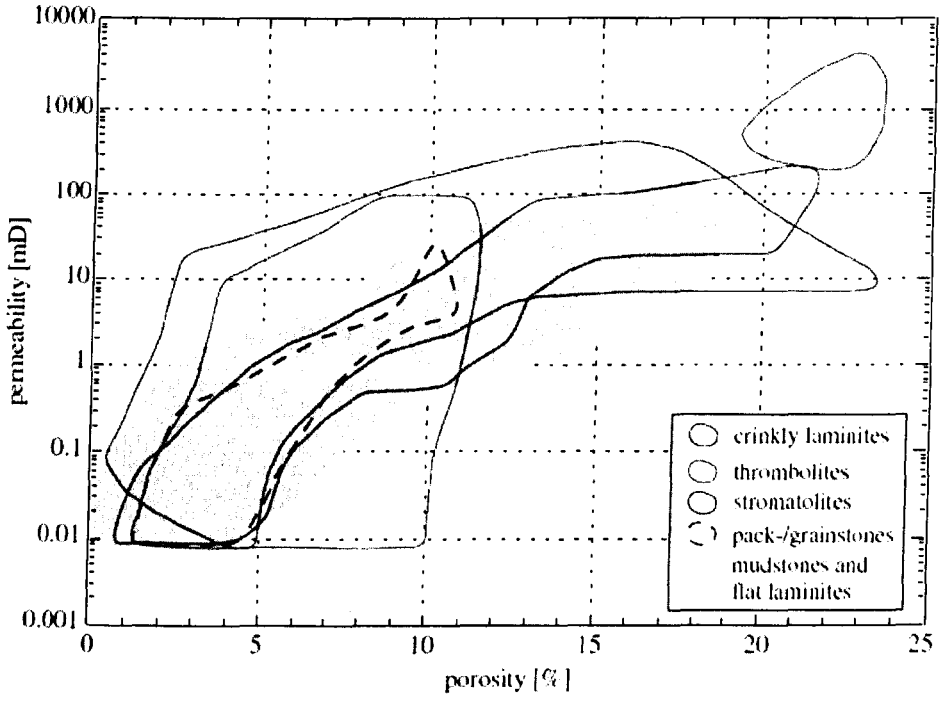

Figure 2-8: The range of porosities and permeabilities of different facies association in the carbonate stringer of Ara group. After (Schrooder, 2000).

Table 2-1: average Porosities, core plug permeabilities, and water saturation of different stringers from different wells incorporated in this study.

Wells	year of drilling	stringer	av. Porosity	average permeability mD	Sw %
BB1	1978	A4C	12.4		2.8
BB2	1978	A4C	13.7	150	3.1
BB3	1980	A4C	11.2	50	2.8
BB4	1981	A4C	8.4	20	61
BB5	1983	A4C	7.1	0.1	38
BBS1	1979	A4C	13.8	10-100	4.7
BBN1	1980	A4C	9		7.2
BBN1	1980	A3C	7.4	0.1	9.5
BBN2	1983	A4C	6.9	0.1	4
Durra1	1983	A3C	9.5	<1	5
Kaukab1	1983	A3C	9		10
Nassir1	1976	A4C	18.2		7.7
Omraan1	1980	A5C	17.2	310	5.6
Omraan1H3	1997	A4C	9.9		
Omraan1H3	1997	A3C	6.1		
Shamah1	1990	A3C	11	Tight	14

2.6 *Huqf source rocks and crude oils*

The distribution of hydrocarbons in the carbonate stringers that are encased by sea of salts provide a prime indication that the oil might have originated from within the salt and stringers or from pre-salt source rocks (e.g.Al-Marjeby & Nash, 1986). Although there are several source rock intervals present within Huqf group, the Huqf characterized oils are geochemically very similar and appear to be a mixture of all these intervals (Grantham *et al.*, 1988; Taylor *et al.*, 2003). Grantham *et al.*, (1988)'s study indicated that the Huqf oils found within the salt are correlated well with the source rocks found in carbonate stringers. However, no details were presented for this correlation, only an indication for an extensive study.

The organic intervals found within the Ara group were already mentioned above based on the work done by Mattes & Conway Morris, (1990). Those are dark, laminated, calcareous shales or dolomites with high sulphur and clay content and variable amount of silt. Kerogenous organic material as well as exsudatinite was also detected indicating the source potential of these intervals (Mattes & Conway Morris, 1990). The best source rocks of these intervals with high TOC (>2%) contain structureless kerogen of type II, probably derived from cyanobacterial origin (Mattes & Conway Morris, 1990). Those intervals are normally deposited under anoxic waters

with high salinity and very strong stratification and high productivity at the surface waters (e.g.Tyson, 1994). The carbonate stringers time equivalent sediments in deep basin and eastern margin show characteristically excellent source rocks, and these are the Al-Shomou silicillyte (or Athel silicillyte) and the U shales (Al-Siyabi, 2005).

The other potential source rocks in the Huqf supergroup are the Buah formation (Terken & Frewin, 2000) and the argillaceous dolomitic Shuram Formation (Terken & Frewin, 2000; Visser, 1991) from the Middle Huqf supergroup. Terken & Frewin, (2000) suggested U shale (equivalent toA4C) and Athel Silicillyte (stringers equivalent) Formations as two main source rocks for Huqf oils. An extensive study by Shell revealed other potential source rocks in the Huqf group (Taylor *et al.*, 2003). This study showed that the best source intervals for oils in carbonate stringers are from the Middle Huqf, specifically the Lower Shuram and the Upper Masira Bay Formations (TOC: 2-6%, HI: 200-900). According to this study, the intra-salt Athel Silicillyte, the U shale (A4C) and the Thuleilat shale are excellent source candidates as they are thick oil prone source rocks with very high TOC (TOC:2.5-5%, HI: 50-800). Other intra-salt organic rich intervals are thin beds and localised as they were found only by few wells (Taylor *et al.*, 2003). Amthor *et al.*, (2005), confirm these observations about the source potential of intrasalt source rocks.

The salt provides a challenge of how the oils migrated through the salt and locked in the carbonate beds (e.g.Al-Siyabi, 2005) and the present organic rich beds within the salts could not generate the whole volume of oils found in these stringers (Al-Siyabi, 2005; Taylor *et al.*, 2003). Besides, there are signatures of pre-salt source rocks (the Middle Huqf) (Taylor *et al.*, 2003). The oils in carbonate stringers are most probably mixtures from oils sourced from within the salt and from other Pre salt source rocks (Taylor *et al.*, 2003). This is further supported by the similarity between those oils and other Huqf oils (Grantham *et al.*, 1988; Terken & Frewin, 2000).

The oils sourced from the Huqf source rocks are found to occur in Precambrian to Tertiary reservoirs along the eastern flank of the South Oman Salt Basin (Grantham *et al.*, 1988). They also occur within early Cambrian intra-salt carbonate and siliceous stringer reservoirs (e.g. AlShomou Silicillyte and Thuleilat shale) in the central part of the basin (Amthor *et al* 1998). Huqf sourced oils show a

very low pristane/phytane ratio and contain significant amount of steranes (Grantham *et al.*, 1988). They are also characterized by a predominance of C_{29} steranes and X-compounds (Figure 4-20) and as well as highly negative carbon isotope values (Grantham *et al.*, 1988; Terken & Frewin, 2000). Statistical evaluation allowed correlation of different Huqf oils to the possible source rocks candidates (Taylor *et al.*, 2003). Some oils show more similarity to one source than the others (intra salt and presalt sources) and some show mixing behaviour between different sources suggesting that the Huqf oil charge was from different sources (Taylor *et al.*, 2003). According to the same source, the oils found in carbonate stringer A2C of Rabab and Sakhiya show close affinity to Shuram source rock, whereas the oils found in Dhahaban South A1C and Harweel Deep -1 A3C have intermediate biomarker and isotopic ratio.

2.7 Thermal history

It is not easy task to predict the thermal history for pre-Devonian source rocks due to the lack of vitrinite in source rocks of this age. Other means of estimating burial temperature and maturity are not as such reliable. The burial and thermal history of these source rocks were mainly relying on maturity estimates from Apatite Fission Track Analysis (AFTA) data and reflectance of solid hydrocarbons and oils (Terken *et al.*, 2001; Toth, 2001; Visser, 1991). Three different studies were done to evaluate the thermal and burial history of Oman in general and south Oman salt basin particularly, and these are Terken *et al.*, (2001), Toth, (2001), and Visser, (1991). The outcome of each of these studies will be outlined here.

Visser (1991) presented modeled burial histories of the Middle and the Upper Huqf source rocks using data from 97 exploration wells from all over the Oman Basins. The data used are wells information, depositional/erosional isopach maps and seismic data as well as Apatite Fission Track Analysis (AFTA) data and maturity estimates from hydrocarbon reflectance. According to Visser (1991)'s model, the northwest Oman had the main oil charge during Mesozoic, when most of the traps were already formed. Whereas, the maximum temperature was reached in the central and southeastern part of Oman about 400Ma, causing the end of the oil generation.

Most of the traps formed after this time, thus Visser (1991) suggested that the oils might have been trapped temporarily in pre salt reservoirs or in intrasalt carbonate stringers, and then remigrated once the traps formed during Mesozioc.

Terken *et al.*, (2001) evaluated the charge timing and risks of petroleum systems of Oman including the late Precambrian to early Cambrian petroleum system. According to their study, the maximum Burial temperatures in south Oman were reached during deposition of the Haima supergroup (Middle Cambrian-Early Silurian) and that the oil generation in Ghaba Salt Basin and south Oman salt Basin occurred mostly during early Palaeozoic (Terken *et al.*, 2001). They suggested that early expelled oil was probably initially trapped in Nafun reservoir rocks sealed by Ara salt and/or trapped in carbonate and silicillyte stringers encased in Ara salt, and that the remigration to the post salt reservoirs occurred due to the retreat of the salt edge at late Paleozoic and early Mesozoic due to halokinetic movements. They postulated that large parts of north and central Oman depend on long distance lateral migration (about 300km) from Huqf and Q kitchens from the northwest of Oman. This distance was determined by using the empirical relationship between the ratio of shielded and unshielded benzocarbazoles isomers and the migration distance (Larter *et al.*, 1996). Most of the oils in the South Oman Salt Basin might have come from Cambrian-Ordovician charge, which was stored in middle Huqf and intrasalt carbonates initially and then remigrated from traps below Ara salt due to the retreat of the salt edge. According to Terken *et al*, (2001)'s model, most of the gas is interpreted to form as a result of thermal cracking of liquid hydrocarbons trapped in deep reservoirs. However, this is proven to be not favorable by Toth (2001) who concluded that there was no gas produced by thermal cracking of hydrocarbon liquid.

Toth, (2001) presented 1D and 3D models to predict mainly the gas potential, from the Intra-salt and the Middle Huqf source rocks and also the gas and oil charge as well as the secondary migration routes for these petroleum systems. These models were based on data from 41 wells from the South Oman salt basin, mainly from the Greater Marmul area, the Greater Birba area and the Harweel cluster. The burial histories curves (Figure 2-9) indicate an initial high subsidence phase during Precambrian to Cambrian (500-400Ma) followed by uplift and nondeposition period within Devonian-carboniferous (400-250Ma), ending with a period of renewed low

subsidence phase from Mesozoic to Cenozoic (250-0Ma). All wells in this study show that the present day depth is equal or greater than the maximum burial depth reached 400Ma. From this model, two pulses of charges were predicted from these source rocks: 500-400 and 250-0Ma, separated by a period of uplift, non-deposition, and low paleosurface temperatures. Oil to gas cracking was proved unlikely in the intra-salt stringer reservoirs of south Oman based on these models. Secondary migration occurred from centre to eastern flank.

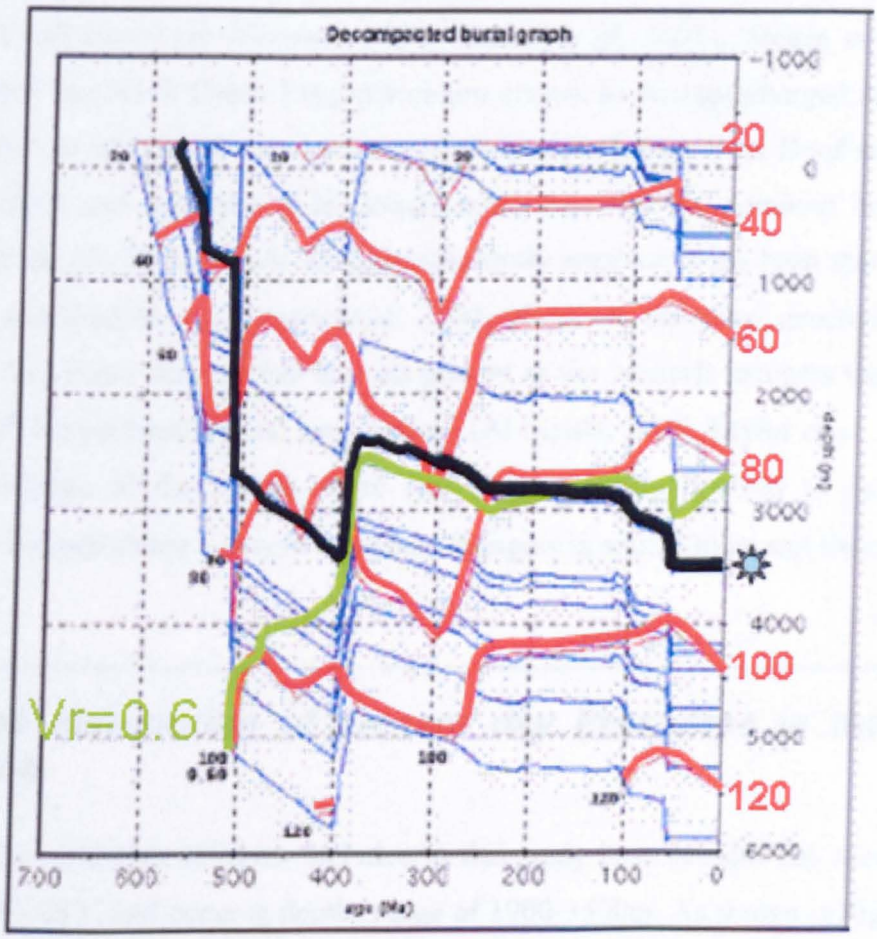

Figure 2-9: Burial curves of different formations (blue lines) in well BBN-1 as well as burial temperatures (red lines). The black solid line is the burial curve of the Intrasalt (e.g. U (A4C)) source rock.

Both Visser (1991)'s and Terken *et al*, (2001)'s models agree that the main oil charge from Huqf source rocks occurred during early Palaeozoic, and that the generated oils were locked first in temporary reservoirs (presumably intrasalt stringers), before it remigrated to post salt reservoirs due to retreat of salt in Eastern Flank. While Toth (2001) suggested there was probably another important charge occurred in the period of Mesozoic onwards, which contributed to the accumulations

present in the South Oman Salt basin from Huqf source rocks. However, all these models failed to discriminate between intrasalt charge and presalt charges.

2.8 Migration and trapping styles in south Oman Salt Basin

The major control on the trapping in South Oman Salt Basin was the Ara salt movements, while the retreat of the salt edge is the main control in charge timing to the post salt reservoirs (Howard, 1991; Terken *et al*, 2001). Terken *et al.*, (2001) interpreted the South Oman Huqf petroleum system to be supercharged and laterally filled prior to salt dissolution by the early Paleozoic charge from Huqf source rocks (both presalt and intrasalt). It is already mentioned that the common belief of the origin of the oils in carbonate stringers (the study reservoirs) has been that they were entirely self charged (e.g. Frewin *et al.*, 2000). However, the recent geochemical work done on this basin showed that the oils present in the intrasalt stringers were derived from both intrasalt and presalt source rocks (Al-Siyabi, 2005; Taylor *et al.*, 2003). To the knowledge of the author, there was not any study devoted to evaluate the migration of petroleum fluids in carbonate stringers in south Oman salt basin.

2.9 The distribution of present day Pressures in the study area

The carbonate stringers included in this study have present day temperatures range of 61-88°C and occur at depths range of 1900-3500m. As shown in Figure 2-10, there is significant variability of formation pressures (RFT) measured for different reservoir units ranging from hydrostatic pressure such as in A4C and A3C of well BBN1 to near lithostatic pressure such as in A3C reservoir unit of well Kaukab1. It is not obvious though why they behave in this manner. One possibility is that, all these overpressured reservoirs were lifted to lithostatic pressure by some mechanism and then dropped keeping the same gradient as lithostatic pressure gradient (Paul Taylor *pers. comm.*). It is obvious that there are significant differences in formation pressures between A3C and A4C reservoir units, confirming that they are not connected. It is not readily obvious if there is significant pressure difference between Birba A4C reservoir units (well BB1-BB5) and Birba south A4C reservoir unit. The A3C of well

Kaukab1 looks if it is in communication with the A3C of well Durra1. However, this does not necessary indicate that they are in flow communication.

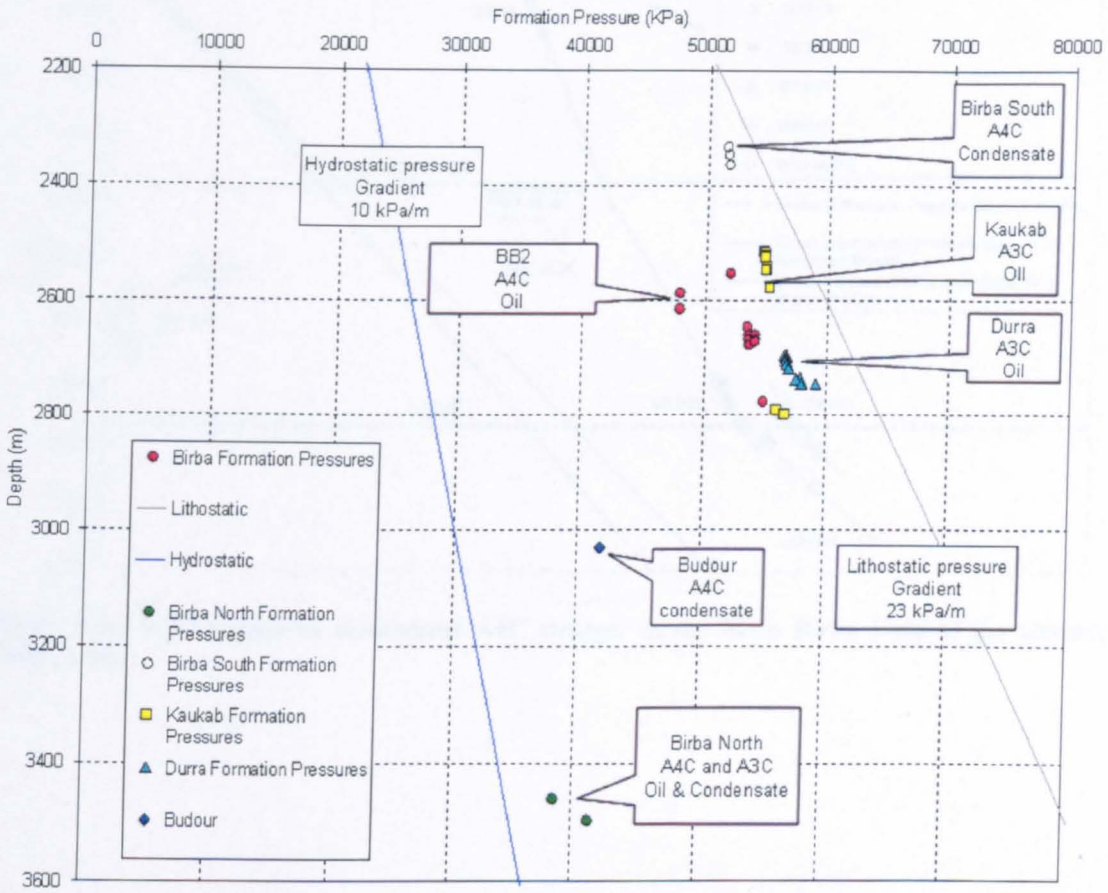

Figure 2-10: the overall distribution of RFT pressures throughout carbonate stringers, obtained from different producing wells. The Birba formation pressures are plotted in Figure 2-11.

Figure 2-11 shows the pressure profile versus depth throughout the A4C carbonate stringer in the main Birba Field. Apparently, wells BB5, BB3 and BBS1 are in communication and that the change in gradient is due to change in density of the fluids. A4C stringer at well BB5 appears to be in the water leg, while A4C of BB3 seems to be in the oil leg, which grades up to gas in BBS1 (A4C). The same aquifer seems to be shared by A3C reservoir unit of BB3. A4C of BB4 was found water bearing when it was drilled in 1981, (Protoy *et al.*, 1995). However, it appears to have oil stains when examining the core rocks. There is a fault separating BB41 from the remaining Birba wells, and pressure data indicates that this fault is sealing and BB4 appears to be more overpressured than the rest of the wells in the Main Birba Field.

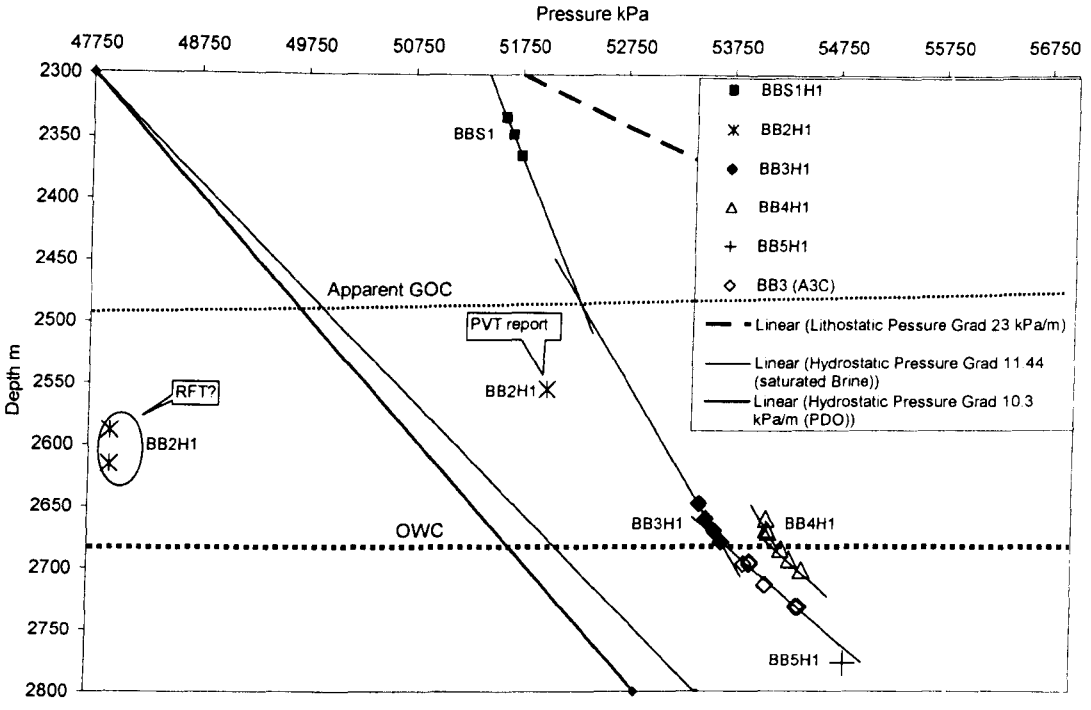

Figure 2-11: RFT pressures throughout A4C stringer in the Main Birba Field of the Greater Birba Area.

Chapter 3 : Experimental

3.1 Introduction

In this chapter, a detailed review of all experimental and data analysis techniques employed in this study as well as detailed description of the samples and data incorporated into the study. This study involves various types of data obtained by different methods and from different sources. Most of the analyses were performed in University of Newcastle upon Tyne. Some of the analyses were done in Shell labs (Rijswijk and Houston) and iso-analytical LTD (UK) as will be stated later.

The samples were taken from 11 wells distributed throughout the Greater Birba area as illustrated in Figure 3-1. Figure 3-1 also shows the samples taken from each well and the reservoir unit the sample were taken from. The oil samples was indicated by codes starting with O and the reservoir units was indicated with symbols starting with A. it is very important to understand the reservoir units stratigraphically because we have samples taken from the same well but from different reservoirs. A detailed explanation of reservoir units has been done in a previous chapter (chapter 2, see Figure 1-2 & Figure 2-3).

In this chapter, only the methods that were carried out by the author will be explained in details. The other types of data such as measurements of physical properties conducted in Shell (Houston) will be mentioned in the corresponding chapter. PVT modelling and all related analysis to it will be explained fully in chapter 7.

The solvents used in this study, unless otherwise stated, were redistilled in an Oldershaw column. Any glassware used was cleaned with Dichloromethane (DCM) and then rinsed with distilled water and finally dried in an Oven at approximately 60°C. The glassware was rinsed again with DCM directly before use. The surfaces of the core rock samples were removed using a hard wire brush and then washed by DCM in order to remove any man made contaminations.

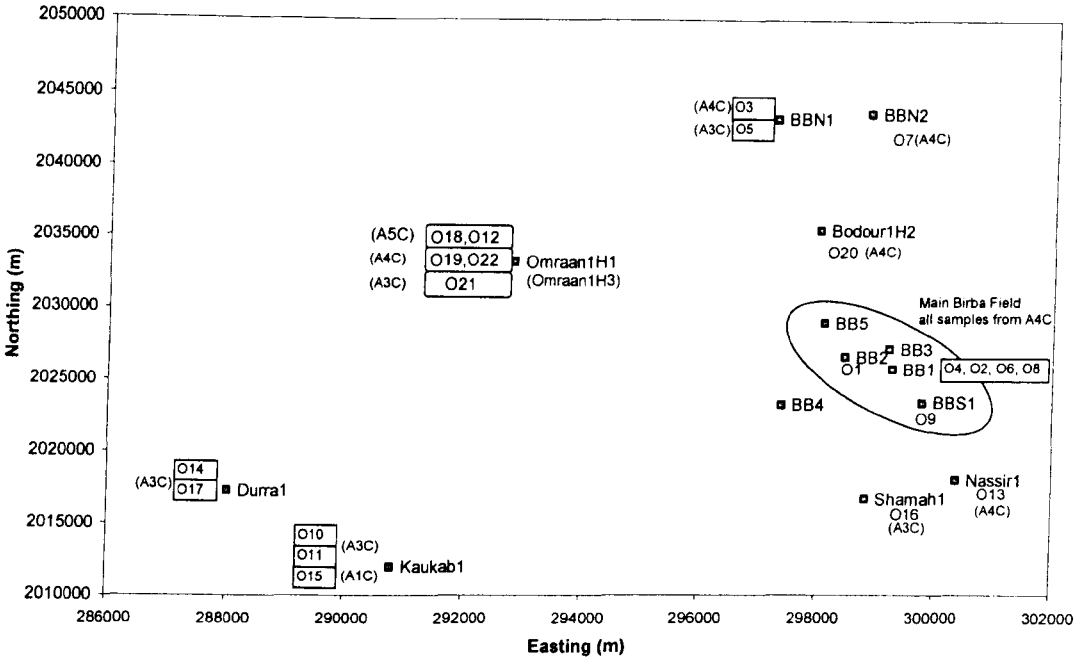

Figure 3-1: The distribution of the wells and the samples taken from each well. The samples start with O, the reservoir unit start with A, and well name is above the locating symbol.

3.2 Samples and data incorporated into the study

Figure 3-2 and Table 3-2 show a flow chart and lists of all experiments and analyses performed on the available samples for the study in the analytical labs of university of Newcastle upon Tyne. Twenty-two dead oil samples and 20 reservoir core rocks were available for this study as well as other data provided by Shell. The twenty-two oil samples are from 11 different wells distributed throughout the Greater Birba area as illustrated in Figure 2 2. They are mainly from two reservoir units; the A4C and A3C carbonate stringers of Infracambrian age. There were two oil samples from A5C and one sample from A1C available for the study. The samples are believed to be representative of the Greater Birba Area in South Oman Salt Basin because there is a sample from each of the oil-bearing wells in the area except those drilled very recently, from which it was not possible to acquire any sample. The wells cover an area of more than 400 km2.

All oil samples were analysed by Iatroscan (thin layer chromatography), gas chromatography-Flame ionization detector, and fractionated into hydrocarbons and polar fractions by solid phase extractions method and the hydrocarbons fractions were

then fractionated by silver nitrate impregnated solid phase extraction method into saturated and aromatic hydrocarbons. All fractions were analysed by gas chromatography-mass spectrometry. Carboxylic Acid fractions were isolated from each oil sample and analysed by gas chromatography. Number of oil samples was analysed by gas chromatography-flame photometric detector. These experiments are illustrated by the flow chart in Figure 3-2 and Table 3-1.

Ten samples of the oil samples were sampled during production tests and two samples were sampled by repeated formation tests. O5 oil sample is a swapped sample from the core obtained from the A3C section of well BBN1. The other oil samples are probably produced type of oils. In some wells, a number of oil samples were taken from the same well and reservoir unit at different times or at different depths. There are four samples taken from A4C of well BB1 as illustrated in the table below. Three of these were taken before the gas injection development that took place in 1993, and the other one is about 6 years later. This will help to see the effect of gas breakthrough on the nature of the oil in BB1 and BB2. Two oil samples were taken from A3C of Kaukab1 and probably two years between them (Not definite). Five oil samples were sampled from Omraan1H3, two from A4C, and two from A3C, taken at different times and two from A5C reservoir units taken at different times from different depths. Details about the different sampled reservoir units are illustrated in chapter 2 (Figure 2-4, 2-5).

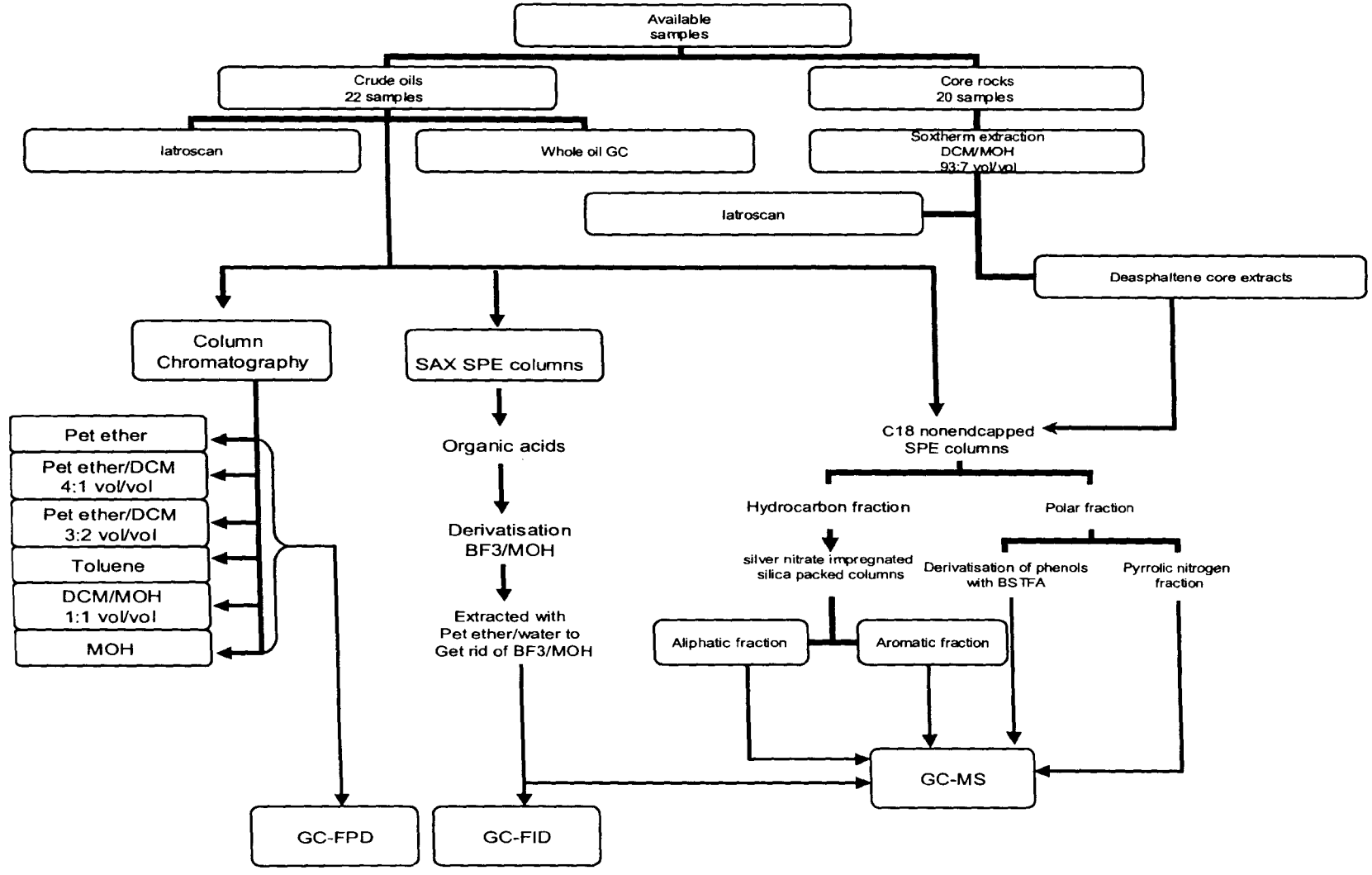

Figure 3-2: Flow chart of all experiments and analysis performed on the available samples for this study at University of Newcastle upon Tyne.

Table 3-1: List of the oil samples (left) and reservoir core rocks (right). The left table shows the producing wells, the sampling dates, sampling depths, sampled reservoir unit and the type of the sample for each oil sample. The right table shows the well, depths and extracts yields for each reservoir rock sample.

Wells	Sample ID	Sampling year	TVD (m)	Stringers	Age	type of sample
BB1	O2	1988	2536.5	A4C	Neoproterozoic III-Cambrian (550-543Ma)	Ukn
BB1	O4	1983	2533.1-2556.0	A4C		Ukn
BB1	O6	1999	2588.3-2556.1	A4C		Ukn
BB1	O8	1988	2533.1-2533.4	A4C		Ukn
BB2	O1	1982	2583.4-2589.5	A4C		WH
BBS1	O9	1987	2329.7	A4C		PT
BBN1	O3	1980	3455.1-3471.5	A4C		Ukn
BBN1	O5	1981	3558.1	A3C		swabbed from core
BBN2	O7	1983	3597.8-3612.8	A4C		PT
Nasser1	O13	1982	1998.6	A4C		Ukn
Budour1H2	O20	2003	2971.59	A4C		Ukn
Omraan1	O12	1982	2601.7-2626.7	A5C		PT
Omraan1H3	O18	1997	2939.1-3201.6	A5C		Ukn
Omraan1H3	O19	1997	2939.1-3201.1	A4C		Ukn
Omraan1H3	O21	1997	3111.5-3201.5	A3C		Ukn
Omraan1H3	O22	2001	2939.1-3201.1	A4C		Ukn
Shamah1	O16	1992	2385.7-2389.7	A3C		Ukn
Durra1	O14	1982	2691.0-2712.2	A3C		PT
Durra1	O17	1982	2695.1	A3C		RFT
Kaukab1	O10	1989	2513.6-2551.6	A3C		PT
Kaukab1	O11	1987	2513.6-2551.6	A3C		PT
Kaukab1	O15	1989	2897.0	A1C		RFT

sample ID	Wells	Depth (ft)	Depth (m)	Extract yields mg/g rock
D16	BB2	9283	2829.46	6.83
D17	BB2	9287	2830.68	3.60
D6	BB2	9306.1	2836.47	7.56
D13	BB2	9578	2919.37	4.99
D18	BB3	9531.5	2905.20	6.18
D4	BB3	9574.5	2918.31	14.21
D3	BB3	9599.9	2926.05	11.69
D5	BB4	9532.5	2905.51	8.79
D11	BB4	9543.9	2908.98	19.33
D20	BB4	9547.0	2909.93	13.21
D12	BB4	9589.9	2917.76	12.91
D19	BB4	9572.5	2923.00	8.49
D7	BB4	9628.4	2934.61	5.04
D1	BB4	9645.9	2940.07	2.29
D21	BB4	9652.0	2941.93	6.21
D14	BB5	9845	3000.76	3.44
D10	BB5	9942.5	3030.47	3.05
D2	BB5	9982.5	3042.67	3.84
D8	BBS1	8481.5	2585.01	4.89
D9	BBS1	8500	2590.80	3.08

PT= Production test sample, RFT= Repeated formation test sample, empty boxes means that the type of these samples is unknown.

Table 3-2: The available data for the study. Please see figure 3-4 and figure 3-5 to understand the stratigraphy of the reservoir units (stringers), e.g A4C or A4 means the fourth carbonate layer in Ara group.

Crude oil samples														
Sample ID	Wells	TVD (m)	Stringers	Sample analysis										
O4	BB1	2533.1	A4	IATROSCAN	GC (n-alkanes and isoprenoid alkanes	GC (organic acids and n-acids)	GC (Light hydrocarbons)*	GCMS (Aromatic hydrocarbons)	GCMS (Alkyl Carbazoles)	GCMS (Alkyl phenols)	GC-IRMS (Whole oil δ13C)*	^{38}S isotopes**	Physical and chemical bulk properties*	
O6	BB1	2537.1	A4											
O8	BB1	2533.1	A4											
O2	BB1	2536.5	A4											
O1	BB2	2583.4	A4											
O9	BBS1	2329.7	A4											
O3	BBN1	3455.1	A4											
O7	BBN2	3597.8	A4											
O13	Nassir1	1998.6	A4											
O20	Bodour1H2	2971.6	A4											
O19	Omraan1H3	2939.1	A4											
O22	Omraan1H3	2939.1	A4											
O14	Durra1	2693.0	A3											
O17	Durra1	2695.1	A3											
O11	Kaukab1	2513.6	A3											
O10	Kaukab1	2513.6	A3											
O16	Shamah1	2385.7	A3											
O5	BBN1	3557.8	A3											
O21	Omraan1H3	3111.5	A3											
O18	Omraan1H3	2939.1	A5											
O12	Omraan1H1	2601.7	A5											
O15	Kaukab1	2896.9	A1											
Gas samples														
G3	Birba South-1H1	2329.7	Gas composition and compound specific Isotopic analysis data*											
G1	Birba-1H1	2533.1												
G2	Birba-2H1	2583.4												
G4	Budour 1h2	2971.6												
G5	Kaukab1	2513.6												
Reservoir core rocks														
D5	BB4H1	2655.9	A4C	Soxtherm extraction	latroscan of extracts	GC (n-alkanes and isoprenoids alkanes)	GCMS (Saturate biomarkers)	GCMS (Aromatic hydrocarbons)						
D11	BB4H1	2659.4	A4C											
D20	BB4H1	2660.4	A4C											
D12	BB4H1	2668.2	A4C											
D19	BB4H1	2673.4	A4C											
D7	BB4H1	2685.1	A4C											
D1	BB4H1	2690.5	A4C											
D21	BB4H1	2692.4	A4C											
D14	BB5H1	2752.5	A4C											
D10	BB5H1	2782.2	A4C											
D2	BB5H1	2794.4	A4C											
D18	BB3H1	2660.3	A4C											
D4	BB3H1	2673.4	A4C											
D3	BB3H1	2681.1	A4C											
D16	BB2H1	2580.0	A4C											
D17	BB2H1	2581.2	A4C											
D6	BB2H1	2587.0	A4C											
D13	BB2H1	2669.9	A4C											
D8	BBS1H1	2337.9	A4C											
D9	BBS1H1	2343.7	A4C											
* acquired by Shell, Rijswiik and Houston														
** acquired by Iso-Analytical Ltd. UK														

3.3 Techniques and experiments performed in this study

3.3.1 Soxtherm extraction

Crushed reservoir core samples were extracted using a soxtherm extraction apparatus. All cellulose double thickness extraction thimbles and cotton wool were pre-extracted in a soxhlet for 24 hours using an azeotropic solvent mixture of Dichloromethane/Methanol (DCM/MeOH) at 93:7 (by volume). A weighed amount (25-40g) of a crushed reservoir core sample was placed in to a pre-extracted cellulose extraction thimble. The cellulose thimble plugged with pre-extracted cotton wool, was then suspended in the extraction jars using metal ring clips. About 200 ml of an azeotropic solvent mixture of DCM/MeOH (93:7 by volume) was poured into the extraction thimbles. A spatula of activated cupper turnings were added to the extraction jars in order to remove any elemental sulphur from the extracts. The sample was then extracted using a Gerhardt Isotherm extraction apparatus at an oil bath temperature of 150°C for 6 hours. Extracts were collected and concentrated (2-3ml of final solution) using a Buchi rotary evaporator at 30°C. An aliquot of the concentrated extract was transferred to a pre-weighed vial and the solvent was reduced to dryness in a stream of dry nitrogen in order to quantify the amount of total extractable material.

3.3.2 Thin layer chromatography-FID (Iatroscan)

The Iatroscan offers a fast and relatively accurate method for quantifying aliphatic and aromatic hydrocarbons as well as non-hydrocarbons in rock extracts and crude oils (Karlsen & Larter, 1991). The principle of this technique involves the application of a small volume of sample (3μl) of solution of oil or rock extract to chromatographic rods and development of the rods in a series of solvents to separate the various compound classes. Each separated fraction (saturated HC, aromatic HC, resins, and asphaltene) is then detected and quantified by moving the rod through a flame ionisation detector. Iatroscan analysis was carried out using Chromarod-S III silica rods and an Iatroscan MK-5 analyser equipped with a flame ionisation detector (FID). The rods need to be burned in the analyser directly before the sample

application to remove any contaminant could be on the rods. A three microlitres of each sample of concentration of about 5 mg/ml was applied to two rods in duplicate. The first two rods in each set of rods were always spotted with calibration oil standard which is oil O6. Therefore, every set of rods can take four samples and standard oil each time (the standard oil will be explained later). Development of rods is done using three types of solvents, hexane, toluene, and dichloromethane (DCM) /methanol (/MOH) (93:7 by volume). The rods were first eluted in hexane to 100% of the rod length, and left to dry. Then they were eluted in toluene up to 60% and left to dry and finally they were eluted in freshly prepared DCM: MeOH (93:7 by volume) up to 30% of the silica-coated rod length and completely dried in an oven of 60°C for 90 seconds. The results were collected and processed using computer package called Atlas. The results will be in the form of four peaks, saturated HC, aromatic HC, NSO, and asphaltene orderly for each sample (Figure 3-3). Each sample was run in duplicate and the average was taken of the two results.

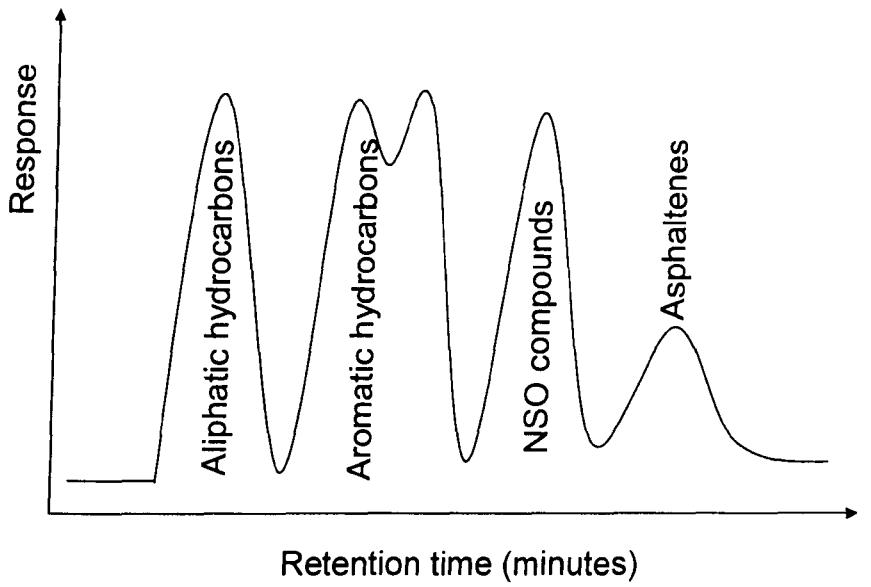

Figure 3-3: : Iatroscan TLC-FID chromatogram (diagram) showing the four fractions resulting from development of the sample in 3 different solvents with increasing polarity.

Thin Layer Chromatography-Flame Ionisation Detection (TLC-FID) Iatroscan screening method was performed in all oil samples and core extracts and calibrated using one of oils from well BB1, which is oil sample O6. The calibration standard oil was first deasphalted to get the accurate amount of asphaltene. The asphaltene was precipitated from 100 mg aliquot of this oil sample in an excess of hexane volumes, then left overnight in the fridge. The sample was then centrifuged to allow the whole

asphaltenes to precipitate and removed. Then the asphaltene separated was accurately weighed. The maltene (remaining petroleum) was separated into aliphatic, aromatic and NSO fractions using a 50 cm column chromatography packed by silica and alumina. The results of this separation as following: 45% for saturated Hydrocarbons fraction, 38.6% for aromatic hydrocarbon fraction, 16.2% for NSO fraction and 0.2% for asphaltene fraction. The problem of this oil is that it has very low asphaltene content. The calibrated results are shown and illustrated in Table 3-3. The calibration was necessary as the Iatroscan give higher response for the aromatic hydrocarbons than saturated hydrocarbons. One of the possible reasons behind this behaviour is the high hydrogen flow need to be used in the Iatroscan FID (Karlsen & Larter, 1991). However, it has been observed that high sulphur asphaltene/resins in high sulphur source rocks give higher response that those in low sulphur source rocks (Karlsen & Larter, 1991). Therefore, it is likely that the high FID response of aromatic fraction is due to high content of aromatic sulphur compounds in this fraction (see chapter 6.4).

Table 3-3: comparison between the non-calibrated and calibrated data. i.e. the amount of each fraction before applying response factor (left) and after applying it (right). For more details, consult the text.

	noncalibrated				Calibrated			
	Saturates	Aromatics	NSO	Asphaltene	Saturates	Aromatics	NSO	Asphaltene
O1	25.49	54.53	18.52	1.46	58.84	33.76	7.28	0.12
O16	32.30	52.07	8.78	6.85	67.28	29.09	3.11	0.52

The above standard oil was analysed with every patch of samples (maximum 4 samples) to calculate the response factor for the different fractions of oil (aliphatic HC, aromatic HC, NSO and Asphaltene). The response factors for the oil suite were calculated for each fraction (aliphatic hydrocarbons, aromatic hydrocarbons, resin and asphaltene fractions) in all samples using fractions isolated from the calibration standard oil (O6) by column chromatography.

$$\text{Response factor (RF)} = \frac{\text{Area of standard} \times 100}{\text{Standard conc.} \times \text{Volume standard solution applied onto rod (3 } \mu l)}$$

Where:

*Standard means any of the four fractions (saturated HC, aromatic HC, resins, asphaltene fractions) obtained by column chromatography separation of the standard oil (O6).

**Standard conc. = % of individual fractions of the standard oil (O6) x concentration of oil O6 x vol. of oil loaded (3ul).

Therefore, the percentage of a particular fraction of a particular oil can be calculated using the equation below:

Equation 2 2:

$$F(\%) = \frac{\text{Area F}}{\text{Sum of areas of all fractions x RF std}}$$

Where:

F= the fraction normalised to the total identified area (e.g saturated hydrocarbons)

RFstd= response factor of fraction F.

3.3.3 Solid phase extraction

Solid phase extraction is a simple sample preparation technique based on the principle of liquid-solid chromatography using commercially available cartridges packed with different chromatographic sorbents that can produce clean fractions of saturated and aromatic hydrocarbon fractions as well polar fraction and acid fractions. This technique can perform rapid separation (up to 40 samples a day) and mitigate any cross contamination problems by minimizing sample handling, and using the minimum of the solvents (Bennett *et al.*, 1996; Bennett & Larter, 2000). Three types of SPE columns were used in this study: 4ml C18-nonendcapped SPE columns, 4ml silver nitrate impregnated silica packed columns, and 6ml SAX SPE columns and each of these columns will be described carefully accordingly. The first type of columns was used to isolate polar compounds from hydrocarbons. The second type of columns was used to separate aliphatic and aromatics. The third type was used to isolate acid fraction from the crude oils. Each one of these will be explained later in this chapter.

Internal standards were used to perform quantification on saturated hydrocarbons, aromatic hydrocarbons, carbazoles and phenols. Squalane and 1,1-binapthyl internal standards were used to quantify saturated and aromatic hydrocarbons respectively. A mixture of squalane and 1,1-binapthyl were propared by dissolving 2.24mg Squalane and 0.51mg 1,1-Binapthyl in hexane and bottled in 25ml-volumetric flask. D8-carbazole internal standard was used to quantify carbazoles and D6-phenol was used to quantify phenols in crude oils. D8-carbazole

internal standard was prepared by adding 1.0 mg D8-cabazole to 25ml of mixture of hexane and toluene (9:1; by volume) and bottled in 25ml-volumetric flask. D6-phenol internal standard was also prepared by dissolving 1mg D6-Phenol in 25ml of mixture of hexane and toluene (9:1; by volume) and bottled in 25-volumentric flask. The later two internal standards were added to the sample in the SPE column before isolating non-hydrocarbons. The squalane was added to the hydrocarbon fraction before separating aliphatic and aromatics hydrocarbons. The concentrations of these standards were carefully monitored and recorded to account for the small losses of the standards with increasing consumption of them in experiments.

3.3.3.1 Isolation and analysis of polar compounds

The polar compounds were isolated using four millilitre Isolute C18 (non-end capped) SPE columns which are packed with silica (2ml). The columns were cleaned with 6ml DCM, left to dry overnight, and then conditioned by eluting 3ml hexane prior to sample loading and the residual solvent was removed with gentle air flush. 5µl of D8-carbazole and 3µl of D6-phenol were injected into the column loaded with the sample. An aliquot of oil (60-90 mg) was loaded into the column directly into the top frit of the cartridge. In some cases, a positive pressure may be needed to force the sample in to the frit. Small amount of hexane (0.5ml) was used to wash the column sides from any oil remains. After allowing the solvent height to fall to the level of the frit, another half millilitre of hexane was added to allow continued elution until the sovent level reached the frit. Four millilitres of hexane were added to elute the total hydrocarbons fraction. A gentle air flush was then applied to the column to remove the residual solvent with the remaining hydrocarbons and the tip of the column was washed with small amount of hexane. The hexane fraction was kept in a 10ml vial and stored in fridge waiting to be subsequently fractionated in to aliphatic and aromatic fraction. The polar compound fraction was eluted from the SPE column with 5ml DCM. Half millilitre of the five millilitre of DCM was used to wash the column sides and left to elute to the level of the frit. The remaining solvent was added to elute the whole polar fraction and the tips of the cartridge were washed. The DCM fraction were evaporited down to 0.5 ml and divided equally for analysis of carbazoles and phenols, i.e. 0.25 ml for each. The 250µl polar fraction for carbazoles was further

reduced to 100µl and transferred to 150µl tapered inserts in auto sampler vials and sealed. The samples were submitted for GCMS analysis.

3.3.3.1.1 Analysis of pyrrolic nitrogen compounds by GCMS

Alkylcarbazoles were analysed on a Hewlett Packard 6890 GC (split/splitless injection at 310 °C) coupled with a Hewlett Packard 5973 mass selective detector (electron impact voltage, 70 eV; filament current, 220 µA; source temperature, 200 °C; multiplier voltage, 1600 V; interface temperature, 300 °C). The chromatography was done on a HP-5 fused silica capillary column (30m x 0.25 mm i.d. x 0.25 µm film thickness). The gas chromatograph oven was first held at 40 °C for 3 minutes, programmed from 40 °C to 200 °C at 10 °C/min temperature ramp, then from 200 °C to 310 °C at 4 °C/min temperature ramp, and held at 300 °C for 14 minutes. Helium was used as carrier gas at a flow rate of 1ml/min and pressure of 50KPa. The mass spectrometer was operated in selective ion monitoring (SIM) mode. The fragment ions monitored for the carbazoles, benzocarbazoles and dibanzocarbazoles are:

Compound	Molecular Ion (M+)
Carbazole	m/z 167
C1alkylcarbazoles	m/z 181
C2alkylcarbazoles	m/z 195
C3 alkylcarbazole	m/z 209
Benzocarbazoles	m/z 217

The concentrations of individual compounds were calculated using the following formula, assuming a response factor of 1; this analysis is therefore only semi-quantitative:

$$C\ (\mu g/g\ oil) = \left(\frac{1000}{Wt.S.}\right) x IS(\mu g) x \left(\frac{A_C}{A_{IS}}\right)$$

Where:

C = Compound to be quantified;
Wt S = weight in mg of the sample applied to the SPE cartridge;
IS (µg) = weight of D8-carbazole added to the pyrrolic nitrogen fractions;
A_C = peak area of the alkylcarbazole isomer;
A_{IS} = the peak area of the D8-carbazole.

3.3.3.1.2 Analysis of oxygen compounds (alkylphenols) by GCMS

Alkyl phenols cannot be easily chromatographed using standard stationary phases used in gas chromatography because the phenolic hydroxyl group interacts with the solid phase leading to deterioration of chromatographis resolution. Therefore, the alkyl phenols are better analysed as trimethylsilyl (TMS) ether derivatives obtained through derivitization with N,O-Bis (trimethylsilyl) trifluoroacetamide (BSTFA) (Figure 3-4). The polar compounds fractions for alkyl phenol analysis were evaporited to 100-200µl and transferred to 3ml vials. A 100µl of BSTFA was added to each sample and the vials were immediately sealed. The vials were thoroughly mixed and then kept in an oven at 60°C for an hour. This will result in replacement of hydrogen with trimethylsilyl group. The samples were then transferred to 250µl inserts fitted in 1ml auto sampler vials to be submitted for GCMS analysis. The concentrations of individual compounds were calculated using the above formula in section 3.3.3.1.1, using response factors reported by Bennett *et al.* (2006).

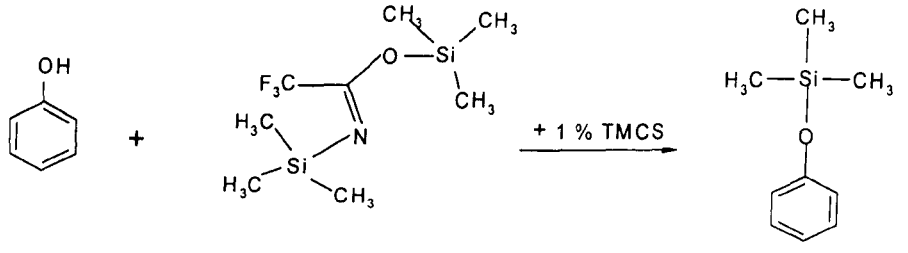

Figure 3-4: The Derivatisation of phenol with BSTFA to produce trimethylsilyl (TMS) ether derivatives.

3.3.3.2 Isolation of aliphatic and aromatic hydrocarbons

This is done by silver nitrate impregnated silica packed columns. These are not available commercially because silver nitrate is very photosensitive and so they need to be prepared in-house. Bennett & Larter (2000) developed this method at University of Newcastle. Thirty grams Keisel gel (60G) and 3 grams silver nitrate were mixed well in a 400 ml conical flask with 60 ml distilled water to make about 40 columns. The mixture-containing flask was covered completely with aluminium foil (a small hole needed to allow the escape of water vapours) and put in a drying oven at 60°C for one to two weeks. After allowing the mixture to dry out completely, the columns were prepared by taking approximately 550mg of the silica added to each

empty reservoir column and carefully compacted using a glass rod. These prepared columns need to be used immediately for optimum efficiency otherwise light might affect the silver nitrate in the silica.

The prepared columns were cleaned by allowing 5 ml hexane to elute through. Positive pressure was needed to force the solvent through. This was done by a plastic syringe installed on each column with a fitting PTFE adaptor and manual pressure. The hexane fractions obtained from previous method were evaporited down to 1ml. Ten microlitres of squalane (2mg squalane/ml hexane) and 1,1-binapthyl (0.3mg/ml hexane) internal standards were added to the 1ml hexane fraction of each sample. Then 100μl of the hexane fraction was loaded in to the silver nitrate impregnated silica packed column. The aliquot was injected directly into the top frit of the column. The frit and column wall were washed by 0.5ml taken from 2ml hexane. A positive pressure was needed to force this amount to the level of the frit. The remaining 1.5ml hexane was all added to elute the aliphatic fraction. After that, a gentle air flush was applied to elute the residual solvent and sample retained in the silica and finally the tip of the column was rinsed thoroughly with hexane. The aliphatic fraction of each sample was collected in a 10ml vial. Four millilitres were added to extract the aromatic fraction from the column.

The aliphatic and aromatic fractions were reduced to 1ml and 0.5ml respectively and transferred to 1.5ml auto sampler vial to be submitted for GCMS analysis. The quantification will be done based on squalane internal standard for aliphatic biomarkers and 1,1-binapthyl internal standard for aromatic hydrocarbons.

3.3.3.3 Isolation of acid fraction

This was done using commercially available 6ml Isolute SAX SPE columns (SAX for Strong Anion Exchange). The whole procedure was developed by (Jones *et al.*, 2001) and modified by (Aitken, 2004) at university of Newcastle upon Tyne. An empty 6ml glass reservoir was fit on each SAX column using fitting adaptors. The SAX SPE columns were cleaned using 10ml hexane followed by 10ml hexane/DCM mixture (1:1 by volume). A gentle air flush was then applied to each column to

remove the retained solvent using a syringe and adaptor. The empty reservoir was then removed. An aliquot of an oil sample (150-400mg) was accurately weighed and recovery standard (10µl of 1.044 mg/ml solution containing adamantine and 5β-cholanic acid) was added to each sample. The samples were then loaded in to the SAX SPE column directly into the frit. The samples were loaded slowly and carefully to make sure that they are absorbed by the frit and the silica. Some thick oil samples were thinned by adding a small amount of DCM and forced through the frit by applying a gentle positive pressure using a syringe and adaptor. Then, the empty glass reservoirs were installed again on the top of each column and the developing solvents were added. A blank was run along with every set of samples analysed. This is done by adding recovery standards to a separate SAX SPE column.

The samples were first developed by 20ml of a mixture of hexane/DCM (1:1 by volume) followed by 25ml DCM to elute the interferents and the tips of the column were rinsed by small amount of both hexane and DCM. This elute was discarded and the remaining petroleum in the column should be now mainly organic acids. The acids were eluted with 50ml of a mixture of diethyl ether and formic acid (50:1 by volume) and the elutants were collected in 100ml round bottom flasks. The acid fractions were then evaporited down to 1ml using rotary evaporator. They were then transferred by DCM to 10ml vials and blown under nitrogen to dryness to remove the formic acid completely. To assure this, the samples were left over night after being dried by nitrogen steam. The samples were washed by 1ml DCM and evaporited to dryness to ensure that the samples are all in the bottom of the vials.

The acids fractions were then derivatised using BF3/methanol. The samples were re-dissolved in 1ml DCM and 1ml BF3/methanol solution was added to each sample. The vials were then capped well and left in an oven at 60°C for one hour. The samples were then transferred to quick fit test tubes to be extracted by petroleum ether and distilled water and get rid off the BF3/methanol. Three millilitres of petroleum ether were added to each sample followed by 10ml distilled water. The mixtures were shaken vigorously and left to settle for 10 minutes. The organic acids were then extracted by petroleum ether and form a coloured layer on top of the water. This layer was pipetted off carefully and transferred into 20ml vials. This petroleum extraction was done another three times for each sample to make sure that all acids were transferred to the vial. The extracts were then blown down to dryness and the sides of

the vials were washed with DCM and blown to dryness again to make sure that the sample in the base of the vial.

The acids fractions might still have some residual alkanes. Therefore, the samples were eluted through 6ml plastic silica column with 4ml hexane and the elutants which would have contained alkanes were discarded. The final step was to elute the acids with 10ml of a mixture of Hexane and DCM (3:7 by volume) in 10ml vials. The samples were then concentrated to the base of the vial and transferred to 250µl inserts fitted in 1ml vials. Five microlitres of an internal standard (2mg/ml 1-phenyl-1-cyclohexanecarboxylic acid solution) were added to each sample. The samples were then submitted to GC and GC-MS analysis.

3.3.4 Gas chromatography with a Flame Ionization Detector

The whole oils, core extracts and acid fractions were analysed by a Fisons (Carlo Erba) Gas chromatography 8000 series equipped with automatic split/splitless injector and flame ionization detector. The samples were chromatographed on HP-5 fused silica capillary column (30m x 0.25mm i.d. x 0.25 um film thickness). For whole oils and extracts and acids fraction, the gas chromatograph oven was temperature programmed from 50°C to 300°C at a ramp rate of 4°C/minwith initial and final hold times of 2 and 20 minutes, respectively. The carrier gas used was hydrogen with a column pressure of 50 kPa. The GC data were acquired and processed on Atlas chromatographic software.

The whole oils and extracts were prepared in DCM solution at concentrations of about 5mg/ml and an amount of squalane standard at concentration of 2mg/ml hexane was added to each sample to quantify resolvable alkanes but especially the n and isoprenoid alkanes. The quantification of n-alkanes and isoprenoids were performed using this equation:

Equation 3-1:

$$X\ (ug/g) = \left(\frac{1000}{Wt}\right) \times C_{IS}\ (\mu g) \times \left(\frac{A_x}{A_{IS}}\right)$$

Where,

X = concentration of individual alkanes (μg/g of oil or extract);
Wt = weight of oil or extract sample in mg, that was added into the original SPE column;
C_{IS} = concentration (μg) of the internal standard (squalane in hexane) added to the sample,
A_X = peak area of the alkane in the chromatogram
A_{IS} = peak area of the internal standard (squalane) in the chromatogram

3.3.5 Gas chromatography-mass spectrometry

All aliphatic and aromatic hydrocarbon fractions as well as acid fraction were analysed by GC-MS. The GC-MS analyses were carried out using a Hewlett-Packard 6890 gas chromatograph fitted with split/splitless injector (280°C) and interfaced to an HP 5973 Mass Selective Detector (electron voltage 70 eV, source temperature 230°C, interface temperature 310°C). Chromatography was performed on an HP-5 fused silica capillary column (phenyl-methyl silicone stationary phase; 30m long, 0.25mm internal diameter, and 0.25mm film thickness). Helium was used as carrier gas at a flow rate of 1ml/min and column pressure of 51.1 kPa. The mass spectrometer was operated in selective ion monitoring (SIM) mode for both fractions as well as full scan mode for a limited number of aliphatic and aromatic hydrocarbon fractions.

A fast heat temperature program was used to analyse the biomarkers (steranes and tricyclic terpanes and hopanes). The temperature used was 40°C to 175°C at 10°C/min, then 175°C to 225°C at 6°C/min, then 225°C to 300°C at 4°C/min, and finally the temperature was held at 300°C for 20 minutes. A slow heating rate temperature program was used in the case of aromatic hydrocarbon compounds. The oven temperature was first held at 40°C for 5 minutes and then programmed from 40°C to 300°C with a 4°C/min temperature ramp, the oven then held at 300°C for 20 minutes.

The aliphatic hydrocarbons and the aromatic hydrocarbons were submitted in 1ml hexane and 0.5ml DCM solutions, respectively, for GC-MS. The quantification were performed based on squalane internal standard for aliphatic and 1,1-binapthyl for aromatic hydrocarbons.

$$X_{b(a)}\ (\mu g/g\ \text{oil, extract}) = (\frac{1000}{Wt}) x C_{IS}(\mu g) x (\frac{A_{b(a)}}{A_{IS}})$$

Where,

$X_{b(a)}$ = concentration (μg/g of oil or extract) of the compound to be quantified (biomarker or aromatic hydrocarbon);
Wt = weight in mg of oil or rock extract that was loaded into the original SPE columns
C_{IS} = concentration in μg of surrogate standard (squalane in hexane) added to the sample
$A_{b(a)}$ = area of biomarker or aromatic hydrocarbon;
A_{IS} = area of squalane or 1,1-binaphthyl internal standards

Note that quantitative values were not corrected for differences in mass spectral response between the various compounds and the corresponding standards. The concentrations reported in this study are therefore semi-quantitative assuming relative response factors between target analytes and the standards of 1.

3.3.5.1 Reproducibility of the GC-MS data

In this study, the molecular differences between different oil samples are relatively small thus reproducibility of the instrument and separation techniques are critical and very necessary. To assess method reproducibility, I analyzed one of the Birba field oils (O8) in triplicate at the same time as the other oils were analysed. The concentrations and parameters of saturate biomarkers and aromatic biomarkers are shown in Table 2 4 and Table 2 5, respectively. Table 3-4 shows that the most of the measurements of concentrations of different biomarkers and aromatic hydrocarbons have Coefficient of variations of 1-6%. This is a lot less that the coefficient variations obtained from the whole data set of the studied oils (CV>10%). This indicates that the variations between the oils in terms of concentrations is real and reflects that these oils were affected by either genetic differences or post-generation processes.

The coefficient of variations for aliphatic hydrocarbons and aromatic hydrocarbons parameters though show very small values and most of the measurement indicate CV of less than 1 to 3, but the aromatic parameters show

relatively larger coefficient variation than aliphatic parameters. The aliphatic parameters of the studied oils (except for condensates and known different oils (O5 and O15) show coefficient variations greater than 4 except for C_{29}%αββ/ααα+αββ which shows very CV of 0.8. therefore, the variations revealed by statistiscal evaluation (PCA) is real and may reflect facies-maturity related variations as suggested in chapter 4.

Table 3-4: The reproducibility of the concentrations (μg/g) of saturated biomarkers and aromatic hydrocarbons. SD is for standard deviations and CV is for coefficient of variation.

Aliphatic biomarkers (μg/g)											
Run Number	C23βαTRI	C24 TETRA	Tm	C29αβ	C30αβ	C21+22 preg	C27 αββ 20R+S	C29 αββ 20R+S	Sum Tricyclics	Sum Stereranes	Sum hopanes
1	768.3	118.8	338.9	855.8	203.4	299	205.4	904.5	2986.9	2581.0	4425.4
2	714.1	112.5	322.0	814.7	187.7	280	213.9	864.2	2830.3	2490.6	4213.7
3	746.9	119.0	335.7	832.4	194.6	298	215.9	888.9	2966.1	2565.1	4315.4
Mean μg/g	743	117	332	834	195	292	212	886	2928	2546	4318
SD	27.29	3.71	8.97	20.63	7.90	10.53	5.54	20.34	85.08	48.24	105.91
CV%	3.67	3.18	2.70	2.47	4.05	3.60	2.62	2.30	2.91	1.90	2.45
aromatic hydrocarbons (μg/g)											
Run Number	C20TAS	C21TAS	C21MAS	C22MAS	2-MN	BiPhen	Fluorene	Phenanthre	1-MP	DBT	BT
1	17.8	16.8	35.3	37.1	554.7	64.3	21.2	91.3	73.7	104.4	276.3
2	16.7	15.5	34.0	37.2	530.6	62.9	20.2	88.2	70.5	102.4	242.9
3	16.8	15.0	36.7	36.8	598.2	69.5	22.9	94.9	76.6	108.8	303.1
Mean μg/g	17	16	35	37	561	66	21	91	74	105	274
SD	0.59	0.92	1.36	0.21	34.27	3.46	1.33	3.32	3.05	3.32	30.12
CV%	3.47	5.83	3.86	0.57	6.11	5.27	6.20	3.63	4.14	3.15	10.99

Table 3-5: The reproducibility of aliphatic and aromatic biomarkers.

Aliphatics biomarkers parameters							
Run Number	C23/C21Triβα	Ts/(Tm+Ts) %	Homohopane Index	Tri/hop	Pregnanes/ Steranes	C29% αββ/ααα+αββ	Hopanes/ steranes
1	3.18	13	0.18	0.66	0.19	58	1.39
2	3.13	12	0.17	0.66	0.19	58	1.36
3	3.08	12	0.17	0.67	0.20	58	1.36
Mean	3.13	12.31	0.17	0.66	0.19	58.35	1.37
SD	4.72E-02	3.38E-01	9.48E-04	7.51E-03	3.00E-03	3.21E-02	1.61E-02
CV%	1.51	2.75	0.54	1.13	1.56	0.06	1.18
Aromatic parameters							
Run Number	MA/MA+T	MPI-1	MNR	DNR-1	TNR1	MDR	DBT/P
1	0.74	0.88	1.10	3.10	0.48	2.29	1.14
2	0.74	0.88	1.10	3.07	0.49	2.31	1.16
3	0.76	0.87	1.10	3.03	0.46	2.28	1.15
Mean	0.74	0.88	1.10	3.06	0.48	2.29	1.15
SD	1E-02	4E-03	2E-03	3E-02	2E-02	1E-02	9E-03
CV%	1.6	0.5	0.2	1.1	3.8	0.6	0.8

3.4 Data Analysis: Principal component analysis

Due to the small variations observed in the studied oils, statistical evaluation was needed to unravel any pattern in these variations. Principal component analysis (PCA) was the data analysis technique chosen in this study to perform this evaluation. PCA can be used to identify the cross relationship between various parameters and compounds and hence might help to provide new cross plots distinguishing between various oil groups especially when failing the conventional parameters to reveal any distinction. The principal of this method is reducing large sets of data to small number of variable controlling most of the variation between samples. This method can be consulted in more details in statistics textbooks to understand the theoretical background of this method. However, a very concise summary of the theoretical background of this method would be done here.

Multivariate methods (PCA is one of them) are extremely powerful because they allow one to manipulate more variables that can otherwise be incorporated. Principal component analysis is a way of identifying patterns in data and expressing their similarities and differences. It describes the variations of a set of multivariate data by giving a set of uncorrelated components called principal component which are linear combinations of the original variables.

It is fundamental to all multivariate data analysis is the concept of similarity and dissimilarity and concept of distance or proximity. the similarity and dissimilarity can be measured by a measure (d) which is basically how close one object from the other in two or three or n dimensions. The distance between two points in a plane (2D) is the length of the path connecting them. In the plane, the distance between the points (x1, y1) and (x2, y2) is given by the this equation (Pythagorean theorem):

$$d = \sqrt{(x_2 - x_1)^2 + (y_2 - y_1)^2}.$$

In three dimensions, the distance between the two points (x_1, y_1, z_1) and (x_2, y_2, z_2) is

$$d = \sqrt{(x_2 - x_1)^2 + (y_2 - y_1)^2 + (z_2 - z_1)^2}.$$

In general, the distance between points x and y in n dimensions is given by:

$$d = |\mathbf{x} - \mathbf{y}| = \sqrt{\sum_{i=1}^{n} |x_i - y_i|^2}\,.$$

The more dissimilar the two objects is the greater distance between them. This distance, which is also called Euclidean distance, is used by data transformation of PCA to identify the parameters that are close to each other to define the principal component.

Principal component analysis manipulates the data using matrix transformations. Matrix is an array of numbers arranged in raws and columns. Any matrix containing n objects (raws) and m variables (columns) can be represented as collection of n-points in multidimensional space or m-space. Our visualization system can not visualize more than 3 dimensions; however space of 3 dimensions does exist.

Say we have a 3x2 (3 raws and 2 columns) matrix with 3 objects (oil or core extracts samples) and 2 variables (e.g. sterane compound) as illustrated in Figure 3-5. The average of each of these variables is calculated which in this case 7 for both of them and then subtracted from the raw data in matrix A to form matrix B. a cross plot of the two variables for the three objects should be drawn as below. A straight line is then fitted to these points so that the distance of these points is minimized to be as small as possible, using the method of least squares (Davis 2002).

	Matrix A			Matrix B	
Objects	V1	V2		V1-mean (V1)	V2-mean (V2)
1	5	4		-2	-3
2	6	2		-1	-5
3	10	8		3	1
Mean	7	7		0	0

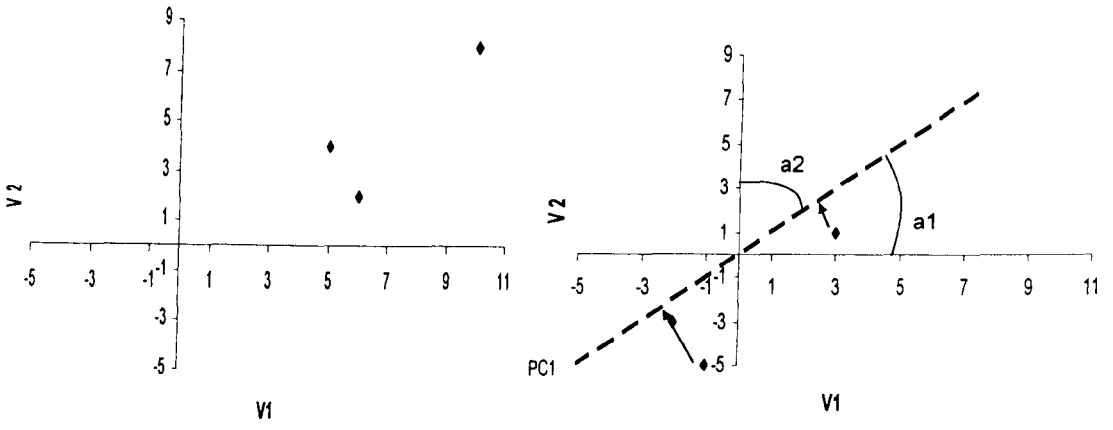

Figure 3-5: Example of PCA analysis.

Data matrix A containing the raw data and the positions of the samples are plotted in the cross plot of V1 versus V2 blow the matrices. Data matrix B containing the residuals of data matrix after subtracting the mean from the original data. A best fit line is draown through the points of matrix B using the least squares method.

So to determine the least-square regression line we must find the slope a and the y-intercept b of the line, then we know the line's equation. The slope is related to quantities S_{xx}, S_{yy}, and S_{xy}, which are calculated using these equations:

Where

$$S_{xx} = \sum x^2 - \frac{(\sum x)^2}{n}$$

$$S_{yy} = \sum y^2 - \frac{(\sum y)^2}{n}$$

$$S_{xy} = \sum xy - \frac{(\sum x)(\sum y)}{n}$$

And the slope (a) is calculated using this equation:

Slope $a = S_{xy} / S_{xx}$

The y-intercept is related to the averages (means) of x and y by:

b = (mean of y) - (mean of x) * a

This best fit line is no more than the principal component eigenvector. The amount of the variance each variable contributes to the principal component eigenvector (loadings) is calculated as cosine of the angle between the best fit line and the original axis (V1 and V2) in m-space (a1 and a2) as shown in Figure 3-5. The principal component scores are obtained by projecting each point down on to the principal component eigenvector as illustrated in Figure 3-5. The products of the scores and loadings from the residual matrix are then subtracted from the data matrix B. This would remove all the variance in the eigenvector from the data. A new matrix is then constructed and the process is repeated. The second series of data points is generated and a best fit line through them is defined, which represent another principal component orthogonal to the first one. The process is repeated several times till the residuals of the variables or objects are zero.

An important assumption of this method is that the data itself must be valid. These methods do not use the same logic of statistical inference that dependence methods do and there are no particular measures that can overcome problems in the data. Therefore, these methods are only as good as the input you have. Any more details regarding the theoretical background of PCA, they can be consulted in statistics books such as Davis 2002.

The input data were normalized concentrations of all or some compounds (variables) for each sample. The number of the variables used varies depending on the type of data used such as biomarkers or aromatic hydrocarbons or ratios. The PCA computer programme used in this project is the "SPSS version 10 for Windows". The output data are principal component scores and loadings. Scores are numbers that express the influence of an eigenvector (PC) on a specific sample or describes the contribution of each PC to each data point. Loadings express the influence of original variable within the principal component. The distribution of PC scores and loadings can identify the source of the variability in the dataset by pulling the main or principal components that explain this variation which are defined above. Each component is

controlled by number of compounds or variables (loadings). Usually, most of the variations are explained by the first two or three principal components. Therefore, the cross plots of the first two components can reveal the various groups of oils. The PCs are, by definition, orthogonal to each other, such that no variance explained by one PC will contribute to another. PCA can be considered as a data reduction technique capable of handling large volumes of data and able to extract the subtle significant differences between the samples.

PCA has been used by a number of authors to analyse geochemical data, e.g. Kvalheim, 1987 for oil-source rock correlation studies, (Bigge & Farrimond, 1998) and (Parfitt & Farrimond, 1998) to find out the extent of biodegradation in a suit of oil seeps along the Dorset coast and Mupe Bay in the Wessex Basin (South of England). The PCA computer programme used in this project is the "SPSS version 10 for Windows".

Chapter 4 Reservoir Geochemistry of the Greater Birba area

4.1 Introduction

The main aim of this chapter is to use geochemical techniques to characterize the petroleum fluids of the Greater Birba area. The objectives of this part of the project are:

- To obtain a geochemical characterization of the petroleum fluids from the Greater Birba area.
- To identify secondary processes that the petroleum fluids may have been subjected to.
- To perform an oil-oil correlation using conventional geochemical parameters and statistical evaluation.
- Evaluation of the biomarker and aromatic hydrocarbon data obtained from core extracts and their implications.
- Geochemical evaluation of surface gas samples obtained from some of the studied wells.

4.2 Experimental

Forty-two samples were collected and analysed for this study - 22 oil samples and 20 reservoir core plugs. Table 4-1 shows the details of the crude oil samples incorporated in this study and Figure 4-1 shows the spatial distribution of the wells studied. Six oil samples were taken during production tests, while only two samples were taken by repeat formation test. Only Oil O1 (well BB1) was sampled from the wellhead, while the types of the rest of oil samples are not known; they were probably produced samples. 19 oil samples out of the 22 crude oil samples are black oils (i.e. API gravity <45°) and the other three samples are gas condensates. Not all the 19 oil samples are from different locations (i.e. wells and reservoir units). Four samples were from the A4C reservoir unit of well BB1 (O2, O4, O6, & O8); probably all of them are produced oil samples collected at the wellhead and the differences between them are in the depths and/or sampling year. Two samples (One RFT sample and one production test sample) were from the A3C reservoir unit of well Durra1 and two samples (One RFT sample and one production test sample) were from A3C reservoir unit of well Kaukab1. The samples were all included to show that the regularities

found between samples are not down to production effects. During the discussion, the sample ID will be referred to more often than wells because of this reason. However, the well name and reservoir unit will be often put in bracket after each sample. It must also be mentioned that term "reservoir" used often for carbonate stringers throughout this chapter and the whole thesis, has a similar meaning to stratigraphic unit, i.e. term reservoir does not mean one interconnected body of oil as used by many studies. In fact, from pressure data, carbonate stringers or carbonate reservoir units exist mostly as overpressured fragmented segments due to the halokinetic movements. The reservoir core rock samples are listed and explained later in this chapter (section 4.4.8).

Table 4-1: crude oil samples incorporated in this study, with the wells, reservoir units, year of sampling, depth (True vertical depth), type of samples, and physical type of samples (e.g. Black oil or condensate).

Wells	Sample ID	Sampling year	TVD (m)	Stringers	Age	type of sample	Note
BB1	O2	1988	2536.5	A4C	Neoproterozoic III-Cambrian (550-543Ma)	Ukn	oil
BB1	O4	1983	2533.1-2556.0	A4C		Ukn	oil
BB1	O6	1999	2588.3-2556.1	A4C		Ukn	oil
BB1	O8	1988	2533.1-2533.4	A4C		Ukn	oil
BB2	O1	1982	2583.4-2589.5	A4C		WH	oil
BBS1	O9	1987	2329.7	A4C		PT	Condensate
BBN1	O3	1980	3455.1-3471.5	A4C		Ukn	Condensate
BBN1	O5	1981	3558.1	A3C		swabbed from core	oil
BBN2	O7	1983	3597.8-3612.8	A4C		PT	oil
Nasser1	O13	1982	1998.6	A4C		Ukn	oil
Budour1H2	O20	2003	2971.59	A4C		Ukn	Condensate
Omraan1	O12	1982	2601.7-2626.7	A5C		PT	oil
Omraan1H3	O18	1997	2939.1-3201.6	A5C		Ukn	oil
Omraan1H3	O19	1997	2939.1-3201.1	A4C		Ukn	oil
Omraan1H3	O21	1997	3111.5-3201.5	A3C		Ukn	oil
Omraan1H3	O22	2001	2939.1-3201.1	A4C		Ukn	oil
Shamah1	O16	1992	2385.7-2389.7	A3C		Ukn	oil
Durra1	O14	1982	2691.0-2712.2	A3C		PT	oil
Durra1	O17	1982	2695.1	A3C		RFT	oil
Kaukab1	O10	1989	2513.6-2551.6	A3C		PT	oil
Kaukab1	O11	1987	2513.6-2551.6	A3C		PT	oil
Kaukab1	O15	1989	2897.0	A1C		RFT	oil

WH = the sample was taken at the wellhead, PT: the sample was taken during production test, RFT = the sample was taken during repeated formation test. Ukn = Unknown.

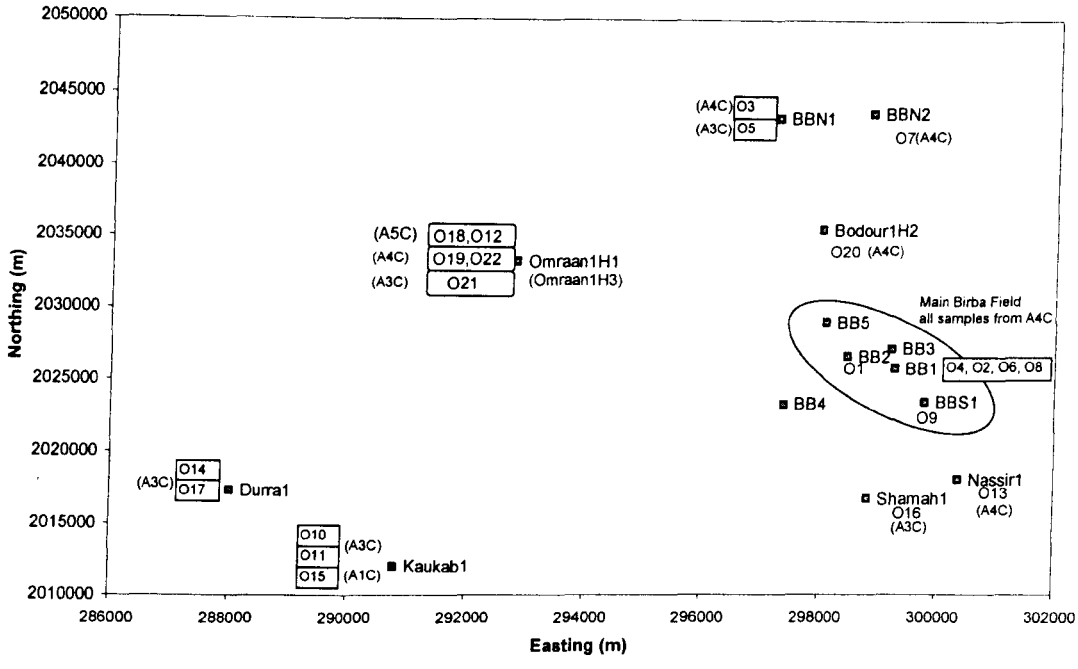

Figure 4-1: The distribution of the wells and oil samples (with letter O) assigned to their reservoir units (with letter A). The condensates are O9 (BBS1), O20 (Budour1), and O3 (BBN1). Several samples are from Omraan1 from three different stringers.

Figure 4-2 shows a schematic diagram of the geochemical methods, which were used in the analysis of the samples. The core samples were crushed and powdered by using a Tema mill. They were then extracted using the Soxtherm extraction method. Cotton wool and cellulose extraction thimbles were pre-extracted in a Soxhlet apparatus for 24 hours using an azeotropic mixture of dichloromethane (DCM) and methanol (MeOH) (93:7 by volume). A weighed amount (25-40g) of rock powder was added to the pre-extracted thimbles and then they were extracted in a Soxtherm apparatus for 6 hours using an azeotropic mixture of DCM: MeOH (93:7). Antibumping granules and activated cupper turnings were added to the solvent before extraction. After extraction, the solvent volume was reduced to 10ml using a Buchi Rotavapor. The content of extractable organic material was determined by removing a known aliquot, evaporating to dryness, and weighing.

Iatroscan analysis (thin layer chromatography-flame ionisation detection (TLC-FID)) was performed on all 20 core extracts as well as the 22 oil samples, using one of the Birba oils (O6, BB1H as a calibration standard) according to the method of (Karlsen & Larter, 1991). The standard was initially deasphaltened by mixing a 40-fold (v/v) excess of hexane with about 100mg of the oil and leaving overnight at 4°C.

The asphaltenes fraction was then separated from the maltene fraction by centrifugation. The maltenes were fractionated using open column silica chromatography on silica. The aliphatic hydrocarbons, aromatic hydrocarbons and a 'polar' fraction were eluted with petroleum ether, DCM, and methanol, respectively.

Core extracts were all deasphaltened using the above method. The twenty-two oil samples and the eighteen core extracts were analysed using gas chromatography. The twenty two oil samples and fourteen of the core extracts were separated in to hydrocarbons and polar fraction using Solid Phase Extraction method described by Bennett *et al.* (1996). The hydrocarbons fraction was then separated in to aliphatic and aromatics using silver nitrate impregnated silica gel described by Bennett and Larter (2000). Fourteen oil samples were sent to Houston Shell centre (USA) to be analysed for physical properties and metal content. Three gas samples were analysed for composition and compound specific isotopes analysis for the purpose of this project. In addition to that, $\delta^{13}C$ isotopic data of whole oil, saturated hydrocarbon fraction and of aromatic hydrocarbon fraction were provided by PDO (Petroleum development of Oman, sultanate of Oman) for number of the study oils.

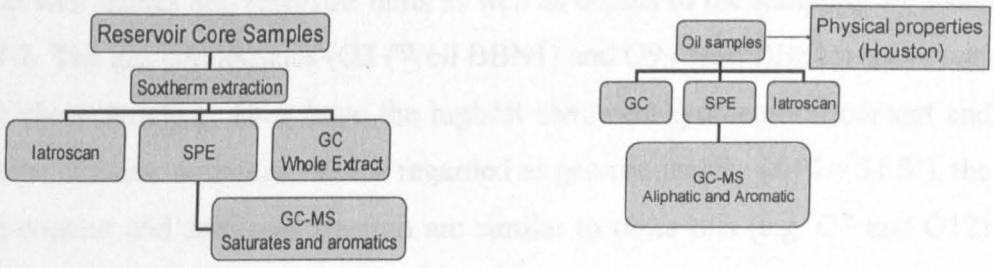

Figure 4-2: Schematic overview of geochemical methods used in the analysis of oil samples and crushed reservoir core samples. The physical properties and metals contents were measured in Shell labs in Houston, USA. SPE = solid phase extraction method.

4.3 Results and discussion

4.3.1 Facies characterization

4.3.1.1 Bulk geochemical composition

The bulk properties that were measured for these oils are listed in Table 4-2 and the distribution of the wells and oil samples is shown in Figure 4-1. The majority of the crude oils had API gravity in the range 28-35° and have high sulfur contents (>1.6 wt %). There are three gas condensates (O3 (Well BBN1), O9 (Well BBS1), O20 (Well Budour1H2) with high API gravity (>46°) and two of these (O9, O20) also have a high sulfur content (>3 wt%). Only oil O13 from well Nasser-1 shows a comparatively low API gravity (23.9°). Most of the oils are saturate rich except for Birba oils, which show only slightly higher content of saturated hydrocarbons over aromatic hydrocarbons (Figure 4-3). The majority of the oil samples have also low asphaltene content. Saturated and aromatic hydrocarbons (HC) fractions comprise between 42 to 68 and 22 to 41% of the oil, respectively. The NSO and asphaltene fractions range between 4 to 24%, and 0 to ca. 1.7% respectively (Table 4-2).

The well names and reservoir units as well as depths of the sampling are listed in Table 4-2. The gas condensates (O3 (Well BBN1) and O9 (Well BBS1)) show very distinctive characteristics. They have the highest saturated hydrocarbon content and no asphaltene content. Although O20 is regarded as gas condensate (API = 51.5°), the asphaltene content and saturated fraction are similar to other oils (e.g. O7 and O12) that are regarded as black oils. This gas condensate also has the highest sulphur content of all oils, as mentioned previously. The bulk compositions are illustrated in a histogram in Figure 4-3. The main Birba field oils (see Figure 4-1 for location) other than condensate O9, show the lowest content of saturates relative to the other oils but the highest aromatic content of all and relatively higher in NSO content than others except for O13. The oil O13 shows the lowest API gravity (23.9°) and the highest asphaltene content (1.7%) and NSO (24%) but has 45% saturated hydrocarbons, which is similar to Main Birba field oils (e.g. O1&O2). Saturated to aromatic hydrocarbon ratio is above unity for all oils but varies considerably, from 1.08 (O1) to 2.91 (O5).

Table 4-2: The bulk properties of petroleum fluids of Greater Birba area. Stringers = carbonate stratigraphic unit (e.g. A4C is Ara carbonates 4th cycle, and A1C>A3C>A4C>A5C in terms of age). TVD is true vertical depth.

Well	Sample ID	TVD (m)	Stringers	API°	Sulfur wt%	Sat%	Aro%	NSO%	Asp%	sat/aro
BB1	O2	2536.5	A4C	28.30	3.03	45	40	15	0.2	1.13
BB1	O4	2533.1	A4C	28.50	3.03	45	41	14	0.1	1.12
BB1	O6	2588.3	A4C			53	34	13	0.1	1.55
BB1	O8	2533.1	A4C		3.00	47	38	15	0.1	1.22
BB2	O1	2583.4	A4C	28.00	2.97	42	39	18	0.2	1.08
BBS1	O9	2329.7	A4C	46.10	3.24	63	31	6	0.0	2.01
BBN1	O3	3455.1	A4C	49.20	1.65	68	26	6	0.0	2.64
BBN1	O5	3558.1	A3C		2.5	64	22	14	0.7	2.91
BBN2	O7	3597.8	A4C	31.60	2.05	56	32	11	0.4	1.72
Nassir1	O13	1998.6	A4C	23.70	3.16	45	30	24	1.7	1.50
Budour1H2	O20	2971.6	A4C	51.50	4.70	56	32	12	0.5	1.77
Omraan1	O12	2601.7	A5C	30.20	2.11	54	32	13	0.5	1.66
Omraan1H3	O18	2823.6	A5C	29.80	2.10	54	36	10	0.3	1.49
Omraan1H3	O19	2939.1	A4C	31.00	1.90	57	33	10	0.4	1.76
Omraan1H3	O21	3111.5	A3C	31.00	1.90	62	34	4	0.0	1.82
Omraan1H3	O22	2939.1	A4C	30.90	2.10	53	36	10	0.7	1.46
Shamah1	O16	2385.7	A3C	29.40	2.46	53	37	8	1.1	1.43
Durra1	O14	2693.0	A3C	34.60	1.97	63	27	10	0.1	2.38
Durra1	O17	2695.1	A3C	33.00	2.02	56	30	14	0.2	1.85
Kaukab1	O10	2513.6	A3C	30.20	2.39	52	37	11	0.4	1.43
Kaukab1	O11	2513.6	A3C	29.10	2.4	52	37	10	0.5	1.40
Kaukab1	O15	2896.9	A1C	32.60	0.78	59	29	11	0.6	2.05

Sat %= 100 * (C_{15+} saturated hydrocarbons/ (saturated hydrocarbons + aromatic hydrocarbons + NSO + asphaltenes), Aro = %aromatic hydrocarbons as above, NSO = %NSO as above, Asp = %asphaltene as above, and sat, aro, NSO and Asp are obtained from Iatroscan.

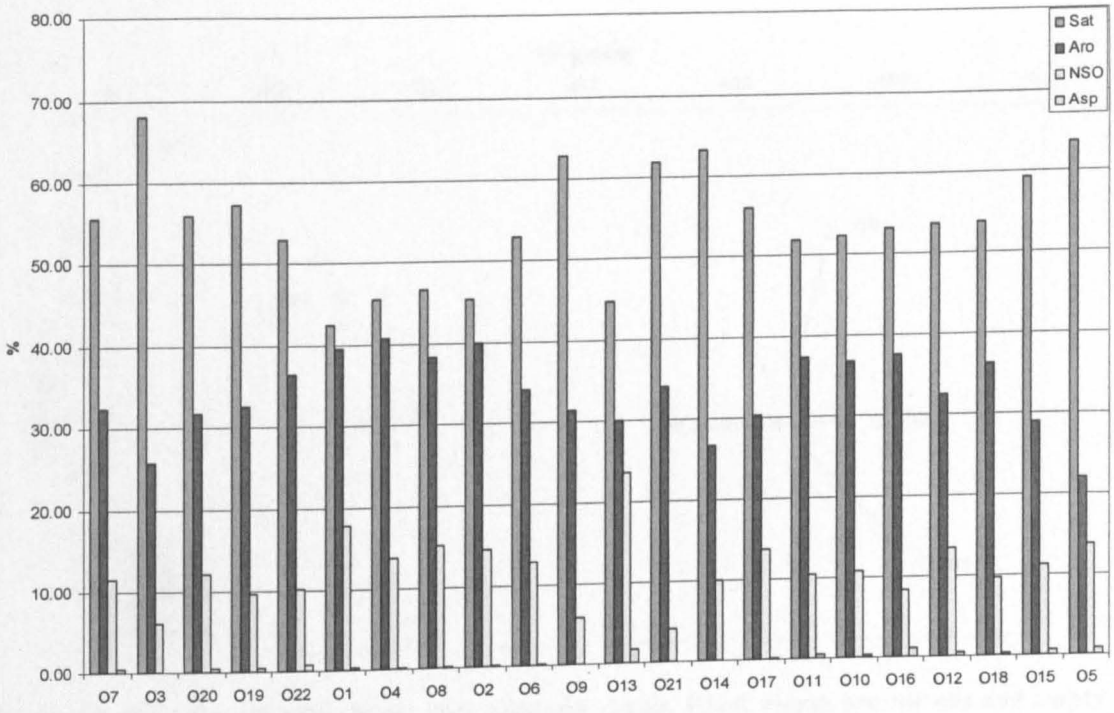

Figure 4-3: Bulk composition (from Iatroscan analysis) of the Greater Birba area oil.

There is a clear increase of API gravity with depth per reservoir unit A4C and A3C oils (Figure 4-4). However, there is no overall trend when all oils are presented. The lack of any geographic (compare Figure 4-4 with Figure 4-1) or depth trend in the distribution of the gas condensates reflects the complexity of the filling in this area. The API vs. depth gradient of A4C black oils seems steeper than that for A3C oils. A5C oils show more or less similar API gravities. API gravity is negatively correlated with sulfur for most of the oils (Figure 4-5). There is a clear decrease in sulfur content in A4C by going from south east (Well BB1 (e.g. O4) and well Nassir1 (O13) to north and north west (BBN2 (O7), Omraan1 (e.g. O19)) and same increase of sulfur content in A3C oils by going from north west (Durra 1 (e.g. O14) and Omraan1 (O21)) to south east (Shamah1 (O16), Kaukab1 (e.g. O11)) (Figure 4-6). These sulfur trends are accompanied by API decrease, which suggests some common control on both properties as suggested by Figure 4-5.

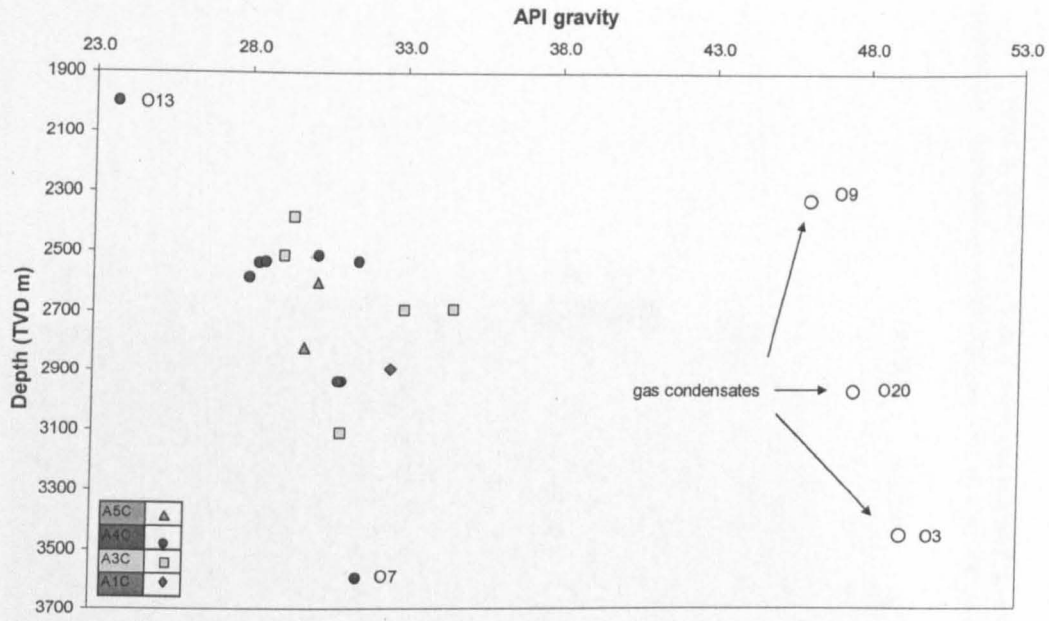

Figure 4-4: Variation in API gravity with reservoir depth. Filled shapes are for oils and empty shapes are for condensates. Different shapes are for different stratigraphic units (reservoir units).

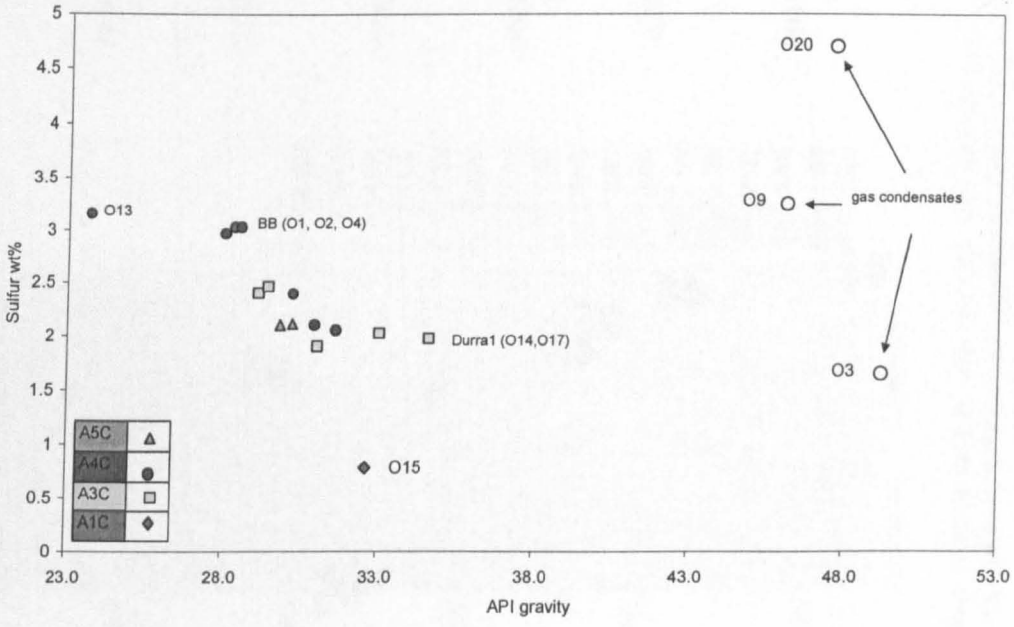

Figure 4-5: Variation in API gravity versus sulphur content (wt %). Filled shapes are for oils and empty shapes are for condensates. Different shapes are for different stratigraphic units (reservoir units).

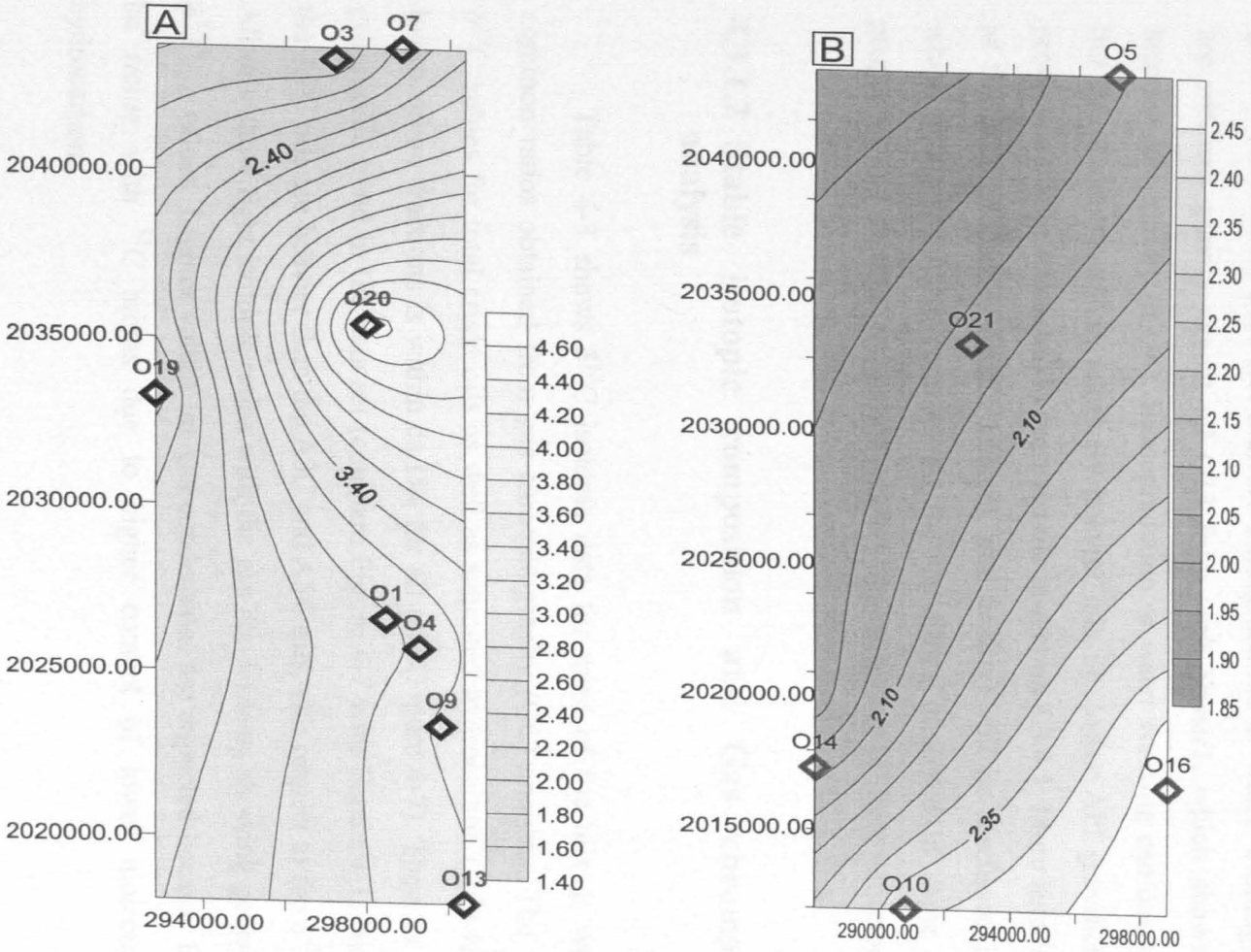

Figure 4-6: The distribution of sulphur content in A4C oils (A) and A3C oils (B) using easting and northing (m) of the well location (equivalent to latitude and longitude). Notice that the sulphur is high in both stringers but generally relatively higher in A4C and there is general increase trend from west to east.

A negative correlation between API gravity and sulfur content of oils has been previously reported in studies (e.g. Hughes *et al.*, 1985). It reflects the occurrence of most of the sulfur compounds in the polar fraction (NSO and Asphaltenes) and this often has a negative correlation with API gravity (unless there is a high content of sulfur compounds in the saturated and aromatic hydrocarbon fractions). The API gravity distribution does not indicate biodegradation or water washing, as most oils are medium gravity except oil O13 from well Nassir1, which shows a relatively heavier API gravity (23.9°). Biodegradation or water washing can concentrate sulfur but this should result in relatively heavier oils i.e. lower API gravities. These two processes will be discussed in more details in section 4.3.4.1. More details about some of the bulk properties (sulfur content, and acidity) will be discussed in chapter 6, which focuses on the controls on the variations observed in some of the bulk properties and attempts to provide a better understanding of these variations.

4.3.1.2 Stable isotopic composition and Gas chromatographic analysis

Table 4-3 shows $\delta^{13}C$ isotopic data for most of the oils as well as some common ratios obtained from gas chromatography (GC) analysis. The variation in $\delta^{13}C$ values for total crude oils as well as saturated hydrocarbon (HC) and aromatic hydrocarbon fractions is within ca.1‰ for all oils (Figure 4-7). There is no obvious geographic trend in the data set (compare Figure 4-7 with Figure 4-1) but generally, the A4C oils are heavier than the A3C and A5C oils with respect to the $\delta^{13}C_{sat}$ values. All oils show light isotopic ratios with the gas condensates showing generally lighter $\delta^{13}C_{total}$ values. Lighter values for gas condensates are expected because they should be richer with ^{12}C atoms due to higher content of lower molecular weight hydrocarbons.

Table 4-3: $\delta^{13}C$ isotopic data and some common ratios from gas chromatographic analysis of the whole oils and chromatographic fractions. (Pr=pristane, Ph=phytane, C_{17}&C_{18}=*n*-C_{17}&*n*-C_{18} alkanes. CPI=Carbon preference Index (*n*-alkanes) = 2*(C_{23}+ C_{25}+ C_{27}+ C_{29})/ [C_{22} + 2*(C_{24} + C_{26} + C_{28}) + C_{30}).

well	Sample ID	TVD (m)	Stringers	$\delta^{13}C$ Whole oil	$\delta^{13}C$ Sat	$\delta^{13}C$ Aro	Pr/Ph	Pr/C17	Ph/C18	CPI
BB1	O2	2536.5	A4C	-34.7	-34.6	-34.7	0.52	0.31	0.68	1.05
BB1	O4	2533.1	A4C	-34.7	-34.6	-34.6	0.53	0.33	0.76	1.04
BB1	O6	2588.3	A4C	nd	nd	nd	0.56	0.33	0.67	1.02
BB1	O8	2533.1	A4C	-34.6	-34.6	-34.7	0.51	0.31	0.74	1.03
BB2	O1	2583.4	A4C	nd	nd	nd	0.50	0.33	0.80	1.07
BBS1	O9	2329.7	A4C	-35.2	-34.5	-34.8	0.54	0.30	0.65	1.07
BBN1	O3	3455.1	A4C	-34.9	-34.9	-34.4	0.60	0.31	0.68	1.02
BBN1	O5	3558.1	A3C	nd	nd	nd	1.34	0.80	0.72	0.98
BBN2	O7	3597.8	A4C	-34.4	-34.4	-34.5	0.60	0.37	0.79	1.04
Nassir1	O13	1998.6	A4C	-34.2	-34.6	-34.4	0.48	0.34	0.85	1.05
Budour1H2	O20	2971.6	A4C	-35	-35.2	-34.9	0.62	0.34	0.70	1.02
Omraan1	O12	2601.7	A5C	-34.7	-34.8	-34.6	0.49	0.34	0.82	1.03
Omraan1H3	O18	2823.6	A5C	-34.6	-34.7	-34.8	0.50	0.33	0.82	1.07
Omraan1H3	O19	2939.1	A4C	-34.6	-34.6	-34.9	0.50	0.35	0.79	1.06
Omraan1H3	O21	3111.5	A3C	-34.6	-34.7	-34.9	0.48	0.34	0.84	1.06
Omraan1H3	O22	2939.1	A4C	-34.7	-34.7	-34.7	0.55	0.33	0.82	1.10
Shamah1	O16	2385.7	A3C	nd	nd	nd	0.48	0.36	0.85	1.05
Durra1	O14	2693.0	A3C	-34.8	-34.8	-34.6	0.47	0.32	0.84	1.05
Durra1	O17	2695.1	A3C	-35	nd	nd	0.51	0.35	0.81	1.04
Kaukab1	O10	2513.6	A3C	-34.9	-35	-34.9	0.53	0.32	0.75	1.04
Kaukab1	O11	2513.6	A3C	-34.1	nd	nd	0.64	0.28	0.58	1.06
Kaukab1	O15	2896.9	A1C	nd	nd	nd	0.46	0.35	0.86	1.05

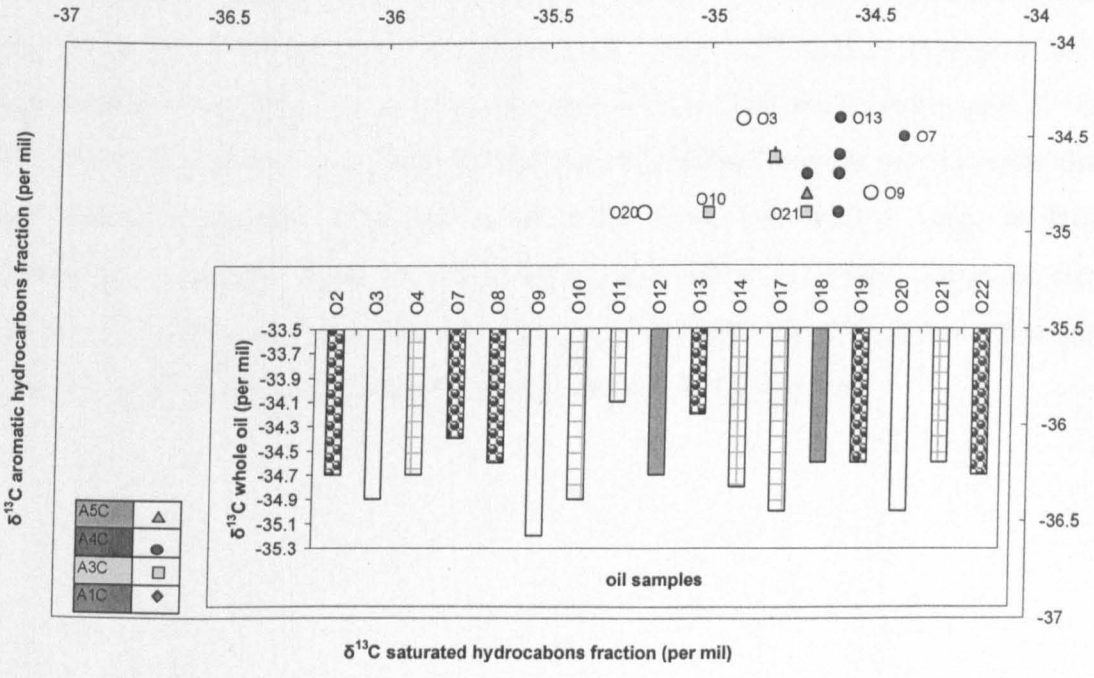

Figure 4-7: A cross-plot of $\delta^{13}C_{Sat}$ (Saturated hydrocarbons) versus $\delta^{13}C_{Aro}$ (Aromatic hydrocarbons) and a histogram of $\delta^{13}C_{Tot}$ (whole oil) values. Different shapes are for different reservoir units; the filled shapes are for oils and Empty circles and columns are condensates.

Almost all of the oils in the different reservoir units (carbonate stringers) and the different wells in the Greater Birba area show generally similar gas chromatograms as shown in Figure 4-8 & Figure 4-9, the exception being oil sample (O5) from the A3C reservoir unit of well BBN1 with relatively higher abundance of C_{17}-C_{27} *n*-alkanes and very big loss of C_{15-} n-alkanes. For most of the samples, the *n*-alkanes occur in a smooth distribution in the carbon number range C_{15+} but there is a slight odd over even predominance between *n*-C_{11} to *n*-C_{15}. This is noticed in all of the black oils but not in the gas condensates (O3 (well BBN1), O9 (well BBS1), & O20 (well Budour1H2)) which show smooth *n*-alkane envelopes over the entire carbon number range (Figure 4-9). The relative abundance of the lower carbon number *n*-alkanes (<C_{15}) varies between different oils and even between the oils from the same reservoir (carbonate stringer) and the same well. The greatest loss of C_{15-} is observed in O1 (well BB2) and O22 (well Omraan1H3) and this may be due to evaporative loss during storage or sample preparation. All samples show a pristane/phytane (Pr/Ph) ratio of 0.6 or less, except for oil O5 (well BBN1), which also shows a different GC fingerprint (Figure 4-8). The carbon preference index (CPI) of the higher molecular weight n-alkane envelopes (*n*-C_{22}-*n*-C_{30}) for all oils is around one. Pristane/*n*-C_{17} ratios are in the range from 0.28 to 0.37 with an average of 0.33; and phytane/*n*-C_{18} ratios are in the range from 0.58 to 0.86 and averages at 0.77. Oil O5 (well BBN1) is exceptional in the data set as it shows a higher pr/*n*-C_{17} ratio than the other samples but is similar in the other ratio. The narrow range in these parameters, especially Ph/*n*-C_{18} which shows relatively wider range, shows no clear geographic or stratigraphic trend, although generally, A4C oils show lower ratios than both A3C and A5C oils (with some overlap) as clear in Figure 4-10.

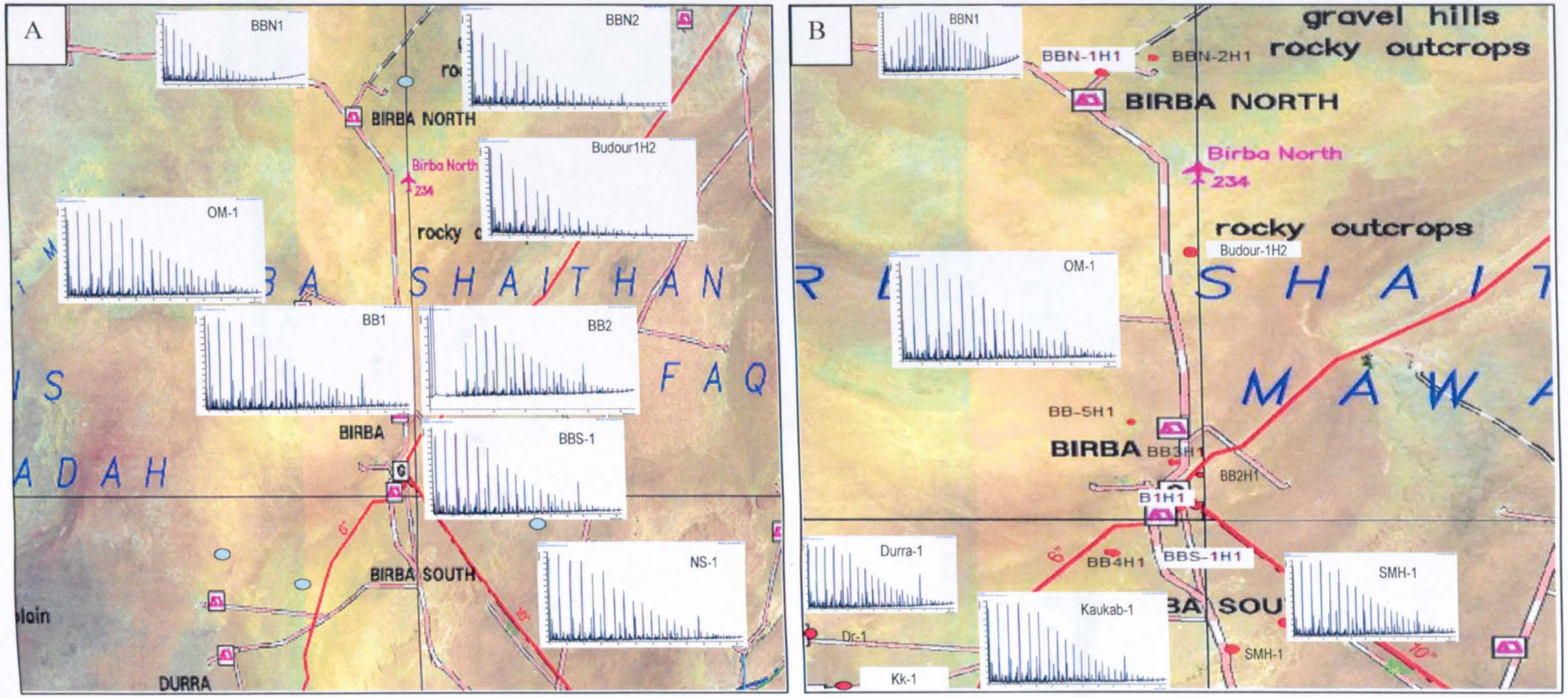

Figure 4-8: GC fingerprints for selected whole oil samples from A4C (A) and A3C (B) oils coupled with the geographic map to illustrate the distribution of the wells.

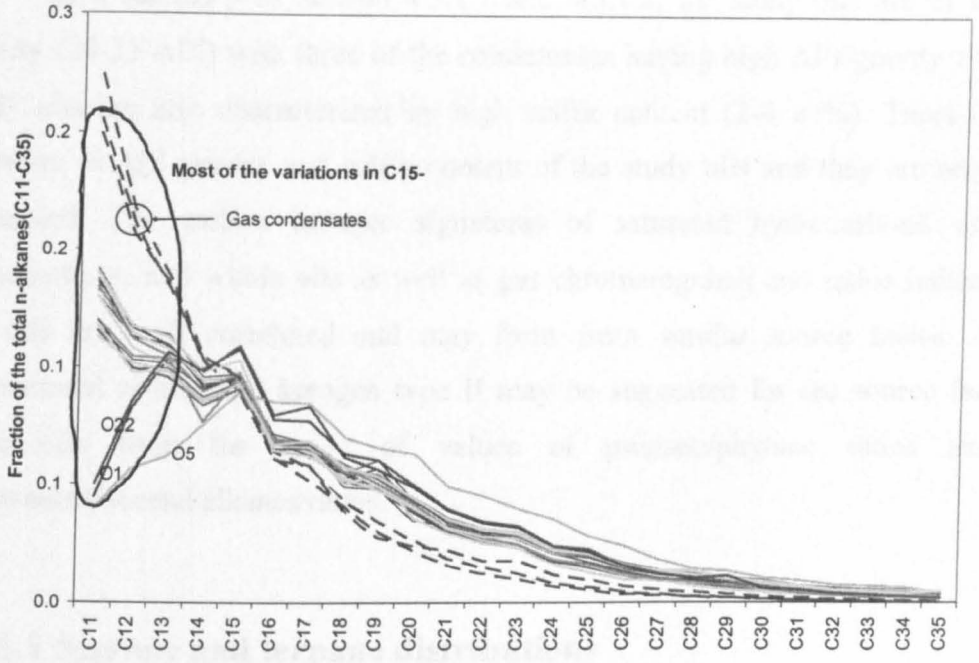

Figure 4-9: Relative abundance of n-alkanes for all sampled oils. O5 shows different n-alkane envelope that has relatively higher C_{19} to C_{27} envelope. Loss of C_{15-} *n*-alkanes in O22 and O1 may be due to evaporative loss during sample storage.

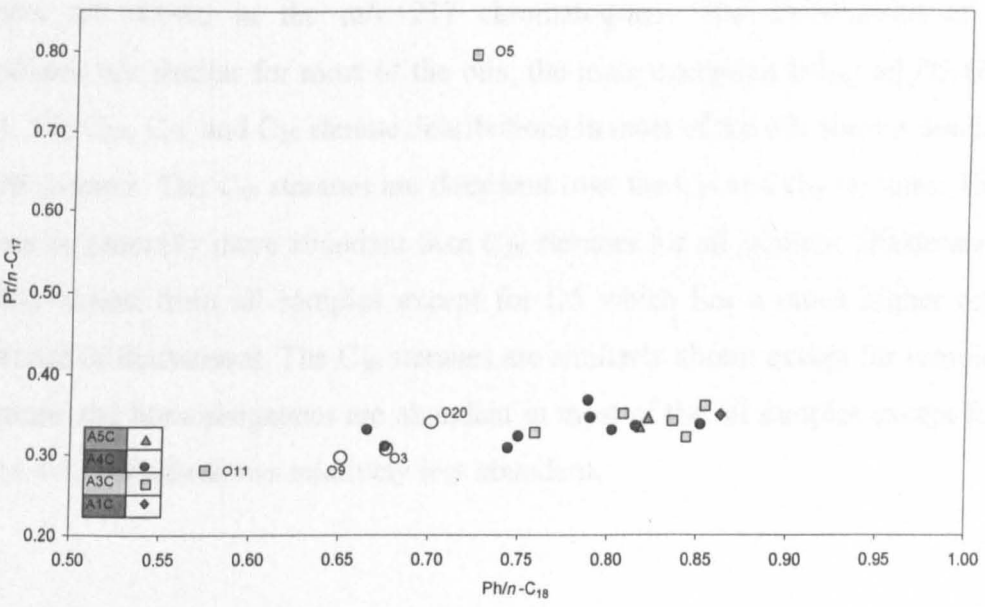

Figure 4-10: Cross plot of pristane/*n*-C_{17} against phytane/*n*-C_{18} for all oils. Pristane/*n*-C_{17} ratios vary from 0.28 to 0.37 with an average of 0.33; and phytane/*n*-C_{18} ratios ranges from 0.58 to 0.86 and averages at 0.77.

In a summery of section 4.3.1.1 and 4.3.1.2, the study oils are of medium gravity (28-35°API) with three of the condensates having high API gravity >45. The study oils are also characterized by high sulfur content (2-4 wt%). There is large variation in API gravity and sulfur content of the study oils and they are negatively correlated. The carbon isotopic signatures of saturated hydrocarbons, aromatic hydrocarbons, and whole oils as well as gas chromatograms and ratios indicate that the oils are well correlated and may form from similar source facies. Anoxic depositional setting and kerogen type II may be suggested for the source facies of these oils from the range of values of pristane/phytane ratios and the isoprenoids/normal alkanes ratios.

4.3.1.3 Sterane and terpane distributions

Typical mass chromatograms of regular steranes (m/z 217), αββ steranes (m/z 218), and diasteranes (m/z 259) are shown below with peaks identified (Figure 4-11). The identification of C_{21} and C_{22} pregnanes, C_{27}, C_{28} and C_{29} ααα and αββ (20S+R) steranes are shown in the m/z 217 chromatogram. The distributions of these compounds are similar for most of the oils, the main exception being oil O5 (Figure 4-12). The C_{27}, C_{28}, and C_{29} sterane distributions in most of the oils show a dominance of αββ isomers. The C_{29} steranes are dominant over the C_{27} and C_{28} steranes. The C_{27} steranes is generally more abundant than C_{28} steranes for all isomers. Diasteranes are virtually absent from all samples except for O5 which has a much higher relative abundance of diasteranes. The C_{30} steranes are similarly absent except for sample O5. Pregnanes and homopregnanes are abundant in most of the oil samples except for O5 (Figure 4-12) which shows relatively less abundant.

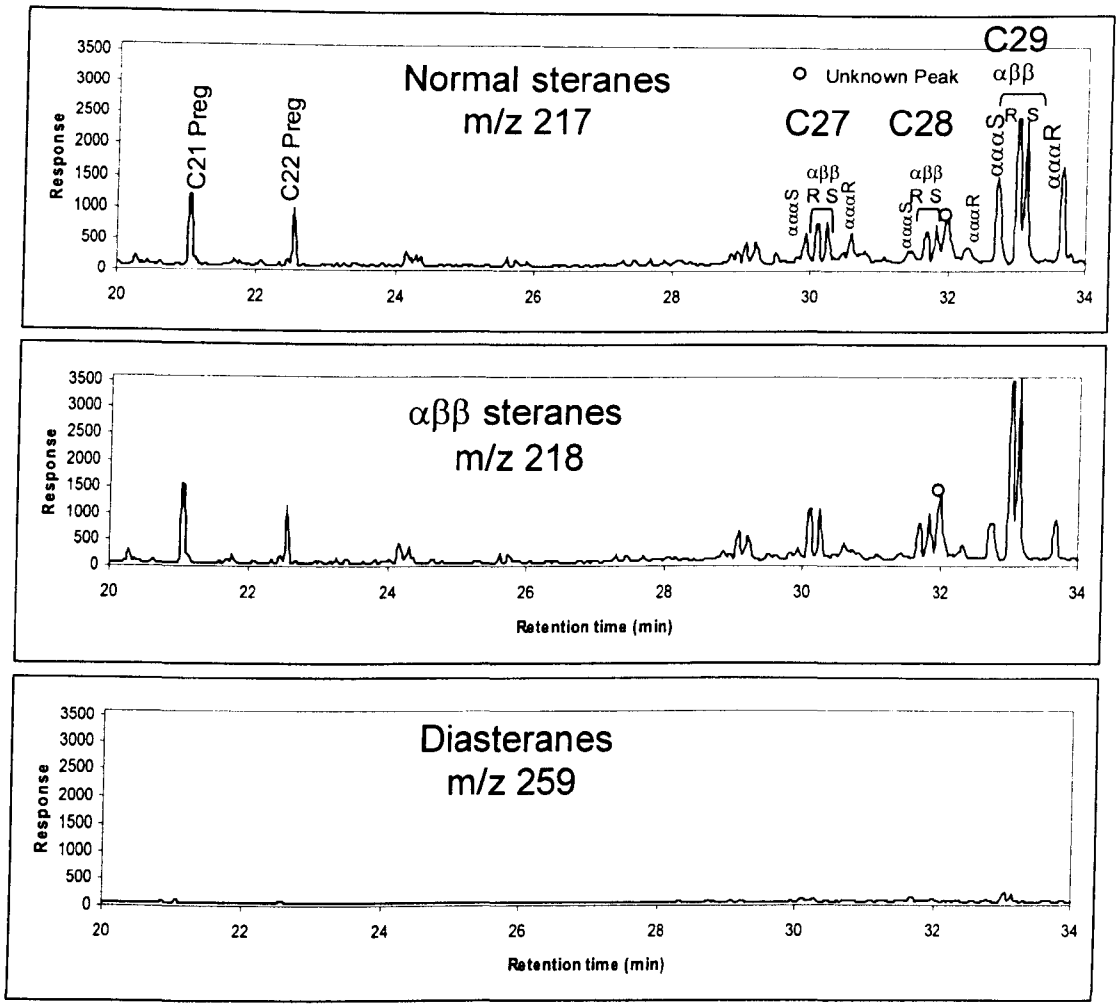

Figure 4-11: Representative mass chromatograms of steranes (m/z 217), iso-steranes (m/z 218), and diasteranes (m/z 259), for Oil O4 from A4C reservoir unit of well BB1.

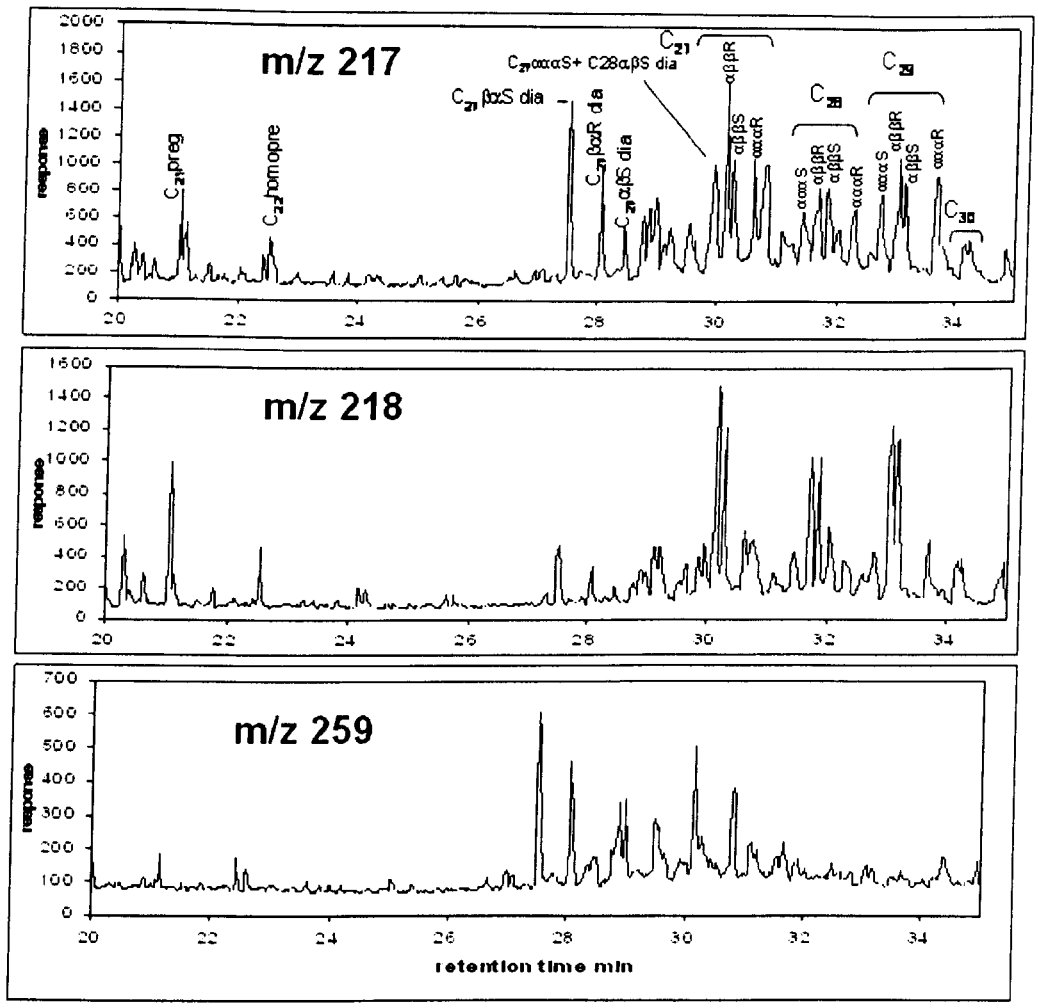

Figure 4-12: The distribution of steranes, diasteranes, and αββ steranes in oil O5.

The predominance of C_{29} steranes usually indicates a terrestrial source for the organic matter. However, as land plants didn't evolve before the Devonian, the C_{29} dominance in the pre-Devonian oils has been attributed to an algal origin (Volkman, 1986). Other studies have indicated that C_{29} sterols can be derived from brown and green algae (Moldowan *et al.*, 1985 and references therein) and diatom cultures (Volkman *et al.*, 1981) as well as cyanobacteria (e.g. Fowler & Douglas, 1984). The absence of the C_{30} steranes from all samples except for O5 can also be interpreted as evidence of the absence of C_{30} sterane precursors. Moldowan *et al.*, 1985 interpreted this absence in petroleum older than 500 Ma due to a delay in the evolution of marine organisms that had C_{30} sterols. However, C_{30} steranes were subsequently detected e.g. in bitumen extracts from Precambrian Chuar rock in Arizona (J) and 2700 Ma old extracts from the Pilbara Craton, Australia (Brocks *et al.*, 1999). Oil O5 (A3C, well BBN1), of Infracambrian age, shows small amounts of C_{30} steranes and so may support the observation from the analysis of the Chuar and Pilbara rock extracts.

However, none of the samples shows 4-methyl steranes, as expected for Palaeozoic samples. O5 (A3C, well BBN1) also differs from the other samples in other respects: e.g., the C_{27} steranes are generally higher than C_{29} in O5 (A3C, well BBN1). Most samples contain very small amount of diasteranes; this indicates a non-clastic or carbonate source for the oil because the rearrangement process of steranes to diasteranes in source rocks during thermal stress is believed to be catalysed by the acidic sites on clays (Rubintsein et al., 1975; Sieskind et al., 1979). However, other studies have shown that the primary control on the abundance of diasteranes is clay rich minerals (Moldowan *et al.*, 1992; Palacas *et al.*, 1984). Moldowan *et al.*, 1986 suggested that diasterane abundance was controlled by the redox conditions during the deposition of organic matter. Oil O5 is again different in having significantly more diasteranes than other oil samples (Figure 4-12). These characteristics might suggest a different environment of deposition (shaley source rock) but possible contamination cannot be ruled out. Pregnanes and homopregnanes were reported in evaporitic source rocks deposited in hypersaline environment (ten Haven et al., 1985); however Wingert & Pomerantz, 1986 proposed a thermal origin from steranes. They showed that 5α (H), 14α (H), 17β (H) pregnanes and homopregnanes isomers coelute with the thermodynamically less stable 5α (H), 14α (H), 17α (H) compounds and so they concluded that αββ pregnanes and homopregnanes are predominant in highly mature oil samples.

Most of the oils in the sample set show relatively high abundances of terpanes (Figure 4-13), which originate from bacterial (prokaryotic) membrane lipids (Ourisson et al., 1979; Ourisson et al., 1982). Representative chromatograms of terpanes for O4 and O5 are shown in Figure 4-13. The distributions of hopanes (Figure 4-13) in most of the samples are very similar; the exceptions are samples O5 (BBN1 (A3C)) and O15 (Kaukab1 (A1C)). The majority of the samples show a predominance of the $C_{29}\alpha\beta$ and $C_{30}\alpha\beta$ hopanes, with the former being more abundant than the latter. This predominance is reversed ($C_{30}>C_{29}$) in samples O15 and O5 (Figure 4-13). This indicates a similar origin for most of the samples except for O5 and O15. Similar hopane distributions have been attributed to organic rich evaporite-carbonate source rocks e.g. (Clark & Philp, 1989; Connan *et al.*, 1986; Zumberge, 1984). The abundance of 18α(H)-22,29,30-trisnorneohopane (Ts) is low in most of the

study samples, whereas that of the regular 22,29,30-trisnorhopane (Tm) is high. The difference in relative abundance of the two isomers is smaller in O5 and (to a lesser extent) in O15 but Tm remains more abundant than Ts. One of the main possible reasons behind the low Ts is that most of the oils in the study area were derived from carbonate source facies, because these facies lack of clays which are believed to play an important rule to convert Tm to Ts during diagenesis (McKirdy et al., 1983). Gammacerane is abundant in most of the samples but virtually absent from O5. Gammacerane is derived from tetrahymanol, produced by ciliates feeding on bacteria (Sinninghe Damsté *et al.*, 1995). The high abundance of gammacerane is typical of highly reducing hypersaline environment (Peters *et al.*, 2005) and powerful indicator of stratified water column conditions during the accumulation of organic matter (Sinninghe Damsté *et al.*, 1995). The relatively high abundance of the C_{35} homohopanes also suggests a hypersaline environment of deposition (Zumberge, 1984) and/or a highly reducing sulphidic depositional setting (Moldowan *et al.*, 1992; Peters & Moldowan, 1991). C_{29}Ts can be measured in samples O5 and O15, whereas in the rest of oil suite it was not possible to be detected. The 28,30-Bisnorhopane (BNH) is desmethylhopane and is good indicator for clay poor anoxic depositional setting (Mello & Maxwell., 1990; Mello *et al.*, 1988) and may also be indicator of highly sulphidic source rocks (Curiale *et al.*, 1985). BNH is thought to be derived from chemoautotrophic bacteria that grow at the oxic-anoxic interface (Peters *et al.*, 2005).

The abundant tricyclic terpanes (C_{19}-C_{29}) were present in most of the oil samples studied, and a representative mass chromatogram (obtained for sample O4) is shown in Figure 4-13. The distribution of the tricyclics shown in Figure 4-13 indicates the mature character of the oil, with βα isomers and the low molecular weight tricyclics being predominant (Peters *et al.*, 2005). This is a typical feature of most of the samples, the exception being sample O5, which shows very low relative abundances of tricyclics. The C_{23}βα isomer is the most prominent tricyclic terpane in most of the oils; this is a feature that has been attributed to carbonate-evaporite sourced oils (Palacas et al., 1984). The very low abundance of C_{26+} tricyclics relative to lower tricyclics (C_{19}-C_{25}) in most of the oils suggests carbonate source (Peters *et al.*, 2005). The C_{24} tetracyclic terpanes show relatively high abundances, a feature which

has been associated with evaporitic facies (Connan & Dessort, 1987b) and evaporite-carbonate facies (Palacas et al., 1984). This compound is also reported in oils believed to be sourced from terrigenous organic matter (Peters *et al.*, 2005 reference therein) and it is common in marine oils sourced from mudstone to carbonate source facies (Peters *et al.*, 2005). However, a carbonate-evaporite source is more appropriate source for these oils as not much evidence of land input has been found.

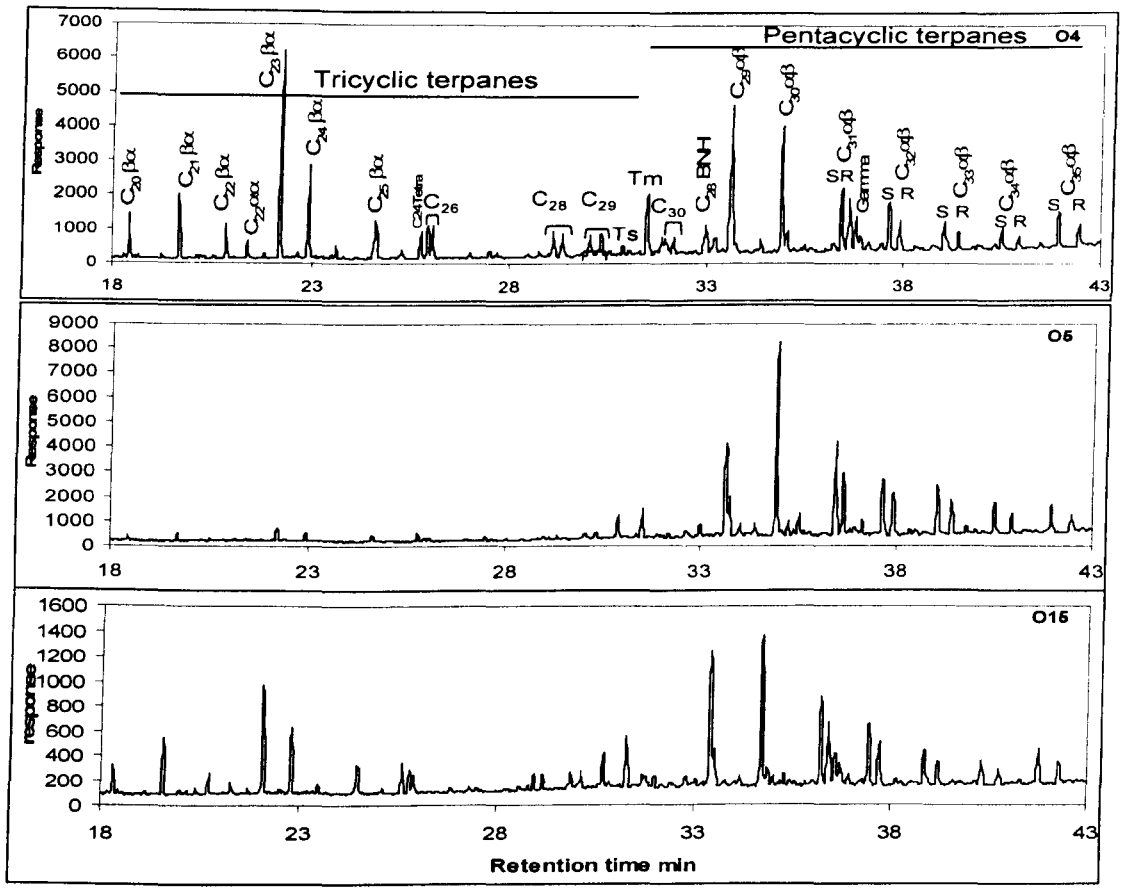

Figure 4-13: The distribution of tri- and pentacyclic terpanes in sample O4 (representative of the majority of samples) and samples O5 and O15 (which are different).

Selected facies-sensitive aliphatic hydrocarbon biomarker parameters are shown in the Table 4-4. The ternary diagram (Figure 4-14) shows relationship between samples based on the relative abundance of the C_{27}, C_{28}, and C_{29} ααα (20R) steranes. This diagram was proposed to differentiate different depositional environments (Moldowan *et al.*, 1985) but mainly to differentiate groups of oils from different organic facies of the same source rock (e.g. Grantham *et al.*, 1988). C_{27} and C_{28} steranes have been reported to indicate different algae and C_{29} steranes has been reported to indicate land plants input (Peters & Moldowan, 1993) but may also be derived from algae (Volkman, 1986). Most studied oil samples fall in a very narrow

cluster in the ternary plot, for the exception being oil sample O5 (A3C, well BBN1). The same principal is applicable in using C_{27}/C_{29} and C_{28}/C_{29} steranes ratios. However, the principal use of C_{28}/C_{29} steranes is to infer the age of the oils and source rocks. Moldowan *et al.*, 1985 reported a general decrease in C_{29} steranes and increase in C_{28} steranes through geologic history. The C_{28} steranes increase is thought to be due to increased diversification of phytoplankton assemblages such as diatoms (Moldowan *et al.*, 1985). A C_{28}/C_{29} steranes ratio less than 0.5 was observed for lower Palaeozoic oils and older, while a ratio greater than 0.7 is for Upper Jurassic to Miocene (Grantham & Wakefield, 1988). All studied oils show a C_{28}/C_{29} steranes ratio less than 0.5 confirming the observation made by Grantham & Wakefield, 1988 , the exception being O5 (A3C, well BBN1) which might be contaminated with some oil during sampling,. The other parameters listed in Table 4-4 are described in Appendix 4-2. The Gammacerane index (Gammacerane/$C_{30}\alpha\beta$) and homohopane index (C35$\alpha\beta$ hopane/(sum of C_{31}-C_{35} $\alpha\beta$ hopanes) are powerful indicator of stratified column and water salinity respectively as discussed above. The C_{24}Tetracyclics/$C_{23}\beta\alpha$Tricyclics ratio is important to distinguish different groups of oils sourced from carbonate and evaporate facies (Aquino Neto *et al.*, 1983). Tetracyclic compounds are thought to originate by thermal or microbial fragmentation of E-ring in hopanes or may be from bacteria through biosynthetic route or from terrigenous precursors (Peters *et al.*, 2005). C_{24} Tetracyclics are more abundant in oils sourced from carbonate and evaporite source rocks or from terrigenous organic matter (Connan & Dessort, 1987a). The C_{26}(S+R)Tricyclics/C_{25}(S+R)Tricyclics is another parameter that is useful to distinguish between lacustrine and marine oils (Peters *et al.*, 2005). The 28,30-Bisnorhopane (BNH) /$C_{30}\alpha\beta$ 17α hopane is a common source parameter but is readily affected by thermal maturity and so it is only useful for oils with similar thermal stress (Curiale *et al.*, 1985). The standard deviation in most of the other parameters is less than 0.08 (8%), which is within the error range (10%). Although the homohopane index shows only small variation, the data suggest that the oils from the main Birba Field (e.g. O4 from well BB-1) show lower ratios than the surrounding oils. There is significant overlap between data from oils from different stringers and it is difficult to distinguish between them. Gas condensate O20 (A4C, well Budour-1H2) is the only sample that looks very different from the rest. Although, maturity can also affect the homohopane ratio, the gas condensate O20 (A4C, well

Budour-1H2) does not differ in other maturity sensitive parameters. Large variations (% Standard deviation= 23-36%) are seen in the ratios of the saturated hydrocarbon biomarker classes in most oils. The cross-plot of tricyclic terpanes (C_{19}-C_{29})/ C_{27}-C_{35} 17α Hopanes ratio versus C_{27}-C_{35} 17α Hopanes/ C_{27}-C_{29} steranes (S+R, ααα+αββ) ratio, shown in Figure 4-15, reveals a negative correlation and apparent grouping among the sample set. The hopanes/steranes ratio has been reported to increase with maturation (Peters & Moldowan, 1993), but it has also been reported to decrease with maturation of coal (Norgate *et al.*, 1999). The tricyclic terpanes (C_{19}-C_{29})/ C_{27}-C_{35} 17α Hopanes ratio has been reported to increase with thermal stress due to the higher stability of tricyclics (van Graas, 1990). Although maturity may result in this relationship, this is not supported by maturity parameters which shows most of the oils display similar maturity (discussed later section 4.3.2).The trend line observed from Figure 4-15 may suggest mixing of oils with condensate charge. This is obvious from the end members based on these ratios, the gas condensates and the other end member is A3C oils (e.g. O14 (well Durra-1), and O11 (well Kaukab-1)). A theoretical mixing model was calculated assuming two end members, a gas condensate resembling the composition of Budour-1H2 gas condensate (O20) and oils resembling the composition of Kaukab-1 oil (O11). The model suggests that the variations are likely to be related to mixing with condensate charge. For the reasons why I choose these two end members, refer to chapter seven (section 7.3.1, 7.4, and 7.5).

Table 4-4: Selected facies sensitive parameters based on saturated hydrocarbon biomarkers. All parameters and terms are explained below the table, and in Appendix 4-1 and the full definitions of the compounds are listed in Table 1-1 in chapter 1. the condensates are shaded and denoted with (GC).

Sample ID	Wells	stratigraphy	depth (m)	C_{27} St %	C_{28} St%	C_{29} St %	C_{27}/C_{29} (St)	C_{28}/C_{29} (St)	Homohopane Index	Gammacerane Index	$C_{29}\alpha\beta/C_{30}\alpha\beta$ H	BNH/$C_{29}\alpha\beta$H	C_{26}Tri(S+R)/ C_{25}Tri(S+R)	C_{24}Tetr/$C_{23}\beta\alpha$Tri	Tric/Hop	Hop/ster	Triterp/Ster
O1	BB2	A4C	2583.35	17	16	68	0.25	0.23	18	0.29	1.24	0.23	0.99	0.17	0.73	1.65	2.86
O2	BB1	A4C	2536.46	17	16	68	0.25	0.23	17	0.30	1.21	0.23	0.93	0.16	0.70	1.68	2.86
O3	BBN1	A4C (GC)	3455.09	17	17	66	0.26	0.26	18	0.24	1.47	0.15	0.89	0.14	1.34	1.43	3.36
O4	BB1	A4C	2533.06	19	15	66	0.28	0.23	18	0.28	1.24	0.23	0.91	0.16	0.68	1.66	2.79
O5	BBN1	A3C	3557.8	40	25	35	1.15	0.73	11	0.02	0.51	0.20	0.76	0.92	0.08	2.78	2.99
O6	BB1	A4C	2537.06	19	14	67	0.29	0.21	17	0.28	1.26	0.23	0.97	0.16	0.66	1.70	2.82
O7	BBN2	A4C	3597.75	16	17	67	0.24	0.25	19	0.32	1.51	0.14	0.86	0.19	0.65	2.01	3.31
O8	BB1	A4C	2533.06	16	15	69	0.23	0.22	18	0.30	1.24	0.23	0.91	0.15	0.67	1.71	2.87
O9	BBS1	A4C (GC)	2329.71	21	15	65	0.32	0.23	15	0.24	1.22	0.22	0.92	0.07	1.00	1.40	2.81
O10	Kaukab	A3C	2513.58	15	16	69	0.22	0.23	21	0.32	1.25	0.20	0.94	0.16	0.47	2.23	3.26
O11	Kaukab1	A3C	2513.58	14	19	67	0.21	0.28	19	0.34	1.26	0.17	0.89	0.15	0.53	2.24	3.42
O12	Omraan1H1	A5C	2601.71	17	14	69	0.25	0.21	19	0.32	1.30	0.21	0.87	0.19	0.51	2.11	3.17
O13	Nassir1	A4C	1998.6	15	15	70	0.21	0.22	19	0.31	1.14	0.23	0.97	0.15	0.53	2.08	3.19
O14	Durra1	A3C	2692.97	19	16	66	0.29	0.24	20	0.31	1.30	0.19	0.91	0.17	0.48	2.14	3.17
O15	Kaukab	A1C	2896.94	20	14	66	0.30	0.22	15	0.22	0.96	0.08	0.84	0.29	0.42	1.54	2.19
O16	Shamah1	A3C	2385.69	18	14	68	0.26	0.21	20	0.33	1.22	0.23	0.86	0.17	0.47	2.20	3.23
O17	Durra1	A3C	2695.07	17	16	67	0.26	0.24	21	0.34	1.27	0.24	0.98	0.17	0.45	2.28	3.30
O18	Omraan1H3	A5C	2823.61	18	14	67	0.27	0.21	19	0.31	1.33	0.20	0.89	0.18	0.53	2.07	3.17
O19	Omraan1H3	A4C	2939.1	17	16	67	0.26	0.24	20	0.30	1.29	0.20	0.91	0.19	0.48	2.16	3.18
O20	Bodour1H2	A4C (GC)	2971.59	21	18	62	0.33	0.29	9	0.27	1.35	0.25	0.96	0.10	1.80	0.94	2.63
O21	Omraan1H3	A3C	3111.51	18	14	68	0.27	0.21	20	0.33	1.30	0.21	1.03	0.19	0.47	2.16	3.18
O22	Omraan1H3	A4C	2939.1	19	14	67	0.29	0.21	19	0.32	1.32	0.19	0.98	0.18	0.54	2.03	3.10
STD ex O5&O15				1.75	1.32	1.77	0.03	0.02	2.69	0.03	0.08	0.03	0.05	0.03	0.34	0.36	0.23

Key to abbreviations: St = steranes (αααR), Homohopane Index= C35αβ hopane/(sum of C_{31}-C_{35} αβ hopanes); Gammacerane Index=/C_{30}αβ; H = 17α hopanes; Tri=Tricyclics; Tetra=Tetracyclics; Tric/Hop=sum of tricyclic terpanes (C_{19}-C_{29})/sum of C_{27}-C_{35} 17α Hopanes. Hop/ster= sum of C_{27}-C_{35} 17α Hopanes/ sum of C_{27}-C_{29} steranes (S+R, ααα+αββ); Triter/ster=(Sum of tricyclics (C_{19}-C_{30}) and C_{27}-C_{35} 17α Hopanes)/ sum of C_{27}-C_{29} steranes (S+R, ααα+αββ); STD ex O5 and O15=standard deviations of all samples except for O5 and O15.

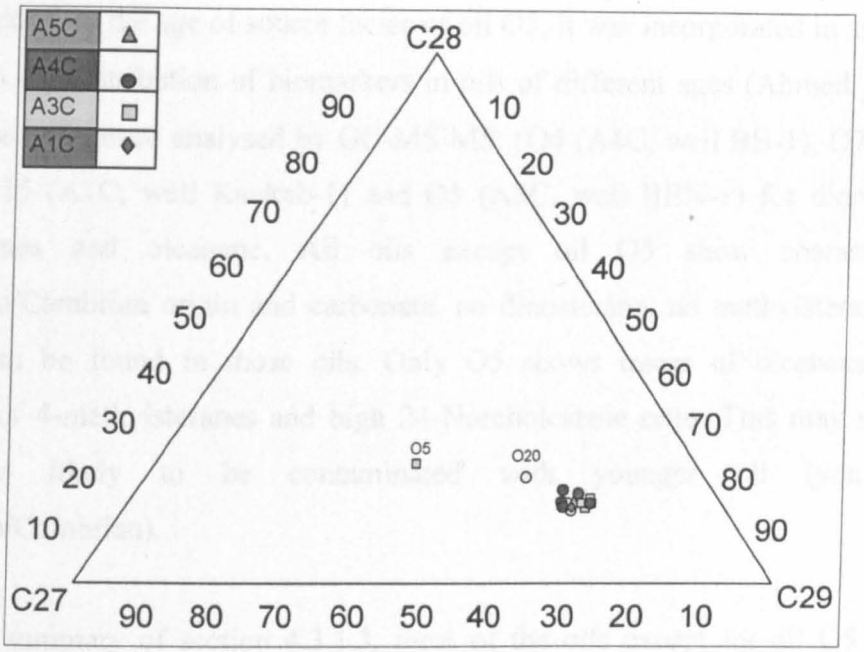

Figure 4-14: Ternary diagram showing the relative abundance of the C_{27}, C_{28}, and C_{29} ααα R normal steranes.

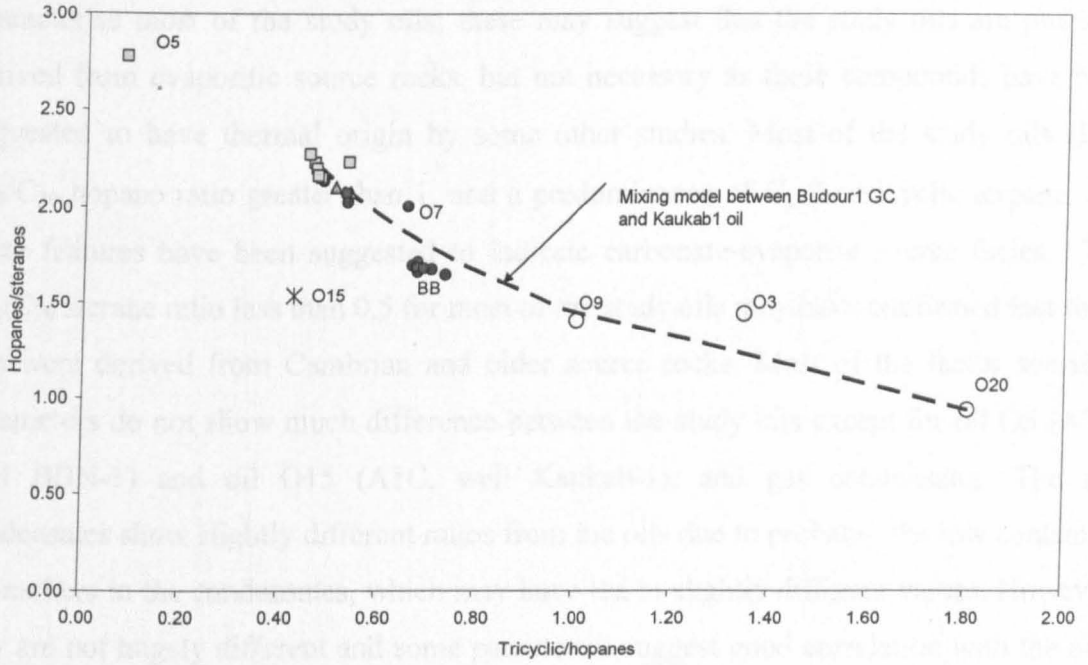

Figure 4-15: A cross-plot of ΣC_{19}-C_{29} tricyclics/ΣC_{27}-C_{35} 17α hopanes versus ΣC_{27}-C_{35} 17α hopanes/C27-C29 steranes (S+R, ααα+αββ). The legend is in Figure 4-4. the mixing model was done assuming two end members, gas condensate having similar composition to Budour gas condensate (O20), and an original oil having similar composition to Kaukab1 oil (O11).

To confirm the age of source facies of oil O5, it was incorporated in an MSc study focusing on the distribution of biomarkers in oils of different ages (Ahmed, 2004). Four of the studied oils were analysed by GC-MS-MS: (O4 (A4C, well BB-1), O7 (A4C, well BBN-1), O15 (A1C, well Kaukab-1) and O5 (A3C, well BBN-1) for dinosteranes, 4-methylsteranes and oleanane. All oils except oil O5 show characteristics of Precambrian/Cambrian origin and carbonate, no dinosterane, no methylsteranes, and no oleanane can be found in those oils. Only O5 shows traces of oleanane, and high abundance of 4-methylsteranes and high 24-Norcholestane ratio. This may suggest that the oil is likely to be contaminated with younger oil (younger than Precambrian/Cambrian).

In a summary of section 4.3.1.3, most of the oils except for oil O5 from A3C stringer of well BBN-1, are dominated by C_{29} steranes (all isomers), and this was attributed to algal origin. Very high abundance of pregnanes and homopregnanes characterise most of the study oils; these may suggest that the study oils are probably derived from evaporitic source rocks, but not necessary as these compounds have been suggested to have thermal origin by some other studies. Most of the study oils show C_{29}/C_{30} hopane ratio greater than 1, and a predominance of $C_{23}\beta\alpha$ tricyclic terpane, and these features have been suggested to indicate carbonate-evaporite source facies. The C_{28}/C_{29} sterane ratio less than 0.5 for most of the study oils may have confirmed that these oils were derived from Cambrian and older source rocks. Most of the facies sensitive parameters do not show much difference between the study oils except for oil O5 (A3C, well BBN-1) and oil O15 (A1C, well Kaukab-1), and gas condensates. The gas condensates show slightly different ratios from the oils due to probably the low content of biomarkers in the condensates, which may have led to slightly different values. However, they are not hugely different and some parameters suggest good correlation with the oils. There is large variation observed in the tricyclic terpanes (C_{19}-C_{30})/ C_{27}-C_{35} 17α Hopanes ratio and the C_{27}-C_{35} 17α Hopanes/ C_{27}-C_{29} steranes (S+R, ααα+αββ) ratio, which is interpreted here that it may have been caused by mixing of a condensate charge with the original oil.

4.3.1.4 Aromatic biomarkers and hydrocarbons

The aromatic fractions were analyzed by GC-MS in SIM mode. Representative chromatograms for some of the ions monitored are shown in Figure 4-16. The ions and compounds discussed in this study are m/z 253 (Monoaromatic steroid hydrocarbons (MAS)), m/z 231 (Triaromatic steroid hydrocarbons (TAS)), m/z 142+156+170 (Alkylnaphthalenes), 178+192+206 (Alkylphenanthrenes) and m/z 184+198 (Alkyldibenzothiophenes). Figure 4-16 shows representative chromatograms for aromatic steroid hydrocarbons and the representative chromatograms for the rest of the aromatic ions are illustrated in Appendix 4. 3.

Aromatic biomarkers and hydrocarbon ratios are often useful in determining the thermal maturity of organic matter (Hase & Hites, 1976) (Johns, 1986; Radke, 1987) but they can also provide valuable information on source organic matter. The C_{27}-C_{28}-C_{29}-ring monoaromatic steroid hydrocarbons are thought to be derived from sterols with side chain double bond during early diagenesis (Moldowan & Fago, 1986) and they can provide a more powerful source correlation than the steranes (Peters *et al.*, 2005). A star plot showing the relationship between the oils based on relative abundance of Monoaromatic steroid hydrocarbons (MAS) is shown in Figure 4-17. Most samples plot tightly together suggesting similar source, the exceptions being samples O20 (an A4C condensate from well Budour1h2), O5 (A3C, well BBN-1), and O15 (A1C, well Kaukab-1). Most samples are dominated by $C_{29}\beta$ and $C_{28}\alpha$ (S and R) monoaromatic steroid hydrocarbons. A dominance of C_{29} monoaromatic steroid hydrocarbon has been attributed to marine carbonate sourced oils (Peters *et al.*, 2005). Sample O15 (A1C, well Kaukab-1) has a similar star shape to the majority of the samples but differs slightly in the relative amount of different isomers. Samples O5 (A3C, well BBN-1) is very different, suggesting different source. Most of the oil samples show very low relative abundances of dia C-ring monoaromatic steroids. Triaromatic steroid hydrocarbons (TAS) can originate from monoaromatic steroid hydrocarbons (MAS) via aromatization and loss of a methyl group but this is not the only mechanism and there must be other sources as there is often no correlation between C_{27}/C_{29} MAS ratio and C_{26}/C_{27} TAS ratio (Peters *et al.*, 2005). The distribution of high molecular weight triaromatic steroid hydrocarbons (C_{26}-C_{27}-C_{28}) is also similar for most of the oils, the exception again being sample O5 (A3C, well BBN1). Most of the oils show a predominance of C_{28} (S+R) TAS whereas O5 (A3C, well BBN1)

is dominated by $C_{26}R+C_{27}S$ TAS. This is again due to difference in source facies for O5 or being contaminated with younger oil than the rest of the study oils, as already discussed in section 4.3.1.3. The triaromatic steroid hydrocarbons distribution shows that condensate O20 (well Budour-1h2) and O15 (A1C, well Kaukab-1) are correlated well with other oils.

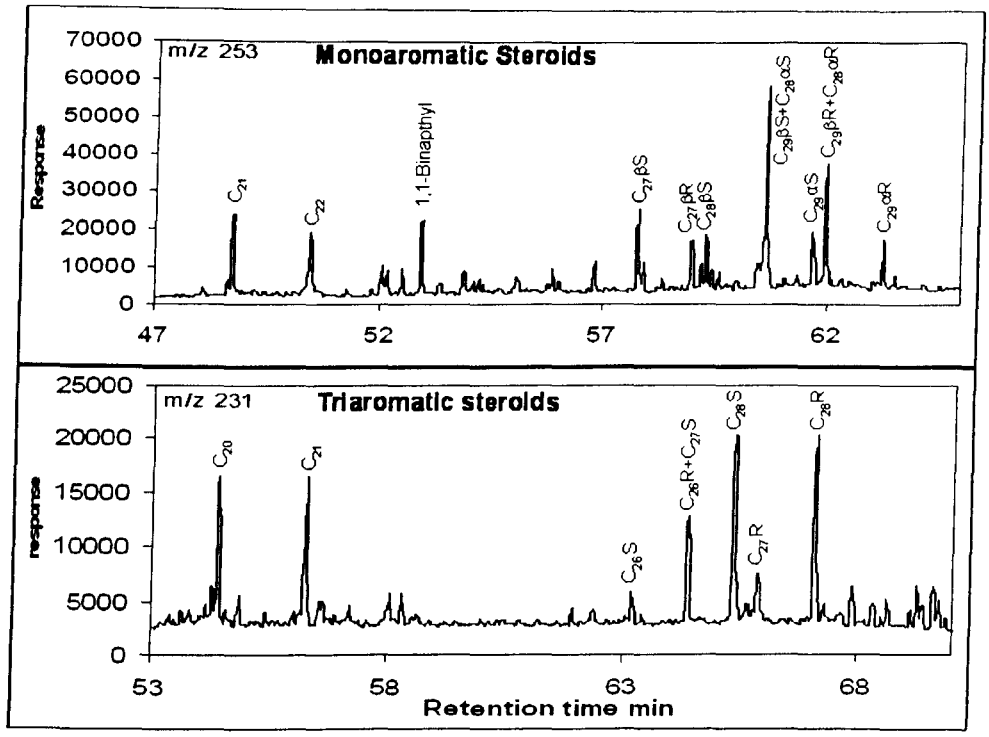

Figure 4-16: Representative mass chromatograms for aromatic steroid hydrocarbons, Monoaromatic and Triaromatic.

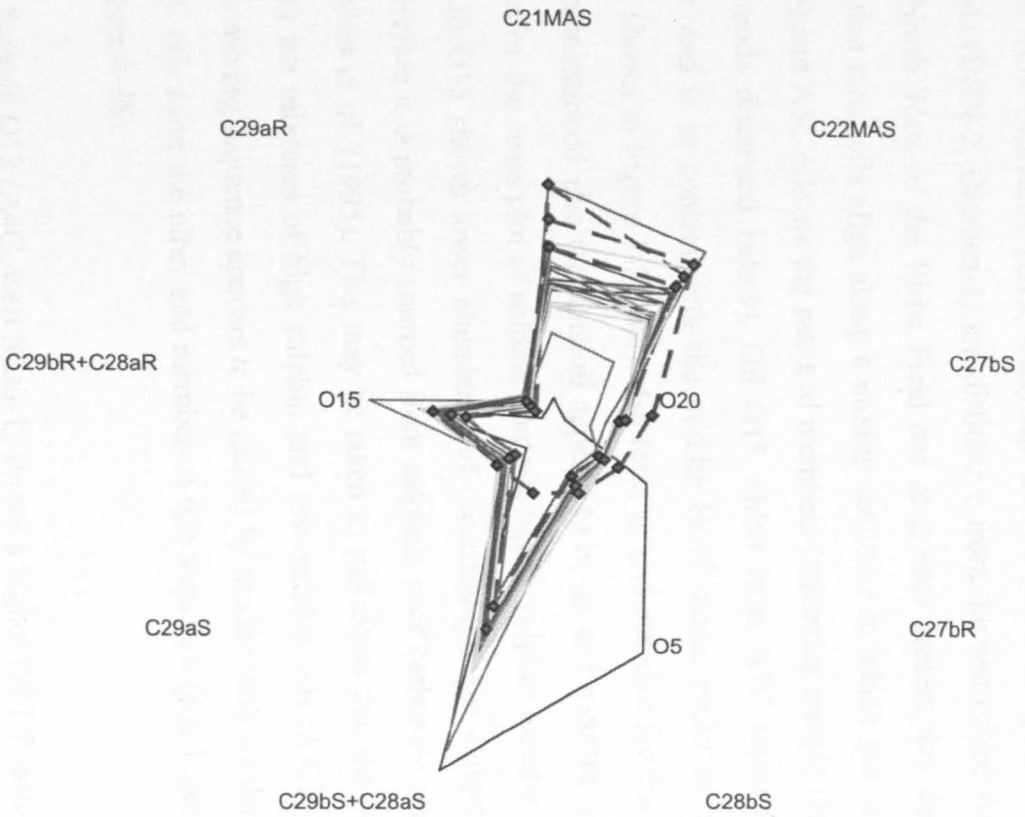

Figure 4-17: A star plot showing the relative abundance of different monoaromatic compounds and isomers to establish correlation between the oils. (a = α, b = β)

The cross-plot of the DBT/P (Dibenzothiophene/Phenanthrene) ratio versus Pr/Ph ratio, shown in Figure 4-18, clusters most of the samples within a very short range of values. Most of the samples fall between the so-called "Zone 2" and "Zone 1B" (Hughes *et al.*, 1995). Zone 1B is proposed for oils from mixed carbonate, marine marl, and lacustrine sulphur rich source rocks and Zone 2 is proposed for oils from sulphur-poor carbonate source rocks according to Hughes *et al.*, (1995). Generally, A3C oils (Durra-1, Kaukab-1, Shamah-1, Omraan-1) and A5C oils (Omraan-1) show lower ratios than A4C oils (Birba Field, Nassir-1, gas condensates), but there is an overlap caused by the samples from Omraan-1 (O19, O22) and BBN-2 (O7). Geographically, the overlapping A4C oils (BBN-2, Omraan-1) are distinctive from the rest of the A4C oils as they both occur North West of the Birba Field and at greater present day depths. The cross-plot shows that most oils align along a mixing sequence in which gas condensates (O9, O20 and O3) and A3C oils are the two end members (assuming sample O13 to be excluded on the grounds discussed below). Oil O15 which from A1C reservoir unit (the deepest stringer and is in contact with the middle Huqf source rocks as clear from the cross section shown in Figure 1-2), may also form an end member for this mixing sequence. It must be mentioned also that this oil appears to be an end member in a mixing sequence revealed by the cross plot of sulphur contents versus sulphur isotopic $\delta^{34}S$ ratios in Figure 6-30. Oil O15 shows lower abundance of dibenzothiophene compared to phenanthrene and therefore it is probably sourced from sulphate poor carbonate source rocks according to Hughes *et al.* (1995). This may be taken as indication that the oils in A4C and A3C stringers are mixtures of high sulphur and low sulphur oils (6.4.3). However, the most obvious mixing sequence appears to be caused by mixing with condensate charge and that the A3C oils form the other end member of this sequence (e.g. Figure 4-15, Figure 4-28, and Figure 4-38).

Sample O13 (A4C, well Nasir-1) shows a higher DBT/P ratio because it probably has a contribution from a different source. This sample also shows a very high sulphur content (3.16 wt %) and the lowest API gravity (23°) of all study oils, as will be discussed later, but it shows no sign of biodegradation, despite the fact that it has high TAN (1.4 mgKOH/g oil) too. It also shows a higher asphaltene content than the other samples. These characteristics suggest that oil O13 (A4C, well Nassir-1) was either water washed (will be investigated later) or affected by a different source. In other respects, this oil shows similar characteristics in the steranes and terpanes distributions to the other oils

surrounding the main Birba Field (Table 4-4). Oil sample O5 (A3C, well BBN-1) is exceptional sample again that are probably derived from different source rocks or have been contaminated with younger oil. Sample O5 falls in the middle of sulphate poor carbonate source rocks (Zone 2) and marine shale source rocks (Zone 3) zones Although sample O5 shows different geochemical characteristics which indicate different origin, this possibility is less likely valid geologically. Oil O5 was sampled from A3C reservoir unit from well BBN1 in the study area; it was swabbed from core rocks rich in oil taken from this well and stored to a bottle. It was sampled from A3C at BBN-1, which is not very far from the rest of the field. Therefore, this is more likely to be contaminated sample and not reflecting the original oil in A3C unit of BBN1 as also concluded from the previous section.

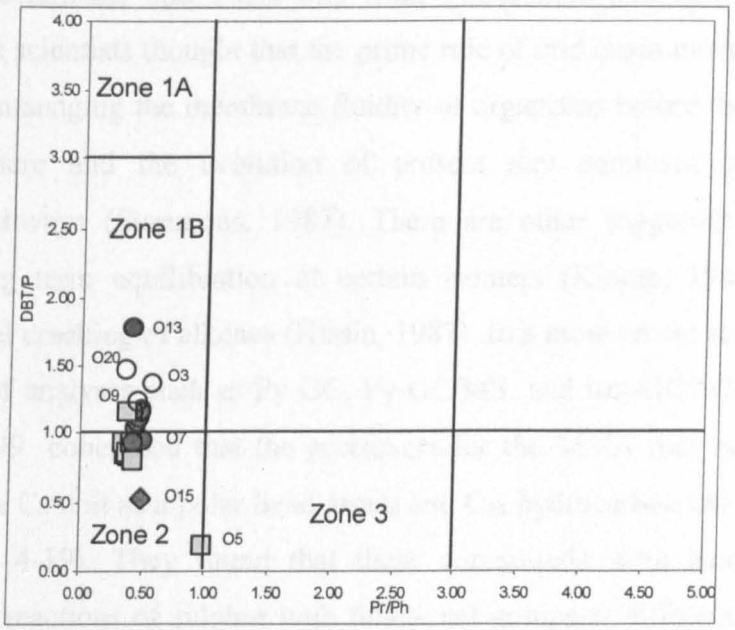

Figure 4-18: A cross-plot of dibenzothiophene/phenanthrene versus Pr/Ph (left) and the concentrations of DBT and Phenanthrene versus the DBT/Phenanthrene ratio (right). Zone 1B is mixed carbonate, marine marl, and lacustrine sulphur rich source rocks, Zone 2 is sulphur-poor carbonate source rocks. Zone 1A is lacustrine sulphur rich, and Zone 3 is marine shale source rocks.

4.3.1.5 Mid chain monomethyl alkanes (X-compounds)

The 'X-compounds' are isomers of mid chain branched monomethyl alkanes (MMA), first identified by Grantham *et al.* (1990) in gas chromatograms of the saturated hydrocarbons from Huqf and Q type crude oils in Oman. According to Grantham *et al.* (1990), their occurrence in an Omani oil indicates a possible contribution from Huqf source rocks (the oldest sedimentary rocks in Oman of Precambrian to Cambrian age, (Grantham *et al.*, 1990)). Mid-chain branched monomethyl alkanes (MMA) have been found in various sediments and crude oils ranging in age from modern to Precambrian (Fowler & Douglas, 1987; Hold *et al.*, 1999; Klomp, 1986). These monomethyl alkanes were attributed to several origins, mainly direct biological contributions (Fowler & Douglas, 1987), or diagenetic products formed by transformation of functionalised lipid precursors such as carboxylic acids (Summons, 1987), This compounds were found mainly in the sediments and crude oils from Proterozoic and early Palaeozoic age. Therefore, some scientists thought that the prime rule of mid chain methylation of n-alkyl lipids to be for managing the membrane fluidity of organisms before the development of an oxic biosphere and the evolution of present day dominant oxygen-dependent desaturation pathways (Summons, 1987). There are other suggested origins such as products of long term equilibration of certain isomers (Klomp, 1986) or from acid catalysed thermal cracking of alkenes (Kissin, 1987). In a more recent study that involved different types of analyses such as Py-GC, Py-GC/MS, and irm-GC/MS (Py=Pyrolysis), Hold *et al.*, 1999 concluded that the precursors for the MMA may have been mainly C_{28+} lipids with a C_6 unit as a polar head group and C_{24} hydrocarbon tail at the 12- or 13-position (Figure 4-19). They found that these compounds were incorporated in the kerogen through reactions of sulphur with functional groups at different positions in the precursor lipids as clear in Figure 4-19.

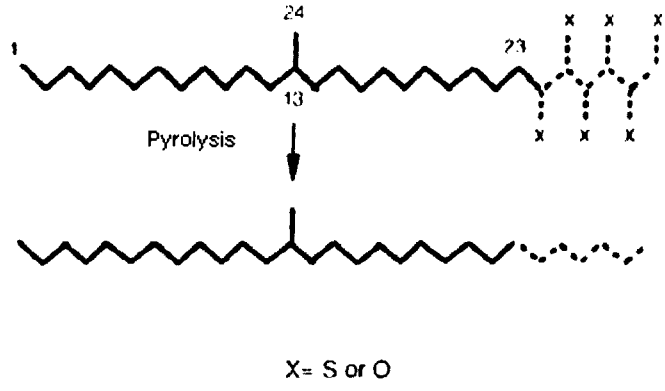

Figure 4-19: proposed mechanisms for the formation of Mid chain monomethyl alkanes (Hold *et al.*, 1999).

12-methyl and 13-methyl mid chain monomethyl alkanes have been identified in the study oils by GCMS using m/z 182 and m/z 196 respectively, by tentative comparison with Hold *et al* (1999) study. Typical distributions as well as structures of the X compounds or MMA studied are shown in the mass chromatograms in Figure 4-20. All oils in the study area have high abundance of the X compounds (4000-9000ppm in the oils and 9000-12000ppm in the gas condensates). Their abundances are plotted in Figure 4-21 as fractions of total X compounds. Most of the oil samples show similar distributions and abundances; the exception being sample O5 (A3C reservoir unit of well BBN1), which has both a very different distribution of X compounds and the lowest overall concentration (4277ppm) again suggesting a different source. All other samples, including gas condensates and oil O15 (from A1C reservoir unit of well Kauka1), show similar distributions for both the12-methyl and 13-methyl compounds. However, the gas condensates and the A3C oils seem to be end members of a mixing sequence while the A4C oils span the whole range. The gas condensates, as expected, show higher amounts of C_{15}-C_{18} compounds, relatively low amounts of C_{20}-C_{30} compounds and similar relative amount of C_{19} in both isomers. This might support the proposed mixing theory, whereby the original oils were mixed with a condensate charge. The high amount of these compounds in condensates suggests that these condensates originated from one of the Huqf source rocks.

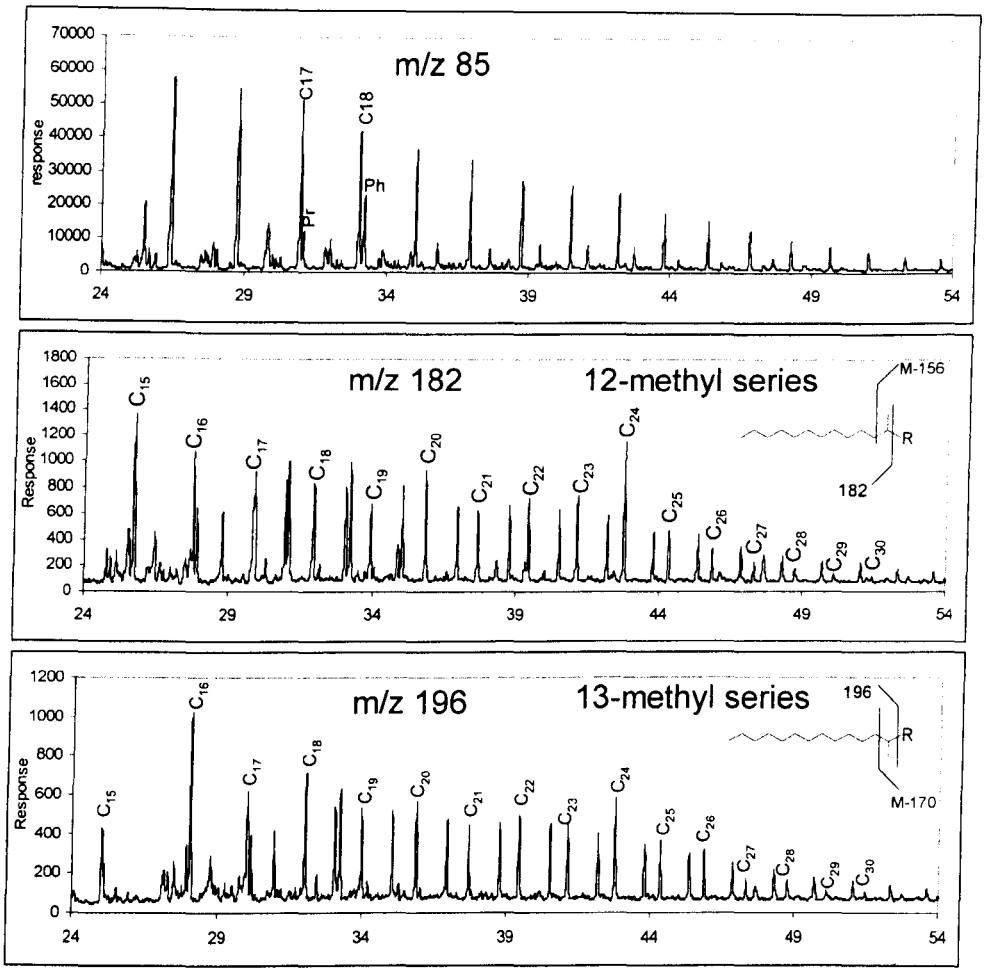

Figure 4-20: Representative mass chromatograms showing typical distribution of X compounds in the oils (for O1).

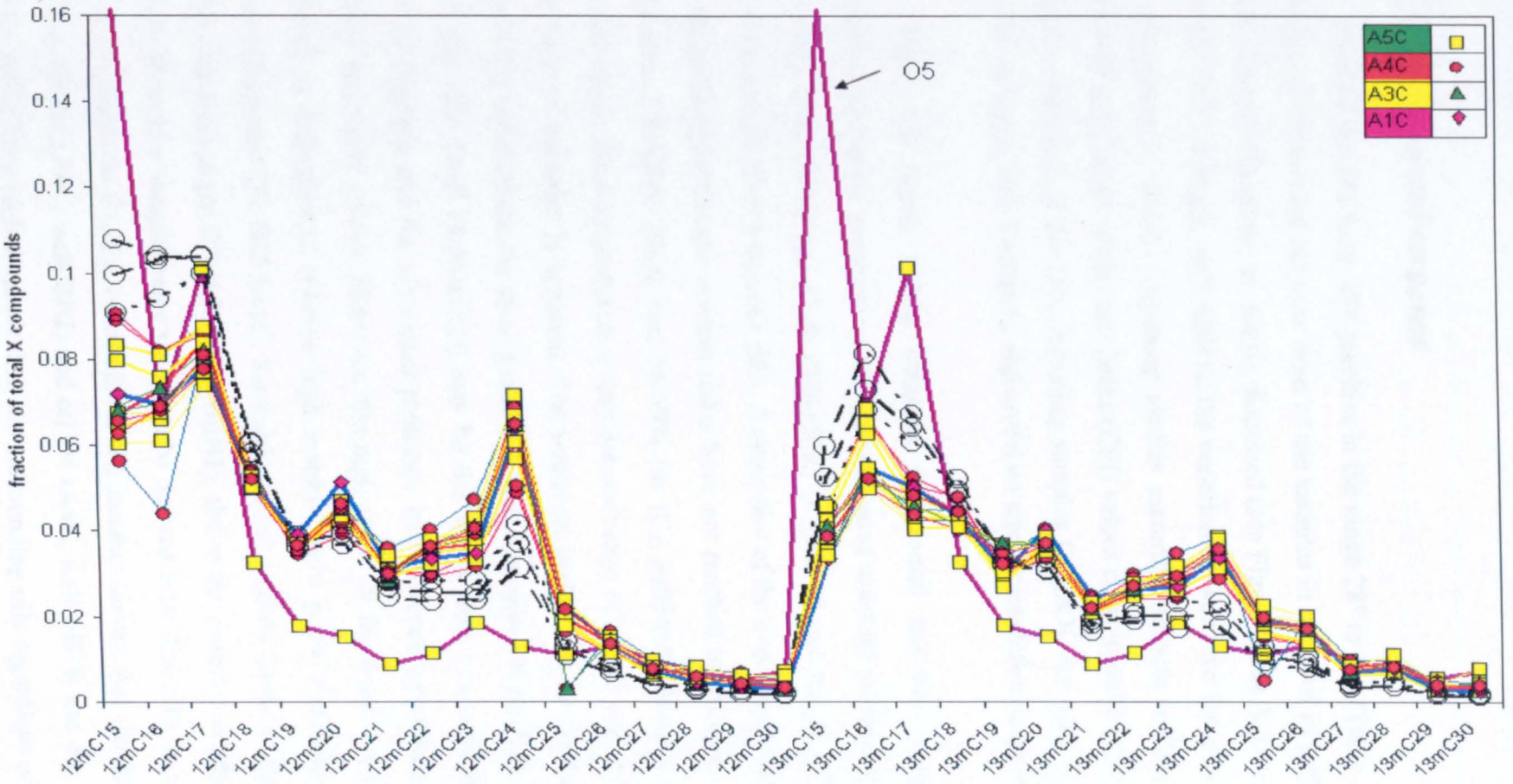

Figure 4-21: Relative abundance of X compounds (12 methyl series and 13-methyl series) for all oil samples. Notice similar distribution for most of the oil samples except for O5. Filled shapes are oils distinguished by reservoir units, and empty circles are condensates.

4.3.2 Maturity characterization

4.3.2.1 Steranes and terpanes

Most of the oils have API gravities in the range 28° to 35° (Table 4-2). There are no significant differences between most of the samples in terms of isoprenoid ratios and isoprenoid/*n*-paraffin ratios, as already discussed (see Figure 4-10). With the exception of sample O5 (A3C stringer, well BBN1), the variation between the samples with regard to these parameters is small, suggesting similar maturity. Smooth n-alkane distributions (Figure 4-9) and Carbon preference Index (CPI) values close to unity (Table 4-3) indicate the mature character of the oils, including samples O5 (A3C stringer, well BBN1) and O15 (A1C stringer, well Kaukab1), and reveal no significant difference in maturity.

Table 4-5 shows values obtained for several maturity sensitive saturated hydrocarbon biomarker parameters. The sterane-based maturity parameters are [C_{29} αββ/ (ααα+αββ) (20R+20S)] and [20S/ (20S+20R) (C_{29}ααα)] and the (C_{21}-C_{22} pregnanes)/ [C_{27}-C_{29} (ααα+αββ, S+R)] steranes ratio. A cross-plot of the first two parameters in Figure 4-22, shows that the sterane isomers ratios have not reached equilibrium level (49-54% for [C_{29}ααα 20S/(20S+20R)], and 56-59% for [C_{29} (αββ/(ααα+αββ)]) (Peters *et al.*, 2005). However, the data comprise a very narrow range of values and no discrimination on the basis of maturity is apparent. The relatively higher values for these parameters (Figure 4-22) obtained for the three gas condensates (samples O3 (well BBN1), O9 (well BBS1), and O20 (well Budour1h2)) may be due to the very low quantities of steranes present (1-20ppm), and the associated problems with accurate measurement (leading to unreliable molecular ratios). However, the high ratios in the condensates may also be interpreted as indicative of relative high maturity or a phase fractionation effect e.g. Pregnanes/Steranes. Oil O15 (A1C, Kaukab1) shows slightly lower maturity relative to the other oils and sample O5 (A3C, well BBN1), shows the lowest maturity of all samples. However, these two samples were shown to be derived from different facies. The ratio of C_{21}+C_{22} pregnanes to C_{27}-C_{29} (ααα+αββ, S+R) steranes shows that the oils of the Birba field, [e.g. oil O1 (A4C, well BB2) and oil O4 (A4C, well BB1)] and the well BBN2 oil (O7 from A4C) have higher values than the surrounding oils regardless of reservoir unit. Although this might be attributed to maturity, other controls can also result in a similar

effect e.g. phase fractionation or mixing with condensate charge. In fact, a possible maturity effect is not supported by API gravity, sulphur content and other maturity indicators (will be discussed later in this section). Phase fractionation might be a possible control on the difference between the gas condensates and the oil, and this will be discussed later in Section 4.3.4.3. Phase fractionation though has little effect on high molecular weight hydrocarbons as will be discussed later in Phase fractionation section (section 4.3.4.3). Therefore, it is more likely that the variations in the C_{21}+C_{22} pregnanes to C_{27}-C_{29} (ααα+αββ, S+R) steranes ratio is affected by mixing with a condensate charge.

Table 4-5: Some maturity sensitive saturated hydrocarbon biomarker parameters for the oils. Standard deviations (STD) for most of the study oils except condensates (O3, O9, & O20), O5 (A3C, well BBN1) and O15 (A1C, well Kaukab1) are listed at the bottom of the table. The shaded samples are gas condensates (assigned by GC). All the parameters listed here are explained and referenced in Appendix 4-1, and the compounds are fully defined in Table 1-1.

Sample code	Wells	stratigraphy (stringer)	depth (m)	$(C_{20}+C_{21}Tri)/(C_{23}+C_{24}Tri)$	C_{23}/C_{21} Tri βα	C_{23}/C_{24} Tri βα	$C_{28}+C_{29}Tri/C_{29}$-C_{33} H	$C_{23}βα$ Tri /$C_{30}αβ$ H	Ts/(Tm+Tm) %	C_{31} (H) 22S/(22R+22S) %	22S/(22S+22R) % (C_{32}-C_{35}) H	Pregnanes/ Steranes	C_{29}% (st) αββ/ααα+αββ	C_{29}% (st) 20S/(20S+20R)
O1	BB2	A4C	2583.4	0.40	3.06	2.24	0.17	1.18	11	51	59.78	0.22	58	50
O2	BB1	A4C	2536.5	0.42	2.97	2.36	0.17	1.13	13	51	62.78	0.20	58	51
O3	BBN1	A4C (GC)	3455.1	0.46	2.72	2.35	0.26	2.09	12	67	56.80	0.36	58	54
O4	BB1	A4C	2533.1	0.41	3.14	2.37	0.17	1.10	12	52	61.71	0.19	59	51
O5	BBN1	A3C	3557.8	0.61	1.41	1.09	0.03	0.04	48	58	60.03	0.22	45	44
O6	BB1	A4C	2537.1	0.42	3.06	2.40	0.16	1.06	12	51	61.80	0.19	58	51
O7	BBN2	A4C	3597.8	0.44	2.79	2.30	0.15	1.08	11	49	59.77	0.23	58	50
O8	BB1	A4C	2533.1	0.40	3.08	2.28	0.19	1.29	12	55	60.61	0.19	58	51
O9	BBS1	A4C (GC)	2329.7	0.43	3.00	2.40	0.22	1.67	11	51	57.95	0.22	59	52
O10	Kaukab	A3C	2513.6	0.39	3.17	2.28	0.12	0.78	11	53	61.17	0.16	58	51
O11	Kaukab1	A3C	2513.6	0.42	3.20	2.08	0.12	0.68	10	53	62.20	0.18	58	51
O12	Omraan1H1	A5C	2601.7	0.42	2.93	2.09	0.13	0.81	11	52	60.89	0.18	58	49
O13	Nassir1	A4C	1998.6	0.37	3.34	2.45	0.13	0.90	9	52	61.40	0.16	58	49
O14	Durra1	A3C	2693.0	0.39	3.18	2.31	0.12	0.84	13	52	61.35	0.17	58	49
O15	Kaukab	A1C	2896.9	0.44	2.34	1.84	0.11	0.53	41	55	59.24	0.12	56	51
O16	Shamah1	A3C	2385.7	0.39	3.28	2.23	0.12	0.78	11	52	60.36	0.15	57	49
O17	Durra1	A3C	2695.1	0.38	3.30	2.00	0.12	0.60	14	53	60.68	0.16	59	51
O18	Omraan1H3	A5C	2823.6	0.41	3.06	2.22	0.13	0.89	14	52	61.31	0.18	57	49
O19	Omraan1H3	A4C	2939.1	0.39	3.10	2.16	0.12	0.77	10	52	60.31	0.17	58	49
O20	Bodour1H2	A4C (GC)	2971.6	0.51	2.58	2.37	0.35	3.04	24	51	65.08	0.30	59	53
O21	Omraan1H3	A3C	3111.5	0.41	3.03	2.18	0.12	0.78	14	52	60.06	0.17	59	49
O22	Omraan1H3	A4C	2939.1	0.42	3.05	2.36	0.14	0.89	12	52	60.60	0.17	58	50
STD (except condensates, O5 and O15)				0.03	0.18	0.12	0.05	0.53	3.25	1.21	1.27	0.04	0.52	1.11

Key to abbreviations: Tri = tricyclics, St = steranes, H = hopanes, Pregnanes/steranes = (C_{21}+C_{22} pregnanes)/ [sum of C_{27}-C_{29} steranes (S+R, ααα+αββ)].

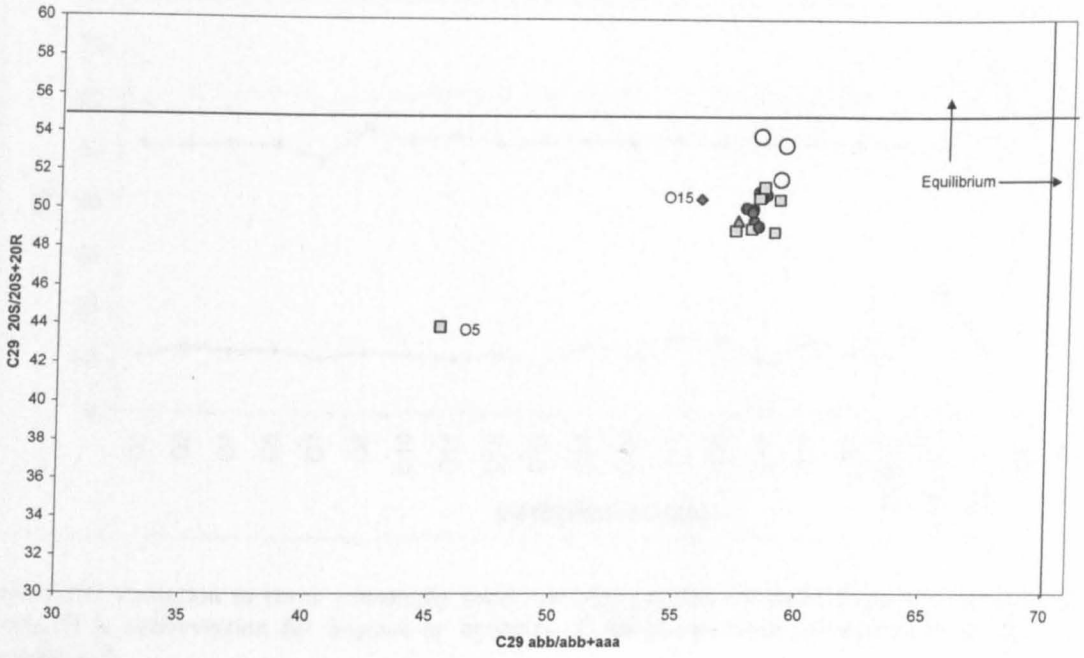

Figure 4-22: A cross-plot of C_{29} sterane isomer ratios: S/S+R (ααα+αββ) versus αββ/ααα+αββ (S+R). Empty circles are gas condensates and filled shapes are oils.

The 22S/(22S+22R) ratio for 17α(H), 21β (H)-homohopane and the C_{32}-C_{35} 17α extended hopanes, and the Ts/(Ts+Tm) ratio [Ts = 18α(H)-22,29,30-trisnorneohopane, Tm = 17α(H)-22,29,30-trisnorhopane] generally show little variation in the sample set (Figure 4-23). Samples O5 (A3C, well BBN1) and O15 (A1C, well Kaukab1) show exceptionally high %Ts, but this may relate to the observation that these samples are probably from different facies (see section 4.3.1). Some gas condensates show odd ratios in some of these parameters. The gas condensate O20 (A4C, Budour1h2), for example, has relatively high %Ts and is very similar to other samples with respect to the other two parameters whereas the BBN-1 gas condensate (O3) shows a relatively high C_{31}αβ homohopane 22S/ (22S+22R) ratio. These variations may be attributable to errors in the measurement of very low amounts of biomarkers in the gas condensates. The extended hopanes parameters had reached equilibrium as indicated from the range of the values (60%, (Peters & Moldowan, 1991).

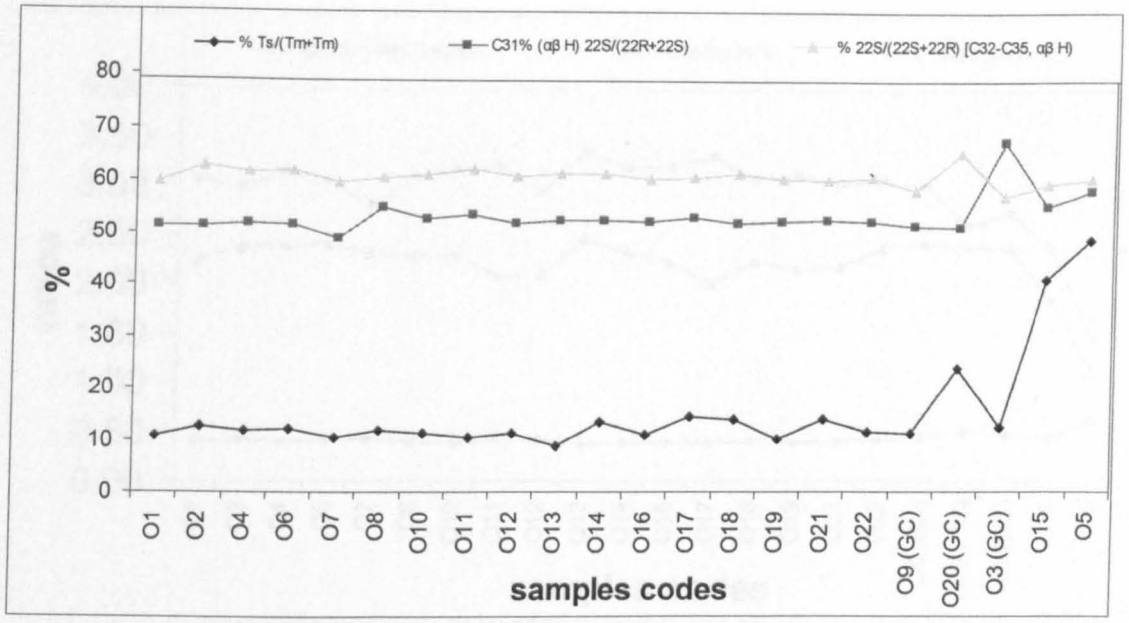

Figure 4-23: Variation in three commonly used maturity sensitive hopane biomarker parameters in the oils. H is abbreviation for hopane or hopanes. These parameters are described in text and in Appendix 4. 2

Selected maturity ratios based on the tricyclics are plotted in Figure 4-24. They show similar values for most of the oils except for samples O5 and O15, which are considered to be from different source facies (section 4.3.1). The gas condensates show similarity to the oils and suggest the possibility that they might be derived from the oils. However, this does not necessarily rule out mixing effects or phase fractionation. The biomarkers maturity parameters used here have small range of high boiling points and might not be affected by phase fractionation as a ratio (see section 4.3.4.3).

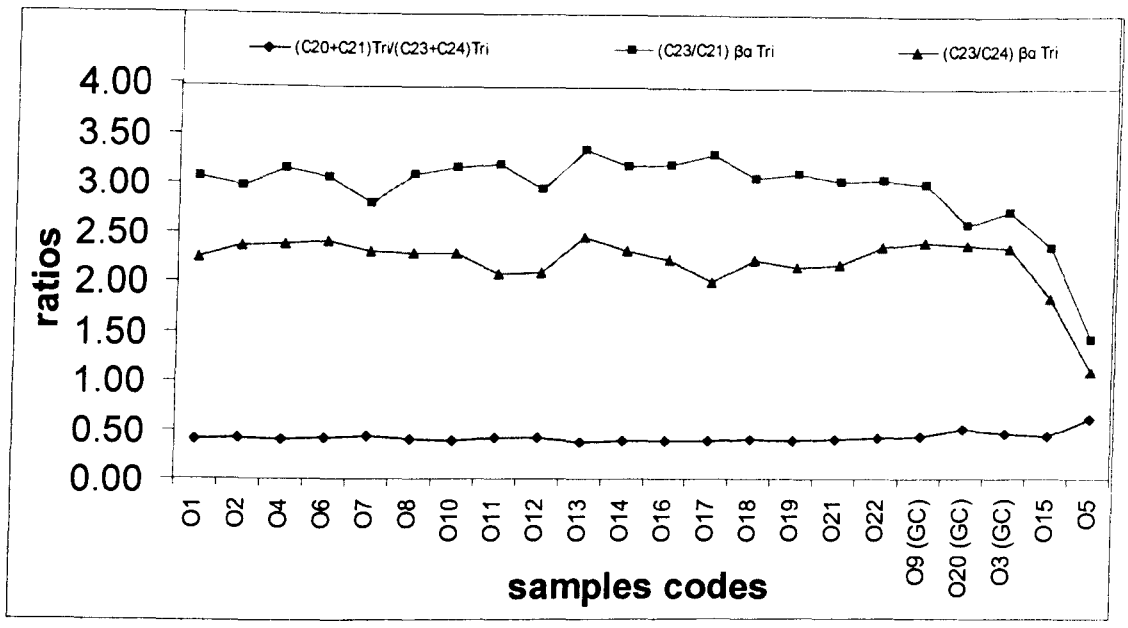

Figure 4-24: Three maturity sensitive parameters based on tricyclic aliphatic hydrocarbons. Tri=Tricyclics, e.g. C_{23}/C_{24} Tri βα = C_{23} βα Tricyclic terpane/C_{24} βα Tricyclic terpane.

The absolute concentrations of the C_{19}-C_{29} tricyclics, C_{27}-C_{35} 17α hopanes, and C_{27}-C_{29} steranes are plotted in Figure 4-25. The plot again distinguishes between the oils from the Birba field (A4C) and those from the surrounding wells (mainly A3C and A5C)), as found using the cross plot of tricyclics/hopanes versus hopanes/steranes in Figure 4-15. Relatively low concentrations of these compounds among oils are found in the oil sample O7 (A4C, well BBN-1) in the north followed by the Birba Field oils (e.g. O1 and O4) and then the rest of the oil samples with the exception of oil samples O5 (A3C, BBN-1) and O15 (A1C, Kaukab-1). The gas condensates [O9 (well BBS-1), O3 (well BBN-1), and O20 (well Budour-1H2)] show the lowest concentrations of these biomarkers (800-2000ppm). These gas condensates are also distinguished in having higher abundances of C_{19}-C_{29} tricyclic terpanes than either C_{27}-C_{29} (ααα+αββ, S+R) steranes or C_{27}-C_{35} 17α hopanes. These observations indicate some maturity differences between oils, but taking the biomarker data as a whole, it is suggested that maturity effects are relatively minor in the area, and the main control on the variations observed in absolute concentration of biomarkers is more likely to be mixing oils with condensate charge (section 4.3.3). The oils with lower biomarkers concentrations exhibit higher n-alkane concentrations, suggesting that there might be dilution effect caused by mixing of normal oil with alkane rich condensate charge (more details in section 4.3.3).

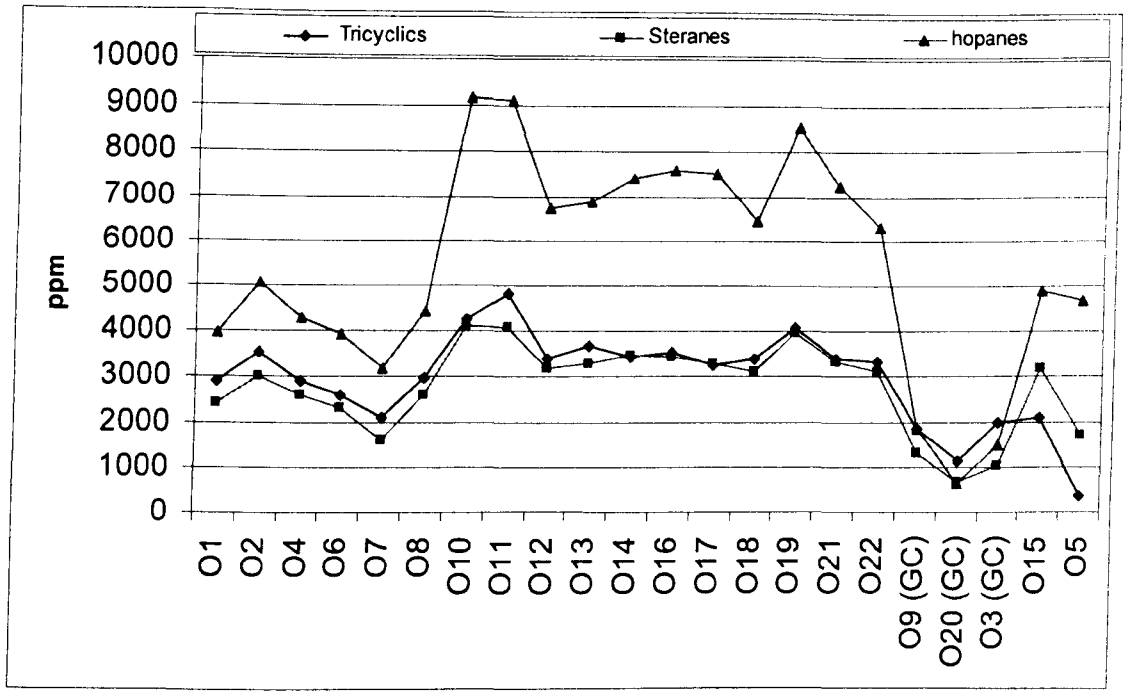

Figure 4-25: Absolute concentrations of C_{19}-C_{30} tricyclic terpanes, C_{27}-C_{29} ($\alpha\alpha\alpha$+$\alpha\beta\beta$, S+R) steranes or C_{27}-C_{35} 17α hopanes. The gas condensates samples are assigned by GC in brackets near the sample codes.

4.3.2.2 Aromatic hydrocarbon biomarkers and aromatic hydrocarbons

Aromatic biomarkers and hydrocarbons are useful in determining thermal maturity of the organic matter because they are thought to form through complex transformations of naphthenic and olefinic natural product precursors (Hase & Hites, 1976) during diagenesis and catagenesis (Johns, 1986; Radke, 1987). Table 4-6 shows values obtained for several aromatic maturity parameters, described and referenced in Appendix 4. 2. The first two parameters, Triaromatic steroid hydrocarbons $C_{20}/(C_{20}+C_{28})$ ratio and Monoaromatic steroid hydrocarbons I/(I+II) ratio ($\sum C_{20}$-$C_{22}/\sum C_{27}$-C_{29}) are based on thermal cracking of higher molecular weight homologues to low molecular weight homologues under thermal stress (Peters & Moldowan, 1993). The rest of the molecular parameters are

- MPI1 = [1.5*(2-Methylphenanthrene + 3-methylphenathrene)/(Phenanthrene + 1-methylphenanthrene + 9-methylphanthrene)]
- MPR = 2-methylphenanthrene/1-methylphenanthrene
- F1 =((3-methylphenanthrene+ 2-methylphenanthrene)/(3-methylphenanthrene+2-methylphenanthrene+1-methylphenanthrene + 9- methylphenanthrene)

- F2 = 2-methylphenanthrene/(3- methylphenanthrene +2- methylphenanthrene +1-methylphenanthrene +9- methylphenanthrene)
- MNR = 2-methylnaphthalene/1-methylnaphthalene
- DNR1 = [(2,6-dimethylnaphthalene+2,7-dimethylnaphthalene)/1,5-dimethylnaphthalene]
- TNR1 = [2,3,6-trimethylnaphthalene/(1,3,5-Trimethylnaphthalene+1,4,6-trimethylnaphthalene)]
- MDR1 = 1-Methyldibenzothiophene/dibenzothiophene

These parameters are based on the methyl transfer reactions under the action of heat. Methyl transfer reactions include methylation, steric strain remethylation and demethylation, depending on the reactivities of different methyl positions and the available sources of methyl groups under increasing temperature (Radke, 1987). With increasing temperature, the methylation is the dominant process, until beyond the maximum of the C_{15+} hydrocarbon generation curve at a mean reflectance of 0.9 $\%R_o$; at which the sources of the methyl groups become exhausted and possibly steric strain derived reactions (remethylation) become dominant at range of mean reflectance of 0.9-1.3$\%R_o$. Beyond the mean reflectance of 1.3$\%R_o$, the demethylation is probably the dominant process (Radke, 1987). Most of these ratios used here are increased with increasing thermal maturation except for MDR1 until mean reflectance $\%R_m$ of 1.3$\%R_o$, beyond which, these ratios are not valid. Although MDR1 should increase in principal, this occurs early in the oil window and reaches its maxima very early and then decreases after then (Radke, 1987). The empirical linear relationship between MPI1 and measured reflectance has been well established with vitrinite reflectance values between $\%R_m$ 0.67-1.35, (Radke *et al.*, 1982a; Welte *et al.*, 1984). The calibration of these two parameters has suggested a new maturity parameter termed calculated vitrinite reflectance (VRE) (Radke & Welte, 1983).

The data set generally shows a narrow range in values for most of the parameters. VRE values (0.81-0.94$\%R_o$) based on MPI-1(range: 0.69-0.90) (assuming the measured vitrinite reflectance <1.35$\%R_o$), indicate that most of the oils are mature and high in the oil window (Radke & Welte, 1983). Interestingly, the gas condensate samples O9 (well BBS-1) and O3 (well BBN-1) show values similar to the geographically associated oils,

Oil O4 (A4C, well BB-1) and oil O7 (A4C, well BBN-1) respectively. The largest variation between oil samples is observed in MPR and DNR-1. A cross-plot of these two parameters distinguishes different groups of oils (Figure 4-26). Oils O5 (A3C, well BBN-1) and O15 (A1C, well Kaukab-1), as usual, show different characteristics to the rest of the oils and appear less mature but this is more likely due to the different origin for those two oils as illustrated before (e.g. Figure 4-15, Figure 4-18 & Table 4-4). MPR parameter groups most of the rest of the oils together in a tight range as clear from Figure 4-26. The gas condensate O3 (A4C, well BBN-1) and O7 (A4C, BBN-2) are from geographically close wells in the BBN block (Northern area in the Greater Birba Area); these oil samples appear to have a relatively low maturity; however, other evidence presented previously (e.g. low biomarker content, Figure 4-25) indicate high maturity characteristics for these two oils. This apparent contradiction in maturity signals is indicative of complexities arising from the mixing of oils. The DNR-1 ratio distinguishes the A4C oils (mainly Birba oils) as one group and the A3C and A5C oils as another group and indicates that the latter is of higher values. Some overlap is seen in the data from the Omraan-1 samples, which span most of the study stringers (A4C, A3C, and A5C), but they show generally similar characteristics. Apparently, one of the A4C oils, oil O13 (A4C, well Nassir-1), shows a lower maturity values than the rest. Although, this apparently concords with its occurrence at shallow depth (i.e. earlier filling) and with its API gravity of 23.9°, other evidence presented previously (O13 shows similar maturity ratios (e.g. Figure 4-23) to the rest of the oils) and discussed again later shows that this oil should not be of lower maturity than the rest of the A4C oils. This variation may again be indicative of facies variations. The maturity sequence suggested by the DNR-1 ratio also conflicts with evidence previously presented and again might suggest facies mixing. Although, Radke *et al.*, 1986 showed experimentally that naphthalenes are better maturity indicators than phenanthrenes, in this study both are suggested to be affected by facies. Gas condensate O3 (A4C, well BBN-1) and O7 (A4C, well BBN-2) are also distinguishable in a cross-plot of $C_{20}/(C_{20}+C_{28})$ Triaromatic steroid (TA) hydrocarbons ratio versus I/(I+II) monoaromatic steroid (MA) hydrocarbons ratio (=short chain MA/Long chain MA). The gas condensate O3 (A4C, well BBN1) and oil O7 (A4C, well BBN2) appear here to have a higher maturity than the rest of the oils, which contradicts the observations from Figure 4-26, suggesting facies variations again. O5 and O15 again plot differently due to their different origins.

Generally, A4C oils are suggested to be of higher maturity than A3C oils and A5C oils although there is a large overlap between them. No significant variation in the data set can be noticed for F1, F2, and MNR except for oils O5 (A3C, well BBN-1) and O15 (A1C, Kaukab-1), which is considered to be due to a source difference. Although there is relatively wide range in TNR-1 values (0.41-0.63), there is no apparent trend and the variation is probably due measurement errors related to the small amounts of compounds present in the samples.

Table 4-6: Values for selected maturity sensitive aromatic hydrocarbon parameters for all oil samples. The definitions of these parameters are listed below the table and refer to Appendix 4-1 for references.

Sample code	Wells	stratigraphy (stringer)	depth (m)	TA $C_{20}/C_{20}+C_{28}$	MA I/(I+II)	MPI-1	VRE (MPI-1)	MPR	F1	F2	MNR	DNR-1	TNR1	MDR1
O1	BB2	A4C	2583.4	0.33	0.31	0.86	0.92	1.41	0.47	0.32	1.09	3.22	0.60	0.64
O2	BB1	A4C	2536.5	0.39	0.33	0.88	0.93	1.41	0.47	0.32	1.07	3.02	0.44	0.66
O3	BBN1	A4C (GC)	3455.1	0.56	0.47	0.77	0.86	1.21	0.43	0.29	0.97	3.02	0.44	0.58
O4	BB1	A4C	2533.1	0.37	0.33	0.89	0.93	1.44	0.47	0.33	1.07	3.06	0.43	0.66
O5	BBN1	A3C	3557.8	0.26	0.05	0.52	0.71	0.72	0.38	0.19	0.96	2.71	0.53	0.80
O6	BB1	A4C	2537.1	0.41	0.35	0.91	0.94	1.45	0.47	0.32	1.06	3.08	0.47	0.67
O7	BBN2	A4C	3597.8	0.52	0.51	0.77	0.86	1.24	0.43	0.29	0.99	3.35	0.56	0.69
O8	BB1	A4C	2533.1	0.35	0.32	0.88	0.93	1.46	0.47	0.32	1.10	3.10	0.48	0.65
O9	BBS1	A4C (GC)	2329.7	0.45	0.39	0.85	0.91	1.39	0.47	0.31	1.09	3.24	0.43	0.64
O10	Kaukab	A3C	2513.6	0.36	0.31	0.86	0.91	1.41	0.47	0.32	1.03	3.54	0.44	0.72
O11	Kaukab1	A3C	2513.6	0.34	0.30	0.87	0.92	1.45	0.48	0.33	1.04	3.60	0.62	0.74
O12	Omraan1H1	A5C	2601.7	0.40	0.35	0.86	0.92	1.47	0.48	0.33	1.03	3.69	0.58	0.62
O13	Nassir1	A4C	1998.6	0.38	0.34	0.69	0.81	1.35	0.45	0.29	1.00	2.41	0.48	0.41
O14	Durra1	A3C	2693.0	0.37	0.30	0.88	0.93	1.44	0.48	0.32	1.04	3.57	0.61	0.70
O15	Kaukab	A1C	2896.9	0.22	0.20	0.54	0.72	0.79	0.35	0.22	0.80	2.18	0.41	0.65
O16	Shamah1	A3C	2385.7	0.35	0.27	0.90	0.94	1.51	0.49	0.33	1.10	3.51	0.53	0.65
O17	Durra1	A3C	2695.1	0.32	0.28	0.89	0.93	1.45	0.48	0.33	1.02	3.64	0.61	0.68
O18	Omraan1H3	A5C	2823.6	0.38	0.34	0.89	0.93	1.44	0.47	0.32	1.00	3.42	0.41	0.66
O19	Omraan1H3	A4C	2939.1	0.36	0.35	0.86	0.91	1.39	0.47	0.32	1.01	3.44	0.42	0.68
O20	Bodour1H2	A4C (GC)	2971.6	0.56	0.45	0.86	0.92	1.34	0.47	0.31	1.12	3.16	0.52	0.56
O21	Omraan1H3	A3C	3111.5	0.45	0.42	0.85	0.91	1.35	0.44	0.30	0.97	3.31	0.63	0.73
O22	Omraan1H3	A4C	2939.1	0.41	0.38	0.86	0.91	1.37	0.46	0.31	1.03	3.46	0.43	0.66
STD				0.08	0.09	0.11	0.06	0.20	0.03	0.04	0.07	0.39	0.08	0.08

Key to abbreviations: TA $C_{20}/(C20+C_{28})$ ratio = Triaromatic steroid hydrocarbons $C_{20}/(C_{20}+C_{28})$, MA I/(I+II) ratio = (ΣC20-C22)/(ΣC27-C29) monoaromatic steroid hydrocarbons, MPI1 = 1.5*(2-Methylphenanthrene+3-methylphenathrene)/(Phenanthrene+1-methylphenanthrene+9-methyl-phenanthrene), MPR = (2-methylphenanthrene/1-methylphenanthrene), F1 = (3-methylphenanthrene+ 2-methylphenanthrene)/(3-methylphenanthrene+2-methylphenanthrene+1-methylphenanthrene + 9-methylphenanthrene), F2 = 2-methylphenanthrene/(3- methylphenanthrene +2- methylphenanthrene +1-methylphenanthrene +9- methylphenanthrene), MNR = 2-methylnaphthalene/1-methylnaphthalene, DNR1 = (2,6-dimethylnaphthalene+2,7-dimethylnaphthalene)/1,5-dimethylnaphthalene, TNR1 = 2,3,6-trimethylnaphthalene/(1,3,5-Trimethylnaphthalene+1,4,6-trimethylnaphthalene) and MDR1 = (1-Methyldibenzothiophene /dibenzothiophene)

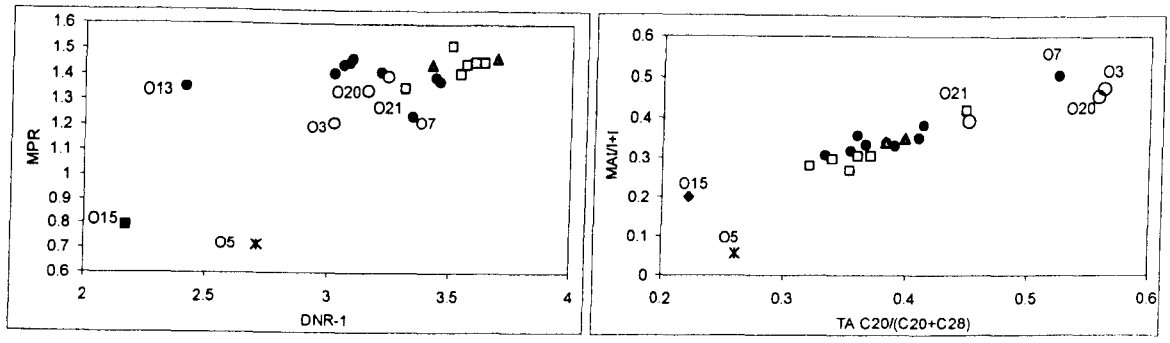

Figure 4-26: Cross plots of MPR (2-MP/1-MP) versus DNR-1 ((2, 6-DMN+2, 7-DMN)/1, 5-DMN) on the left and MA I/(I+II) versus TA $C_{20}/(C_{20}+C_{28})$.

Figure 4-27 shows a cross-plot of total aromatic hydrocarbons abundance versus aromatic biomarkers concentrations. Oils O5 (A3C, well BBN-1) and O15 (A1C, well Kaukab-1) are again shown to be different from the rest of the samples and this is probably another consequence of different origins. Both samples contain the lowest amount of aromatic hydrocarbons, although they contain similar amounts of aromatic biomarkers. Most of the A3C and A5C oils cluster together and show only a small variation in relative abundance of the aromatic biomarkers, whereas the A4C oils are more variable in terms of aromatic hydrocarbons but show similar amounts of aromatic biomarkers. There is no apparent geographic or spatial trend in the distribution of the aromatic hydrocarbons. well BBN-2 oil (O7 from A4C) shows the highest amount of aromatic hydrocarbons, suggesting facies variation rather than maturity difference because it contains a similar amount of biomarkers (both aliphatic and aromatic) as the Birba oils (e.g. O4 from A4C of well BB1). The same argument can be used for sample O13 (A4C, well Nasser1). It is very interesting to note that gas condensates contain similar amounts of aromatic hydrocarbons to Birba oils (e.g. O4 from well BB1) and very low amounts of aromatic biomarkers. The variation in aromatic hydrocarbon concentration in the A4C oils cannot be explained by maturity as they show similar amounts of aromatic biomarkers. The difference between the A4C oils in one group and the A5C/A3C oils in another group in both aromatic hydrocarbons and aromatic biomarkers might suggest facies control which is supported by other evidence previously mentioned. The effect of phase fractionation on these parameters is discussed later 4.3.4.3). My preliminary conclusion here is that although maturity effects cannot be ruled out, the main processes responsible for the slight differences between the samples are probably mixing of oils.

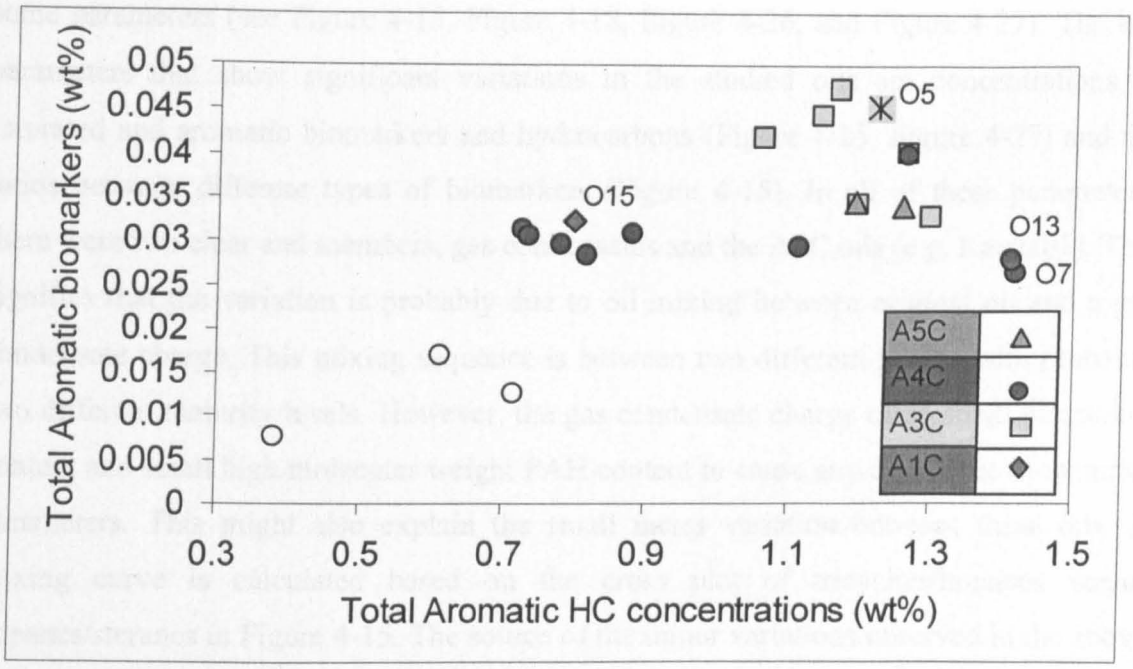

Figure 4-27: A cross-plot of relative abundance of total aromatic biomarkers (Triaromatic steroid hydrocarbons (ΣC_{20}-C_{21}+ΣC_{26}-C_{28}) Monoaromatic steroid hydrocarbons (ΣC_{20}-C_{22}+ΣC_{27}-C_{29})) and relative abundance of total aromatic hydrocarbons (C_0-C_2 alkylphenanthrenes+ C_0-C_3 alkylnaphthalenes+ C_0-C_3 alkylbenzothiophenes + C_0-C_1 alkyldibenzothiophenes + C_0-C_1 alkylflourenes + C_0-C_1 alkylbiphenyls). Empty shapes are condensates and filled ones are oils.

4.3.3 Oil- condensate mixing and dilution effects

Due to the small differences found between various groups of samples, it was difficult to draw a clear conclusion about the facies and maturity control. This section was meant to summarize all evidence used to support one against the other and weigh them. There is clear evidence that the studied oils (with the exception of oil O5 (A3C, well BBN1), oil O15 (A1C, well Kaukab1)) are from similar source facies and were generated at the same level of thermal stress, which was indicated by the small variations observed in carbon isotopic ratios of the whole oil, saturated hydrocarbons and aromatic hydrocarbons as well as some of the GC ratios (Table 4-3, Figure 4-7). It was also suggested by the small variations observed in several facies parameters (Table 4-4) such as sterane carbon numbers distribution (Figure 4-14) or monoaromatic steroid hydrocarbons carbon numbers distribution (Figure 4-17) and maturity parameters of saturated hydrocarbons (Table 4-5) such as sterane isomer ratios (S/(S+R) of $C_{29}\alpha\alpha\alpha$ and $\alpha\beta\beta/(\alpha\alpha\alpha+\alpha\alpha\beta)$ of C_{29} (S+R)) (Figure 4-22) and %Ts/(Ts+Tm) ratio (Figure 4-23) and by the small variations observed in some of the maturity sensitive parameters of aromatic hydrocarbons such as MPI1 (Table 4-6). However, there are still major variations among

some parameters (see Figure 4-15, Figure 4-18, Figure 4-26, and Figure 4-27). The key parameters that show significant variations in the studied oils are concentrations of saturated and aromatic biomarkers and hydrocarbons (Figure 4-25, Figure 4-27) and the ratios between different types of biomarkers (Figure 4-15). In all of these parameters, there were two clear end members, gas condensates and the A3C oils (e.g. Kaukab1). This signifies that the variation is probably due to oil mixing between original oil and a gas condensate charge. This mixing sequence is between two different phases with probably two different maturity levels. However, the gas condensate charge carry small biomarker content and small high molecular weight PAH content to cause any difference in maturity parameters. This might also explain the small facies variation between these oils. A mixing curve is calculated based on the cross plot of tricyclics/hopanes versus hopanes/steranes in Figure 4-15. The source of the minor variations observed in the above parameters might possibly be migration of these oils through tight and organic/petroleum rich carrier rocks. This results in small and unpredicted variation of molecular ratios as observed in some of the parameters such as MPR and DNR1 (e.g. Figure 4-26). Secondary processes effect will be also investigated later as well as statistical evaluation of these small facies and maturity variations to confirm this proposal (mixing of the original oils with a separate gas condensate charge).

It is expected that increasing maturity of the source will produce oils with low biomarker content and high low molecular weight *n*-alkanes. Since maturity effect is not thought to be a major control in the geochemical variations of the studied oils from the above argument, another process must lead to oils with similar maturity but lower biomarker content. The concentrations of *n*-alkanes are plotted against both the biomarker contents and aromatic hydrocarbon contents in Figure 4-28. Interestingly, there is an inverse relationship between both the two properties and n-alkanes concentrations. There are three main groups of oils, gas condensates, Birba Field oils and surrounding oils (A5C and A3C and two A4C oils). This suggest that there might have been a flooding of high *n*-alkanes content petroleum fluid charge depleted of biomarkers and mixed with the original oil that was similar to the A3C and A5C oils. This effect can be called "Dilution effect". This seems to affect mainly Birba oils and might have led to the formation of gas condensates. There are larger variations in A4C oils as we have a clear increase of *n*-alkanes and decrease of both biomarkers and aromatics from North West (well Omraan1, O19) and South East (well Nassir1, O13) through Birba oils (O1, O4) to gas condensates.

Gas condensates do not follow depth trend and two of them were situated in association with down dip oils. Riemens *et al* (1985) tried to prove that the gas condensate in A4C of well BBS1 (O9) is the gas cap of the oil found in A4C stringer of well BB2 (O1) using PVT modeling and interference pressure testing. The observation here suggests that the condensate found in A4C stringer from well BBS1, can be possibly the gas cap. However, the formation of the gas cap was not because of the gravity segregation as Riemens *et al* stated (further supported by PVT modeling in this study), it might have been formed because of the mixing with a gas condensate charge that increased the gas saturation of the original oil until forming gas from this mixture. This might be supported by the failure of Riemens *et al* (1985)'s model to predict the composition and properties of the oils found in A4C up dip of at well Birba 1 oils. Significant evidence will be presented throughout the thesis that the mixing theory of the oils with condensates is more likely than gravity graded column. This charge might have migrated vertically through faults or migrated up dip in A4C from the North.

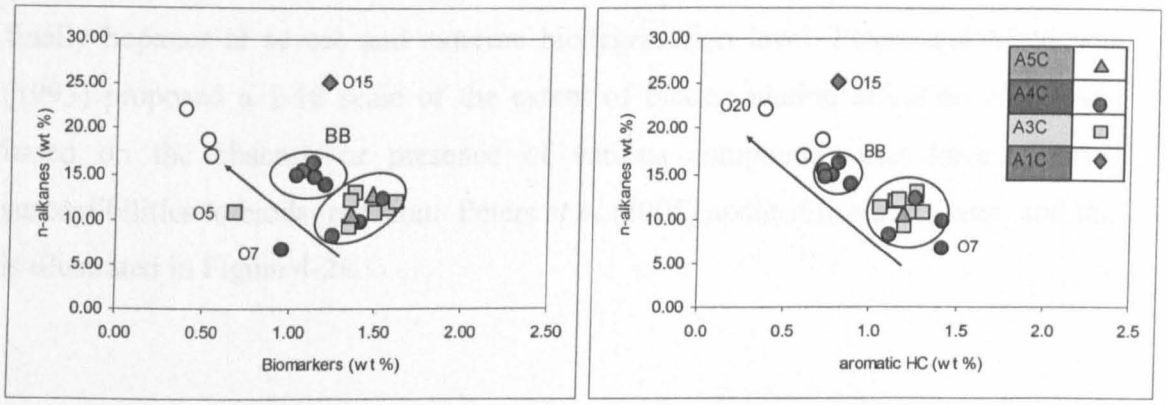

Figure 4-28: The cross plot between n-alkanes wt% (n-C_{11}-n-C_{30}) versus Biomarkers concentration (C_{20}-C_{29} Tricyclics, C_{21}-C_{29} Steranes, C_{27}-C_{35} hopanes, C_{21}-C_{29} monoaromatic steroid hydrocarbons, C_{20}-C_{28} Triaromatic steroid hydrocarbons) in the left plot and versus aromatic hydrocarbons concentration wt% (C_0-C_2 alkylphenanthrenes+ C_0-C_3 alkylnaphthalenes+ C_0-C_3 alkylbenzothiophenes + C_0-C_1 alkyldibenzothiophenes + C_0-C_1 alkylflourenes + C_0-C_1 alkylbiphenyls) in the right plot. Empty circles are gas condensates and filled shapes are oils.

4.3.4 Secondary alteration processes

4.3.4.1 Biodegradation and water washing

It is important to investigate these two processes, as there is no clear-cut control on geochemical variations seen so far. Biodegradation is an in-reservoir alteration process caused by living organisms primarily bacteria, that alter and/or metabolize various classes of compounds of crude oils under certain conditions such as low temperature, low salinity, and nutrients availability (Peters & Moldowan, 1993). The *n*-alkanes are usually the first compounds to be favorably consumed by bacteria (Peters & Moldowan, 1993). Therefore, any biodegraded oil is characterized by absence or low content of *n*-alkanes. The next highly susceptible compounds are alkylcyclohexane followed by alkylbenzenes, then acyclic isoprenoids, then alkylnaphthalenes, then bicyclic alkanes, then alkylphenanthrenes, then steranes and finally hopanes at severe and extreme biodegradation level. Peters and Moldowan (1993) proposed a 1-10 scale of the extent of biodegradation effect on crude oils, based on the absence or presence of various compounds that have different susceptibilities to biodegradation. Peters *et al* (2005) updated this scale later, and this is illustrated in Figure 4-29.

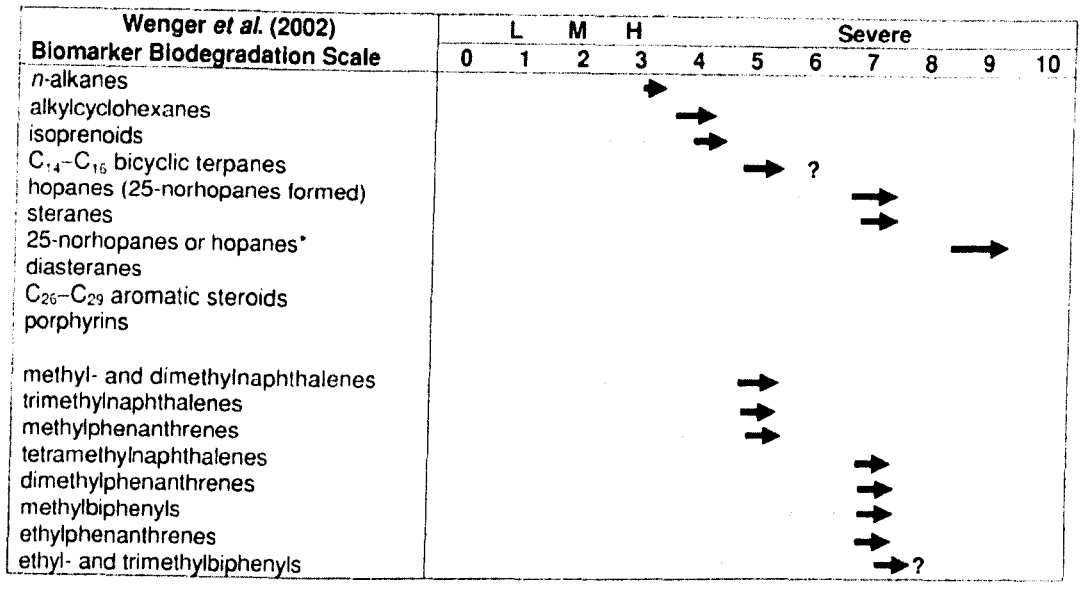

Figure 4-29: Peters *et al* (2005)'s biodegradation scale with a 10 point quasi-stepwise biodegradation sequence for the compound groups.

The study oils are characterized by high acidity (TAN = up to 1.24) and high sulfur content (S = up to 3.24), which are potential indicators for biodegradation (Meredith *et al.*, 2000; Peters *et al.*, 2005). However, Medium API gravities and saturated hydrocarbon rich oils such as the studied oils (28-52°API, saturated hydrocarbons/aromatic hydrocarbons greater than 1) do not suggest that biodegradation or water washing has affected these oils. Most of the oils show smooth *n*-alkane envelopes (Figure 4-8 & Figure 4-9) and contain very high abundance of *n*-alkanes (10-32 wt%). This suggests that these oils have not been altered by biodegradation and they can be ranked in Peters *et al* (2005) scale in the bottom of the scale where the biodegradation level is zero. The acidity and sulfur in the study oils will be explored later in chapter 6 (section 6.3 and 6.4). It may be important to mention here that Meridith *et al* (2000) found some non degraded high sulfur oils exhibiting high TAN but with very low content of carboxylic acids, which are similar to the crude oils in this study (section 6.3).

It is already mentioned that there is large variation observed in C_{27}-C_{35} 17α Hopanes/ C_{27}-C_{29} steranes (S+R, ααα+αββ) (i.e. hopanes/steranes) ratio; this ratio can be affected by high level biodegradation (severe, >level 5 in Peters et al 2005 scale). Although the study oils show no sign of even the lowest level of biodegradation (full suite of *n*-alkanes are not affected), it is useful to discuss the possibility of the

biodegradation effect on this ratio in case if the low levels of biodegradation are camouflaged by fresh oil charges. The distribution of C_{27}-C_{29} steranes (S+R, ααα+αββ) shows no indication of biodegradation (Figure 4-11). Furthermore, if steranes are biodegraded, there will be higher variations in C_{21}-C_{22} pregnanes/C_{27}-C_{29} steranes ratio and that is not the case in this study (Table 4-5). Same argument can be drawn for 17α hopanes, if they are biodegraded, they should have been converted to, at least some, to 25-norhopanes (Peters *et al.*, 2005; Peters & Moldowan, 1991; Welte *et al.*, 1982) (when oils reach and exceed severe biodegradation level 5 in Peters et al (2005) scale). No 25-norhopane (or 10-desmethylated hopanes) occurrence can be detected in any of the studied oils including oil O13 (A4C, well Nassir1) (Figure 4-30). Therefore, it is difficult to think of biodegradation as a possible control on hopanes/steranes ratio (Figure 4-15). Wardroper *et al.*, (1984) indicated that the light tri-aromatic steroids C_{20} and C_{21} are less resistant to biodegradation and/or water washing than high molecular weight ones (Wardroper *et al.*, 1984). Although there is variation in C_{20}/(C_{20}+C_{28})-triaromatic steroid hydrocarbons (TAS) ratio, this was attributed to mixing with condensate charge as this agrees well with other geochemical characteristics; mainly API gravity and sulfur distribution (higher TAS cracking ratios characterize high sulfur and low API gravities oils). If this parameter is controlled by biodegradation, we will expect that those oils with lower ratio will have higher sulfur content and lower API gravity and this is not the case (Figure 4-26). Furthermore, if the biodegradation or/and water washing have active control, there should be inverse relationship between the ratio of light TAS to heavy TAS and light monoaromatic steroid hydrocarbons (MAS) to heavy MAS (Wardroper *et al.*, 1984) which is not seen in Figure 4-26.

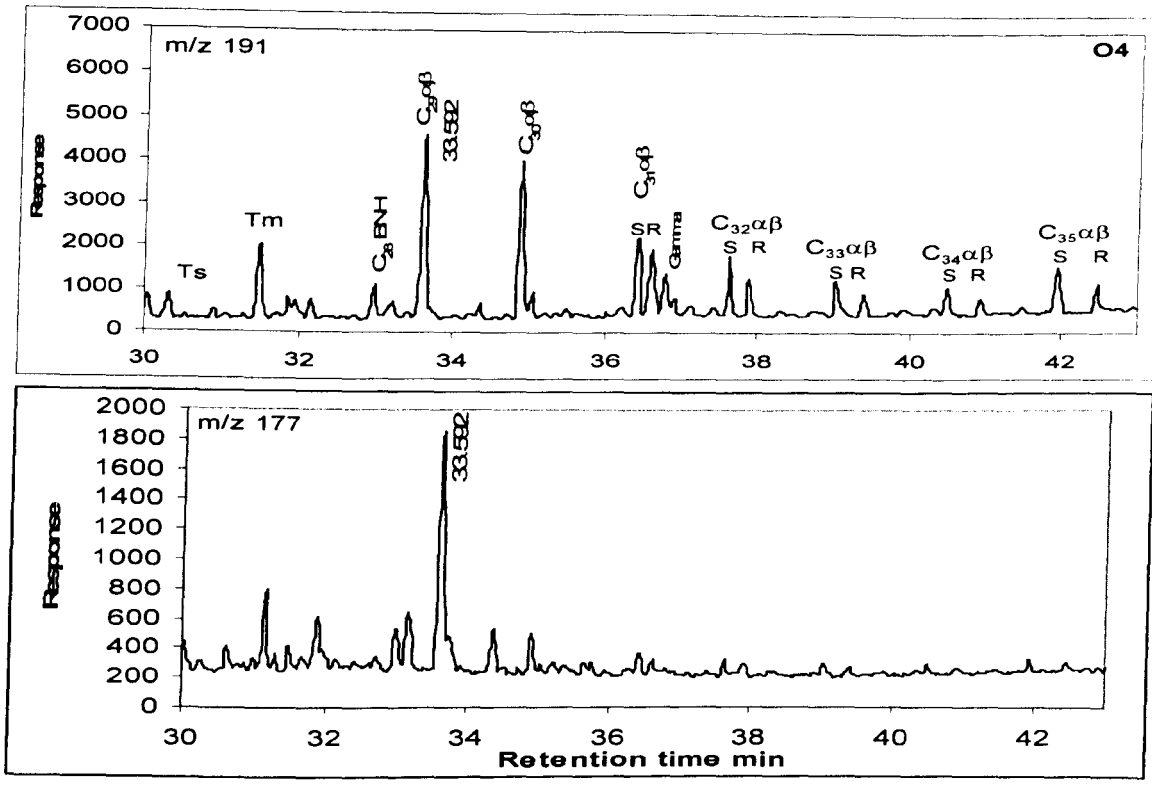

Figure 4-30: representative chromatograms of hopanes (top) and 25-norhopanes (bottom) for oil O13 from A4C reservoir unit of well Nassir1.

Oil O13 (well Nasser-1, A4C reservoir unit) shows the lowest API gravity and the highest acidity (TAN=1.24mgKOH/g oil) and high sulfur content (3.14wt %) in the Greater Birba area. Yet there is no sign of biodegradation as mentioned above. This oil shows the lowest content of benzene and toluene of all oils including gas condensates (Benzene: 0.14 wt% and Toluene: 0.53 wt% of oil, Table 5-9). Therefore, it is important to investigate the effect of water washing on higher molecular weight hydrocarbons of this oil and compare it with rest of the oils. In order to investigate the water washing, the relative distribution of alkylated phenanthrene, alkylated naphthalene and alkylated dibenzothiophenes are normalized and plotted for all samples (Figure 4-31). Oil O13 (well Nasser-1, reservoir A4C) and O5 (Well BBN-1, reservoir A3C) are very different from the rest by having relatively higher lower homolog in all of them. The cross plot of phenanthrene/ (Methylphenanthrene + Dimethylphenanthrene) ratio versus dibenzothiophene/ (Methylbenzothiophene+ Dimethylbenzothiophene) ratio illustrate this more clearly. This is opposite to what can be caused by water washing (Huang *et al.*, 2003b). Huang et al (2003) observed that the lower homologs of the above polyaromatic hydrocarbons are easily washed than the higher homologs as the light homologs are more soluble in water than higher

homologs. Therefore, the differences seen in oil O13 are more related to oil mixing and highly likely to be mixed with a lighter oil or gas condensate charge. This is supported by the geological setting of these carbonate stringers. These stringers are almost completely encased by salt and therefore it is difficult to imagine an active oil-water contact, unless the water washing occurred during migration through the carrier beds towards the reservoir. Furthermore, the formation waters in these accumulations are highly saline, which also limits the possibility of the water washing effect. The water washing caused by migration might be a possibility behind the lower benzene and toluene content in this oil, although facies variations effect is also a possibility.

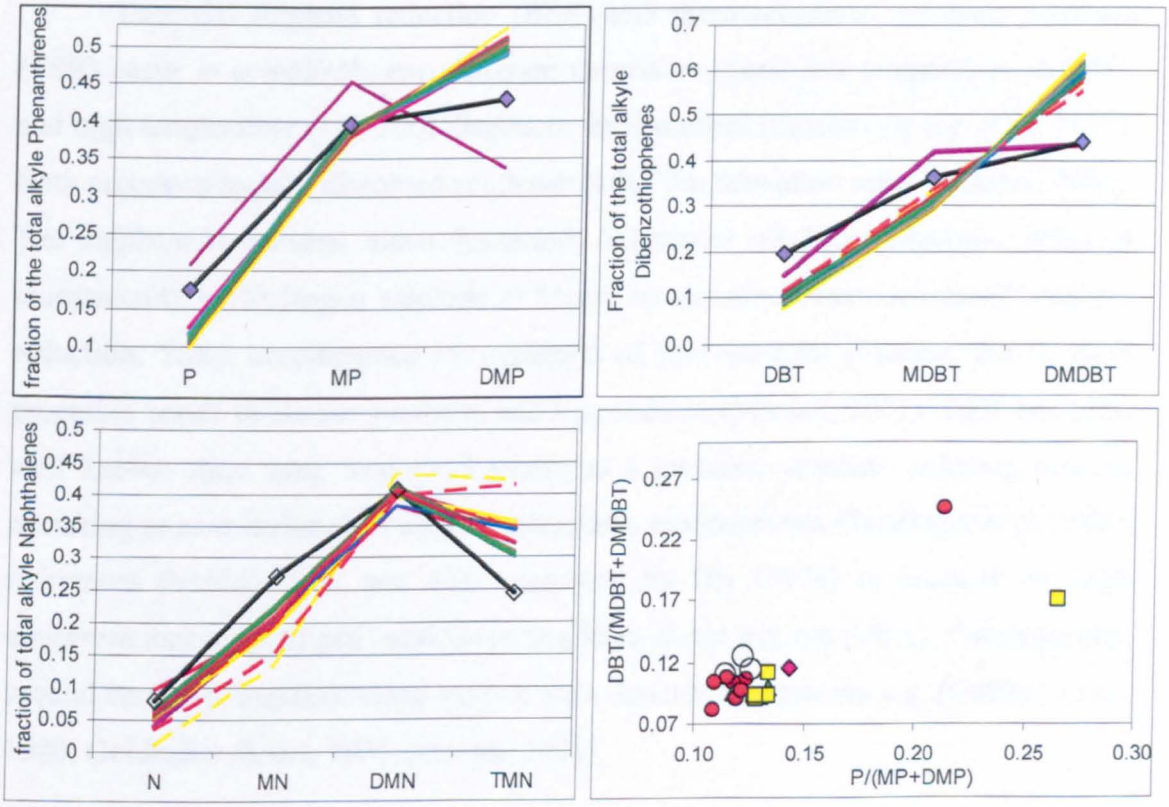

Figure 4-31: the relative distribution of alkyl homologues for Phenanthrenes (top left), Dibenzothiophenes (top right) and Naphthalenes (Bottom left). The bottom-right plot shows a cross plot of the ratios of dibenzothiophene to the sum of methyl and dimethyl dibenzothiophenes in the y-axis and the ratio of phenanthrene to the sum of methyl and dimethyl phenanthrene in the x-axis. The line with diamond is for O13 and the other distinctive line is for O5. all these compounds are shown in chromatograms in Appedix 4-3.

4.3.4.2 Thermochemical and bacterial sulphate reduction

Some of the oils if not most are characterized by high sulfur content (2-5%) and the gases produced from these fields consist of H_2S content of 0.7-4 vol. %. Therefore, it was important to investigate the possibility of thermochemical sulphate reduction (TSR) and bacterial sulphate reduction (BSR) in these fields. However, there is limitation for this investigation as it was not possible to provide sulfur isotopic data of hydrogen sulfide for this study and so the investigation will focus on previously published geochemical consequences of these two processes.

Bacterial sulphate reduction (BSR) and thermochemical sulphate reduction (TSR) occur in completely two different thermal regimes, low temperature (0-80°C) and high temperature (100-200) diagenetic environment respectively e.g. (Orr, 1977). Both processes require dissolved sulphates (SO_4^{2-}) in formation water (Machel, 2001). The sulphate is reduced either bacterially (Bacterial sulphate reduction, BSR) or inorganically by hydrogen sulphide at higher temperature (thermochemical sulphate reduction, TSR), accompanied by oxidation of hydrocarbons (Machel, 2001). Both processes result in similar products and by-products (Machel, 2001). BSR has been well known since long time (>55 years) as a common sulphate reducing process occurring in near surface and shallow diagenetic environments (Trudinger *et al.*, 1985, references therein). TSR was first suggested by Orr (1974) to account for high concentrations of hydrogen sulphide in Big Horn Basin in Utah (USA). Subsequently, several empirical and theoretical studies were done on this process e.g. (Gaffney *et al.*, 1980; Goldhaber & Orr, 1995; Machel, 2001).

Temperature is the most important controlling factor on both BSR and TSR. BSR occurs at low temperature range up to 60-80°C ($0<T<60\text{-}80^{\circ}C$), which is equivalent to vitrinite reflectance levels of 0.2 to 0.3%R_o and depths less than 2000-2500m at normal geothermal gradients. Whereas TSR occurs in diagenetic geological environment of temperature range of 100°C to 150°C and may occur at even higher temperatures up to 200°C e.g. (Goldhaber & Orr, 1995; Machel *et al.*, 1995; Trudinger *et al.*, 1985; Worden *et al.*, 1995). This temperature range is equivalent to vitrinite reflectance levels of 1.0 to 4.0%R_o (Figure 4-32) and depths of about 2000 to 6000m (Machel, 2001), and some studies suggest even as low as 80°C (Orr, 1977).

Figure 4-32 shows a schematic diagram of the relationship between hydrocarbon generation, destruction, thermal maturity and temperatures of the reservoir/source rock.

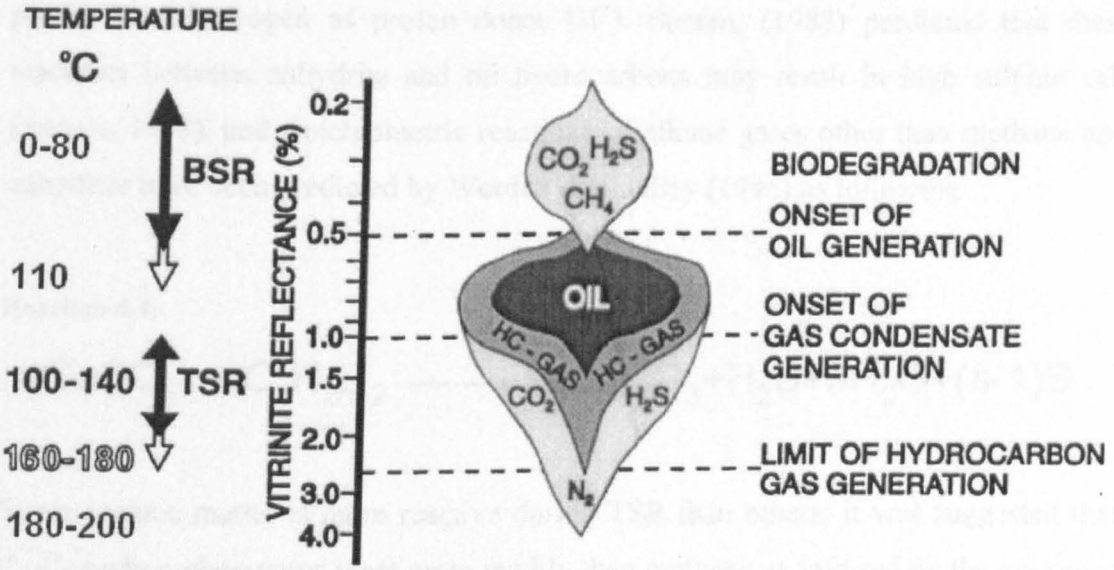

Figure 4-32: schematic diagram of the relationship between hydrocarbon generation, destruction, thermal maturity, and temperature. Modified after (Machel *et al.*, 1995)

The overall reaction of these two processes:

Reaction 4-1

$$\text{Anhydrite } (CaSO_4) + \text{hydrocarbons (e.g. } CH_4) \longrightarrow \text{calcite } (CaCO_3) + H_2S + H_2O \pm S \pm CO_2$$

For thermochemical sulphate reduction, several studies showed empirically that this reaction (Reaction 4-1) only occurs in the presence of hydrogen sulphide or other low valence state sulphur compounds and consists of two reactions (Reaction 4-2&Reaction 4-3) e.g. ((Krouse *et al.*, 1988; Worden & Smalley, 1996), references therein).

For methane (CH_4) as an example for hydrocarbons:

Reaction 4-2

$$CaSO_4 + CO_2 + 3H_2S \longrightarrow \text{calcite } (CaCO_3) + 3H_2O + 4S$$

Reaction 4-3:

$$4S + CH_4 + 2H_2O \longrightarrow 4H_2S + CO_2$$

Reaction 4-2 represents the reduction of sulphate in the presence of hydrogen sulphide, and the replacement of anhydrite by calcite. The oxidation of hydrocarbons is represented by reaction 4-3 by the elemental sulphur produced by reaction 6-2 in the presence of hydrogen as proton donor (H^+). Sassen, (1988) predicted that these reactions between anhydrite and oil hydrocarbons may result in high sulphur oils (Sassen, 1988), and stoichiometric reactions of alkane gases other than methane and anhydrite have been predicted by Worden & Smalley (1996) as following:

Reaction 4-4:

$$n\mathrm{CaSO_4} + \mathrm{C}_n\mathrm{H}_{2n+2} \longrightarrow n\mathrm{CaCO_3} + \mathrm{H_2S} + n\mathrm{H_2O} + (n\text{-}1)\mathrm{S}$$

Some organic matter is more reactive during TSR than others; it was suggested that C_2-C_5 hydrocarbon gases react more readily than methane as inferred by the existence of many sour gas reservoirs lacking C_2-C_5 hydrocarbons, yet they have methane and hydrogen sulphide as well as other non hydrocarbons gases (Peters *et al.*, 2005). All these reactions (Reactions 4-2, 4-4) produce elemental sulphur, calcite and water, and they utilize sulphate dissolved in pore water and oil-water contact (Krouse *et al.*, 1988; Orr, 1974). The anhydrite exists as a crystalline solid within the rock matrix, but it dissolves in formation waters (coexisting with hydrocarbons) and this provide transport for sulphate to the TSR system, i.e. can be reduced by hydrocarbons in the presence of hydrogen sulphide e.g. (Orr, 1974). Worden & Smalley (1996) argued that most of the sulphates are locked as solid anhydrites and very low amount of sulphate will be available in the aqueous phase. However, a direct reaction between (solid) anhydrite and (liquid) hydrocarbons is unlikely because the anhydrite have got higher surface affinity for water than non-polar hydrocarbons and there is always a thin layer of water separating anhydrite from hydrocarbons (Cross, 1999 , references therein). Therefore, although it is necessary to have aqueous sulphate, this appears to be rate limiting factor for TSR due to the low amount of sulphate dissolved in formation water (Worden & Smalley, 1996).

From these reactions, we can track the evolution of sulphur and carbon isotopes of hydrogen sulphide, hydrocarbons, anhydrite and pyrites if present. With progressing TSR, The hydrogen sulphide is produced by overall reaction 4-1 or 4-4

but specifically by reaction 4-3 from the reduction of elemental sulphur. This means that the anhydrite-derived sulphur will comprise hydrogen sulphide produced. Therefore, TSR produced hydrogen sulphide will be enriched in ^{34}S and thus the sulphur isotopic $\delta^{34}S$ ratio will approach that for anhydrite (Machel, 2001; Machel *et al.*, 1995). This is the case also for sulphur in hydrocarbons; the elemental sulphur and polysulphide can be incorporated into the hydrocarbons and so with increasing the sulphur species, the sulphur isotopes $\delta^{34}S$ will shift towards that for anhydrite. As TSR increases, the amount of hydrogen sulphide and carbon dioxide increases, while the amount of hydrocarbons decreases. The source of carbons in carbon dioxide is hydrocarbons and so the carbon isotopes $\delta^{13}C$ in carbon dioxide will decrease (^{12}C is more preferentially oxidized than ^{13}C), while $\delta^{13}C$ of the hydrocarbons (especially saturates, (Manzano *et al.*, 1997)) will decrease. This is all expected from those reactions. However, those isotopic trends were determined empirically and the reactions above were predicted according to these trends as well as other observations such as petrographic data (Cross, 1999; Machel, 2001).

$\delta^{34}S$ in crude oils varies from -7.5 to +25% relative to Diablo meteorite's (standard)(Gaffney *et al.*, 1980) . It can be used to evaluate mechanisms of formation of hydrogen sulphide and its relationship to the associated sulphates (Gaffney et al., 1980) as discussed above. It is proposed that very low or no fractionation occurs during sulphur incorporation reactions during early diagenesis (Orr, 1974). However, with increasing temperature, the fractionation increases and may reach up to 20 per mil depending on temperature, while the migration was reported to cause no fractionation in this ratio (Orr, 1974). Therefore, source facies and maturity are the main controls on the variations in this ratio (Gaffney et al., 1980; Orr, 1974), as well as thermochemical or/and bacterial sulphate reduction e.g. (Manzano *et al.*, 1997). The effects of bacterial/thermochemical sulphate reductions are very often similar to thermal maturation. Table 4-7 shows the effect of the two different processes: thermal maturation and TSR (BSR should have similar effect as TSR on the listed parameters (Machel, 2001; Machel *et al.*, 1995)).

Table 4-7: comparison between the effects of TSR and thermal maturation. Similar effects to TSR but to less extent are expected for BSR

Parameters	Increasing TSR	Increasing maturation	References
C_{15+} Sat/Aro	Decreases	Increases	(Manzano *et al.*, 1997)
Sulphur content	Increases	Decreases	(Orr, 1974)
Elemental sulphur	Increases	-	(Machel, 2001)
API gravity	Increases or decreases but increases at high level of TSR	Increases	(Manzano *et al.*, 1997; Orr, 1974)
GOR Sm^3/Sm^3	-	Increases	(Orr, 1974)
S/N		Increases	(Orr, 1974)
H_2S concentration	Increases at higher rate	Increase at lower rate	(Worden & Smalley, 1996)
$\delta^{34}S$ (crude oil)	Increases and approaches sulphate $\delta^{34}S$	Does not change or slightly increases	(Gaffney *et al.*, 1980; Orr, 1974; Thode, 1981)
$\delta^{34}S$ (H_2S)	Approaches sulphate	Little change	(Gaffney *et al.*, 1980; Krouse *et al.*, 1988; Orr, 1974)
$\delta^{13}C$ of CO_2	Decreases (becomes lighter)	-	(Krouse *et al.*, 1988; Orr, 1974)
$\delta^{13}C$ of Saturated HC	decreases	increases	(Manzano *et al.*, 1997; Peters *et al.*, 2005)
$\delta^{13}C$ of aromatic HC	Should not change	Increase	Expected
$\delta^{13}C$ of whole oil	increases	increases	(Orr, 1974; Sassen, 1988)

Table 4-8 shows the data used in this study to investigate the possibility of TSR in the study reservoirs. Similar effects on the parameters can be expected for the BSR process since both of them can be described by Reaction 4-1. However, BSR is less likely to occur since no sign for biodegradation effect can be found by examining the C_{15+} composition (section 4.3.4.1, this chapter), and the C_3-C_8 composition (section 5.5.3.4, chapter 5) of the study oils. In addition to that, only little or no organic acids were found in these oils although they are characterized with high TAN values as well as high sulphur content. Therefore, BSR might not occur in the study

oils. If there is sulphate reduction in the studied reservoirs, it is more likely to be thermochemical sulphate reduction.

Present day Reservoir temperatures in the Greater Birba Area range from 61° to 88°C. Burial history of the area has not been well modeled and therefore it is difficult to tell if the reservoir is cooling or heating up. One temperature profile was suggested by a broad study of carbonate stringers in the South Oman Salt Basin by Toth, (2001). This indicates that Intra salt stringer (e.g.A4C) was only buried to up to 80°C, which is not enough for TSR to occur (Figure 4-33). The presence of diamondoids in BBN2 (unpublished PDO data) indicates that the carbonate stringers might have been buried deeply at higher temperature. However, the presence of diamondoids might be related to a high maturity condensate charge mixed with the original oil in place as proposed in this study.

Table 4-8: Geochemical and isotopic data that can control or be affected by TSR/BSR in the study oils. H_2S wt% is the dissolved hydrogen sulphide in oils and condensates.

Sample ID	well	TVD (m)	Stratigraphy	Temperaturre °C	Sulfur content wt%	H_2S mol%	CO2 mol%	API° gravity	NSO %	Asp %	C_{15+} Sat/aro	VRE (MPI-1)	Whole oil $\delta^{34}S$	Saturates $\delta^{13}C$
O1	BB2	2583.4	A4C	71	2.97	1.17	3.84	28.00	17.8	0.24	1.74	0.92		
O2	BB1	2536.5	A4C	69.4	3.03			28.30	14.5	0.17	1.84	0.93		-34.6
O3	BBN1	3455.1	A4C	80	1.65			49.20	6.1	0.01	4.29	0.86	15.85	-34.9
O4	BB1	2533.1	A4C	69.4	3.03	2.29	3.39	28.50	13.8	0.10	1.81	0.93	12.81	-34.6
O5	BBN1	3558.1	A3C		2.5				13.7	0.70	4.72	0.71		
O7	BBN2	3597.8	A4C	88	2.05			31.60	11.5	0.43	2.78	0.86	14.15	-34.4
O9	BBS1	2329.7	A4C	68.3	3.24	0.90	2.84	46.10	5.7	0.00	3.26	0.91	12.96	-34.5
O10	Kaukab1	2513.6	A3C	72	2.39			30.20	10.8	0.37	2.21	0.91		-35
O11	Kaukab1	2513.6	A3C	72	2.4	3.55	5.87	29.10	10.4	0.50	2.26	0.92	13.57	
O12	Omraan1	2601.7	A5C	74	2.11			30.20	13.5	0.50	2.69	0.92	13.13	-34.8
O13	Nasser1	1998.6	A4C	61	3.16	3.83	6.03	23.70	23.6	1.69	2.43	0.81	11.72	-34.6
O14	Durra1	2693.0	A3C	72	1.97			34.60	9.9	0.07	3.87	0.93	13.96	-34.8
O15	Kaukab1	2896.9	A1C		0.78			32.60	11.2	0.63	3.32	0.72	17.00	
O16	Shamah1	2385.7	A3C	74.5	2.46			29.40	8.4	1.10	2.31	0.94	13.07	
O17	Durra1	2695.1	A3C	72	2.02	2.39	4.99	33.00	13.7	0.15	3.01	0.93		
O18	Omraan1H3	2939.1	A5C		2.1			29.80	9.7	0.30	2.41	0.93		-34.7
O19	Omraan1H3	2939.1	A4C		1.9			31.00	9.7	0.41	2.85	0.91		-34.6
O20	Budour1H2	2971.6	A4C	75.6	4.7	0.93	3.68	51.50	12.1	0.47	2.88	0.92	12.84	-35.2
O21	Omraan1H3	3111.5	A3C		1.9			31.00	4.1	0.00	2.95	0.91		-34.7
O22	Omraan1H3	2939.1	A4C		2.1			30.90	10.1	0.68	2.37	0.91	13.00	-34.7

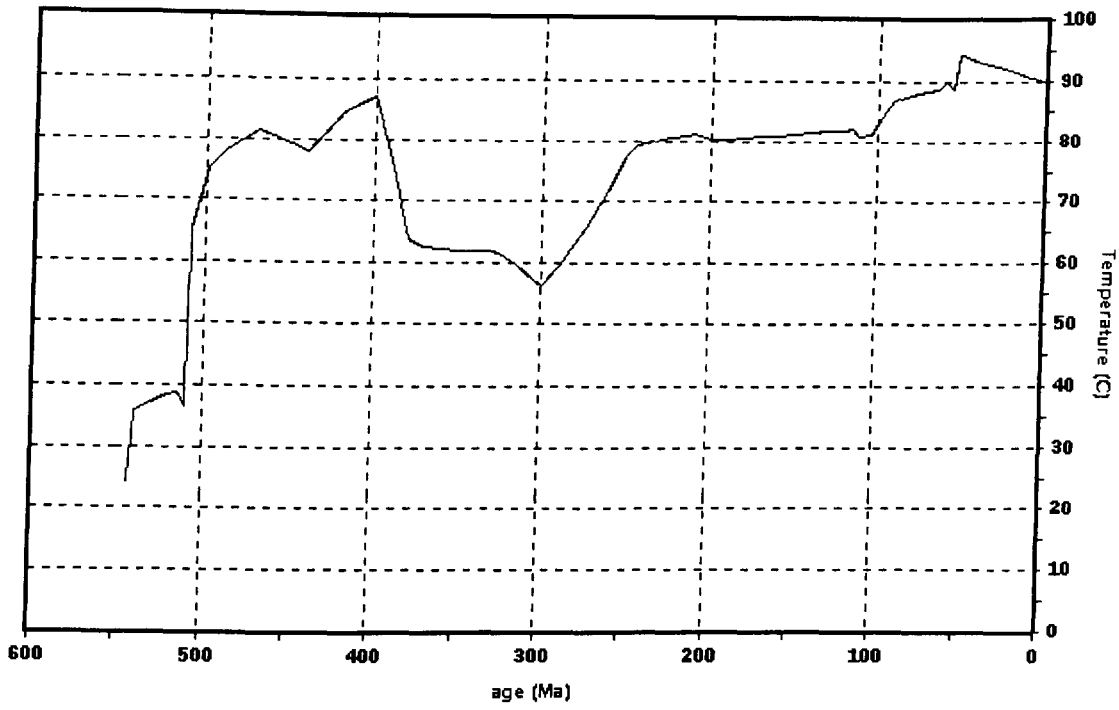

Figure 4-33: The temperature history curve of the A4C stringer that most of the high sulphur oils and condensates are from.

Figure 4-34 shows cross plots of some of the important parameters to discern the effect of TSR/BSR in the study oils. Apparently, there is good relationship between the amount of carbon dioxide and hydrogen sulphide in the study oils. It generally distinguishes between two main groups, one is the gas condensates and A4C oils, and the other group is the A3C oils, despite the overlapping caused by A4C oils. However, there is no good relationship between API gravity and the amount of hydrogen sulphide in the oils. If TSR/BSR process is working in these reservoirs, we would expect a decrease in API gravity with increase in abundance of hydrogen sulphide; this is not evident in the study oils as clear from Figure 4-34 (B). The presence of gas condensates (empty circles) form some sort of relationship between API gravity and amount of hydrogen sulphide. The gas condensates are expected to have higher API gravity and less ability to dissolve hydrogen sulphide. However, this may also suggest that the condensate charge that is proposed in this study to have mixed with the oils in the study area was not rich in hydrogen sulphide. Furthermore, there is no isotopic evidence (in the available data) for the presence of TSR/BSR effects. Carbon isotopic ratio for saturated hydrocarbons is expected to decrease with

increasing abundance of carbon dioxide, because the saturated hydrocarbon are preferentially oxidized than other class of compounds. This is not evident in the study oils in Figure 4-34 (C). The most interesting relationship is revealed by the cross plot of sulfur content versus sulfur isotopic ratios of the whole oils in Figure 4-34. There is a clear but general decrease in sulfur isotopic ratio of the whole oil with increasing sulfur content in the study oils. This relationship suggests that TSR/BSR processes are less likely to be responsible of increasing sulfur content in the study oils. The mean sulfur isotopic ratio of anhydrite in the study carbonate stringers is 38.0±5‰. If the sulphur content has been increased by incorporating polysulphides formed by TSR/BSR reactions through the available functional groups in the hydrocarbons, the bulk sulphur isotopic signature of the sulphur in the study oils will shift towards that of reservoir, which is not the case here. However, this is not enough to eliminate TSR or BSR completely; it only suggests that they are not the major control on the variations of sulfur content. Apparently, the sulfur isotopes of the sulfur was probably decreased by incorporating more light sulfur compounds, which is coherent with the mixing theory proposed in this study. Sulphur isotopes are explained in more details in chapter 6 (section 6.4).

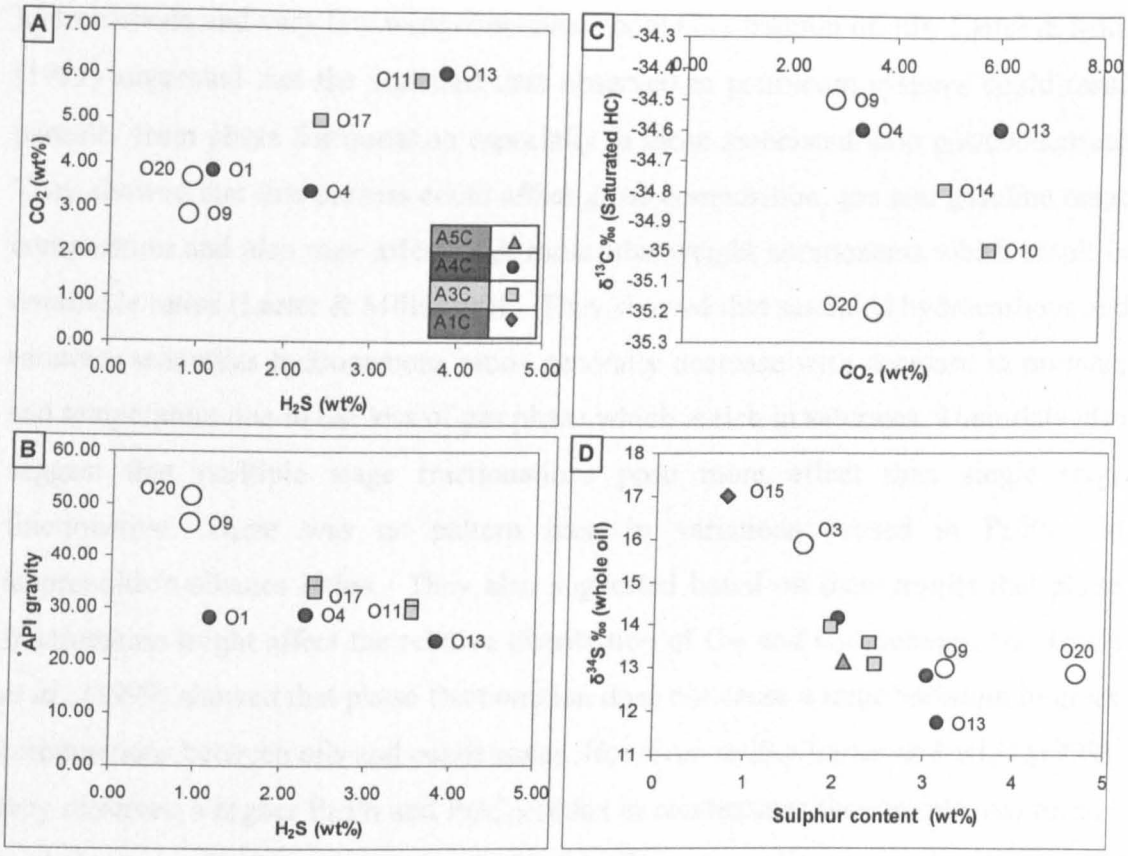

Figure 4-34: cross plot of various parameters to discern the TSR effects in oil compositions, A) a cross plot of amount of hydrogen sulphide content versus amount of carbon dioxide in some of the study oils (these are obtained from PVT oil samples, either surface or borehole samples) B) a cross plot of hydrogen sulphide versus API gravity of the study oils C) a cross plot of carbon isotopic ratio of bulk saturated hydrocarbons amount of carbon dioxide in some of the study oils and D) a cross plot of the sulphur content versus the sulphur isotopic ratio of whole oil for the study crude oils. The missing data were not measured at the first place.

4.3.4.3 Phase Fractionation

The association of gas condensates and oils in carbonate reservoirs in the Greater Birba area provided the motivation to investigate the phase fractionation effect in the study oils. This process is investigated in the light hydrocarbon of the study oils in chapter 5. In this section, the focus will be on C_{15+} hydrocarbons. The mechanism of phase fractionation is basically separating gas rich petroleum from liquid phase which is accompanied by dissimilar distributions of different components between the two phases depending on compound fugacity and boiling point e.g. (Thompson, 1987). Several empirical studies that investigated this process experimentally (Larter & Mills, 1991; Thompson, 1987; Thompson, 1988; van Graas *et al.*, 2000); most of these studies focused on the effect of phase fractionation on light

hydrocarbons and very few were concerned about C_{15+} fraction of oils. Larter & Mills (1991) suggested that the scattered data observed in petroleum systems could result partially from phase fractionation especially in those associated with gas/condensate. They showed that this process could affect gross composition, gas and gasoline range composition and also may affect high molecular weight components which result in unreliable ratios (Larter & Mills, 1991). They showed that saturated hydrocarbons and saturates/aromatics hydrocarbons ratios generally decrease with decrease in pressure and temperature due to the loss of gas phase which is rich in saturates. Their data also suggest that multiple stage fractionations pose more effect than single stage fractionation. There was no pattern seen in variations caused in Pr/Ph and isoprenoids/n-alkanes ratios. They also suggested based on their results that phase fractionation might affect the relative distribution of C_{27} and C_{29} steranes. van Graas *et al.*, (1999) showed that phase fractionation does not cause a large variation in gross compositions between oils and condensates. However, unlike Larter and Mills (1999), they observed a higher Pr/Ph and Pr/C_{17} ratios in condensates than in oils. According to their study, Ph/C_{18} ratios were similar in oils and condensates and did not vary during experiment and $C_{17}/ (C_{17}+C_{27})$ ratios show higher values in condensates than in oils. Higher Pr/Ph ratios for condensates compared to oils were also reported by other authors (Curiale & Bromley, 1995; Dzou & Hughes, 1993). Molar Slope factor (SF) is a measure of the decrease in n-alkanes concentrations with increasing chain lengths (Thompson, 2000a; Thompson, 2000b). These studies show that normal oils should have a slope factor lower than 1.2 and the condensates from thermal origin should be about 1.2 and phase fractionation produced gas condensates should show a higher slope factor. The effect of phase fractionation was also investigated in C_{15+} aromatic hydrocarbons. Some aromatic HC are sensitive to normal conditions and might be evaporated during sampling and sample preparation like C_1 and C_2 -naphthalenes. Methyl phenanthrene indices were observed to be affected slightly but not significantly by phase fractionation (Dzou & Hughes, 1993; Larter & Mills, 1991) and this difference were found within the analytical error margin by another study (van Graas *et al.*, 2000). However, a large variation was thought to be induced by phase fractionation in these parameters according to Thompson (1991). England et al (1991) found that phase fractionation may alter the relative abundance of saturated hydrocarbons, aromatic HC and NSO compounds. According to their study, many biomarkers ratios were significantly altered and concentrations of biomarkers were

lower in condensates as opposed to parent oils. They also show that minor alteration occurs in ratios involving compounds isomers of molecules with similar carbon numbers like MPI and significant alterations occurs in ratios involving compounds of different C-number or different numbers of aromatic rings like $C_{20}/(C_{20}+C_{28})$ Tricyclic aromatic steroids. Generally, most of the studies show that phase fractionation increases low molecular weight compounds in gas rich phase and concentrate high molecular weight compounds in liquid rich phase and this is most obvious in gas condensate and oil systems.

Table 4-9 shows some of the above reported parameters that can be affected by phase fractionation. Most of the parameters show small variations (Standard deviations) that are within measurement errors. However, some of the parameters show higher values for the gas condensates than the oils (n-alkanes ratios, alkylnaphthalenes/alkylphenanthrenes and TAS $C_{20}/(C_{20}+C_{28})$. This is probably because of the effect of phase fractionation but maturity effects cannot be ruled out as these condensates have been found to have thermal origin (chapter 5). Only the bulk property (saturates HC/aromatic HC) and alkylnaphthalenes/ alkylphenanthrenes show significant variations. Regarding the later ratio, the standard deviation is more controlled by O13, which also shows different values in some of the parameters, otherwise most of the oils show close range of values. Oil O13 shows high content of alkylnaphthalenes and depleted in alkylphenanthrenes (highest ratio) which is probably an indication of mixing facies. This can not be phase fractionation in this case because this oil shows the lowest API gravity of all oils (API 23.9) and high sulfur content (>3 wt%).

Table 4-9: Selected parameters that are reported they can be affected by phase fractionation. GC parameters are derived from m/z 85 chromatograms.

Sample ID	Wells	TVD (m)	Stratigraphy	Sat/Aro	Pr/Ph	Pr/*n*-C_{17}	Ph/*n*-C_{18}	nC_{10}/ (*n*-C_{10}+*n*-C_{25})	*n*-C_{17} / (*n*-C_{17}+*n*-C_{27})	MSF	C_{27}/C_{29} Steranes	MPI1	Naph/Phen	TAS C20/ (C_{20}+C_{28})
O1	BB2	2583.4	A4C	1.08	0.43	0.29	0.79	0.83	0.91	1.21	0.35	0.86	4.54	0.33
O2	BB1	2536.5	A4C	1.13	0.45	0.28	0.73	0.84	0.91	1.20	0.34	0.88	5.06	0.39
O3 (GC)	BBN1	3455.1	A4C	2.64	0.57	0.27	0.67	0.95	0.96	1.34	0.35	0.77	7.32	0.56
O4	BB1	2533.1	A4C	1.12	0.47	0.28	0.72	0.84	0.92	1.22	0.37	0.89	4.68	0.37
O5	BBN1	3558.1	A3C	2.91	0.99	0.57	0.74	0.46	0.89	1.13	1.08	0.52	4.84	0.26
O7	BBN2	3597.8	A4C	1.72	0.50	0.24	0.65	0.80	0.93	1.26	0.37	0.77	4.87	0.52
O9 (GC)	BBS1	2329.7	A4C	2.01	0.46	0.27	0.79	0.93	0.97	1.30	0.35	0.85	8.27	0.45
O10	Kaukab1	2513.6	A3C	1.43	0.39	0.27	0.81	0.77	0.92	1.21	0.31	0.86	4.87	0.36
O11	Kaukab1	2513.6	A3C	1.40	0.36	0.26	0.84	0.73	0.91	1.21	0.30	0.87	5.47	0.34
O12	Omraan1	2601.7	A5C	1.66	0.38	0.25	0.78	0.71	0.91	1.18	0.33	0.86	4.55	0.40
O13	Nasser1	1998.6	A4C	1.50	0.40	0.26	0.77	0.82	0.92	1.20	0.31	0.69	8.54	0.38
O14	Durra1	2693.0	A3C	2.38	0.37	0.25	0.84	0.80	0.92	1.23	0.31	0.88	5.83	0.37
O15	Kaukab1	2896.9	A1C	2.05	0.48	0.21	0.55	0.87	0.92	1.28	0.34	0.54	4.62	0.22
O16	Shamah1	2385.7	A3C	1.43	0.34	0.26	0.86	0.77	0.91	1.18	0.28	0.90	5.10	0.35
O17	Durra1	2695.1	A3C	1.85	0.37	0.24	0.87	0.78	0.91	1.23	0.28	0.89	5.41	0.32
O18	Omraan1H3	2939.1	A5C	1.49	0.41	0.26	0.84	0.72	0.91	1.22	0.29	0.89	4.61	0.38
O19	Omraan1H3	2939.1	A4C	1.76	0.41	0.28	0.86	0.75	0.91	1.22	0.28	0.86	4.37	0.36
O20 (GC)	Budour1H2	2971.6	A4C	1.77	0.36	0.20	0.74	0.95	0.97	1.33	0.47	0.86	8.14	0.56
O21	Omraan1H3	3111.5	A3C	1.82	0.42	0.29	0.88	0.84	0.94	1.25	0.41	0.85	5.64	0.45
O22	Omraan1H3	2939.1	A4C	1.46	0.42	0.24	0.73	0.80	0.92	1.20	0.29	0.86	4.49	0.41
Std except O5&O15				0.41	0.06	0.02	0.07	0.07	0.02	0.05	0.05	0.05	1.41	0.07

Key to abbreviations: sat/aro = C15+ saturated hydrocarbons / aromatic hydrocarbons ratio (sat and aro are % of Σ (saturated HC+ aromatic HC + NSO + asphaltenes), Pr = pristane, Ph = Phytane, TAS = triaromatic steroid hydrocarbons. MSF = the ratio of molar concentrations of two successive *n*-alkanes averaged for C_{11}-C_{30} (e.g. C_{11}/C_{12}, C_{12}/C_{13}...etc).

4.3.5 Statistical evaluation of geochemical variations in Greater Birba Area petroleum fluids

4.3.5.1 Steranes and terpanes

It has been shown above that there is no significant variation in most of the geochemical ratios. Therefore, statistical evaluation was needed to explore the significance of any variation in composition. The wells and samples incorporated in this study are listed in Table 4-10 and shown in Figure 4-35. Principal Components Analysis (PCA) was performed on saturated hydrocarbons fraction of oil samples using absolute concentrations of 47 biomarkers. Oil O5 (A3C, BBN1) and gas condensates (O3 (well BBN1), O9 (well BBS1), and O20 (well Budour1h2) were excluded from the statistical evaluation because they always show noticeable difference from the rest of the group.

Table 4-10: the oil samples used in this study. Most of these samples were incorporated in the statistical evaluation except for O5, and gas condensates. TVD is true vertical depth.

Wells	Sample ID	Sampling year	TVD (m)	Stringers	Age	Note
BB1	O2	1988	2536.5	A4C	Neoproterozoic III-Cambrian (550-543Ma)	oil
BB1	O4	1983	2533.1-2556.0	A4C		oil
BB1	O6	1999	2588.3-2556.1	A4C		oil
BB1	O8	1988	2533.1-2533.4	A4C		oil
BB2	O1	1982	2583.4-2589.5	A4C		oil
BBS1	O9	1987	2329.7	A4C		Condensate
BBN1	O3	1980	3455.1-3471.5	A4C		Condensate
BBN1	O5	1981	3558.1	A3C		oil
BBN2	O7	1983	3597.8-3612.8	A4C		oil
Nasser1	O13	1982	1998.6	A4C		oil
Budour1H2	O20	2003	2971.59	A4C		Condensate
Omraan1	O12	1982	2601.7-2626.7	A5C		oil
Omraan1H3	O18	1997	2939.1-3201.6	A5C		oil
Omraan1H3	O19	1997	2939.1-3201.1	A4C		oil
Omraan1H3	O21	1997	3111.5-3201.5	A3C		oil
Omraan1H3	O22	2001	2939.1-3201.1	A4C		oil
Shamah1	O16	1992	2385.7-2389.7	A3C		oil
Durra1	O14	1982	2691.0-2712.2	A3C		oil
Durra1	O17	1982	2695.1	A3C		oil
Kaukab1	O10	1989	2513.6-2551.6	A3C		oil
Kaukab1	O11	1987	2513.6-2551.6	A3C		oil
Kaukab1	O15	1989	2897.0	A1C		oil

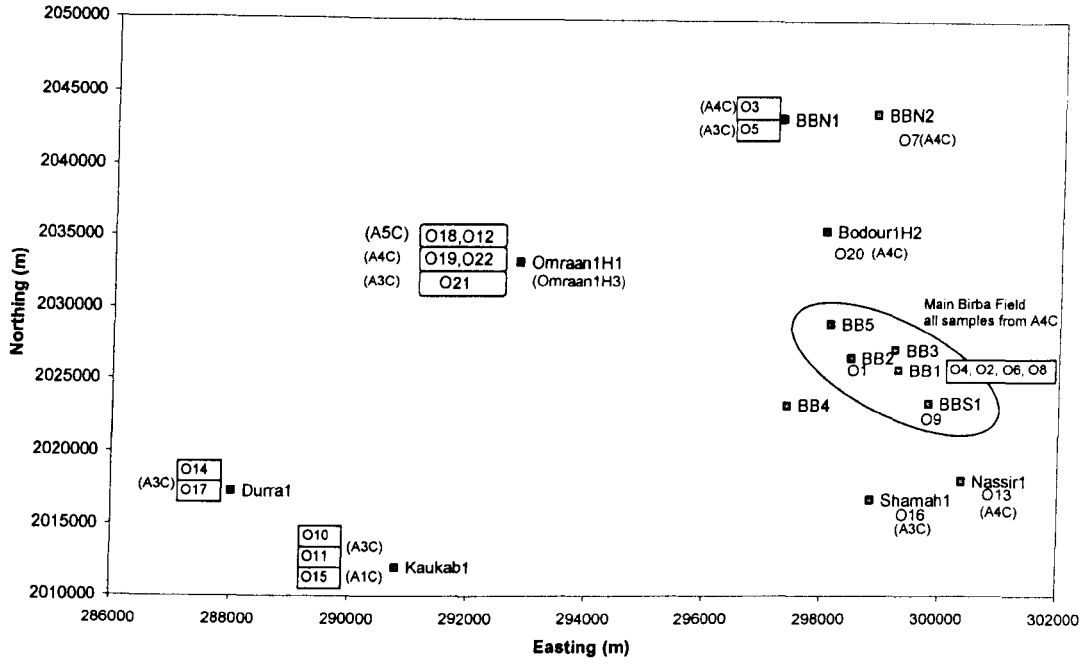

Figure 4-35: The geographic locations of the oil samples evaluated statistically.

The results are shown by Figure 4-36 & Figure 4-37. The first two principal components explain most of the variance (80%). Figure 4-36 shows a cross plot of these two principal components. Clearly, there is a clear distinction between different stringers' oils; although there is overlap by few samples. Two oil samples from A4C (O19 and O22) cluster with the other A3C and A5C oil samples. These are from well Omraan 1H3 and as clear from the plot, they are grouped together with other oils from well Omraan1 (O12 (A5C), O18 (A5C), and O21 (A3C)). This might suggest that these are either co-mingled produced oils or the stringers in this area are in communication. Oil O15 was already shown that it is probably sourced by different facies and indeed, it is clearly separated by both principal components.

The main variance is explained by the first principal component (65.8%) which is controlled mainly by the ratio of sum of tricyclics, Tm, Gammacerane, pregnanes and C_{29} steranes (all isomers) to the sum of hopanes and C_{27}+C_{28} steranes (all isomers) as clear from Figure 4-37. The second principal component explains 14.2% of the variance and gives moderate to high positive loadings for C_{24} tetracyclics, Ts, pregnanes, C_{27} αββ, C_{28} αββ and C_{29} ααα and moderate to high negative loadings for Tm, C_{28} Bisnorhopane, C_{29}αβ hopane, Gammacerane, and C_{35} homohopane. Therefore, the second principal component is more controlled by facies

variations. Because of the similarity between both groups in many geochemical characteristics, there was probably mixing between oils from two similar sources with small differences between them. This could be achieved by mixing with condensate like charge with small content of biomarkers as proposed before.

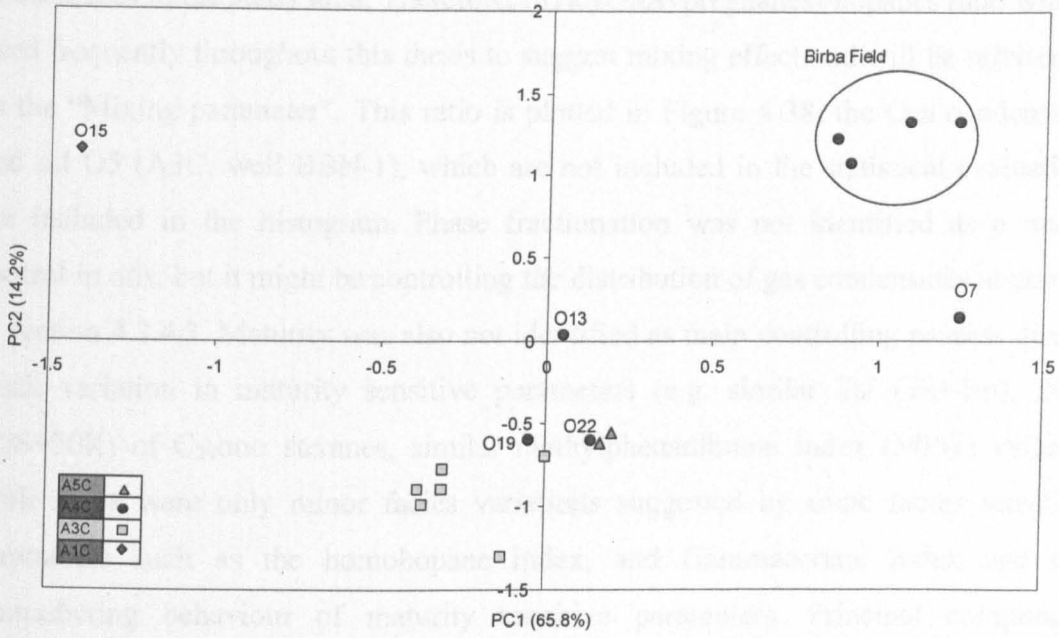

Figure 4-36 A cross plot of PC1 versus PC2 of 17 oil samples, derived from Principal component analysis on 47 saturated hydrocarbon biomarkers. Refer to Figure 4-35 and Table 4-10 for the locations and the description of the samples used.

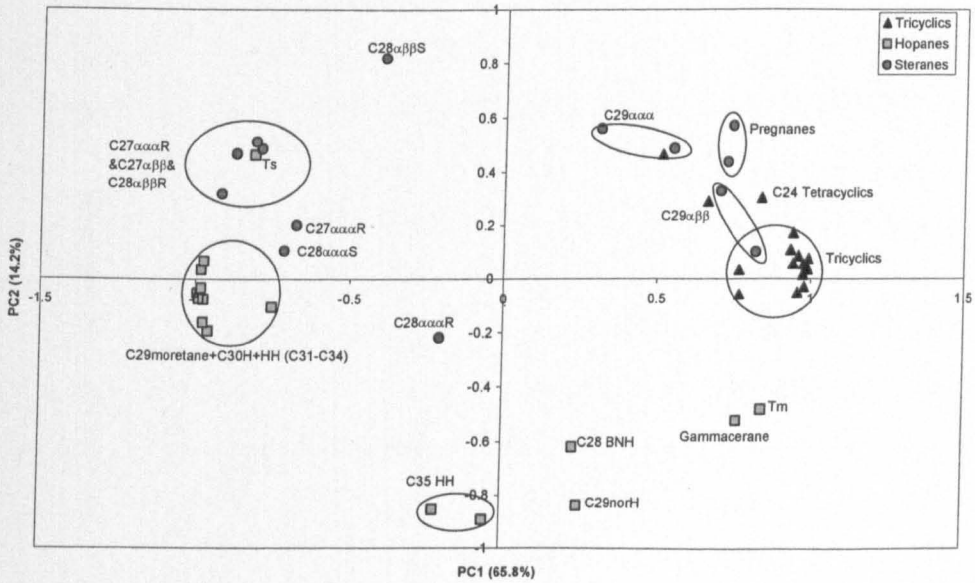

Figure 4-37: PC1 and PC2 loadings of the 47 biomarkers included in the principal component analysis for the 17 oil samples.

Therefore, the first principal component supports the proposed theory in this study that the study oils are mixtures of the original oils with a condensate charge. The ratio between light biomarkers (Tricyclics and pregnanes) to the higher molecular weight biomarkers (hopanes) should distinguish between various groups of oils and condensates in the study area. Therefore, (Tricyclics+pregnanes)/hopanes ratio will be used frequently throughout this thesis to suggest mixing effect and will be referred to as the "Mixing parameter". This ratio is plotted in Figure 4-38, the Gas condensates and oil O5 (A3C, well BBN-1), which are not included in the statistical evaluation, are included in the histogram. Phase fractionation was not identified as a major control in oils, but it might be controlling the distribution of gas condensates as shown in section 4.3.4.3. Maturity was also not identified as main controlling process due to small variation in maturity sensitive parameters (e.g. similar Ts/ (Ts+Tm), 20S/ (20S+20R) of $C_{29}\alpha\alpha\alpha$ steranes, similar methylphenanthrene Index (MPI1) values), while there were only minor facies variations suggested by some facies sensitive parameters such as the homohopane index, and Gammacerane Index and the contradicting behaviour of maturity sensitive parameters. Principal component analysis enlarged these variations as suggested by the 14% variance explained by facies related parameters in Figure 4-37.

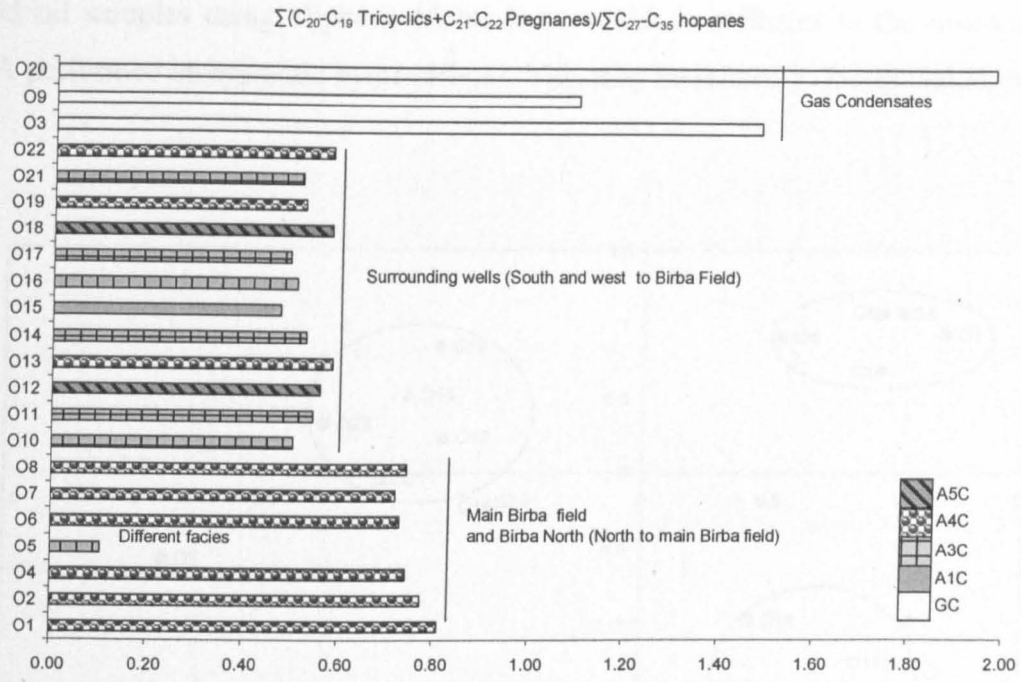

Figure 4-38: Histogram showing the PCA derived parameter ((Tricyclics+pregnanes)/hopanes) for all 22 oil samples including gas condensates. Refer to Figure 4-35 for the geographic distribution of the samples.

4.3.5.2 Aromatic biomarkers and hydrocarbons

Principal component analysis was also performed on 16 samples using the concentrations of 51 compounds of aromatic biomarkers and hydrocarbons listed in Appendix 4. 6. Few samples were excluded from the whole set because they can be distinguished from others very clearly. The results are illustrated by the cross plot of the first two principal components in Figure 4-39 and the cross plot of loading of the 51 components in Figure 4-40. The first two principal components explain about 58.8% of the variation. Three main groups can be distinguished from the plot of the first two components, A, B, and C. Group A consists of all well Omraan1 and well Omraan1H3 oils in the north west of Greater Birba Area as well as well Shamah1 in the South east and group B includes well BB1 and well BB2 oils in the main Birba field and group C consists of well Durra1 and well Kaulkab1 oils in the south west of Greater Birba area. It is very important to notice that the resulted grouping is different to that found by using aliphatic biomarkers in the previous section but does not contradict it. This distinguishes further between surrounding wells to Birba field (Group B), in to two groups (mainly Omraan1 and Omraan1H3 samples) and C (Durra1 AND Kaukab1). However, O7 from well BBN2 was grouped with Birba

Field oil samples using aliphatic biomarkers, which is different to the outcome of PCA performed on aromatic hydrocarbons. This may be related to facies variation.

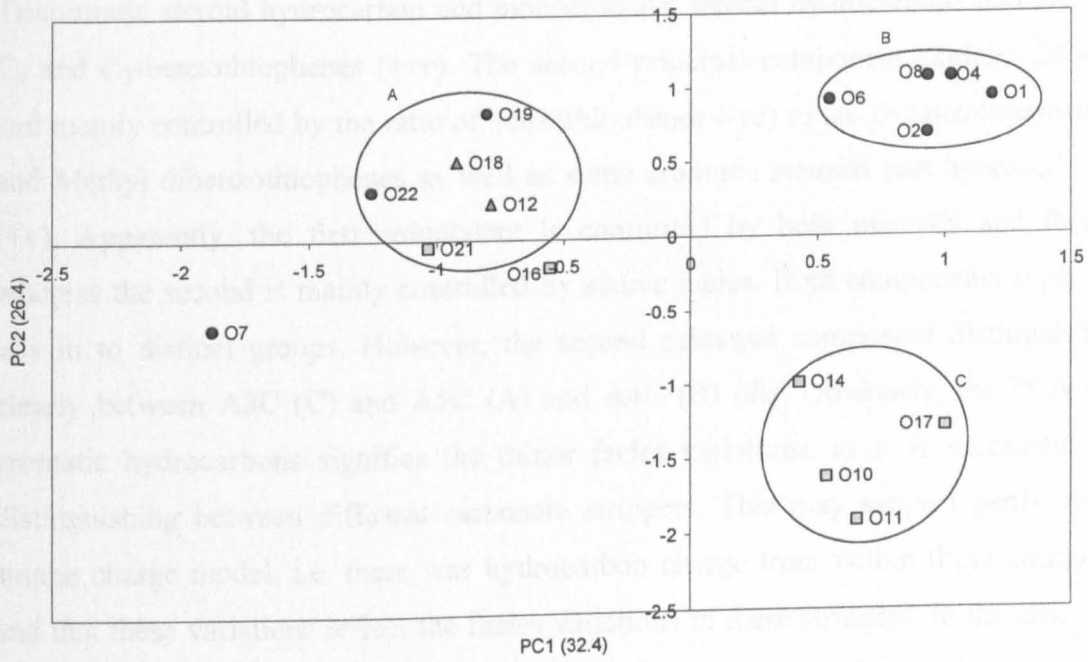

Figure 4-39: A cross plot of PC1 versus PC2 of 16 oil samples, derived from Principal component analysis on 51 aromatic hydrocarbons and biomarkers. Refer to Figure 4-35 and Table 4-10 for the locations and the description of the samples used. The amount of variations explained is put in brackets (%) near each principal component.

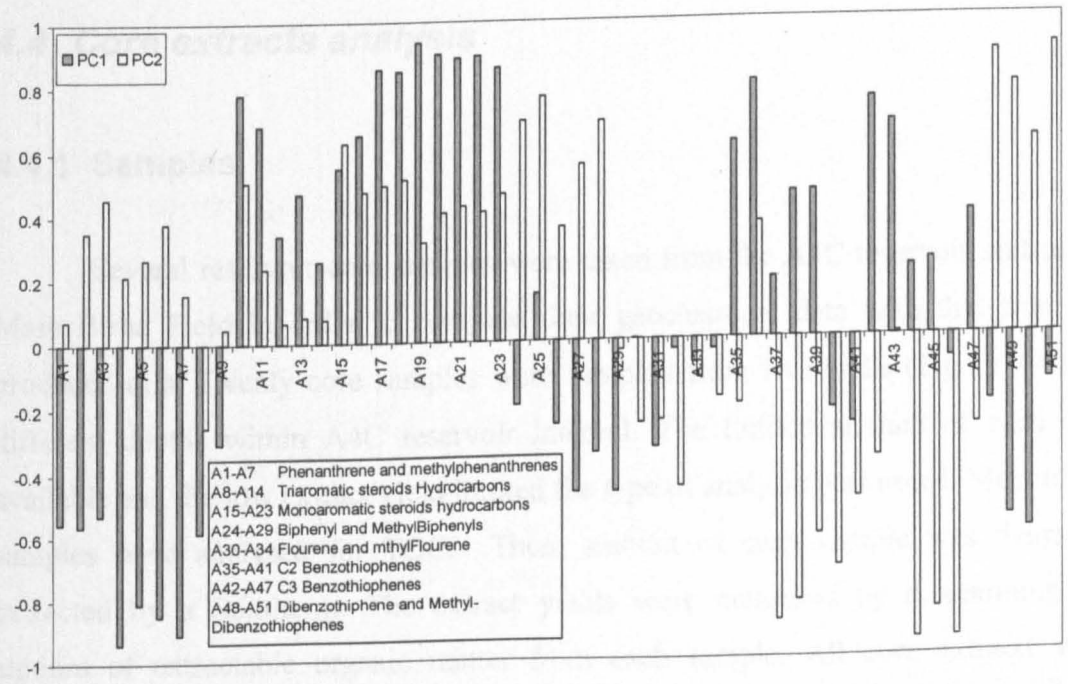

Figure 4-40: PC1 and PC2 loadings of 51 aromatic hydrocarbons and biomarkers for 16 oil samples. The full definitions of the compounds used are listed in Appendix 4. 6.

The first principal component explains 32.4% and mainly controlled by the relative proportions of phenanthrene and methylphenanthrene and the low molecular weight Triaromatic steroid hydrocarbons (-ve) versus the high molecular weight Triaromatic steroid hydrocarbon and monoaromatic steroid hydrocarbons and few of C_2 and C_3-benzothiophenes (+ve). The second principal component explains 26.4% and mainly controlled by the ratio of benzothiophenes (-ve) to the Dibenzothiophenes and Methyl dibenzothiophenes as well as some aromatic steroids and hydrocarbons (+v). Apparently, the first component is controlled by both maturity and facies whereas the second is mainly controlled by source facies. Both components separate oils in to distinct groups. However, the second principal component distinguishes clearly between A3C (C) and A5C (A) and A4C (B) oils. Obviously, the PCA on aromatic hydrocarbons signifies the minor facies variations, as it is successful to distinguishing between different carbonate stringers. This may support partly self-source charge model, i.e. there was hydrocarbon charge from within these stringers and that these variations reflect the facies variations in these stringers. In the absence of reliable basin modeling studies and detailed geochemical correlations that compare between these oils and the kerogens of host facies this is difficult be proved.

4.4 Core extracts analysis

4.4.1 Samples

Several reservoir core samples were taken from the A4C reservoir unit of the Main Birba Field in order to compare their geochemical data with that from the produced oils. Twenty core samples were sampled from five wells (Figure 4-41) at different depths within A4C reservoir interval. The limited amount of each core available and the low extract yield limited the type of analysis performed. Most of the samples were analysed for TOC. Then, amount of each sample was thermally extracted by a Soxtherm. The extract yields were measured by determining the amount of extractable organic matter from each sample. All core extracts were analysed by Iatroscan for bulk compositions. Eighteen of these samples were deasphalted (asphaltenes was removed from each sample by centrifugation) and the

maltene fractions were analysed by GC. Thirteen of the maltene fractions were separated by the pre-packed C18-nonendcapped SPE columns into hydrocarbons and non-hydrocarbons. The hydrocarbons fractions were further separated by silver nitrate impregnated silica into aliphatic and aromatic hydrocarbons, which were subsequently analysed by GC-MS (full method is described in chapter 3).

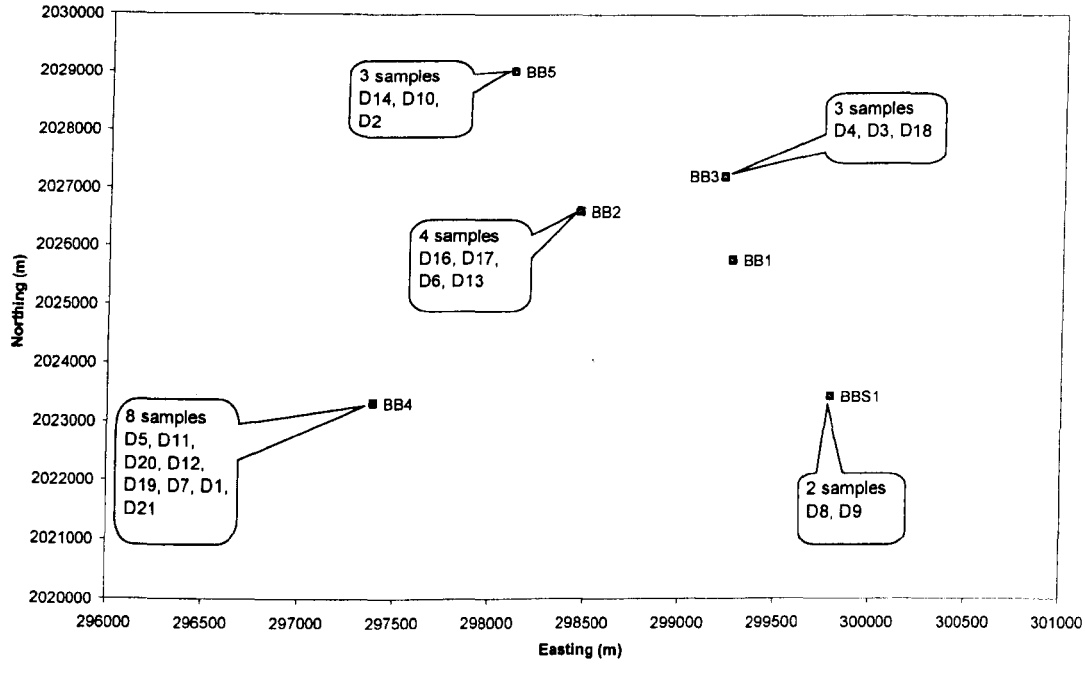

Figure 4-41: The location of the wells, from which the core samples were taken. D8 and D9 are samples taken from gas zone in well BBS1.

4.4.2 Extract yields, bulk compositions and whole oil chromatograms

Table 4-11 shows the extract yields (weight of the solvent extractable organic matter/weight of the core sample extracted), TOC, the bulk composition and few GC derived ratio. It is clear that TOC is very low for a reservoir core sample. This may be due to that most of the petroleum is in the fractures of the carbonate stringers. This is supported by the poor relationship between TOC or extract yields and porosity as illustrated in Figure 4-42. Carbonate stringers reservoirs in the Greater Birba area are characterised by low quality (tight porosity and permeability). The low TOC may suggest that the reservoir rocks are not rich in organic matter. However, this study

was not based on high density sampling; therefore this implication should be taken with caution.

Table 4-11: The bulk composition of core extracts and *n*-alkane/isoprenoid ratios. All core samples were taken from A4C carbonate stringer.

sample ID	Wells	Depth ft	TVD (m)	TOC%	Extract yields mg/g rock	Porosity%	Sat mg/g	Aro mg/g	NSO mg/g	Asp mg/g	Pr/Ph	Pr/C17	Ph/C18
D16	BB2	9306.0	2580.0	0.52	6.83	5.10	2.73	0.31	9.86	0.28	0.32	0.33	0.88
D17	BB2	9578.0	2581.2	0.97	3.60	1.40	6.37	1.91	10.15	0.87	0.34	0.33	0.99
D6	BB2	9283.0	2587.0	0.53	7.56	15.10	0.80	0.60	0.59	0.02	0.25	0.57	0.89
D13	BB2	9287.0	2669.9	0.15	4.99	7.30	1.35	0.32	0.71	0.04	0.35	0.50	1.14
D18	BB3	9599.9	2660.3	0.61	6.18	12.50	4.47	2.86	13.49	0.75	0.29	0.33	0.99
D4	BB3	9574.5	2673.4	0.40	14.21	9.70	0.67	0.44	0.46	0.02	0.37	0.41	0.76
D3	BB3	9531.5	2681.0	0.23	11.69	11.50	0.65	0.44	0.46	0.03	0.31	0.42	0.76
D5	BB4	9645.9	2655.9	0.26	8.79	1.70	0.51	0.12	0.31	0.05	0.46	0.34	0.82
D11	BB4	9532.5	2659.4	0.25	19.33	11.40	12.37	6.44	9.52	0.38	0.48	0.37	0.69
D20	BB4	9628.0	2660.4	0.15	13.21	11.40	2.89	1.93	3.37	0.39	*no GC*	*no GC*	*no GC*
D12	BB4	9543.9	2668.2	0.35	12.91	13.10	5.64	3.78	4.38	0.64	*no GC*	*no GC*	*no GC*
D19	BB4	9589.9	2673.4	0.20	8.49	5.00	0.48	0.25	1.56	0.21	0.44	0.31	0.71
D7	BB4	9572.7	2685.0	0.50	5.04	8.00	1.05	0.90	2.13	0.42	0.43	0.32	0.73
D1	BB4	9547.0	2690.5	0.60	2.29	8.90	0.31	0.16	0.42	0.07	0.50	0.28	0.54
D21	BB4	9652.0	2692.3		6.21	8.20	7.52	4.67	8.46	0.35	0.37	0.34	0.66
D14	BB5	9982.5	2752.5	0.30	3.44	4.70	0.36	0.14	0.16	0.01	0.44	0.39	0.94
D10	BB5	9942.5	2782.2	0.59	3.05	10.30	0.32	0.15	0.22	0.04	0.40	0.36	0.77
D2	BB5	9845.0	2794.4	0.70	3.84	1.30	0.56	0.20	0.40	0.05	0.54	0.31	0.60
D8	BBS1	8481.0	2337.9	0.40	4.89	12.60	0.29	0.10	0.28	0.04	0.23	0.30	0.86
D9	BBS1	8500.0	2343.7	0.84	3.08	5.90	0.30	0.11	0.29	0.05	0.23	0.48	1.23

Key: TVD = true vertical depth, TOC = total organic carbon, sat (Iatroscan) = saturated hydrocarbons yields in mg/g rock, aro (Iatroscan) =aromatic hydrocarbons yield in mg/g rock, Asp (Iatroscan) = asphaltene in mg/g rock. Pr =pristane, Ph = phytane.

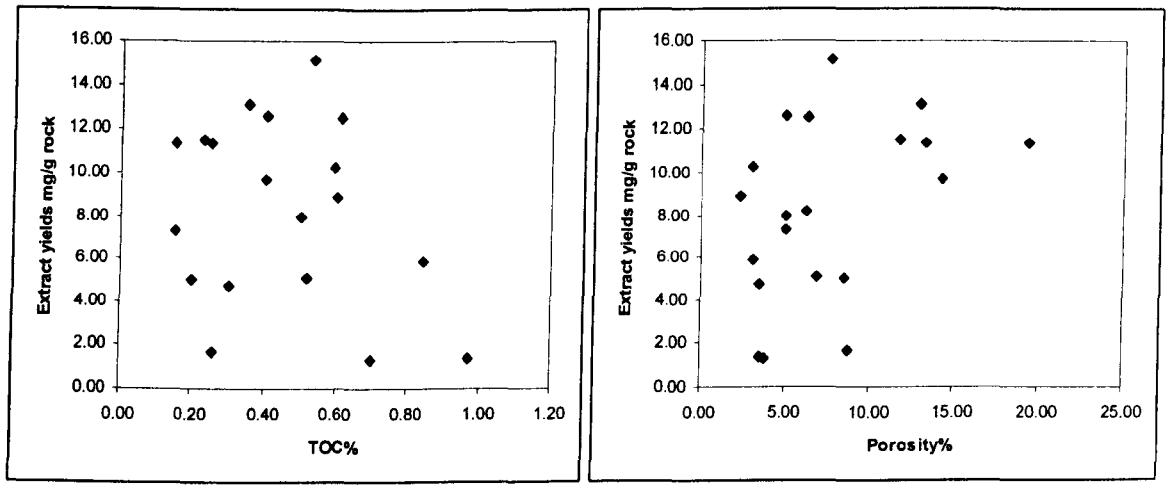

Figure 4-42: a cross plot of extract yields versus TOC (left), and porosity (right).

The bulk compositions of the core extracts are dominated by saturated hydrocarbons in most samples but there are large lateral and vertical variations as obvious from Figure 4-43. The very low extract yields (<10mg/g rock) as shown in Table 4-11 might be the source of the high variability observed in the bulk compositions of the studied samples. Wells BB2 and BB3 are characterized by relatively high polar concentrations in the top of the stringer (polar fraction>40%, 10-13mg/g) (Figure 4-43), while most of the other core samples are saturate rich. All three samples indicate normal oils in BB5, however, this well was not successful and

A4C was found water bearing. The pressure data indicate that this well is in the water leg (section 2.9). The presence of this bitumen in water leg (this bitumen has similar characteristics to oils in oil leg) may suggest vertical migration as proposed in this study. Another possible scenario is that this water zone was oil leg initially but then some oil was leaked and cause shrinkage of oil leg. Higher density of samples was taken from BB4 (eight samples) which is dried well. In this well, the saturated hydrocarbons decrease whereas aromatic HC increase towards the middle of the interval, which exhibits the highest content of polars (>8mg/g). This well was found tight and there was no enough driving pressure to produce oil (PDO internal report).

The samples were taken from cores, which are about 25 years old and kept in temperatures 20 to 30°C. Gas chromatograms of these extracts show substantial losses of lower (C_{10}-C_{15})) and middle (C_{16}-C_{20}) molecular weight n-alkanes. Table 4-11 shows several common n-alkane/isoprenoid parameters although these might not be reliable due to the reason above. However, all samples show similar Pr/Ph ratios (<0.55) and no major variation between most of the samples in the ratios of isoprenoids to *n*-alkanes. These extracts correlate well with produced oils in terms of these ratios (Figure 4-45).

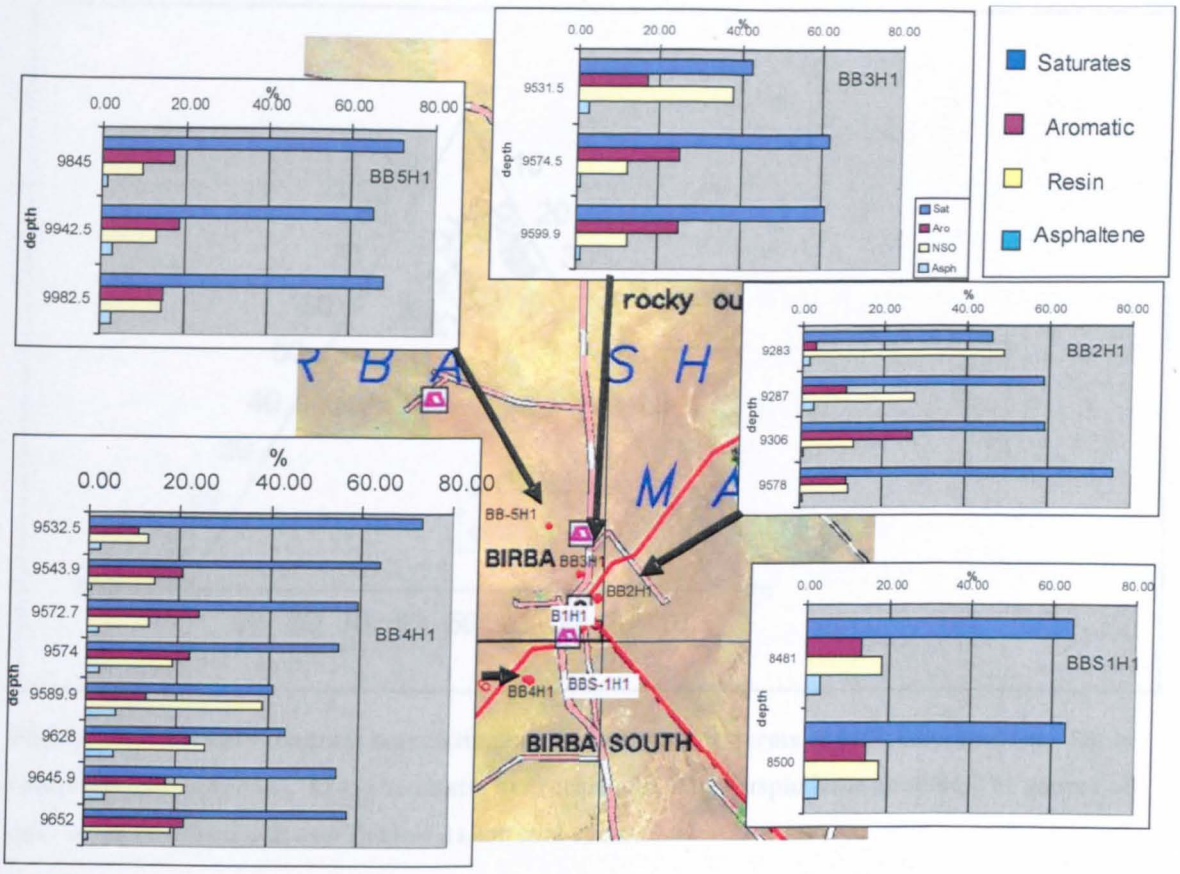

Figure 4-43: The bulk composition (SARA analysis by Iatroscan) of core extracts from five wells in Birba Field. Depths are in feet.

The bulk compositions of extracts versus produced oils are shown in Figure 4-44. Although the extracts show higher NSO + Asphaltene content as expected from reservoir rocks, they correlate fairly well with the produced oils except for D16, D18, and D12, which were characterised by higher NSO content. The relative distributions of the C_{27}-C_{29} steranes were also used to compare extracts and produced oils. They all cluster in a very narrow range of percentages as shown in Figure 4-44. It is expected that reservoir core extracts should show slightly different bulk composition to oils by having higher NSO compounds and asphaltene and lower saturates. The difference depends on the quality of the reservoir rocks, the lower the quality the higher the difference. Figure 4-45 shows that the core extracts are probably not genetically different from produced oils. They cluster together with some scatter in core extracts suggesting that there are small facies differences.

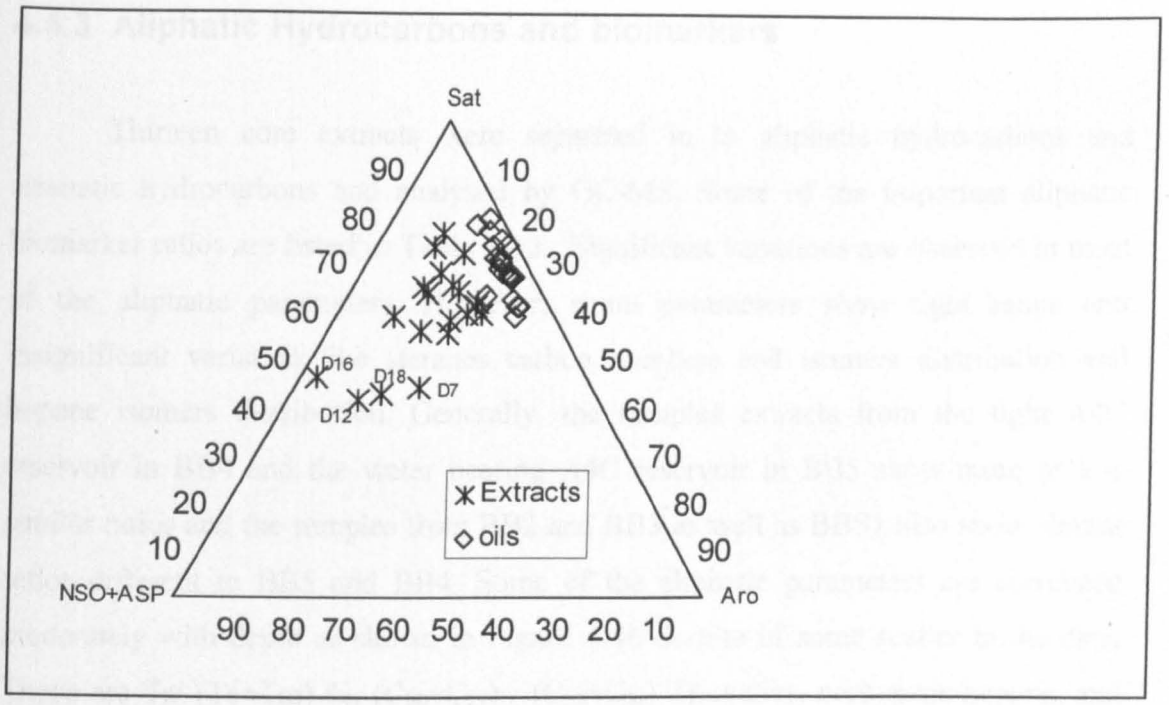

Figure 4-44: Ternary diagram correlating oils and extracts in terms of bulk compositions. Sat is saturated hydrocarbons, Aro is aromatic hydrocarbons, Asp = asphaltene content. The source of data is Table 4-2 for oils and Table 4-11 for core rocks.

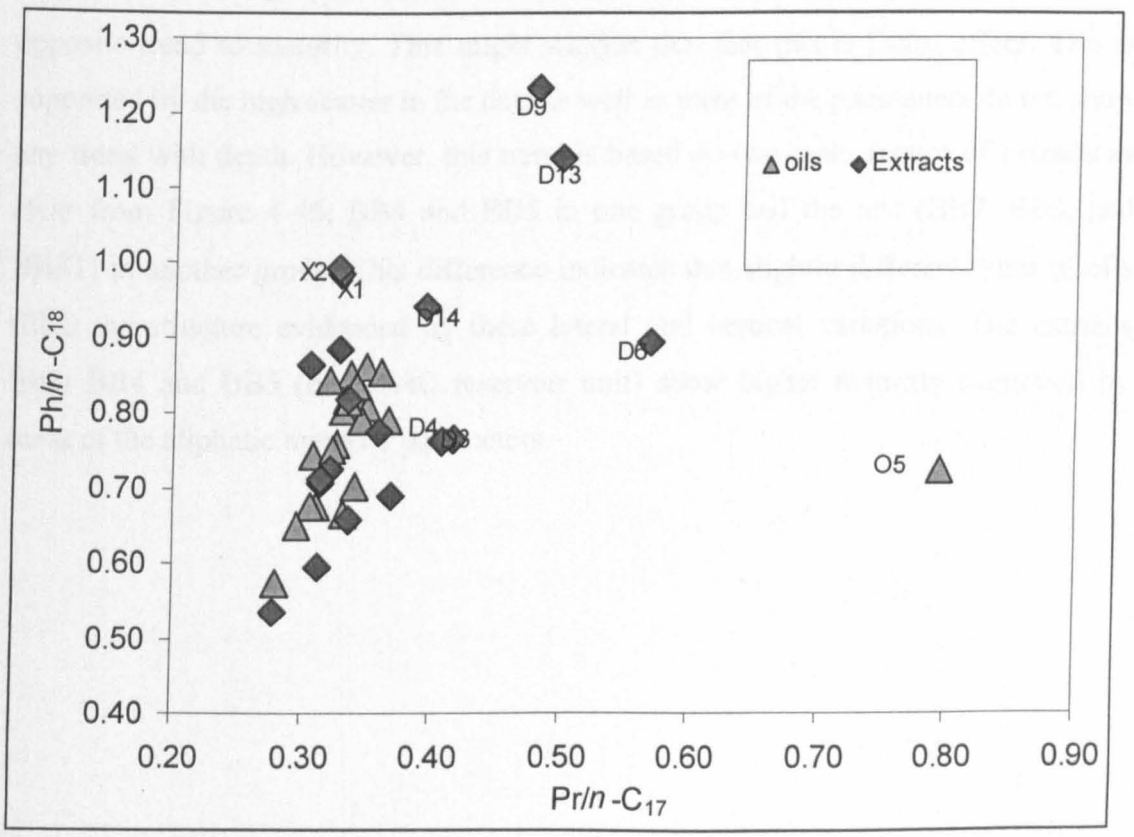

Figure 4-45: Pr/n-C_{17} versus Ph/n-C_{18} of the whole oils and extracts.

4.4.3 Aliphatic Hydrocarbons and biomarkers

Thirteen core extracts were separated in to aliphatic hydrocarbons and aromatic hydrocarbons and analysed by GC-MS. Some of the important aliphatic biomarker ratios are listed in Table 4-12. Significant variations are observed in most of the aliphatic parameters. However, some parameters show tight range and insignificant variation like steranes carbon numbers and isomers distribution and hopane isomers distribution. Generally, the samples extracts from the tight A4C reservoir in BB4 and the water bearing A4C reservoir in BB5 show more or less similar ratios and the samples from BB2 and BB3 as well as BBS1 also show similar ratios different to BB5 and BB4. Some of the aliphatic parameters are correlated moderately with depth as shown in Figure 4-46 despite of some scatter in the data. Those are Ts/ (Ts+Tm) %, (C_{20}+C_{21}) / (C_{23}+C_{24}) Tricyclics, norhopane/hopane, and C_{28}+C_{29} Tricyclics/ C_{29}+$C_{30}\alpha\beta$ hopanes. The first three parameters show increase with depth whereas the last parameter decreases with depth. while Ts/(Ts+Tm)% and norhopane/hopane may suggest that this increase is probably related to maturity, the parameters (C_{20}+C_{21})/(C_{23}+C_{24}) and (C_{28}+C_{29} Tricyclics)/(C_{29}+$C_{30}\alpha\beta$ hopanes) show opposite trend to maturity. This might suggest that that this is facies effect. This is supported by the high scatter in the data as well as most of the parameters do not show any trend with depth. However, this trend is based on two main groups of extracts as clear from Figure 4-46, BB4 and BB5 in one group and the rest (BB2, BB3, and BBS1) in another group. This difference indicates that slightly different types of oils filled the structure evidenced by these lateral and vertical variations. The extracts from BB4 and BB5 (both A4C reservoir unit) show higher maturity suggested by most of the aliphatic maturity parameters.

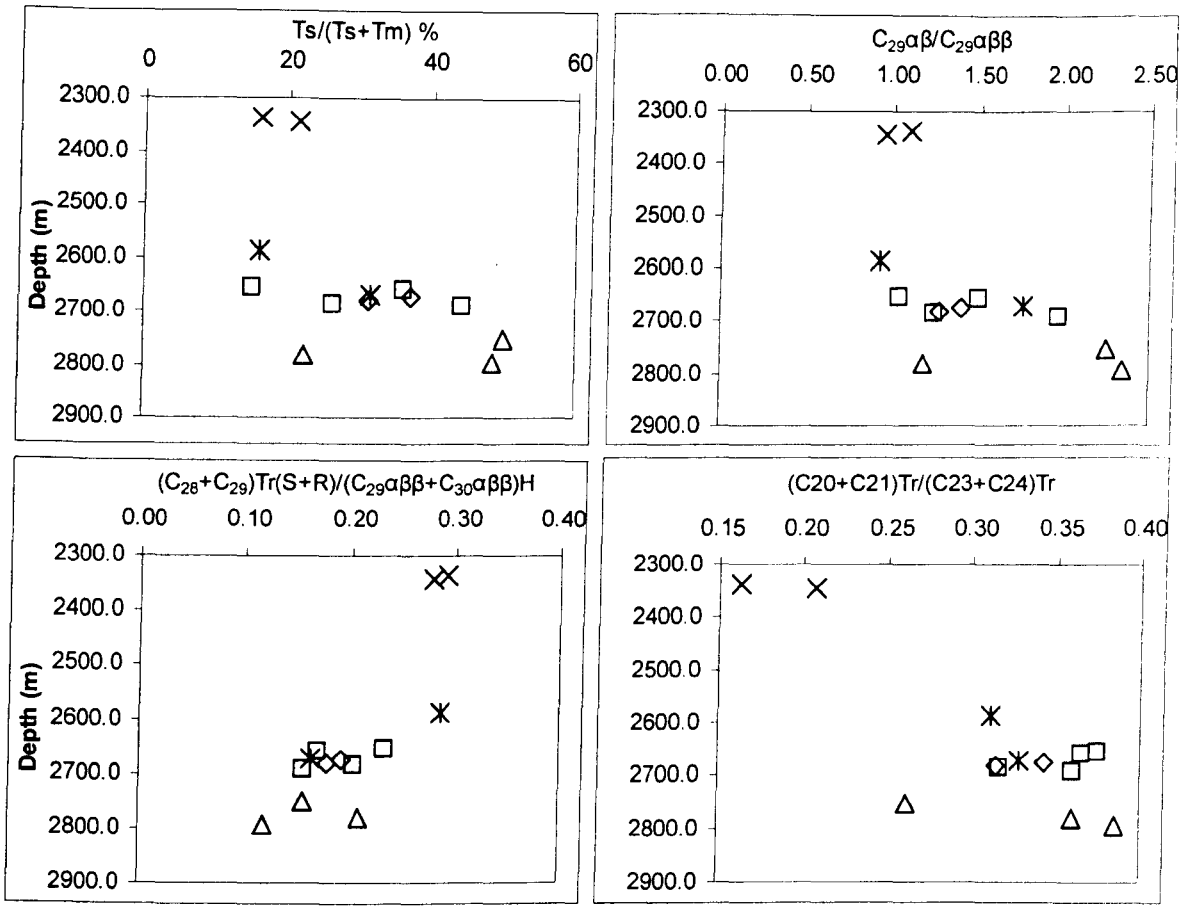

Figure 4-46: The relationship between some aliphatic hydrocarbon biomarker parameters and depth for all wells. BBS1 (cross), BB2 (Asterisks), BB3 (diamonds), BB4 (Squares), and BB5 (Triangles). ab = αβ, Tr = Tricyclics.

Figure 4-47 shows that the core extracts are well correlated with oils except for few samples using sterane carbon number distributions. The aliphatic maturity parameters ($(C_{20}+C_{21})/(C_{23}+C_{24})$, %Ts/ (Ts+Tm), $C_{21}+C_{22}$ pregnanes/C_{27}-C_{29} steranes, $\%C_{29}\alpha\beta\beta/(\alpha\alpha\alpha+\alpha\beta\beta)$ and $\%C_{29}S/(S+R)$)) show that the core extracts are relatively more mature than produced oils. This indicates that the fresh new charges of oil that flooded the Birba Field were from another source of lower maturity. There were no big variations among maturity parameters identified in produced oils and so the filling direction of these new charges cannot be predicted.

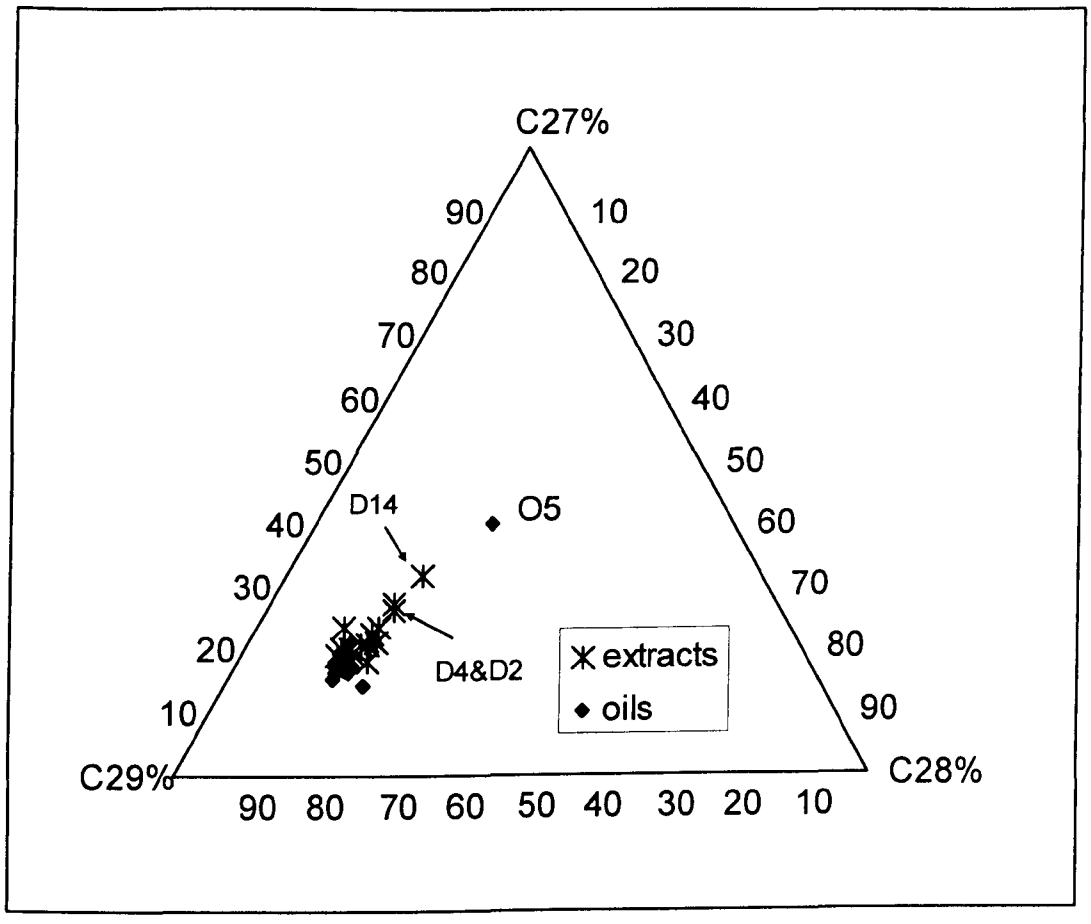

Figure 4-47: Ternary diagram correlating extracts and oils using the relative abundance of the C_{27}, C_{28}, and C_{29} steranes.

Table 4-12: Aliphatic hydrocarbon biomarker ratios for core extracts. Most of these parameters are defined in Appendix 4. 2.

Wells	Sample ID	Depth (m)	Ts/(Tm+Ts)%	Ts/$C_{30}\alpha\beta H$	C_{32}% 22S/(22R+22S)	Gammacerane Index	$(C_{20}+C_{21})Tr$ / $(C_{23}+C_{24})Tr$	C_{28}/C_{29} (Tri)	C_{23}/C_{21} (Tri)	C_{23}/C_{24} (Tri)	C_{26}/C_{25} Tri(S+R)	C_{24}Tetra/ C_{23}Tri
BBS1	D8	2337.9	16	0.10	58	0.17	0.16	1.31	5.98	2.12	1.00	0.22
BBSI	D9	2343.7	21	0.16	56	0.19	0.21	2.17	5.11	2.05	0.99	0.16
BB2	D6	2587.0	16	0.12	59	0.25	0.31	0.99	3.69	2.18	0.96	0.16
BB4	D5	2655.9	15	0.09	59	0.28	0.37	1.11	3.32	2.46	0.98	0.15
BB4	D11	2659.4	36	0.35	57	0.21	0.37	1.54	3.33	2.41	0.82	0.27
BB2	D13	2669.9	32	0.28	55	0.13	0.33	1.01	3.57	2.27	1.22	0.33
BB3	D4	2673.4	37	0.39	61	0.19	0.34	1.32	3.56	2.37	0.92	0.27
BB31	D3	2681.1	31	0.14	60	0.25	0.31	1.17	3.70	2.35	0.97	0.29
BB4	D7	2685.1	26	0.20	56	0.15	0.32	1.79	4.14	2.66	0.97	0.19
BB4	D1	2690.5	44	0.46	59	0.09	0.36	1.47	3.88	2.76	1.09	0.39
BB5	D14	2752.5	50	0.62	60	0.11	0.26	1.20	4.25	1.98	0.90	0.62
BB5	D10	2782.2	22	0.17	58	0.23	0.36	1.73	3.34	2.47	0.96	0.18
BB5	D2	2794.4	48	0.55	59	0.13	0.38	1.16	3.33	2.73	0.88	0.52
STD			12.24	0.18	1.85	0.06	0.07	0.35	0.79	0.25	0.10	0.15
Sample	**Sample ID**	**Depth**	$C_{23}Tri/C_{30}\alpha\beta H$	$C_{24}Tetr/C_{30}\alpha\beta H$	$[(C_{28}+C_{29})$ Tri(S+R)] /(C29αβ+C30αβ)H	C27%St	C28%St	C29%St	Preg/St	C29% αββ/(αββ+ααα)	C29% 20S/(20S+20R)	$C_{29}\alpha\beta/C_{29}\alpha\beta\beta$
BBS1	D8	2337.9	1.20	0.26	0.41	19.34	21.08	59.58	0.18	57.18	46.95	1.09
BBSI	D9	2343.7	1.47	0.24	0.39	18.45	20.30	61.25	0.19	59.76	54.59	0.94
BB2	D6	2587.0	1.60	0.26	0.40	22.11	22.25	55.65	0.25	59.10	46.04	0.92
BB4	D5	2655.9	1.32	0.19	0.30	19.62	21.60	58.78	0.21	58.18	45.13	1.03
BB4	D11	2659.4	1.12	0.30	0.20	20.03	22.34	57.63	0.24	57.63	44.86	1.51
BB2	D13	2669.9	0.79	0.26	0.19	22.07	17.00	60.93	0.19	58.41	45.94	1.76
BB3	D4	2673.4	1.16	0.31	0.24	26.13	21.03	52.84	0.24	57.67	44.62	1.40
BB31	D3	2681.1	0.79	0.23	0.22	17.02	23.12	59.86	0.16	57.73	46.07	1.28
BB4	D7	2685.1	1.40	0.26	0.26	19.77	15.29	64.94	0.24	60.17	49.58	1.24
BB4	D1	2690.5	0.65	0.25	0.19	21.71	19.72	58.57	0.15	54.92	45.92	1.97
BB5	D14	2752.5	0.62	0.38	0.19	30.47	22.51	47.03	0.16	54.62	46.21	2.25
BB5	D10	2782.2	1.47	0.27	0.26	17.90	18.08	64.03	0.24	58.73	46.06	1.19
BB5	D2	2794.4	0.51	0.27	0.13	24.91	22.18	52.91	0.19	55.52	46.87	2.35
STD			0.37	0.05	0.09	3.76	2.38	4.91	0.04	1.74	2.63	0.48

4.4.4 Aromatic hydrocarbons and biomarkers

Table 4-13 show selected parameters obtained from aromatic biomarkers and hydrocarbons distribution. Some of the parameters show tight range of values for most of the samples, however a number of them shows large variation that could tell about the history of the reservoir filling. There is poor correlation between those parameters and depths for all samples (Figure 4-48). Therefore, those parameters with large variation are analyzed by statistical evaluation using principal component analysis.

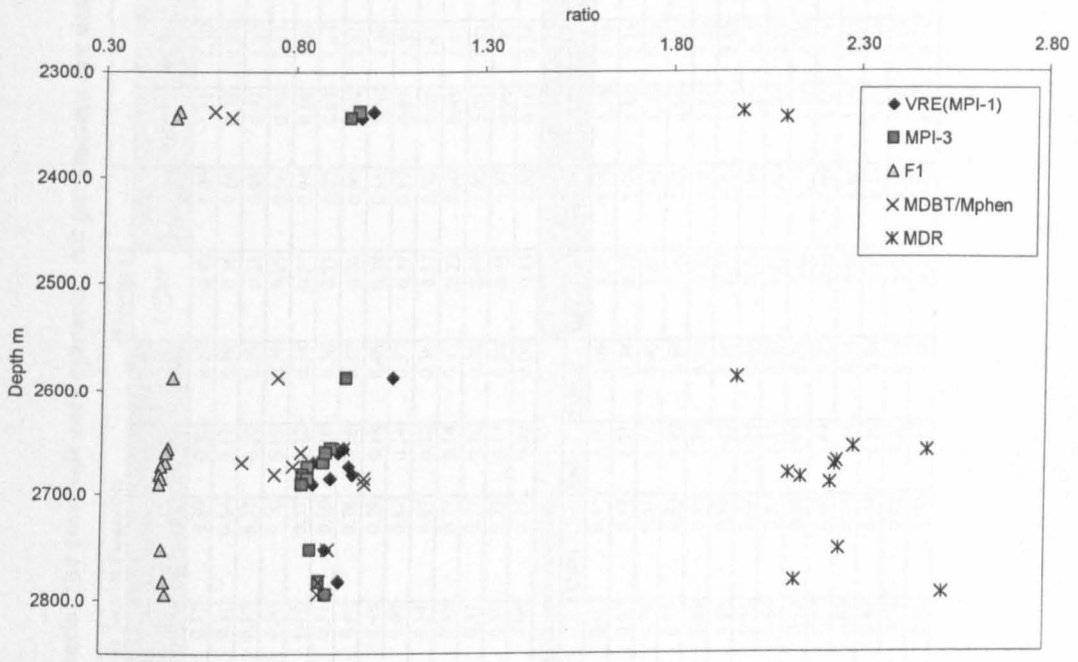

Figure 4-48: some aromatic parameter show poor correlation and minor variation in some other with depth. See Appendix 4. 2.

Table 4-13: Selected aromatic parameters to characterise the reservoir core extracts. All parameters are described and listed in Appendix 4-2.

			Triaromatic and Monoaromatic Steroids Parameters						Fluorenes		Phenanthrene and alkyl Phenanthrenes parameters							
Wells	TVD (m)	Sample ID	TA $C_{20}/(C_{20}+C_{28})$	TA $C_{26}20S/C_{28}20S$	TA $C_{27}20R/C_{28}20R$	MA/ (MA+TA)	MA I/(I+II)	TA (I/I+II)	F/∑MF	VRE (MPI-1)	MPI-1	MPR	MPR-1	MPI-2	MPI-3	MPR-9	F1	F2
BB2	2587.0	D6	0.27	0.12	0.37	0.39	0.20	0.34	0.48	1.06	1.11	1.39	1.48	1.33	0.94	2.17	0.48	0.29
BB2	2669.9	D13	0.31	0.10	0.31	0.64	0.17	0.39	0.36	0.86	0.76	1.37	0.59	1.03	0.88	0.76	0.47	0.32
BB3	2673.4	D4	0.32	0.11	0.37	0.71	0.20	0.39	0.21	0.95	0.92	1.31	1.15	1.24	0.84	1.52	0.46	0.31
BB31	2681.1	D3	0.31	0.12	0.36	0.70	0.19	0.38	0.29	0.96	0.94	1.33	1.29	1.27	0.83	1.76	0.45	0.31
BB4	2655.9	D5	0.27	0.10	0.39	0.57	0.22	0.34	0.27	0.94	0.89	1.49	0.81	1.23	0.90	1.13	0.47	0.33
BB4	2659.4	D11	0.29	0.12	0.37	0.69	0.16	0.36	0.23	0.92	0.87	1.44	0.80	1.18	0.89	1.10	0.47	0.32
BB4	2685.1	D7	0.31	0.14	0.40	0.76	0.20	0.37	0.26	0.90	0.84	1.31	0.88	1.15	0.84	1.10	0.46	0.31
BB4	2690.5	D1	0.41	0.13	0.43	0.79	0.18	0.46	0.39	0.86	0.76	1.29	0.69	1.04	0.83	0.89	0.45	0.31
BB5	2752.5	D14	0.32	0.12	0.40	0.82	0.14	0.37	0.37	0.89	0.82	1.33	0.77	1.11	0.85	1.01	0.46	0.31
BB5	2782.2	D10	0.29	0.12	0.34	0.67	0.22	0.36	0.52	0.93	0.88	1.41	0.86	1.20	0.88	1.16	0.47	0.32
BB5	2794.4	D2	0.40	0.15	0.46	0.77	0.14	0.45	0.29	0.90	0.83	1.41	0.69	1.12	0.89	0.93	0.47	0.32
BBS1	2337.9	D8	0.30	0.14	0.37	0.71	0.16	0.38	0.66	1.00	1.01	1.41	0.96	1.24	0.97	1.30	0.49	0.30
BBSI	2343.7	D9	0.30	0.11	0.31	0.73	0.17	0.38	0.45	0.97	0.96	1.45	0.84	1.19	0.94	1.23	0.49	0.30
STD			0.04	0.01	0.04	0.11	0.03	0.04	0.13	0.06	0.10	0.06	0.26	0.09	0.05	0.38	0.01	0.01

			Naphthalene and alkyl naphthalene parameters						Alkyldibenzothiophene					C_2&C_3 AlkylBenzothiophene		Biphenyls Parameters		
Wells	TVD (m)	Sample ID	MNR	DNR-1	DNRx	TNR1	ENR	TMNR-1	MDR1	MDR4	MDR2,3	MDR	(2+3-MDBT)/1-MDBT	C/F	3+4/6	DBF/Bp	4MBP/Bp	DBT/P
BB2	2587.0	D6	1.28	3.80	0.89	0.52	2.09	1.09	1.91	3.78	3.10	1.98	1.62	0.59	0.62	0.25	0.46	0.62
BB2	2669.9	D13	0.94	2.98	0.67	0.63	1.91	0.74	0.93	2.09	1.44	2.25	1.55	0.82	0.64	0.15	0.20	0.38
BB3	2673.4	D4	1.01	2.89	0.78	0.51	1.76	0.41	1.07	2.41	1.76	2.24	1.64	0.66	0.50	0.06	0.56	0.75
BB31	2681.1	D3	1.05	2.98	0.75	0.53	1.90	0.68	1.24	2.62	2.00	2.12	1.61	0.65	0.54	0.07	0.50	0.72
BB4	2655.9	D5	0.76	2.53	0.63	0.57	1.68	0.76	0.72	1.65	1.21	2.29	1.68	0.67	0.72	0.06	1.26	0.96
BB4	2659.4	D11	0.88	2.51	0.64	0.60	1.63	0.78	0.75	1.85	1.32	2.49	1.77	0.52	0.63	0.05	0.94	0.75
BB4	2685.1	D7	0.91	2.21	0.64	0.51	1.54	0.63	0.73	1.56	1.25	2.15	1.72	0.49	0.68	0.05	0.70	1.02
BB4	2690.5	D1	0.94	2.49	0.68	0.52	1.57	0.70	0.65	1.46	1.07	2.23	1.64	0.49	0.67	0.09	1.14	0.90
BB5	2752.5	D14	0.85	2.60	0.63	0.50	1.75	0.81	0.68	1.53	1.19	2.25	1.75	0.58	0.66	0.07	0.59	0.87
BB5	2782.2	D10	1.29	2.60	0.77	0.60	1.84	0.47	0.98	2.08	1.53	2.14	1.57	0.58	0.59	0.06	0.37	0.73
BB5	2794.4	D2	0.87	2.39	0.63	0.51	1.66	0.74	0.65	1.65	1.14	2.53	1.74	0.48	0.58	0.07	1.56	0.78
BBS1	2337.9	D8	1.12	3.38	0.88	0.54	1.70	0.84	1.17	2.33	1.87	1.99	1.60	0.51	0.64	0.21	0.41	0.48
BBSI	2343.7	D9	1.05	2.63	0.74	0.61	1.77	0.95	1.05	2.20	1.78	2.10	1.70	0.56	0.62	0.13	0.40	0.50
STD		STD	0.16	0.44	0.09	0.05	0.15	0.18	0.35	0.63	0.55	0.16	0.07	0.10	0.06	0.07	0.40	0.19

Principal component analysis was performed on those highly variable aromatic parameters (see Figure 4-50 to know these parameters). It reveals two main groups (Figure 4-49); these are BB4 and BB5 in one group and the BB3 and BBS1 in another group. BB2 can also be included in the second group. They are separated mainly by the first principal component (PC1) which explains about 43% of the variance. PC1 gives high positive loadings (Figure 4-50) for MA/(MA+TA), MPI-2, MDR, 4MBp/Bp and DBT/P and high negative loadings for MDR1, MDR4 and MDR2,3. Therefore, PC1 is controlled by both maturity and facies variations. Notice that most of the parameters are dibenzothiophene and methyl dibenzothiophenes ratios. Most of these are controlled by both maturity and facies even DBT/P (Cumbers *et al.*, 1987; Huang & Pearson, 1999; Peters & Moldowan, 1993; Radke *et al.*, 1986). Therefore, these two groups can only indicate different oil charges flooded the reservoir. This will help when these extracts are compared with the oils using these distinguishing parameters. BB5 (A4C) reservoir is at present under the OWC, and deeper with respect to other Main Birba Field wells, therefore this might potentially indicate filling direction. This distinction cannot be due to water washing because BB4 is correlated well with BB5 and yet it is above OWC. However, this indicate that the latest oil charge did not reach A4C in BB4 suggesting that the sealing fault that separate the BB4 block was there before this charge.

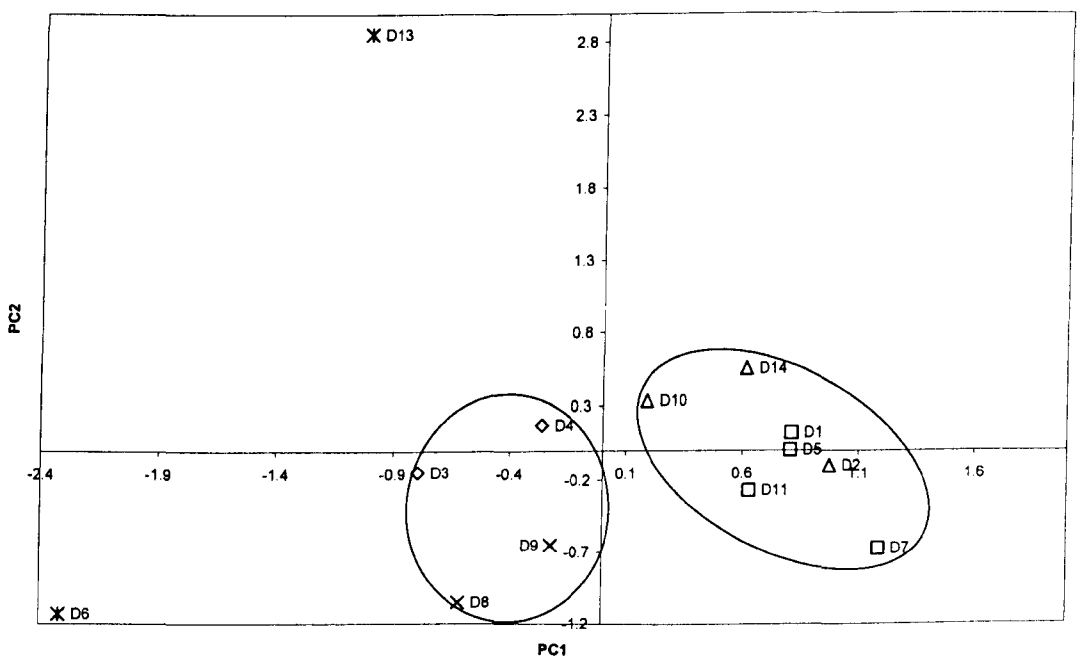

Figure 4-49: PC1 (43%) vs. PC2 (20%) of highly variable aromatic parameters. BBS1 (cross), BB2 (Asterisks), BB3 (diamonds), BB4 (Squares), and BB5 (Triangles)

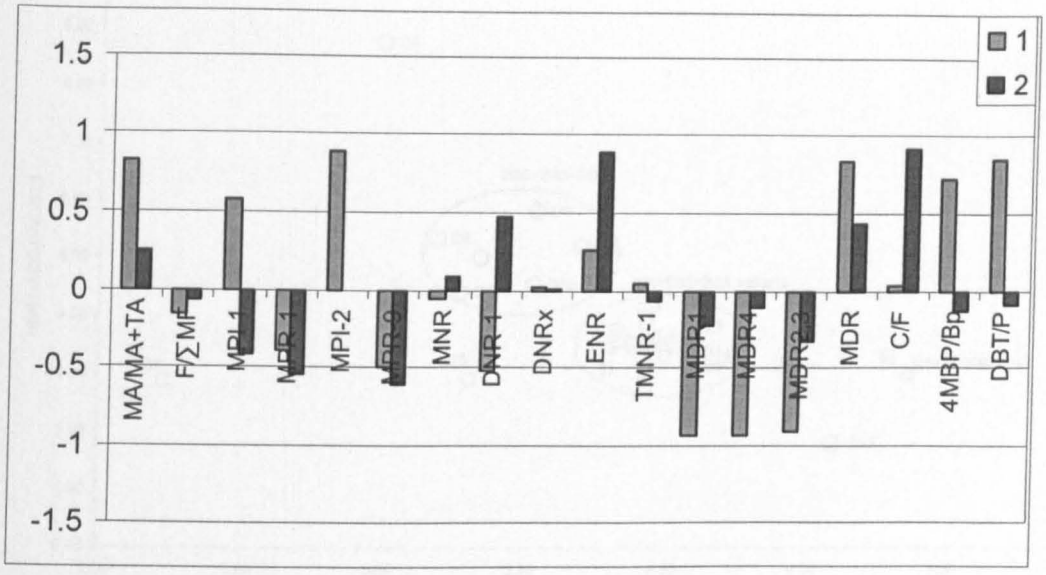

Figure 4-50: PC1 and PC2 loadings

Comparing reservoir extracts and produced oils might be useful. A cross plot of some highly variable parameters that distinguish between the two groups of extracts (derived from PCA analysis) for both oils and extracts to correlate them. This plot reveals that the oils in A4C and A3C reservoirs are similar to the oils in the water leg in BB5 and oil stain in the tight A4C reservoir of BB4. Both of the reservoirs in these wells are presently deeper than the other extracts from producing wells. It is possible that the oils in the carbonate stringers at present day reflects new charge different to that present in the bitumen. It is also important to note that the oils extracted from condensate zones are similar to other oils but different to the condensates. This suggests that the oil was there before the arrival of condensate charge that displace oil downwards.

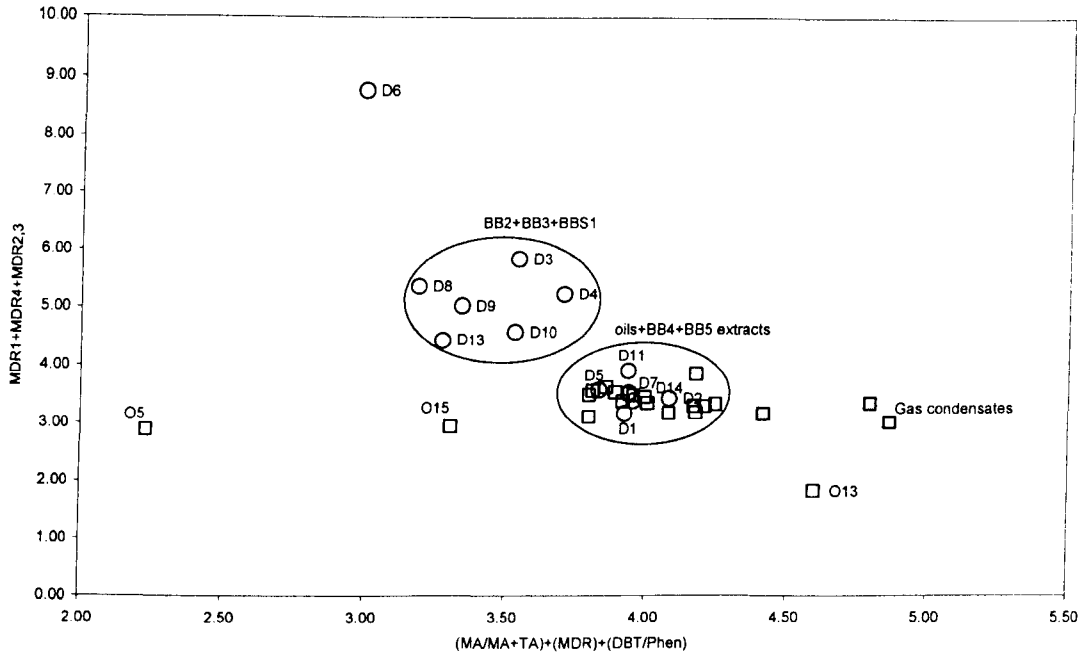

Figure 4-51 a cross plot of selected ratios for both oils and reservoir rock extracts. Gas condensates are filled squares, while the extracts and the oils are empty circles and squares respectively.

4.5 Gas analysis

4.5.1 Introduction

There are two main sources of natural gases in petroleum systems, bacterial and thermogenic gases (Tissot & Welte, 1984). Bacterial gases result from either microbial fermentation of light hydrocarbons or carbonate reduction and they are exclusively composed of methane (>99 vol. %) with a lighter methane carbon isotopic signature (<-55‰) (Rice & Claypool, 1981). Thermogenic gases are generated from any type of maturing kerogen (Tissot & Welte, 1984). However, the C_{2+} is generated mainly from kerogen type I and II because humic Kerogen or type III source rock expels mainly methane. At the early catagenesis, gas forms mainly from kerogen in source rocks concurrently with oil whereas at late thermal stages, the gas are generated by thermal cracking of oil and residual kerogen (Pepper & Dodd, 1995). The initial gases generated at low thermal maturity (<0.5 Ro%) are relatively dry but with increasing maturation, they become more wet (Hunt, 1995) and gas wetness (C_{2+}) might reach about 80% of the whole gases in some cases (Whiticar, 1994). As the gases become late mature (1.3-2 Ro%), they become methane rich again due to the cracking of oil and residual kerogen (Hunt, 1995). For high quality source rocks (Hydrogen Index>600 mg g /C), the oil to gas cracking window was predicted to vary in the range of 155-205°C, according to first order kinetic model and at heating rate of 2°C/Ma (Pepper & Dodd, 1995).

Most of the information from gas samples are stored in five saturated aliphatic compounds: methane, ethane, propane, and butane, while the higher carbon number hydrocarbons (C_5-C_7) are subjected to severe fractionation due to the possibility of pressure-temperature induced condensation during production and/or sampling (Whiticar, 1994). The relative proportions of C_1-C_4 normal alkanes in a gas sample are routinely used to classify any natural gas sample e.g. (Jenden & Kaplan, 1989; Prinzhofer & Huc, 1995; Zou *et al.*, 2006). Higher homologs than methane are better interpretive tools than methane because methane are ubiquitous and form by several

sources (Whiticar, 1994). Gas wetness is one of the tools that are used routinely to classify gases; this ratio has different definitions such as below:

Gas wetness (vol. %) $=(C_2+C_3+iC_4+nC_4)/(C_1+C_2+C_3+iC_4+nC_4) \times 100$ (Whiticar, 1994)

$= C_1/C_2$ .....from (Claypool, 1974)

$= 1/\Sigma C_{2+}$ from (Faber, 1987) in (Whiticar, 1994)

$= C_1/(C_2+C_3)$ Bernard Parameter from (Whiticar, 1994)

Bernard parameter can be used to assess the thermal maturity of the gas accumulation as described in Table 4-14.

Table 4-14: Gas wetness as an indicator for thermal maturity.

$C_1/(C_2+C_3)$ (Bernard parameter)	Thermal maturity level of gas
≈5	*When Generated from Kerogen type I/II*
>20	*Mature*
>50	*overmature*

Berner & Faber (1988) proposed mathematical expressions that relate the relative amounts (vol. %) of methane, ethane, and propane in an unaltered thermogenic natural gas to the level of thermal maturity (% R_o) specifically for sapropelic source rocks. These relationships are described by the equation and the diagram below. Methane is dominating at all stages of generation, and it increases with thermal maturity, (Berner & Faber, 1988).

% methane = $9.1 \ln(\% R_o) + 93.1$

% ethane = $-6.3 \ln(\% R_o) + 4.8$

% propane = $-2.9 \ln(\% R_o) + 1.9$

Non-hydrocarbon compounds such as N_2, H_2S, and CO_2 are often very important species in Natural gases, and store important information to petroleum geochemistry (Jenden & Kaplan, 1989; Whiticar, 1994). . The amount of sulphide depends on the source rock composition and the temperature (Orr, 1977). Sulphide (HS^-, H_2S) is abundant in marine environment and results from bacterial sulphate reduction (Orr, 1977). At deeper depths and higher temperatures, It can also result from thermal cracking (>120°C) of organic sulphur compounds especially in

evaporite-carbonate kerogens and generated oils (Orr, 1974; Orr, 1977). It can also be formed by thermochemical sulphate reduction, which has to be initiated by hydrogen sulphide (Orr, 1974). The natural gas that contains hydrogen sulphide greater than 1 vol. % is classified as Sour gas, and the sour gas may contain up to 30% hydrogen sulphide (Internet).

Carbon dioxide is also derived from several sources; mainly it is derived from degradation of organic matter, inorganic dissolution of carbonates at high temperatures (by the release of oxygen bearing groups) or degassing of the mantle (Cai *et al.*, 2002). Carbon dioxide can also be formed by diagenetic remineralisation such as decarboxylation of organic acids or secondary alteration such as biodegradation or oxidation of hydrocarbons (Pallasser, 2000; Whiticar, 1994).

Nitrogen is abundant in natural gases derived from red beds and humic source rocks (Jenden 1989). It is also derived from metamorphic rocks and igneous rocks in the crust and mantle (Jenden 1989). Nitrogen content may reach 90% of the gas accumulation such as those found in the eastern Zechstein Formation (Weinlich, 1991). Nitrogen is thought to be derived by the release of nitrogen bearing groups from organic matter, the release of ammonia from clays at elevated temperatures and from mantle (Jenden 1989, references therein). Atmospheric nitrogen and dissolved meteoric nitrogen may provide additional important source as proposed by (Coveney *et al.*, 1987). Although kerogens may contribute to the nitrogen content in natural gases, they have insufficient nitrogen content to generate the levels of nitrogen found in natural gases (Krooss *et al.*, 1995). Fractionation of gases due to pressure decline during production may affect the nitrogen as well as methane as proposed by Weinlich (1991) in (Whiticar, 1994).

Natural gases can also be characterised and distinguished reliably by stable isotope signatures of specific compounds. The carbon and hydrogen isotope signature of a natural gas can provide us useful information about the source type (kerogen types and source facies) of the gas and thermal maturity of the source rocks (Whiticar, 1994). Secondary processes affecting the natural gases and mixing can be identified and distinguished by the use of isotope signature together with the molecular compositions of the gases (Whiticar, 1994). The distribution of isotopes is primarily

controlled by several factors: the isotope ratios of the precursor's organic material, hydrocarbon generation and expulsion processes, migration, trapping and destruction of natural gas (Whiticar, 1994). The carbon isotopes in thermogenic hydrocarbons are thought to be controlled by the kinetic isotope effects KIE. KIE theory predicts that the light hydrocarbons generated from reactive kerogen through saturation of the alkyl group cleaved from the kerogen, will be enriched in the lighter isotope relative to the remaining reactive kerogen. If we take carbon isotopes, $^{12}C_{alkyl}$-$^{12}C_{kerogen}$ bonds will break far more easily than $^{12}C_{alkyl}$-$^{13}C_{kerogen}$, $^{13}C_{alkyl}$-$^{12}C_{kerogen}$ or $^{13}C_{alkyl}$-$^{13}C_{kerogen}$ bonds. Therefore, the light hydrocarbons generated will have lighter $^{13}C/^{12}C$ ratios than the source kerogen. This is thought to be also applicable to microbial gas, whereby methane is depleted in the heavier isotope relative to the source microbial material (Whiticar 1992). The magnitudes of the kinetic isotope effects are frequently larger than for thermo catalytic or cracking processes (Whiticar, 1994). The magnitude of the isotope separation decreases with increasing thermal maturation of the source organic matter, and generally decreases with decreasing source quality ($\alpha_{kerogen\ I/II,hc}$> $\alpha_{kerogen\ III,hc}$). It also decreases with carbon number; i.e. $\alpha_{org,hc}$ is methane>ethane>propane>butane. If the hydrocarbons appear enriched in ^{13}C relative to the source organic matter, this may indicate the presence of secondary effects such as mixing of inorganic methane (e.g. volcanic or mantle), oxidation of hydrocarbons, or sometimes sampling and production artefacts. The isotopic exchange after the formation of hydrocarbons, with carbon bearing species such as water, carbon dioxide or kerogen is believed to be negligible at normal diagenetic and catagenetic pressure and temperature conditions and times (Galimov *et al.*, 1972).

Equation 4-1

$$\alpha_{A,B} = R_A/R_B$$

Equation 4-2

$$\alpha_{org,hc} = (^{13}C_{org}+10^3)/(^{13}C_{hc}+10^3)$$

Methane can be formed by several sources, which is not the case for the higher homologs such as ethane; therefore the distribution of isotopes in higher homologs could give us a better idea about the source and maturity level of the natural gas (e.g. Clayton (1991), James (1983), Whiticar (1986)). Coexisting species with

hydrocarbons such as carbon dioxide and organic acids may give us valuable information about the different bacterial methane formation pathways (Whiticar 1986).

Several diagrams were proposed to characterize natural gases based on various empirical studies. Some of these are listed below:

- A cross plot of $C_1/\Sigma C_n$ versus $\delta^{13}C_{CH4}$ was used by Stahl (1977) to define different thermogenic gas types.
- A cross plot of C2+ (vol. %) versus $\delta^{13}C_{CH4}$ was used particularly for reservoired natural gases to distinguish between bacterial source and organic matter.
- Bernard diagram defined as $C_1/(C_2+C_3)$ versus $\delta^{13}C_{CH4}$ is used to distinguish between different types of gases and this suites surface sediment gases and seepages. It can be used to distinguish thermogenic gas from dry bacterial gas, late mature gas, or coal derived gas. This diagram can also be sued to assess secondary effects such as mixing and oxidation effects where the primary end member gases are known. (Whiticar and Faber 1986). This diagram will be used to correlate the natural gases from the Greater Birba area.
- A cross plot of $\delta^{15}N$ and $\delta^{13}C_{CH4}$ versus volume percent N_2 and a cross plot of $\delta^{15}N$ versus $\delta^{13}C_{CH4}$ have been reported to distinguish between different sources of nitrogen and methane, and may help to distinguish between different natural gases. (Jenden1988, Gerling 1988, and Weinlich 1991). Jenden 1988 used these plots to characterize gases from Sacramento basin; he found that most of the high nitrogen gases exhibit isotopically heavy methane >-25‰, although few of them show lighter methane than -25‰. He interpreted these variations due to mixing of nitrogen rich gas with thermogenic and microbial gas.

Faber (1987) proposed mathematical equations (eq 4-3-4-5) to estimate the thermal maturity of natural gases using the carbon isotope of methane, ethane and propane based on empirical relationship between maturity and carbon isotopic

signatures of these hydrocarbon generated from kerogen type I and type II. The thermal maturity estimated from ethane and propane is more representative of the thermal maturity of the natural gas than that estimated from methane; methane is readily altered by several processes while ethane and propane have got only minor sources such as bacteria and the main source is kerogenous organic matter (Oremland 1988). They are not readily altered by secondary processes such as oxidation (Whitica and Faber 1986). There are equations proposed to estimate the thermal maturity of natural gases sourced from humic sources (kerogen type III), however, we will not list them here as they are not applicable to the study, since the proposed source for the associated oils is evaporite-carbonate facies of kerogen type IIS.

$$\delta^{13}C_{CH4}\ (‰) = 15.4 \log_{(10)} \%Ro - 41.3 \quad \text{----------Equation 4-3}$$

$$\delta^{13}C_{C2H6}\ (‰) = 22.6 \log_{(10)} \%Ro - 32.2 \quad \text{----------Equation 4-4}$$

$$\delta^{13}C_{C3H8}\ (‰) = 20.9 \log_{(10)} \%Ro - 29.7 \quad \text{---------- Equation 4-5}$$

The above equations can be modified to calculate the relationship between carbon isotope signatures of methane-ethane, methane-propane, and ethane-propane according to these equations (Whiticar, 1994):

$$\delta^{13}C_{C2H6}\ (‰) = 1.47\ \delta^{13}C_{CH4}\ (‰) - 28.41 \quad \text{--------Equation 4-6}$$

$$\delta^{13}C_{C3H8}\ (‰) = 1.36\ \delta^{13}C_{CH4}\ (‰) - 26.35 \quad \text{------- Equation 4-7}$$

$$\delta^{13}C_{C3H8}\ (‰) = 0.93\ \delta^{13}C_{C2H6}\ (‰) - 0.08 \quad \text{----------Equation 4-8}$$

Faber 1987 compare between ethane and propane carbon isotopic signatures for natural gases from kerogen type I and II and found the best fit regression line is given by this equation below:,

$$\delta^{13}C_{C3H8}\ (‰) = 0.93\ \delta^{13}C_{CH4}\ (‰) - 0.55 \quad \text{--------- Equation 4-9}$$

While Jenden & Kaplan (1989) formulated these equations based on empirical correlations (Jenden & Kaplan, 1989):

$$\delta^{13}C_{C2H6}\ (‰) = 0.245\ \delta^{13}C_{CH4}\ (‰) - 17.8 \text{ ---------- Equation 4-10}$$

$$\delta^{13}C_{C3H8}\ (‰) = 0.27\ \delta^{13}C_{CH4}\ (‰) - 18.0 \text{ ---------- Equation 4-11}$$

It is not uncommon to find a natural gas as admixture of gases from different source rocks of different maturities e.g. (Jenden *et al.*, 1993). Once the natural gas is expelled, several processes may alter the natural gas properties: the molecular and isotopic signatures. Some of these processes are in-reservoir thermal cracking (Prinzhofer & Huc, 1995), microbial oxidation such as bacterial sulphate reduction (Aplin & Coleman, 1995; Cai *et al.*, 2002; Pallasser, 2000)), migration related fractionation (Stahl, 1977; Thompson, 1979), and thermochemical sulphate reduction (Krouse *et al.*, 1988). These processes are very easily discerned if they are reflected by a series of samples at various degrees, but in some other cases, these cannot be discerned.

No solid evidence for isotopic fractionation was found during migration towards the trap (Whiticar, 1994) although it was suggested by some workers (e.g. Stahl 1977). The molecular fractionation during migration or redistribution of hydrocarbons was proved significant by Thompson 1979 and other workers. Microbial oxidation of hydrocarbons leads to changes in gas compositions, by enriching the altered gases with higher homologs and heavier isotopes by consuming methane and light isotopes respectively. This process is controlled by fractionation factor between $\alpha_{CO2\text{-}CH4}$ of values of 1.025 and 1.004 (Whiticar 1992). Ethane and propane are less susceptible to bacterial oxidation (Whiticar, 1994).

4.5.2 Gas samples

Five gas samples (surface samples from well head) are incorporated in this study and these samples are from 5 different wells and 2 reservoir units as shown in Figure 4-52. The gas samples were analysed at Shell labs in Rijswijk (Netherland). They were analysed for the molecular compositions and carbon isotopic ratios, but the

concentrations of gas compounds were not measured and sulphur isotopic ratio for H_2S was also not determined. Oxygen and nitrogen isotopic ratio were provided for carbon dioxide and nitrogen.

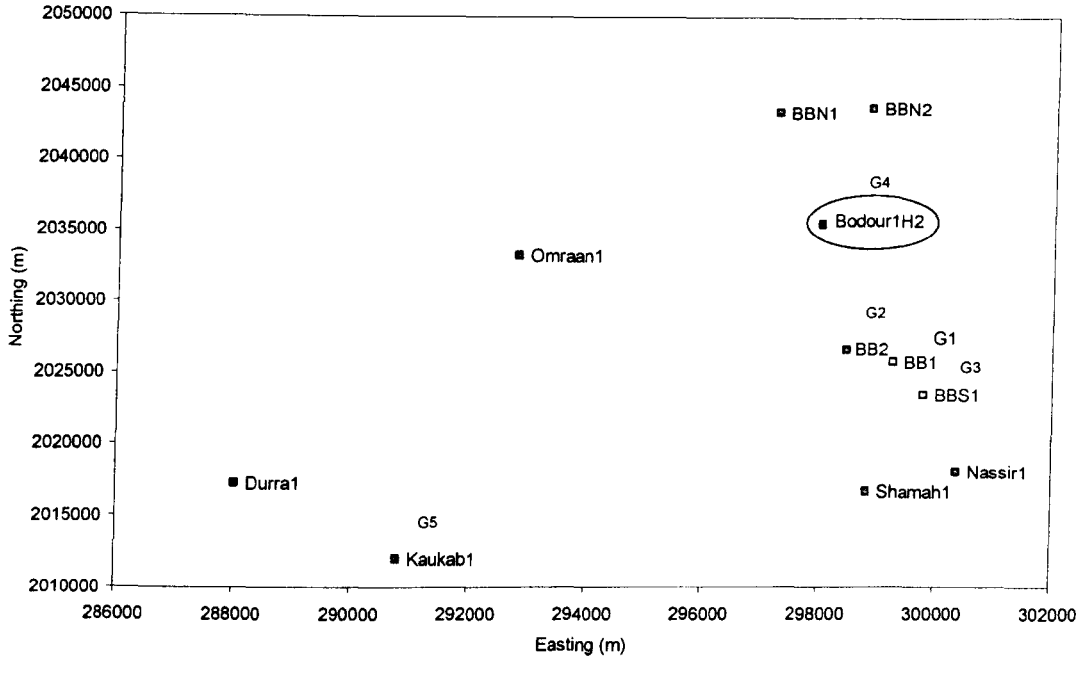

Figure 4-52: Locations of wells that the samples were taken from. Four gas samples (G1-G4) were taken from A4C reservoir unit and one sample (G5) was taken from A3C reservoir unit.

4.5.3 Results and discussion

The molecular composition and the isotopic data of five gas samples from Greater Birba area are shown in Table 4-15. The molecular composition is dominated by methane with a minor proportion of ethane, propane, and carbon dioxide making up (11.1-13.9 vol.%) and very tiny amount of butane, pentane, the plus fraction (C_6+), hydrogen sulphide (H_2S) and nitrogen (N_2). It is very clear from the table that samples G4 (well Budour1h2, A4C reservoir unit) and G5 (well Kaukab1, A3C reservoir unit) are slightly different to the other gas samples. G5 is characterized by relatively very high H_2S (4.8 vol. %) and higher CO_2 (5 vol. %) with relatively lower content of C_2-C_{6+}. G4 (well Budour1h2) is different by having higher contents of C_2-C_{6+} than the rest of samples.

Table 4-15: The molecular composition (Top) and the compound specific isotopic analysis of five gas samples from Greater Birba area.

			Gas Composition vol%										
Sample code	**Wells**	**stringer**	**C_1**	**C_2**	**C_3**	***i*-C_4**	***n*-C_4**	***i*-C_5**	***n*-C_5**	**C_6^+**	**N_2**	**CO_2**	**H_2S**
G1	Birba-1	A4C	83.3	5.2	2.4	0.23	0.7	0.115	0.24	0.43	0.89	4.8	1.61
G2	Birba-2	A4C	83.7	5.2	2.6	0.28	0.86	0.154	0.32	0.39	1.36	4.4	0.71
G3	Birba South-1	A4C	82.5	5.3	2.7	0.27	0.82	0.148	0.3	0.88	0.86	4.8	1.48
G4	BUDOUR-1H2	A4C	80.2	6.4	3.2	0.36	1.39	0.33	0.79	1.43	1.01	4.1	0.7
G5	KAUKAB-1	A3C	82.4	4.3	1.8	0.16	0.4	0.06	0.09	0.33	0.67	5	4.8
			Compound specific Isotopic Analysis ‰										Ratio
			C_1	**C_2**	**C_3**	***i*-C_4**	***n*-C_4**	***i*-C_5**	***n*-C_5**	**$\delta^{13}C_{CO2}$**	**$\delta^{18}O_{CO2}$**	**$\delta^{15}N$**	***i*-C_4/*n*-C4**
G1	Birba-1	A4C	-41.3	-42.5	-39.7	-35.5	-38.6	-35.4	-36.8	-11.7	37.5	-2.2	0.3
G2	Birba-2	A4C	-41.5	-42.7	-39.8	-35.8	-38.3	-35.4	-36.8	-11.4	37.7	-4.4	0.3
G3	Birba South-1	A4C	-41.4	-42.6	-39.7	-35.6	-38.6	-35.5	-36.8	-11.8	37.4	-6.8	0.3
G4	BUDOUR-1H2	A4C	-41.1	-44.6	-39.8	-36.2	-38.5	-35.8	-37	-8.7	37	-7.1	0.2
G5	KAUKAB-1	A3C	-42.4	-39.8	-38.4	-34.8	-37.1	-34.6	-37	-11	38	nd	0.4

Characterization of natural gases is complicated by several sources and processes that affect their compositions and isotopic ratios as mentioned in the above literature review such as source facies, maturity and mixing as well as other important secondary processes such as oxidation, TSR, BSR, biodegradation, in-reservoir thermal cracking and cap leakage. One of the most important diagrams to classify natural gases is the Bernard diagram. Figure 4-53 shows this diagram for all five gases and clearly, all gases fall within thermogenic origin range. All gas samples show high wetness (<12), which indicates thermal origin for these gases. The carbon isotopic signature of methane is also within the range of thermal origin reported in literature (e.g. -47 to -37 for sapropelic kerogen and -30 to -21 for humic kerogen from Whiticar (1994)).

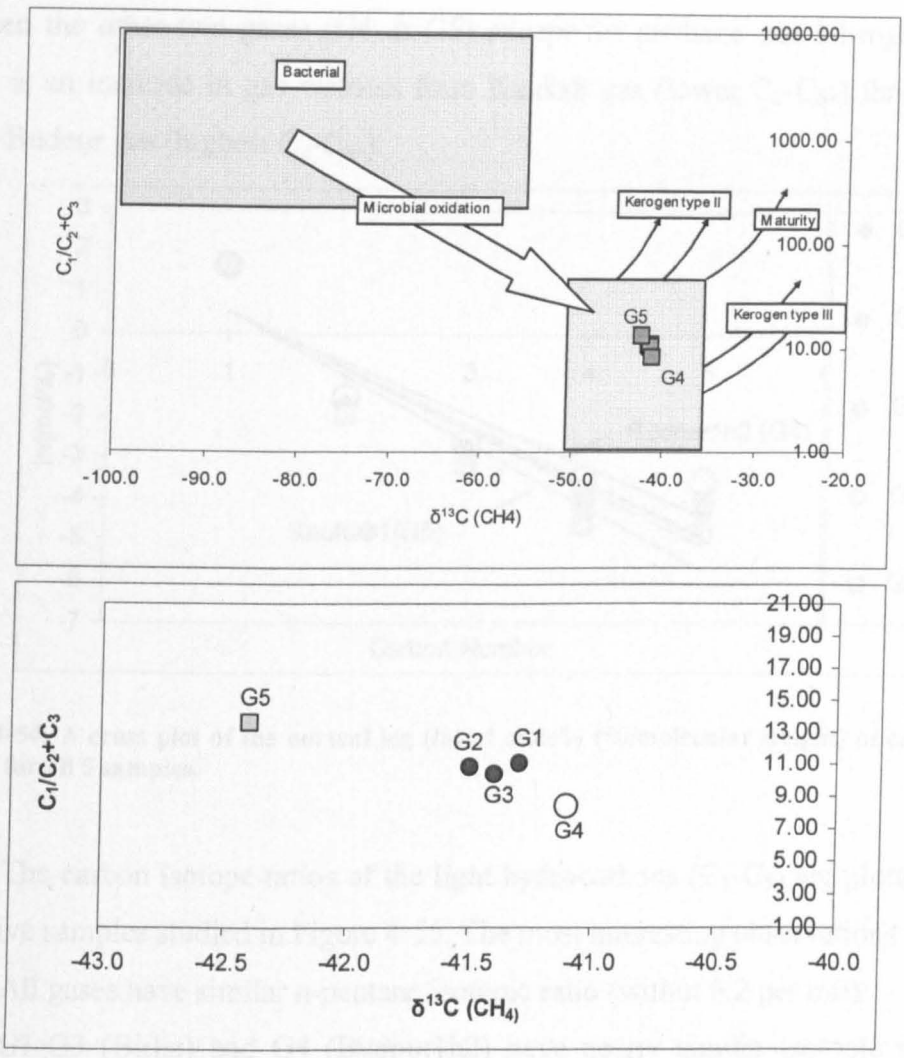

Figure 4-53: Bernard diagram to classify the gases based on the gas dryness and the carbon isotopic ratio of methane.

The normal logs of mole percentage of each hydrocarbon component are plotted for all samples in Figure 4-54. The plot shows that Birba gases are well correlated whereas the gases from well Budour1h2 and well Kaukab1 (G4 and G5 respectively) are slightly different. Budour1h2 gas seems to have higher content of C_2-C_5 whereas Kaukab1 gas shows lower content of these components. They all have similar proportion of methane. The high amount of methane in all gas samples results on steeper predicted trend line. This might suggest that the dominating methane might have come as a later thermal charge from depleted source rock or dried gas was charged in. This might come obvious when isotopic data are involved in the discussion. There is a consistent trend by going from Budour1h2 (G4) through Birba (G1-G3) to Kaukab1 (G5) gas; the molecular contents of Birba gases are always in

between the other two gases (G4 & G5) except for methane and Nitrogen content. There is an increase in gas wetness from Kaukab gas (lower C_2-C_{6+}) through Birba gas to Budour gas (highest C_2-C_{6+}).

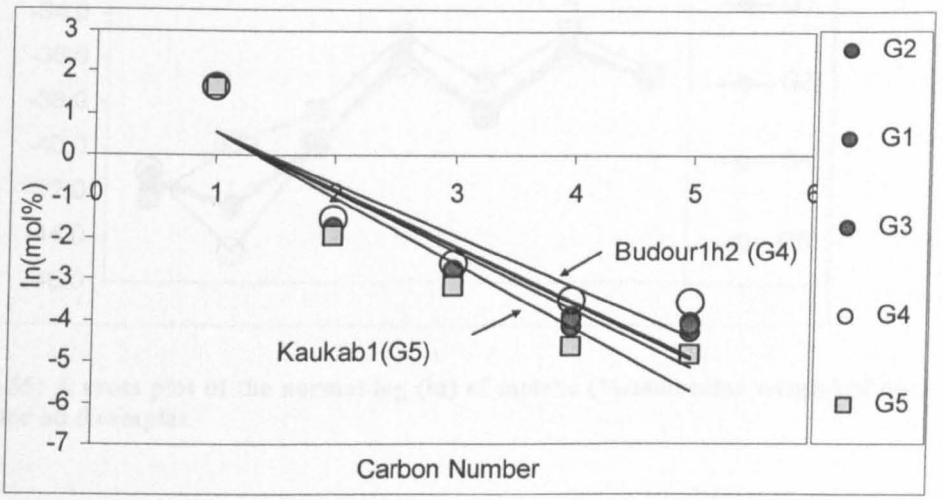

Figure 4-54: A cross plot of the normal log (ln) of mole% (%/molecular weight) of each carbon number for all 5 samples.

The carbon isotope ratios of the light hydrocarbons (C_1-C_5) are plotted for all of the five samples studied in Figure 4-55. The most interesting observations are

1. All gases have similar n-pentane isotopic ratio (within 0.2 per mil).
2. G1-G3 (Birba) and G4 (Budour1h2) have nearly similar isotopic ratios for butanes and propane and methane (<0.3‰).
3. G5 has heavier carbon isotopic ratios than others for most of the compounds except for methane.
4. G4 (Budour1h2) has lighter isotopic ratio of ethane than for other 3 Birba samples (G1-G3).
5. G1-G4 are characterised by isotopically heavier methane than ethane.

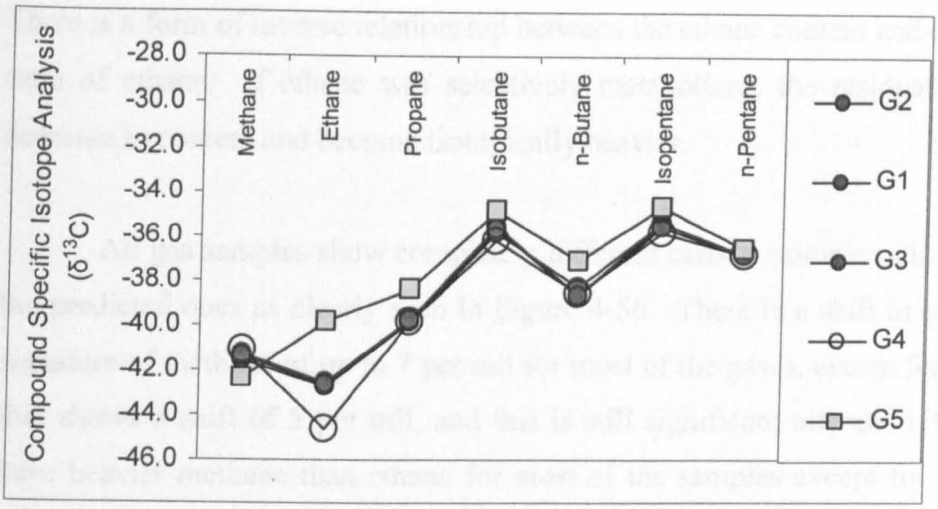

Figure 4-55: A cross plot of the normal log (ln) of mole% (%/molecular weight) of each carbon number for all 5 samples.

Clearly, Figure 4-55 shows that the gases in Ara carbonates (stringers) of the Greater Birba area have been subjected to secondary alteration and this alteration is expressed mainly in the methane and ethane. Carbon isotopic ratios for propane to pentane are similar for most of the gases except for the gas G5 from A3C reservoir unit of well Kaukab1. Therefore, in an attempt to predict the original isotopic composition of these gases, equations 4-7 & 4-8 were used to calculate the original carbon isotopic ratio for ethane and methane, before they were altered using the carbon isotopic signature of propane as a known factor assuming that propane has not been subjected to any alteration (i.e. $\delta^{13}C$ of methane and ethane were calculated from equations 4-7 and 4-8 respectively). Figure 4-56 shows a comparison between the real data and the predicted data (only $\delta^{13}C$ of CH_4 and C_2H_6 are predicted). It clearly shows that Birba gases and Budour1h2 gas have similar carbon isotopic signatures for methane and ethane, which is predicted anyway as we calculated them using propane carbon isotopic ratio which is more or less similar for these gases. By comparing the ethane carbon isotopic ratios, Birba gases seems to have similar actual ratios to the predicted ones, which reflect that these gases were probably not subjected to any secondary alteration to their ethane isotopic compositions, while Kaukab1 and Budour1h2 gases were probably altered. However, ethane carbon isotopic ratio exhibits the highest fractionation between gas samples. Assuming the data are reliable, ethane might have been altered by selective biodegradation. However, there is no evidence supporting this hypothesis except the scatter in ethane carbon isotopic ratio.

There is a form of inverse relationship between the ethane content and carbon isotopic ratio of ethane. if ethane was selectively metabolised, the residual ethane would decrease in content and become isotopically heavier.

All gas samples show completely different carbon isotopic ratio of methane to the predicted ones as clearly seen in Figure 4-56. There is a shift in carbon isotopic signature of methane of up to 7 per mil for most of the gases, except for Kaukab1 gas that shows a shift of 5 per mil, and this is still significant alteration. Generally, we have heavier methane than ethane for most of the samples except for Kaukab1 gas. This may result from mixing with a heavier and drier gas or oxidation effect (bacterial or inorganic) (e.g. Jenden *et al.*, 1993) or leakage of the cap rocks (Prinzhofer & Huc, 1995) or perhaps leakage of the sampling bottles.

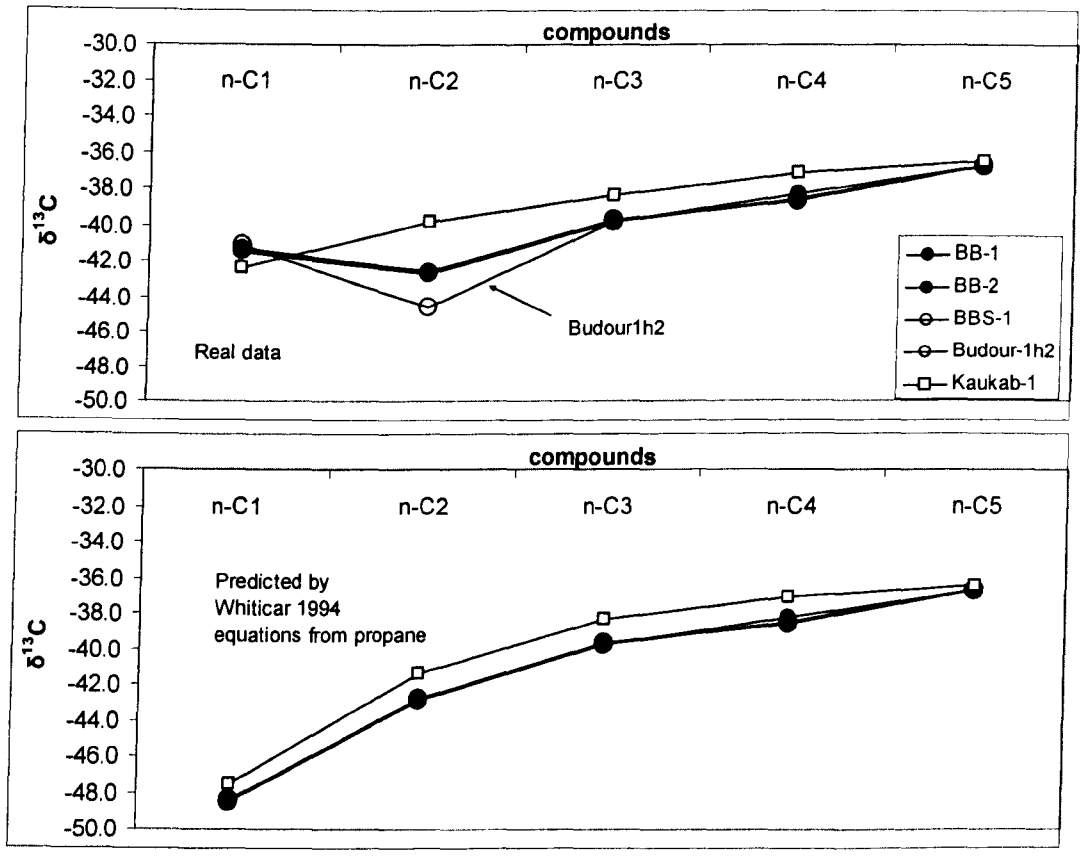

Figure 4-56: Comparison between the real carbon isotopic ratio for the light normal alkanes and the calculated carbon isotopic ratios using Whiticar (1994) equations. Only $\delta^{13}C$ of methane and ethane were calculated using $\delta^{13}C$ of propane by equations 4-7 and 4-8.

Figure 4-56 shows that well Kaukab1 gas shows slightly heavier carbon isotopic ratios for ethane through to normal butane than the other gases. This might suggest that this gas has relatively higher thermal maturity than the other gases. Since methane and ethane are thought to be altered, we used carbon isotopic ratio for propane to estimate the maturity of these gases as listed in Table 4-16. The estimated thermal maturity appears to be very low and probably question the empirically derived equation used to estimate it. Well Budour1h2 gas, which appears different in some characteristics to Birba gases (G1-G3), it shows similar maturity to them. Although, Berner (1989) formulated these equations specifically for kerogen type I and type II source rocks, the low thermal maturity values given for the study gases in Table 4-16, probably indicate that these equations are not applicable to the study oils, and cautions must be taken as they can not be taken as universal measure for thermal maturity of various gases.

Table 4-16: calculated thermal maturity level for the study gas samples.

Sample code	Wells	stringer	$\%R_o$
G1	Birba-1	A4C	0.33
G2	Birba-2	A4C	0.33
G3	Birba South-1	A4C	0.33
G4	BUDOUR-1H2	A4C	0.33
G5	KAUKAB-1	A3C	0.38

Since the most significant feature in the gas composition, of the study gases are the isotopically heavy methane, this might help us to understand most of the variations observed in the study gases and so it is going to be discussed in details. As mentioned above, several processes may results in isotopically heavier methane over ethane, mixing, oxidation, cap rock leakage or bottle sampling leakage. Methane can be oxidised by several processes most likely sulphate reduction processes (bacterial and inorganic). These processes should results in lower abundance of methane by consuming it through oxidation, and results in enriching the residual methane in heavy carbon isotopes. They should also result in higher content of isotopically lighter carbon dioxide, and higher abundance of hydrogen sulphide. While we have isotopically heavier methane than ethane, the relative amount of methane does not vary significantly between the study gases (range: 80.2-83.7 vol.%) even for the gas

sample from well Kaukab1, which does not show isotopically heavier methane than ethane. Figure 4-57 shows various cross plots to investigate the possibility of the oxidation effect on the study gases. A poor relationship was obtained for carbon isotopic ratio of carbon dioxide versus the relative amount of carbon dioxide and hydrogen sulphide in the study gases. However, these plots distinguish between the three types of gases, Budour 1h2 (G4), Birba (G1-G3) and Kaukab1 (G5) gases. A better correlation was obtained for carbon dioxide content versus carbon isotopic ratio of methane and oxygen isotopic ratio of carbon dioxide. There is a decrease in carbon dioxide abundance with increasing heavy carbon isotopes of methane and decreasing heavy oxygen isotopes. This can not be related to oxidation, as the expected trend should be opposite; with oxidation, the carbon in carbon dioxide molecules is derived from hydrocarbons' light carbon isotopes, and the oxygen is derived from the water light isotopes coexisting with these hydrocarbons. Therefore, either progressive oxidation there is an increase in carbon dioxide content accompanied by increasing heavy isotopic ratio of methane (depleted from ^{12}C) and probably decreasing oxygen isotopic ratio. Therefore, the correlation between CO_2 content versus $\delta^{13}C$ of CH_4 and $\delta^{18}O$ of CO_2 might not explain the origin of the isotopically heavy methane and the carbon dioxide. Two possible sources for carbon dioxide, inorganic dissolution of carbonates in catagenesis by the release of oxygen bearing groups, or as part of dry gas charge mixed with the original gases in the study area.

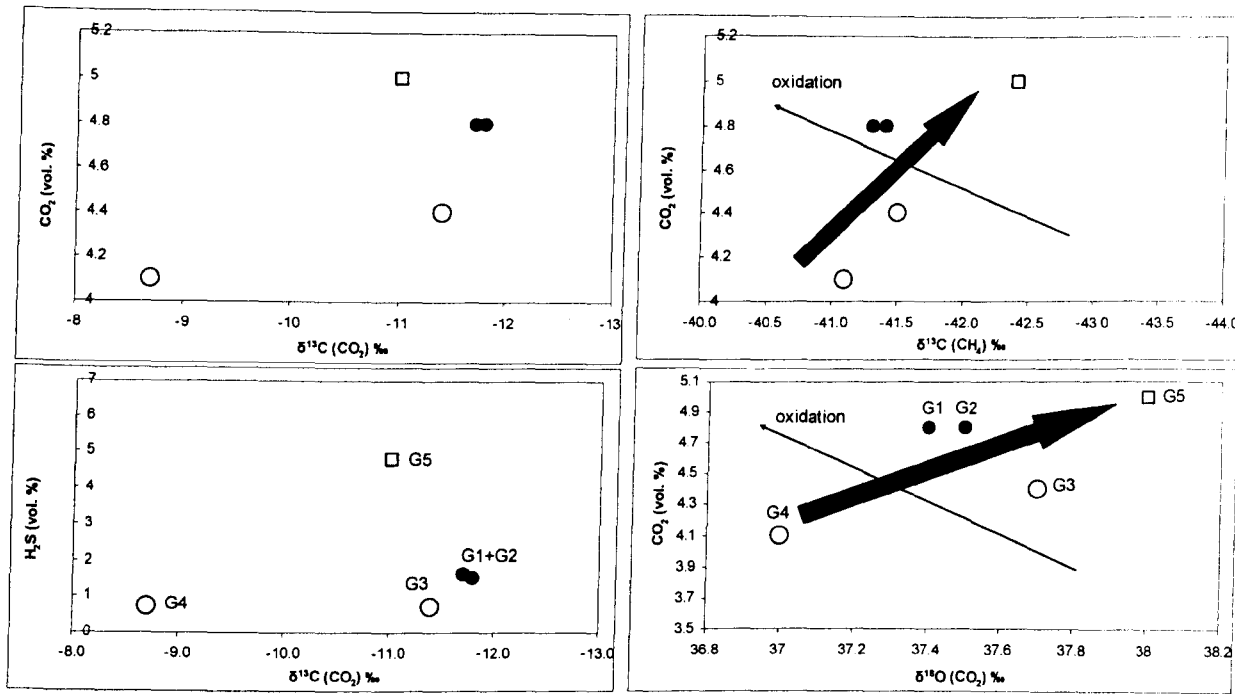

Figure 4-57: Cross plots of carbon dioxide content (vol.%) versus $\delta^{13}C$ of CO_2 (Top left), carbon dioxide content versus $\delta^{13}C$ of CH_4 (top right), hydrogen sulphide versus $\delta^{13}C$ of CO_2 (bottom left), carbon dioxide content (vol.%) versus $\delta^{13}C$ of CO_2 (bottom right).

Mixing with dry and isotopically heavy gas was also studied. Jenden (1993) studied various gases (oil associated and non-associated) in the northern Appalachian Basin (western central New York). He interpreted the variations in cross plots of carbon isotopic ratio of methane versus that for ethane and the cross plot of $\delta^{13}C$ (C_2-C_1) versus $\delta^{13}C$ (C_3-C_2), he interpreted them as mixing sequence between two thermogenic derived gas end members, under mature, wetter and isotopically lighter gas , and overmature, drier, and isotopically heavier gas. Some of his studied gases have the heavy methane characteristic similar to the gases in this study (Figure 4-59). He predicted the mixing models corresponding to the two end members according to the equation below:

The concentration of any light hydrocarbons is given by:

Equation 4-12:

$$C_i^M = (f * C_i^A) + ((1-f) * C_i^B)$$

Where A and B are gases, i is a light hydrocarbon, C is the concentration, and f is the fraction of the component A or B in the mixture. While the isotopic ratio is approximated by:

Equation 4-13

$$I_i^M = [f * C_i^A * I_i^A + (1-f) * C_i^B * I_i^B]/C_i^M$$

Where I is the compound isotopic ratio of a light hydrocarbon.

I attempted to apply this model to the study oils, using two hypothetical end members, one is a dry over mature heavy methane, and the other one is calculated using Whiticar (1994) equations (eq 4-7 & 4-8) (Only methane and ethane were calculated from propane isotopic ratio and the other hydrocarbons in the hypothetical end member have the same carbon isotopic ratios to those in actual gases). Jenden (1993) stated in his equation that the concentration of a compound should be used, but the list of their hypothetical end members were shown in relative percentages (vol %) not the concentration. Unfortunately, we only have the relative volume percentages for the study gases, and therefore, we are going to used these instead of the concentrations. Figure 4-58 shows this model as well as the actual data. The model predicts that the present day gases are mixtures of a dry heavy gas with the original predicted gas (calculated by Whiticar 1994) at ratio of 1.94:1 (By vol %) respectively. This is a hypothetical model, but it is supported by PVT modelling. There is no clear evidence of the presence of this dry methane.

Table 4-17: The hypothetical end members used to calculate the mixing model for the study gases

$\delta^{13}C_1$	$\delta^{13}C_2$	$\delta^{13}C_3$	$\delta^{13}C_4$	$\delta^{13}C_5$	vol.% C_1	vol.% C_{2+}
-48.5	-42.8	-39.7	-38.6	-36.8	50	<50%
-39.4	-	-	-	-	100	≈0

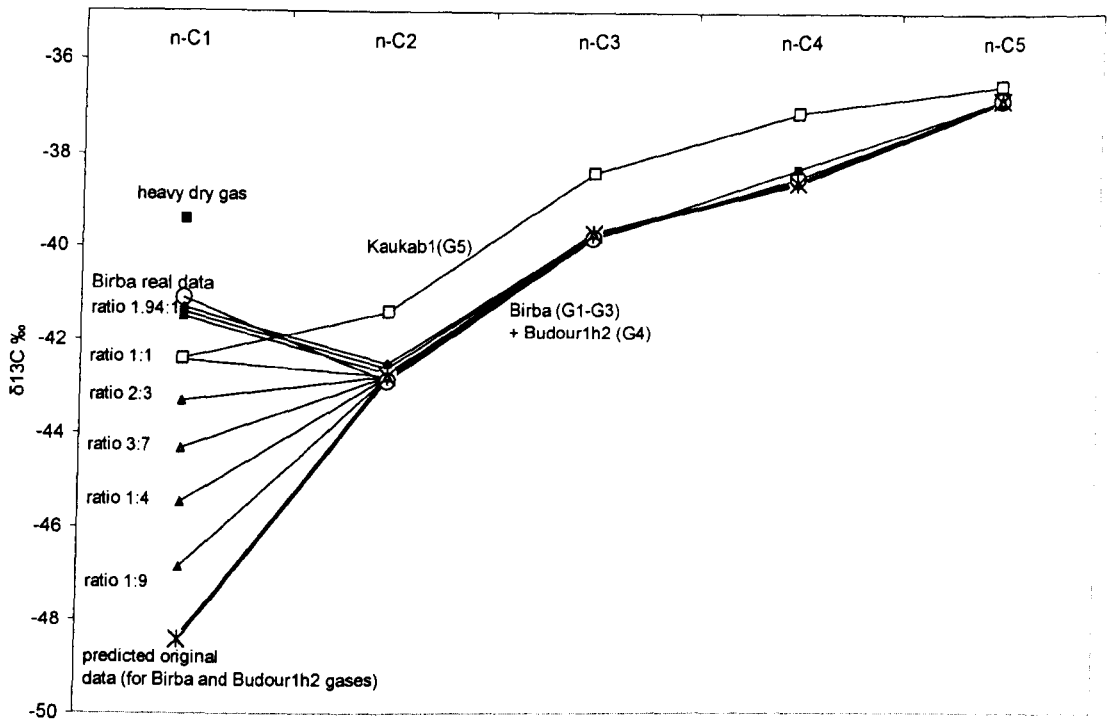

Figure 4-58: the proposed mixing model to account for the isotopically heavy methane in the study gases.

Prinzhofer and Huc (1995) reinterpreted Jenden (1993) data and they found that the main controls on the variations observed in the gases of Appalachian Basin are thermal maturation accompanied by leakage from the gas cap as shown in Figure 4-59. They successfully calculated the proportion of gas leaked as 15% according to the equation below (equation 4-14, V is probably the velocity of an isotope leaking, and M for Molecular mass of the isotope). They set their model with isotopic fractionation factors proportional to the inverse of the square root of the molecular mass and with a 15% of leakage. This model might also be applicable to the study gases. Unfortunately, we could not measure the possible leakage in the study gases due to the lack of explanation of how to measure the leakage in their paper.

$$\frac{V_1}{V_2} = \sqrt{M_2 / M_1}$$ ----------**Equation 4-14**

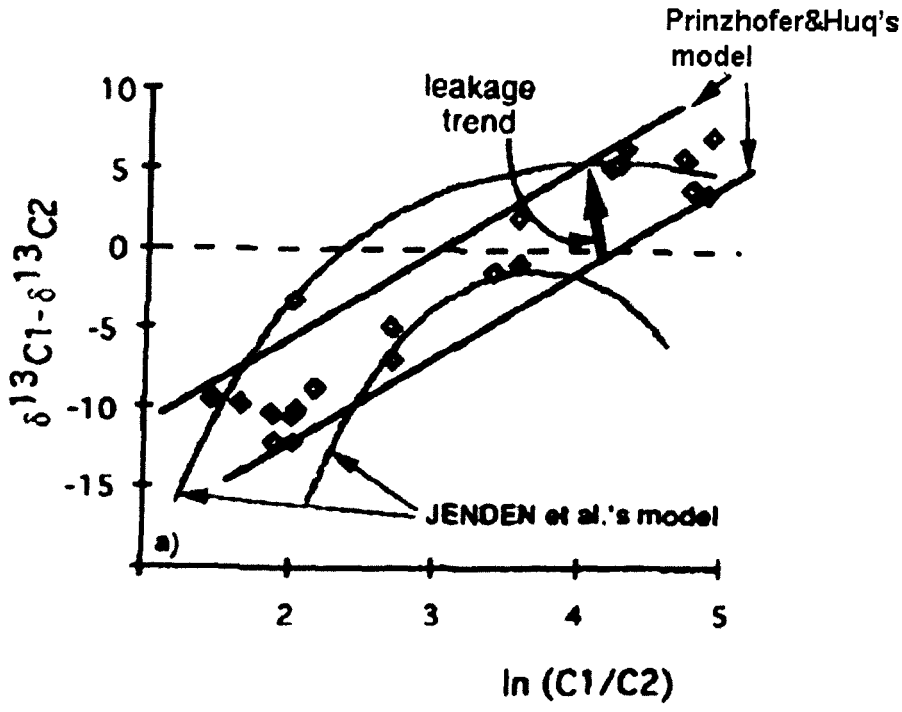

Figure 4-59: comparison between Jenden et al (1993) mixing model and Prinzhofer & Huc (1995) model to explain the heavy methane in the gas accumulations from Appalachian Basin. After (Prinzhofer & Huc, 1995).

In a summary, five surface gas samples from two carbonate stringers were studied using the relative volume percentages and isotopic ratios of light hydrocarbons and some of non-hydrocarbons gases. The aim of this work is to investigate the origin and the geochemical processes that these gases have been subjected to, which might help us to understand the variability observed in the physical properties in the Greater Birba area crude oils. The limited number of gas samples was a potential problem in arriving at clear-cut conclusion. However, it was suggested here that these gases might have been altered by mixing with relatively heavier methane and/or affected by cap rock leakage (anhydrite). The carbon isotopic ratio of ethane exhibits significant variation. It suggested that this might be attributed to selective biodegradation that have metabolized ethane.

4.6 Conclusions

The aim of this work was to assess the reservoir geochemistry of petroleum fluids in the Greater Birba area and to correlate them with each other using the available samples and data provided for this study. Most of the study oils in the Cambrian-Precambrian carbonate stringers in the Greater Birba area are probably sourced from organic rich evaporate-carbonate facies deposited in hypersaline and reducing environment. Most of the oils show more or less similar geochemical characteristics. No sign of biodegradation and water washing was found in all oils. Most of the oils are probably from mature source in the middle of oil window estimated by VRE based on MPI-1 and they show very similar maturities. There are only minor facies and maturity variations observed in the study oils. Statistical evaluation of biomarkers and aromatic hydrocarbons of most of the oils except for O5, O15 and condensates reveal that the main variations are in the relative proportion of the light biomarkers to the heavy biomarkers. The two main groups of the oils statistically evaluated are Birba and Birba North oils (wells, BB1, BB2, BBN2) in one group and the rest was in another group, which are mainly A3C/A5C oils including the rest of the A4C oils (e.g. O13 and O22). Therefore, the main variation in geochemistry was found in the ratio of light biomarkers to heavy biomarkers and the concentrations of biomarkers. This is suggested to be related to a gas condensate mixing with normal oil causing dilution of biomarkers by *n*-alkanes, as supported by the inverse relationship between n-alkanes versus biomarkers concentrations.

High sulfur content cannot be attributed to thermochemical/bacterial sulphate reduction because no indication can be found for these two processes. Although, the carbonate reservoirs in this study are of low temperatures no geochemical or isotopic evidence could be found to suggest the BSR effect. For example, there is apparent trend between the sulfur isotopes of the whole oil, and the amount of sulfur content, which is opposite to what is expected from TSR/BSR effect.

The core extracts analyses indicate that the fresh new charges of oil that flooded the Birba Field were from another source of lower maturity. There were no big variations among maturity parameters identified in produced oils and so the filling direction of these new charges cannot be predicted. It is possible that the oils in the

carbonate stringers at present day reflects new charge different to that present in the bitumen. It is also important to note that the oils extracted from condensate zones are similar to other oils but different to the condensates. This suggests that the oil was there before the arrival of condensate charge that displace oil downwards. It is also concluded here that the latest oil charge did not reach A4C in BB4 suggesting that the sealing fault that separate the BB4 block was there before this charge.

Gas analysis suggests that the heavy methane observed in the study gases ($\delta^{13}C$ of methane > $\delta^{13}C$ of ethane) might be related to mixing of relatively heavy dry gas with normal gases or leakage of the cap rock (which is anhydrite). It might also be related to unusual ethane biodegradation, suggested from the significant variation observed in the carbon isotopic ratio of ethane.

Chapter 5 Light hydrocarbons: oil-oil and oil-condensate correlations and the origin of gas condensates in the Greater Birba area

5.1 Introduction

The Greater Birba area is over 480 km^2 in extent and has been explored by more than 20 wells, 14 of which are involved in this study. Significant variations were observed in the physical properties (e.g. API gravity, Sulfur content, TAN) of produced oils from those producing wells. The main aim of the work in this chapter is to use the geochemistry of light hydrocarbons to understand these variations and controls behind them. The particular objectives are listed below:

- Geochemical characterization of light hydrocarbons
- Oil-oil and oil-condensate correlations
- Identifying secondary processes that those petroleum fluids were subjected to.

Since chapter 4 concluded that there was probably mixing of original oils with a condensate charge, it is very important to study the compositions of light hydrocarbons to test this hypothesis. The greater Birba area is characterized by occurrence of gas condensates. These will be correlated with the oils and investigated to find out the origin of these condensates i.e. are they of thermal origin or phase fractionation origin.

5.2 Geological setting

The South Oman Salt Basin formed during the Neoproterozoic in response to wrench faulting and rifting (Loosveld et al., 1996), or possibly as an intra-cratonic depression in the foreland of an orogenic belt (Immerz *et al.*, 2000). During Neoproterozoic III – Early Cambrian time it was filled by 3 - 6 km of clastic, carbonate and evaporitic sediments of the Huqf Supergroup (Gorin et al., 1982; Loosveld et al., 1996) that overlie Pan-African basement. The upper part of the Huqf Supergroup consists of the evaporite-carbonate cycles of the Ara Group (Figure 5-1). Deposits of the Ara Group record a period of important basin restriction related to rapid subsidence and renewed tectonic activity (Mattes & Conway Morris, 1990).

The Ara group consists of six evaporite-carbonate cycles, which are believed to be tecton-eustatic cycles i.e. subsidence and sea level changes. These cycles are termed A1 to A6 from bottom to top (Figure 5-1, Figure 5-2). All cycles have a similar stratigraphy. The carbonate units within these cycles are called carbonate stringers and are termed AxC, whereas AxE for Evaporites, where x is the cycle number. The main producing unit in the Greater Birba area are A3C and A4C. most of the oil samples involved in this study are from these two stringers in addition to three samples from A5C and A1C stringer. The geochemistry of the salt indicates a marine source for brines that deposited the evaporates (Schrooder, 2000). The thickness of carbonate stringers varies but ranges between 50 and 150 m. To the southeast in the eastern flank of the basin, the Greater Birba Area was probably bounded by a carbonate platform lacking evaporites, because of either non-deposition or post-depositional dissolution.

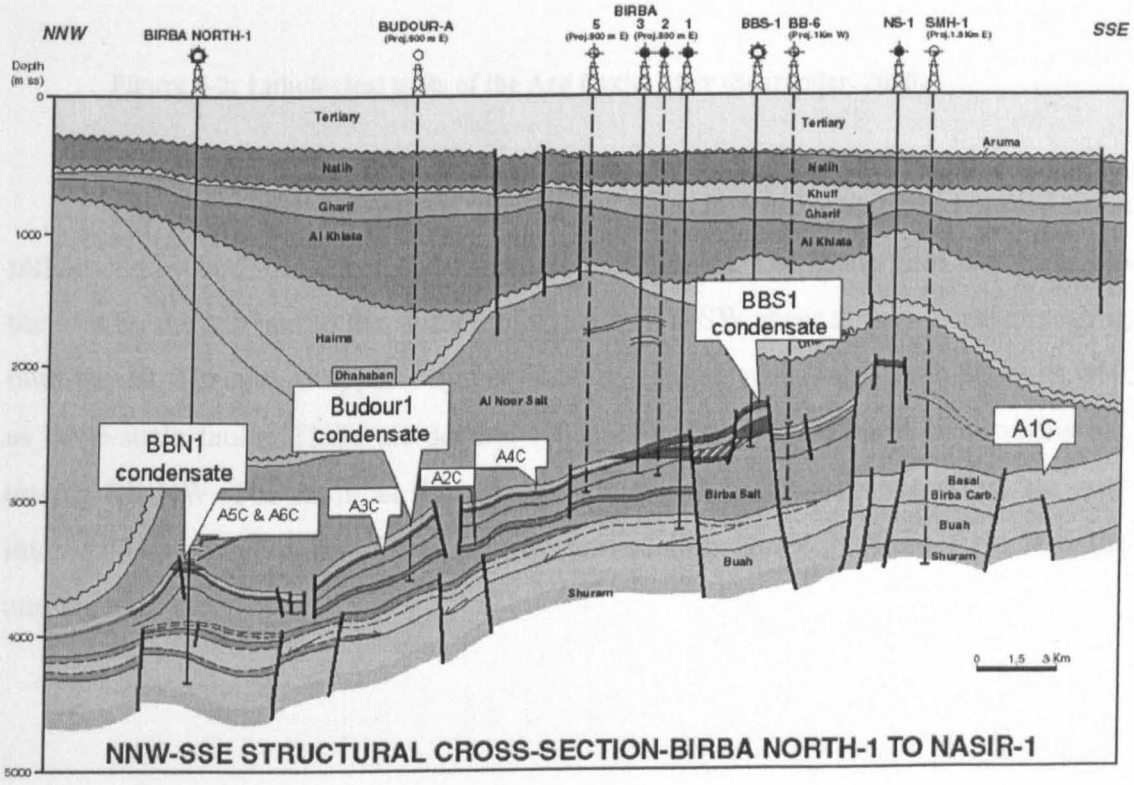

Figure 5-1: NNW-SSE structural cross section of carbonate stringers from well Birba North 1 to Nasir1.

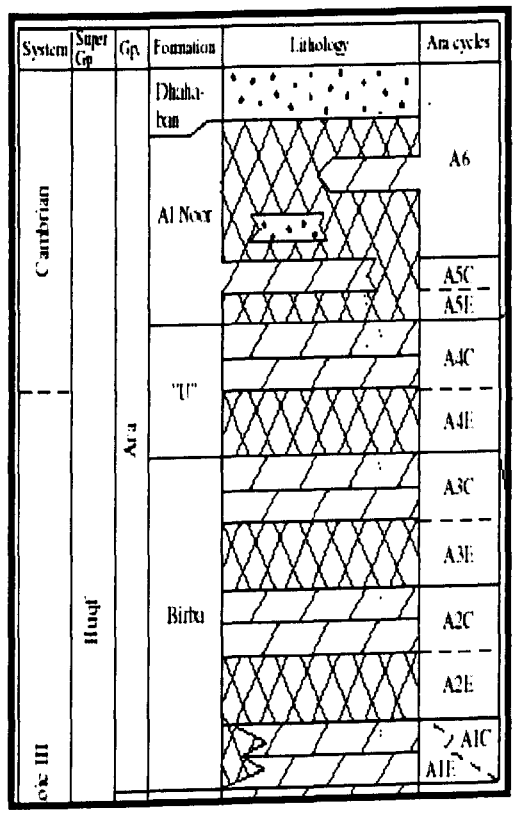

Figure 5-2: Lithological units of the Ara Cycles after (Schrooder, 2000).

The structural history of the Birba field is very complex because it is influenced by both halokinetic and tectonic movements. The Birba field is bounded to the east by the salt and to the south by the major NE-SW shear zone, i.e. major sealing fault trends. The area is apparently very heavily faulted with small-scale faults as well as large-scale faults. There are several types of faults with different orientations but mainly SE-NW. The faults at the A4 stringer, which is the main reservoir, are very intense. The distribution of sealing and non-sealing faults in Birba field remains unresolved.

5.2.1 Literature review: The light hydrocarbons and their geochemical applications

The term "light hydrocarbons" (LHC) is used here for the gasoline range hydrocarbons up to nonane, but mainly C_4-C_9. The study of LHC is important because they may contain over 50% of the carbon in petroleum (Mango, 1997). The main light hydrocarbons consist of four classes: normal alkanes (e.g. n-heptane), isoalkanes such as 2-Methylhexane (2-MH), cycloalkanes such as alkylcyclopentanes (e.g. 1,1-DMCP) and alkylcyclohexanes (e.g. MCH), and aromatics (e.g. Toluene) (see Figure 5-3). The C_7 LHC received more attention because C_7 isomers are easily resolvable by standard chromatographic methods, and they are less prone to alteration by sampling and storage evaporation (Peters *et al.*, 2005). Figure 5-4 shows a typical gas chromatogram of 45.8 API gravity gas condensate and Table 5-1 lists all light hydrocarbons used in this study and some of them reviewed in this section.

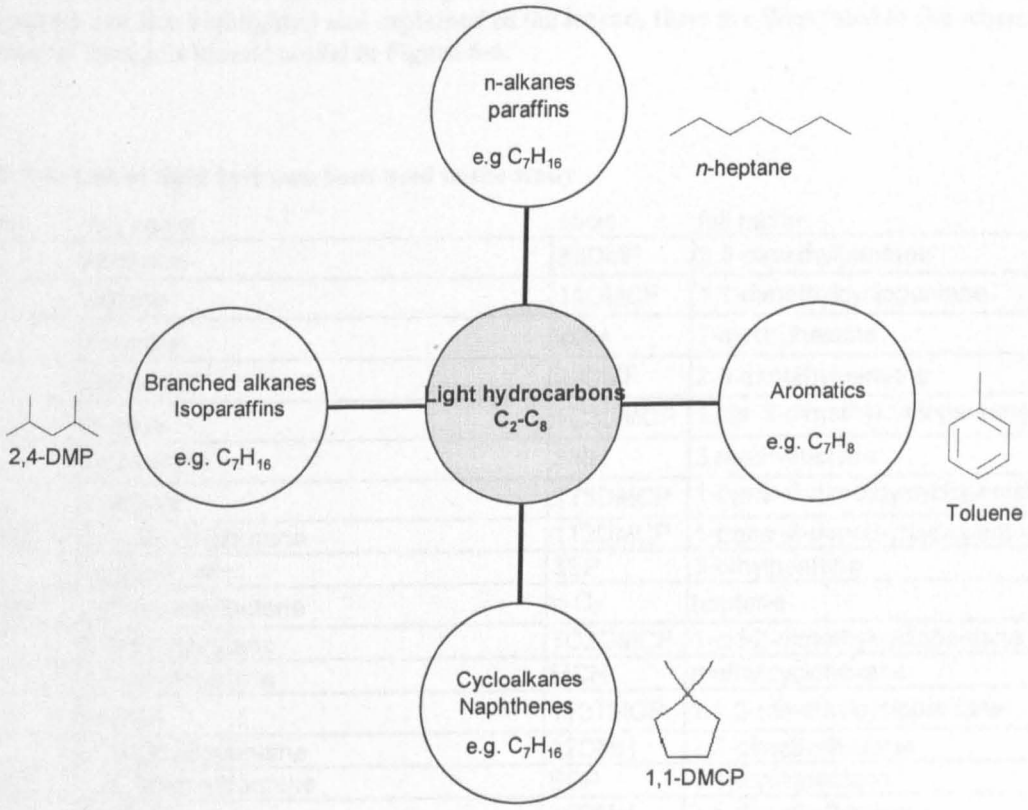

Figure 5-3: The four main classes of light hydrocarbons in petroleum with very important examples, used in this study.

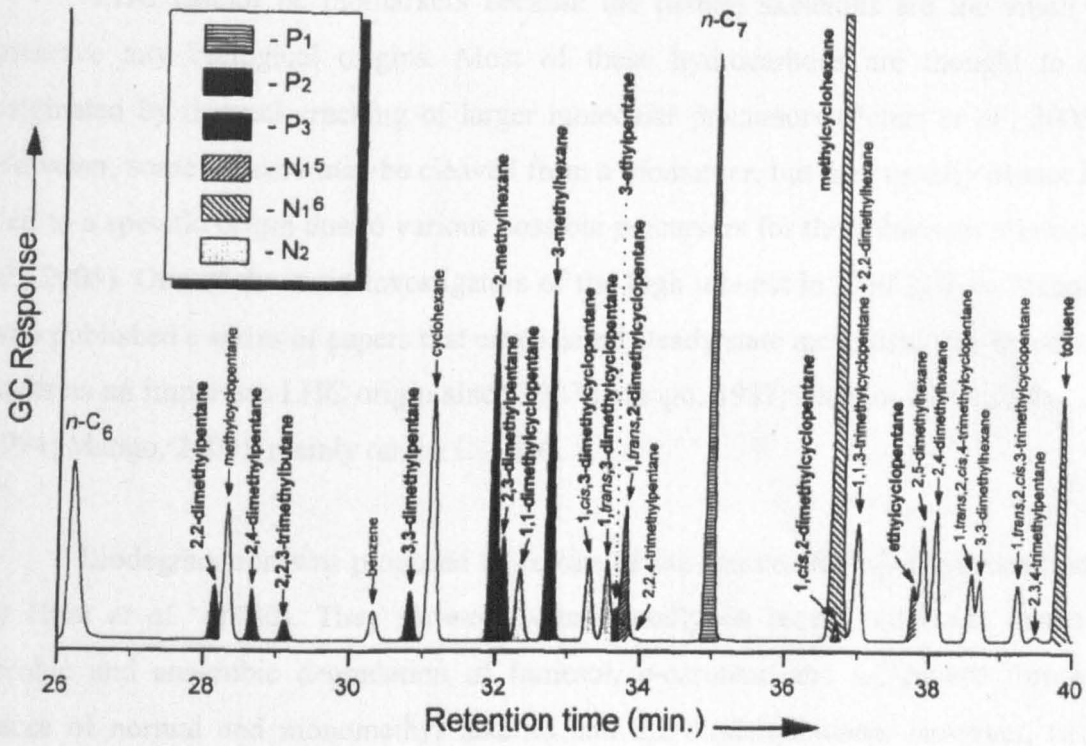

Figure 5-4: Partial whole oil gas chromatogram of a condensate of API gravity of 45.8°. Mango's parameters are also highlighted and explained in the legend, these are illustrated in the schematic diagram of Mango's kinetic model in Figure 5-6.

Table 5-1: List of light hydrocarbons used in the study

short	full name	short	full name
n-C_1	Methane	33DMP	3,3-dimethylpentane
n-C_2	ethane	11DMCP	1,1-dimethylcyclopentane
n-C_3	propane	2MH	2-methylhexane
IC_4	isobutane	23DMP	2,3-dimethylpentane
n-C_4	butane	1C3DMCP	1-*cis*-3-dimethylcyclopentane
IC_5	isopentane	3MH	3-methylhexane
n-C_5	pentane	1T3DMCP	1-*trans*-3-dimethylcyclopentane
22DMB	2,2-dimethylbutane	1T2DMCP	1-*trans*-2-dimethylcyclopentane
CP	cyclopentane	3EP	3-ethylpentane
23DMB	2,3-dimethylbutane	n-C_7	heptane
2MP	2-methylpentane	1C2DMCP	1-cis-2-dimethylcyclopentane
3MP	3-methylpentane	MCH	methylcyclohexane
n-C_6	hexane	113TMCP	1,1,3-trimethylcyclopentane
MCP	methylcyclopentane	22DMH	2,2-dimethylhexane
22DMP	2,2-dimethylpentane	ECP	ethylcyclopentane
BENZ	benzene	25DMH	2,5-dimethylhexane
24DMP	2,4-dimethylpentane	223TMP	2,2,3-trimethylpentane
223TMB	2,2,3-trimethylbutane	1T2C4TCP	1-trans-2-cis-4-trimethylcyclopentane
CH	cyclohexane	TOL	Toluene

LHC cannot be biomarkers because the carbon skeletons are too small to preserve any biological origins. Most of these hydrocarbons are thought to be originated by thermal cracking of larger molecular precursors (Peters *et al.*, 2005). However, some isomers may be cleaved from a biomarker, but they usually cannot be tied to a specific origin due to various possible precursors for these isomers (Peters *et al.*, 2005). One of the main investigators of the high interest in LHC is F.D. Mango, who published a series of papers that emphasised steady state metal catalysis in source rocks as an important LHC origin since 1987 (Mango, 1987; Mango, 1990b; Mango, 1994; Mango, 2000); mainly on the C_7 LHC.

Biodegradation was proposed to be one of the sources for light hydrocarbons by Hunt *et al.*, (1980). They showed experimentally on recent sediments that an aerobic and anaerobic degradation of farnesol, b-carotene and a-2-pinene formed traces of normal and monomethyl alkanes and 2,2-dimethylbutane. However, two main origins for light hydrocarbons in petroleum have received more attention and acceptance, the most widely accepted thermal cracking theory (Hunt, 1995), and kinetic steady state metal catalysis theory (Mango, 1990b; Mango, 1992; Mango, 1996).

Mango (1987) found that there are invariant abundance ratios of some LHC, constant for similar sourced oils (Mango, 1987). He argued that these constant ratios could not be explained by thermal cracking or acidic mineral catalysis (Mango, 1990b). According to Mango, (1990b), the higher stability of higher hydrocarbons and the compositions of the LHC do not favour the thermal cracking origin for LHC, and the absence of equilibrium state in LHC does not support the acidic clays as catalysis. If the light hydrocarbons originate by thermal cracking of higher hydrocarbons, we would expect the light hydrocarbons distribution resemble the distribution of the primary structures that dominate the higher hydrocarbons such as *n*-allkanes and isoprenoids; *n*-alkanes should crack to *n*-alkane and isoprenoids should crack to isoprenoids. Although there are evidences that suggest that the light hydrocarbon might be related to biotic precursors or primary structures, Mango doubted that these precursors can explain the amount of related light hydrocarbon products (e.g.Mango, 2000). Some of these evidences, Kissin (1991) showed that the isoprenoids can be related to certain isoalkanes (e.g. 2-methylpentane and 2-methylhepatne from cracking of pristane and phytane). *n*-alkylcyclohexannes and *n*-alkylbenzenes may

crack to form methylcyclohexane and toluene (Ji-Zhou Dong *et al.*, 1993), while 2—methylalkanes and 3-methylalkanes may potentially be products of iso- and anteisoalkanes cracking (Mango, 1997, references therein). Mango argued that the primary structures (n-alkanes and isoprenoids) do not often dominate the light hydrocarbons as they do the higher molecular weight hydrocarbons; i.e. there is progressive decrease in dominance with decreasing carbon number from C_{10} and lower. Figure 5-5 compares between primary cracking products and the typical distribution of LHC in crude oils. it is clear that only the primary products that appear in the chromatogram (above), while the secondary products such as 3-methylheptane, isoalkanes and cycloalkanes are apparently no present. Such distribution have not been cited anywhere (Mango, 1997), and the same argument was used against acid catalysis .

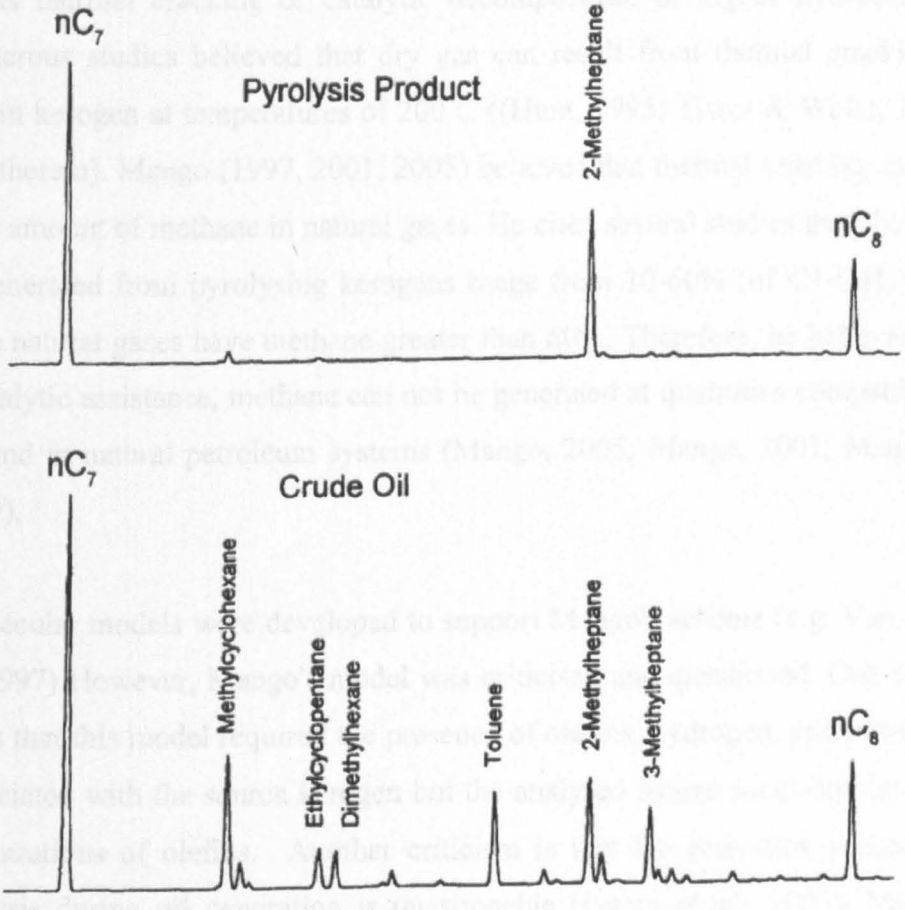

Figure 5-5: Comparison between C5-C8 primary products from cracking a mixture of natural products found in petroleum (top) and the typical distribution of C5-C8 light hydrocarbons in crude oils (Bottom). The pyrolysis was performed on a mixture of n-pentadecane, pristane, cholestane, which was heated in a sealed glass at 390°C for 3 hours and then it was hydrogenated to remove the olefins (Mango, 1997).

Mango proposed that these invariant ratios result from steady state transition metal catalysis reactions (Mango, 1990b; Mango, 1992; Mango, 1996; Mango, 2000). According to Mango's scheme (Mango, 1990b), methyl hexanes originate from a common *n*-heptane precursor and the dimethylpentanes (DMP) are daughter products of the methylhexanes; these reactions are catalysed by transition metal catalyst forming a three ring (cyclopropyl) intermediate. These isoheptanes keep constant ratio (2MH+2,4DMP)/(3MH+2,3-DMP) over a wide range of concentrations and called this ratio K1. Mango (1990) developed the scheme further, and included five and six ring closures for the origin of cyclic alkanes and tolune, and predicts other invariant ratios, K2, K3, and K4.

One of the important arguments is the origin of dry gas via one of the two mechanisms thermal cracking or catalytic decomposition of higher hydrocarbons. while numerous studies believed that dry gas can result from thermal cracking of petroleum in kerogen at temperatures of 200°C ((Hunt, 1995; Tissot & Welte, 1984), references therein). Mango (1997, 2001, 2005) believed that thermal cracking can not explain the amount of methane in natural gases. He cited several studies that show the methane generated from pyrolysing kerogens range from 10-60% (of C1-C4), while most of the natural gases have methane greater than 60%. Therefore, he believed that without catalytic assistance, methane can not be generated at quantities compatible to what is found in natural petroleum systems (Mango, 2005; Mango, 2001; Mango & Elrod, 1999).

Molecular models were developed to support Mango's scheme (e.g. Van Duin & Larter, 1997) However, Mango's model was criticised and questioned. One of the criticisms is that this model required the presence of olefins, hydrogen, and transition metals associated with the source kerogen but the analysed source rock samples lack high concentrations of olefins. Another criticism is that the activation process of metal catalysis during oil generation is questionable (Peters *et al.*, 2005). Mango, (2000) admitted that initial oils generation result from thermal decomposition of kerogen and the metal catalysis decompose saturated hydrocarbons to light hydrocarbons and the natural gases result from the decomposition of light hydrocarbons via the same mechanism (Mango, 2000).

Equation 5-1: The origin of light hydrocarbons and gas by metal catalysed kinetic reactions (M* for metal calalyst) after (Mango, 2000)

$$\text{Kerogen} \xrightarrow{\Delta} \text{oil} \xrightarrow{[M^*]} \text{LHs} + \text{Wet Gas} \xrightarrow{[M^*]} \text{Dry Gas}$$

A schematic representation of the kinetic model proposed by Mango (1990b) is illustrated in Figure 5-6. There are three types of intermediate ring-closures in the kinetic scheme: the 3-carbon ring closure (Isoparaffins), the 5-carbon ring closure, and the 6-ring closures (carbocyclic products+toluene) as illustrated in the diagram below for the heptane species and also by Equation 5-2.

Equation 5-2: The three key ring-closures in Mango's scheme.

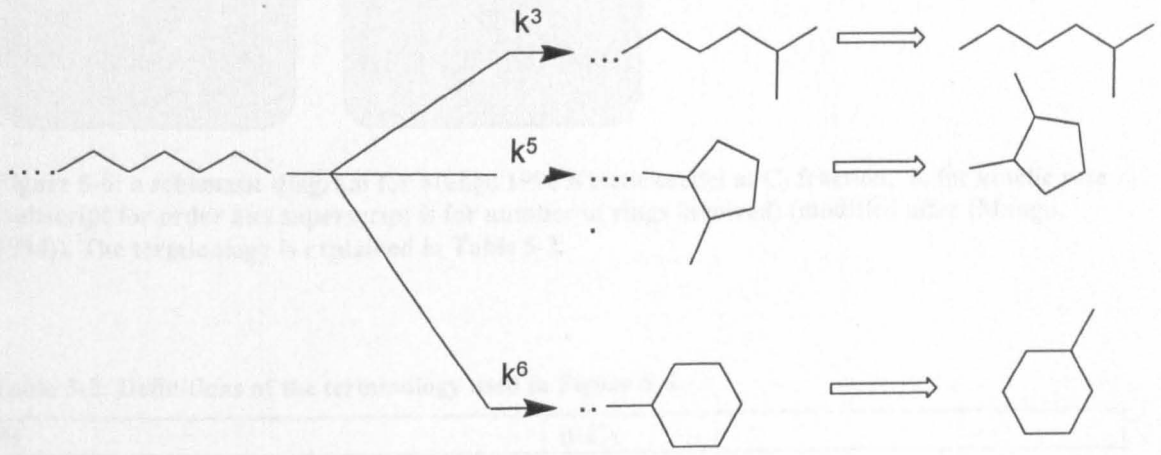

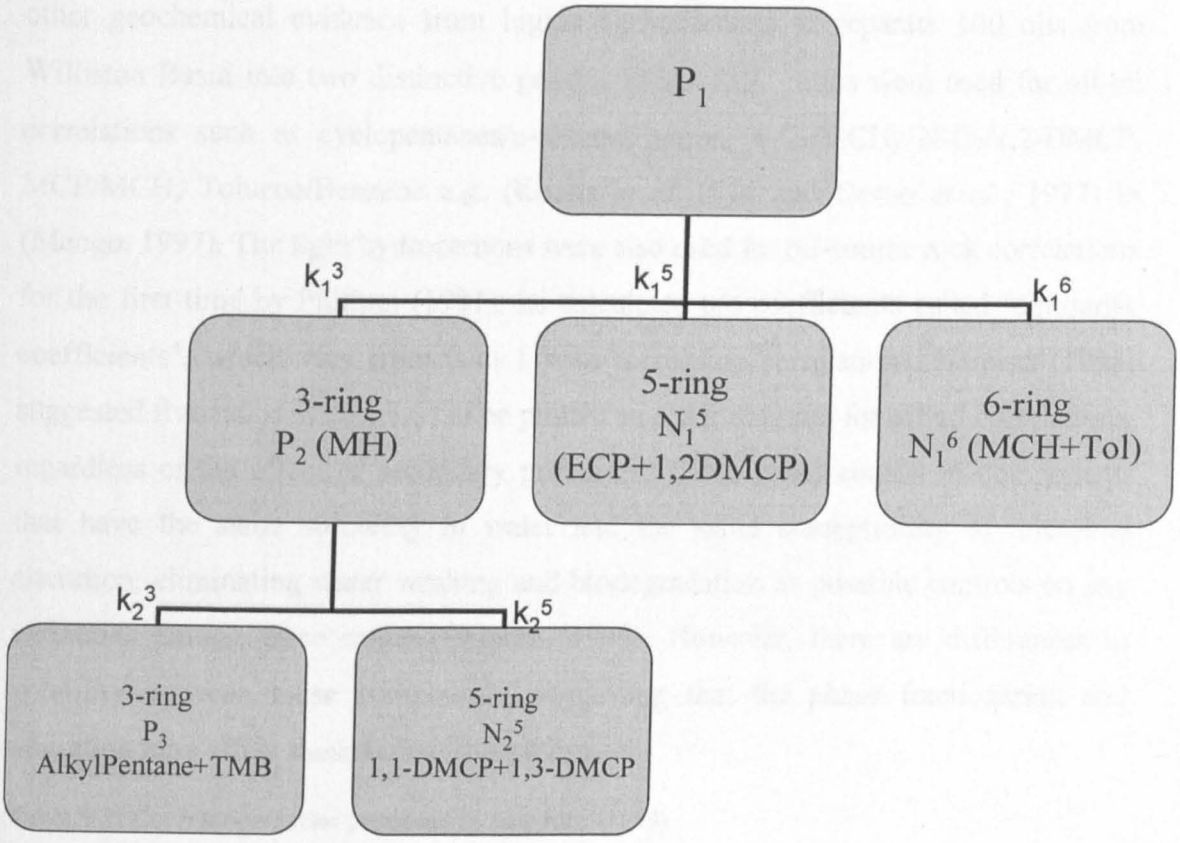

Figure 5-6: a schematic diagram for Mango 1990 Kinetic model at C_7 fraction. K for kinetic rate (subscript for order and superscript is for number of rings involved) (modified after (Mango, 1994)). The terminology is explained in Table 5-2.

Table 5-2: Definitions of the terminology used in Figure 5-6.

P1	n-C_7
P2	2MH+3MH
P3	3EP+23DMP+22DMP+33DMP+233TMB
N^5_1	ECP + 1*c*2-DMCP + 1*t*2-DMCP
N^5_2	1,1-DMCP + c-l,3-DMCP + t-1,3-DMCP
N^6_1	MCH+Tol

n-C7 = *n*-heptane, MH = methyl hexane, EP = ethyl pentane, DMP = dimethyl pentane, TMB = trimethyl butane, DMCP = dimethyl cyclopentane, ECP = ethylcyclopentane, MCH = methylcyclohexane, Tol = toluene.

Light hydrocarbons were not used often in oil-oil and oil-source correlations during early history of petroleum geochemistry (e.g. Williams, 1974). The low interest in the LHC in this field was down to their accepted origin by thermal cracking, which means limited geochemical information can be obtained from their distribution; they were used more frequently to describe the secondary effects such as biodegradation and water washing (Peters *et al.*, 2005). Williams (1974) used ternary plot of normal alkanes, isoalkanes, and cycloalkanes in the C_4-C_9 range together with

other geochemical evidence from higher hydrocarbons to separate 100 oils from Williston Basin into two distinctive groups. Other LHC ratios were used for oil-oil correlations such as cyclopentanes/n-alkanes ratios, *n*-C_7/MCH, N-C_7/1,2-DMCP, MCP/MCH, Toluene/Benzene e.g. (Koons *et al.*,1974 and Deroo *et al.*, 1977) in (Mango, 1997). The light hydrocarbons were also used for oil-source rock correlations for the first time by Philippi (1981), he calculated ten coefficients called "similarity coefficients", which vary from 0 to 1 with increasing correlations. Halpern (1995) suggested five ratios (Table 5-3) to be plotted as a star diagram for oil-oil correlations, regardless of the effect of secondary processes. These ratios consist of components that have the same solubility in water and the same susceptibility to microbial alteration, eliminating water washing and biodegradation as possible controls on any variations among these ratios (Halpern, 1995). However, there are differences in volatility between these compounds, suggesting that the phase fractionation and migration may affect those ratios (this study).

Table 5-3: Correlation ratios proposed by Halpern (1995)

Name	Ratio	Δ BP (°C)	Δ Solubility (ppm)
C1	2,2-DMP/P3	-5.8	-0.6
C2	2,3-DMP/P3	4.8	0.3
C3	2,4-DMP/P3	-4.5	-0.6
C4	3,3-DMP/P3	1.1	0.9
C5	3-EP/P3	8.5	-2.0

Several invariant ratios were proposed by Mango's model (1987-2000), and these have are proved to be powerful for oil-oil and oil-source rock correlations e.g. (Eneogwe, 2004; Jiang & Li, 2002; ten Haven, 1996). These are listed in Table 5-4.

Table 5-4: Mango Invariant ratios. Key to abbreviations is in Table 5-1.

K1 = "(2MH+2,4DMP) /(3MH+2,3-DMP)" (Mango, 1987),

K2 = " P3/(P2+N_2^5)" (Mango, 1990b),

K3 = "(2MH+ 3,3DMP+3EP)/(3MH+2,4DMP)" (Mango, 2000)

K4 = "(2MH+1,3(*cis*+*trans*)DMCP)/(3MH + 1,1DMCP)" (Mango, 2000).

These ratios are expected to be constant in all oils sourced from the same or similar source. However, other parameters must be used in conjunction with these invariant ratios, because similar values of Mango invariant ratios do not necessary indicate the same source (ten Haven, 1996). Eneogwe (2004) used K1 (Table 5-4) and the ratio between the concentrations of methylhexanes to ln (P_3/N_2) (P_3 and N_2 are illustrated and defined in Figure 5-6 and Table 5-2) to differentiate between two groups of oils from the offshore Eastern Niger Delta in Nigeria. Jiang & Li (2002) used K1 (Table 5-4) along with a ternary plot of n-C_7 vs. (MCH+Tol) vs. (iso-C_7+DMCPs)) (abbreviations explained in Table 5-1) to group oils from Williston Basin in USA into several genetic groups giving well defined Bakken/Madison grouping with overlapping due to mixing (Jiang & Li, 2002). K1 and K2 and a cross plot of P_2 vs. N_2/P_3 together with other parameters (e.g. carbon Isotope values of saturated hydrocarbons and aromatic hydrocarbons) were used to separate oils and condensates into different genetic oil sets (ten Haven, 1996). Mango (1997) used a cross plot of concentrations of methylhexanes against ln(P_3/N_2) and a cross plot of concentration of *n*-heptane against ln(ΣCyclopentanes/ΣCyclohexanes) to distinguish Midland oils from both Sabine Parish (Luisiana, USA) and Eugene Island (Gulf of Mexico) oils.

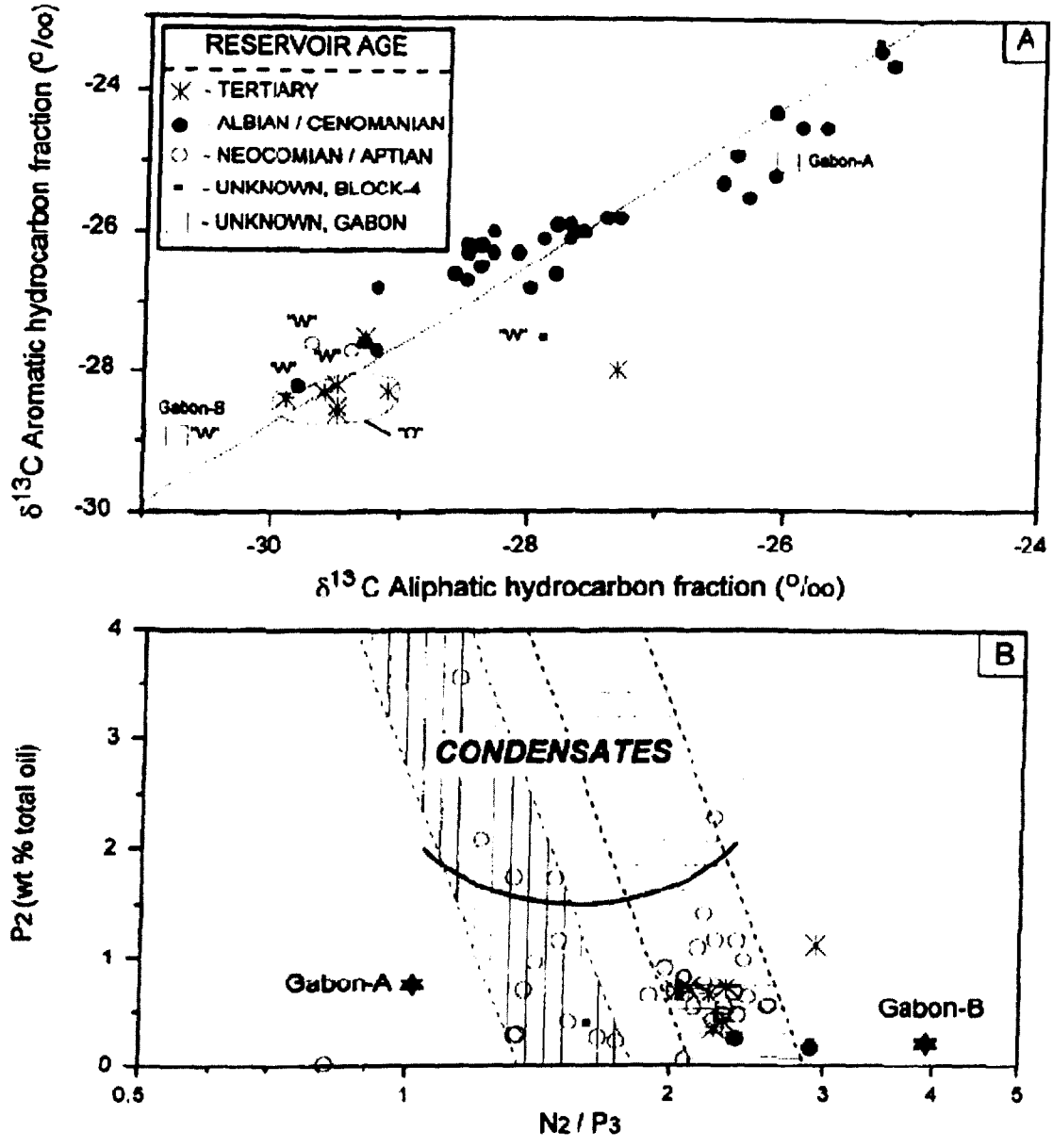

Figure 5-7: cross plots used by Ten haven (1996), to study oils/condensates from Block 2, North Angola.

Compound specific isotopic analysis (CSIA) (referring to $\delta^{13}C$) was recognised to be a reliable correlation tool, specifically for condensates and oils. Whiticar & Snowdon (1999) correlated 40 oils and gas condensates from different ages and source rocks using CSIA ($\delta^{13}C$), and found that $\delta^{13}C$ of individual gasoline range hydrocarbons (C_4-C_9) are powerful indicators of different source rocks and ages. They further concluded that these results suggested a steady state kinetic relationship for the formation of oil and gas, and not thermodynamic relationship. They also stated that $\delta^{13}C$ of non-straight chained alkanes are better diagnostic ratios than normal alkanes.

Pasadakis *et al.* (2004) performed multivariate statistical analysis (PCA) on crude oils from the Williston Basin North America. They used various data from different fractions including gasoline-range hydrocarbon data to identify four oil families. They included in their statistics: normal, cyclic and branched alkanes from C_6 to C_8 as well as toluene and benzene (Pasadakis *et al.*, 2004).

Light hydrocarbons can also provide significant information about their sources, maturity and post expulsion history. The post expulsion history includes the changes induced by the migration process (Thompson, 1988) and in-reservoir alteration processes such as gas washing (Meulbroek *et al.*, 1998; Thompson, 1987), phase-separation related fractionation (Larter & Mills, 1992), biodegradation (George *et al.*, 2002; Masterson *et al.*, 2001), thermochemical sulfur reduction (Rooney, 1995), and water washing (George *et al.*, 2002). Mixing of oils and condensates is also a very important process that lead to considerable alteration of LHC composition (Chen *et al.*, 2003).

The amounts of light hydrocarbons in crude oils correlate well with maturity; the amount of LHC in unaltered oils might be <15% in low maturity oils, 25-40% in mid oil window expelled oils, and thermal condensates may reach 100% (Peters *et al.*, 2005). Higher abundance of light hydrocarbons can also be related to source type; it has been found that type II kerogen release higher yields of LHC than type III kerogen in mature sediments (Leythaeuser *et al.*, 1979). The loss of LHC can be attributed to biodegradation (Masterson *et al.*, 2001), water washing (George *et al.*, 2002), or thermochemical sulphate reduction (TSR) (Rooney, 1995). Thermal maturation and mixing with condensate charge increases the abundance of LHC (Chung *et al.*, 1998), while evaporative fractionation, can have the effects of increasing (in the gas phase) or decreasing (in the residual oil) the abundances of light hydrocarbons (Thompson, 1987).

Thompson (1983) used the cross plot of heptane [H=100**n*-C_7/(ΣCH thro to MCH) excluding 1-cis-2-DMCP, see Table 5-1] and isoheptane [I=(2MH+3MH)/(1,3-DMCP(*cis*+*trans*)+1-*cis*-2-DMCP)] values to distinguish the effects of source, maturity and biodegradation on various cuttings and outcrop samples. The cross plot of these two ratios allows recognising two different maturation curves from aliphatic

and aromatic kerogens, based mainly on the variations of isoheptane values. Aliphatic kerogens are relatively rich in normal alkanes and aromatic kerogens are rich in isoalkanes (Thompson, 1983). It has been found that carbonate/marl source rocks generally have a trend above the aliphatic curve; the highly aliphatic source rocks from lacustrine facies give higher heptane ratios; and the marine (type II) and prodeltaic (type II/III) source rocks generally fall in between the two curves (Peters et al., 2005).

Precambrian oils were found to be depleted in cycloalkanes relative to normal and isoalkanes (Mango, 1994). MCH was thought to be derived from terpenoids and carotenoids of non-marine facies (Clayton *et al.*, 1991) and is found to be the largest peak in those oils sourced from terrigenous coals and coaly shales (Peters *et al.*, 2005). Toluene was suggested to originate from coals and lignin (Leythauser 1979). It has also been reported to occur at high abundance in marine sulphur rich carbonate-evaporite sourced oils, which was attributed to the sulphur-catalysed diagenetic cyclization and aromatization of normal alkanes (Sinninghe Damasté *et al.*, 1993). The ternary plot of P1/CP/P2 was used to distinguish between marine (Iso-rich) and terrigenous (CP rich) source rocks (Dai, 1992). The ternary plots of $P1/N_2^5+N_1^5/$ MCH and $N_2^5+N_1^5/P2/N_1^6$ were used to differentiate between marine (rich in *n*-C_7 & MH) and coal (rich in cyclic & Toluene) source rocks (Odden *et al.*, 1998). The ternary plot of $N_2^5+N_1^5/P2/N_1^6$ was also used to distinguish between different oils families (Obermajer *et al.*, 2000). Ten Haven (1996) used a ternary plot of Isoheptanes/Cyclopentanes/Cyclohexanes to distinguish lacustrine (Iso-rich) from terrrgenous (CH-rich) oils in Vietnam (ten Haven, 1996).

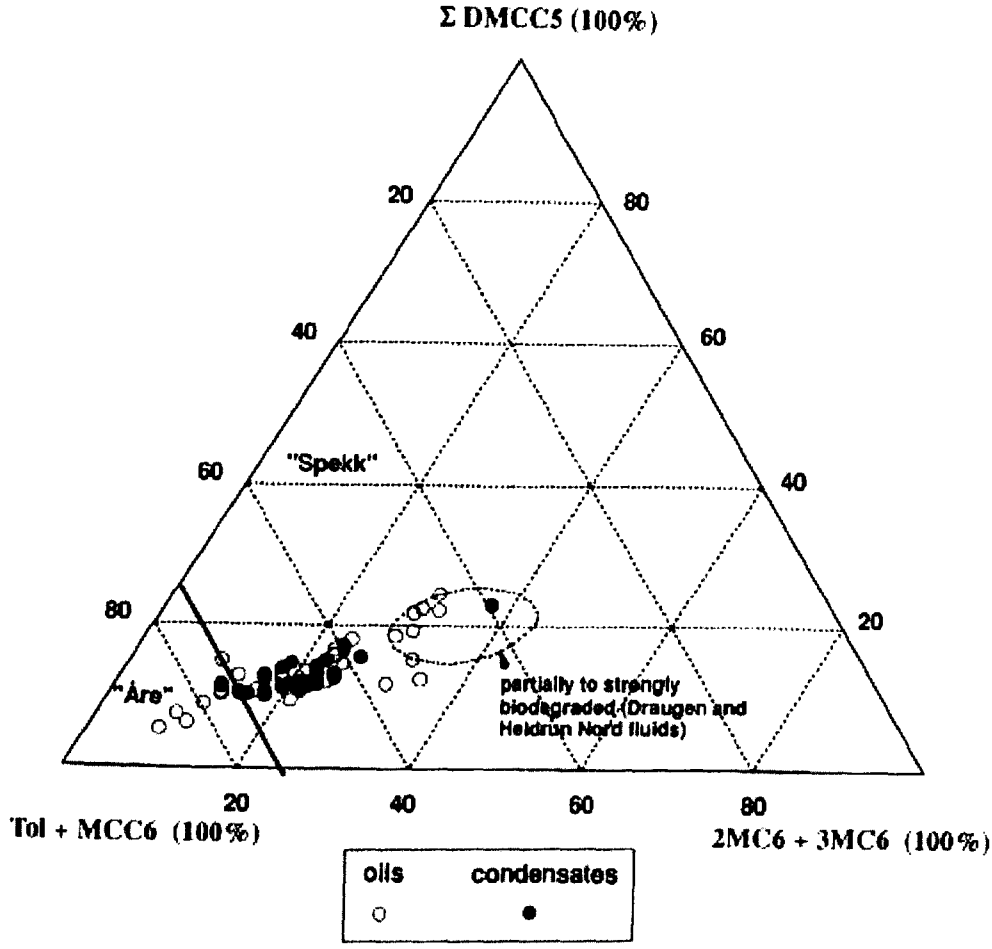

Figure 5-8: $N_2^5+N_1^5/P2/N_1^6$ ternary plot used by Odden *et al.*, (1998) to differentiate between thermal extracts of early Jurassic coaly Are formation and Late Jurassic marine shaly Spekk formation for Mid-Norway.

Hunt *et al.* (1980) reported that there is an increase in the ratio of tertiary carbon LHC species to quaternary carbon LHC species with the depth of maximum yield for LHC such as 2,2DMB/2,3DMB and 2,4DMP/2,3DMP, suggesting them as maturity indicators (Hunt *et al.*, 1980). Schaefer & Littke, (1988) observed a strong correlation between vitrinite reflectance and three C_7 ratios: J, V and R1 described below (Equation 5-3). All of these ratios systematically increase with increasing maturity. However, the relationship between these ratios and vitrinite reflectance can be affected by source facies (Chung *et al.*, 1998).

Equation 5-3: Schaefer maturity parameters (V, and J) from (Schaefer & Littke, 1988). It also shows an empirically determined equivalences (R_V, R_J, and R1) for vitrinite reflectance based on these parameters. abbreviations are explained in Table 5-1.

$$V = C_7 \text{ paraffins (acyclic alkanes)/naphthenes}$$

$$R_V = 1.0 + 1.8 * \log V$$

$$J = (2MH+3MH)/1,2\text{-}(cis+trans)\ DMCP$$

$$R_J = 0.84 + 1.1 * \log J$$

$$R1 = 1,\text{-trans-2-DMCP}/1\text{-CIS-2-DMCP}$$

The cross plot of heptane (H) and Isoheptane (I) values was also suggested as a maturity indicator as well as a source indicator (Table 5-5); the oils from the same kerogen should vary along the aliphatic or aromatic curves depending on their maturity, with the higher the values the higher the maturity (Thompson, 1979; Thompson, 1983). Thompson, (1979) attributed this temperature related changes to the thermal cracking of higher polycyclic hydrocarbons such as triterpanes, to cyclopentanes and cyclohexanes, which undergo ring opening under increasing thermal stress and thus the formation of relatively highly stable acyclic alkanes (Thompson, 1979). Mango (1990a) argued that the cycloalkanes are more stable than the open chained alkanes, and thus the higher polycyclic hydrocarbons were less likely to be the source for light cycloalkanes (Mango, 1990a).

Two ratios based on isoalkanes were reported as excellent maturity indicators; these are 2-MH/3-MH and 2,4-DMP/2,3-DMP (Mango, 1987), with the latter being better indicator of temperature of generation according to the kinetic steady state metal catalysis model (Mango, 1990b). Mango believed that the 2,4-DMP/2,3-DMP ratio is independent of source and time of residence in sediments. BeMent *et al.* (1995) compared 2,4-DMP/2,3-DMP ratios of a large set of oils and extracts of various ages and kerogen types, with calculated vitrinite reflectance determined from maximum burial temperatures for each of the source rocks. They concluded that this ratio is independent of kerogen type and heating rate confirming Mango's above speculations, and is strongly related to the temperature of generation. They used this calibration to formalize an equation to calculate the temperature at which the oil was generated based on 2,4-DMP/2,3-DMP ratio (Equation 5-4). They found that the unaltered

primary oils are generated at a temperature range of 95 °C to 140 °C with an average of 125 °C. They also reported good correlations between this ratio and API gravity for genetically related oils. Mango (1997) claimed that this equation can be calculated from his data published in (Mango, 1990b). Some studies confirmed this significant discovery e.g. (Chung *et al.*, 1998). However, other studies reveal that this ratio can be source dependent, has poor correlation with API gravity, and poor correlation with source rock temperature (Peters *et al.*, 2005 , and references therein). The poor correlation between this ratio and API gravity can be related to the secondary processes that alter the oils and make them no longer reflect the original oils. The absence of correlation between maturity biomarkers and this ratio may reflect mixing of light and heavy hydrocarbon components of different maturity (Peters *et al.*, 2005).

Equation 5-4 : The temperature at which the oil is generated from the source rocks (BeMent *et al.*, 1995).

$$°C_{temp}=140+15\ \ln(2,4\text{-DMP}/2,3\text{-DMP})$$

Kornaki and Mango (1996) (in Peters *et al.*, 2005) proposed a calculated value to evaluate whether the light hydrocarbons of crude oils have been subjected to secondary alteration or not; they called it "primesum value". The full description was listed in Peters *et al* (2005). The C_7 distributions can be described as linear combinations of three end members, *a* (Methylcyclohexane+ Toluene), *b* (dimethylpenetanes), and *c* (Methylhexanes+alkylcyclopentanes) and the sum of the coefficients of the three end members should sum to one. These coefficients are expressed as, *a*, *b* and *c*. The calculations of these coefficients are performed using the listed in equations below.

Equation 5-5: K for kinetic rate , K3 for 3 ring closure, K5 for 5 rings closure and 6 for 6 rings closure, (Figure 5-6, Equation 5-2)

$$K^3=P_2+P_3+N_2/P_3$$

$$K^5=N_2^5+N_1^5/2P_3$$

$$K^6=N^6{}_1/P_3$$

Then, the mixing of these theoretical end members is defined by the following equations:

Equation 5-6

$$\ln(K^3)=a(1.64)+b(1.11)+c(2.65)$$

$$\ln(K^5)=a(0.76)+b(3.62)+c(3.12)$$

$$\ln(K^6)=a(3.98)+b(1.46)+c(1.51)$$

Finally, the primesum can be determined by performing matrix inversion on the previous equations to get the coefficients, using these equations:

Equation 5-7

$$a= -0.0197 \ln(k^3)-0.1199 \ln(k^5) +0.28226 \ln(k^6)$$

$$b= 0.2436 \ln(k^3)-0.1745 \ln 9k^5)-0.0671 \ln(k^6)$$

$$c=0.2875 \ln(k^3)+0.1473 \ln(k^5)-0.1469 \ln(k^6)$$

Kornacki and Mango (1996) stated that the oils that yield a primesum value of 1, have not been subjected to secondary alteration and classified as original oils. Those oils with a primesum value of 0.8 and positive coefficients (a, b and c), might have been biodegraded, and those with primesum values greater than one might have been affected by TSR. However, primesum values can be affected by source facies and also the oils derived from carbonate source rocks were found to yield a primesum of greater than 1. Furthermore, some TSR-altered oils were found to yield a primesum of 1 like other unaltered oils (Peters *et al.*, 2005).

Phase fractionation is one of the most important secondary processes that can result in significant alteration of gross compositions and amounts of LHC. Phase fractionation is caused by several processes including differential migration of gas and liquid (Larter & Mills, 1992), addition of methane (or gas rich) charge to reservoired oil, and leakage of gas cap through faults to form an independent condensate accumulation at shallower depth (Thompson, 1987). This process is initiated by the exsolution of gas from the parent petroleum fluid because of decrease of pressure. This phenomena was first suggested by Silverman (1965) as a phase separation process (Silverman, 1965) and then reintroduced and modified by Thompson (Thompson, 1987; Thompson, 1988) in the form of evaporative fractionation as a

result of admixture of migrating methane with the emplaced oil. The separation of the gas phase involves the transfer of material of low and intermediate molecular weight in to the vapour phase. The light components will be distributed unevenly in the gas and liquid phase prior to separation depending on their vapour-liquid equilibrium constants. Therefore, this will result into different relative abundance in the two phases and so some ratios can be formulated. The dissolution of any given compound in gas phase is controlled by its vapour pressure or fugacity (Thompson, 1987). The fugacity (f) is controlled by the molecular weight (e.g. $f_{methane} > f_{ethane} > f_{propane}$), isomeric structure (for identical molecular weight, e.g. $f_{1\text{-cis-2-DMCP}} > f_{1,1\text{-DMCP}}$), hydrocarbon class (e.g. $f_{aliphatic} > f_{aromatic}$) and the composition of the mixture of hydrocarbons involved (Thompson, 1987). All aromatic hydrocarbons except benzene can form transitory complexes of higher molecular weight by inducing polarity in other molecules because of their polar structures. This should restrict the escape of the aromatic compounds to the gas phase, and enrich them in the liquid phase. (Thompson, 1987; Thompson, 1988). K. Thompson investigated this process by conducting a series of experiments on normal oils repeatedly recharged with methane to saturation, and then releasing the pressure and collecting the gas (Thompson, 1987). The residual oil becomes more depleted in light hydrocarbons and enriched in aromatic hydrocarbons after each methane charge is removed. Normal and branched paraffins partition into the gas phase more readily than aromatic and cyclic hydrocarbons. Therefore, the residual oil is expected to be enriched in aromatic and cyclic hydrocarbons, and the vapour phase/gas condensate is expected to be enriched in paraffins and branched alkanes. Subsequent addition of methane would result in both residual oil and gas condensates becoming more enriched in aromatic and cyclic paraffins, and depleted in normal alkanes and branched alkanes, relative to the previous residual oil (Thompson, 1987). Thompson (1987) stated that this process can be easily screened by a cross plot of normal alkanes/napthenes and aromatics/normal alkanes, and proposed several ratios based on experiments and empirical observations. Thompson (1987) used the cross plot of F (*n*-heptane/ methylcyclohexane) versus B (Toluene/*n*-heptane) to describe the effect of evaporative fractionation as well as other possible processes (Figure 5-9). The three compounds used in these ratios have the same carbon number and approximately similar molecular weight (*n*-heptane (100.2) methylcyclohexane (98.19) and Toluene (92.13); thus their distributions are mainly controlled by molecular structure, which determines the solubility of a particular

compound in gas and oil. Maturity, biodegradation and TSR processes can also be monitored by the cross plot of F and B. With increasing maturity, toluene and normal heptane are enriched in oils and so increase F and B (Thompson, 1987; Thompson, 1988) The effect of TSR and biodegradation on these parameters in oils is reviewed in more detail later in this section. Thompson (1987) found that super mature oils (VRE>1.2) should have the ratio F>1.5 with normal oils (unaltered and have normal maturity) having F=0.4-0.8 and B=0.2-0.6. However, F was found to be largely influenced by source facies; algal rich source rocks within the oil-window can yield F as high as five (Table 5-6) (Peters *et al.*, 2005).

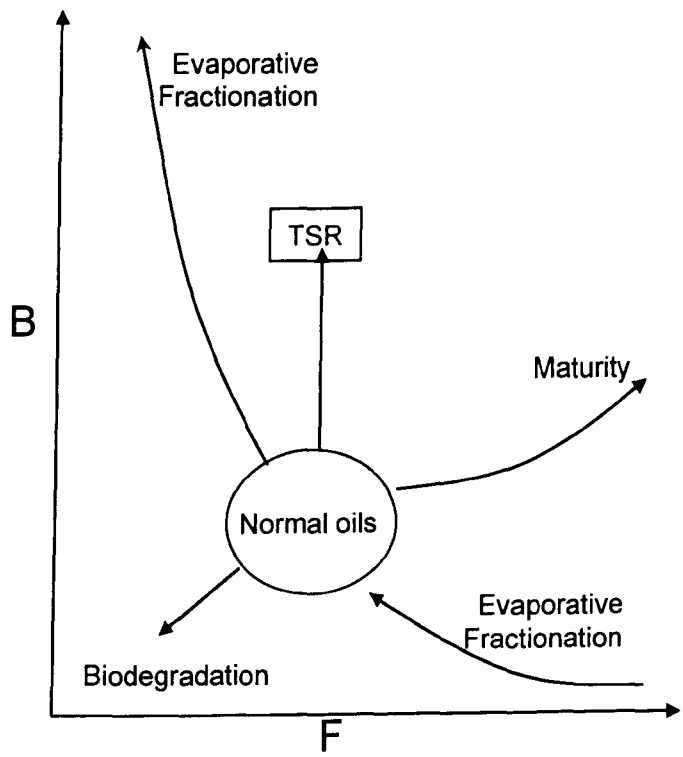

Figure 5-9: B-F diagram illustrating the effect of various processes on both ratios; slightly modified after (Thompson, 1987). B and F are explained in Table 5-5.

Table 5-5: Thompson's ratios of Light hydrocarbons (C_6-C_8). The abbreviations are explained in Table 5-1.

Ratio	Definition	Property assessed
A	Benzene/n-C6	Aromaticity (Fractionation)
B	Toluene/n-C7	Aromaticity (Fractionation)
X	Xylene (m&p)/n-Octane	Aromaticity (Fractionation)
C	(*n*-C_6+*n*-C_7)/CH+MCH	Paraffinicity (Maturity)
I	(2MH+3MH)/1,3-DMCP(*cis*+*trans*)+1-*cis*-2-DMCP	Paraffinicity (Maturity)
F	*n*-C_7/MCH	Paraffinicity (Maturity)
H	100**n*-C_7/(ΣCH thro to MCH) excluding 1-cis-2-DMCP	Paraffinicity (Maturity)
R	*n*-C_7/2-MH	Normality (branching)
U	Ch/MCP	Normality (branching)

Table 5-6: The source dependency of Thompson's ratio F (Peters *et al.*, 2005). The range of values for F (*n*-heptane/Methylcyclohexane) reported from different source facies.

Source facies	F
Thompson's range	0.4-0.8
Marine shales	0.4-1.5
Marine carbonates	0.4-5.0
Tertiary coals	0.1-0.5

Carpentier *et al* (1996) conducted evaporative fractionation experiments at a temperature of 134 °C and pressure release from 335 to 240 bars and then to ambient conditions; oils and condensates were collected from both stages. Minor variations were found between the recombined oil and the liquid phase at 240bar, while large variations were observed in the ratios (e.g. B, definition in Table 5-5) measured between the liquid and the gas phase at 240bar. Significant fractionations were found between different chemical families for a particular carbon number; the gas condensate was enriched in normal and isoalkanes, depleted in cycloalkanes, and strongly depleted in aromatics. The normal alkanes and isoalkanes of the same carbon numbers, show only slight differences in partitioning, with the isoalkanes

showing slightly more affinity for the gas phase. Cyclic alkanes and the aromatics exhibit relatively more affinity for the liquid phase than normal alkanes. Carpentier *et al* (1996) calculated Thompson's paraffinicity and aromaticity indices (listed in Table 5-5 and illustrated in Figure 5-9) in the first stage-liquid, gas and recombined oil; they confirmed Thompson's evolution trends. No partition variations were observed for compounds of similar carbon number within the same chemical family (e.g. isoalkanes). They also suggested that the ratios of n-alkanes/aromatic and isoalkanes/aromatic were possible parameters to distinguish phase separation effect for genetically related oils. There is a good correlation between the partition coefficients and critical temperatures for each individual compound, and no correlation with boiling point (aromatics have higher critical temperatures than normal alkanes) (Carpentier *et al.*, 1996). Although they found that the composition could be modelled accurately by Equations of state (EOS), the properties of the recombined fluids such as bubble point pressure, gas oil ratio, and densities were not accurately predicted by the model.

Meulbroek *et al.* (1998) designed a computer-based model to predict phase fractionation caused by migrating gas charge into oil accumulation and this model was applied to South Eugene Island Block 330 in US Gulf coast. The model was mainly based on examination of the effects of different amounts of added methane to normal oil on the paraffinicity, and aromaticity indices proposed by Thompson, as well as the n-alkane distribution of a large petroleum database. The more methane migrated to the system, the higher the aromaticity and the lower the paraffinicty in the fractionated oils, while the distribution of *n*-alkanes is progressively depleted in lower normal alkanes as gas washing progresses (Meulbroek *et al.*, 1998).

van Graas *et al.* (2000) conducted a six stage differential evaporation experiment starting with single phase fluid and constantly decreasing pressure for 6 pressure steps and collected the gas phase at each stage. It was found that small molecules were preferentially dissolved in gas phase, under both ambient conditions (1bar, 15 C) or elevated pressure and temperature. According to their work, pressure is the main control on the partitioning of a particular compound to gas or liquid phase. They stated that it was difficult to formalize general rules for the behaviour of individual parameters (van Graas *et al.*, 2000).

Van Graas *et al.* (2000) found that carbon isotope ratios of individual compounds were not affected by phase fractionation, while the carbon isotope ratios of hydrocarbon fractions are affected, which is believed to be due to the change in composition. Carpentier *et al* (1996) measured carbon isotopic ratios of individual compounds from C_9 to C_{13} and found that there is minor fractionation between recombined oils and residual oils, but the condensates are consistently lighter isotopically. The $\delta^{13}C$ of C_6-C_7 could not be measured due to their losses during sample preparation (Carpentier *et al.*, 1996). Carbon isotope ratios of the whole oils subjected to phase fractionation, were found to be relatively heavier for the residual oils and lighter for the condensates (gas phase) (Curiale & Bromley, 1996; Dzou & Hughes, 1993; Masterson *et al.*, 2001).

Light hydrocarbons can be easily affected by evaporation at room temperatures, complicating the ratios and trends of LHC. Evaporation of light hydrocarbons can result from the sampling, storage and preparation of the samples for analysis (Carnipa-Morales *et al.*, 2003). Thompson (1987) used the ratio of Benzene/hexane and xylene/n-octane to assess this problem. He suggested that this process is accompanied by sharp increase in the first ratio and no change in the second ratio (Thompson, 1987). Carnipa-Morales *et al.* (2003) performed series of experiments to evaluate this potential problem as well. They found that several parameters are easily affected by this type of evaporation, such as Thompson parameters (aromaticity and paraffinicity and other ratios listed in Table 5-5), Halpern correlation parameters (listed in Table 5-3) and transformation ratios (listed in Table 5-7), as well as Mango's ternary plots (e.g. Figure 5-8). The cross plot P2 vs. N2/P3 (these are explained in Table 5-2) was found not generally affected by evaporation. Carnipa-Morales *et al.* (2003) stressed on the importance of storage preservation conditions of oil samples and speculated that the samples used by different workers in this field (such as Mango and Thompson) must have been well preserved.

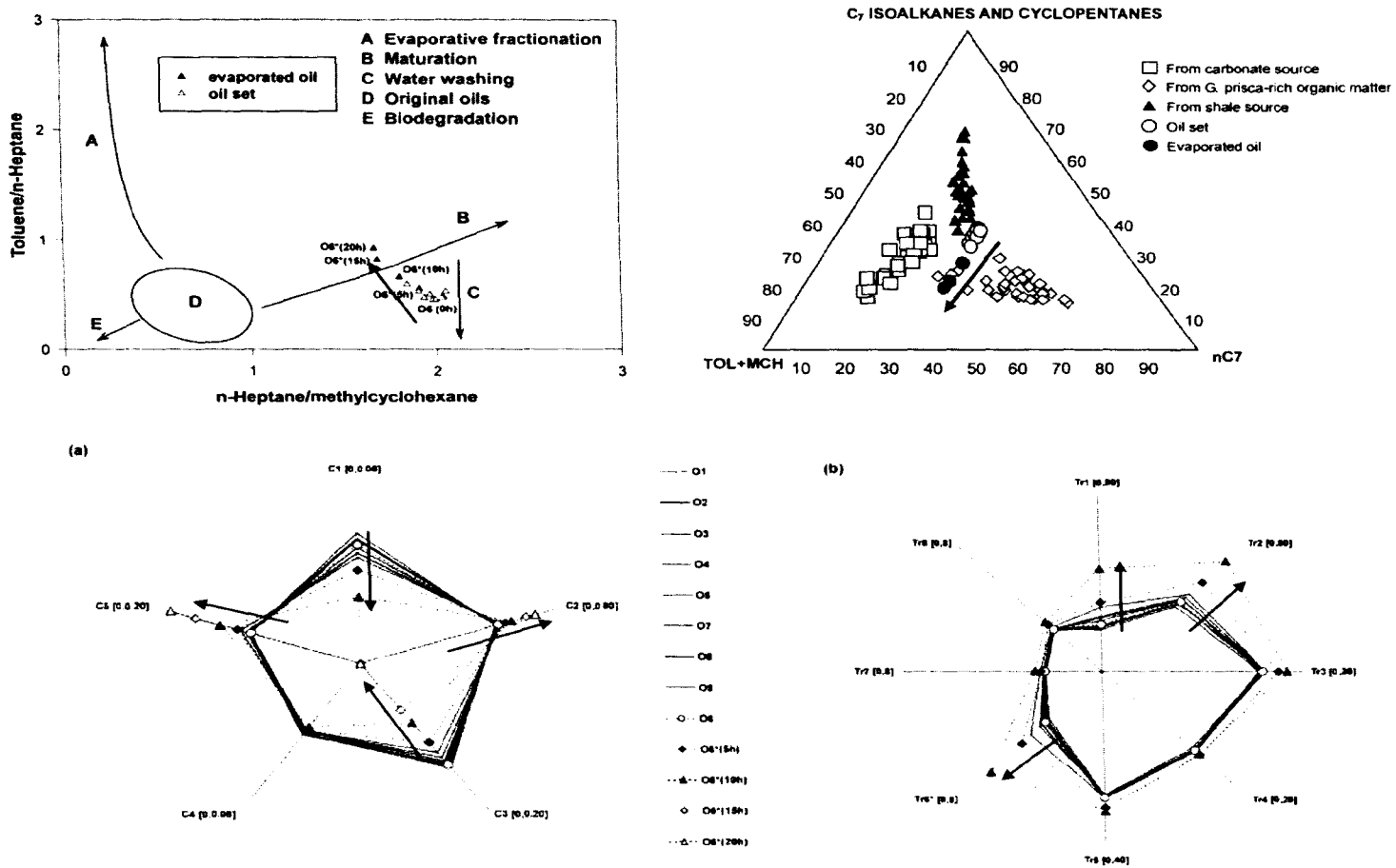

Figure 5-10: the effect of room temperature evaporation on some of the common LHC ratios. The solid black arrow indicate the effect of room temperature evaporation with increasing time.

Several studies have reported the effects of biodegradation and water washing. The susceptibility of any compound to be attacked by microbes depends on its carbon skeleton, degree of alkylation, and position of alkylation (George *et al.*, 2002). George *et al.* (2002) stated that the carbon skeleton controlled biodegradation series is expected to be as following: MH>1,2-DMCP&1,3-DMCP >MP&1,1-DMCP (with decreasing solubility). It was also noted that biodegradation decreases with increasing degree of alkylation (George *et al.*, 2002). The compounds with adjacent alkyl groups (1,1 or 1,2 or 1,2,3) were found to have higher resistance than those with widely positioned groups (George *et al.*, 2002). Branched alkanes with alkyl groups (group near to the either ends of the molecule) were found to be more susceptible to microbial attack than those with alkyl groups in the middle (2MH>4MH>3MH, i.e. susceptibility to biodegradation decreases) (George *et al.*, 2002). Thompson (1987) suggested that the relative decrease of ratios F and B indicates biodegradation, because normal heptane is selectively removed by microbes and toluene is extracted by water washing which may co-occur with biodegradation. Kornacki and Mango (1996) (in Peters *et al.*, 2005) proposed that a primesum value (explained in by Equation 5-5 & Equation 5-6 & Equation 5-7) less than 0.8 and positive coefficients is indicator of biodegradation. Biodegradation can also affect the compound specific isotopic values. Biodegraded oils tend to be enriched in ^{13}C because ^{12}C is more easily utilised by micro organisms; the lighter hydrocarbons tend to be isotopically heavier than heavier hydrocarbons (George *et al.*, 2002). Halpern (1995) suggested eight C_7 ratios (TR1-8) as indicators of alteration caused by biodegradation, water washing and evaporation, and proposed that they were better normalised collectively as a star diagram (Halpern, 1995). Seven of these ratios (TR2-TR8) measure the level of biodegradation in the oils by going from TR8 (most resistant) to TR2 (most prone) and six of these have 1,1-DMCP as the denominator, which is believed to be the most resistant light hydrocarbon to biodegradation by Halpern (1995). TR8 is the ratio of methyhexanes to dimethylpentane, which is believed to be the most resistant to microbial attack. TR6 is a measure of evaporation due to the large difference in boiling point between the nominator and denominator (Δ 11.7°C) (Halpern, 1995).

Table 5-7: Transformation ratios proposed by Halpern (1995). Δ is the difference between the nominator and denominator. The Solubility in water.

Name	Ratio	Δ BP (°C)	Δ Solubility (ppm)
TR1	Toluene/1,1-DMCP	22.8	496
TR2	*n*-C7/1,1-DMCP	10.6	-21.8
TR3	3-MH/1,1-DMCP	4.0	-21.4
TR4	2-MH/1,1-DMCP	2.2	-21.5
TR5	P2/1,1-DMCP	3.2	-21.4
TR6	1-*cis*-2-DMCP/1,1-DMCP	11.7	-11.0
TR7	1-*trans*-3-DMCP/1,1-DMCP	3.0	-4.0
TR8	P2/P3	6.0	-0.6

The removal of hydrocarbons by leaching to the water (water washing) is a phenomenon that can have a great impact in the composition of hydrocarbon column (Lafargue & Le Thiez, 1996). The first Halpern transformation indicator (TR1) in Table 5-7, is a measure of water washing because it is based on the large difference in solubility between the nominator (Toluene) and denominator (1,1-DMCP) (Δ 496ppm) (temperature was not stated) (Halpern, 1995). Lafargue & Le Thiez (1996) conducted experiments to investigate the effect of water washing on hydrocarbons. They found that water washing is a slow process affecting mainly the most soluble compounds (Benzene, toluene, xylene), followed by normal alkanes and then the cycloalkanes. Cycloalkanes should be more soluble than normal alkanes, which is opposite to the observed trend. Lafargue & Le Thiez (1996) attributed this to what they call "co-solvent effect" or mixing effect. The water washing effect was also found to increase with increasing temperature and water flow rate and decreases with increasing the hydrocarbon column height (Lafargue & Le Thiez, 1996). Lafargue & Le Thiez (1996) suggested the cross plot of benzene/*n*-C_6 versus toluene/*n*-C_7 as evidence for a water washing effect; both ratios should be expected to decrease with water washing (Lafargue & Le Thiez, 1996). George *et al* (2002) suggested the cross plot of MCH/Tol versus 3MP/Benz to distinguish the water washing effect. Water washing effects should be associated with increases in both of the ratios because of large difference in solubility between nominator and denominator in each ratio (George *et al.*, 2002).

Thermochemical sulphate reduction (TSR) is another secondary alteration process that can alter the gasoline range hydrocarbon composition significantly. Increasing TSR is associated with a preferential increase in cycloalkanes relative to the acyclic alkanes, which results in a drop in isoheptane value (I) and an increase in the Heptane value (H) (Peters *et al.*, 2005) (H & I defined in Table 5-5). TSR can also increase B (Tol/n-C7), and causes little effect on F (n-C7/MCH) in moderate TSR reservoirs, while in severely altered TSR oils, B drastically increases and F is reduced (Peters *et al.*, 2005). TSR has been also reported to disturb Mango's invariance ratios (K1, K2, K3, & K4) (Whiticar & Snowdon, 1999) and usually yields a K1 value greater than 1 . This TSR affected oils plot off the normal trend line of these ratios. Compound specific Isotopic analysis (CSIA) of gasoline range hydrocarbons is a very powerful analysis to detect the effect of TSR in condensates and oils (Whiticar & Snowdon). Whiticar & Snowdon (1999) showed that that the carbon isotope ratios of the gasoline-range fraction of condensate samples from Brazeau River are strongly influenced by TSR. The light hydrocarbons of these TSR affected condensates appear to be enriched in ^{13}C relative to those unaffected TSR (greater than 10‰) and that the *n*-alkanes are most affected by TSR (Figure 5-11) (Whiticar & Snowdon, 1999). Rooney (1995) studied the effect of thermochemical sulphate reduction in CSIA and revealed that TSR affects more readily condensates (heavier carbon isotopic ratios) than oils and specifically saturated hydrocarbons fraction, which may be shifted up to 3‰ (Rooney, 1995).

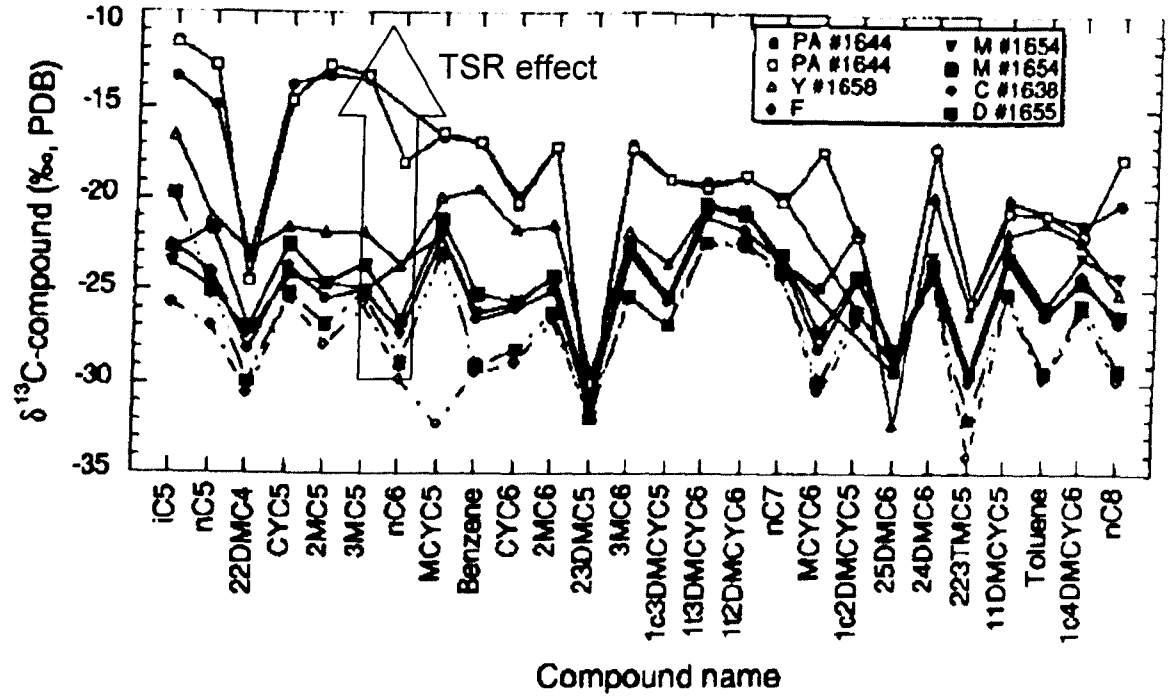

Figure 5-11: The effect of Thermochemical sulphate reduction on the $\delta^{13}C$ of individual light hydrocarbons of condensates and crude oils from Brazeau River (Western Canada). PA and Y are condensates.

Chung *et al.* (1998) used the light hydrocarbons of oils as well as biomarkers and isotopic data from C_{15+} fractions to identify mixing sequences between oils derived from Kimmeridge Clay Formation, Heather formation and Brent coal in the North Sea (Chung *et al.*, 1998). Light hydrocarbons were also used together with other biomarker parameters and concentrations to identify significant input from the Bakken shale into the Madison Group reservoirs in the Canadian Williston Basin (Jiang & Li, 2002). Jarvie & Lundell (2001) used a ternary plot $P_1/ N_1^6/(P_2+ P_3+N_1^5+N_2^5)$ (these parameters are defined in Figure 5-6 & Table 5-2) to identify mixing of oils in the Williston Basin (Jarvie & Lundell, 2001). Rooney *et al.* (1998) used compound specific isotope analysis of light hydrocarbons to distinguish biodegraded and normal oil mixing in Clair field, West Shetland, by comparing CSIA of LHC released from the pyrolysis of the asphaltenes in the oil (Rooney *et al.*, 1998).

5.3 Sampling and data analysis

The light hydrocarbons (LHC) data were acquired from the Shell database at Petroleum Development of Oman (PDO). The data available for this section were 14 oil samples from 10 wells and 3 different reservoir units. Unfortunately, a number of oils in the Greater Birba area were not analysed by Shell for light hydrocarbons. Figure 5-12 and Table 5-8 shows the samples used in this study and the distributions of the wells. A typical chromatogram of light hydrocarbons used is shown earlier in Figure 5-4.

Table 5-8: The wells, reservoir units, and petroleum of the studied samples.

sampleID	Well	Well code	TVD m	Reservoir unit	Sample type
O2	BIRBA-1	BB1	2536.46	A4C	Oil
O3	BIRBA NORTH-1	BBN1	3455.09	A4C	Condensate
O4	BIRBA-1H1	BB1	2533.06	A4C	Oil
O7	BIRBA NORTH-2	BBN2	3597.75	A4C	Oil
O8	BIRBA-1	BB1	2533.06	A4C	Oil
O9	BIRBA SOUTH-1	BBS1	2329.71	A4C	Condensate
O12	OMRAAN-1	Om1	2601.71	A5C	Oil
O13	NASIR-1	NS1	1998.6	A4C	Oil
O14	DURRA-1	Durr1	2692.97	A3C	Oil
O17	DURRA-1	Durr1	2695.07	A3C	Oil
O18	OMRAAN-1H3	Om1h3	2823.61	A5C	Oil
O19	OMRAAN-1H3	Om1h3	2939.1	A4C	Oil
O20	BUDOUR-1H2	Bud1h2	2971.59	A4C	Condensate
O21	OMRAAN-1H3	Om1h3	3111.51	A3C	Oil
O22	OMRAAN-1H3	Om1	2939.1	A4C	Oil

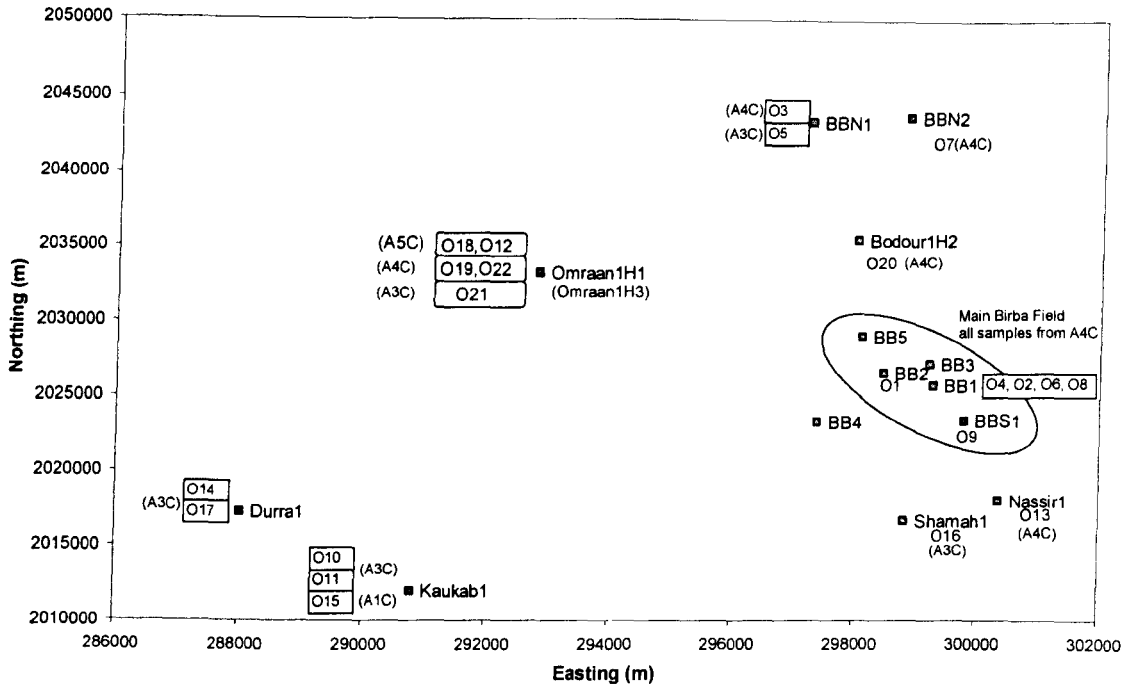

Figure 5-12 The distribution of the wells and oil samples (with letter O) assigned to their reservoir units (with letter A).

5.4 Results

Histograms of the abundances of light hydrocarbons for two representative oils and a gas condensate are shown in Figure 5-13. Normal heptane has the highest abundances in the oils followed by normal hexane. Isoalkanes are next in abundance after normal alkanes, while the cycloalkanes are extremely low. Table 5-9 shows the abundance of light hydrocarbons quantified ($<C_8$) in Greater Birba Area oils. Some of the peaks were very small and could not be quantified, especially C_2-C_4 compounds. Gas condensates show the highest content of light hydrocarbons (>160 mg/g oil), while the oils contain a range of 26-78 mg/g oil of LHC.

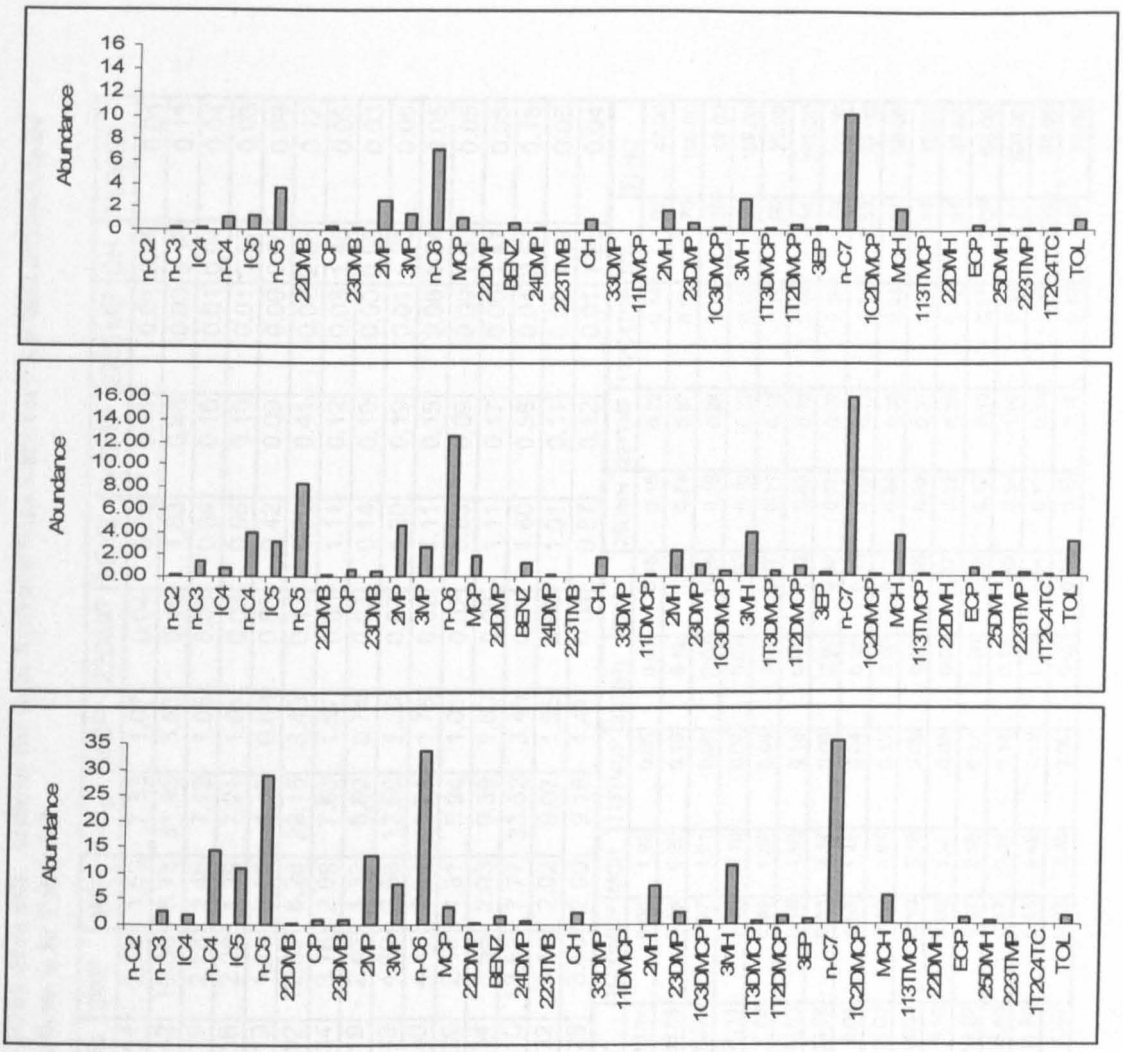

Figure 5-13: the abundances (mg/g oil) of individual hydrocarbons for oil O14 (top), O14 (Middle) and O20 (Bottom, condensate). Similar distributions are observed in other samples.

Table 5-9: The concentrations (mg/g oil) of light hydrocarbons in Greater Birba area oils. some of the light hydrocarbons were very low and difficult to be quantified. The samples are described in Table 5-9 and the key to abbreviations is in Table 5-2.

sampleID	n-C_2	n-C_3	IC_4	n-C_4	IC_5	n-C_5	22DMB	CP	23DMB	2MP	3MP	n-C_6	MCP	22DMP	BENZ	24DMP	223TMB	CH	33DMP
O2		0.03	0.10	0.87	1.39	3.82	0.04	0.28	0.21	2.68	1.53	7.33	1.07	0.04	0.65	0.11	0.01	0.95	0.04
O3		0.05	0.31	3.68	5.82	17.39	0.17	0.94	0.82	10.88	6.73	31.45	3.53	0.16	1.63	0.48	0.03	3.10	0.13
O4		0.11	0.14	1.12	1.25	3.80	0.03	0.28	0.19	2.58	1.46	7.19	1.06	0.03	0.64	0.10	0.01	0.94	0.04
O7				0.01	0.35	1.78	0.02	0.21	0.16	2.28	1.39	7.21	1.04	0.03	0.55	0.10	0.01	0.97	0.03
O8					0.28	0.70	0.01	0.12	0.10	1.29	0.85	4.13	0.68	0.03	0.42	0.09	0.00	0.65	0.03
O9		0.51	1.06	8.32	9.99	23.18	0.18	1.09	0.92	12.32	6.28	29.15	3.43	0.13	1.70	0.41	0.02	2.66	0.12
O12		0.55	0.71	2.88	2.45	5.07	0.07	0.51	0.34	3.16	2.09	7.86	1.57	0.05	1.11	0.12	0.03	1.46	0.05
O13				0.20	0.81	2.60	0.03	0.13	0.19	2.46	1.32	6.60	0.74	0.03	0.14	0.10	0.00	0.58	0.03
O14	0.17	1.34	0.74	3.84	3.22	8.28	0.08	0.56	0.43	4.62	2.63	12.58	1.89	0.07	1.20	0.19	0.01	1.70	0.05
O17		0.72	0.66	3.65	3.15	7.87	0.07	0.52	0.40	4.16	2.41	11.21	1.78	0.02	1.11	0.15	0.06	1.54	0.05
O18		0.14	0.16	0.87	1.12	2.90	0.03	0.27	0.20	2.15	1.31	5.94	1.01	0.02	0.63	0.09	0.00	1.03	0.05
O19		0.16	0.28	1.68	2.07	5.61	0.07	0.47	0.34	3.56	2.03	9.39	1.60	0.08	1.11	0.17	0.00	1.47	0.05
O20		2.68	2.14	14.40	10.87	28.84	0.29	1.20	1.10	13.52	7.77	33.62	3.48	0.21	1.68	0.56	0.04	2.57	0.15
O21		0.24	0.30	1.98	2.13	5.67	0.05	0.44	0.32	3.43	2.02	9.07	1.56	0.06	1.01	0.11	0.00	1.49	0.05
O22		0.32	0.35	2.37	2.27	6.10	0.04	0.43	0.28	3.49	2.00	9.18	1.41	0.04	0.87	0.12	0.01	1.25	0.04

sampleID	11DMCP	2MH	23DMP	1C3DMCP	3MH	1T3DMCP	1T2DMCP	3EP	n-C7	1C2DMCP	MCH	113TMCP	22DMH	ECP	25DMH	223TMP	1T2C4TCP	TOL	∑LHC
O2	0.06	1.76	0.63	0.23	2.84	0.21	0.48	0.24	10.34	0.06	1.92	0.05	0.03	0.48	0.15	0.22	0.14	1.00	42.00
O3	0.19	6.68	2.34	0.77	10.76	0.69	1.62	0.91	38.88	0.18	6.20	0.18	0.12	1.49	0.54	0.87	0.55	5.70	166.00
O4	0.06	1.68	0.65	0.22	2.82	0.22	0.48	0.24	10.26	0.07	1.91	0.06	0.02	0.46	0.13	0.24	0.15	1.38	42.00
O7	0.08	1.52	0.75	0.21	2.87	0.24	0.50	0.24	11.14	0.08	2.19	0.06	0.02	0.50	0.16	0.22	0.18	1.92	39.00
O8	0.05	1.24	0.49	0.16	2.10	0.16	0.36	0.18	7.55	0.05	1.52	0.04	0.01	0.37	0.11	0.18	0.12	0.96	25.00
O9	0.19	5.61	2.19	0.60	9.03	0.61	1.64	0.75	30.43	0.16	4.90	0.15	0.07	1.23	0.43	0.72	0.44	4.34	165.00
O12	0.11	1.90	0.85	0.53	2.98	0.32	0.74	0.29	12.08	0.11	3.14	0.09	0.02	0.62	0.15	0.22	0.19	3.59	58.00
O13	0.06	1.39	0.56	0.22	2.29	0.21	0.45	0.19	8.01	0.05	1.41	0.04	0.00	0.30	0.09	0.12	0.11	0.53	32.00
O14	0.12	2.41	1.08	0.43	3.89	0.39	0.88	0.36	16.03	0.12	3.65	0.11	0.00	0.77	0.24	0.35	0.31	5.24	80.00
O17	0.12	2.12	0.99	0.24	3.75	0.37	0.80	0.32	14.03	0.10	3.19	0.09	0.03	0.66	0.02	0.31	0.22	3.10	70.00
O18	0.06	1.24	0.68	0.20	2.31	0.18	0.47	0.17	9.36	0.08	1.93	0.06	0.00	0.37	0.12	0.15	0.12	1.61	37.00
O19	0.08	1.69	0.96	0.26	3.21	0.34	0.64	0.24	12.56	0.07	2.58	0.12	0.00	0.55	0.12	0.19	0.17	2.09	56.00
O20	0.16	7.44	2.27	0.73	11.27	0.74	1.77	1.02	35.46	0.17	5.34	0.15	0.12	1.43	0.54	1.00	0.56	4.71	200.00
O21	0.08	1.65	0.89	0.28	3.14	0.37	0.69	0.25	11.90	0.11	2.49	0.12	0.00	0.54	0.17	0.18	0.20	2.03	55.00
O22	0.07	1.69	0.78	0.24	2.96	0.24	0.57	0.25	11.42	0.05	2.05	0.06	0.02	0.38	0.13	0.16	0.12	1.27	53.00

Heptane (H) values versus Isoheptane (I) values (Thompson, 1983) distinguish different groups of oils and condensates (Figure 5-14). The curve through the oils of Greater Birba area is similar to those proposed by Thompson for aliphatic and aromatic type kerogen. Figure 5-15 shows the cross plot of paraffinicty and aromaticity indices suggested by Thompson. The same grouping can be observed in this plot.

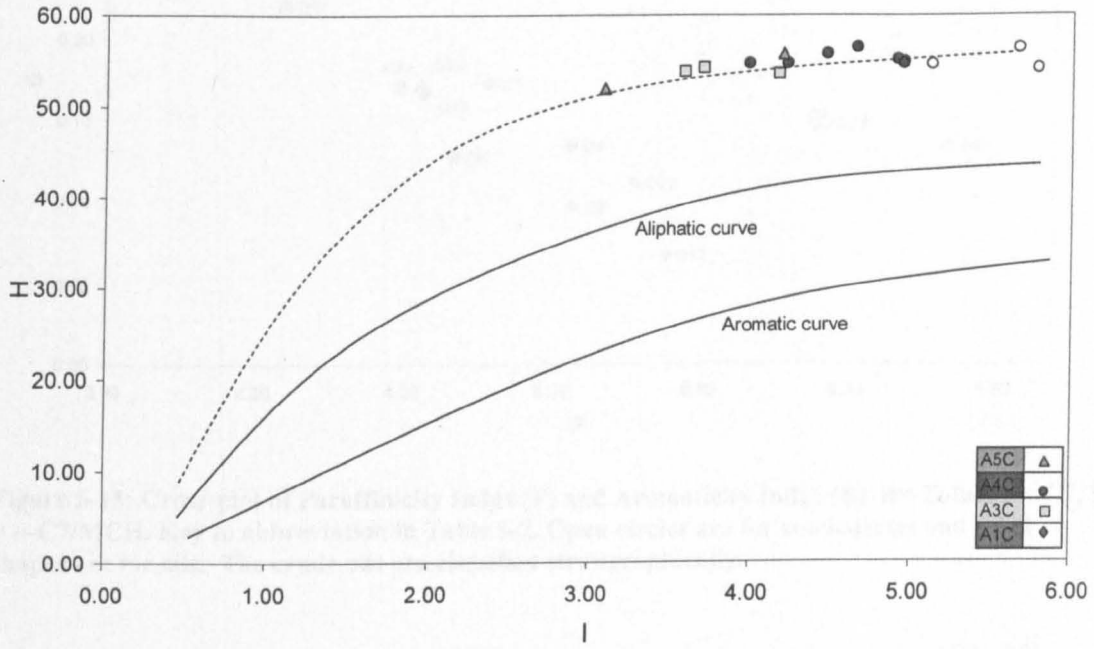

Figure 5-14: cross plot of Heptane value versus Isoheptane value (definition in Table 5-5). H = 100*n-C7/(ΣCH thro to MCH) excluding 1-cis-2-DMCP, I = (2MH+3MH)/1,3-DMCP(cis+trans)+1-cis-2-DMCP. Key to abbreviations in Table 5-2. Open circles are for condensates and filled shapes are for oils. The crude oils are classified stratigraphically.

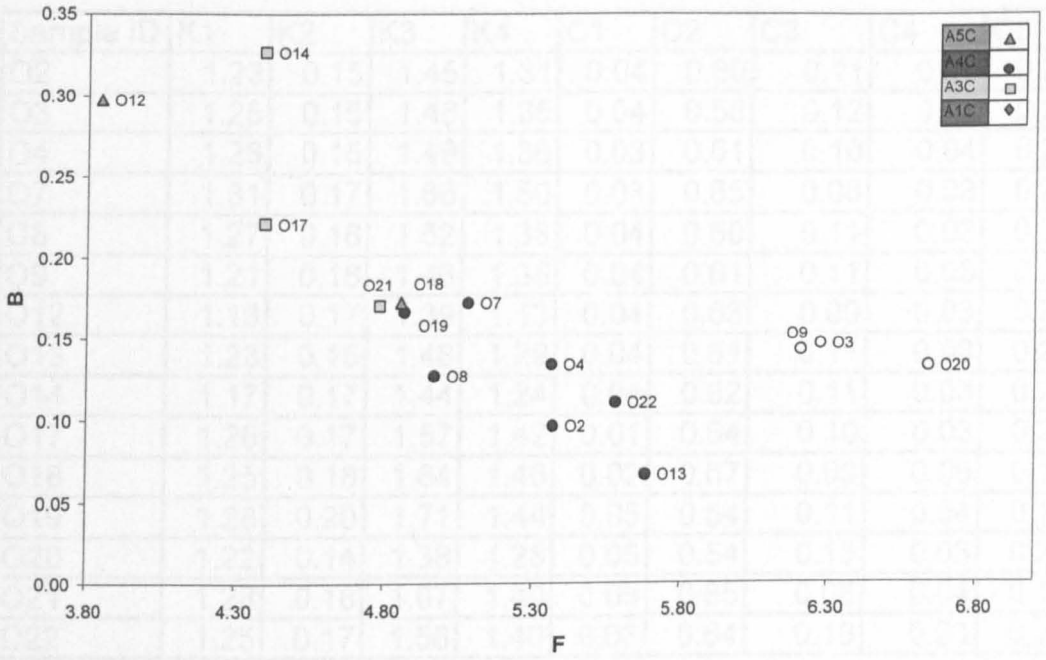

Figure 5-15: Cross-plot of Paraffinicity Index (F) and Aromaticity Index (B). B= Toluene/*n*-C7, F = *n*-C7/MCH. Key to abbreviation in Table 5-2. Open circles are for condensates and filled shapes are for oils. The crude oils are classified stratigraphically.

Table 5-10 shows lists of Halpern's correlation parameters (C1-C5) and Mango's invariant ratios (K1-K4) for the studied oils. Both types of ratios were illustrated in Figure 5-16 and Figure 5-17. Clearly, both illustrations indicate good correlation between oils and gas condensates.

Table 5-10: The correlation ratios proposed by Mango (1987-2000) and (Halpern, 1995). These parameters are explained in Table 5-4 for Mango's invariant ratios and in Table 5-3 for Halpern correlation parameters.

Sample ID	K1	K2	K3	K4	C1	C2	C3	C4	C5
O2	1.23	0.15	1.45	1.31	0.04	0.60	0.11	0.03	0.23
O3	1.25	0.15	1.46	1.35	0.04	0.58	0.12	0.03	0.23
O4	1.26	0.15	1.49	1.36	0.03	0.61	0.10	0.04	0.23
O7	1.31	0.17	1.66	1.50	0.03	0.65	0.08	0.03	0.21
O8	1.27	0.16	1.52	1.38	0.04	0.60	0.11	0.03	0.22
O9	1.21	0.16	1.46	1.35	0.04	0.61	0.11	0.03	0.21
O12	1.13	0.17	1.39	1.13	0.04	0.63	0.09	0.03	0.21
O13	1.23	0.15	1.48	1.29	0.04	0.61	0.11	0.03	0.21
O14	1.17	0.17	1.44	1.24	0.04	0.62	0.11	0.03	0.21
O17	1.26	0.17	1.57	1.42	0.01	0.64	0.10	0.03	0.21
O18	1.25	0.18	1.64	1.46	0.02	0.67	0.09	0.05	0.17
O19	1.28	0.20	1.71	1.44	0.05	0.64	0.11	0.04	0.16
O20	1.22	0.14	1.38	1.28	0.05	0.54	0.13	0.03	0.24
O21	1.28	0.18	1.67	1.40	0.05	0.65	0.08	0.04	0.18
O22	1.25	0.17	1.56	1.40	0.03	0.64	0.10	0.03	0.20

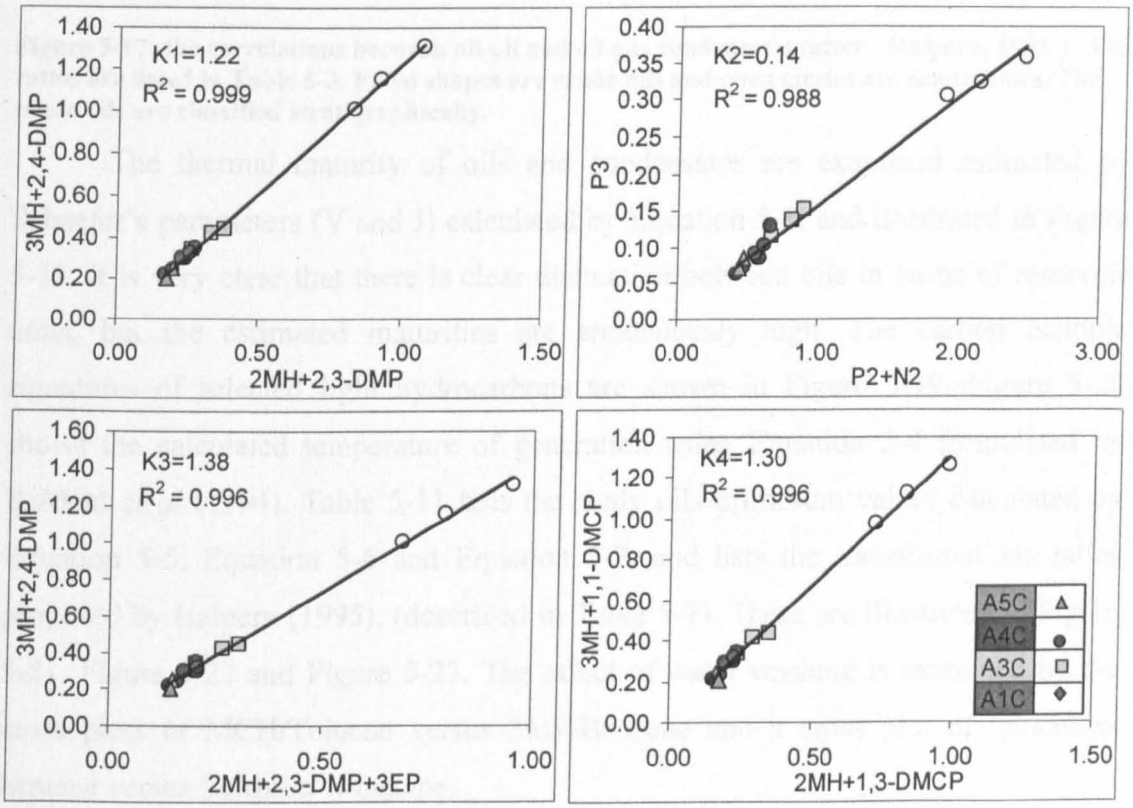

Figure 5-16: Invariance ratios proposed by Mango (1987-2000). Filled shapes are crude oils and open circles are condensates. The crude oils are classified stratigraphically. Key to abbreviations in Table 5-2.

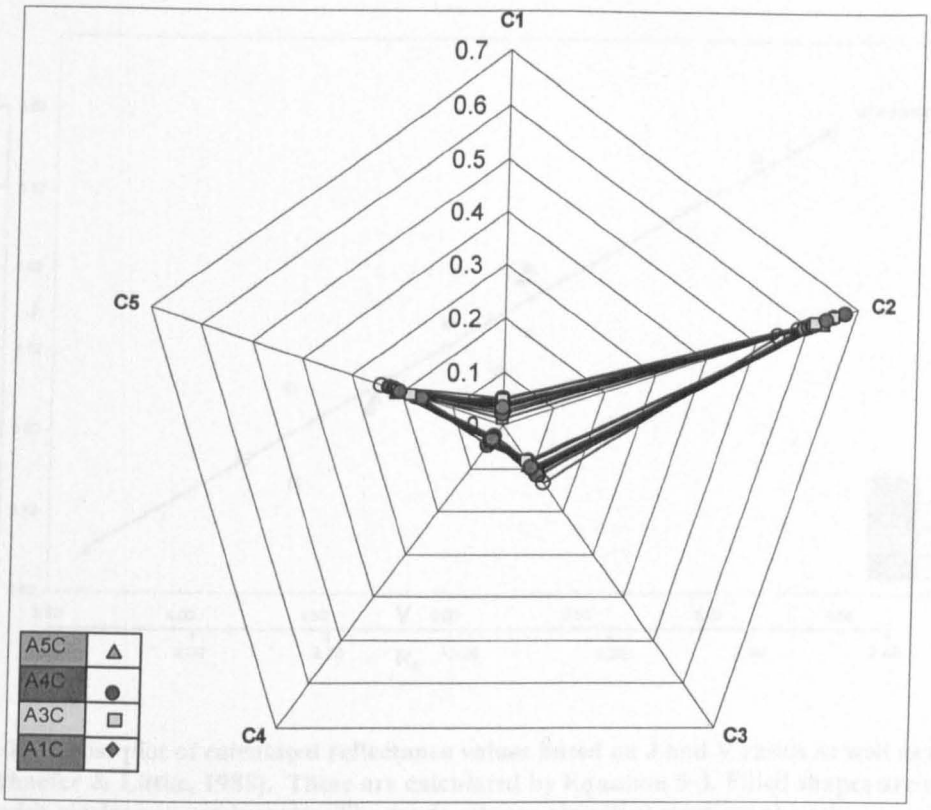

Figure 5-17: the correlations between oil-oil and oil-gas condensates (after Halpern, 1995). The ratios are listed in Table 5-3. Filled shapes are crude oils and open circles are condensates. The crude oils are classified stratigraphically.

The thermal maturity of oils and condensates are examined estimated by Schaefer's parameters (V and J) calculated by Equation 5-1, and illustrated in Figure 5-18. it is very clear that there is clear distinction between oils in terms of reservoir units, but the estimated maturities are anomalously high. The carbon isotopic signatures of selected light hydrocarbons are shown in Figure 5-19. Figure 5-20 shows the calculated temperature of generation using Equation 5-4 formulated by BeMent *et al* (1994). Table 5-11 lists the study oils primesum values calculated by Equation 5-5, Equation 5-6 and Equation 5-7, and lists the transformations ratios proposed by Halpern (1995), (described in Table 5-7). These are illustrated in Figure 5-21, Figure 5-22 and Figure 5-23. The effect of water washing is examined by the cross plots of MCH/Toluene versus 3MP/Benzene and a cross plot of toluene/*n*-heptane versus Benzene/ *n*-hexane.

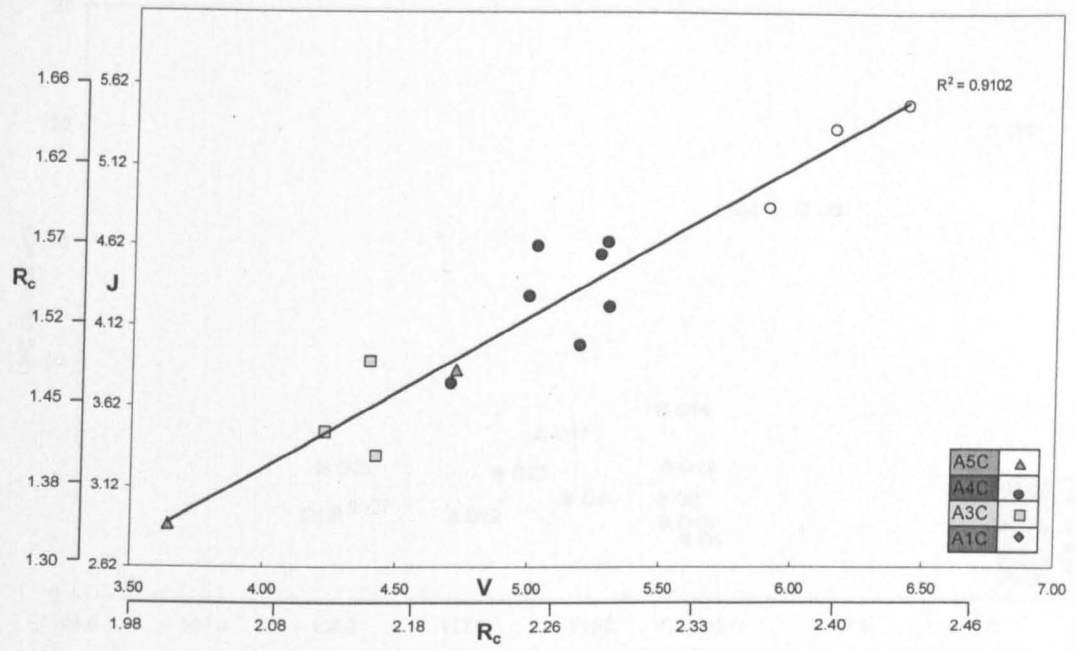

Figure 5-18: Cross plot of calculated reflectance values based on J and V ratios as well as the two ratios (Schaefer & Littke, 1988). These are calculated by Equation 5-3. Filled shapes are crude oils and open circles are condensates. The crude oils are classified stratigraphically.

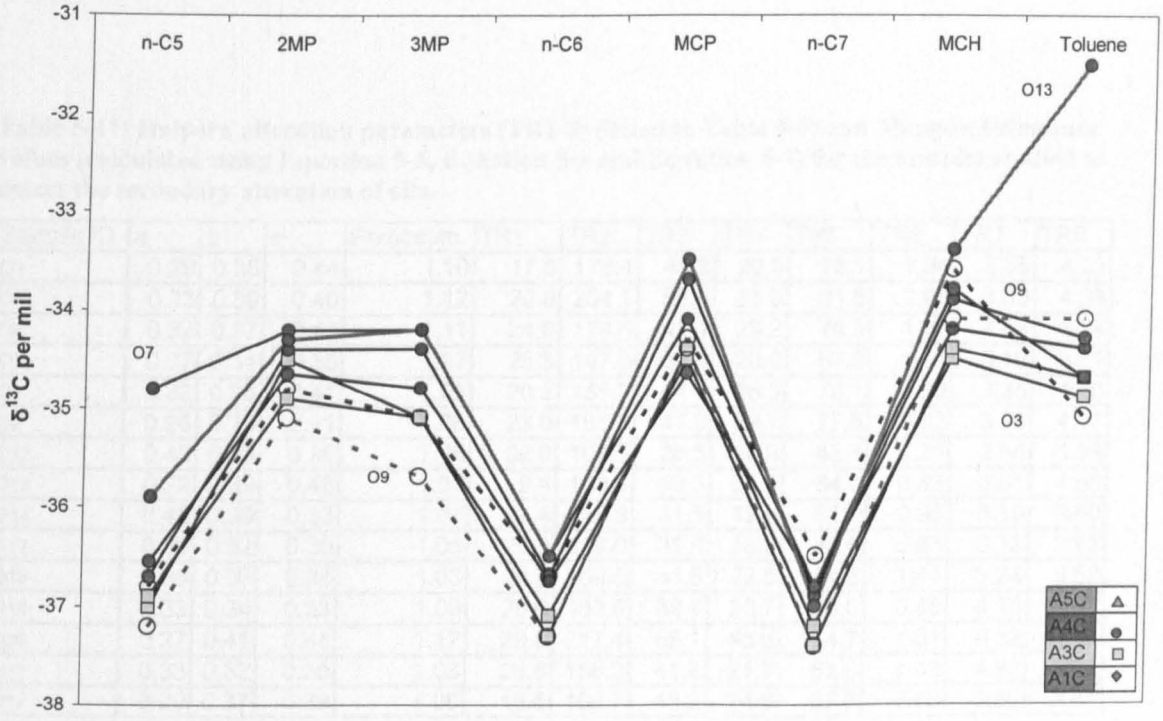

Figure 5-19: $\delta^{13}C$ for a number of selected light hydrocarbons. Filled shapes are crude oils and open circles are condensates. The crude oils are classified stratigraphically.

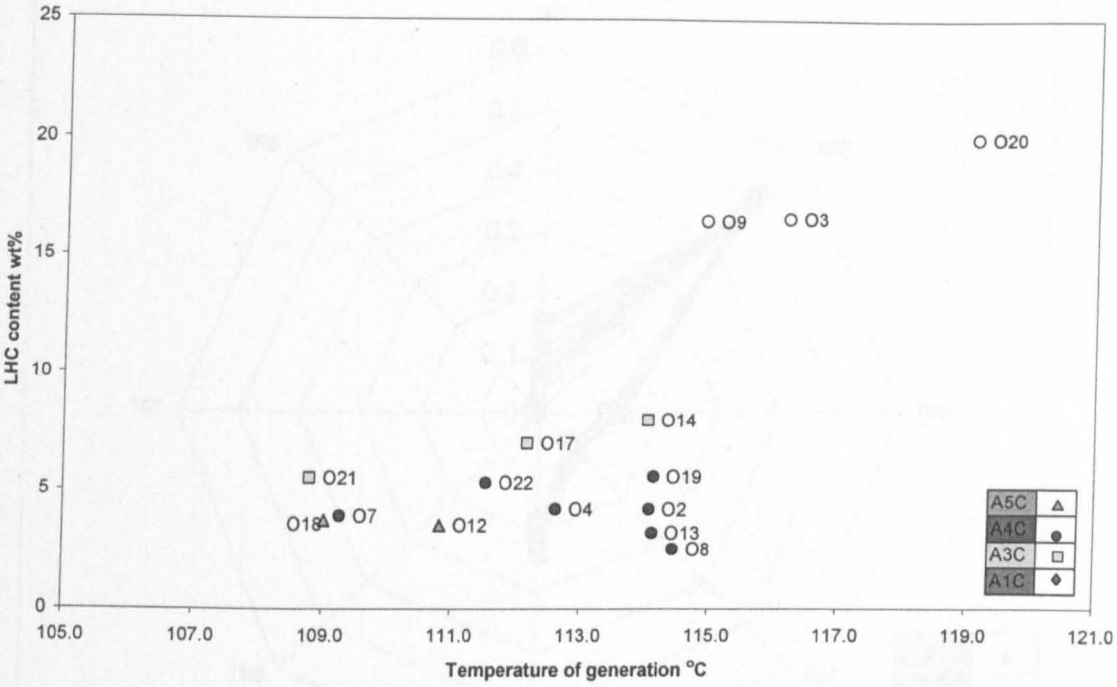

Figure 5-20: Cross plot of LHC (wt%) versus temperature of generation (°C). The temperatures of oil generations were calculated using an empirical equation stated in Equation 5-4 after (BeMent *et al.*, 1994). Filled shapes are crude oils and open circles are condensates. The crude oils are classified stratigraphically.

Table 5-11: Halpern alteration parameters (TR1-8) (listed in Table 5-7) and Mango's Primesum values (calculated using Equation 5-5, Equation 5-6 and Equation 5-7) for the samples studied to detect the secondary alteration of oils.

Sample ID	*a*	*b*	*c*	Primesum	TR1	TR2	TR3	TR4	TR5	TR6	TR7	TR8
O2	0.29	0.38	0.44	1.10	17.0	175.4	48.2	29.9	78.1	1.04	3.65	4.32
O3	0.33	0.39	0.40	1.12	29.9	204.1	56.5	35.0	91.5	0.96	3.63	4.33
O4	0.32	0.37	0.42	1.11	24.0	178.6	49.1	29.2	78.3	1.20	3.88	4.24
O7	0.37	0.34	0.36	1.07	25.3	147.0	37.9	20.0	57.9	1.01	3.10	3.81
O8	0.32	0.36	0.41	1.09	20.2	158.7	44.1	26.0	70.1	1.00	3.35	4.10
O9	0.28	0.39	0.41	1.08	23.0	161.3	47.9	29.7	77.6	0.82	3.26	4.06
O12	0.43	0.29	0.35	1.06	32.0	107.5	26.5	16.9	43.4	0.95	2.84	3.59
O13	0.22	0.39	0.46	1.07	9.4	140.8	40.3	24.5	64.8	0.83	3.61	4.05
O14	0.45	0.30	0.33	1.07	42.4	129.9	31.5	19.5	51.1	0.96	3.19	3.60
O17	0.39	0.32	0.35	1.06	26.3	119.0	31.8	18.0	49.8	0.83	3.12	3.83
O18	0.36	0.33	0.34	1.03	29.2	169.5	41.8	22.5	64.3	1.41	3.24	3.52
O19	0.33	0.34	0.33	1.00	25.6	153.8	39.4	20.7	60.0	0.88	4.15	3.27
O20	0.27	0.41	0.44	1.12	28.9	217.4	69.1	45.6	114.7	1.04	4.52	4.44
O21	0.33	0.32	0.38	1.03	26.6	156.2	41.2	21.7	62.9	1.42	4.83	3.53
O22	0.29	0.37	0.39	1.06	18.6	166.7	43.2	24.6	67.8	0.80	3.50	3.81

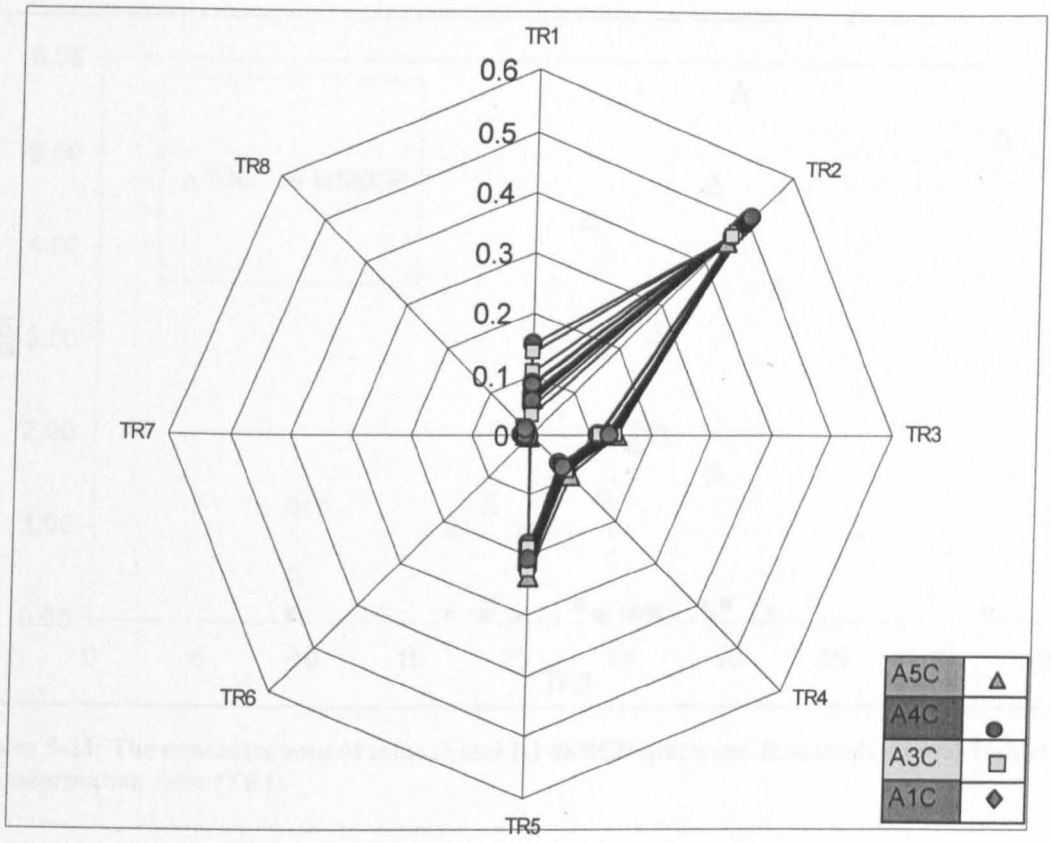

Figure 5-21: The normalised star distributions of Halpern (1995) Transformation ratios in the studied oils. Filled shapes are crude oils and open circles are condensates. The crude oils are classified stratigraphically.

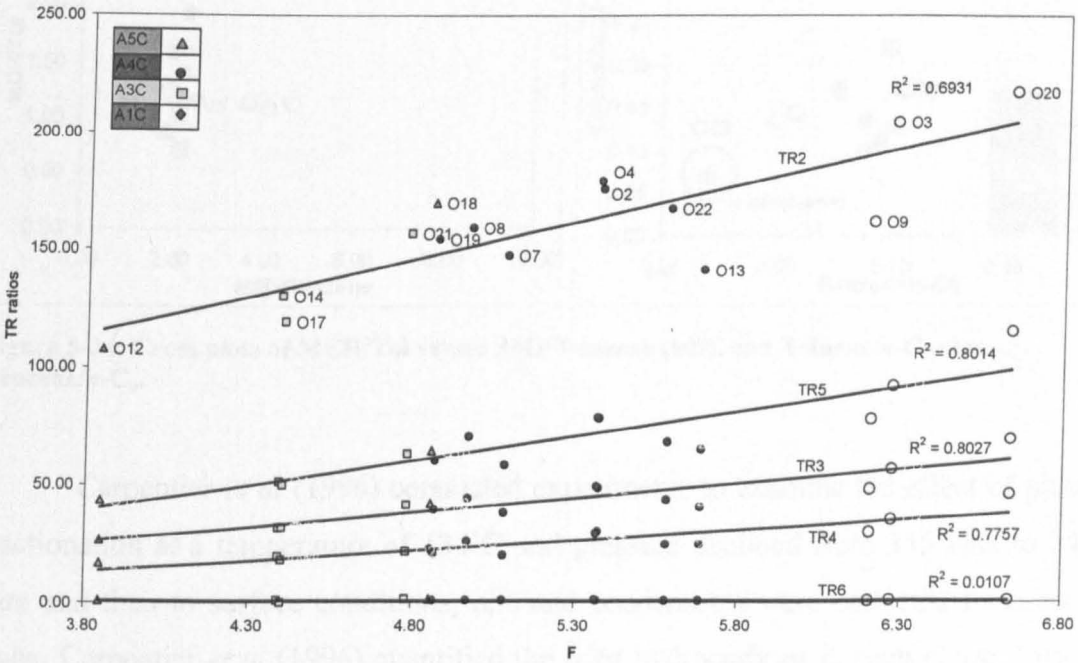

Figure 5-22: The cross plot of different Halpern Transformations ratios against paraffinicty Index F (Table 5-5) of the oils and condensates. Filled shapes are crude oils and open circles are condensates. The crude oils are classified stratigraphically.

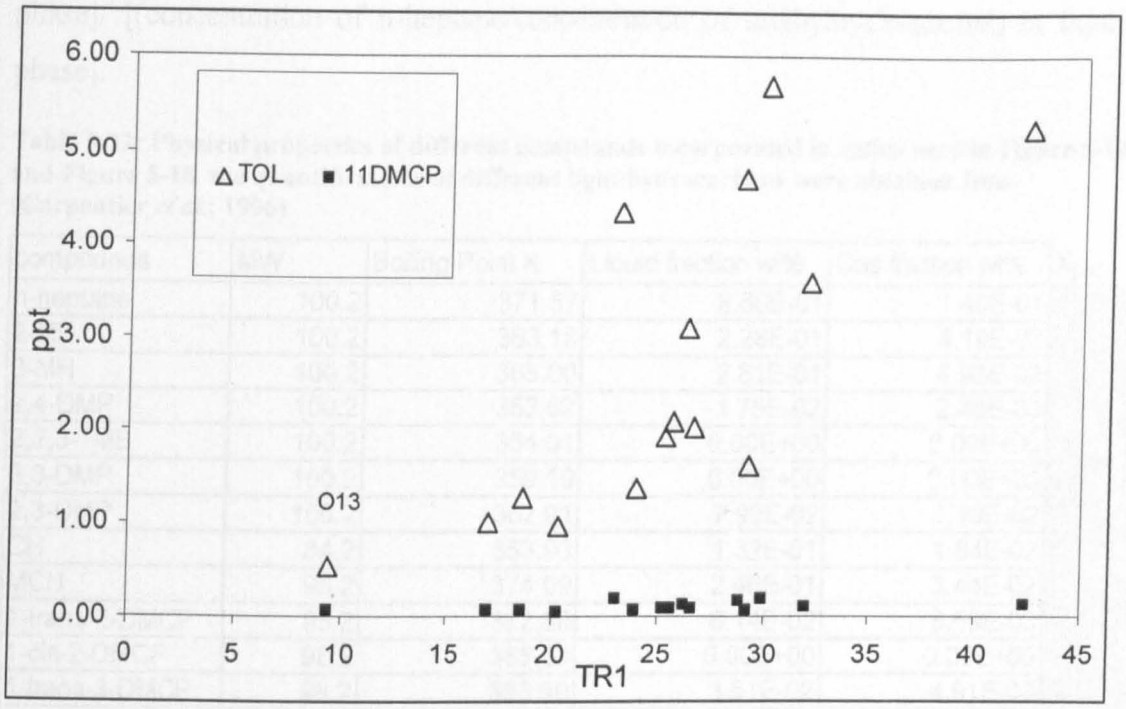

Figure 5-23: The concentrations of toluene and 1,1-DMCP (parts per thousands) versus Halpern Transformation ratio (TR1).

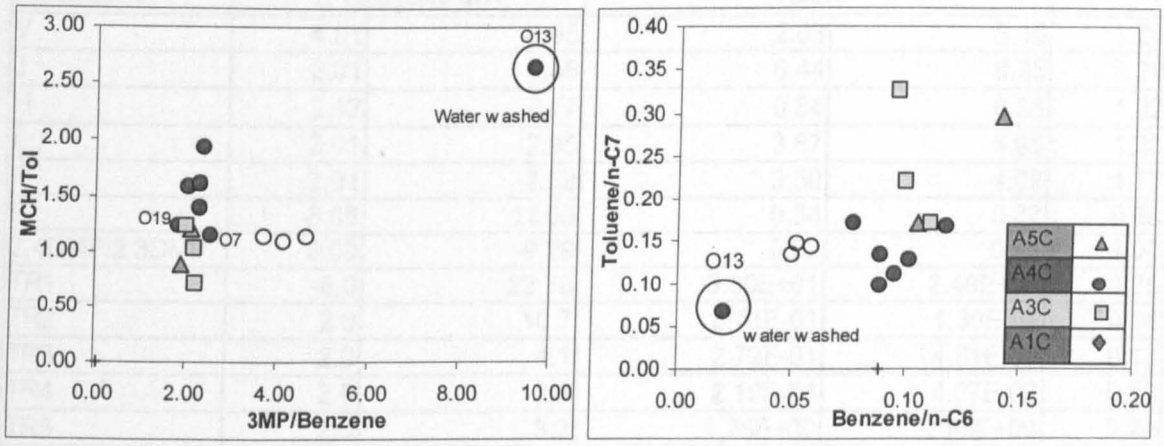

Figure 5-24: Cross plots of MCH/Tol versus 3MP/Benzene (left), and Toluene/*n*-C_7 versus Benzene/*n*-C_6.

Carpentier *et al* (1996) conducted experiments to examine the effect of phase fractionation at a temperature of 134°C and pressure declined from 335 bars to 240 bars and then to surface conditions; oils and condensates were collected from each stage. Carpentier *et al* (1996) quantified the light hydrocarbons in each phase. I used their quantifications to calculate the parameters I used in this study in liquid and gas phases to assess the effect of phase fractionation. The ratio of each parameter in liquid and gas phase is called $X_{G/L}$ where X is the parameter (e.g. for parameter F, $X_{G/L}$ = $F_{G/L}$= [(concentration of n-heptane/concentration of methylcyclohexane) in gas

phase]/ [(concentration of n-heptane/concentration of methylcyclohexane) in liquid phase].

Table 5-12: Physical properties of different compounds incorporated in ratios used in Figure 5-14 and Figure 5-18. the quantifications of different light hydrocarbons were obtained from (Carpentier *et al.*, 1996)

compounds	MW	Boiling Point K	Liquid fraction wt%	Gas fraction wt%	$X_{(G/L)}$
n-heptane	100.2	371.57	8.60E-01	1.40E-01	
2-MH	100.2	363.18	2.28E-01	4.19E-02	
3-MH	100.2	365.00	2.81E-01	4.93E-02	
2,4-DMP	100.2	353.62	1.75E-02	2.46E-03	
2,2,3-TMB	100.2	354.01	0.00E+00	0.00E+00	
3,3-DMP	100.2	359.19	0.00E+00	0.00E+00	
2,3-DMP	100.2	362.91	7.90E-02	1.10E-02	
CH	84.2	353.93	1.32E-01	1.84E-02	
MCH	98.2	374.09	2.46E-01	3.44E-02	
1-trans-2-DMCP	98.2	372.50	6.14E-02	8.59E-03	
1-cis-2-DMCP	98.2	365.00	0.00E+00	0.00E+00	
1-trans-3-DMCP	98.2	363.90	3.51E-02	4.91E-03	
1-cis-3-DMCP	98.2	364.71	3.51E-02	4.91E-03	
1,1-DMCP	98.2	360.90	8.77E-03	1.23E-03	
Tol	92.1	383.60	2.89E-01	3.05E-02	
Parameters	$\Delta T_{boiling}$ and MW		Ratios		
V	4.01	-3.65	2.83	3.38	1.20
J	2.01	0.46	6.44	8.25	1.28
H	3.12	6.77	0.84	0.86	1.02
I	2.01	-2.95	3.87	4.95	1.28
F	2.01	-2.52	3.50	4.08	1.17
B	-8.06	12.03	0.34	0.22	0.65
2,4DMP/2,3DMP	0.00	-9.29	0.22	0.22	1.00
TR1	-6.0	22.70	3.30E+01	2.49E+01	0.75
TR2	2.0	10.7	8.51E-01	1.39E-01	0.16
TR3	2.0	4.1	2.72E-01	4.81E-02	0.18
TR4	2.0	2.3	2.19E-01	4.07E-02	0.19
TR5	2.0	3.2	1.76E+00	2.99E+00	1.70
TR7	0.0	3.0	2.63E-02	3.68E-03	0.14
MCH/Toluene	6.0	-9.5	8.5E-01	1.1E+00	1.33

5.5 Discussion

5.5.1 Kerogen type and source correlations

Thompson (1983) used the cross plot of heptane (H =100*n-C_7/(ΣCH through to MCH) excluding 1-cis-2-DMCP)) and Isoheptane (I=(2MH+3MH)/1,3-DMCP(*cis*+*trans*)+1-*cis*-2-DMCP) values (e.g. Figure 5-14) to distinguish the effect of source, maturity and biodegradation on various cuttings and outcrop samples. The cross plot of these two ratios allows recognition of two different maturation curves for oils generated from aliphatic and aromatic kerogens respectively. Aliphatic kerogen is relatively rich in normal alkanes and aromatic kerogen is rich in isoalkanes (Thompson, 1983). Comparing the studied oils and Thompson's curves reveals that the Thompson set of values is not universal (Figure 5-14). Thompson (1983) established these curves based on mainly extracts of cuttings and outcrop samples, which were largely marine shales. It has been found that carbonate/marl source rocks generally have a trend above the aliphatic curve; the highly aliphatic source rocks from lacustrine facies give higher heptane ratios; and the marine (type II) and prodeltaic (type II/III) source rocks generally fall in between the two curves (Peters *et al.*, 2005). It has been found that Precambrian oils are depleted in cycloalkanes relative to normal and isoalkanes (Peters *et al.*, 2005). The studied oils show relatively higher heptane and isoheptane values and so the maturation curve is above the aliphatic kerogen curve proposed by Thompson (1983). This may be indirect evidence supporting the oils were sourced from carbonate-evaporite source rocks. Alternatively, the high H and I values (listed in Table 5-5) in the studied oils may be related to the age of the source rocks, as those oils were proposed to be sourced from Pre or Infracambrian source rocks (Grantham *et al.*, 1988).

Although the studied oils have already been identified as similar oils sourced from the same or similar source rocks (chapter 4), it has been proposed that those oils were mixed with a condensate-like charge that dilutes the biomarker content in those oils (chapter 4). Therefore, it is important to try to correlate those oils using their light hydrocarbon contents and identify variations, and the controls on these variations. Mango (e.g. Mango 2000) proposed two types of C_7 ratios: invariant ratios and ring preference ratios. The invariant ratios should be constant in all oils sourced from the

same source rocks (Mango, 2000). Therefore, these are powerful parameters for oil-oil and oil-source rock correlations. Figure 5-16 shows the four ratios proposed by Mango and applied to the studied oils. It is very clear according to Mango's (2000) theories that the oils and even the gas condensates are probably sourced from the same source, since all oils and gas condensates fall on the same correlated line. Very small variations are observed in K4 (Figure 5-16), which might be related to the effect of secondary migration related facies impurities. Halpern (1995) suggested five ratios (C1, C2, C3, C4, C5) to be plotted as a star diagram in order to correlate oils, regardless of the effect of secondary processes. These ratios consist of components that have the same solubility in water and the same susceptibility to microbial alteration, eliminating water washing and biodegradation as major controls on any variations among these ratios (Halpern, 1995). However, there are differences in volatility between these compounds, suggesting that the phase fractionation and migration may affect those ratios, as will be discussed in section 5.5.3.1. Figure 5-17 shows that the studied oils correlate well and suggest that they are all likely to be from the same source.

5.5.2 Maturity

It is already mentioned in previous section that the studied oils plot along a maturation curve similar to that proposed by Thompson (1983) for aliphatic kerogen derived oils. The same author used the cross plot of heptane (H) and Isoheptane (I) values (listed in Table 5-5) to classify oils in terms of maturity; the types are normal paraffinic oils, mature, supermature and biodegraded oils as described in Table 5-13. The studied oils show extremely high values for both ratios. Generally, Figure 5-14 shows higher maturity for A4C and gas condensates than A3C and A5C oils. The studied oils have been already proven to be of similar maturity based on C_{15+} hydrocarbons ratios and that the oils are within the oil window (Chapter 4). Therefore, the maturity level suggested by the light hydrocarbons parameters might indicate the maturity of a separate condensate charge mixed with the oils or indicate that the oils and condensates are sourced from highly paraffinic source rocks. According to Thompson's ranges for different maturity levels (Table 5-13), the studied oils fall in the range of super-maturity level for both H and I values (defined in Table 5-5). However, the high values for these two ratios are probably consequence of the oils

being sourced from highly paraffinic source rock, which is likely to be carbonate-evaporite source rock (Peters *et al.*, 2005). The effect of phase fractionation on these ratios will be investigated later (Section 5.5.3.2).

Table 5-13: Classification of oils based on Heptane and Isoheptane values (Thompson, 1983).

Class	Heptane value (H)	Isoheptane value (I)
Normal, Paraffinic	18-22	0.8-1.2
Mature	22-30	1.2-2.0
Supermature	30-60	2.0-4.0
Biodegraded	0-18	0-0.8
The studied oils	>51	>3

Another plot of maturity parameters is shown in Figure 5-18. These shows the calculated vitrinite reflectance based on two maturity parameters J and V [J = (2MH+3MH)/1,2-(*cis*+*trans*) DMCP; V= paraffins (acyclic alkanes)/naphthenes] (as in Equation 5-3) proposed by (Schaefer & Littke, 1988). The ratio J is based on the ratio between the normal heptane to the C_7 naphthene, while the ratio J is based on the ratio of isoheptanes to cyloalkanes. These two ratios were calculated in extracts of source rocks (Lias Є shales, Saxony Basin, Germany) at various depths from different locations. They were observed to increase with maturity and correlate well with measured vitrinite reflectance on these rocks. Good correlation has been obtained between these two ratios on the studied oil samples Figure 5-18. However, the calculated reflectance again indicated super mature source for gas condensates, in agreement with H vs. I cross plot shown in Figure 5-14. The effect of source on the range of these ratios cannot be ruled out as these ratios were observed to be facies dependent e.g. (Chung *et al.*, 1998), and highly likely reflecting the carbonate-evaporite type of oils. Generally, Figure 5-18 shows that there is maturation sequence from A3C/A5C oils through A4C oils to gas condensates. This can be also described as mixing sequence knowing that the C_{15+} hydrocarbons indicate similar maturities for the oils.

The temperatures of generation for the studied oils are calculated from 2,4DMP/2,3DMP ratio using Equation 5-4 according to (BeMent *et al.*, 1994). They were cross-plotted versus the light hydrocarbons content (C_3-C_7) in Figure 5-20. The oils appear to be generated at temperatures equivalent to vitrinite

reflectance of 0.7 to 0.9% (Younes & El-Ghamri, 2006), similar to those suggested by aromatic hydrocarbons parameters (chapter 4). Clearly, from Figure 5-20, there is no clear difference between A4C and A3C/A5C oils; both types of oils span a wide range. The gas condensates have relatively higher values than both types of oils. Although the ratio (24DMP/23DMP) has been proposed as an excellent maturity parameter (BeMent *et al.*, 1994; Mango, 1990b), a claim supported by other studies e.g. Chung *et al.* (1998), facies and in-reservoir alteration processes can affect this ratio (Peters *et al.*, 2005). The wide overlapping calculated temperature of generations of the oils might be caused by the effect of reservoir alteration processes such as evaporative fractionation and possibly migration; which has affected the 2,4DMP/2,3DMP maturity indicator. However, Figure 5-19 shows the compound specific isotope analysis values of selected light hydrocarbons, which shows that A4C tend to have heavier carbon isotope ratios than both A5C and A3C oils indicating that A4C have higher maturity than A5C/A3C oils.

The above arguments can be summarized as that there are maturity differences between A5C/A3C oils and A4C oils, due to mixing with a higher maturity condensate charge. Although this conclusion is supported by the carbon isotopic signature of selected light hydrocarbons as shown in Figure 5-19, the gas condensates show lighter carbon isotopic values than expected especially for the low molecular weight light hydrocarbons. This might have been a consequence of phase fractionation effect. This will be discussed in more details in section 5.5.3.2.

5.5.3 Secondary processes

5.5.3.1 Phase fractionation

It is already mentioned (chapter 4) that the gas condensates in Greater Birba area probably have both thermal and phase fractionation origins. The cross plot of F (=*n*-C_7/MCH) and B (=Toluene/*n*-C_7) (Figure 5-9) reveals interesting trend among the studied oils. Paraffinicity increases and aromaticity decreases from A3C/A5C oils to A4C oils. The gas condensates show the highest values of paraffinicity, while they have more or less similar values for aromaticity as for A4C oils. This is also

supported by the cross plot of A versus C which reveals a similar trend to B-F trend (not shown, see Table 5-5&Table 5-9). If evaporative fractionation (by addition of methane) did occur, those oils with lower paraffinicity and higher aromaticity (i.e. A5C and A3C oils) should be regarded as the residual oils and the A4C oils as the parent oils. However, the gas condensates are distributed and associated with the oils in A4C reservoir unit, suggesting that the possible fractionation should have occurred to A4C oils and not A3C and A5C oils. If A4C oils are the residual oils and the A5C/ A3C oils are the parent oils, the trend would be opposite to the trend proposed by Thompson (1987). Besides, it is difficult to describe the gas condensates present in A4C as the exsolved gas from the parent oils for number of reasons: firstly, the condensates are highly paraffinic but the aromaticity is similar to that for A4C oils (i.e. associated oils); secondly, one of the condensates (O9 of well BBS1) is proved to be in contact with the oil leg (e.g. O4 of well BB1) down dip. The oil O3 is probably also in equilibrium contact with O7 in Birba North block from using rft pressures (there are no PVT data from both of these BBN oils, thus so it is difficult to confirm). The lower content of light hydrocarbons in A4C oils are due to compositional gradient (or phase separation) that is a consequence of gas-condensate-oil mixing.

Thompson's evaporative fractionation involves physical separation of two phases as result of methane added to the system. However, in the Greater Birba area, crude oils coexist with gas condensates in the same reservoir unit, and one of these condensates is proved to be in contact with the oil leg down dip. Maturity and mixing are probably the main mechanisms that caused this trend in B and F (defined in Table 5-5) in oils in Figure 5-9. However, the effect of evaporative fractionation cannot be totally ruled out, as the mixing of a gas rich phase with normal oils can also cause partitioning of paraffins to the gas phase and thus enriching the condensates with normal alkanes, similar to the effects of phase separation process (Carpentier *et al.*, 1996; Larter & Mills, 1991). There is no difference in aromaticity between condensates and A4C oils possibly because it is overprinted with the condensate charge, as the aromatics are the lowest in these oils (Table 5-9). A better model for the origin of gas condensates, which also explains the large paraffinicity variation between oils, is that the original oils in A4C were admixed with gas condensates of relatively higher maturity. This model is further supported by the PVT modelling done on the studied oils (chapter 6). The next section will discuss the maturity and

phase fractionation effect together, to check if the phase fractionation can or cannot be ruled out as a control on the variations observed between oils.

5.5.3.2 Maturity versus Phase fractionation

Maturity difference was suggested by several parameters and relationships; these are the cross plot of heptane (H) and isoheptane (I) values (Figure 5-14), the cross plot of Schaefer parameters (J and V) (Figure 5-18), and the compound specific isotopic analysis $\delta^{13}C$ values of selected light hydrocarbons (Figure 5-19). It is also suggested to a lesser extent by the temperatures of generation predicted from the maturity ratio 2,4-dimethylpentane to 2,3-dimethylpentane (Figure 5-20). However, it is also possible that some of the above parameters might have been affected by phase fractionation, and this possibility is supported by the fact that the distribution of condensates are found all in one reservoir unit (A4C, in the studied area) and some of them associated with oils down dip. Figure 5-20 shows wide range of overlapping temperature of generation between A3C/A5C oils and A4C oils. In addition, the proposed higher maturity A4C oils should have higher total light hydrocarbons, and aromatic LHC than those of lower maturity; but this is not apparent in the data in Table 5-9 and Figure 5-20.

In order to weight these two factors, the above maturity parameters were evaluated by investigating the susceptibility of them to be affected by phase fractionation. Carpentier *et al.*, (1996) conducted PVT experiments and thermodynamic modelling to investigate the affinity of the low to middle molecular weight hydrocarbons ($<C_{20}$) for the gas and liquid phases, which are produced by single and multiple flashes to lower pressures below saturation (Carpentier *et al.*, 1996). According to their study, normal alkanes and isoalkanes partition preferably to the gas phase, while naphthenes and aromatic LHC have a high affinity for the liquid phase. Most of the maturity parameters used here rely on the ratio between different compound classes such as the ratios of normal alkanes to aromatics (e.g. B= Toluene/ n-C_7), and the ratios of isoalkanes to cyclic alkanes (e.g. I=(2MH+3MH)/1,3-DMCP (*cis*+*trans*)+1-*cis*-2-DMCP & J= (2MH+3MH)/1,2-(*cis*+*trans*) DMCP). Therefore, the ratios J, V (Figure 5-18, calculated by Equation 5-3), F, B (Figure 5-15, defined in

Table 5-5), I (Figure 5-14, defined in Table 5-5), and Methylcyclohexane/Toluene are expected to be affected by phase fractionation. Table 5-12 confirms this expectation and shows that these ratios are strongly affected by phase fractionation ($X_{G/L}$ values are greater or lesser than 1). Phase fractionation effect can also alter transformation ratios (listed and defined in Table 5-7) proposed by Halpern (1995). However, the ratios H (Figure 5-14) and 2,4DMP/2,3DMP (or temperature of generation, Figure 5-20) shows values of $X_{(G/L)}$ of 1 or very close to 1, suggesting that these ratios keep constant and have not been affected by phase fractionation. Therefore, the maturity effect is probably a more favoured explanation for the variations between the studied oils. This is also supported by the compound specific analysis of the light hydrocarbons (Figure 5-19). The $\delta^{13}C$ values of the selected compounds in gas condensates always overlap with those values in the A4C oils, suggesting similar maturities of the condensates to the oils in A4C reservoir unit. However, Figure 5-19 shows that the condensates have similar carbon isotopic ratios for *n*-C_7, MCH, and Toluene to A4C oils, but lighter isotope ratios for *n*-C_5, 2-MP, 3-MP, and *n*-C_6 with minor overlap. Carpentier *et al.* (1996) stated that the condensates from phase fractionations show consistently lighter ^{13}C isotopic ratios than residual oils. Therefore, the gas condensates also show signs of phase fractionation. The author believes that this is related to the vertical compositional gradients observed in the Birba Field and probably does occur in other A4C related oil accumulations as a result of mixing of the oils with higher maturity condensate charges.

5.5.3.3 Thermochemical sulphate reduction (TSR)

Thermochemical sulphate reduction has been investigated in the C_{15+} hydrocarbon analysis (Chapter 4), and the conclusion was that there was no solid evidence for its effects in the studied oils. The temperature regime, amount of sulfur, concentration of H_2S supported this conclusion. However, these pieces of evidence are not enough to rule out the effect of this process completely. Thermochemical sulphate reduction has a significant effect on the light hydrocarbons and can alter their distribution e.g. (Whiticar & Snowdon, 1999).

The $\delta^{13}C$ of a number of light hydrocarbons for some of the studied oils are shown in Figure 5-19. Compound Specific Isotopic analysis (CSIA) of gasoline range

hydrocarbons is a very powerful analysis to detect the effect of TSR in condensates and oils (Whiticar & Snowdon, 1999), since they the remaining hydrocarbons enriched in ^{13}C and so show heavier carbon isotopic ratios. There are no significant variations in the carbon isotopic ratios for most of the compounds. However, the A4C oils have consistently higher ratios than the A3C oils (only O10 and O11 from well Kaukab1). Although this could be related to TSR, it more likely reflects the effect of maturity, in agreement with other maturity parameters. Furthermore, the study of Rooney (1995) revealed heavier carbon isotopic ratios in TSR altered condensates and not oils (Rooney, 1995). Interestingly, the gas condensates show lighter isotopic ratios for most of the compounds and were similar to those of the A3C oils; this is consistent with the observations from the whole oil carbon isotopic ratio analysis (chapter 4). This can be related to the effect of the preferential partitioning of lighter carbons to gas phase than in liquid phase during phase separation. The last observation little evidence of the effect of TSR in the studied oils. The oil O13 shows a very heavy carbon isotopic ratio for toluene which might be related to water washing or source impurities, as will be discussed next section.

5.5.3.4 Biodegradation and water washing

No indications of biodegradation and water washing were observed in the C_{11+} hydrocarbons analysis of the studied oil. However, it is important to eliminate these effects from light hydrocarbons because biodegradation and water washing can be expressed clearly in the gasoline-range hydrocarbons data. Table 5-11 show some of the ratios have been used to detect the biodegradation and water washing. These are TR2-7 for biodegradation and TR1 for water washing, suggested by Halpern, 1995 (listed and defined in Table 5-7). The transformation ratios (TR2-7) are based on the susceptibility of the numerator in each ratio to microbial attack, and high resistance of 1,1-DMCP as a denominator (Halpern, 1995). The TR1 ratio is based on the high solubility difference between the Toluene and 1,1-DMCP and thus it is a good indicator of water washing; other processes such as maturity, TSR and phase fractionation enrich oils with aromatics. TR6 can be used to measure the effect of phase fractionation due to the large difference in boiling point between numerator and denominator, which is the largest in this ratio (22.8°C difference) (Carpentier *et al.*,

1996; Thompson, 1987). Figure 5-21 show the normalised star plot of all Halpern transformation ratios. Clearly, most of the oils fall in the same type of star plot confirming the same source for the oils and condensates. TR2-7s do not show major variations in normalised star diagram, ruling out the effect of the biodegradation in the studied oils. The fact that TR6 does not show large variations as in Figure 5-21, confirms that boiling point is not the only factor that determines the evaporative fractionation; vapour pressure or fugacity is as important as boiling point (Peters *et al.*, 2005) and might be more important under the reservoir conditions. However, each individual ratio without star plotting shows large variations as listed in Table 5-11. Five of these ratios were plotted versus paraffinicty index F in Figure 5-22 . This reveals very good correlation of most of these ratios with paraffinicty Index (F) except for TR6, suggesting the same control can be assigned to these as to paraffinicty. Both mixing and evaporative fractionation is possibly controlling these ratios. In summary, there is no evidence for biodegradation in light hydrocarbons as well as high molecular weight hydrocarbons.

The TR1 ratio is a good indicator of water washing. Toluene is highly water soluble relative to 1,1-DMCP (Δ Solubility=496ppm). Generally, A4C oils have lower ratios than for A3C and A5C oils with overlap between them. Figure 5-23 confirms this observation showing that the TR1 increase results from the increase of toluene concentrations and not from the decrease of 1,1DMCP concentration. Figure 5-24 shows the cross plot of MCH/Tol versus 3MP/Benzene c.f. (George *et al.*, 2002) and the cross plot of Toluene/*n*-C_7 versus Benzene/*n*-C_6 c.f. (Lafargue & Le Thiez, 1996), which were used as indicators of water washing. Clearly, only O13 shows a major indication of water washing. The other oils show large variations in toluene ratios, while the condensates are separated by benzene ratios. The light hydrocarbon fraction of the A4C oils shows higher maturity characteristics (Figure 5-14, Figure 5-18, and Figure 5-19). Therefore, the variations in TR1 and other toluene ratios in Figure 5-24, can be interpreted here as to be due to maturity differences between A4C oils and A3C/A5C oils. The O13 oil shows the highest TR1 ratio, the lowest toluene concentration, the heaviest $\delta^{13}C$ isotopic value of toluene, high paraffinicity, and the lowest aromaticity as well as the cross plot of some of the water washing sensitive parameters as in (Figure 5-24). Apparently, this oil was selectively altered by severe water washing. However, the carbonate stringers are well encased in salts and the

water if present will be highly saline. This may lower the possibility of the water washing effect on this oil. Therefore, another possibility is that this oil has been affected by facies variations.

5.6 Conclusions

The light hydrocarbons suggest that the oils and condensates were sourced from carbonate source rocks, which is inferred from the cross plot of heptane and isoheptane values, confirming the same conclusion from chapter 4. The level of the maturity could not be determined; several ratios (e.g. V) suggested super mature sources, however these ratios depend on the source facies and cannot give us a definite value for the maturity. Nevertheless, these suggest relative difference in maturity between A4C and A3C/A5C oils; A4C oils are relatively higher maturity than A3C/A5C oils. The Condensates are probably higher maturity than both types of oils based on the above maturity ratios and this was also suggested to a less extent by compound specific carbon isotope analysis and the high heptane (H) value. There was no sign for biodegradation and TSR in the area. The oil O13 was probably water washed suggested by isotopically heavier toluene and other parameters, but alos facies effect should not be ruled out.

It is proposed that mixing with condensate and gas charge resulted in formation of gas phase (condensate) and liquid phase (oil) causing phase fractionation effect, and these two processes (mixing and phase fractionation) were responsible for the distribution patterns of oils and condensates. The mixing led to the formation of gas caps by increasing saturation pressure. The gas-oil mixture equilibrated and eventually form compositional grading column. It is propose that the phase fractionation indications are signs of this grading/segregation, as suggested by the increase of gross amount of light hydrocarbons, from A4C oils (that should be phase fractionated) to A3C/A5C oils to condensates.

Chapter 6 Geochemistry of the non-hydrocarbons of crude oils and condensates of the Greater Birba area.

6.1 Occurrence and distribution of pyrrolic nitrogen compounds in crude oils and condensates from the Greater Birba area

6.1.1 Introduction

Nitrogen-containing compounds are of ubiquitous occurrence in petroleum and source rocks (nitrogen content of petroleum is usually in the range 0.1 - 2.0 wt% (Li *et al.*, 1995). In petroleum, nitrogen compounds are found mainly in the relatively polar and high molecular weight fractions (e.g. in the so-called 'NSO fraction' and in the asphaltenes), occurring predominantly as aromatic heterocycles, with neutral pyrrolic structures dominating over basic pyridinic forms (Wilhelms, 1992). It is thought that pyrrolic nitrogen compounds are not derived directly from biological precursors but rather they arise as diagenetic artefacts during the reworking of nitrogen-containing sedimentary organic matter, or via the incorporation of inorganic nitrogen species (NH_4^+) into organic carbon skeletons (Li *et al.*, 1995). Clegg *et al.* (1997) suggested that the alkylcarbazoles and alkylbenzocarbazoles might have originated from alkaloids derived from terrestrial plants and blue-green algae, whereas Li *et al.* (1995) suggested that they were more likely to be the products of condensation reactions involving proteins and pigments.

Some of the more important nitrogen compounds found in petroleum are the alkyl carbazoles and the benzocarbazoles, these having been proposed as potential indicators of secondary migration distance (Bennett *et al.*, 2002; Larter *et al.*, 1996). The molecular structure and carbon numbering system of alkylcarbazoles and the benzocarbazoles are shown in Figure 6-1. The alkylcarbazoles can be categorised into three main groups based on the position of alkyl-substituents relative to the active pyrrole (NH) functionality (see Figure 6-1) (Li *et al.*, 1995):

- Pyrrolic N-H shielded isomers: where an alkyl group is substituted in position 1 and position 8 e.g. 1,8-dimethylcarbazole
- Pyrrolic N-H partially shielded isomers: where an alkyl group is substituted in either position 1 or position 8 e.g. 1,4-dimethylcarbazole

- Pyrrolic N-H exposed isomers: where the alkyl group substitution is in positions other than 1 or 8.

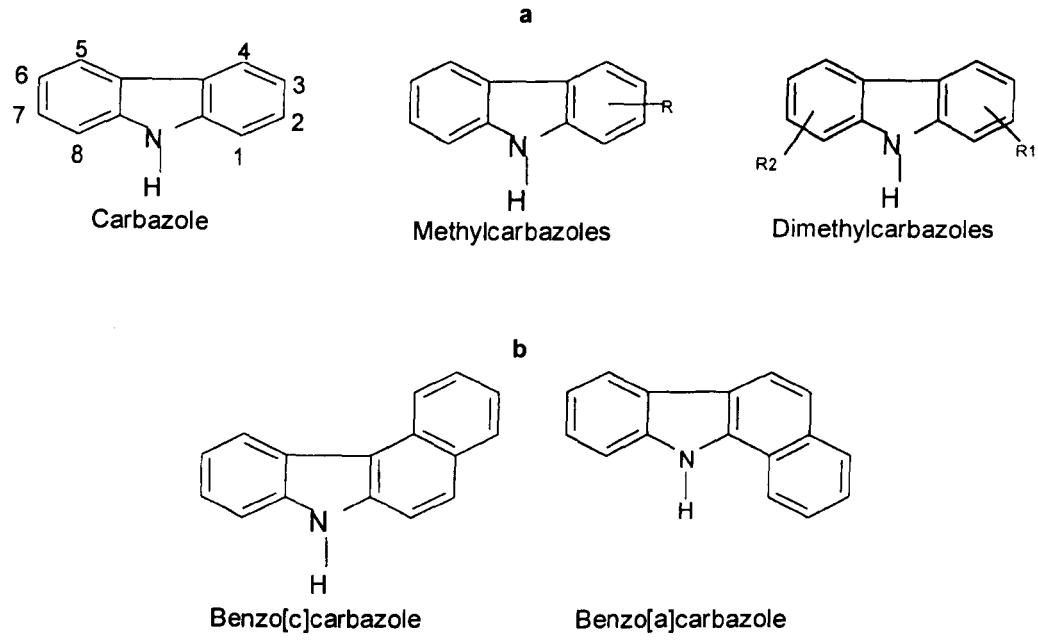

Figure 6-1: Molecular structure of (a) C0-C2 alkylcarbazole and (b) benzocarbazole isomers. For methylcarbazoles, R, R1 and R2 = CH3.

Several processes are proposed to influence the distribution of carbazoles and benzocarbazoles; these include source facies (Bakr & Wilkes, 2002; Clegg *et al.*, 1997), thermal maturity (Clegg *et al.*, 1998), primary migration (Bennett *et al.*, 2002; Li *et al.*, 1997), secondary migration (Larter *et al.*, 1996; Li *et al.*, 1995), and biodegradation (Huang *et al.*, 2003a).

Clegg *et al.* (1997) found that facies variations exert an important control on the distribution of alkylcarbazoles and alkylbenzocarbazoles. They reported that the anoxic carbonate facies (wackstones) of the Keg River Formation in the Western Canada Sedimentary Basin were characterised by high abundances of high molecular weight alkylcarbazoles (C_4-C_5 alkyl homologues), while the regressive marlstones deposited under restricted higher salinity conditions showed a higher content of carbazole and 1-methylcarbazole. Clegg *et al.* (1997) also found that the regressive carbonate facies of the Upper Keg River Formation in the Western Canada Basin showed similar relative distributions of different methylcarbazole isomers to those of Jurassic Posidonia shales of the Lower Toarcian in Northern Germany, in that 1-methylcarbazole occurred in higher abundance than the other methylcarbazole

isomers. It was also possible to distinguish between the different carbonate facies by cross-plots of 4-methylcarbazole/ (4-+2-methylcarbazole) and 3-methylcarbazole/ (3-+2-methylcarbazole) against the Rock-eval hydrogen index; the facies with lower hydrogen indices (marlstones) were characterised by relatively high methylcarbazole ratios compared to the anoxic wackstones.

Thermal maturity is another major control on the distribution of alkylcarbazoles and alkylbenzocarbazoles. (Li *et al.*, 1997) found that in a carbonate source rock maturation sequence the total concentration of C_0-C_3 alkylcarbazoles and non-alkylated benzocarbazoles in source rock bitumens increased with increasing maturity over the range of 0.45 to 1.3% R_o. Clegg *et al* (1997) found that the effect of maturity on the alkylcarbazole isomer distribution is similar to that observed for alkyldibenzothiophenes and phenanthrenes, and they proposed that the carbazoles become more alkylated with increasing maturity up to a maturity level of 0.88% R_o, after which demethylation becomes the more dominant process. These authors found that 1-methylcarbazole and 1,8-dimethylcarbazole are the thermally most stable isomers of the methylcarbazoles and dimethylcarbazoles, respectively, and proposed several alkylcarbazole isomer-based ratios which appear to be sensitive to maturity variations (see Table 6-1). These ratios were reported to show systematic changes with maturity up to 0.88% R_o (Clegg *et al.*, 1997).

Table 6-1: Alkylcarbazole isomer ratios which appear to be sensitive to maturity (from Clegg *et al.*, 1977).

Ratio	Response to increasing maturity
$\frac{\text{1-methylcarbazole}}{\text{1-methylcarbazole+4-methylcarbazole}}$	Increase
$\frac{\text{1-methylcarbazole}}{\text{1-methylcarbazole+2-methylcarbazole}}$	Increase
$\frac{\text{1-methylcarbazole}}{\text{1-methylcarbazole+3-methylcarbazole}}$	Increase
$\frac{\text{2-methylcarbazole}}{\text{2-methylcarbazole+3-methylcarbazole}}$	Increase
$\frac{\text{3-methylcarbazole}}{\text{3-methylcarbazole+4-methylcarbazole}}$	Decrease
$\frac{\text{4-methylcarbazole}}{\text{4-methylcarbazole+carbazole}}$	Increase
$\frac{\text{3-methylcarbazole}}{\text{3-methylcarbazole+2-methylcarbazole}}$	Increase
$\frac{\text{1,8-methylcarbazole}}{\text{1,8-methylcarbazole+1-ethylcarbazole}}$	Increase

Molecular fractionation of alkylcarbazoles and benzocarbazoles has been shown to occur both during the migration of petroleum from source rocks to the carrier bed (primary migration) and during migration through the carrier bed to the reservoir (secondary migration) (Bennett *et al.*, 2002; Larter *et al.*, 1996; Li *et al.*, 1995). When petroleum migrates through the carrier system, alkylcarbazole isomers with an exposed NH group tend to be sorbed more strongly by mineral surfaces and are thus removed from the migrating petroleum, which consequently becomes enriched in NH-shielded isomers (alkyl group in position 1 and 8) (Larter *et al.*, 1996; Li *et al.*, 1992; Li *et al.*, 1995). Partitioning of the NH-shielded isomers is thought to be restricted principally by steric effects associated with the alkylation position with respect to the active pyrrolic functionality. Li *et al.* (1995) found that migrating petroleum also becomes enriched in higher molecular weight alkylcarbazole homologues relative to lower molecular weight homologues.

Petroleum migration may also lead to systematic molecular fractionation within the benzocarbazoles. Evidence from field studies (Larter *et al.*, 1996) showed in source-related oils from the Western Canada Sedimentary Basin that there was a decrease in benzocarbazole concentration and a decrease in the relative abundance of benzo[a]carbazole relative to the benzo[c] isomer with increasing migration distance.

This led to the suggestion that the benzocarbazole [a]/[c] ratio could be used as a potential indicator of secondary migration distance (Larter *et al.*, 1996). Larter *et al.* (1996) suggested that during migration there is a preferential removal of the more rod-shaped benzo[*a*]carbazole relative to the sub-spherical benzo[*c*]carbazole due to the sorption of benzocarbazoles from the petroleum onto the clay mineral surfaces and solid organic matter in the carrier bed, resulting in a decrease in the [a]/[c] ratio with increasing migration distance. Larter *et al* (2000) conducted a laboratory-based core-flood experiment using an initially water-wet siltstone, a North Sea crude oil and controlled subsurface conditions of temperature and pressure, in an attempt to simulate secondary migration and determine the effect of on the distribution of benzocarbazoles. They found that the earlier-eluted oils were characterised by lower concentrations of benzocarbazoles and by a lower benzocarbazole [a]/[c] ratio, relative to the original oil. Both concentrations and ratios subsequently increased with increasing elution volume to values comparable to those in the original oil (Larter *et al.*, 2000b). Several later studies have affirmed the potential use of the benzocarbazoles ratio as a migration tracer e.g. (Bakr & Wilkes, 2002; Bennett *et al.*, 2002; Li *et al.*, 1999; Li *et al.*, 1997; Terken & Frewin, 2000; Wang *et al.*, 2004). However, Clegg *et al* (1998) presented convincing evidence from a suite of naturally migrated oils from the Sonda de Campeche area, Gulf of Mexico, that benzocarbazole concentrations and distributions are also influenced by source facies and maturity. They concluded that expulsion and secondary migration exert little or no control on the concentrations and distribution of benzocarbazoles in those basins with short or vertical migration systems, and that both maturity and source facies are the dominant controls. In response, Bennett *et al* (2002) suggested that the petroleum is generated over a narrow maturity interval (0.6-1.0% vitrinite reflectance) and that it may be possible to distinguish between maturity and migration effects in many instances. Furthermore, Li *et al* (1999) reported that source facies and maturity have no influence on either the benzocarbazoles or the alkylcarbazoles in the Rainbow-Shekilie-Zama oils of Western Canada even though these oils show considerable variation in the distribution of saturated hydrocarbons and aromatic hydrocarbons. The effect of maturity on the benzocarbazole ratio has been supported by other studies such as (Clegg *et al.*, 1997; Horsfield *et al.*, 1998).

Huang *et al.* (2003) showed in a suite of oils from the Liaohe Basin, China, that biodegradation can also influence the distribution of alkylcarbazoles and benzocarbazoles in petroleum. These authors found that 1-methylcarbazole is more rapidly degraded than other, more water soluble, methylcarbazole isomers. Since the Birba oils show no evidence of biodegradation, a more in-depth review of the effect of biodegradation on the occurrence of carbazoles in oils is not considered to be directly relevant to the present study.

6.1.2 Occurrence and distribution of carbazoles in the Greater Birba Area oils

The C_0-C_2 alkylcarbazole concentrations in the oils from the Greater Birba area are given in Table 6-2 and the isomer distributions are illustrated by the representative histograms shown in Figure 6-2. The oils low contents of carbazole and alkylcarbazoles, with most of the samples giving total concentrations of less than 20 ppm. The concentrations are typical of Omani crude oils (B. Bowler, NRG, *pers. commun.*), which generally give values of less than 50 ppm. By contrast, some North Sea oils – especially those characterised by short migration distances (<20 km) – have total C_0-C_2 alkylcarbazole concentrations of 100 ppm or more. As discussed previously, the Birba oils are mixtures of petroleum from middle Huqf source rocks as well as from intra-salt source rocks (Section 2.6). As the relative contribution from each source rock is not known, secondary migration distances cannot be measured or assumed. It is therefore not possible to provide a meaningful interpretation of the carbazole data in terms of migration distance – furthermore, as shown later, it appears that other processes (oil-condensate mixing and phase fractionation) may also significantly influence the occurrence and molecular composition of the carbazoles in the Birba oils.

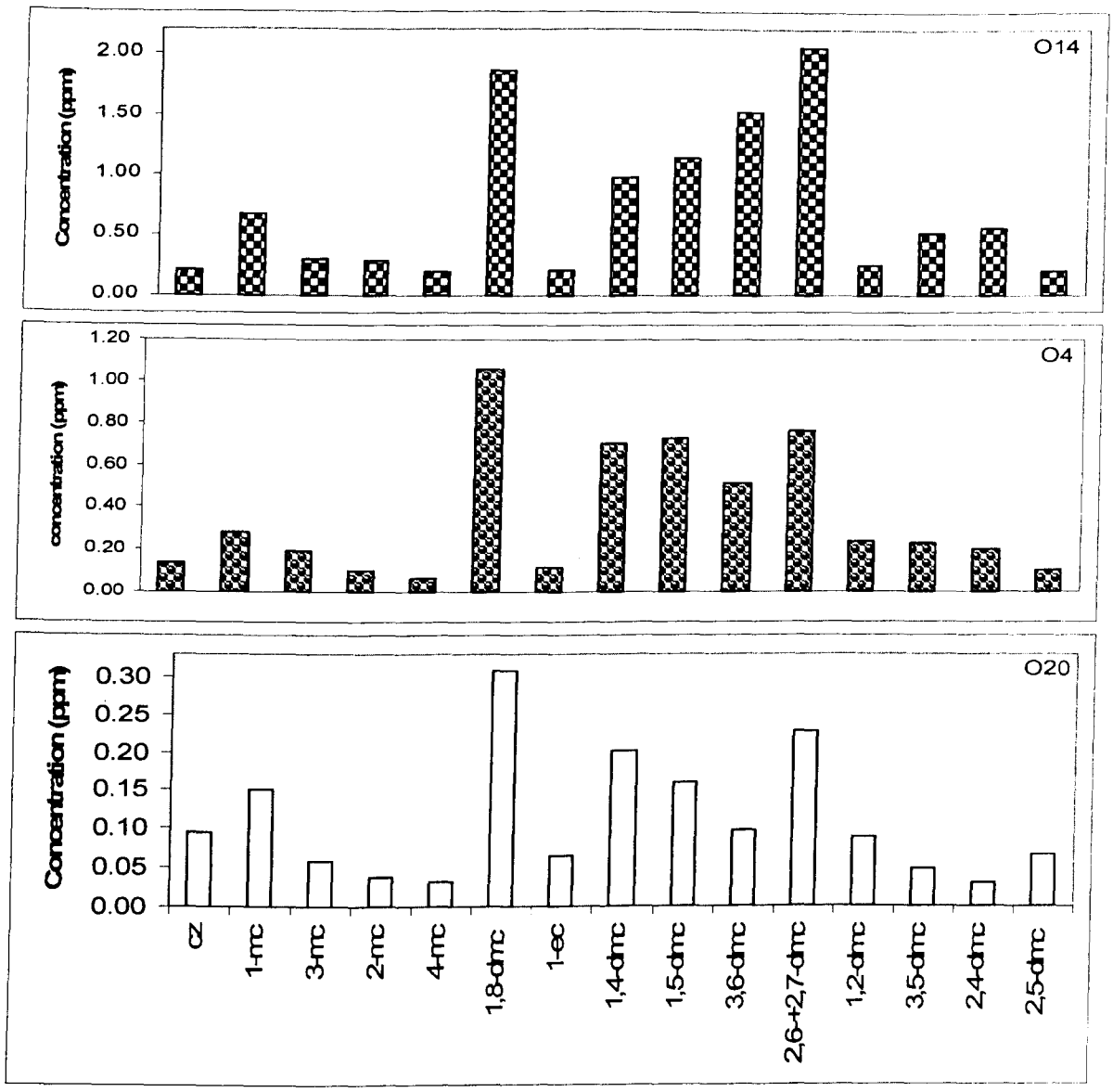

Figure 6-2: Distributions of C_0-C_2 alkylcarbazoles in 3 representative oils from the Greater Birba area sample set; samples O4 (well BB1, A4C), O14 (well Durra1, A3C) and O9 (well BBS1, A4C, condensate). Key to compound name abbreviations (x-axis) is given in Table 6-2.

Table 6-2: The concentrations (ppm) of carbazole and alkylcarbazoles in the Birba oils.

Sample	Wells	TVD (m)	Stringers	cz	1-mc	3-mc	2-mc	4-mc	1,8-dmc	1-ec	1,4-dmc	1,5-dmc	3,6-dmc	2,6-+2,7-dmc	1,2-dmc	3,5-dmc	2,4-dmc	2,5-dmc	Sum
O1	BB2	2583.4	A4C	0.14	0.31	0.05	0.14	0.11	1.31	0.15	0.98	0.53	0.80	0.87	0.34	0.25	0.26	0.12	6.34
O3	BBN1	3455.1	A4C	0.10	0.16	0.05	0.05	0.05	0.47	0.05	0.20	0.19	0.16	0.26	0.04	0.05	0.05	0.03	1.92
O4	BB1	2533.1	A4C	0.14	0.28	0.19	0.10	0.06	1.06	0.11	0.70	0.73	0.51	0.76	0.24	0.23	0.20	0.10	5.43
O5	BBN1	3558.1	A3C	0.96	0.61	1.88	0.22	0.29	1.44	0.03	0.61	3.77	2.29	4.23	2.37	0.87	0.28	0.54	20.38
O6	BB1	2588.3	A4C	0.17	0.35	0.17	0.12	0.05	1.24	0.12	0.91	0.49	0.71	0.81	0.23	0.20	0.15	0.13	5.84
O7	BBN2	3597.8	A4C	0.52	0.48	0.17	0.21	0.17	1.91	0.04	0.94	1.09	1.11	1.93	0.21	0.31	0.44	0.27	9.81
O9	BBS1	2329.7	A4C	0.10	0.21	0.11	0.05	0.04	0.64	0.06	0.39	0.24	0.33	0.40	0.10	0.10	0.10	0.06	2.92
O10	Kaukab1	2513.6	A3C	0.30	0.72	0.27	0.41	0.24	2.39	0.18	1.32	1.66	2.17	2.99	0.51	0.84	1.25	0.24	15.52
O11	Kaukab1	2513.6	A3C	0.21	0.63	0.22	0.34	0.21	2.10	0.19	1.18	1.48	1.92	2.64	0.43	0.71	1.09	0.20	13.53
O12	Omraan1H1	2601.7	A5C	0.21	0.91	0.25	0.32	0.17	3.66	0.49	1.50	2.22	3.09	3.59	0.65	0.69	0.93	0.51	19.19
O13	Nassir1	1998.6	A4C	1.80	3.54	1.14	1.32	1.44	3.20	0.40	2.81	1.80	2.93	5.39	0.52	0.78	1.51	0.49	29.08
O14	Durra1	2693.0	A3C	0.21	0.68	0.31	0.28	0.20	1.86	0.22	0.98	1.14	1.52	2.04	0.25	0.52	0.56	0.21	10.99
O15	Kaukab1	2896.9	A1C	0.32	0.71	0.17	0.21	0.27	0.89	0.11	1.02	0.61	1.12	2.06	0.24	0.23	0.35	0.23	8.54
O16	Shamah1	2385.7	A3C	0.35	1.03	0.60	0.61	0.42	2.10	0.23	1.56	1.15	2.46	3.33	0.60	0.85	1.18	0.46	16.93
O18	Omraan1H3	2939.1	A5C	0.17	0.68	0.18	0.26	0.14	2.59	0.24	1.42	1.27	2.45	2.62	0.28	0.42	0.55	0.40	13.67
O20	Bodour1H2	2971.59	A4C	0.09	0.15	0.06	0.04	0.03	0.31	0.06	0.20	0.16	0.10	0.23	0.09	0.05	0.03	0.07	1.66
O21	Omraan1H3	3111.51	A3C	1.08	0.70	0.23	0.29	0.45	1.91	0.28	1.11	1.26	1.41	1.78	0.71	0.56	0.71	0.64	13.14
O22	Omraan1H3	2939.1	A4C	0.14	0.33	0.11	0.12	0.07	1.32	0.12	0.73	0.61	1.24	1.46	0.21	0.31	0.32	0.20	7.27

Key: cz =carbazole; mc = methylcarbazole (e.g. 1-mc = 1-methylcarbazole); dmc = dimethylcarbazole (e.g. 1,4-dmc = 1,4-dimethylcarbazole); ec = ethylcarbazole; sum = total concentrations (ppm or μg/g) of carbazole and alkylcarbazoles listed in the table; 1-mc/1-ec = concentration ratio of 1-methylcarbazole/1-ethylcarbazole; 1,8-dmc/(2,6-+2,7-dmc) = concentration ratio of 1,8-dimethylcarbazole/(2,6-dimethylcarbazole+2,7-dimethylcarbazole).

Figure 6-2 shows histograms of the distribution of carbazole and alkylcarbazoles in a representative sample from each of the three main groups defined on the basis of biomarkers, aromatic hydrocarbons and light hydrocarbons. The representative samples are O14 (well Durra-1) from the A3C reservoir unit (A3C/A5C group), O4 (well BB-1) from the A4C reservoir unit of the main Birba Field (A4C group), and O20 condensate (well Budour-1H2) from the A4C reservoir unit (condensates group). All samples show generally similar C_0-C_2 alkylcarbazole distributions characterised by relatively high abundances of some dimethylcarbazoles; this is seen even with the gas condensates, as exemplified by sample O20 (well Budour-1H2)). As shown in Fig. 6-2, sample O14 (well Durra-1) has generally higher abundances of alkylcarbazoles than sample O4 (well BB-1), and both of the oils contain higher concentrations of alkylcarbazoles than the condensate (sample O20).

The sum of the C_0-C_2 alkylcarbazoles for each of the samples analysed is plotted in Figure 6-3, which clearly shows that the oils in the A4C reservoir unit have significantly lower C_0-C_2 carbazole contents than most of the other oils. There is generally a >50% difference in alkylcarbazoles content between the A4C oils and the oils from both the A3C and the A5C reservoir units (although only 2 samples from the A5C unit (from Omraan1) were analysed). As expected, the gas condensates were characterised by the lowest content of alkylcarbazoles. Sample O15 (well Kaukab-1) from the deepest reservoir (A1C) has similar alkylcarbazole concentrations to the A4C oils, while sample O5 (well BBN1) from the A3C unit has the second highest content of the sample suite.

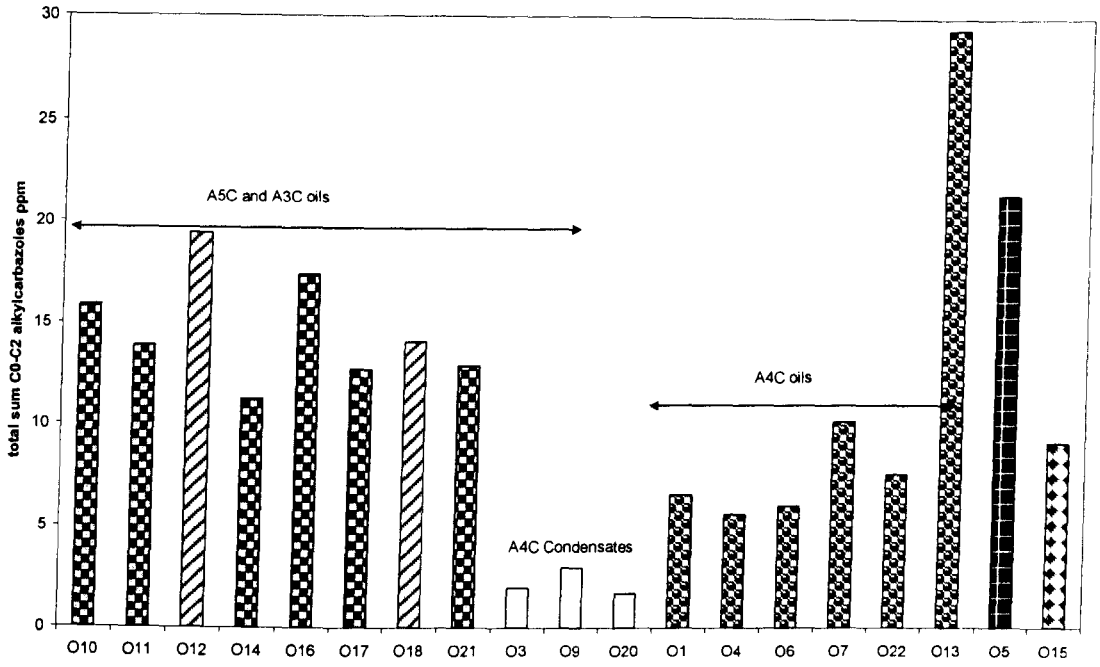

Figure 6-3: Histogram showing the sum of the C0-C2 alkylcarbazoles in the Birba oils.

The highest total content of alkylcarbazoles was found in sample O13 (well Nassir-1) from the A4C reservoir. Sample O13 (well Nassir-1, A4C) is characterized by relatively high NSO compound and asphaltene contents, and by a relatively low API gravity (23.9°). Although this oil (O13) is characterised by lower maturity ratio (VRE based on MPI = 0.86% R_c) (Figure 6-11), several evidences were presented earlier in chapter 4 and chapter 5, indicated that this oils is influenced by facies variations. Therefore, the high content of alkylcarbazoles in this oil might be another consequence of this facies differences. The source rocks and carrier beds in the Birba system are carbonates and yet the total concentrations of alkylcarbazoles are much lower than those reported for oils from the Sonda de Campeche, also a carbonate system (Clegg *et al.*, 1998). Carbonate carrier beds typically have low clay content and so the main loss of alkylcarbazoles during migration probably results from interaction with water rather than sorption on to minerals. The lower concentration of alkylcarbazoles in the Birba oils relative to the oils from the Sonda de Campeche may therefore reflect either a longer migration distance or a difference in source rock type. It should be noted that alkylcarbazole concentrations in the Birba oils are not particularly low when compared to other oils from Oman.

Figure 6-4 shows a cross-plot of the dimethylcarbazole isomer ratio 1,8-dmc/(2,6-+2,7-dmc) (shielded/exposed isomers) and the total concentration of alkylcarbazoles. The data show an interesting correlation, which suggests the possibility of a migration trend. When the ratio is plotted as a contour map, however, (Figure 6-5) it is apparent that there is no particular spatial trend, which might be indicative of a filling direction. However, assuming that this ratio is migration indicator, the spatial distribution of this ratio (which agrees well with the sum of alkylcarbazoles) might suggest that reservoir filling occurred mainly through vertical migration via faults (rather than by lateral migration) and that the main filling point was the Birba field. The mixing curve suggested by other data (oil-condensate mixing taking O11 and O20 as potential end membersis suggested from their PVT behaviour, chapter 7) is calculated and shown in Figure 6-4. Clearly, the mixing trend is different to the trend revealed by the migration ratio versus alkylcarbazoles content, although the mixing effect cannot be ruled out.

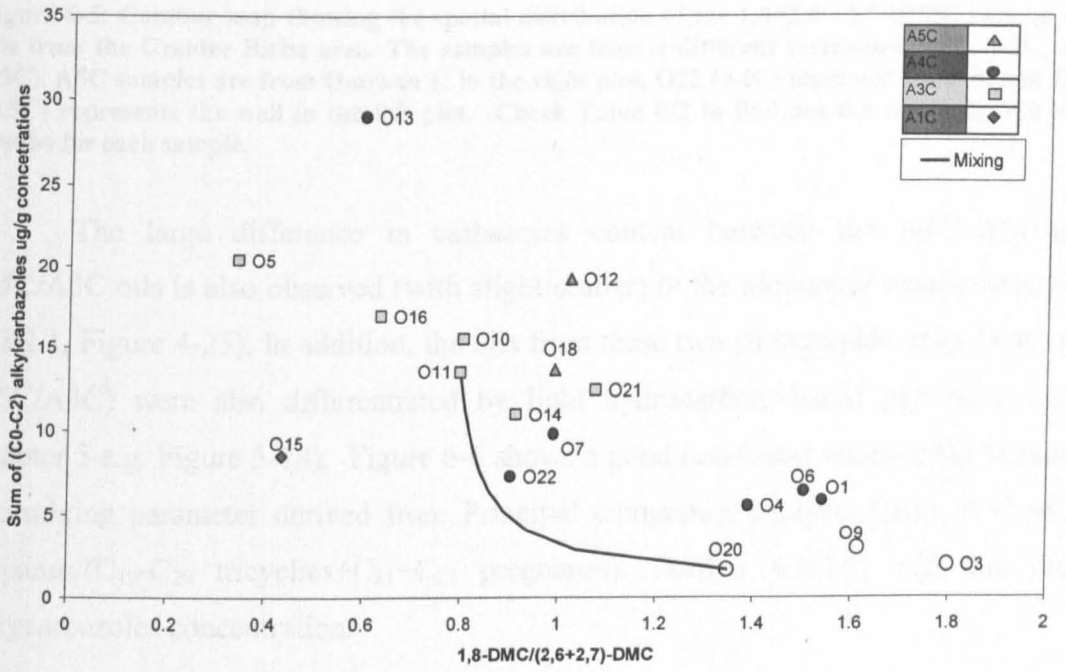

Figure 6-4: Cross-plot plot of the sum of the C0-C2 alkylcarbazoles versus the 1,8-dmc/(2,6-dmc+2,7-dmc) ratio. Key: A4C oils (filled circles for oils and empty circles for condensates), A3C oils (squares), A5C oils (triangles), and A1C oil (diamonds).

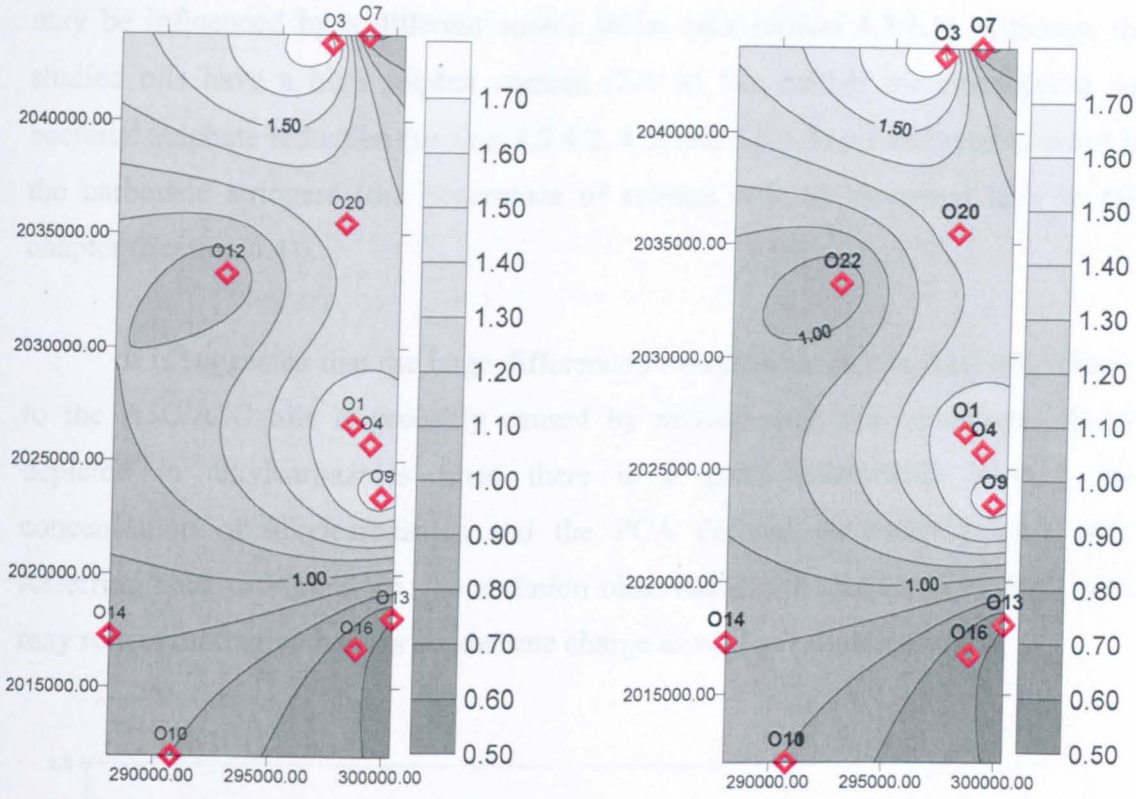

Figure 6-5: Contour map showing the spatial distribution of the 1,8/(2,6-+2,7-)DMC ratio in the oils from the Greater Birba area. The samples are from 3 different reservoirs (A4C, A3C, and A5C). A5C samples are from Omraan 1; in the right plot, O22 (A4C) represent the well and O12 (A5C) represents the well in the left plot. Check Table 6-2 to find out the reservoir unit and depths for each sample.

The large difference in carbazoles content between the A4C oils and A5C/A3C oils is also observed (with slight scatter) in the biomarker content (Section 4.3.2.1, Figure 4-25). In addition, the oils from these two stratigraphic units (A4C vs. A5C/A3C) were also differentiated by light hydrocarbons-based parameters (see chapter 5 e.g. Figure 5-18). Figure 6-6 shows a good non-linear relationship between the mixing parameter derived from Principal component analysis [ratio of C_{27}-C_{35} hopanes/(C_{19}-C_{29} tricyclics+C_{21}+C_{22} pregnanes), Section 4.3.5.1] with the total alkycarbazoles concentration.

Several maturity parameters reveal no major differences between these oils (e.g. $VRE_{MPII} \approx 0.9\%$ R_c, standard deviation = 0.02) and source-related data indicates that they are highly likely to be sourced from similar carbonate-evaporite source rocks (see section 4.3.1, also see Figure 6-11). Furthermore, most of the oils show no sign of biodegradation or water washing; the exception being sample O13 (Nassir1, A4C), which is probably affected by water washing (see section 5.5.3.4) at the light end or

may be influenced by a different source facies (see section 4.3.4.1). Although the studied oils have a high sulphur content (2-3 wt %), neither thermochemical nor bacterial sulphate reduction (section 4.3.4.2, 4.5, and 5.5.3.3) are believed to occur in the carbonate stringers (the occurrence of sulphur will be discussed later in this chapter (Section 6.4)).

It is suggested that the large difference in alkylcarbazoles in A4C oils relative to the A5C/A3C oils is probably caused by mixing with a a condensate charge depleted in alkylcarbazoles since there is a good relationship between the concentration of alkylcarbazoles and the PCA derived parameter (Figure 6-6). Referring back to Figure 6-5, the variation observed in the 1,8/(2,6+2,7)-DMC ratio may reflect mixing with a gas condensate charge as well as migration.

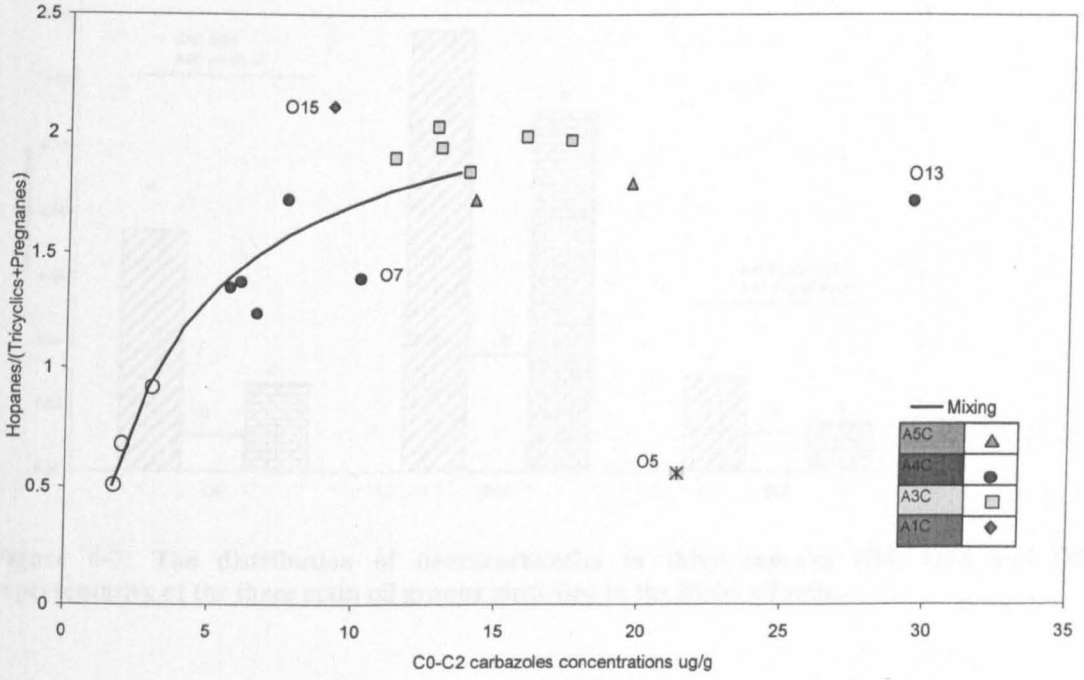

Figure 6-6: Cross plots showing the correlation between the total concentration of C_0-C_2 carbazoles versus the PCA derived parameter (see Chapter 4), Hopanes/ (Tricyclics+pregananes) is the ratio [(ΣC_{27}-C_{35} 17α Hopanes)/ (ΣC_{21}+C_{22} pregnanes+ Σtricyclic terpanes (C_{19}-C_{30}))]. The Mixing curve shown is calculated using O11 (an oil) and O20 (a condensate) as potential end members. Filled shapes are oils and empty circles are condensates from A4C.

6.1.3 Occurrence and distribution of benzocarbazoles

The concentrations of the benzocarbazole isomers in the Birba oils are given in Table 6-3. The total content of benzocarbazoles in the Birba oils is shown graphically in Figure 6-8. Benzo[a]carbazole is the dominant isomer in most of the oils and benzo[b]carbazole is usually the least abundant. Figure 6-7 shows the distribution of benzocarbazoles in three samples representative of the three main oil groups identified on the basis of other data (see Chapter 4 and Chapter 5). Sample O14, representing the A5C/A3C group, shows higher contents of benzocarbazoles than sample O4 which represents the A4C group). The condensates (represented by sample O20) are characterised by very low benzocarbazoles concentrations, reflecting the low content of polar compounds in these fluids.

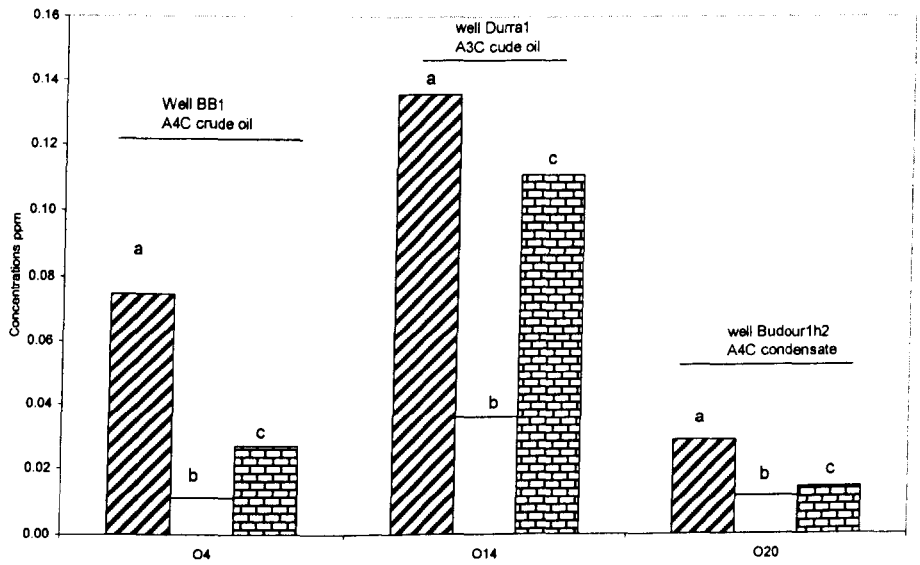

Figure 6-7: The distribution of benzocarbazoles in three samples (O4, O14 and O20) representative of the three main oil groups identified in the Birba oil suite.

Table 6-3: The concentrations (ug/g) of benzocarbazoles in the Birba oils. TVD is tru vertical depth (m)

Sample	wells	TVD	Stringer	benzo[a]carbazole	benzo[b]carbazole	benzo[c]carbazole	sum	[a]/[c]
O1	BB2	2583.4	A4C	0.09	0.02	0.04	0.14	2.25
O3	BBN1	3455.1	A4C	0.04	0.01	0.02	0.06	2.09
O4	BB1	2533.1	A4C	0.07	0.01	0.03	0.11	2.76
O5	BBN1	3558.1	A3C	0.64	0.04	0.28	0.96	2.34
O6	BB1	2588.3	A4C	0.08	0.03	0.07	0.18	1.08
O7	BBN2	3597.8	A4C	0.12	0.07	0.13	0.32	0.93
O9	BBS1	2329.7	A4C	0.03	0.01	0.03	0.07	1.30
O10	Kaukab1	2513.6	A3C	0.16	0.05	0.13	0.34	1.27
O11	Kaukab1	2513.6	A3C	0.15	0.05	0.13	0.33	1.19
O12	Omraan1H1	2601.7	A5C	0.16	0.06	0.15	0.36	1.09
O13	Nassir1	1998.6	A4C	0.21	0.03	0.14	0.38	1.44
O14	Durra1	2693.0	A3C	0.14	0.04	0.11	0.28	1.22
O15	Kaukab1	2896.9	A1C	0.26	0.09	0.21	0.55	1.26
O16	Shamah1	2385.7	A3C	0.21	0.03	0.23	0.47	0.91
O18	Omraan1H3	2939.1	A5C	0.19	0.05	0.18	0.43	1.08
O20	Bodour1H2	2971.6	A4C	0.03	0.01	0.01	0.05	2.01
O21	Omraan1H3	3111.5	A3C	0.20	0.05	0.17	0.42	1.15
O22	Omraan1H3	2939	A4C	0.02	0.04	0.22	0.28	0.09

Benzo[b]carbazole is commonly the least abundant benzocarbazole isomer in oils but it has been reported to occur in higher relative abundance in oils derived from kerogenous deltaic source rock e.g. in areas of the Haltenbanken, offshore mid-Norway. As the Birba oils analysed in this study are believed to be sourced from carbonate-evaporite source rock deposited in a marine environment, it is not unexpected that they have a very low content of benzo[b]carbazole.

Figure 6-9 shows a crossplot of the total benzocarbazoles content against the total alkylcarbazoles content. Both benzocarbazoles and alkylcarbazoles concentrations generally increase from gas condensates through A4C oils to A5C/A3C oils. Oils O5 (A3C, well BBN-1) and O15 (A1C, well Kaukab-1) lie outside of this trend and this may reflect the fact that they are sourced from different facies. The other exception to the general trend is sample O13 (well Nassir1, A4C), which shows an anomalously high content of alkylcarbazoles which is not evident in the benzocarbazoles. The reason for this is unclear, but it might be a possible to be another consequence of this oil being affected by another source, as suggested by other data (e.g. section 4.3.4.1). Although the benzocarbazoles concentration in sample O13 is not particularly high within the context of the data set, the sample does exhibit the highest value within the A4C group of oils. As suggested previously, the alkylcarbazoles concentration is probably controlled by both mixing and migration,

the benzocarbazoles concentrations reveal similar trend to alkylcarbazoles concentrations suggesting similar controls on their distribution.

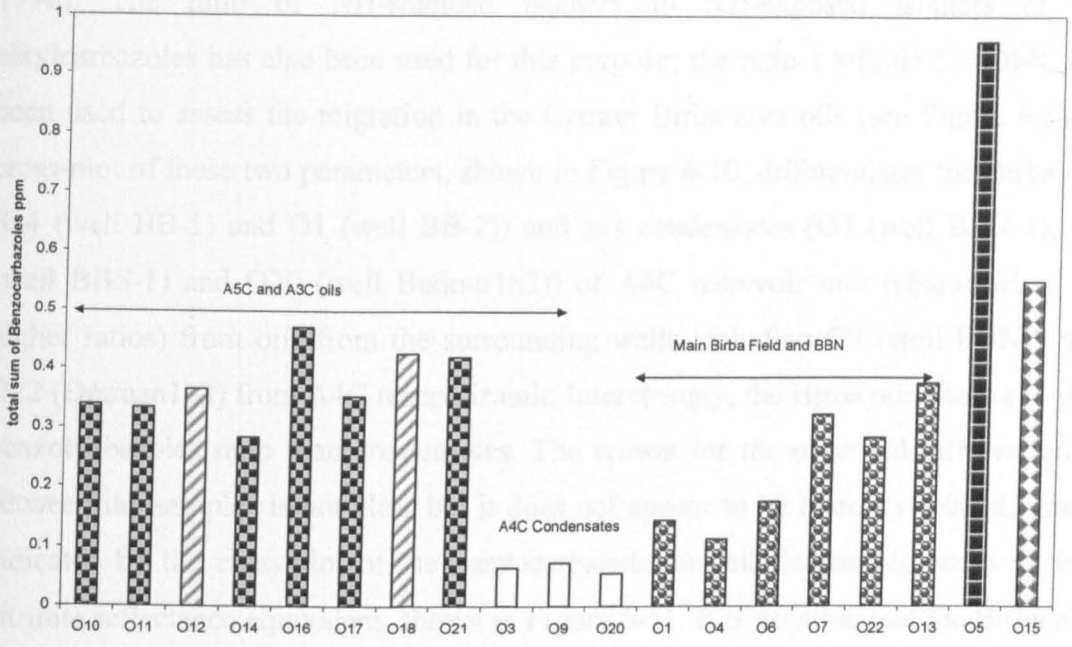

Figure 6-8: Histogram showing the total concentration of benzocarbazoles in the study oils.

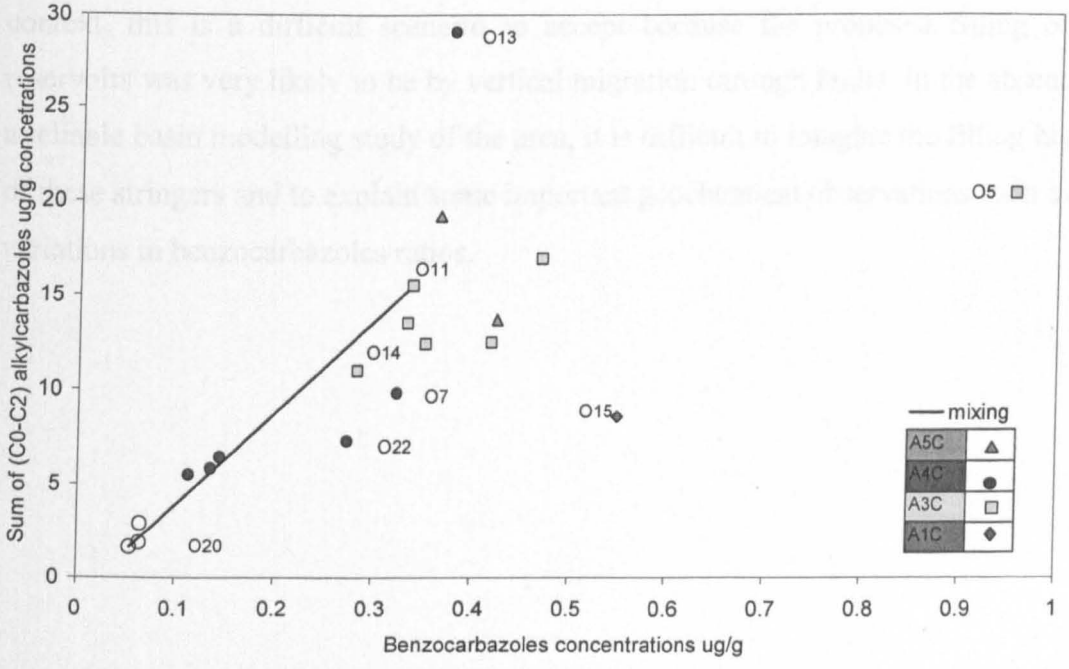

Figure 6-9: Crossplot of the total content of alkylcarbazoles (ug/g oil) versus the total content of benzocarbazoles (ug/g oil) in the Greater Birba area oils. Mixing curve shown is calculated using O11 (an oil) and O20 (a condensate) as potential end members.

The relative abundance of the benzocarbazole [a] and [c] isomers has been proposed as an indicator of petroleum secondary migration distance (Larter *et al.*, 1996). The ratio of NH-shielded isomers to NH-exposed isomers of the alkylcarbazoles has also been used for this purpose; the ratio 1,8/(2,6+2,7)-DMC has been used to assess the migration in the Greater Birba area oils (see Figure 6-5). A cross-plot of these two parameters, shown in Figure 6-10, differentiates the Birba oils (O4 (well BB-1) and O1 (well BB-2)) and gas condensates (O3 (well BBN-1), O9 (well BBS-1) and O20 (well Budour1h2)) of A4C reservoir unit (characterised by higher ratios) from oils from the surrounding wells including O7 (well BBN2) and O22 (Omraan1h3) from A4C reservoir unit. Interestingly, the Birba oils show a higher benzocarbazoles ratio than condensates. The reason for the observed differentiation between the samples is not clear but it does not appear to be maturity-related; this is indicated by the cross-plot of the benzocarbazole and alkylcarbazole ratios against vitrinite reflectance equivalent, shown in Figure 6-11. It is possible that the Birba oils originally (i.e. prior to mixing with condensate) migrated over a longer distance than the other oils, and that later migration of condensates into system resulted in large local variations in carbazoles and benzocarbazoles concentration. In a geological context, this is a difficult scenario to accept because the proposed filling of the reservoirs was very likely to be by vertical migration through faults. In the absence of a reliable basin modelling study of the area, it is difficult to imagine the filling history of these stringers and to explain some important geochemical observations such as the variations in benzocarbazoles ratios.

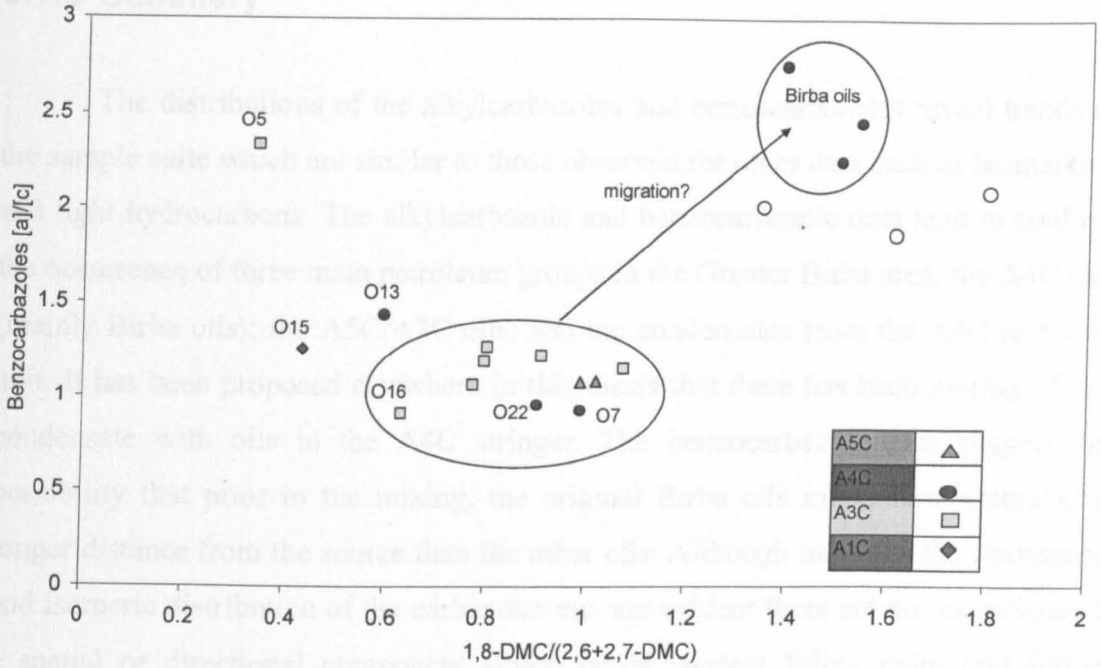

Figure 6-10: Cross-plot of the benzocarbazole [a]/[c] ratio versus 1,8-DMC/2,6+2,7-DMC ratio. The three oil samples on the right of the plot (filled circles) are from the Birba 1 and Birba 2 wells. The open circles denote condensates.

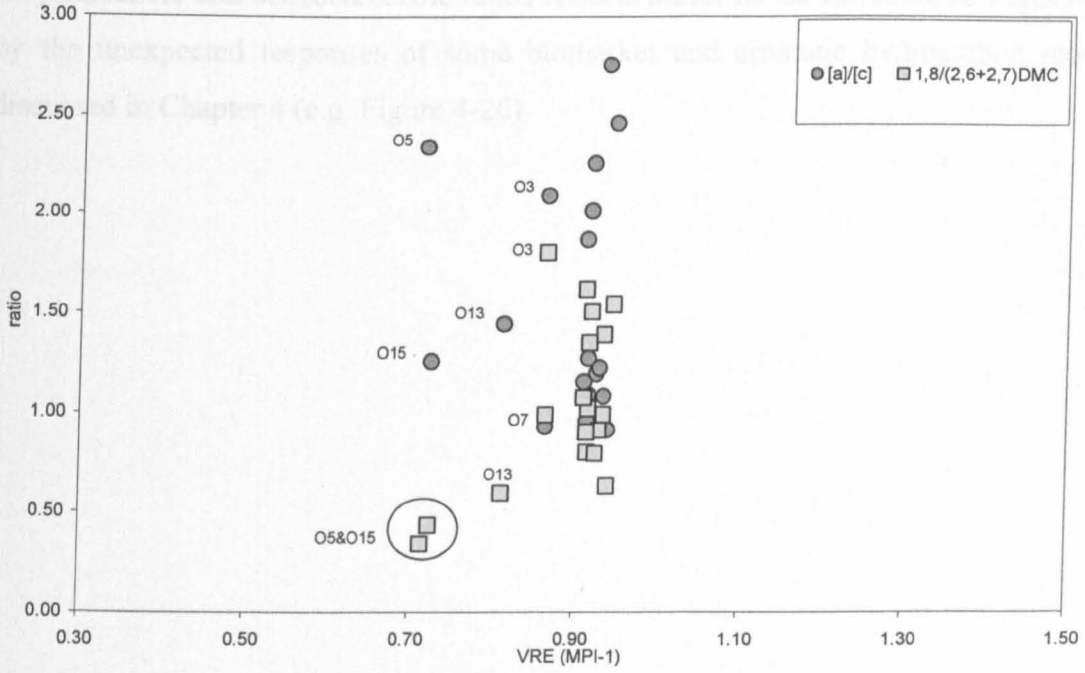

Figure 6-11: Cross-plot of the benzocarbazole [a]/[c] ratio and alkylcarbazole ratio (1,8-dimethylcarbazole/(2,6+2,7-dimethylcarbazoles)) versus vitrinite reflectance equivalent based on the methylphenanthrene ratio (MP1-1 = [1.5(2-methylphenanthrene+3-methylphenathrene) /(phenanthrene+1-methylphenanthrene+9-methylphanthrene)].

6.1.4 Summary

The distributions of the alkylcarbazoles and benzocarbazoles reveal trends in the sample suite which are similar to those observed for other data such as biomarkers and light hydrocarbons. The alkylcarbazole and benzocarbazole data tend to confirm the occurrence of three main petroleum groups in the Greater Birba area: the A4C oils (mainly Birba oils); the A5C/A3C oils; and the condensates from the A4C reservoir unit. It has been proposed elsewhere in this thesis that there has been mixing of gas condensate with oils in the A4C stringer. The benzocarbazole data suggest the possibility that prior to the mixing, the original Birba oils might have migrated a longer distance from the source than the other oils. Although trends in the abundance and isomeric distribution of the carbazoles etc. are evident there are no indications of a spatial or directional component which might suggest filling point and filling direction. This may be taken as supporting evidence that the filling of the reservoirs was most likely vertical via various fault conduits, as proposed in various sections throughout this thesis. The other possibility is that the observed variations in the alkylcarbazole and benzocarbazole ratios reflects minor facies variation, as suggested by the unexpected responses of some biomarker and aromatic hydrocarbon ratios discussed in Chapter 4 (e.g. Figure 4-26).

6.2 *Phenolic compounds*

6.2.1 Introduction

Low molecular weight (C_0-C_3) alkyl phenols are ubiquitous components of petroleum fluids (Ioppolo *et al.*, 1992; Macleod *et al.*, 1993; Taylor, 1994). The abundance and distribution of low molecular weight (C_0-C_3) alkylphenols (the subscript denotes the number of alkyl carbon atoms attached to the benzene ring) have been determined in crude oils (Ioppolo *et al.*, 1992), formation waters (Taylor, 1994) and production waters (Tibbetts *et al.*, 1992).

Figure 6-12 shows the molecular structures and ring numbering system of phenol and the C_1-C_3 alkylphenols quantified in the present study. Phenol isomers with an alkyl group attached to position 2 and/or 6 are termed ortho-substituted phenols; isomers with an alkyl group in position 3 or 5 are termed meta-substituted phenols; and isomers where the alkyl group occurs in position 4 are termed para-substituted phenols. Alkyl substitution adjacent to the reactive OH group has a shielding effect; isomers substituted in both positions 1 and 6 are termed 'OH-shielded' isomers, and isomers substituted in either the 1 or the 6 position are termed 'partially-shielded'. Isomers with no substitution in either position 1 or 6 are termed 'OH-exposed'.

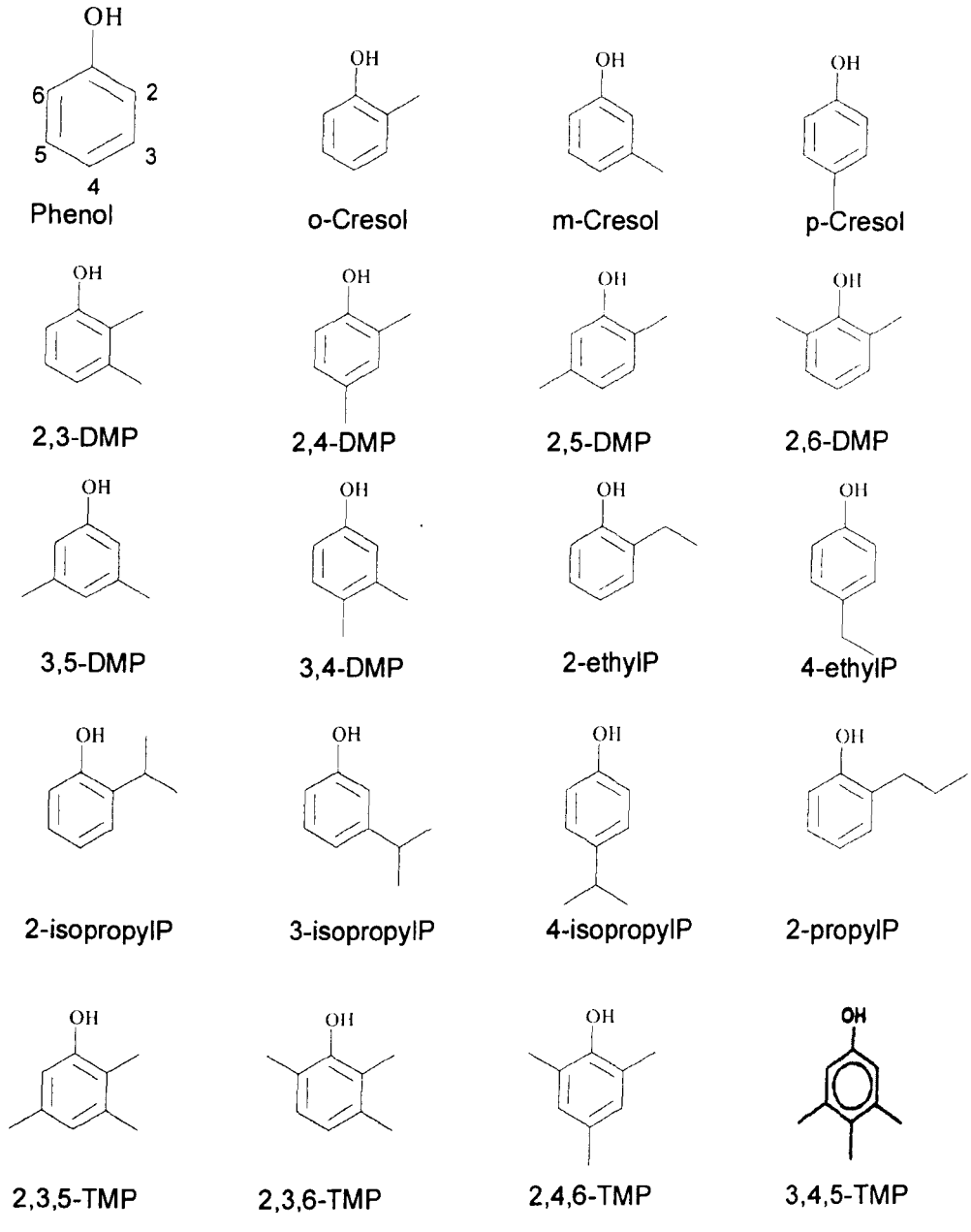

Figure 6-12: Ring numbering system and molecular structures of the C_0-C_3 alkylphenols analysed in this study. Key; DMP = dimethylphenol, TMP = trimethylphenol and P = phenol.

Alkylphenols are characterised by several physical-chemical properties which are of significance to petroleum geochemistry. They are weak acids and can form salts in acid-base reactions (Taylor, 1994). They can also form hydrogen bonds, especially with water, due to the presence of an electronegative oxygen atom in the hydroxyl functional group (Taylor, 1994). This makes the alkyl phenols very water-soluble (Bennett & Larter, 1997; Taylor, 1994) and confers a potentially important role for phenols in the control of wettability; this is the tendency for oil or water to adhere to

rock and it has a major impact on oil production (Taylor *et al.*, 1997). Due to their solubility in water, the occurrence and distribution of phenols in petroleum may be significantly influenced by water-washing (the loss of water soluble compounds from petroleum into an aqueous phase) (Taylor *et al.*, 1997). This process occurs during secondary migration and within the reservoir at the oil/water contact. Phenol and alkylphenols are toxic compounds and they pose a threat to aquatic ecosystems if discharged into the environment in high concentrations (Taylor, 1994).

Although phenolic compounds occur in algae, bacteria and fungi ((Taylor, 1994) and references therein), these are not considered as likely direct sources of alkylphenols in petroleum. The precursors of petroleum alkyphenols are thought to be formed by the incorporation of oxygenated aromatic compounds into kerogen during sedimentation and burial diagenesis (Taylor, 1994). As lignin is thought to be a major source for these oxygenated compounds (Taylor, 1994) kerogen type III might be expected to have higher contents of alkylphenols than kerogen type II. However, kerogen type III was found to have lower contents of alkylphenols than kerogen type II in some studies e.g. (Taylor, 1994) and this was interpreted as being due to the low petroleum yields from kerogen type III (Taylor, 1994). Taylor *et al* (1997) found that oils derived from terrestrial organic matter were characterised by consistently lower alkylphenols concentrations than the marine sourced oils in their database.

No genetic link has been found between source organic matter and low molecular weight (C_0-C_3) alkylphenols; this may reflect the destruction of biological structures during the formation of kerogen or it may be the case that the molecules are too small and insufficiently specific to reflect their biogenic origin (Taylor, 1994). The smallest known phenol biomarkers are C_4 isopropylmethylphenols (IMPs) which have been identified in higher plants (Ioppolo-Armanios et al., 1993). Alkylphenols may also form as the result of condensation reactions between formation water and petroleum (Taylor, 1994).

Processes that can affect the concentrations and distribution of alkylphenols in crude oils are maturation (Senftle *et al.*, 1986), oil/water and oil/mineral partitioning (Taylor *et al.*, 1997), and biodegradation (Taylor, 1994). Larter (1989) conjectured

that phenol precursors are lost from kerogen and coals with increasing rank by catagenic release of oxygenated aromatic species, or breakage of alkyl-oxygen bonds in aryl-alkyl ether species, which are common in lignin, or by reductive dehydroxylation of phenolic hydroxyls to yield aromatic hydrocarbons (Larter, 1989). Simple alkylphenol precursors are inferred to form during catagenic breakdown of the original methyoxyphenol precursors (Venkatesan *et al.*, 1993). According to these authors, alkylphenols concentrations were found to increase with rank up to 0.6% vitrinite reflectance in flash pyrolysates, while phenol itself was found to decrease with rank over the maturity range 0.2-0.6% Vr in coal samples from the Mahakam delta (Venkatesan *et al.*, 1993). Senftle *et al.* (1986) observed a linear decrease in the concentrations of alkylphenols with increasing maturity in the vitrinite reflectance range 0.6 to 1.6% (Senftle *et al.*, 1986). The ratio of phenol to the sum of the C_1-C_2 alkylphenols has been suggested as a sensitive measure of maturity (Taylor, 1994).

Original alkylphenol distributions in petroleum expelled from the source rock may be subsequently modified by transalkylation reactions and isomeric rearrangements to produce mixtures of phenols with a higher thermodynamic stability (Ioppolo-Armanios *et al.*, 1994; Taylor, 1994), references therein). This is evident from the general similarity in distributions of alkylphenols in most oils regardless of the source type, suggesting that thermodynamic equilibrium has been reached (Pigman et al (1954) in (Taylor, 1994).

Alkylphenols are highly water-soluble components with low partition coefficients (the partition coefficient is defined as C_o/C_w where C_o and C_w are the equilibrium concentrations of a given alkylphenol in oil and coexisting water, respectively) (Equation 6-1). Equation 6-1 shows the formulae for calculation of the partition coefficient and of the initial concentration of an alkylphenol in water after equilibration, derived from the original equations for partition coefficients presented by (Taylor *et al.*, 1997).

Table 6-4 shows the oil/water partition coefficients (at half seawater salinity and neutral pH) for some lower molecular weight alkylphenols in a North Sea crude oil at 80°C and 1.01 bars, as determined by Taylor *et al.* (1997). They showed that

both the degree and the location of alkyl substitution on the aromatic ring of the alkylphenol molecule affect the oil/water partition coefficient values; partition coefficients increase with increasing degree of alkylation and with increasing ortho-substitution. The effect of water washing on crude oil can be manifest very clearly by the distribution of the alkylphenols, resulting in a reduction in concentrations of the lowest molecular weight alkylphenols and of non-shielded isomers (para and meta-substituted isomers, see Figure 6-12).

Partition coefficients have been found to be affected by water salinity and by the composition of crude oils, while the general trends – such as P increasing with increasing degree of alkylation - are not affected (Taylor, 1994). Bennett & Larter (1997) studied the effect of temperature, salinity and pressure on the partitioning behaviour of alkylphenols. They found that partition coefficients for alkylphenols increase with increasing brine salinity and decrease with increasing temperature. Increasing the pressure of the oil/brine system up to 340 bars was found to have little effect on the partition coefficient.

Equation 6-1: Formulae for the calculation the partition coefficient and of the initial concentration of a component in oil when equilibrated with water (Taylor *et al.*, 1997).

$$P = C_o / C_w$$

$$C_{oi} = C_o \bullet [(V_w/(V_o \bullet P)) + 1]$$

P = oil/water partition coefficient of component

C_{oi} = initial component concentration in oil (kg m^{-3})

C_o = final equilibrium concentration of component in oil (kg m^{-3})

V_w = volume of oil (m^{-3})

V_o = volume of water (m^{-3}) (at half sea water salinity and neutral pH)

Table 6-4: Oil/water partition coefficient (*P*) for some lower molecular weight alkylphenols, measured at 80°C and 1.01 bar, as reported by (Taylor *et al.*, 1997). (dmp=dimethylphenol; tmp=trimethylphenol)

Compound	*P*	Compound	*P*
phenol	1.3	2-isopropylphenol	54
o-cresol	5.2	2,3-dmp	13
m-cresol	3.4	3,4-dmp	8.6
p-cresol	3.6	2,-propylphenol	47
2-ethylphenol	17	3-isopropylphenol	31
2,5-dmp	15	4-isopropylphenol	31
2,4-dmp	15	2,4,6-tmp	67
2,6-dmp	25	2,3,5-tmp	45
3,5-dmp	10	2,3,6-tmp	60
4-ethylphenol	11	3,4,5-tmp	60

In addition to their partitioning behaviour in oil-water systems, petroleum alkylphenols can also interact with sediment surfaces during (primary and secondary) migration reflecting the hydrophilic nature of the mineral matrix. Interaction may also occur with solid organic matter (kerogen), which is usually hydrophobic. Consequently, the concentrations and distributions of alkylphenols in petroleum may be altered by partitioning with water, minerals and organic matter in the carrier beds during migration and within the reservoir (Larter & Aplin, 1995; Taylor *et al.*, 1997). Larter & Aplin (1995) suggested that oil/rock partitioning would not have a strong influence on alkylphenol distributions in petroleum whereas the absolute concentration of alkylphenols would decrease dramatically with increasing migration distance. The authors proposed that phenols concentrations in a suite of related oils may be used to estimate the volume of water and rock contacted by the oils during secondary migration. Taylor *et al* (1997) showed experimentally that 1 volume of oil (Tampen Spur, N. Sea) which has migrated 25 km through Jurassic sandstones may have equilibrated with up to 20 volumes of rock and water depending on the sorbing phases present (the sorbing phase being organic matter in this example). Lucach *et al.*,

(2002) reported similar effects of secondary migration on petroleum phenols concentrations for a suite of Omani oils from the Ghaba and Fahud Salt Basins (northern part of Oman Interior Basin, Figure 1-1); they observed that the total concentration of C_0-C_3 alkylphenols decreased from 10μg/g to 2μg/g oil) within the first 50km migration distance (Lucach *et al.*, 2002).

As with the alkylcarbazoles, alkylphenol isomers can be classified as shielded, exposed or partially exposed, according to the degree of shielding of the reactive OH group by alkyl substituents. As noted earlier, OH-shielded isomers are alkyl substituted in positions 2 and 6, partially shielded isomers are substituted in position 2 or 6, and OH-exposed isomers are substituted in positions other than 2 and 6. For an oil containing equal amounts of each isomer the ratio of shielded to exposed isomers should be 1.25 and this ratio can be altered by partitioning of exposed isomers into water and onto mineral surfaces (the shielded isomers also partition but at much slower rate) (Taylor, 1994). The partitioning of alkylphenols may start at the moment of petroleum generation within the source rock and continues during primary and secondary migration and within the reservoir until the oil is produced at the surface, due to the continuous contact with water, minerals and organic matter (Taylor *et al.*, 1997; Taylor, 1994).

6.2.1 The occurrence and distribution of alkyl phenols

The distributions and concentrations of low molecular weight (C_0-C_3) alkylphenols have been determined for a subset of 13 oils from the Greater Birba area sample suite (Table 6-6). The samples were from 11 wells and four different reservoirs (stratigraphic units). Seven samples were taken from A4C reservoir unit, three samples from the A3C unit, 2 samples from the A5C unit and 1 sample from the A1C unit. The C_0-C_3 alkylphenols were analysed using GCMS, monitoring the M^+-15 ion i.e. m/z 151 for phenol, m/z 165 for methyl phenols or cresols, m/z 179 for dimethylphenols, and m/z 193 for trimethylphenols. A representative reconstructed ion chromatogram for these ions obtained for sample O14 (A3C, well Durra1) is shown in Figure 6-13, The concentrations of individual phenols in the analysed samples are listed in Table 6-6.

Individual phenols were identified by comparison of retention time with phenols occurring in a reference oil from the Miller field (North Sea, UK) which had previously been characterised by coinjection with authentic phenol standards. Although most of the target compounds in the Birba oils were clearly separated and identifiable under the GC conditions used, there was an anomalously high peak which eluted at a similar retention time to 2,4,6-+2,3,5-trimethylphenol (see Fig. 6-13). The peak is occurred in most of the Birba oils analysed and was especially prominent in the gas condensates. It was not apparent, however, in the Miller oil analysed as a reference with the studied oils, suggesting that it is not a contaminant introduced during the analysis. To double-check this, a comparison was made of the ratio of the response of this peak using the molecular ion (m/z 208) and the M^+-15 ion (m/z 193) for an oil and a condensate from the Birba oil suite, as well as the Miller oil and a synthetic mix of alkylphenols; the results are shown in Table 6-5. The similarity in the ratios suggests that the peak probably fragments in a similar way to the trimethylphenols. This is further supported by the strong similarity in the mass spectrum of this peak and those for trimethylphenols. In the absence of evidence to the contrary, it was assumed that the anomalous compound is a trimethylphenol of unknown identity. For quantification purposes the high peak was assumed to be 2,4,6-TMP and its 'shoulder' was assumed to be 2,3,5-TMP; in practice, both isomers were quantified as one peak because it was not possible to quantify them separately in some samples due to insufficient chromatographic resolution. The sum of the alkylphenols listed in Table 6-1 includes this peak.

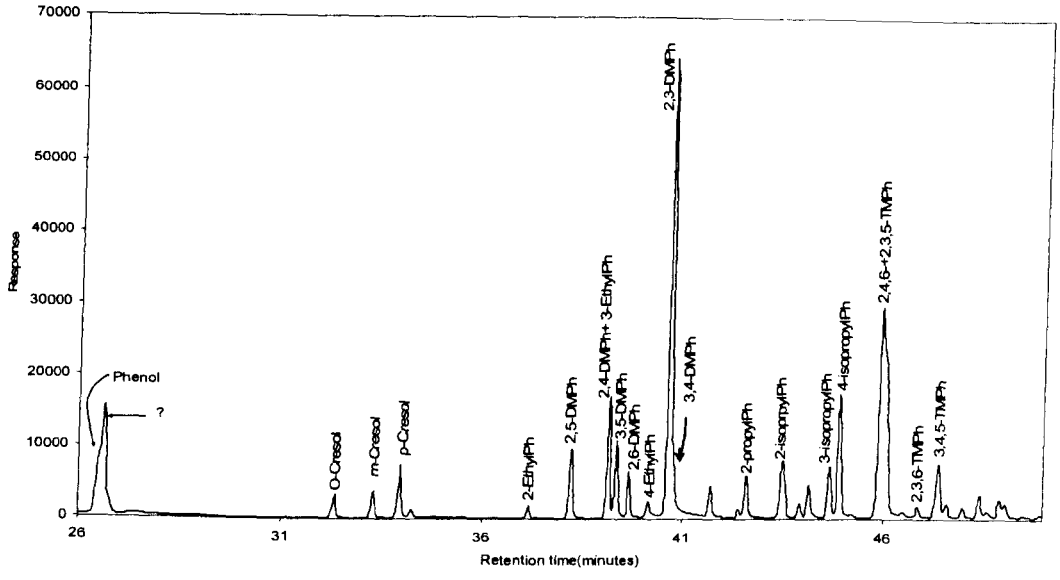

Figure 6-13: Representative reconstructed ion chromatogram of alkylphenols showing sum of four ions m/z 151, 165, 179, and 193. (Sample is O14 (A3C, well Durra 1)).

Table 6-5: Comparison of the integrated area response of an anomalous peak eluting with 2,4,6-tmp and 2,3,5-tmp using the molecular ion (m/z 208) and M^+-15 (m/z 193). Data is shown for two samples from the Birba oil suite (oil O7 and condensate O20), for a synthetic mixture of alkylphenol standards and for Miller oil used as an analytical reference standard.

	Synthetic mix	Miller oil	Oil O7	Condensate O20
M^+	1442001	46581	212131	57805
M^+-15	1261146	36071	176279	46629
Ratio $(M^+-15)/M^+$	0.87	0.77	0.83	0.8

Table 6-6: Concentrations (ug/g) of phenol and C_1-C_3 alkyl phenols in the Birba oils.

sample ID	Wells	Stringer	TVD (m)	Phenol	O-Cresol	M-Cresol	P-Cresol	2-EthylP	2,5-DMP	2,4-DMP+ 3-EthylP	3,5-DMP	2,6-DMP	4-EthylP	2,3-DMP	3,4-DMP	2-isoprpylP	2-propylP	3-isopropylP	4-isopropylP	2,4,6-+2,3,5-TMP	2,3,6-TMP	3,4,5-TMP	Sum
O1	BB2	A4C	2583	0.41	0.12	0.03	0.04	0.10	0.31	0.62	0.09	0.19	0.03	0.16	0.08	0.03	0.21	0.01	0.14	5.79	0.84	0.88	10.1
O3 (GC)	BBN1	A4C	3455	1.73	0.28	0.17	0.32	0.29	1.57	5.65	0.57	2.22	0.41	0.44	0.39	0.09	0.14	0.02	2.19	60.96	8.98	3.42	89.8
O4	BB1	A4C	2533	0.37	0.10	0.03	0.03	0.10	0.26	0.56	0.09	0.31	0.05	0.14	0.07	0.03	0.13	0.01	0.51	6.99	1.50	0.86	12.1
O5	BBN1	A3C	3558	1.03	0.32	0.16	0.18	0.07	0.39	0.83	0.32	0.07	0.05	0.06	0.08	0.41	0.06	0.04	0.40	0.41	0.11	2.32	7.3
O7	BBN2	A4C	3598	0.58	0.11	0.07	0.12	0.08	0.73	2.14	0.54	0.22	0.06	0.29	0.18	0.07	0.10	0.05	0.27	5.64	0.60	2.01	13.9
O9 (GC)	BBS1	A4C	2330	2.09	0.26	0.07	0.09	0.23	0.46	1.20	0.09	0.84	0.11	0.14	0.11	0.10	0.06	0.03	1.15	17.98	3.78	1.10	29.9
O10	Kaukab1	A3C	2514	0.74	0.18	0.08	0.12	0.12	0.80	1.74	1.52	0.30	0.08	0.45	0.31	0.05	0.06	0.02	0.24	5.83	0.65	2.81	16.1
O12	Omraan1H1	A5C	2602	0.64	0.15	0.05	0.06	0.09	0.55	1.01	0.61	0.21	0.06	0.16	0.13	0.03	0.04	0.03	0.07	3.18	0.52	1.34	8.9
O13	Nassir1	A4C	1999	0.50	0.05	0.03	0.24	0.09	0.21	2.07	1.52	0.06	0.34	0.09	0.06	0.21	0.14	0.01	0.11	1.06	0.11	0.87	7.8
O14	Durra1	A3C	2693	0.71	0.20	0.12	0.25	0.11	0.60	1.40	0.64	0.29	0.12	0.09	0.35	0.08	0.06	0.02	0.36	4.26	0.57	1.30	11.5
O15	Kaukab1	A1C	2897	1.40	0.04	0.07	0.04	0.04	0.06	0.11	0.04	0.00	0.04	0.01	0.02	0.04	0.08	0.03	0.03	0.07	0.02	0.07	2.2
O16	Shamah1	A3C	2386	0.85	0.23	0.14	0.09	0.33	1.34	1.85	2.99	0.40	0.18	0.55	0.52	0.08	0.10	0.02	0.45	4.94	0.78	2.92	18.7
O20 (GC)	Bodour1H2	A4C	2972	1.10	0.72	0.25	0.36	0.63	1.24	5.35	0.41	1.90	0.33	0.46	0.42	0.61	0.29	0.29	5.21	118.27	9.81	3.91	151.6

Key: O=Ortho; M=Meta; P=para; Sum= sum of C_0-C_3 alkylphenols; P=phenol (e.g. EthylP=ethylphenol); DMP=Dimethylphenol; TMP=trimethylphenol; shielded = sum of concentrations of [O-cresol+2,3DMP+2,4DMP+2,6DMP+2ethylP+2isopropylP+2propylP+2,3,5TMP +2,3,6TMP+2,4,6TMP], exposed = sum of concentrations of [Phenol+m-cresol+p-cresol+3,5DMP+3,4DMP+4ethylP+3isopropylP+ 4isopropylP+3,4,5TMP]. TVD=true vertical depth.

Figure 6-14 shows histograms of the concentrations of phenol and the C_1-C_3 alkylphenols in eight oil samples from the two main groups within the Greater Birba sample set which were identified using biomarker, aromatic hydrocarbon and light hydrocarbon parameters. One group comprised mainly oils from A4C reservoirs (well BB1 (sample O4), well BB2 (sample O1), well BBN1 (A4C)), and the other group comprised oils from the A3C/A5C reservoirs (well Kaukab1 (sample O10), well Durra1 (sample O14), well Shamah1 (sample O16), well Omraan1 (sample O12)).

Most of the alkylphenol distributions show three maxima; one in the C_0-C_1 range, and one in each of the C_2 and C_3 alkylphenol homologue groups., Phenol is the most abundant peak in the C_0-C_1 range in the most of the samples. All samples show very low contents of cresols compared to phenol and other alkyl phenols. Within the C_2-alkylphenols, the dimethylphenols are much more abundant than the ethylphenols in most of the studied samples. The trimethylphenols are the dominant components of the distribution in almost all of the samples, the exception being sample O13 which shows a dominance of 2,4- and 3,5-dimethylphenol, as indicated in Figure 6-14. The greatest variations in isomer abundance within the sample set are observed among C_3-alkyl phenols; concentrations vary from less than 1μg/g to 139μg/g, with an average of 22μg/g and a standard deviation of 40. The '2,4,6-+2,3,5-TMP' peak predominates in the distribution of alkyl phenols in most of the samples, as shown in Figure 6-14. Although the relative abundance of this peak is variable from sample to sample, it tends to occur in higher abundance in condensates than in oils (Figure 6-14) and accounts for much of the wide variation within the sample set.

Figure 6-14 shows a general similarity in the alkylphenols distribution for most of the samples; the main exceptions are sample O13 (well Nassir1, A4C reservoir unit) and the Birba oils O4 (well BB1) and O1 (well BB2). Oil O13 (Nassir1) differs from the rest of the samples (including others from the same reservoir (A4C)) by its lower abundance of 2,4,6-+2,3,5-trimethylphenols and the dominance of the 2,4- and 3,5-dimethylphenols. This oil showed some geochemical characteristics in its light hydrocarbon composition (e.g. low abundance of benzene and toluene, and a heavy $\delta^{13}C$ isotopic value for toluene, see Section 5.5.3.4) which suggest that the light end may have been affected by water washing.. If the oil has been subjected to water

washing, this should also be expressed in the alkylphenols distribution. Oil O13 (Nassir1) exhibits relatively low contents of phenol and cresols, and of alkylphenols generally within the data set (see Table 6-6). Although this data might suggest a water washing effect, this is apparently contra-indicated by the relatively high abundances of the more-water-soluble 2,4-and 3-5-DMP isomers and relatively low abundances of the less water-soluble 2,4,6- and 2,3,5-DMP isomers. Therefore, water washing can not explain the dominance of dimethylphenols over trimethylphenols in sample O13 compared to other oils in the area as shown in Figure 6-14.

The Birba oil samples O4 (well BB1) and O1 (well BB2) show slightly different distributions of trimethylphenols from the rest of the samples, including the other A4C oils (well BBN1 (sample O7) and well Nassir 1 (sample O13)). Interestingly, the distributions of trimethylphenols and of the other alkyl phenols in these samples are very similar to those obtained for the condensates as shown in Figure 6-15. Generally, A5C and A3C oils (the samples on the right hand side of Figure 6-14) show higher alkylphenols contents than A4C oils (samples on the left hand side of Figure 6-14) but they have much lower alkylphenols contents than the condensates (Table 6-6).

Phenol and alkylphenols have a very high affinity for the gas phase and phase fractionation may partly explain why the condensates have higher contents of alkylphenols than the oils. Another possibility is that it is related to gravitational segregation which followed the oil-condensate mixing, as proposed from the interpretation of light hydrocarbons data (e.g. total amount of light hydrocarbons, paraffinicity and aromaticity, (see Sections 5.5.2 and 5.5.3.2) and partially supported by the observations made in the analysis of higher molecular weight hydrocarbons (e.g. dilution of biomarkers by alkanes (see Section 4.4.5). This is further supported by the relative low phenol concentration in the Birba oils and higher concentrations in the condensates. However, phase fractionation/segregation cannot explain the higher abundance of trimethylphenols relative to the C_0-C_2 alkyl phenols in the condensates. As discussed earlier, alkylphenol concentrations and distributions in petroleum are influenced by source facies, thermal maturity and biodegradation. Most of the oils in the sample set are considered (on the basis of standard hydrocarbon parameters discussed elsewhere in this thesis) to be sourced from similar facies (with only minor

facies variation between them), the exceptions being samples O5 (well BBN1, A3C) and O15 (well Kaukab1, A1C). Most of the oils are of similar maturity, the exceptions being oil O13 (Nassir1, A4C), oil O5 and oil O15, and the condensates (O9 (well BBS1), O3 (well BBN1) and O20 (well Budour1H2) from A4C reservoir unit). Furthermore, there are no geochemical indications of biodegradation in the study oils.

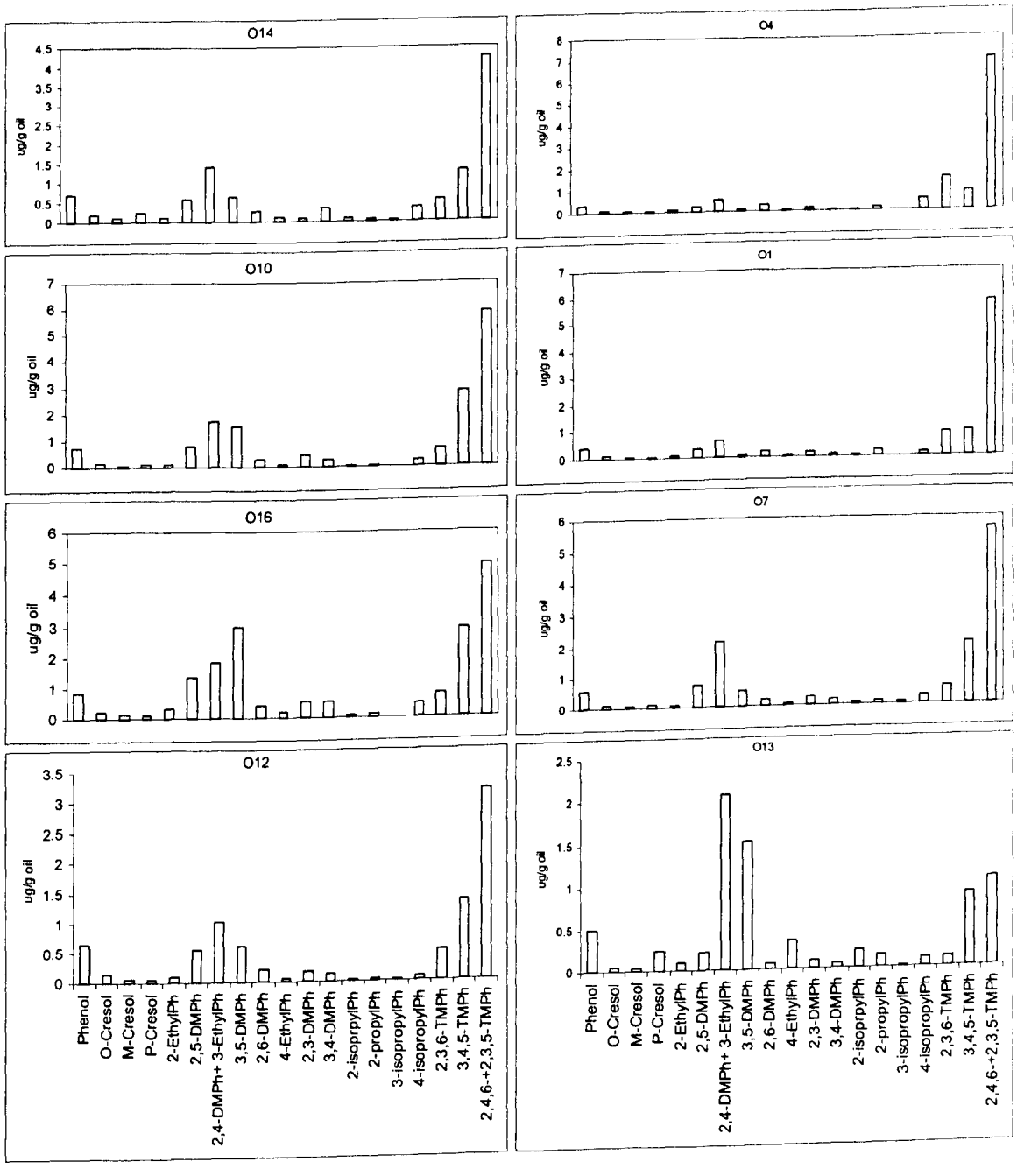

Figure 6-14: Histograms showing the concentrations of individual alkylphenols in eight representative samples from the Birba oil suite. Samples from A4C reservoirs are shown on the right and samples from A5C/A3C reservoirs on the left). Samples not shown here are the condensates – the alkylphenol distributions for these are given in Figure 6-15.

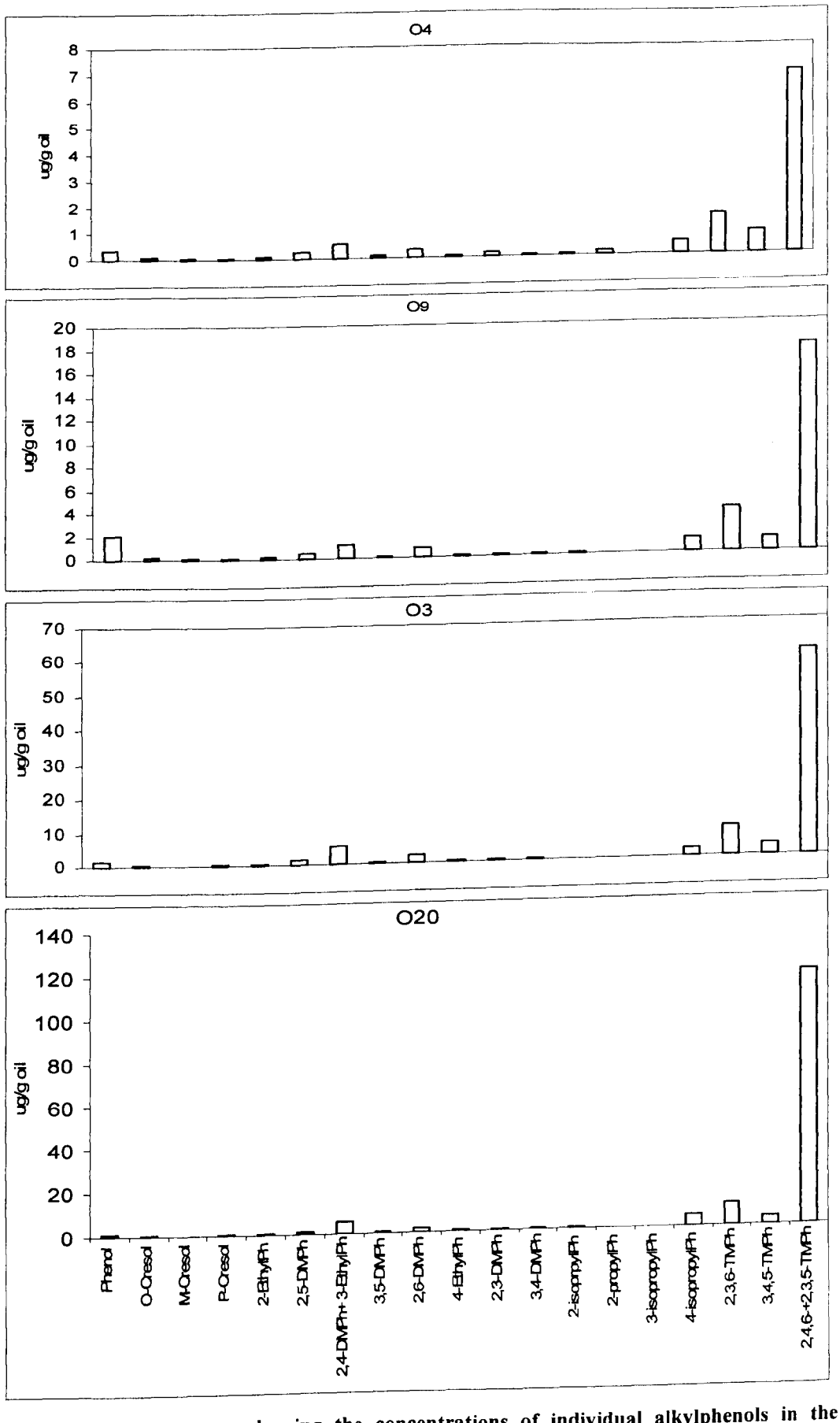

Figure 6-15: Histograms showing the concentrations of individual alkylphenols in the gas condensate samples O3, O9 and O20 and in oil sample O4 from the A4C reservoir unit

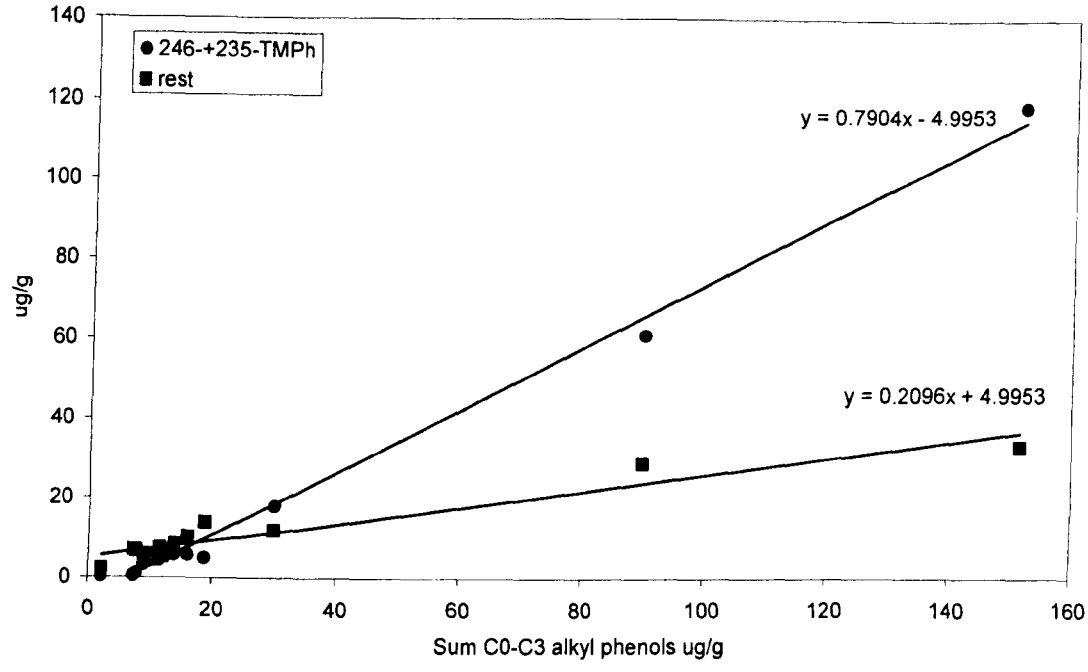

Figure 6-16: Cross-plot of the total alkylphenols content versus 2,4,6-+2,3,5-TMP (the biggest peak in the alkylphenols distribution) (filled stars) and the rest of the alkylphenols (filled squares) in the oils from the Greater Birba area

Water-washing, oxidation and migration are also important processes that can affect the distribution of alkylphenols (Bastow *et al.*, 2003; Bennett *et al.*, 1996; Taylor *et al.*, 1997; Taylor, 1994). Photo-oxidation and autooxidation of phenols occurs when an oil is exposed to light and air for a period of time; ortho- and para-substituted isomers are most affected, while phenol and meta- substituted isomers are least affected (Bastow *et al.*, 2003). Thus, 2,4,6- and 2,3,5-TMP might be expected to be relatively low if the oils had the oil been significantly affected by oxidation, which is not the case in the Greater Birba area oils.

Secondary migration processes (sorption and dissolution) can affect the distribution of alkylphenols dramatically during oil/rock/water interaction. Oil/rock partitioning may account for the low total content of alkylphenols in the studied oils. The carrier beds in the Ara carbonates (the reservoir units e.g. A3C, A4C, A5C etc.) are generally tight (large scale permeability range: 0.01-0.5mD) and organic rich (Schrooder, 2000). These two factors can easily result in a dramatic reduction in the concentration of alkylphenols (Taylor *et al.*, 1997). However, 2,4,6-TMP is not

exceptional in this context and should also be removed yet it occurs in relatively high abundance.

Water washing is another process that can affect the distribution of the alkyl phenols. As mentioned previously, there is no evidence of this process having affected most of the studied oils; the exception is sample O13 which shows some characteristic effects of water washing in the distribution of light hydrocarbons. However, the distribution of alkylphenols in this oil does not show characteristic water-washing effects such as the greater depletion of phenol relative to the cresols and an increase in the relative abundance of shielded to exposed isomers.

It is suggested that the unusual nature of the alkylphenols distribution in sample O13 relative to the other oils in the sample set might be attributed more to facies variation than to the effects of migration. The effect of migration as a possible control on the alkylphenols distribution in the studied oils cannot be ruled out, however, and oil/water/rock interaction during migration through tight carrier beds may at least partially account for the generally low content of alkylphenols and the dominance of the trimethylphenols in these oils (i.e. generally A4C oils might have migrated over a longer distance than A3C/A5C oils). This is further supported by the ratio of shielded /exposed isomers of C_0-C_3 alkylphenols as shown in Figure 6-17.

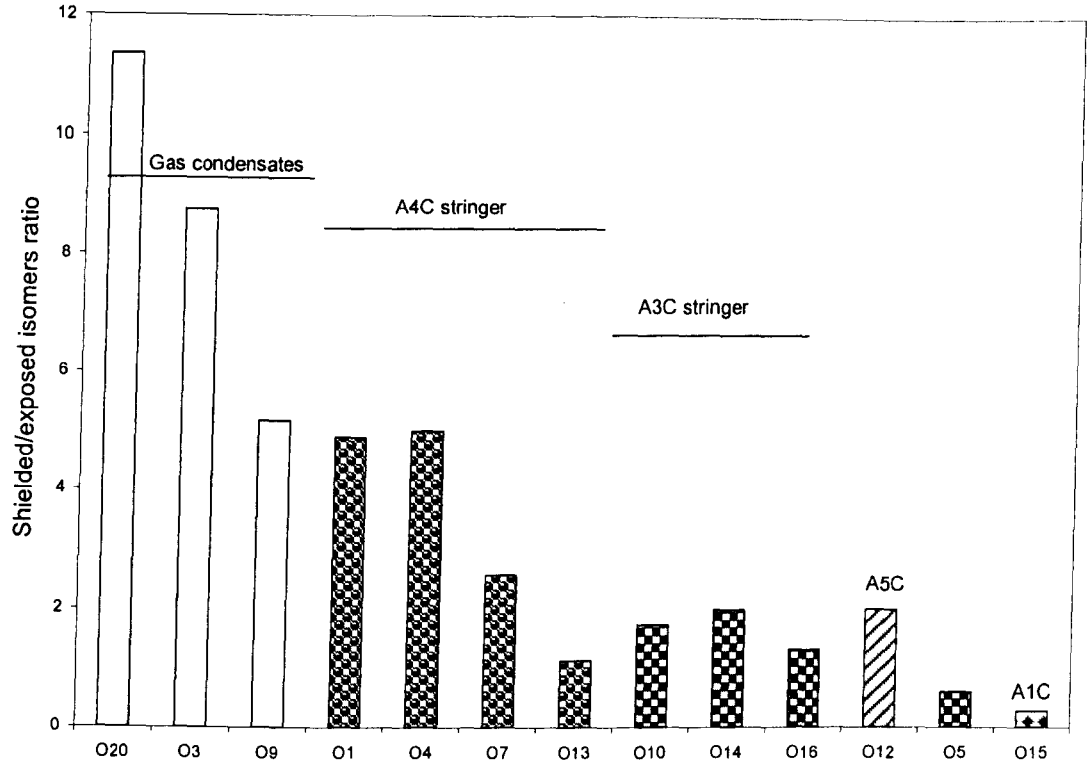

Figure 6-17: Shielded/exposed C_1-C_3 alkylphenol isomer ratios for the Birba oils. Notice that there is a general decrease in the ratio from condensates through A4C oils to A3C/A5C oils.

6.2.2 Summary

Analysis of the C_0-C_3 alkylphenols in a subset of the oils from the Greater Birba area reveals an unusual distribution of alkylphenols with little similarity to those obtained in other studies. The variation in the alkylphenol distribution reflects the same differentiation of groups within the sample set as was identified by other data in this study. The alkylphenols analysis distinguishes three main groups: the A4C oils (mainly Birba oils, well BB1 (O4) and BB2 (O1)); the A3C/A5C oils (e.g. Kaukab1 (O10); and the A4C condensates (e.g. well BBN1 (O3)). The Birba oils are characterised by a lower content of alkylphenols than the A3C/A5C oils, while the condensates have the highest content of alkylphenols. This is attributed to a phase fractionation effect (alkylphenols partition more easily into the gas phase than the liquid phase) resulting from the proposed mixing of condensate with the original oil. It also suggested, on the basis of a relatively high content of shielded alkylphenol isomers, that the Birba oils and condensates might have migrated a longer distance than the other oils. The unusual nature of the alkylphenols distribution in sample O13

(A4C, well Nassir1) cannot be explained as a migration, biodegradation, water washing or thermal maturity effect, and it is suggested that this oil might have originated or influenced by a slightly different source facies.

6.3 Acids in crude oils and condensates from the Greater Birba area

6.3.1 Introduction

The main aim of this study was to identify the main controls on the large variations in some important properties of the petroleum fluids from the Greater Birba area. One of these properties is the acidity of the crude oils; as mentioned earlier, the acidity has important implications in petroleum exploration and production. The oils analysed in this study show significant variations in acidity; the total acid number (TAN) varies from 0.16 to 1.24 mg KOH/g oil in the crude oils and shows very low values, in the range 0.11-0.14 mg KOH/g oil, in the condensates. The aims of this part of the study were to identify the reasons for the high variability in acidity and its effect on other important properties, and to investigate possible correlations between acidity and geochemical observations gained from different types of data.

Organic acids in petroleum were first termed 'naphthenic acids' after the first group of acids to be characterised in petroleum, which were saturated cyclic carboxylic acids. There are, however, many other chemical classes of organic acids in crude oils (Meredith *et al.*, 2000). The acidity of a crude oil is measured by two methods: American Standard Test Method for Acid Number of Petroleum Products by Potentiometric Titration (ASTM D-664) and American Standard Test Method for Acid and Base Number by Colour-Indicator Titration (ASTM D-974) (Intertek-Caleb-Brett, 2006). In both methods, the acidity is measured by its total acid number (TAN) which is the number of milligrams of potassium hydroxide (KOH) required to neutralise the acidity in one gram of oil (Derungs, 1956). The neutralisation end-point in the ASTM D-664 method is defined by a potentiometric reading in millivolts, that compares the initial reading with that of freshly prepared non-aqueous basic buffer solution or with a well defined inflection point. In the ASTM D-974 method, the neutralisation end-point is defined as the colour change of *p*-naptholbenzein in a toluene-water-isopropanol solvent. Both methods can also be used to determine the total base number (TBN) by using hydrochloric acid instead of potassium hydroxide

as the titrating solution and methyl orange instead of *p*-naptholbenzein as the colour indicator (Peters *et al.*, 2005). Oils with a TAN greater than 0.5 mg KOH/g are classified as high acidity oils and these are less desirable due to associated corrosion and refinery problems (Meredith *et al.*, 2000).

The study of organic acids has important implications in petroleum exploration and production. A high acids content in crude oils is usually taken as a potential indicator of biodegradation (Meredith *et al.*, 2000). Most oils with a TAN greater than 1 are biodegraded, and *all* oils with a TAN higher than 2 are biodegraded. A high acids content in oil may result from acids being concentrated by depletion of other organic compounds, or from neoformation of new acids (Peters *et al.*, 2005). Carboxylic acids consist mainly of naphthenic acids, which are believed to originate from the biodegradation of C_{18} (or greater) cycloalkanes, alkylaromatic organic sulphur compounds and possibly polar resins and asphaltenes (Thorn & Aiken, 1998). Meredith *et al.* (1999) reported a good agreement between the total carboxylic acids content of oils and the degree of biodegradation. They determined the acids content by a non-aqueous ion-exchange extraction method and by gas chromatographic analysis of the methyl esters of the acids. There was no correlation between *n*-acids or fatty acids and both TAN and biodegradation. However, a noticeable correlation between the contents of fatty acids and n-alkanes was observed, suggesting that normal alkanes were probably precursors of normal fatty acids (Barakat & Rullkoetter, 1995).

6.3.2 Distribution of acidity (TAN)

Table 6-7 shows the TAN, the total amount of acids isolated and the amount of normal saturated fatty acids in the studied oils from the Greater Birba area, together with some of their important properties and geochemical characteristics. Figure 6-18 shows the spatial (geographical) variation in acidity (TAN) in the three reservoir units in the Greater Birba area; not all samples are represented in the plot because some of the samples are from the same well but from different reservoir units (e.g. in the Omraan 1 well, sample O12 is from the A5C unit and sample O22 is from the A4C unit). Each carbonate stringer covers a large area and wells drilled through it, might

find flowing oils in some parts and while other parts are tight (e.g. in well Shamah1 the A4C was tight and the A3C was flowing oil). Most of the A4C samples are from the eastern part of the Greater Birba area and the samples from the A3C unit are from the western part. The data are plotted spatially in Figure 6-18 regardless of the type of reservoir since the reservoirs are distinguishable as explained in the figure caption. It is very clear that the oils from the Birba field (O1 (well BB2), O4 (well BB1)) and from well Nasser1 (O13) are characterised by high acidity. Oil O12 (well Omraan1H3) from the A5C reservoir unit and oil O15 from the A1C reservoir unit (data in Table 6-7, but not shown in Figure 6-18 because it shares the same well as oil O10) also show high acidity. The A3C oils, sample O7 from the A4C unit, and the condensates from A4C all show low acidity (<0.5 mg KOH/g oil).

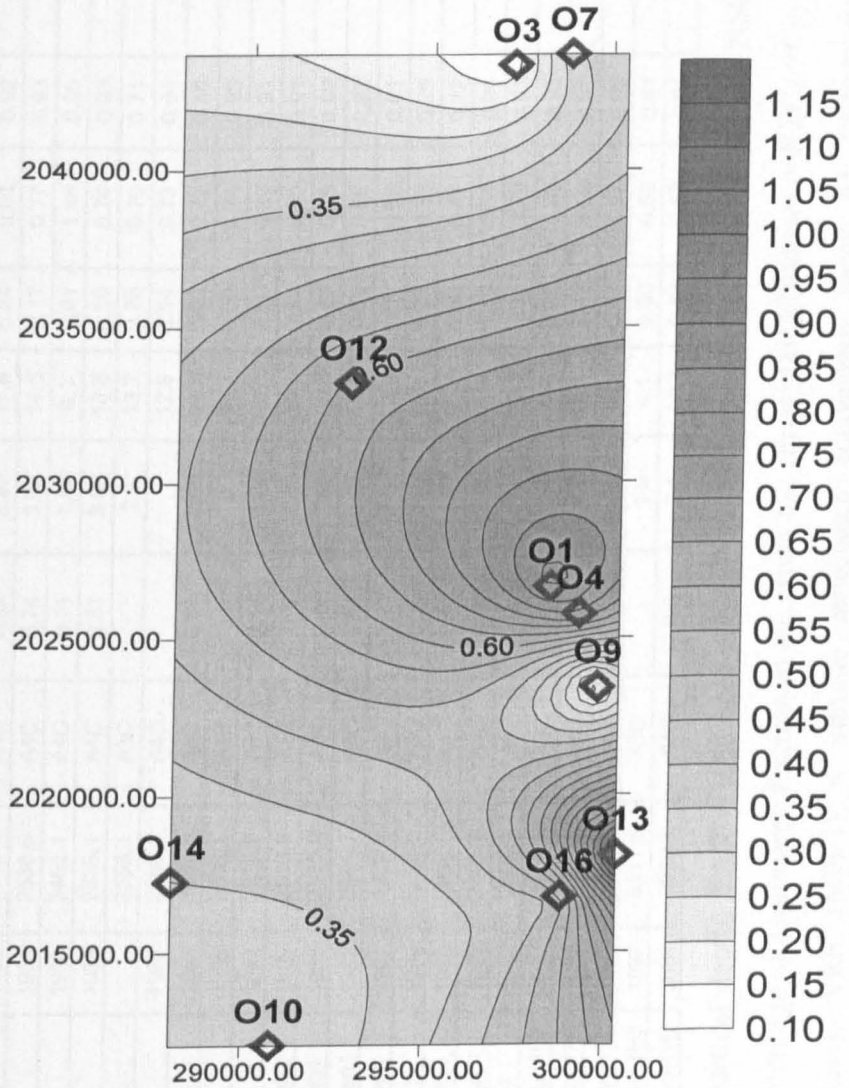

Figure 6-18: The spatial distribution of acidity (TAN) in oils from the Greater Birba area. The sample codes represent 3 reservoir units: A4C (O1, O4, O13, O7 & condensates O9&O3); A3C (O10, O14, O16) and A5C (O12).

Table 6-7: Total acid number, total acids and n-fatty acids concentrations in the studied oils, together with other geochemical characteristics.

Sample ID	well	year	TVD (m)	Reservoirs	TAN mgKOH/g	Sulfur wt%	NSO%	Asp%	Preg+Tric/ Hopanes	VRE (MPI-1)	C29% αββ/(ααα+αββ)	Total alkylphenols ug/g	total acids ug/g	n-acids ug/g
O1	BB2	1982	2583.4	A4C	0.92	2.97	17.8	0.24	0.81	0.92	57.99	10.07	13.9	10.6
O2	BB1	1988	2536.5	A4C	0.74	3.03	14.5	0.17	0.77	0.93	58.37		12.4	6.3
O3	BBN1	1980	3455.1	A4C	0.11	1.65	6.1	0.01	1.48	0.86	58.25	89.85	5.2	2.7
O4	BB1	1983	2533.1	A4C	0.81	3.03	13.8	0.10	0.74	0.93	58.53	12.14	13.6	8.1
O5	BBN1		3558.1	A3C		2.5	13.7	0.70	0.10	0.71	45.38	7.31	21.8	21.8
O6	BB1	1999	2588.3	A4C			12.8	0.14	0.73	0.94	58.20		12.3	5.2
O7	BBN2	1983	3597.8	A4C	0.34	2.05	11.5	0.43	0.72	0.86	57.71	13.87	16.4	10.1
O8	BB1	1988	2533.1	A4C		3	15.1	0.09	0.74	0.93	58.36		12.5	9.9
O9	BBS1	1987	2329.7	A4C	0.14	3.24	5.7	0.00	1.09	0.91	59.09	29.89	4.4	2.0
O10	Kaukab1	1989	2513.6	A3C	0.3	2.39	10.8	0.37	0.50	0.91	58.23	16.07	14.1	12.2
O11	Kaukab1	1987	2513.6	A3C	0.16	2.4	10.4	0.50	0.58	0.92	58.43		9.4	5.4
O12	Omraan1	1982	2601.7	A5C	0.61	2.11	13.5	0.50	0.56	0.92	58.09	8.94	11.9	8.8
O13	Nasser1	1982	1998.6	A4C	1.24	3.16	23.6	1.69	0.58	0.81	58.02	7.77	22.4	15.4
O14	Durra1	1982	2693.0	A3C	0.35	1.97	9.9	0.07	0.53	0.93	57.92	11.53	10.6	8.1
O15	Kaukab1	1989	2896.9	A1C	0.59	0.78	11.2	0.63	0.47	0.72	55.88	2.21	14.3	8.1
O16	Shamah1	1992	2385.7	A3C	0.46	2.46	8.4	1.10	0.51	0.94	57.29	18.75	11.0	4.2
O17	Durra1	1982	2695.1	A3C		2.02	13.7	0.15	0.49	0.93	59.07		13.6	12.1
O18	Omraan1H3	1997	2939.1	A5C		2.1	9.7	0.30	0.58	0.93	57.39		9.3	2.5
O19	Omraan1H3	1997	2939.1	A4C		1.9	9.7	0.41	0.52	0.91	58.20		8.6	5.0
O20	Budour1H2	2003	2971.6	A4C		4.7	12.1	0.47	1.97	0.92	59.27	151.55	8.3	3.6
O21	Omraan1H3	1997	3111.5	A3C		1.9	4.1	0.00	0.52	0.91	58.87		8.0	1.4
O22	Omraan1H3	2001	2939.1	A4C	0.6	2.1	10.1	0.68	0.58	0.91	57.95		16.7	12.0

TVD = True vertical depth; TAN = total acid number; NSO% = normalised percentage of NSO compound fraction in the crude oil; Asp% = normalised percentage of asphaltene fraction in the crude oil; (Preg+Tric)/Hopanes = [(ΣC_{21}+C_{22} pregnanes)+ (Σtricyclic terpanes (C_{19}-C_{30}))]/(ΣC_{27}-C_{35} 17α Hopanes); VRE (MPI-1) = vitrinite reflectance equivalence based on methylphenanthrene index [1.5(2-Methylphenanthrene+3-methylphenathrene)/(Phenanthrene+1-methylphenanthrene+9-methylphenanthrene)].

6.3.3 Controls on TAN

Figure 6-19 shows the variation in TAN with relative content of NSO compounds + asphaltenes in the Birba oils. There is a good correlation (R^2=0.83) between the TAN and the resins content of the oil suggesting that most of the compounds contributing to TAN are in the resins fraction. Although the highest TAN and the highest asphaltenes content in the data set were both found in sample O13 (Nasser 1), there is no consistent correlation between these parameters (most of the oils have very low asphaltene content). It is noticeable that oils from the A3C unit are characterised by consistently low TAN and asphaltene contents, while oils from the A4C unit span the whole range - from highest the TAN in the data set in sample O13 to extremely low TANs in the condensates e.g. sample O3.

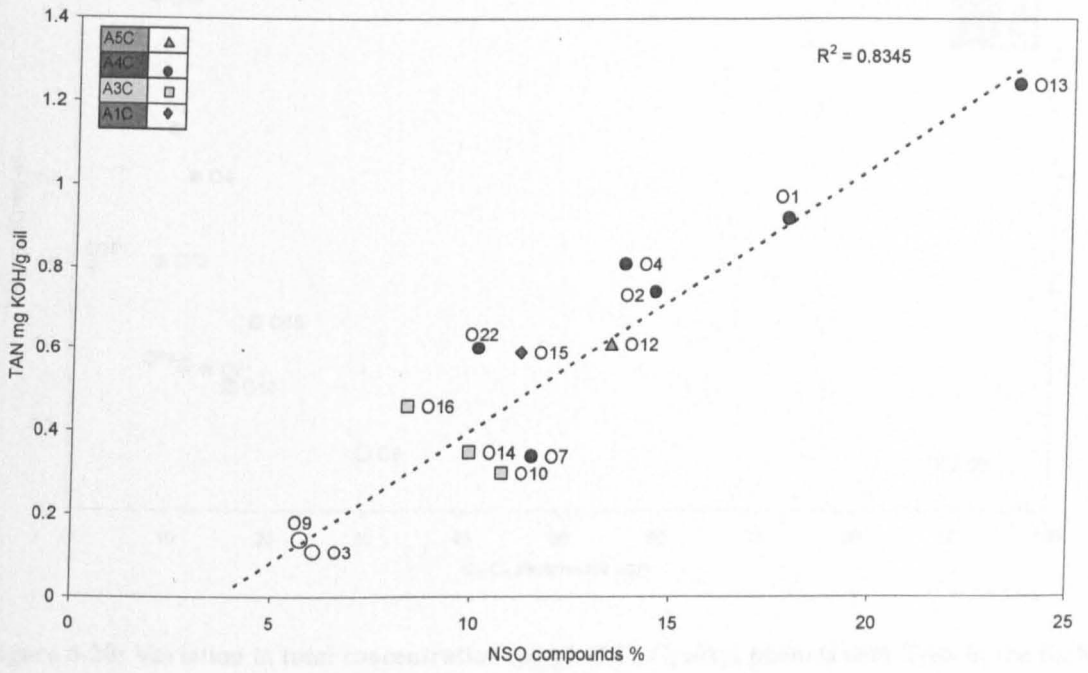

Figure 6-19: Variation in NSO+Asphaltene content (% of total C_{15+}) with total acid number (TAN) for A4C oils (filled circles for oils and empty circles for condensates), A3C oils (squares), A5C oils (triangles), and A1C oil (diamonds).

Phenol and alkylphenols are acidic compounds which partition easily into water and so can contribute to the TAN. The variation in C_0-C_3 alkylphenols concentration with TAN shown in the cross-plot in Figure 6-20 shows a general but weak non-linear negative trend with significant scatter. This suggests that

alkylphenols variations do not control the larger variation observed in TAN. However, it can be inferred from this cross-plot that both properties share at least partially, a common control, since they are inversely related. As discussed previously, the main control on the distribution of alkylphenols in the Birba oils is probably phase fractionation. If this were the case, it would be expected that the alkylphenols content of the oils would have an inverse relationship with acidity since most of the acids are in the heavy fraction (resins). This suggests that phase fractionation may partially control the acidity of the oil by concentrating the acidic compounds in the residual oils (e.g. sample O4), as the volatile compounds partition into the gas phase; this is assuming that phase fractionation truly controls the alkylphenols distribution. The weak nonlinear relationship and the significant scatter in the alkylphenols vs. TAN cross-plot suggest that other controls are more important than phase fractionation.

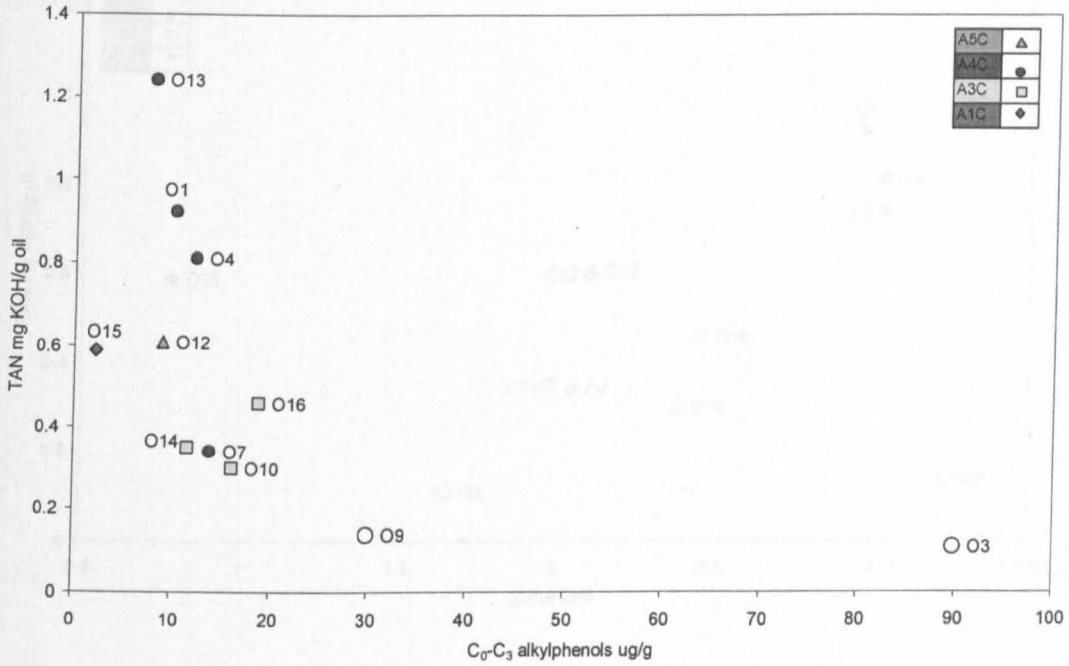

Figure 6-20: Variation in total concentration (µg/g) of C_0-C_3 alkyl phenols with TAN in the Birba oils. Symbols are explained in Figure 6-19. Empty circles are condensates.

The relationship between sulphur content and acidity of the Birba oils is illustrated in Figure 6-21, and a general positive trend between the two properties suggests a common control. This sort of trend might be expected to reflect variation in thermal maturity or biodegradation but as discussed elsewhere in the thesis the Birba oils show similar maturity and are not biodegraded. Phase fractionation might be involved, although it is difficult to envisage this as a major controlling process on the

distribution of sulphur, and this is supported by the significant scatter in the cross-plot. Assuming that there is a real trend in the data in Figure 6-21, the main outliers are samples O9 and O15. Sample O9 (well BBS1, A4C unit) has an unusually high sulphur content for a condensate; this is one of two high sulphur condensates. The other sample outside the main trend was sample O15 from the A1C unit, the deepest reservoir unit sampled, which can be attributed to the different origin for this oil. It has to mentioned here that sulphur content and sulphur isotopes was found to be likely controlled by mixing of oils with high sulphur condensates, and that most of the sulphur is probably in the light fraction and aromatic hydrocarbons fraction. Oil O15 and condensates, which are outliers here, can be possibly the two end-members to this mixing sequence.

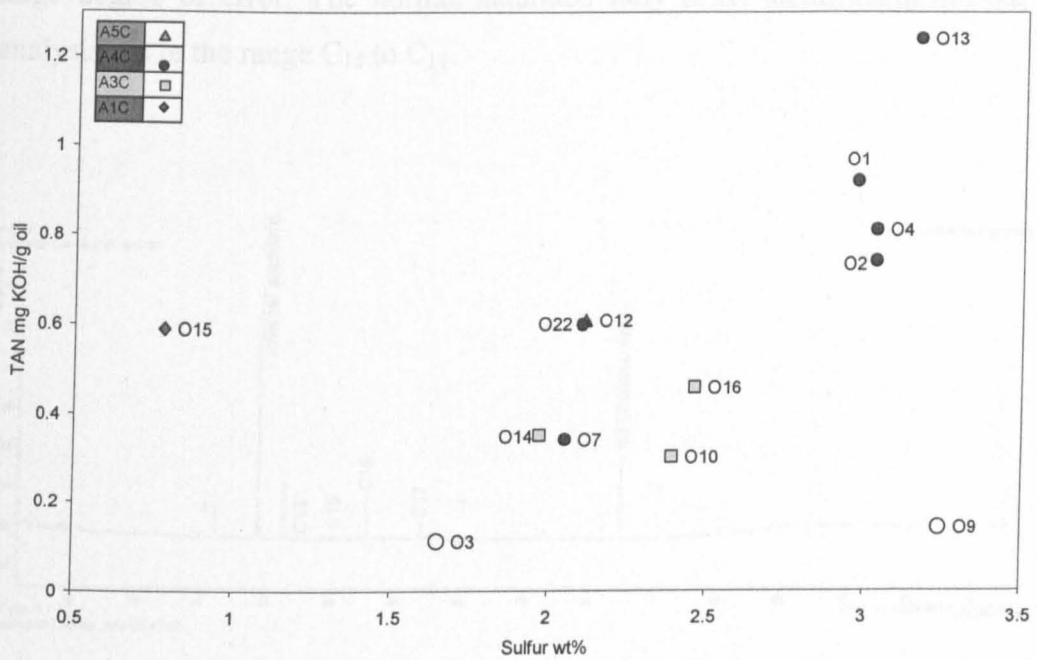

Figure 6-21: Cross-plot showing variation in sulphur content (wt %) with TAN in the Birba oils. Empty circles are condensates.

6.3.4 n-Acids, total acids and TAN

Figure 6-22 shows a gas chromatogram of the derivatised acid fraction from one of the Birba oils (sample O1) characterised by a high TAN, together a chromatogram of the procedural blank. Although this oil is classed as 'high acidity' due to the high TAN (>0.5 mg KOH/g), it is very clear that there are virtually no acids present except for some saturated fatty acids (C_{16} and C_{17}) which may be

contaminants introduced during sample preparation and/or storage. It is also clear from Figure 6-22 that the chromatogram shows no 'hump' or unresolved complex mixture of compounds, as might be expected since this oil is not biodegraded. The method for the quantification of acids by GC analysis is explained in detail in the Experimental Section (Chapter **3**). Quantification of the acids involves choosing a point slightly below the baseline in the chromatogram and integrating the whole area above this point. This is done for the oils and for a procedural blank run with the batch of samples. The integrated area from the blank (including any contamination peaks and standards) is subtracted from that of the oil, the difference being attributed to acid components. If there is no hump in the chromatogram and if the acids occur in very low abundance (as with many of the Birba oils), then this method is prone to a large degree of error. The normal saturated fatty acids identified/quantified in the analysis are in the range C_{14} to C_{17}.

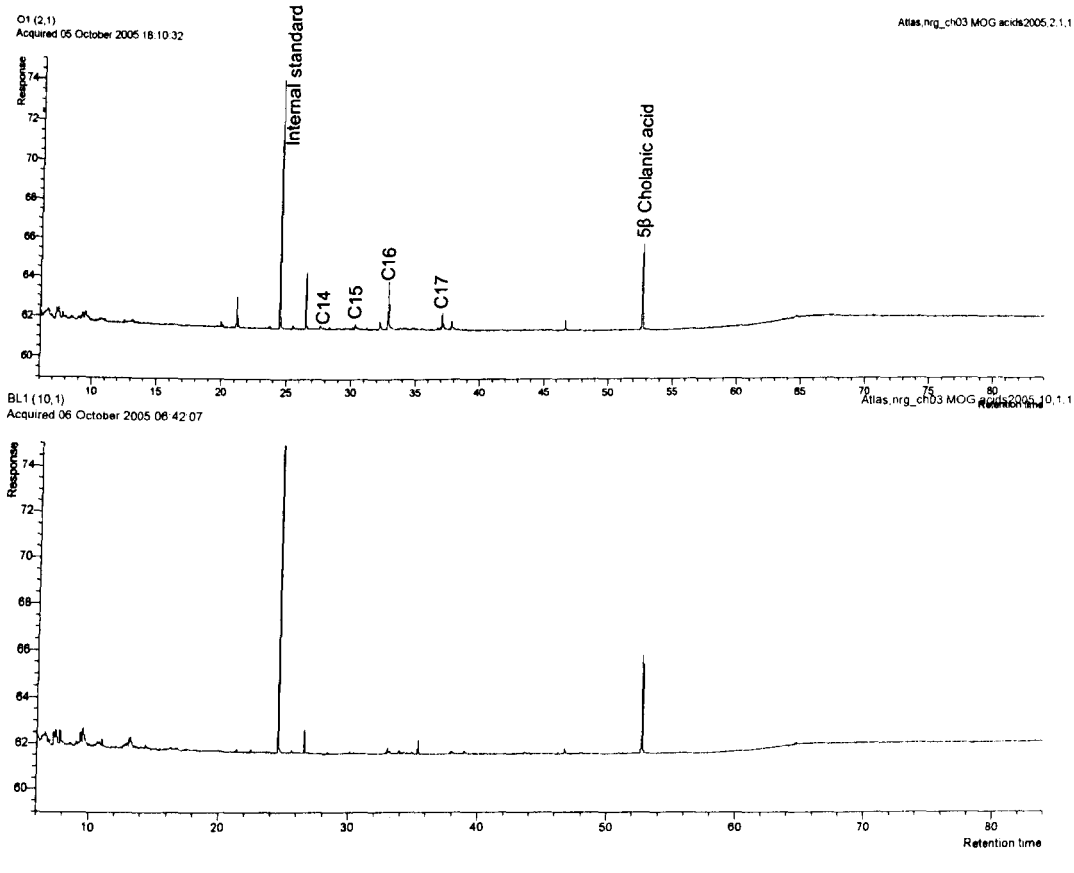

Figure 6-22: Gas chromatogram of the derivatised acid fraction from sample O1 (high TAN) (top) and a procedural blank (bottom) run in the same sample sequence.

The amounts of total acids and *n*-fatty acids and the TAN of the studied oils are given in Table 6-7. The average total acid concentration and the average total *n*-acid concentration for the sample set are 12.3ppm and 8ppm respectively. These relatively low values reflect the fact that none of the oils is biodegraded, as indicated by other geochemical data discussed previously in Chapter 4 and Chapter 5. A poor correlation was found between TAN and the total acids concentration, as illustrated in Figure 6-23, suggesting that the total acids content does not represent the total acid number, at least for the samples analysed in this study. In contrast, Meredith *et al.* (2000) reported a good correlation between total acids content and the TAN, implying that the carboxylic acid fraction was a major contributor to the TAN. However, they also reported that three high acidity oils in their sample suite showed very low acid contents (Meredith *et al.*, 2000). These oils were also characterised by high sulphur contents and Meredith *et al.* (2000) suggested that sulphur might play a role in controlling the TAN. This hypothesis is supported by the moderate positive correlation between sulphur content and the TAN in the present study (Figure 6-21). It is recommended that further investigation of this relationship should be undertaken.

The cross-plot of TAN against total acids content (Figure 6-23) for the Birba samples shows no clear distinction between oils from different reservoirs or from different geographic locations, suggesting the possibility that the variations in total acids content could be due to post-sampling effects.

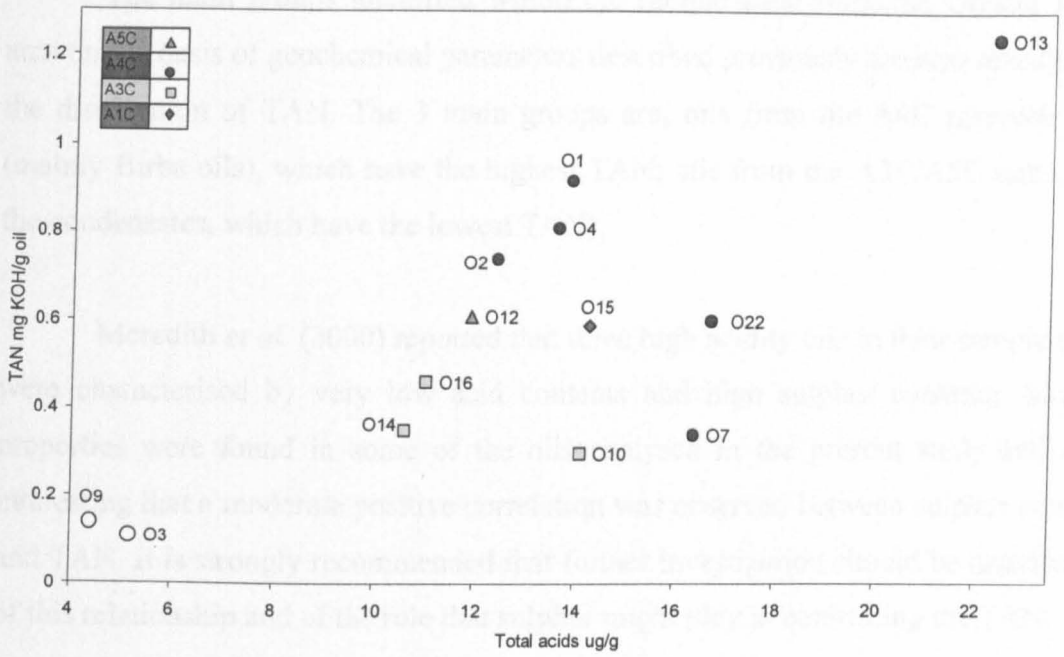

Figure 6-23: Variation in total acids content (ppm) with TAN for the studied oils. Samples O9 and O3 are condensates.

6.3.5 Summary

Several of the oils from the Greater Birba sample set are characterised by high or moderately high acidity, as indicated by the total acid number (TAN). However, when the carboxylic acid fraction was isolated and quantified using chromatographic methods (Aitken *et al.*, 2004), the content of acids in the oils was found to be very low. In contrast to the observations published by Meredith *et al* (2000), there was no correlation between total acids content and TAN.

The TAN showed a good positive correlation with NSO content, suggesting that most of the acids contributing to the TAN are in the resins fraction. Lower molecular weight alkylphenol concentrations tend to vary inversely with TAN and show a non-linear relationship. It is suggested that for the Greater Birba oils the TAN is partially controlled by phase fractionation, with loss of the more volatile components of petroleum into the gas phase leading to concentration of the heavier fractions (such as NSO compounds/resins fraction) in the residual oil.

The main groups identified within the sample suite from the Greater Birba area on the basis of geochemical parameters described previously are also revealed by the distribution of TAN. The 3 main groups are; oils from the A4C reservoir unit (mainly Birba oils), which have the highest TAN; oils from the A3C/A5C units; and the condensates, which have the lowest TAN).

Meredith *et al.* (2000) reported that three high acidity oils in their sample suite were characterised by very low acid contents and high sulphur contents. Similar properties were found in some of the oils analysed in the present study and it is interesting that a moderate positive correlation was observed between sulphur content and TAN. It is strongly recommended that further investigation should be undertaken of this relationship and of the role that sulphur might play in controlling the TAN.

6.4 *Sulphur analysis*

6.4.1 Introduction

Sulphur is the third most abundent element in petroleum and the sixth most abundant in biomass (Hunt, 1995). The study of sulphur is of prime importance for both petroleum and environmental geochemistry. Sulphur in the form of hydrogen sulphide can cause refinery problems such as corrosion and catalyst poisoning (Hunt, 1995). Combustion of sulphur-containing fuels causes global problems like acidification of forests and lakes (Hunt, 1995). The sulphur content of is important to petroleum geochemistry as it can be used as a potential tool for assessing oil quality as well as for determining maturity and the depositional environment of deposition of source rocks (Hunt, 1995).

Sulphate (SO_4^{2-}) is the most stable form of sulphur in anoxic water columns (Orr & Sinninghe Damsté, 1990). Sulphate is utilized by micro-organisms in the water column, and is subsequently converted into biosynthetic organic sulphur compounds (OSC), which accumulate as part of organic matter (Orr & Sinninghe Damsté, 1990). Organic sulphur compounds may be formed by the living organism such as S-bacteria, brown (phaeophyceae) algae, and red (phodophycea) algae (Hunt, 1995). The main biosynthetic organic sulphur compounds that may form by this way are sulphur containing amino acids (custeine and methionine) in proteins, sulpholipids in membranes, and sulphate esters in cell wall carbohydrates, which have soft structures that are easily degraded by microbial and enzymatic processes (Orr & Sinninghe Damsté, 1990). This pathway of sulphur origin in petroleum is suggested to be not a major route for sulphur enrichment in organic matter because of sulphur is of lower abundance in living biomass (6th most abundant element), while it is of higher abundance in petroleum (third most abundant element after hydrogen and carbon) (Orr & Sinninghe Damsté, 1990). Furthermore, the organic sulphur compounds found in petroleum are very different from those biosynthetic organic sulphur compounds (Orr & Sinninghe Damsté, 1990). The main forms of organic sulphur compounds in young sediments are hydrogen sulphide, methyl mercapatan, and dimethyl sulphide,

as well as some oxidised forms such as elemental sulphur, polysulfide, thiosulphate, polythionates, sulphite, and sulphate (Kohnen, 1991; Vairavamurthy *et al.*, 1995).

Several studies have proposed that the main source of sulphur in organic matter is the hydrogen sulphide/polysulphide formed by sulphate reducing bacteria utilizing sulphate in anoxic water at the sediment water interface (in silled basins or high upwelling areas) (e.g. Ivelv *et al.*, 1973; Kohnen, 1991; Kohnen *et al.*, 1989; Orr & Sinninghe Damsté, 1990; Vairavamurthy *et al.*, 1995). Figure 6-24 shows a schematic diagram for the possible origins and fates of sulphur during diagenesis and catagenesis of sediments. Hydrogen sulphide is very reactive and readily oxidized or partially oxidized by various oxidants to be converted to other sulphur forms such as elemental sulphur, polysulphides, sulphite, thiosulphate, and polythionate and eventually sulphate (Vairavamurthy & Zhou, 1995; Yao & Millero, 1995). The sulphur in these forms range in valence state from –II (H_2S, HS^-, S^{2-}) (very reactive) to +VI (HSO_4^-, SO_4^{2-}) (inactive) (Orr & Sinninghe Damsté, 1990). During the very early diagenesis, the reactive sulphur (hydrogen sulphur or any other reactive forms) reacts to form pyrite (Iron Sulphide) and organic sulphur (Orr & Sinninghe Damsté, 1990; Sinninghe Damsté & de Leeuw, 1992; Sinninghe Damsté *et al.*, 1988; Vairavamurthy *et al.*, 1995). Reactions of organic molecules with sulfur in reduced form (higher valence state such as hydrogen sulfide) are believed to play an importent rule in foming macromolecular geopolymers (humic polymers to kerogen to petroleum or coal, Figure 6-24) through di- and plolysulfide cross linking, which help to preserve sedimentary organic matter (Schouten *et al.*, 1995). Organic Sulfur in organic matter in marine sediments was found to be enriched in $\delta^{34}S$ by more than 10 per mil in most cases relative to the sulphur locked in pyrite ($\Delta\delta^{34}S_{(organic\text{-}pyritic)}$=+2.0 to 32.7 parts per mil), which suggests that the two types of sulphur are not exclusively derived from the same origin (Anderson & Pratt, 1995).

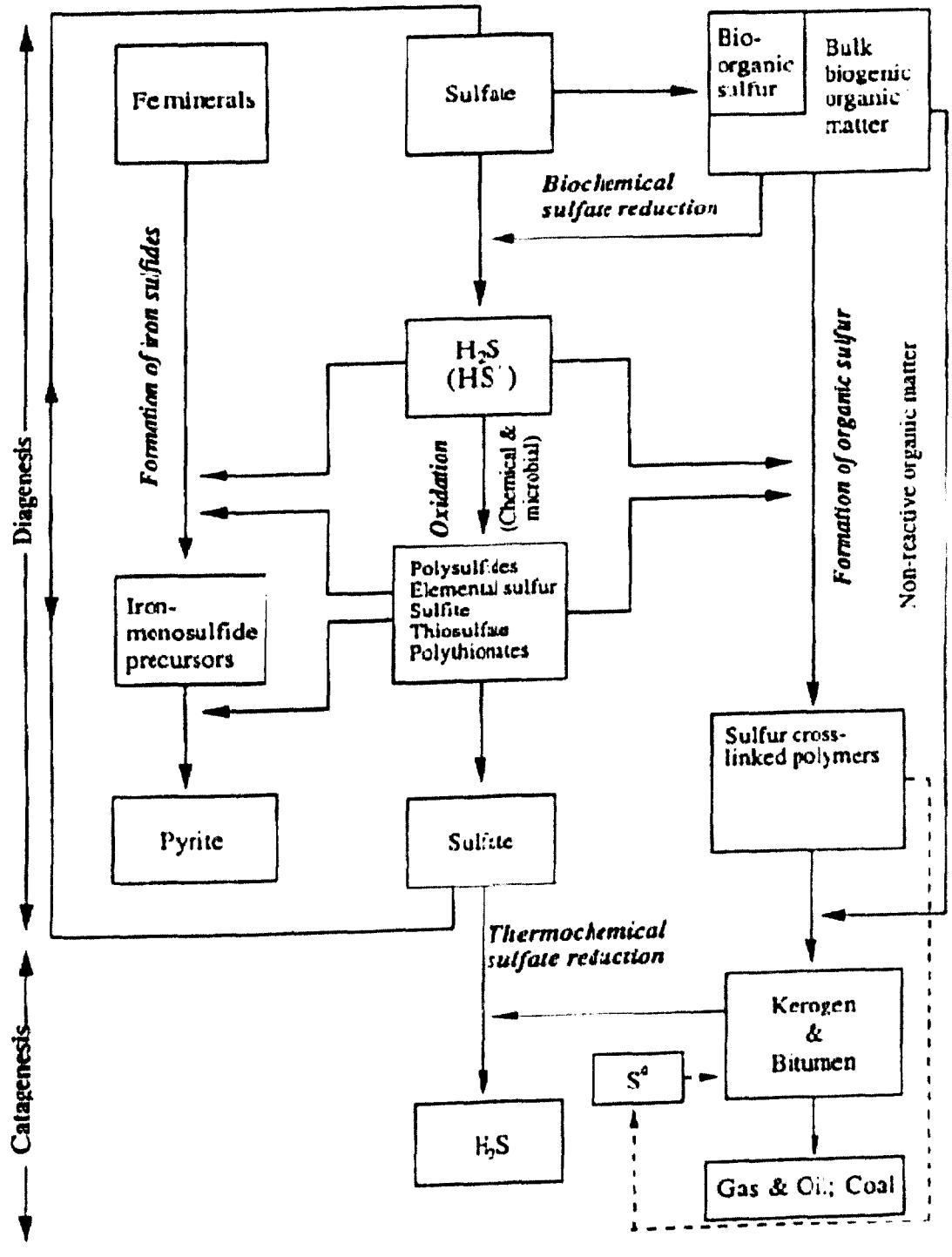

Figure 6-24: Geochemical transformation of sulphur during diagenesis and catagenesis (Vairavamurthy *et al.*, 1995).

In sedimentary environments that have high abundance of iron, reactive sulfur reacts favourably and more quickly with iron and so most of the sulphur become locked as iron sulphide (pyrite) (Tissot & Welte, 1984). Thus, the abundance of sulphur in organic matter is enhanced in iron poor sediments such as carbonate and evaporite facies (Hunt, 1995; Staudt & Schoonen, 1995; Tissot & Welte, 1984).

Clastic source rocks are rich in clays and therefore they generate low sulphur crude oils; iron in clays reacts with sulphur to form pyrite (FeS) (Hunt, 1995; Tissot & Welte, 1984). The relative abundance of iron in clastics and carbonates is 12 to 1 and in sandstones and carbonates is 3 to 1, (Tissot & Welte, 1984). Figure 6-25 shows a schematic diagram of the diagenesis and catagenesis of the sulphur in the two distinctive environments and related source facies.

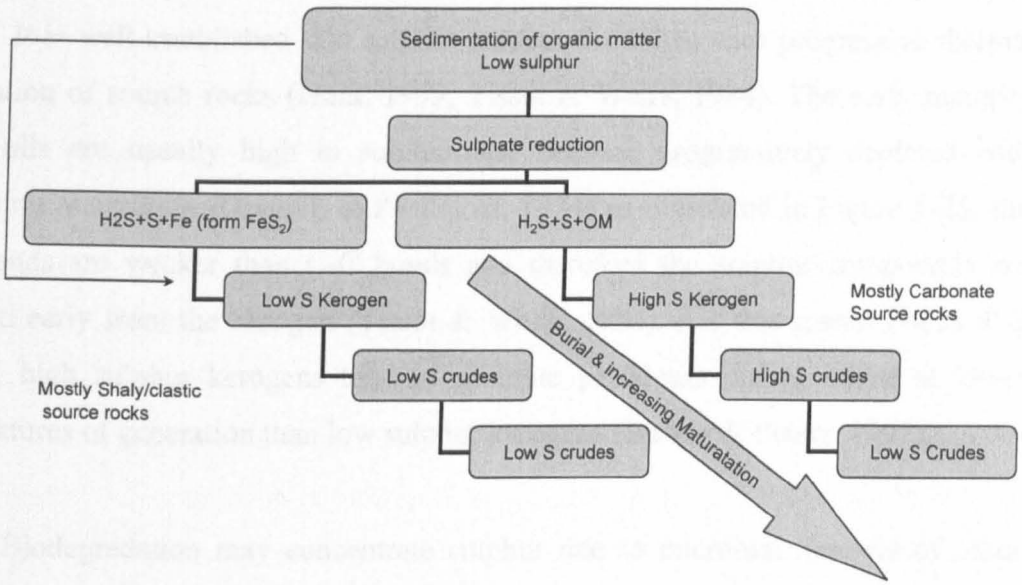

Figure 6-25: diagenesis and catagenesis behind the sulphur origin in petroleums sourced from calstic and carbonate source rocks.

Sulphur content of a crude oil is determined primarily by the source facies (e.g. clastic versus carbonate) (Tissot & Welte, 1984), and thermal maturity (Gransch & Posthuma, 1974; Ho *et al.*, 1974; Orr, 1974). Once the crude oils are generated, other processes may control the abundance and distribution of sulphur in crude oils such as thermal cracking (Sassen, 1988), biodegradation or/and water washing (Bailey *et al.*, 1973; Orr & Sinninghe Damsté, 1990; Thode, 1981), thermochemical sulphate reduction (Gaffney *et al.*, 1980; Goldhaber & Orr, 1995; Orr, 1974; Worden & Smalley, 1996) and bacterial/microbial sulphur reduction (Trudinger *et al.*, 1985).

It has already been mentioned that sulphur content is higher in clay poor sediments such as carbonate or anhydrite deposited in highly reducing conditions. Metals in clays in marine siliciclastic rocks, are attacked more rapidly by the reduced

sulphur to form metal sulphides and lead to low sulphur organic matter deposits (Tissot & Welte, 1984). Most Lacustrine facies are often characterised by low sulphur content because there is usually low sulphates content available (fresh water column) during early diagenesis to incorporate sulphur into the organic matter (Peters & Moldowan, 1993). However, exceptional case histories have been reported for lacustrine source rocks and crude oils that exhibit high sulphur content such as salt lake sediments in China (Fu *et al.*, 1986) and lacustrine oils (S = 7.5wt%). from Rozel Point from North-Western part of Utah (USA) (Sinninghe Damsté *et al.*, 1987).

It is well established that sulphur content decreases with progressive thermal maturation of source rocks (Hunt, 1995; Tissot & Welte, 1984). The early maturity crude oils are usually high in sulphur and become progressively depleted with increasing maturation (Gransch & Posthuma, 1974) as illustrated in Figure 6-25; the C-S bonds are weaker than C-C bonds and therefore the sulphur compounds are released early from the kerogen (Tissot & Welte, 1984). For this reason (weak C-S bonds), high sulphur kerogens tend to generate petroleum during burial at lower temperatures of generation than low sulphur kerogens (Baskin & Peters, 1992).

Biodegradation may concentrate sulphur due to microbial removal of other non-sulphur compounds, preferentially saturated hydrocarbons (Bailey *et al.*, 1973; Hunt, 1995; Peters & Moldowan, 1993). Likewise, sulphur can also be diluted by mixing of high sulphur oil with sulphur poor condensate charge.

Bacterial and thermo-chemical sulphate reduction processes (BSR and TSR respectively) are important sulfur additive processes occurring in reservoirs and source rocks (e.g. Orr, 1974; Vairavamurthy *et al.*, 1995) as illustrated in Figure 6-24. They result in high sulphur crude oils and produce large amount of souring gas (H_2S). BSR occurs at low temperatures less than 80°C, and only contributes less than 5% to the total H_2S in reservoir (Machel, 2001). TSR occurs at high temperatures (T>125-145°C) and may occur at temperatures as low as 100°C (Machel, 2001). TSR produces high concentrations of H_2S. Below 100°C, either high activation energies and/or other kinetic inhibitors cause the slowness or absence of TSR (Cross, 1999). High abundance of thiols in very high maturity oils and condensates are good indicator for

TSR, while low thiols indicate the absence of TSR. (Thode & Monster, 1965). These processes were reviewed in much more details in section 4.3.4.2.

Sulphur contents of oils and bitumen varies between less than 0.05 to 14 wt.% but most of the petroleums have less than 4 wt.% (Hunt, 1995). The crude oils that have sulphur content greater than 1 wt% are classified as high sulphur oils while these are classified as low sulfur oils if sulfur content lower than 1 wt.% (Hunt, 1995). Most of the sulfur is bound to hydrocarbons and very little dissolved in oil as elemental S or H_2S (Hunt, 1995). Sulfur compounds are heavier than structurally equivalent hydrocarbons due to the higher molecular mass of sulphur (32) (Tissot & Welte, 1984). Sulfur compounds can be found in all fractions in low, medium, and high molecular weight fractions; It is thought that half of the total sulphur is in the asphaltene and resins fractions (Hunt 1995). It was found that the sulphur compounds in the light fraction of petroleum were mainly thiophenes and aliphatic sulphides (Poirer & Smiley 1984). Most studies have been on low molecular weight aliphatic and aromatic organic sulfur compounds (Orr & Sinninghe Damsté, 1990) and until recently, very few studies on organic sulfur compounds in asphaltenes and resins have been reported. Most knowledge has been acquired on low molecular weight organic sulfur compounds with 15 atoms and fractions with boiling point below 300°C (Orr & Sinninghe Damsté, 1990). However, most of the sulphur (60-80% of total sulphur) is present in fractions with boiling points greater than 300°C (Sinninghe Damsté *et al.*, 1990). High sulphur kerogen sourced oils always have high sulfur asphaltenes which have S/C ratio greater than 0.035. Sulfur found in petroleum includes thiols (alkyl, cyclic, aromatic), sulphides (alkyl, dialkyl, alkylcycloalkyl, alkylaryl, cyclic, thiaindanes, disulfides), thiophenes (alkyl, thieno)) and benzothiophenes (alkyl, naptho) and elemental sulfur as a minor constituent (Figure 6-26).

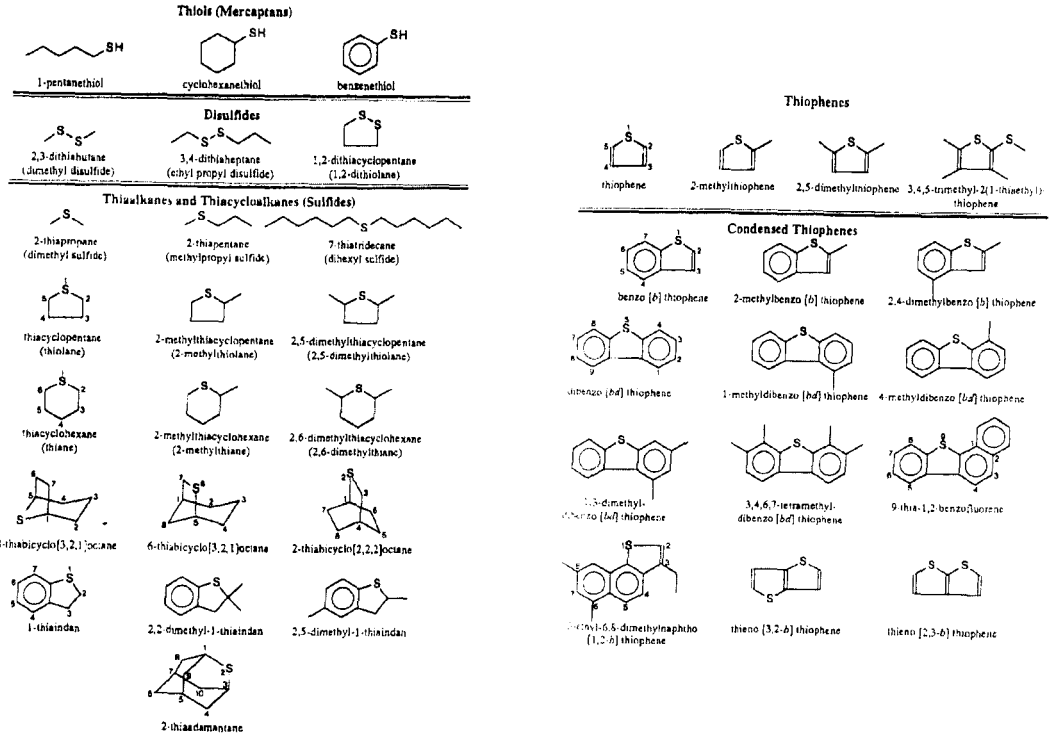

Figure 6-26: Molecular structures of number of thiols and thiophenes. After (Kohnen, 1991).

Sulphur isotopic ratios have been successful correlation tools for crude oils (Gaffney *et al.*, 1980; Orr, 1974; Thode, 1981). They can also be used to evaluate mechanisms of formation of hydrogen sulphide and its relationship to the associated sulphates (Gaffney *et al.*, 1980). $\delta^{34}S$ in crude oils varies from -7.5 to +25% relative to troilite of the Canyon Diablo iron meteorite (standard) (Gaffney *et al.*, 1980). The main control on the sulphur isotopic fractionation is the relative abundance of the sulphate available for the bacterial sulphate reduction during deposition; high degree of isotopic fractionation is expected if plenty of sulphate available such as evaporite depositional setting, while zero or little isotopic fractionation is expected in fresh water depositional setting where the sulphate is so limited (Killops & Killops, 2005). In limited sulphate settings, the sulphate is used up entirely and so the products will carry the same proportions of light and heavy isotopes. With increasing temperature, the sulphur isotopic fractionation increases and may reach up to 20 per mil depending on temperature (Orr, 1974) and some crude oils were found to have as low $\delta^{34}S$ as -10‰ (Killops & Killops, 2005); while migration, biodegradation and water washing have been suggested to be cause no or little isotopic fractionation (Killops & Killops,

2005; Orr, 1974). Therefore, source facies and thermal maturity are the main controls on the variations in this ratio (Gaffney *et al.*, 1980; Orr, 1974). Genetically related crude oils should have $\delta^{34}S$ values within 2‰ (Killops & Killops, 2005; Orr, 1986).

The oils in this study have high sulphur contents and therefore it was important to develop better understanding of sulphur distribution and its relationship with other geochemical features. This study is neither extensive nor in-depth due to the time allowed and the limited data available. Our aim here is attempting to define the controls on sulphur distribution in Greater Birba area oils and understand the origin of it in the oils.

6.4.2 Distribution of sulphur in the study crude oils

The sulphur content (weight %) and sulphur isotopic ratios ($\delta^{34}S$‰) have been determined for the studied oils and listed in Table 6-8 as well as other properties and parameters. Sulphur content was determined by Shell in Houston (USA). The Sulphur content is high in most of the oil samples (>1.9 wt %) except for O15 (A1C, well Kaukab1) and some of the samples exceeds 3wt% sulphur content; even the gas condensates have high sulphur content (>1.65 wt %). Two of these condensates (O9 from well BBS1and O20 from well Budour1h2) show very high sulphur content (>3%), even higher than all oils. Condensate O3 from BBN1 show lower sulphur content (1.65 wt%); this may suggest that this condensate is relatively of higher maturity or from slightly different facies than the other condensates. This condensate (O3) shows significantly heavier sulphur isotopes than the other oils and condensates confirming this suggestion. However, this is not very obvious in other geochemical data incorporated in this study; this condensate show consistently similar geochemical features as the other two gas condensates such as biomarkers and aromatic hydrocarbons ratios. Therefore, it is unknown why this condensate is different to the other condensates.

Table 6-8: The sulphur content and sulphur isotopes of the studied oils as well as number of other properties and parameters. The condensates are marked with GC in brackets. The key to abbreviations is below the table.

Sample ID	well	Sampling year	TVD (m)	Stratigraphy	Sulfur wt%	NSO%	Asp%	(Preg+Tric)/ Hopanes	VRE (MPI-1)	C_{29}% (St) (αββ/ααα+αββ)	$\delta^{34}S$
O1	BB2	1982	2583.4	A4C	2.97	17.8	0.24	0.81	0.92	57.99	
O2	BB1	1988	2536.5	A4C	3.03	14.5	0.17	0.77	0.93	58.37	
O3 (GC)	BBN1	1980	3455.1	A4C	1.65	6.1	0.01	1.48	0.86	58.25	15.85
O4	BB1	1983	2533.1	A4C	3.03	13.8	0.10	0.74	0.93	58.53	12.81
O5	BBN1		3558.1	A3C	2.5	13.7	0.70	0.10	0.71	45.38	
O6	BB1	1999	2588.3	A4C		12.8	0.14	0.73	0.94	58.20	
O7	BBN2	1983	3597.8	A4C	2.05	11.5	0.43	0.72	0.86	57.71	14.15
O8	BB1	1988	2533.1	A4C	3	15.1	0.09	0.74	0.93	58.36	
O9 (GC)	BBS1	1987	2329.7	A4C	3.24	5.7	0.00	1.09	0.91	59.09	12.96
O10	Kaukab1	1989	2513.6	A3C	2.39	10.8	0.37	0.50	0.91	58.23	
O11	Kaukab1	1987	2513.6	A3C	2.4	10.4	0.50	0.58	0.92	58.43	13.57
O12	Omraan1	1982	2601.7	A5C	2.11	13.5	0.50	0.56	0.92	58.09	13.13
O13	Nasser1	1982	1998.6	A4C	3.16	23.6	1.69	0.58	0.81	58.02	11.72
O14	Durra1	1982	2693.0	A3C	1.97	9.9	0.07	0.53	0.93	57.92	13.96
O15	Kaukab1	1989	2896.9	A1C	0.78	11.2	0.63	0.47	0.72	55.88	17.00
O16	Shamah1	1992	2385.7	A3C	2.46	8.4	1.10	0.51	0.94	57.29	13.07
O17	Durra1	1982	2695.1	A3C	2.02	13.7	0.15	0.49	0.93	59.07	
O18	Omraan1H3	1997	2939.1	A5C	2.1	9.7	0.30	0.58	0.93	57.39	
O19	Omraan1H3	1997	2939.1	A4C	1.9	9.7	0.41	0.52	0.91	58.20	
O20 (GC)	Budour1H2	2003	2971.6	A4C	4.7	12.1	0.47	1.97	0.92	59.27	12.84
O21	Omraan1H3	1997	3111.5	A3C	1.9	4.1	0.00	0.52	0.91	58.87	
O22	Omraan1H3	2001	2939.1	A4C	2.1	10.1	0.68	0.58	0.91	57.95	13.00

Key to abbreviations: TVD = true vertical depth, NSO% = (resins fraction*100/(saturated hydrocarbons + aromatic hydrocarbons + resins (NSO) + asphaltenes) from Iatroscan, Asp% = Asphaltene fraction*100 /(saturated hydrocarbons + aromatic hydrocarbons + resins (NSO) + asphaltene), (Preg +Tric)/hopanes = [(C_{21}+C_{22} Pregnanes + ΣC_{19}-C_{29} Tricyclic terpanes)/ ΣC_{27}-C_{35} hopanes], VRE (MPI-1) = vitrinite reflectance equivalence based on MPI-1 (defined in Appendix 4-1), St = steranes (S+R).

Since we have samples from different stratigraphic reservoir intervals it was not easy to plot the spatial distribution of this property for the whole area. Therefore the sulphur content was plotted spatially for A4C and A3C reservoirs separately (Figure 6-27). It is very clear that sulphur increases from west and northwest to east south east in both stringers. Figure 6-27 shows that the A4C oils are relatively high in sulphur than A3C oils. The current theory is that the main control behind the large variations observed in fluid properties is mixing of the original oils with one or multiple charges of condensates (chapter 4 and 5). The higher sulphur content in condensates may rule out the effect of phase fractionation related to compositional grading as the main control behind the variations in fluid properties. Phase fractionation should result in relatively lower sulphur content in condensates and higher in oils. The possible controls behind the distribution of sulphur will be discussed in the next section.

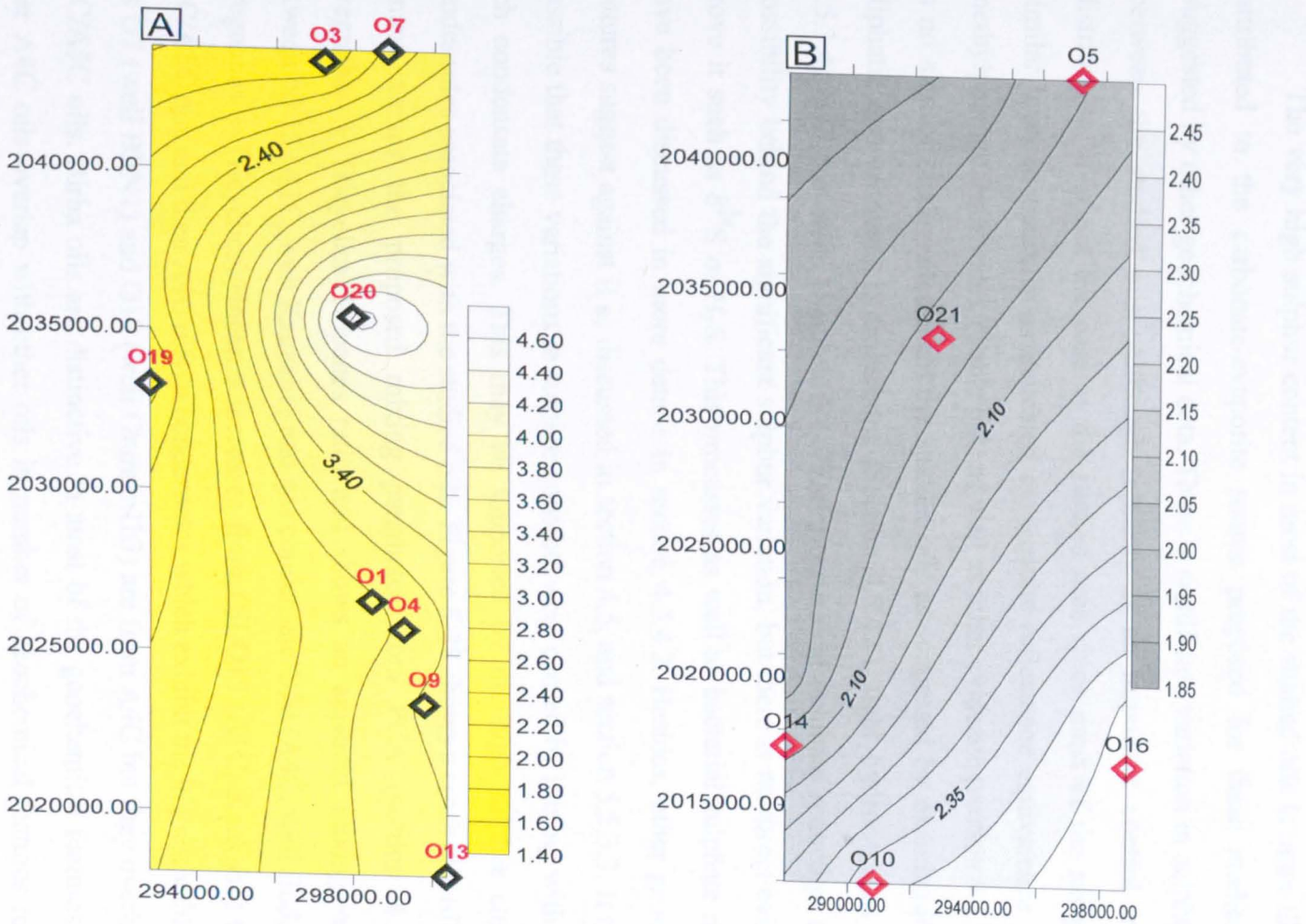

Figure 6-27: The distribution of sulfur content in A4C oils (A) and A3C oils (B). Notice that the sulfur is high in both stringers but generally relatively higher in A4C and there is general increase trend from west to east.

6.4.3 Controls on sulphur

The very high sulphur content in most of the studied oils is more likely to be attributed to the carbonate-evaporite source proposed for these studied oils as suggested by other geochemical data. There is significant variation in sulphur content between the studied oils. Although maturity is an important control in sulphur distribution, it is not the case in the studied area since most of the samples have similar level of maturity as indicated by vitrinite reflectance equivalence based on methylphenanthrene index (Table 6-8) as well as other evidence (section 4.3.2). There is no sign of biodegradation in the studied oils as suggested by examination of the aliphatic and aromatic hydrocarbons (Section 4.3.4.1), light hydrocarbons (Section 5.5.3.4), and the acids (Section 6.4). Thermochemical sulphate reduction can be a possibility behind the significant sulphur variation, but there is no direct evidence to prove it such as $\delta^{34}S$ of H_2S. This processes as well as bacterial sulphate reduction have been discussed in more details in section 4.3.4.2. Besides, other geochemical features suggest against it as discussed in section 4.5, and section 5.5.3.3. It might be possible that these variations in sulphur contents were caused by mixing with sulphur rich condensate charges. This may be supported by the high sulphur content in condensates associated with the studied oils. Figure 6-28 shows a cross plot of sulphur content versus the proposed mixing parameter from PCA (section 4.3.2), Σ (Pregnanes + Tricyclics)/Hopanes ratio and shows an apparent mixing sequence between oil 15 (A1C, well Kaukab1) and gas condensate O20 (A4C, well Budour1h2). (Pregnanes + Tricyclics)/Hopanes increases from Oil O15 (A1C, Kaukab1) through A3C/A5C oils and then A4C oils to condensates which exhibit the highest values. The oils O7 (well BBN1) and O19 (well Omraan1h3) are from A4C but they overlap with A3C/A5C oils. Birba oils are distinctive in most of the geochemical features, while other A4C oils overlap with other oils in number of geochemical features (e.g. O7 (well BBN1) & O19 (well Omraan1h3)).

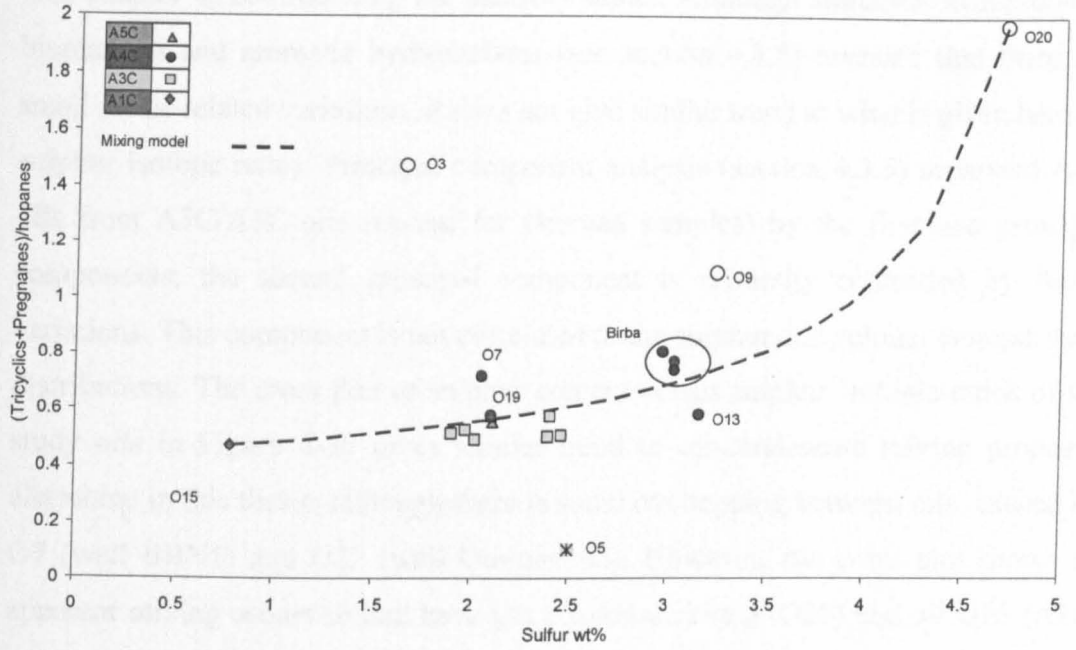

Figure 6-28: Cross plot of sulfur content versus the ratio between sum of tricyclics (C_{19}-C_{29}) and pregnanes (C_{21}-C_{22}) to sum of hopanes (C_{29}-C_{35}). The broken line is a mixing model using O20 and O15 as end members.

In order to confirm the control on sulphur distribution in the studied oils, sulphur isotopes $\delta^{34}S$ of selected oils were determined. Figure 6-29 shows the spatial distribution of $\delta^{34}S$ of whole oils in the study area. Generally, there is an increase in sulphur isotopic ratio from eastern part of area (O4 from A4C of well BB1, O13 from A4C of well Nassir1, O16 from A3C of Shamah and condensates) towards the north and south west. Figure 6-28 shows a cross plot of sulphur content versus sulphur isotopic ratios of the study oils and condensates. There is no clear discrimination between the different groups obtained using other (see chapter 4 and chapter 5). Two gas condensates show similar isotopic ratios [O9 (well BBS1), O20 (well Budour1H2)] to some crude oils such as O4 (well BB1), O22 (well Omraan1h3) and O16 (well Shamah1). Oil O15 (A1C, Kaukab1) has the heaviest sulphur isotopic ratio. This confirms that this oil is derived from different source facies. It is not obvious why O3 (well BBN1) shows a very heavy sulphur isotopic ratio; it may be due to measurement error. O7 (well BBN2) is from geographically similar location to condensate O3 (well BBN1), but O7 shows similar sulphur isotopic ratio as O14 (A3C, well Durra1) which is from far southwest with respect to O7 (well BBN2) and different stratigraphic unit. Maturity effect is ruled out because there was evidence from light hydrocarbons (see chapter 5 and biomarkers

(see chapter 4) contradicting the maturity effect. Although statistical evaluation of biomarkers and aromatic hydrocarbons (see section 4.3.5) revealed that there are small facies related variations, it does not give similar trend to what is given here by sulphur isotope ratios. Principal component analysis (section 4.3.5) separated A4C oils from A3C/A5C oils (except for Omraan samples) by the first two principal components; the second principal component is primarily controlled by facies variations. This component is not correlated to the sulphur and sulphur isotopic ratio distributions. The cross plot of sulphur content versus sulphur isotopic ratios of the study oils in Figure 6-30 gives similar trend to oil-condensate mixing proposed elsewhere in this thesis; although there is some overlapping between oils, caused by O7 (well BBN1) and O22 (well Omraan1h3). However, the cross plot shows an apparent mixing sequence that have gas condensates (e.g. O20) and oil O15 (A1C, well Kaukab1) as the two end members of this sequence. I attempted to calculate a mixing model using these two end members; the mixing curve is shown in the same cross plot of sulphur content versus sulphur isotopic ratios (Figure 6-30) for a direct comparison. The mixing curve shows a nice match with the measured data; it crosses some of the oils and the rest are within 1 per mil. This is supported by the mixing curve calculated between sulphur content and the mixing parameter in Figure 6-28. This mixing sequence was already suggested by one of the important facies indicator, dibenzothiophene/phenanthrene (DBT/P) ratio as shown in Figure 6-32. If we exclude O13 (A4C, well Nassir1), there is apparent mixing trend from condensates through A4C, A3C/A5C oils to O15 (A1C, Kaukab1) oil as clear fromFigure 6-30. this mixing sequence is slightly different ot the mixing sequence suggested by the light hydrocarbons and biomarkers. There is no clear distinction between A4C and A3C/A5C oils in Figure 6-30, as suggested the light hydrocarbon distribution and biomarkers. Oil O15 has been characterised based on several evidences that this oil is sourced from different facies. The presence of this oil in this mixing sequence might suggest that the small facies variation between the oils suggested by several eivences (e.g. Figure 4-39) and mixing with the condensate charge might have both impacted the distribution of sulphur and sulphur isotopes in the crude oils of the Greater Birba area.

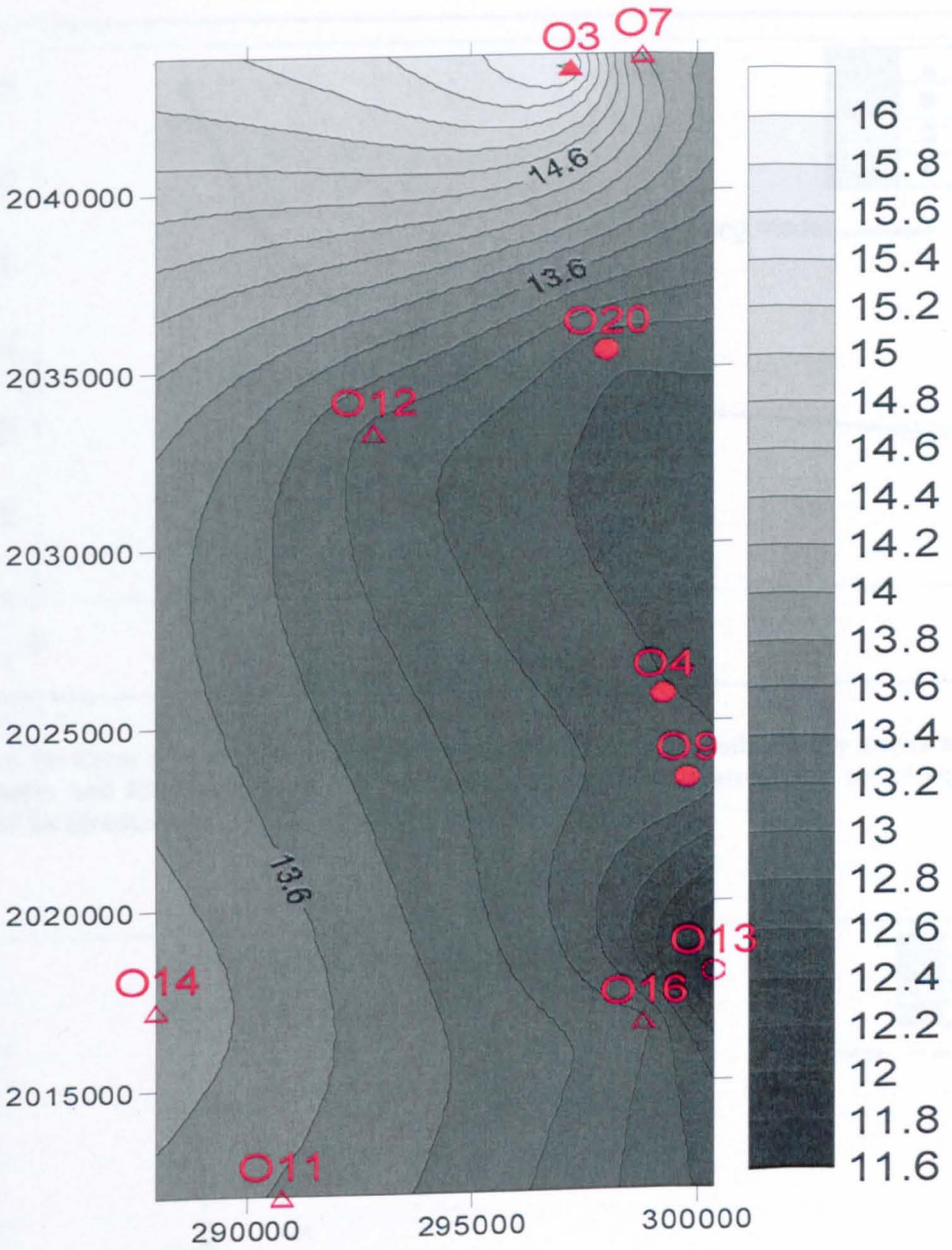

Figure 6-29: The spatial distribution of sulphur isotope ratios $^{34}S/^{32}S$ in the Greater Birba area. The plot excludes O15 (A1C, well Kaukab1) which has the highest sulphur isotopic ratio.

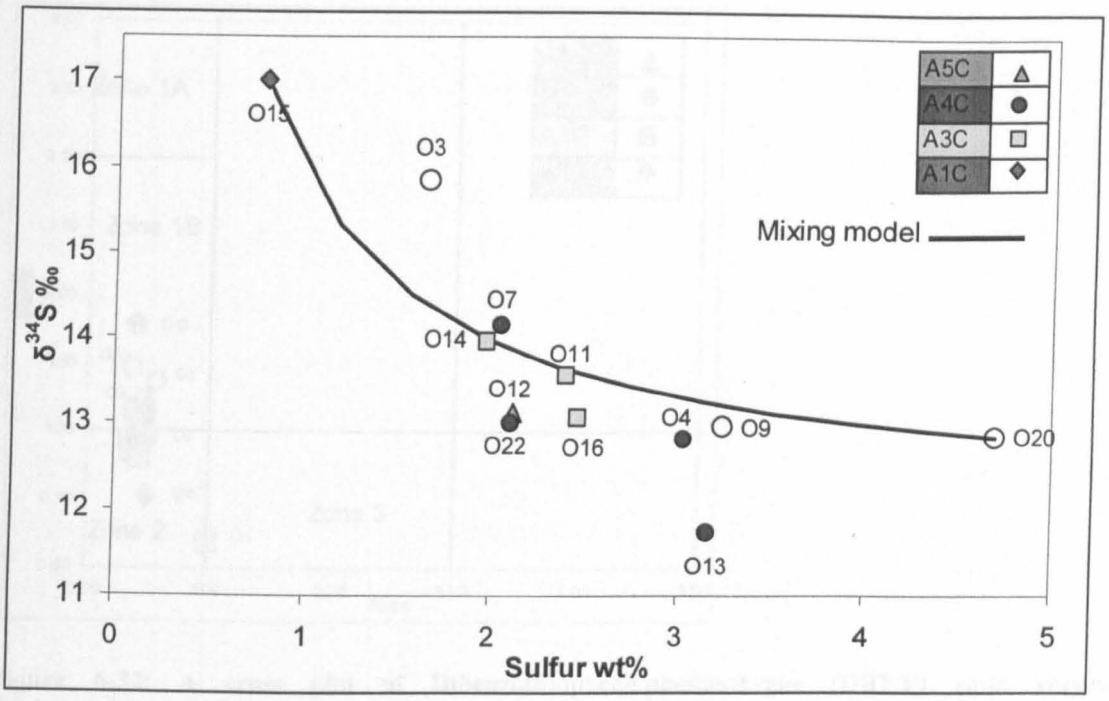

Figure 6-30: Cross plot of sulphur content versus $\delta^{34}S$ of the study oils. Empty circles are gas condensates and filled shapes are oils. the mixing model is calculated using set of equation proposed by (Jenden *et al.*, 1993), and illustrated in section 4.4.

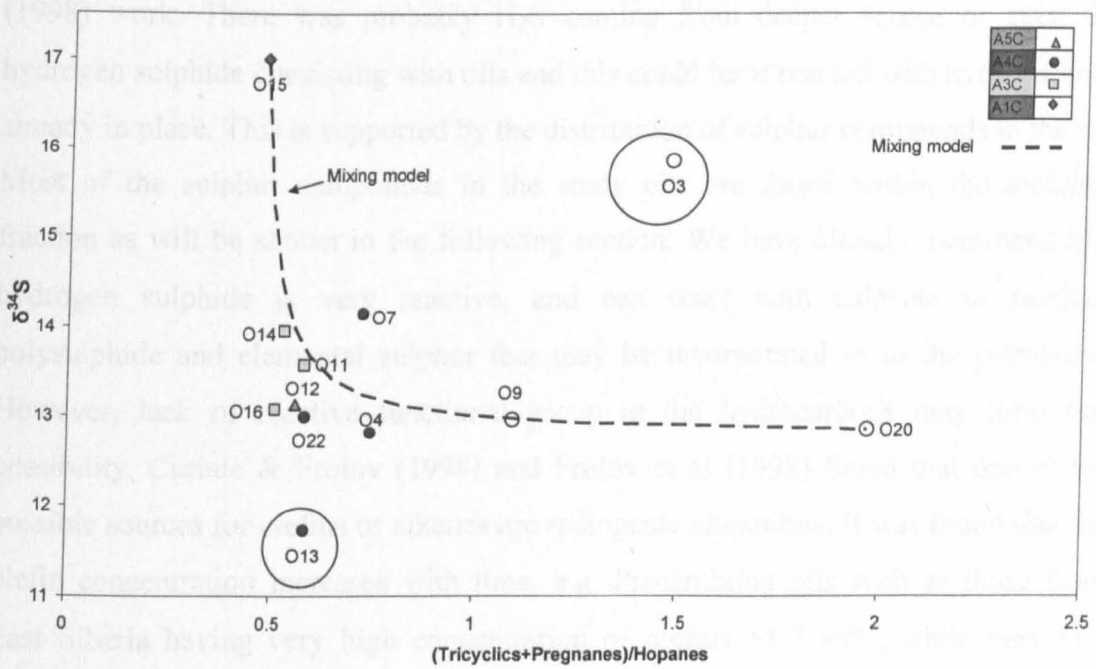

Figure 6-31 cross plot of sulphur isotopic ratios versus mixing parameter (Tricyclics+Pregnanes)/ hopanes. The mixing model shows similar trend to Figure 6-30.

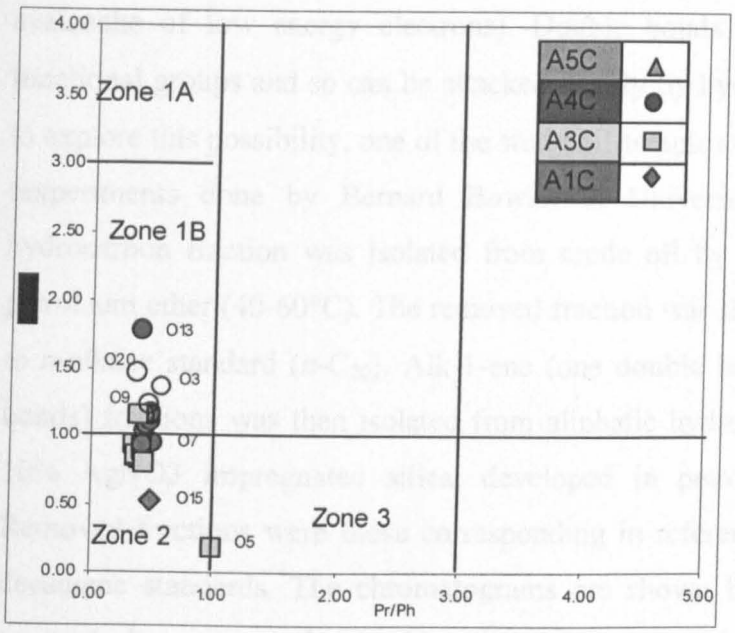

Figure 6-32: A cross plot of Dibenzothiophene/phenanthrene (DBT/P) ratio versus Pristane/Phytane (Pr/Ph) ratio. This is shown already in Figure 4-18.

The other possibility is based on Frolov *et al* (1998) and Curiale & Frolov (1998) work. There was probably H_2S coming from deeper source or even the hydrogen sulphide coexisting with oils and this could have reacted with hydrocarbons already in place. This is supported by the distribution of sulphur compounds in the oil. Most of the sulphur compounds in the study oils are found within the aromatic fraction as will be shown in the following section. We have already mentioned that hydrogen sulphide is very reactive, and can react with sulphate to produce polysulphide and elemental sulphur that may be incorporated in to the petroleum. However, lack of reactive functional group in the hydrocarbons may limit this possibility. Curiale & Frolov (1998) and Frolov et al (1998) found that one of the possible sources for olefins or alkenes are radiogenic alterations. It was found that the olefin concentration increases with time, e.g. Precambrian oils such as those from East Siberia having very high concentration of olefins >1.2 wt%, while very low content of olefins were found in Mesozoic samples (<0.3 wt%) (Curiale & Frolov, 1998). Radiogenic alteration occurs when a high energy α or β or γ particle (10^3-10^7 eV) attacks the alkanes and knock out the low energy electrons (20-80 eV) leading to "non-selctive monomolecular elimination of H_2 from the excited alkane molecules" (Curiale & Frolov, 1998), (excited alkanes means unstable alkanes due to the loss of

avalanche of low energy electrons). Double bonds in alkenes are very reactive functional groups and so can be attacked readily by hydrogen sulphide. In an attempt to explore this possibility, one of the study oil samples (O8) were analysed for olefins (experiments done by Bernard Bowler at Univeristy of Newcastle). Aliphatic hydrocarbon fraction was isolated from crude oil by TLC on silica, developed in petroleum ether (40-60°C). The removed fraction was that corresponding in reference to *n*-alkane standard (*n*-C_{20}). Alk-1-ene (one double bond) and alk-2-ene (2 double bonds) fractions was then isolated from aliphatic hydrocarbons fraction By TLC on 10% AgNO3 impregnated silica, developed in petroleum ether (40-60°C). The Removed fractions were those corresponding in reference to 1-octadecene and 1,9-decadiene standards. The chromatograms are shown below in Figure 6-33. There seems to be some olefins in this oil but not present in large quantity. There is no quantitation for these peaks, however, the concentration of oils was used to analyse these olefins was about 10 mg/ml, which gives an indication that the oils contains very low quantity of alkenes, and hard to be identified. This does not rule out the possibility that most of the alkenes formed this way, were readily attacked by hydrogen sulphide to form secondary sulphur compounds. Therefore, both processes (radiogenic addition of sulphur and oil-condensate mixing) are possible and they probably both contribute to the distribution of sulphur in the crude oils of the Greater Birba area.

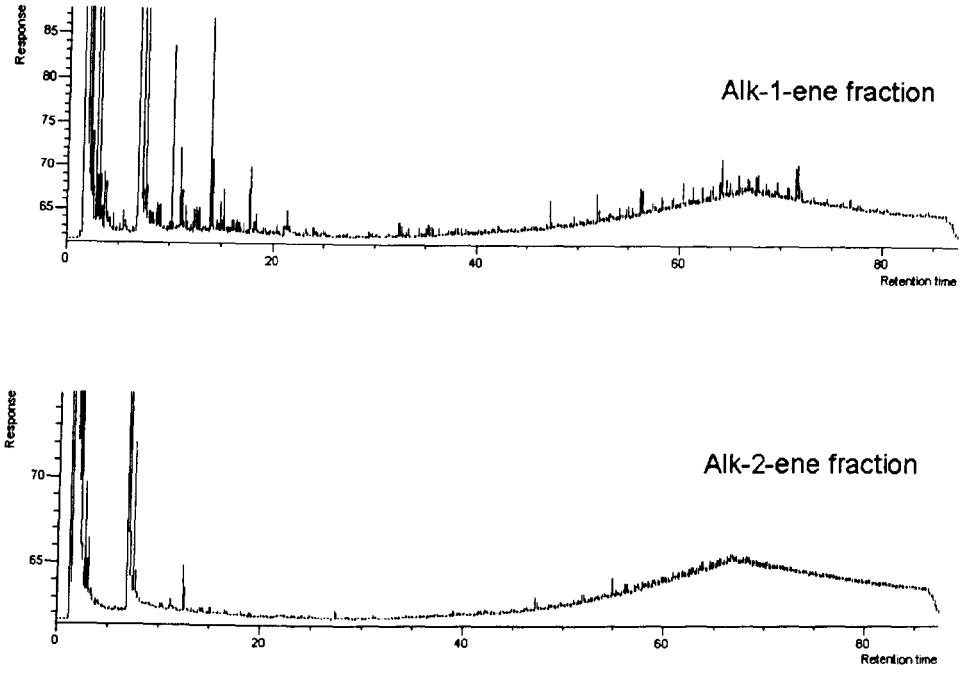

Figure 6-33: GC chromatograms for alkene fractions with one double bonds (top) and two double bonds (bottom).

6.4.4 Where is the petroleum sulphur?

Since mixing of oils with condensate charge has been suggested as a possible factor controlling the distribution of sulphur, we would expect that most of the sulphur is in the low molecular weight fraction (C_{15-}) of oils and condensates. When sulphur content is plotted against C_{15+} bulk compositions, there is an apparent positive relationship between sulphur content and the aromatic hydrocarbon (aromatic HC) and NSO fractions, whereas poor relationship is established with asphaltene fraction (Figure 6-34). Although this may suggest that the most of the sulphur is in the form of aromatic hydrocarbons and resins, the relationship is complicated as can be seen from the plots by the high sulphur condensates and O13, suggesting that other sulphur compounds exist in other fractions especially in the low molecular weight fraction. The high sulphur condensates show similar aromatic HC content with other oils, and this may suggest that significant amount of sulphur compounds exists in the light fraction of these condensates and highly likely in the other oil samples. Oil O13 (A4C, well Nassir1) shows the highest content of both NSO and asphaltene but not aromatic content, suggesting that most of the sulphur compounds in this sample are within the heavy fraction of the oil. Oil O15 (A1C, well Kaukab1) shows aromatic

hydrocarbon content as low as the other A3C/A5C oils but contains significantly lower sulphur content. Oil O5 (denoted with Asterisk) is always excluded from argument since this is interpreted to be derived from different source facies or contaminated with younger oils.

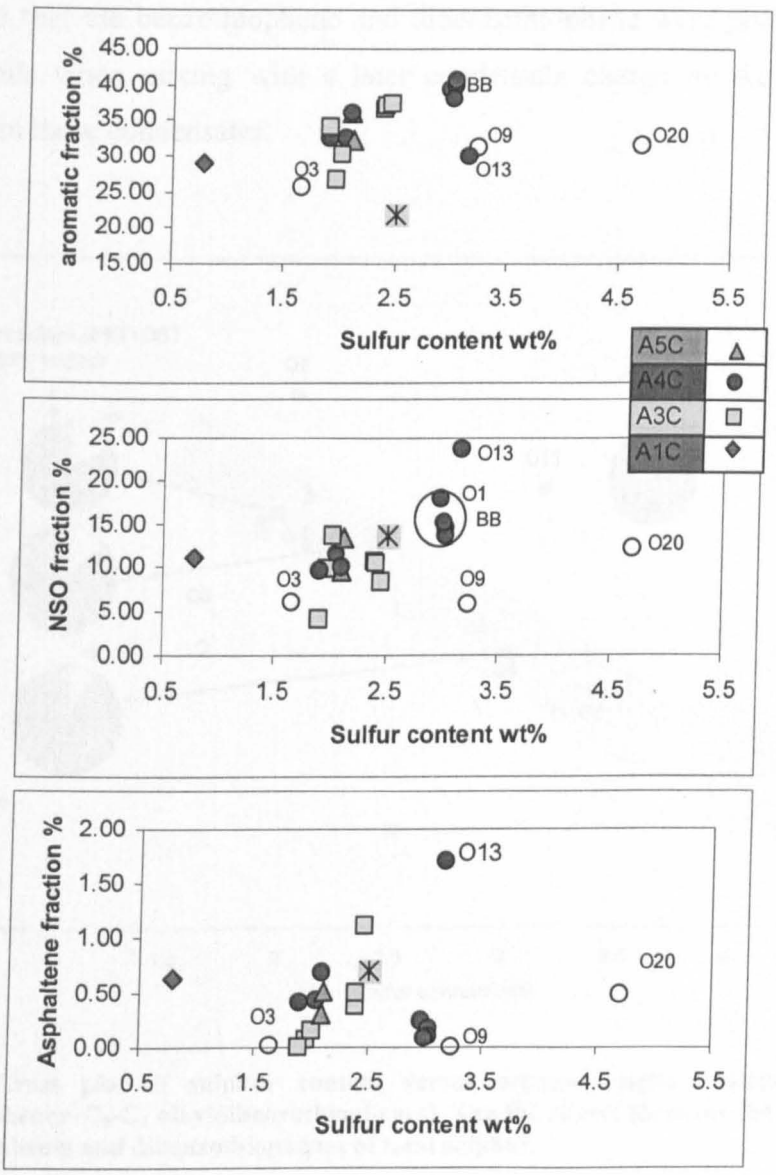

Figure 6-34: cross plots of sulfur content versus bulk compositions (C_{15+}). O5 from A3C of well BBN1 is denoted with Asterisk.

C_0-C_3 alkyl benzothiophenes and C_0-C_2 dibenzothiophenes were identified and the total sum was plotted against sulphur content. Interestingly, most of the oils show generally inversely correlated trend between sulphur content and organic sulphur compounds except for oil O13 (A4C, well Nassir1), O5 (A3C, well BBN1) and O15 (A1C, well Kaukab1), suggesting that they are not the major contributing compounds

to total sulphur content. O13 is an exception to this trend and shows high sulphur content and high benzothiophenes and dibenzothiophenes, although Figure 6-34 shows that most of the sulphur in oil O13 (A4C, Nassir1) is in the NSO and asphaltene fraction, not in aromatic fraction. Therefore, further analysis need to be done to understand the distribution of sulphur compounds in the studied oils. We may suggest here that the benzothiophene and dibenzothiophene were probably partially diluted in oils when mixing with a later condensate charge by the light sulphur compounds in these condensates.

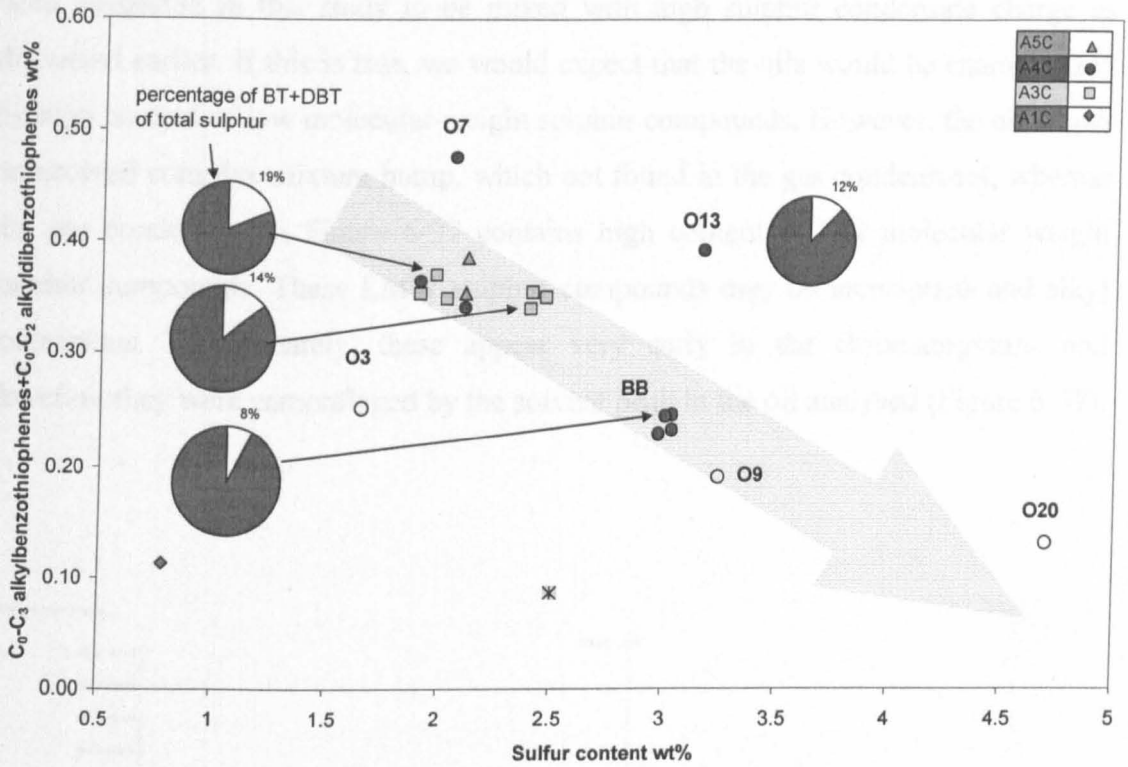

Figure 6-35: Cross plot of sulphur content versus organic sulphur compounds (C_0-C_3 alkylbenzothiophenes+C_0-C_2 alkyldibenzothiophenes). The Pie charts illustrate the percentage of these benzothiophenes and dibenzothiophenes of total sulphur.

Detailed GCMS investigation of aromatic hydrocarbons and aliphatic hydrocarbons fractions did not show other major organic sulphur compounds except traces of alkyl thiols and these are mostly camouflaged or obscured by other compounds in the background. Therefore, six samples of the studied oils were sent to Calgary (Canada) to be analysed by Flame Photometric detector-gas chromatography to find out the sulphur distribution in those high sulphur oils. Four of these oils were fractionated into eight fractions by silica-alumina column chromatography and

different solvents with increasing polarity. About a half gram of each oil was loaded into a silica-alumina packed column filled with petroleum ether. The eight fractions were eluted sequentially in the order of increasing polarity; the type and amount of solvent used to elute each fraction is listed in Table 6-9. The oil samples and fractions were then sent to be analysed by FPD-GC to find out the fractions that contain most of the sulphur compounds.

Figure 6-36 and Figure 6-37 show FPD chromatograms of a high sulphur oil and high sulphur condensate respectively. The high sulphur oil in Figure 6-36 has been suggested in this study to be mixed with high sulphur condensate charge as discussed earlier. If this is true, we would expect that the oils would be characterized by high content of low molecular weight sulphur compounds. However, the oil shows unresolved complex mixture hump, which not found in the gas condensates, whereas the gas condensate in Figure 6-37 contains high content of low molecular weight sulphur compounds. These LMW sulphur compounds may be mercaptans and alkyl mercaptans. Unfortunately, these appear very early in the chromatograms, and therefore they were camouflaged by the solvent peak in the oil analysed (Figure 6-37).

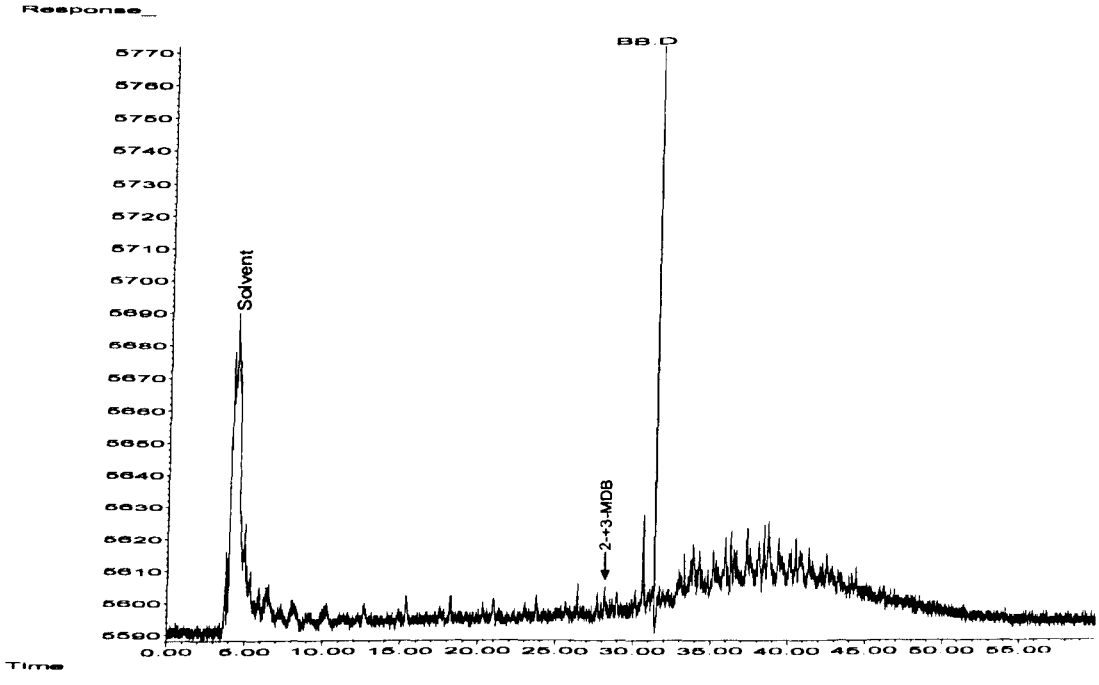

Figure 6-36: FPD chromatogram of an oil exhibiting high sulphur content (S wt%). The chromatogram shows a complex unresolved mixture hump.

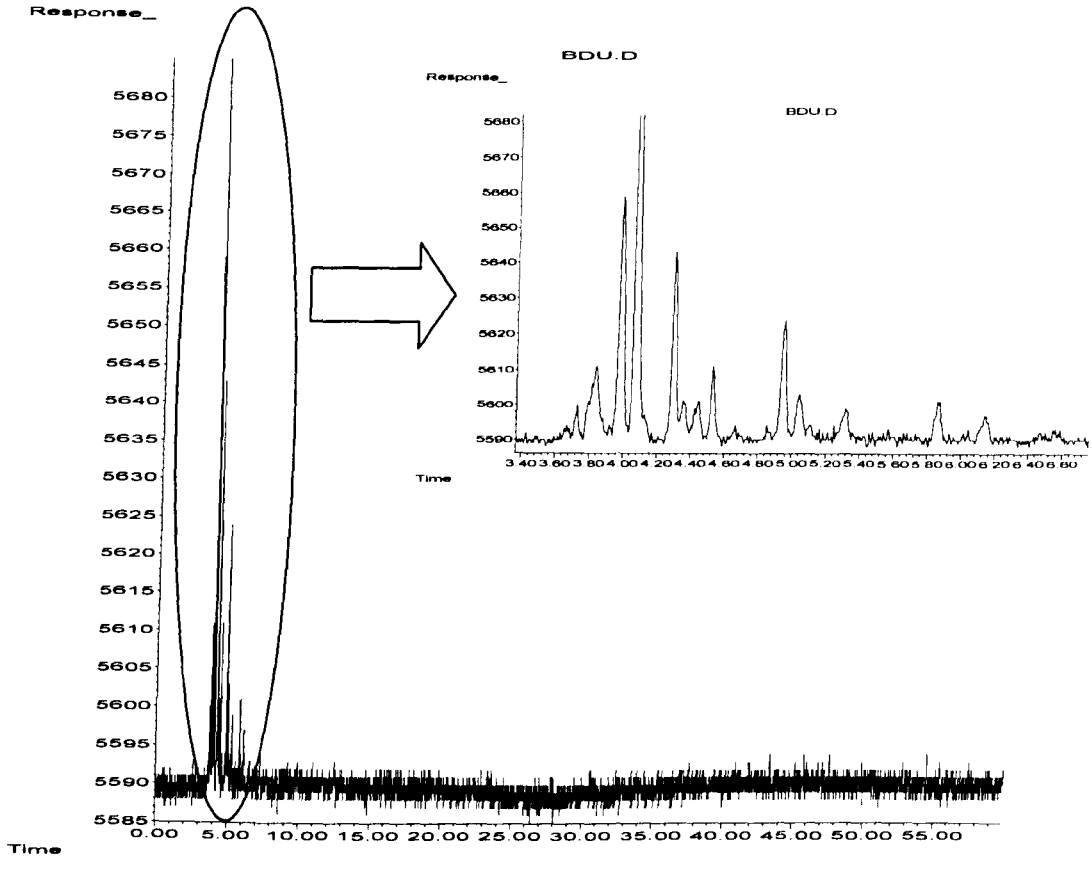

Figure 6-37: FPD chromatogram of a condensate (O20 from well Budour1h2) exhibiting high sulphur content (4.6 wt %). The chromatogram does not shows the complex unresolved mixture hump in the oils shown in Figure 6-36. It shows rather high content of low molecular weight sulphur compounds.

Although it is proposed that the condensate mixed with oils might have increased the sulphur content and subsequently shifted the sulphur isotopic signature to lighter values as shown in Figure 6-30 and Figure 6-31, it is probably appropriate to think according to Figure 6-34, that the aromatic HC fraction contributes significantly to the sulphur content as there is good correlation between sulphur content and C_{15+} aromatic HC fraction. Therefore, it is important to understand the distribution of sulphur compounds in these oils. Figure 6-38 shows FPD traces of BB1 oil and its eight fractions. Interestingly, FPD chromatograms show very low content of sulphur compounds and small unresolved hump. This hump appears in fraction B, C and D. These are aromatic HC fractions suggesting that most of sulphur compounds are within aromatic HC fraction, which supports the positive correlation between sulphur content and aromatic hydrocarbon fraction in Figure 6-34. therefore, although very low sulphur content has been detected by FPD in the studied oils, the positive correlation between sulphur content and aromatic fraction content (Figure 6-34) and the negative correlation with the aromatic sulphur compounds quantified indicate that

there are other aromatic compounds occurring most likely in the hump (recognised in fraction B, C, D, and E) but these were difficult be identified or quantified. The presence of hump indicates that there are enormous amount of aromatic sulphur compounds that can not be resolved easily by GC-MS. These might have formed by reactions of the free highly reactive hydrogen sulphide with the unsaturated aromatic compounds. The sulphur additive mechanism might have been radiogenic formation of alkenes, which were easily attacked by the available hydrogen sulphide. This may be supported by negative trend but poorly correlated between sulphur content versus hydrogen sulphide content dissolved in these oils as shown in Figure 6-39. This is further supported by the fact that the A4C oils and condensates are generally high in sulphur content, and this carbonate stringer was characterized by high content of radioactive Uranium as shown by (Mattes & Conway Morris, 1990), and this stringer was initially called U Formation due to this reason. Therefore, we think that addition of sulphur possibly occurred by mixing with high sulphur gas condensate and probably to less extent the sulphur was added by chemical reactions of hydrogen sulphide with alkenes formed radiogenically in the oils.

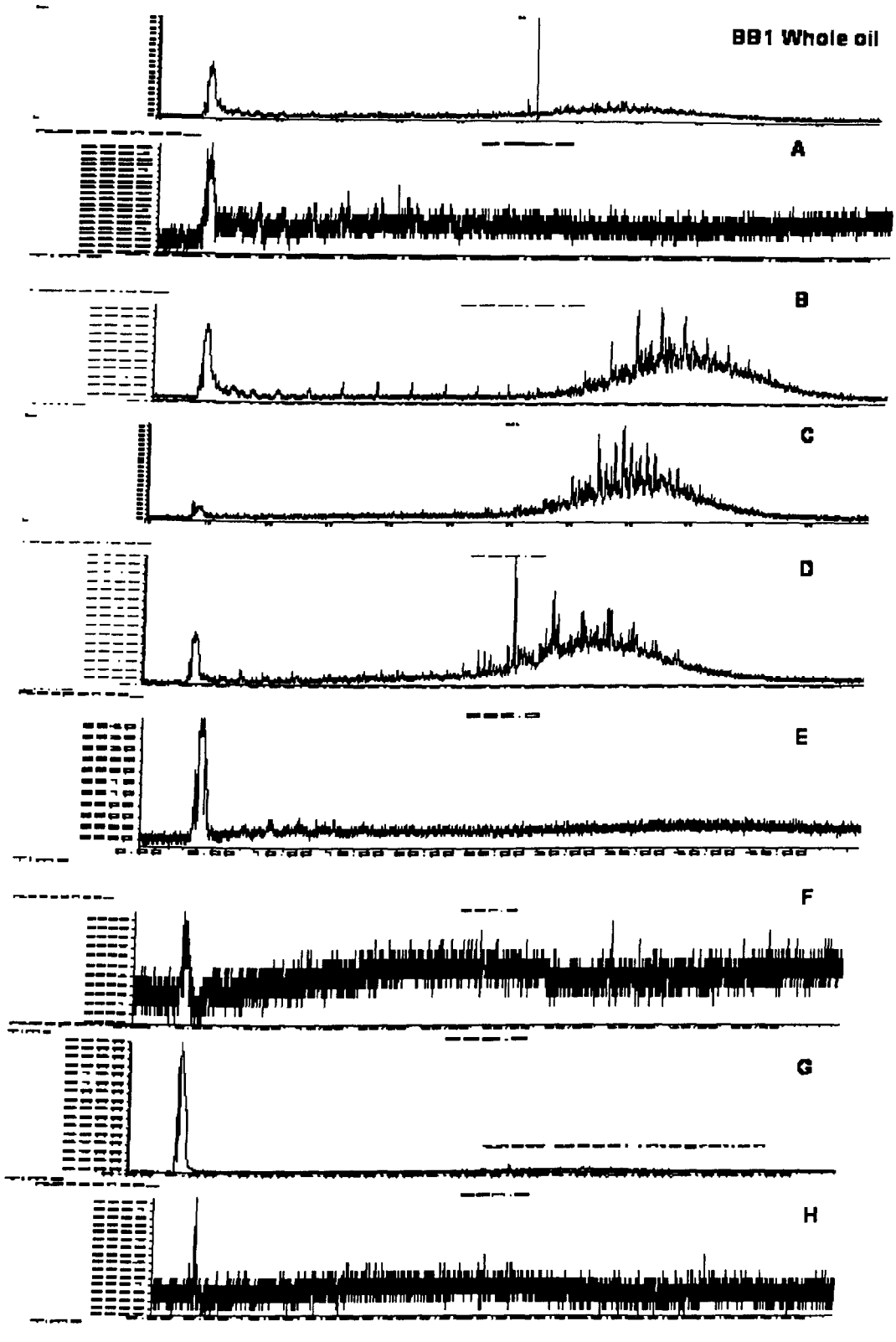

Figure 6-38: FPD-GC traces of an oil from Birba 1 and its eight fractions. The different fractions (A-H) are explained in the text and listed in Table 6-9.

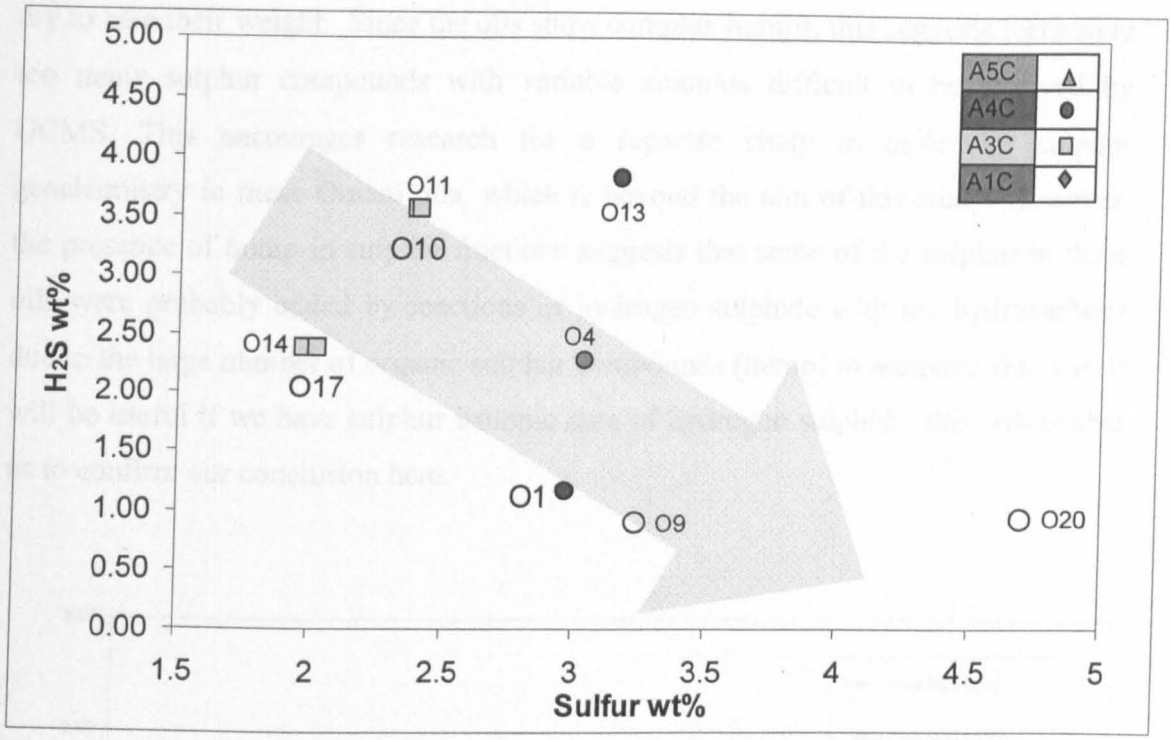

Figure 6-39: cross plot of sulphur content wt% versus hydrogen sulphide content wt% in some of the studied oils (hydrogen sulphide content were obtained from PVT oil samples from correspondent wells and reservoirs. Filled shapes are oils and empty shapes are condensates.

It was difficult to quantify the aromatic compounds from the FPD chromatograms because no standard had been added to the samples. I tried to quantify the humps in the FPDs of the whole oil samples using the known quantity of 2,3-MDBT (measured from GCMS as an internal standard) (Figure 6-36) and list them in Table 6-9. The results do not make sense as the values are too high and there is no correlation with the measured sulphur content. Subsequently, all the fractions were analysed using CNS analyser to measure the amount of sulphur in these fractions. A known amount of chromatographic fraction (in DCM, those fractions obtained by the method described in section 6.4.4) was weighed on to ca. 1g alumina contained in an ashed (600C, 4 hrs) ceramic crucible and the DCM was allowed to evaporate overnight at room temperature. The total carbon, total nitrogen and total sulphur contents of the samples were then determined using an Elementar Vario-max CNS analyser which was calibrated using a sulfadiazine standard.. The results are listed in table Table 6-9. Although, one of the oils show anomalously high sulphur content (8.55wt% by CNS versus 3.03wt% by Shell), the relative distribution of sulphur in these fractions confirmed the FPD analysis as shown in Figure 6-40. The light molecular weight sulphur compounds must have gone as these fractions were blown

dry to take their weight. Since the oils show complex humps, this suggests there were too many sulphur compounds with variable amounts difficult to be resolved by GCMS. This encourages research for a separate study in molecular sulphur geochemistry in these Omani oils, which is beyond the aim of this study. However, the presence of hump in sulphur fractions suggests that some of the sulphur in these oils were probably added by reactions of hydrogen sulphide with the hydrocarbons due to the large number of organic sulphur compounds (hump) in aromatic fraction. It will be useful if we have sulphur isotopic data of hydrogen sulphide, this will enable us to confirm our conclusion here.

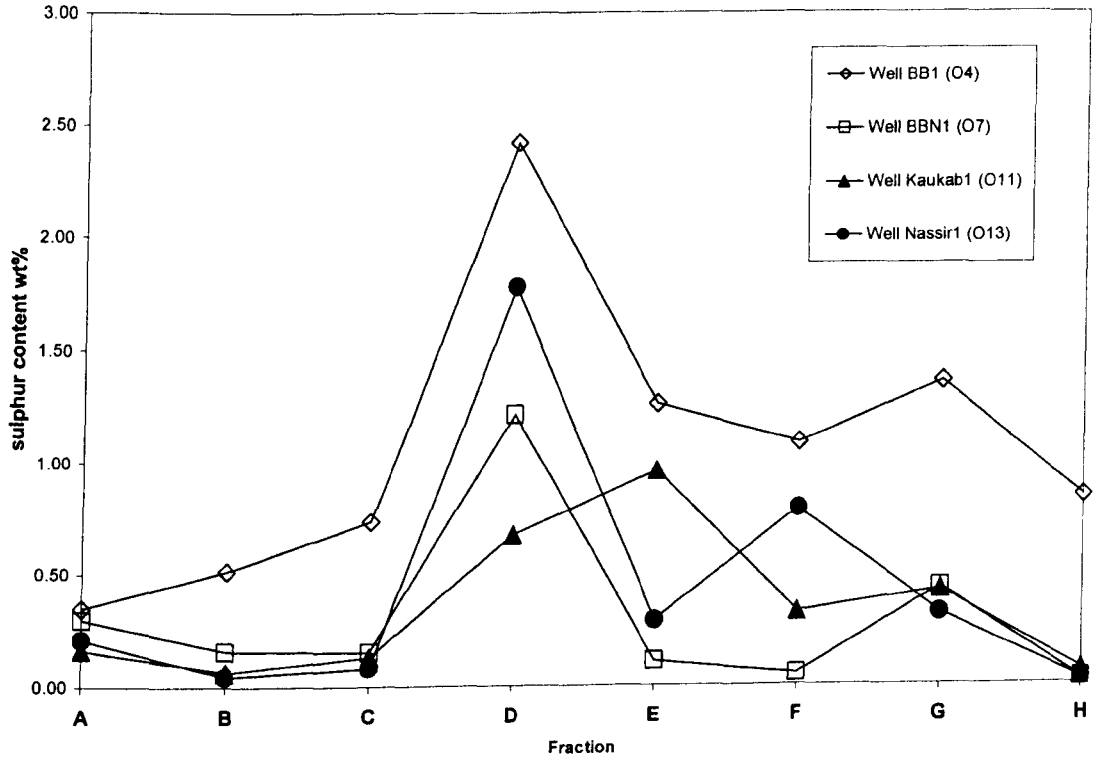

Figure 6-40: the amount as weight percentages of whole oil and distribution of sulphur in the eight fractions of the four oils fractionated by column chromatography.

Table 6-9: fractionation of the oil samples analysed by FPD. NQ means the sulphur content could be quantified due to the very low content of identifiable dibenzothiophenes. Letter O is for sulphur value measured by Shell and letter N sulphur value measured by Iso-analytical Ltd (UK).

	Fraction	Developing solvents	volume ml	weight (mg)	S wt%	Total sulfur (FPD)	sulfur content wt%
well BB1 (O4)		Initial total weight		492.8	8.55	11.4	3.03
	A	Petroleum ether	110	137.1	0.35		
	B	DCM:Pet ether (1:4)	20	16.5	0.51		
	C	DCM:Pet ether (1:4)	35	11.7	0.73		
	D	DCM:Pet ether (2:3)	50	124.3	2.42		
	E	DCM:Pet ether (2:3)	40	12.6	1.26		
	F	Toluene	50	8	1.08		
	G	DCM:M-OH (1:!)	50	33.8	1.35		
	H	Methanol (M-OH)	50	0.1	0.84		
		Recovery %		69.8			
well BBN1 O7		Initial total weight		500.7	2.45	3.10	1.84
	A	Petroleum ether	100	165.4	0.30		
	B	DCM:Pet ether (1:4)	20	17.6	0.16		
	C	DCM:Pet ether (1:4)	40	17.1	0.15		
	D	DCM:Pet ether (2:3)	50	78.3	1.22		
	E	DCM:Pet ether (2:3)	50	5.6	0.11		
	F	Toluene	50	3.2	0.05		
	G	DCM:M-OH (1:!)	45	36.9	0.43		
	H	Methanol (M-OH)	50	7.8	0.03		
		Recovery %		66.3			
well Kaukab1 O11		Initial total weight		507.1	2.80	8.8	2.40
	A	Petroleum ether		160.1	0.16		
	B	DCM:Pet ether (1:4)		9.2	0.06		
	C	DCM:Pet ether (1:4)		13.7	0.13		
	D	DCM:Pet ether (2:3)		46.5	0.67		
	E	DCM:Pet ether (2:3)		44	0.96		
	F	Toluene		11.5	0.32		
	G	DCM:M-OH (1:!)		32.4	0.42		
	H	Methanol (M-OH)		0.8	0.071		
		Recovery %		62.7			
well Nassir1 O13		Initial total weight		500.1	3.53	9.80	3.16
	A	Petroleum ether	100	124	0.21		
	B	DCM:Pet ether (1:4)	20	3.7	0.04		
	C	DCM:Pet ether (1:4)	38	11	0.08		
	D	DCM:Pet ether (2:3)	50	100.8	1.78		
	E	DCM:Pet ether (2:3)	50	13.9	0.29		
	F	Toluene	60	61.7	0.78		
	G	DCM:M-OH (1:!)	48	18.9	0.32		
	H	Methanol (M-OH)	50	0.2	0.03		
		Recovery %		66.8			
BBS1 O9						NQ	3.24
Budour1 O20						NQ	4.6

6.4.5 Summary

Most of the oils have higher sulphur content due to probably high sulphur source facies. However, the study oils show significant variations in sulphur content. Since there is no major facies variations observed in these oils and the assessment of the maturity on these oils reveal similar maturity for them, other controls must be suggested to control the sulphur content variability in the study oils. The significant variability of sulphur (0.7-4.6 wt %) seems to follow the proposed mixing theory throughout this thesis. This is supported by the inverse relationship between sulphur content and sulphur isotopic ratio $\delta^{34}S$, which follows a mixing line between oil O15 and gas condensate. This mixing sequence is different to the mixing sequence suggested by other data. No clear separation between A4C oils and A3C/A5C oils as suggested by light hydrocarbons and biomarker data. it is suggested that a combination of the minor facies variations observed in these oils and mixing with high sulphur condensate might have resulted in slightly different mixing sequence. This is supported by involvement of oil 15 (A1C, well Kaukab1) in this mixing sequence. It is also suggested that the variability of sulphur content migh be related to radiogenic addition of organic sulphur compounds by reactions of hydrocarbons with hydrogen sulphide coexisting with oils.

Chapter 7 PVT modelling of petroleum fluids in the Greater Birba area

7.1 Introduction

7.1.1 Aims and Objectives

Significant variations of bulk properties were observed in petroleum fluids of the Greater Birba area. it has been proposed throughout the whole thesis is that the oils in the Greater Birba area have been subjected to mixing with a condensate charge, that may have played a significant impact in the distribution of their properties. Therefore, it was necessary to investigate the phase behaviour of these fluids thermodynamically using the PVT data available to see if PVT modelling can also confirm this mixing sequence. Unfortunately, there were no PVT samples acquired for some of the oil accumulations in the Greater Birba area. There will be investigations of the phase relationships between the different petroleum fluids in the Greater Birba area and identifying the controls on these relationships and attempting to predict them with the aid of Calsep PVTsim package version 14. Riemens *et al.* (1985) claimed that there is strong compositional grading (i.e. systematic variation of compositions (e.g. methane, ethane ...etc) with depth) due to gravitational effects in A4C reservoir unit of Birba field between well BB2 and well BBS1 (Riemens et al., 1985) (Figure 7-1). This model will be tested and possibly extrapolated to predict the compositions of petroleum fluid from well BB3 down the column as they all (BB2, BBS1, BB3) share the same reservoir (A4C) and were proved to be in connection with each other using interference pressures (Riemens et al., 1985).

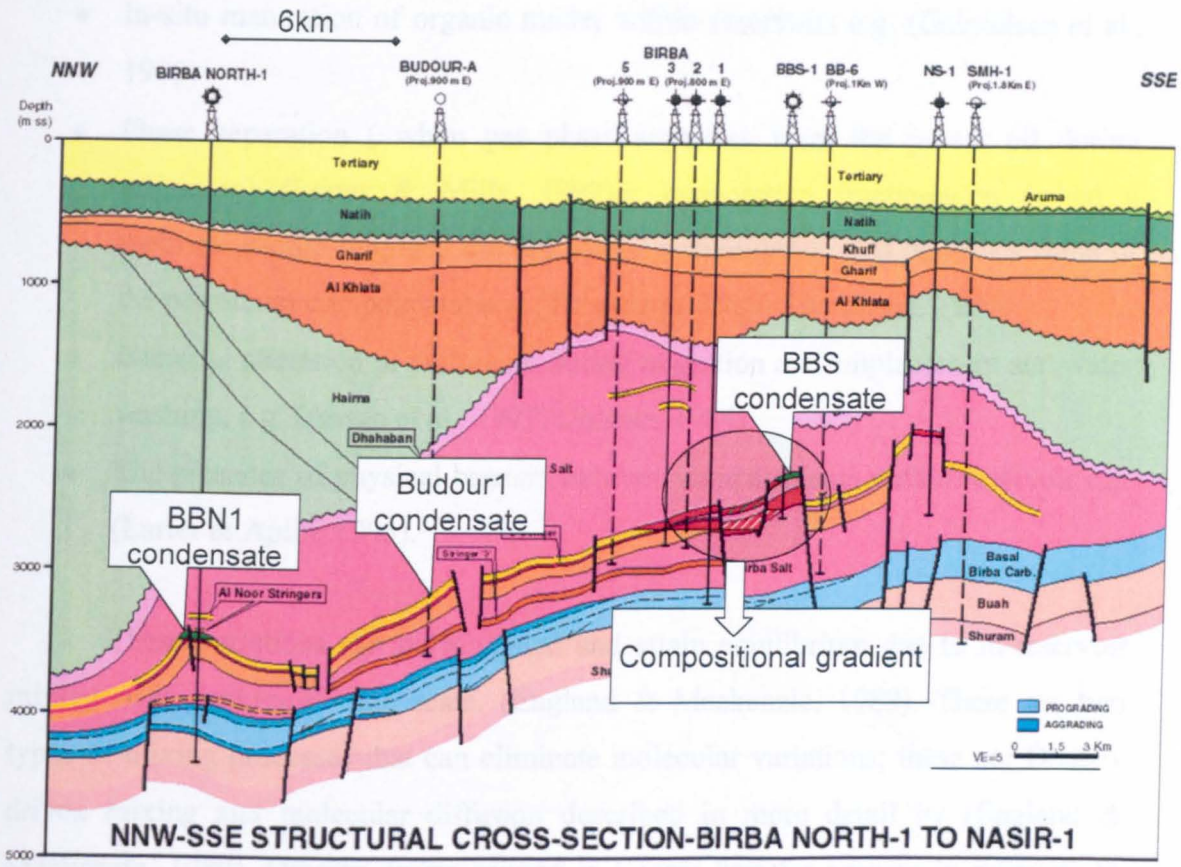

Figure 7-1: A cross section from north north west to south south east of the Greater Birba area. The compositional gradient was observed in Birba from Birba 2 to BBS1 by Riemens *et al* (1985).

7.1.2 Literature review

In-reservoir heterogeneities of petroleum fluids:

Subsurface petroleum fluids are naturally heterogeneous and their character influences their physical and chemical behaviour. Fluids advancing into a trapping reservoir may be of different compositions due to being generated at different times (different maturities) and environments (different sources). Hence, lateral and vertical compositional variations within a reservoir will be expected during the early reservoir life and even in its whole life (Larter & Aplin, 1995). Other factors can result in to these heterogeneities in reservoir fluids during the geological life of the reservoir and that include:

- Secondary migration and reservoir filling e.g. (England & Mackenzie, 1989)
- Mixing of fluids from more than one source or source type e.g. Forties Field and Magnus Field in North Sea (England, 1990)

- In-situ maturation of organic matter within reservoirs e.g. (Gabrielsen et al., 1985)
- Phase separation (when gas phase separates from the parent oil during migration) (Larter & Mills, 1992)or evaporative fractionation (when a methane charge migrates through an oil accumulation and dissolves some of the petroleum components) e.g. (Thompson, 1987; Thompson, 1988)
- Bacterial alteration of petroleum during migration and emplacement and water washing, e.g. (Ahsan et al., 1997; Connan, 1984)
- The presence of physical barriers between compartments within reservoir e.g. (Larter & Aplin, 1995).

These variations can be mitigated and attain equilibrium due to in-reservoir mixing over geological time scale, (England & Mackenzie, 1989). There are two types of mixing processes that can eliminate molecular variations; these are Density driven mixing and molecular diffusion described in more detail by (England & Mackenzie, 1989). Density driven mixing is a mass transfer process in response to filling related density gradients to achieve mechanical equilibrium so that the density of the oil become the same throughout the petroleum reservoir. Diffusive mixing involves molecular movements through the reservoirs vertically and laterally in response to gravity (gravity segregation) or to chemical potential (horizontal concentrations differences of different molecular species) respectively. England and Mackenzie, (1989) established order of magnitude estimates of the rates of in-reservoir mixing processes as shown in Figure 7-2. They concluded that the density driven mixing depends on the permeability, it is rapid at geological scale (timescales of 10000 to a million years) in reservoirs with high field wide permeability (good reservoir quality) and geologically slow in reservoirs with low field wide permeability. They also concluded that diffusive mixing in vertical oil columns is geologically rapid under gravity and form gravitational segregated column (ca. 1Ma), while lateral diffusive mixing of petroleum columns is geologically slow across large fields (time scale of tens of million years). The mean core plugs permeability in the main Birba field in the South Oman Salt Basin varies from 30 to 50mD. England et al.(1987) and (England & Mackenzie, 1989) stated that the large scale permeability is 100 times lower than the core plugs permeability. Therefore, the large-scale permeability in the

main Birba field is 0.3 to 0.5. The time needed for these mixing processes to attain equilibrium is calculated in section 7.3.3.3.

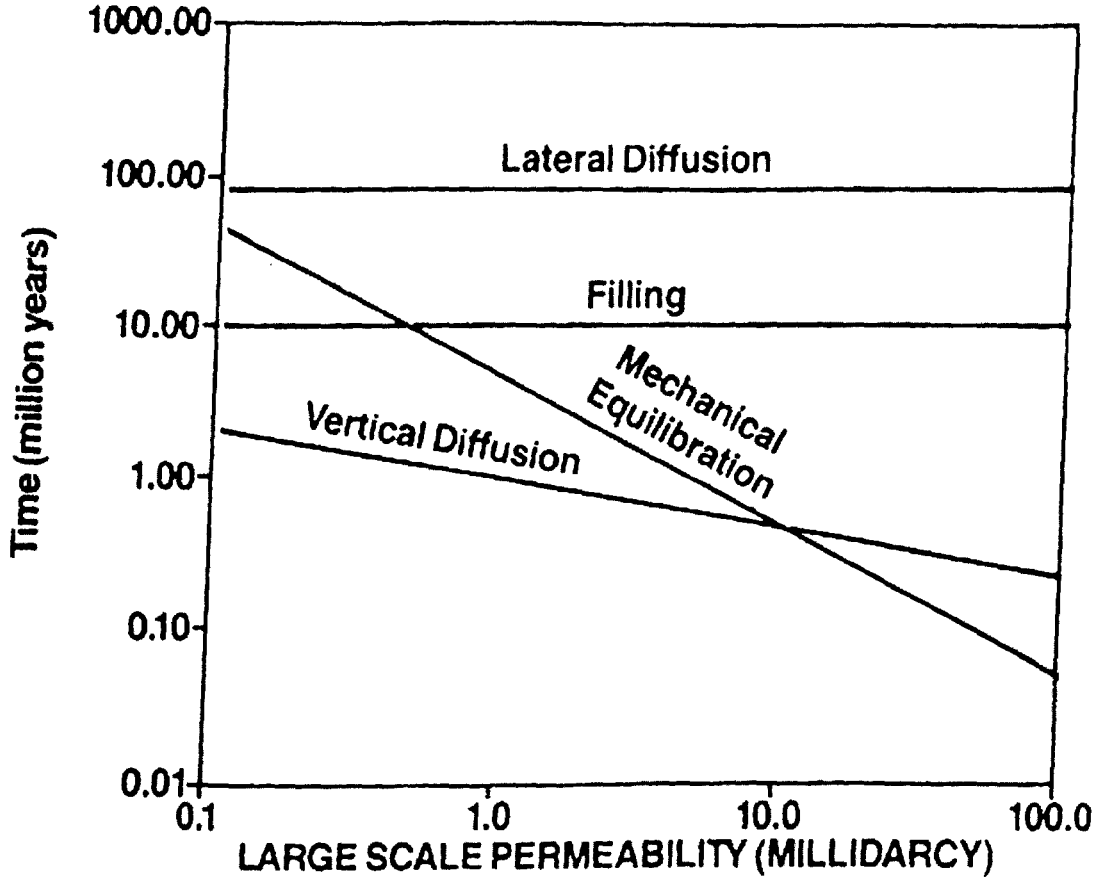

Figure 7-2: order of magnitude estimates of in-reservoir mixing timescales as a function of reservoir wide permeability, after (England & Mackenzie, 1989).

PVT (Pressure-temperature-volume) analysis of petroleum fluids:

Fluid data, either of hydrocarbons (references will be cited later) or even formation waters in reservoir provide reliable and very useful information about reservoir heterogeneity (Cosentino, 2001). The main fluid data concerned here is the PVT (pressure-volume-temperature) properties of the petroleum fluids. Density and viscosity are two main fluid properties and those have been a standard part of reservoir analysis for many years (Meulbroek & MacLeod, 2002). Other PVT properties which are phase-related include (Di Primio et al., 1998):

- Saturation point pressure (Bubble point and Dew point pressures): the pressure at which a new physically distinct petroleum phase (e.g. liquid

and gas) appears in a petroleum fluid during decompression along the Pressure-Temperature gradient. Bubble point pressure marks the pressure where a separation of a gas phase from a supercritical liquid phase occurs, while dew point pressure marks the beginning of formation of a liquid from a supercritical gas phase takes place.

- GOR (Gas to oil ratio) and CGR (gas to condensate ratio): the amount of gas in solution and the amount of condensate in gas respectively.
- Formation volume factor (FVF): the volume of reservoir oil to the volume of the oil in surface conditions or the volume of reservoir liquid to give one standard barrel in surface conditions.

PVT analysis provide a very important tool to characterize the physical properties of reservoired fluids as well as the changes in volume and phase state occurring during production, and hence indicate any heterogeneity in the above properties throughout reservoir either laterally or vertically e.g. (Di Primio et al., 1998). PVT analysis utilizes the composition of the oil (amount of methane, ethane, propane.....etc in the oil) and the bulk initial oil analysis (density, viscosity, gravity) to analyze other bulk properties of oils (see PVT data section). This tool can predict the bulk properties away from the well control using the composition of the analysed oil. The prediction of bulk properties relies on two models, work together (Meulbroek & MacLeod, 2002). The first model is the Equation of State (EOS) which is used to predict the relationships among the intrinsic state properties of pressure, density, and temperature. Given a one-phase mixture of known composition, any of these properties can be predicted as a function of the other two. Fluid phase equilibria models (FPE) are the second set of models that work complementarily with EOS. This set of models predicts the number and composition of phases that minimize the Gibbs free energy of a system. These models require knowledge of the chemical potential of all species in all possible mixtures. EOS-generated volumetric data can predict this quantity, (Meulbroek and MacLeod, 2002).

The phase behaviour of petroleum fluids:

The phase behaviour of the fluids is basically the response of these fluids to the change in PVT conditions. Understanding phase behaviour of the subsurface petroleum is valuable in order to determine its properties. The phase rule states

$$P=C-F+2 \quad \text{----------Equation 7-1}$$

Where P is the number of phases, C is the number of components, and F is the degree of freedom (Danesh, 1998).

Under usual conditions, up to 3 phases may in fact be in equilibrium: petroleum gas, water, and petroleum liquid. The liquid and gas are saturated with respect to each other and the petroleum phases will be saturated with respect to water. Therefore, one need to consider two phases, water saturated petroleum liquid and water saturated petroleum gas, (England et al., 1987). When oil and gas coexist in a petroleum reservoir, they are in equilibrium (saturated with respect to each other) and have saturation pressure equal to reservoir pressure at oil-gas contact as shown in diagram below (Figure 7-3).

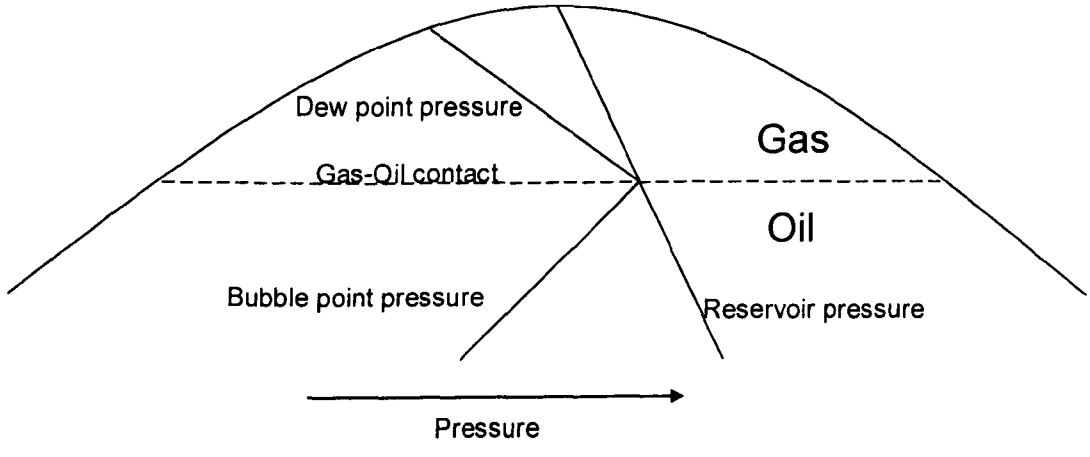

Figure 7-3: Schematic diagram showing a reservoir containing saturated gas and oil phase. The solid straight lines represent different types of pressures, and the broken line is for gas-oil contact.

The phase behaviour of a hydrocarbon mixture at reservoir and surface conditions is determined by its chemical composition and the prevailing temperature and pressure. The composition of petroleum is considered by PVT calculation either to consist of two components, oil (C_{6+}) and gas (C_1-C_5) or 6 components from C_1 to C_6 and C_{7+} is the seventh lumped component, (Danesh, 1998), where C_4 for example includes all compounds consisting of four carbons (e.g. butane, 1-methylpropane, ..etc). C6+ and C7+ are called plus fractions and these include all compounds with 6 carbons or 7 carbons respectively, and above (e.g. C6+ = C6+C7+C8+.....etc). Other PVT studies preferred the plus fraction of C_{10+} (di Primio, 2002, di Primio et al., 1998) or even C_{20+} (no reference cited, this study).

PVT calculations and the phase behaviour are performed using PVT software packages, which use equations of state, (Danesh, 1998). The phase behaviour of a fluid is commonly described using either specific physical properties of the fluids such as formation volume factor, saturation pressure or gas to oil ratio, or by means of a pressure vs. temperature phase diagram (phase envelope) (Di Primio et al., 1998).

The typical phase diagram of a reservoir petroleum system is shown in Figure 7-4). The phase envelope shown here consists of two regions: a monophase region (outside the envelope) and a two phase-region (inside the envelope). The two phase region is enclosed by the bubble point curve (marks the PT conditions where a separation of gas from supercritical liquid phase) and dew point curve (marks the PT conditions where a separation of a liquid phase from a supercritical gas phase). The critical point is the PT point that is located at the intersection of a bubble point curve and a dew point curve, where a coexisting liquid and gas mutually approach each others' compositions and physical properties. The discussion below of the possible phase envelopes and their characteristics are mainly based on (Danesh, 1998) unless stated. A reservoir will contain gas if its temperature is higher than the fluid critical temperature otherwise it contains oil. The production of a reservoir will result in retrograde condensation in the reservoir if the reservoir temperature lies between the critical temperature and the cricondentherm (the maximum temperature at which two phases can coexist); no liquid will form if it is above the later point. The oil in the reservoir with a temperature close to its critical point is more volatile than that at a lower temperature. A small reduction of the pressure below the bubble point in a

reservoir with a temperature just below the critical temperature may vaporize half the oil volume. Critical temperatures of heavy hydrocarbons are higher than those of light hydrocarbons and the critical temperature of heavy hydrocarbons bearing petroleum fluids is normally higher than that for the reservoir. Whereas the temperature of a reservoir mainly composed of methane with a critical temperature of 190.6K will be higher than the mixture critical temperature. When the reservoir pressure falls below the saturation point, the phase diagram is still valid but now the two phase region is entered and production of one or more of the fluids changes the net composition.

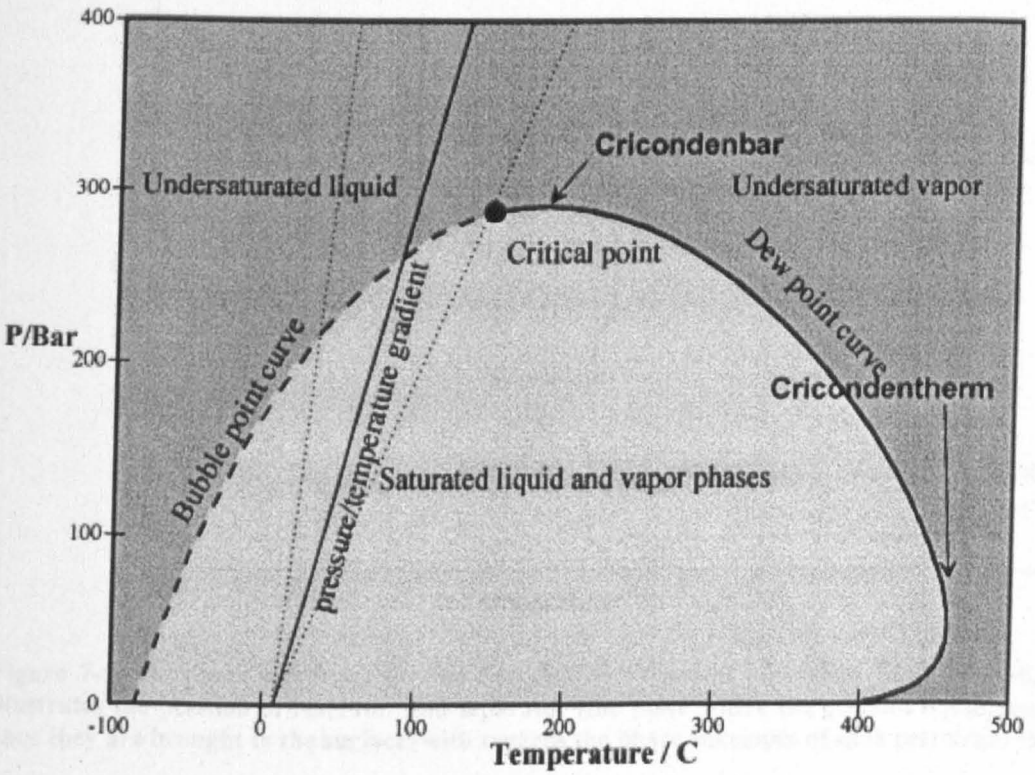

Figure 7-4: Phase envelope of a typical black oil with all terms used in the text. The area enclosed by the dotted lines represents the extent of naturally occurring P/T conditions of reservoirs. After (Di Primio et al., 1998).

Each petroleum fluid has its own phase envelope. The petroleum fluids are classified normally into 5 types, Dry and Wet gas, gas condensate, and volatile oil and black oil (Figure 7-5) depending on their composition. Dry gases are predominantly composed of methane and non-hydrocarbons such as nitrogen and carbon dioxide. The phase envelope is relatively tight and mostly located below the reservoir temperature. There will be not any change in the state of gas from reservoir to the separator (the place where the gas and liquid separated once they are brought to the surface). Wet gas is mainly composed of methane and other light hydrocarbon

components; with its dew point-bubble point envelope is located at pressures and temperatures well below that of the reservoir. A wet gas therefore will not drop out a condensate in the reservoir during depletion (production) as illustrated in Figure 7-5. A condensate may form in the separator because the separator is located inside the envelope (i.e. the PT conditions at the separator which is located on the surface are located within the PT envelope conditions range).(Danesh, 1998)

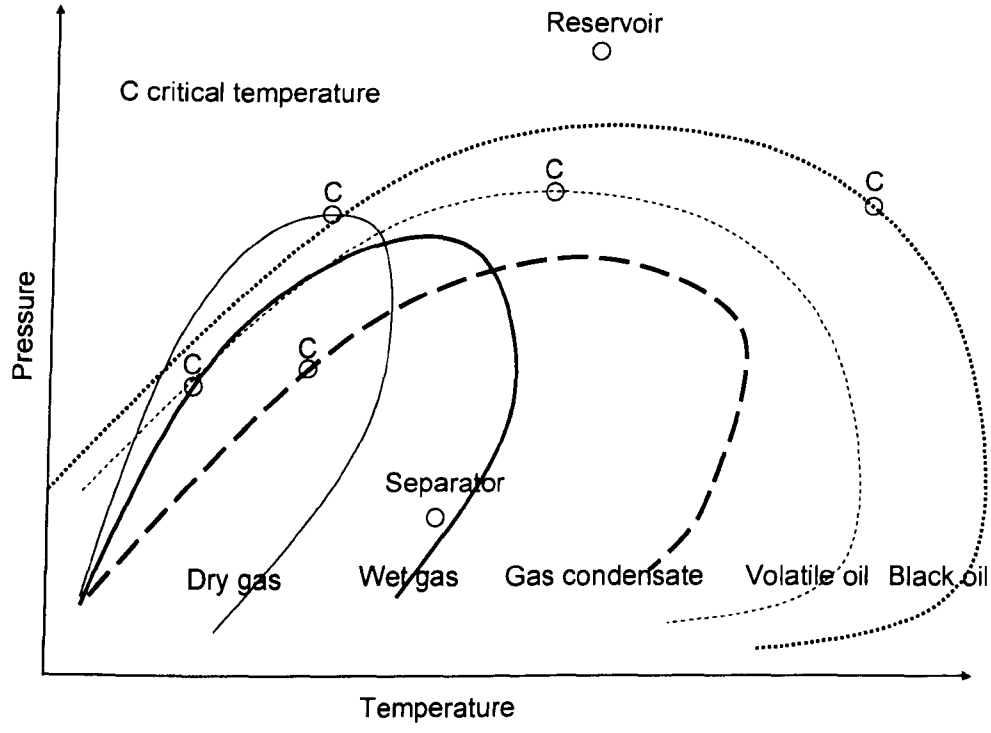

Figure 7-5: the phase envelopes for the five different types of petroleum fluids. The diagram illustrates the position of reservoir and separator (the place where the gas and liquid separated once they are brought to the surface) with regards the phase envelopes of each petroleum fluid.

The presence of relatively heavier hydrocarbons in gas condensates expands the phase envelope relative to a wet gas; hence the reservoir temperature lies between the critical point and cricondentherm (Figure 7-5). The gas will drop out liquid by retrograde condensation in the reservoir, when the pressure falls below the dew point. The amount of potentially condensable hydrocarbons in the reservoir increases with the C_{6+} content of the gas, as heavy hydrocarbons shift the critical temperature toward the reservoir temperature. Whereas gases with a cricondentherm near the reservoir temperature will behave very much like a wet gas. GOR (Gas oil ratio) for a condensate should be less than 10000 and more than 570 Scf/bbl; if it is more than 10000 Scf/bbl it is treated as a wet gas. The producing GOR initially remains constant until the reservoir pressure falls below the dew point and increases thereafter. The

condensation in reservoir has negligible effect on the properties of produced gas, but it can noticeably reduce the gas recovery rate (Danesh, 1998). The liquid dropout reaches a maximum and then decreases by vaporization during pressure depletion (Danesh, 1998). Condensation and loss of valuable compounds in reservoirs could be avoided by maintaining the reservoir pressure above the fluid dew point by gas recycling. Volatile oils have many common features with gas condensates (Figure 7-5), but as they contain more heavy compounds they behave liquid like at reservoir conditions. The phase envelope is wider than that for the gas condensate, with a higher critical temperature due to its larger concentration of heavy compounds. The volatile oil is referred to as near-critical oils because the reservoir temperature is near the critical temperature as illustrated in Figure 7-5. They are called volatile because a small reduction of pressure below the bubble point vaporizes a significant fraction of the oil. Initial GOR ranges from 310 to 570 Scf/bbl. This increases when the reservoir pressure falls below the bubble point pressure during the reservoir life.(Danesh, 1998)

Black oil has the widest phase envelope with its critical temperature well above the reservoir temperature (Figure 7-5). GOR is less than about 310 Scf/bbl and may decrease initially when the reservoir pressure falls below the bubble point, as the evolved gas remains immobile at very low saturations. The GOR then increases sharply as the gas to oil mobility ratio within the reservoir varies inversely with the viscosity ratio, which is typically of two orders of magnitude. The saturation pressure is relatively low.(Danesh, 1998)

The relationship between the chemical compositions and the PVT properties of petroleum fluids:

The strongest compositional influence on subsurface fluid phase behaviour and the physical properties is the quantity of gas "light H/C" dissolved in the liquid phase "oil" (i.e. GOR: gas to oil ratio). The concentration, density, and molecular weight of individual compounds or petroleum compound classes, also have a strong effect, so a precise knowledge of the petroleum composition is necessary. The amount and composition of the gas in the fluid influences its saturation pressure and GOR, "the higher the dissolved lighter gas content the higher the saturation pressure". Plus fraction (the higher molecular weight, C_{10+} or C_{7+} or C_{20+}) has a strong influence on

the position of the Cricondentherm (the highest Temperature at which the gas and oil coexist) and critical point; and indirectly it influences the GOR and Saturation pressure, e.g. a fluid with a high plus fraction; is of high cricondentherm, low GOR and low saturation pressure, (di Primio et al., 1998).

The gas content of the petroleum phase increases sharply with increasing pressure but it decreases slightly with increasing temperature (England et al., 1987). In the other hand, condensates dissolved in gas phase show the same trend with pressure and temperature (England et al., 1987). The density and viscosity are very important properties of petroleum that control the mobility and the migration of subsurface hydrocarbons. These properties are severely affected by the gas or condensate dissolved in petroleum or gas phase respectively (England et al., 1987). The higher the GOR the lower the density and the viscosity of the petroleum, and the same trends are found for the CGR of the gas phase. Therefore, density and viscosity of liquid phase decreases with P-T and those of gas phase increases as shown in Figure 7-6. At some critical P-T, gas saturated oil and condensate saturated gas approach similar composition, and properties and the petroleum will be in the form of single-phase supercritical fluid, (England et al., 1987). Berg (1975) (in England et al., 1987) has shown that the interfacial tension of oil-water remains reasonably constant at 20-40 x 10^{-3}Nm^{-1} with increasing P-T and because the gas phase has similar composition and properties to oil at the critical point and above it, then the gas-water contact has similar value. The rapid decrease of density and water solubility of gas with decrease in P-T conditions causes the interfacial tension of gas-water to rise to about 70 x 10^{-3} Nm^{-1} at the surface. The interfacial tension of oil-gas decreases from 3 Nm^{-1} at STP to 0.02 Nm^{-1} at 40 MPa and 120°C as the two phases approach one another in their properties (England et al., 1987). This implies that the two phases will migrate together as foam due to the similar properties they have, (England et al., 1987).

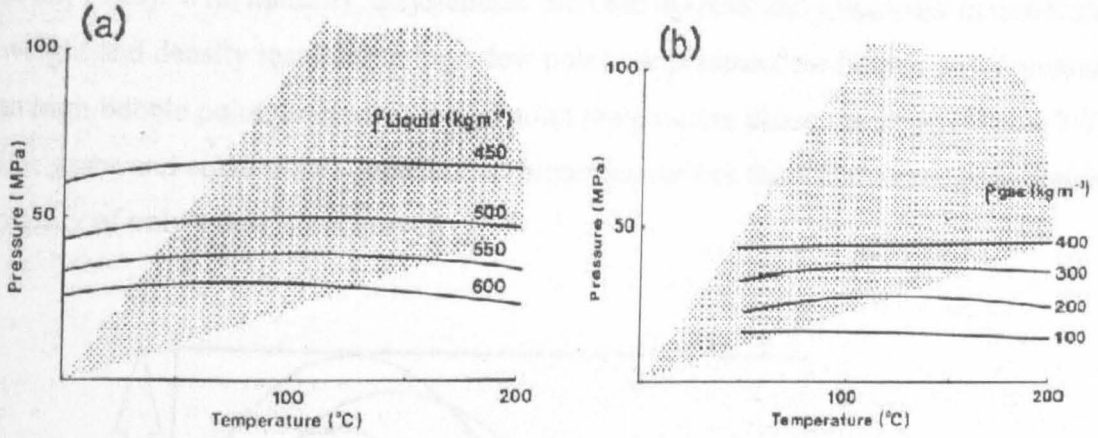

Figure 7-6: isochors (curves of constant density) for gas saturated petroleum liquid (a) and condensate-saturated petroleum gas in P-T space.

The saturation pressure of a petroleum fluid is closely correlated with the GOR and CGR. The higher the GOR the higher the bubble point pressure and the same trend are observed for the CGR and dew point pressure. Dew point temperature increases with the increase of condensates in gas phase, (England, 1990).

Impact of petroleum systems processes on the PVT properties

The main controls on the physical properties of the petroleum: Maturity, source facies, secondary migration and uplift. All of these involve drastic or gradual change in PT conditions of the petroleum or petroleum settings. It is well recorded in literature that GOR of the expelled petroleum increases with maturity systematically, (England et al., 1987, Larter and Aplin, 1995). The heterogeneous expelled petroleum pulses result in a range of GOR between 0.2 to 0.5 kg/kg, (Larter and Mills, 1992, England and Mackenzie, 1989). The variation of GOR across the reservoir may indicate the filling history of the field or the presence of physical barriers to fluid flow. Because the higher the maturity the higher the GOR, the filling direction will be from higher GOR to lower ones, e.g. (Larter et al., 1989). The molecular weight and density also change in a regular fashion with maturity, (di Primio et al., 1998). These three factors (GOR, Molecular weight, and density) are very important controls on phase behaviour. High GOR oils have a bubble point curve extending to high pressures, while petroleum with high proportions of high molecular weight material (and high densities) has dew point curve extending in to high temperatures (Di Primio

et al., 1998). With maturity, a systematic increase in GOR and a decrease in molecular weight and density resulting in high dew point temperature/low bubble point pressure to high bubble point pressure/low dew point temperature phase envelope (Figure 7-7). For gases and condensates generated at higher maturities from the source rock consist mainly of only a dew point curve.

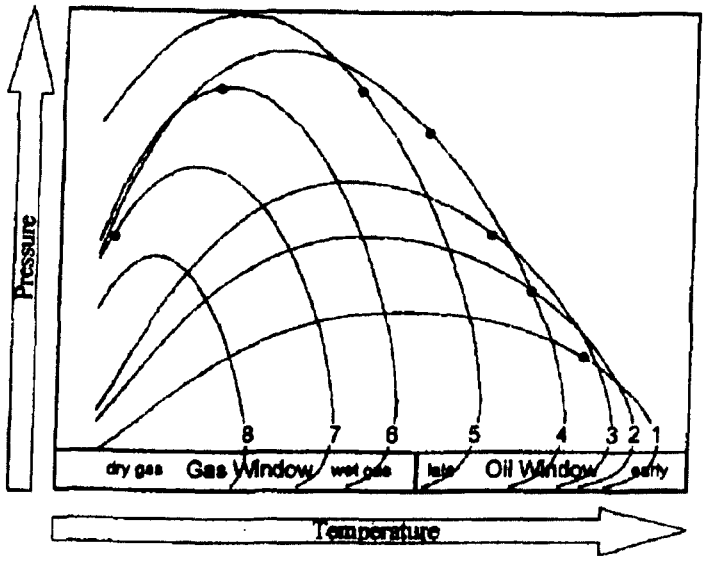

Figure 7-7: evolution of phase envelopes of petroleum with progressive maturation of source rocks. After (Di Primio et al., 1998) levels 1 to 8 represent increasing maturity levels.

Source facies pose an important control on the physical properties of the generated fluids, (di Primio, 2002). High quality source rocks will expel fluids with lower GOR enriched in higher molecular weight compounds. The GOR of the expelled phase depends on the degree of oil cracking in the source rock, which in turn is controlled by the source rock expulsion efficiency and may potentially vary between 1200 and 150 scf/bbl (Larter and Mills, 1992). As the quality of the organic matter decreases, the generated fluids will have increasing proportion of gas leading to higher saturation pressure and lower formation volume factor (di Primio, 2002).

With upward movement or uplift, pressure and temperature decreases resulting in phase separation (development of two phase system) (England *et al.*, 1987; Larter & Mills, 1992) (see Figure 7-8) (Di Primio et al., 1998)), and so differential migration (distinction between the phases due to different properties) , or phase fractionation (e.g. gas washing) (Thompson, 1987). The phase separation might lead to gas and oil

but also might lead to precipitation of a solid phase out of the liquid (di Primio, 2002; Khavari-Khorasani et al., 1998). This precipitation will change the average molecular weight of the migrating petroleum fluid, but it is not taken in account by the PVT software simulation and calculation. It is possible though to calculate the condensation by performing a series of successive flashes to shallower depths. With pressures and temperatures decreasing along an assumed regional pressure/temperature gradient during migration : the phase envelope shrinks in a systematic way, the critical points of the liquids move towards Low PT, MW decreases, bulk density of liquid increases (due to degassing) and of the vapour phase decreases (condensation to a liquid phase). This implies that differential migration of oil and gas should result from this difference in density and viscosity between physically segregated vapour and liquid phases, ((Di Primio et al., 1998)di Primio, 2002).

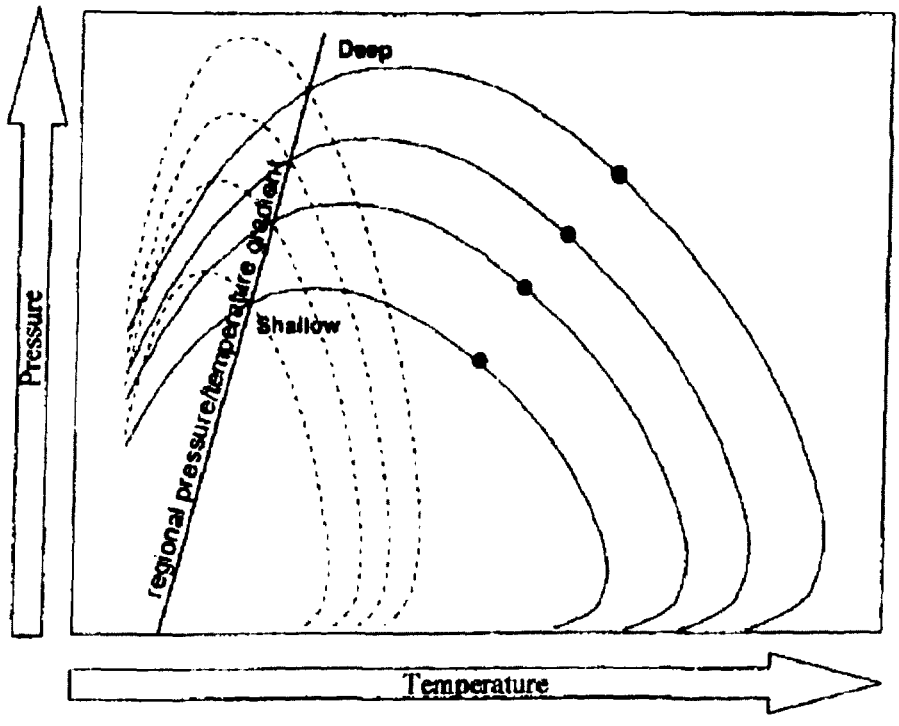

Figure 7-8: Evolution of phase envelopes with uplift or vertical migration for black oils (solid lines) and gas/gas condensates (brocken line). After (Di Primio et al., 1998).

A large difference in viscosity and density can cause fingers of less dense phase of the interface is moving and penetrating the denser phase, (England, 1990, England and Mackenzie, 1989). Phase separation should result in to a systematic decrease in saturation pressure and Formation volume factor. Near vertical

displacement of undersaturated fluids may lead to rapid saturation due to addition of gas without altering formation volume factor (the same volume) (Di Primio et al., 1998). di Primio (2002) used the GOR variation of oils and condensates with depth to assign different oils and gas accumulations the northern half of Quadrant 25 in the Norwegian North Sea to originate from one source rock and that the phase separation results in this distribution of petroleum fluids in (Figure 7-9).

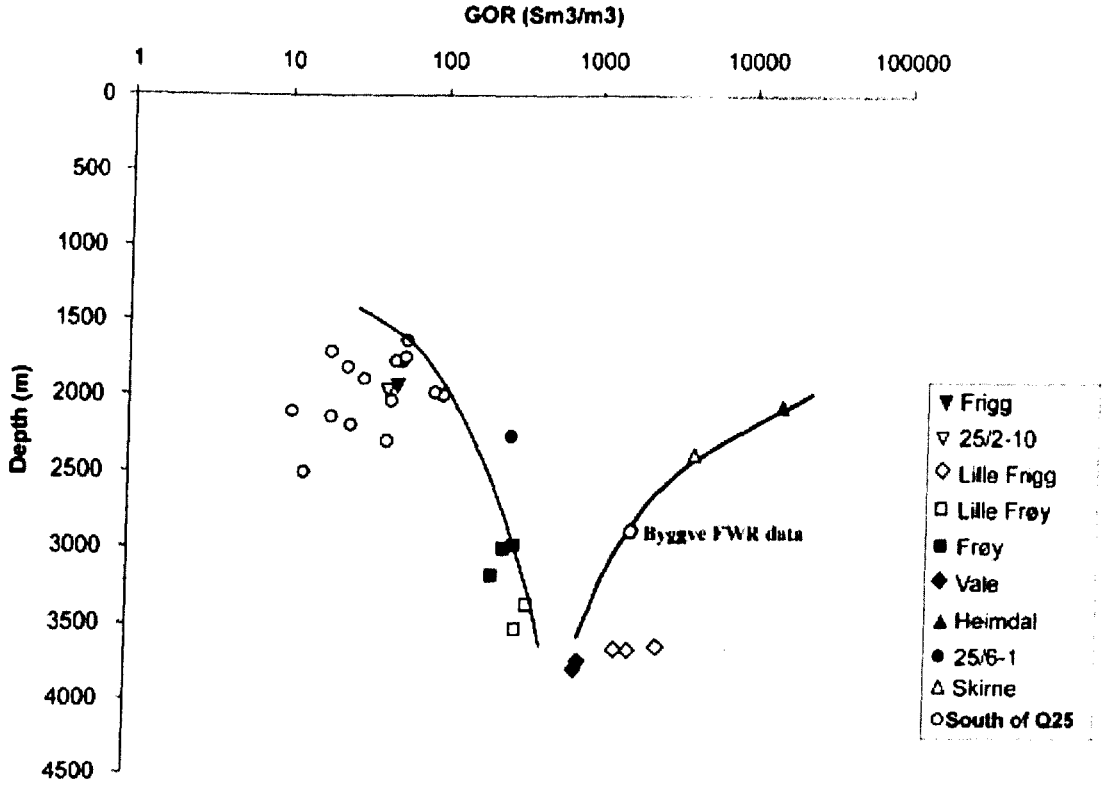

Figure 7-9: Gas oil ratios of different petroleum fluids as a function of depth. Notice that the GOR of oils and condensates converge at GOR similar tot that for Vale oil field, indicating that this oil might be the model fluid.

Secondary effects including mixing, biodegradation and reservoir reburial accompany the genetic effects and migration effects. Mixing of fluids from different source rocks would lead to petroleum properties plotting along a line between the mixing end members. Mixing can be identified by the cross plot of PT phase envelopes as shown in Figure 7-10. Biodegradation of oil leads to its rapid saturation and severely alters its formation volume factor, (Larter et al., 2000). The reburial of the structure may increase the prevailing PT. This will increase the mutual solubility of C_1-C_5 and C_{6+}. For a single-phase reservoir, this will result in a fluid, which is no longer saturated, if there is no excess gas or condensate to dissolve in the oil and gas. This explains partly why unsaturated oils and gases with a wide range of GOR occur

in most petroleum basins (GOR from 0.1 to 100 kg/kg). The wide range of GOR is also mainly controlled by phase separation during migration, (di Primio, 2002).

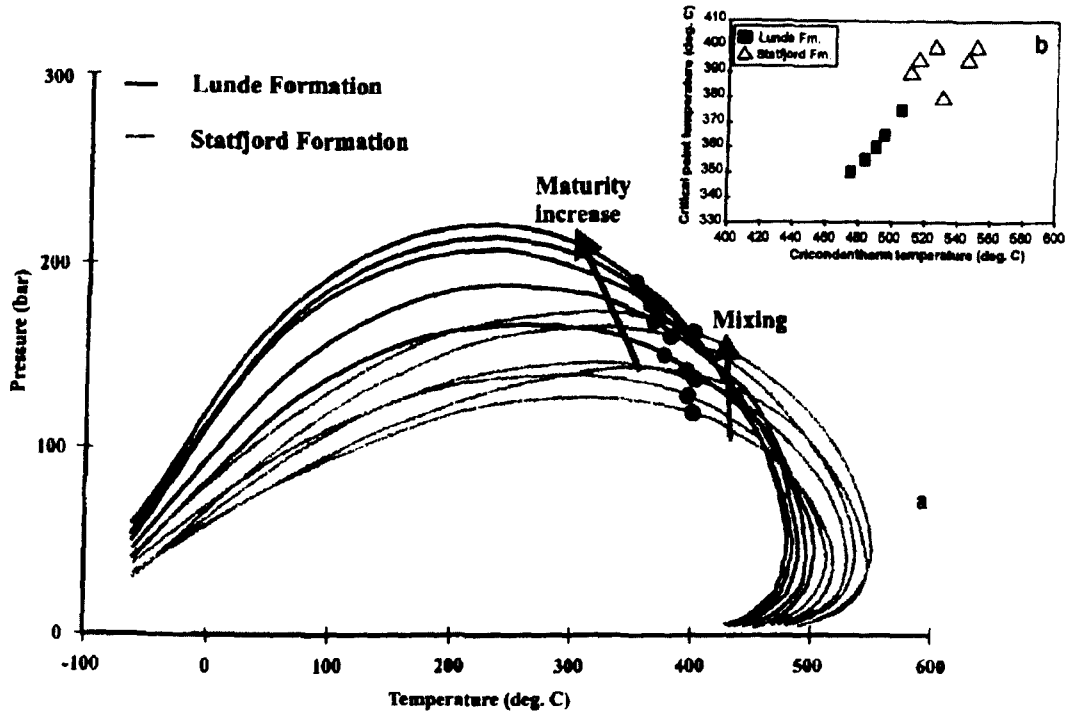

Figure 7-10: mixing sequence revealed by the phase envelopes of petroleum fluids from Snorre Field (Tampen Spur). The top right cross plot shows a mixing line revealed by cross plot of cricondentherm and the critical point temperatures.

In many petroleum systems, the heavy "asphaltene rich" oils are situated at the shallow basin rims and are commonly biodegraded (Tissot & Welte, 1984).. Source maturity and migration related factors all influence the asphaltene content of oils (Hunt, 1995; Tissot & Welte, 1984). Asphaltene content typically decreases with maturity increasing and it ranges from 25% when immature to less than 5% in supermature oils (Hunt, 1995). Khavari-Khorasani et al., (1998) have published an attempt to model asphaltene precipitation towards an understanding of the distribution of heavy oils versus light oils in Gulf of Suez. Asphaltene precipitation is modelled as a liquid-liquid phase fractionation. The fluids with more than 15% asphaltene have very low saturation pressure and therefore will not precipitate any asphaltene in a quite wide range of pressure and temperature. The fluids with asphaltene less than 5% are also not prone to asphaltene precipitation if they have low GOR. Increasing GOR though will increase the probability of asphaltene precipitation because it will depress the asphaltene envelope (saturation pressure) to higher values. The fluids between

those values are more prone to asphaltene precipitation due to the higher saturation pressure with respect to the asphaltene.

Although the above study and other studies mentioned above and later have used fluids generated artificially from source rock samples in order to simulate the PVT flashes to see effects of geological controls on the migrated oils from source to trap, Heum *et al* (1986) has warned that this may impact the prediction of the properties of the reservoir petroleum. Using the composition of the petroleum expelled from a source rock from source artificially (pyrolysis), may lead to over optimistic conclusion concerning the types of the hydrocarbons and GOR because of its failure to model timing effect (residence time). PVT modelling of DST oils provide more realistic picture according to (Heum et al., 1986). The former gives a very low saturation pressure (bubble point and dew point pressure) and low GOR and the later indicated that the petroleum is at state near critical points, (Heum et al., 1986).

Compositional grading

Compositional graded hydrocarbon column is defined as a hydrocarbon column that exhibits systematic variations of composition such as methane and plus fraction (heavy end) with depth. Compositional variations with depth can result for several reasons including temperature and pressure effects and some of these:

- Gravity segregation and asphaltene precipitation, (Belery & da Silva, 1990; Hirschberg, 1984; Schulte, 1980)
- Thermal diffusion, (Belery & da Silva, 1990)
- Thermally induced convection, (Hoier & Whitson, 2001; Whitson & Belery, 1994)
- Non-complete mixing, (England et al., 1987)
- Varying distributions of the hydrocarbon types like paraffin and aromatics within the heptanes plus fraction, (Schulte, 1980).
- Biodegradation and water washing: mainly at the oil water contact e.g. (Anissimov & Bylinkin, 2003; de Oliveira Padua, 1997)

- Methane concentrations that may lead to neighbouring fields having varying of gas saturation. This also includes admixture of gas and gas condensates from deeper reservoirs through faults, e.g. (Montel et al., 2003; Thompson, 2004).
- Multiple source rocks crude oils migrating differentially in to different layers and geological units.

These and others might occur separately or in combination and lead to significant and uncorrelatable variations in fluid composition, both vertically and laterally. It is impossible to model numerically most of these processes due the lack of physical and chemical understanding of the problem and the continuous changing boundary conditions as well as the lack of the needed property data and geological information necessary to build even the simplest physical models (Hoier & Whitson, 2001).

It is already mentioned that one of the important mixing processes in reservoirs was molecular diffusion due to gravity segregation whereby the heavy components sink to the bottom of the column and the light components migrate to the top of the column (England & Mackenzie, 1989). Uniform pressure and temperature lead to the uniformity of fugacity of each component throughout all co-existing phases to attain chemical equilibrium (Danesh, 1998). The uniformity of fugacity is equivalent to the uniformity of concentration for a single-phase fluid (Danesh, 1998). However, the temperature and pressure are not uniform throughout a reservoir; the temperature increases with depth with a gradient of about 0.2-0.3 K/m and even much higher in extreme cases (Danesh, 1998). The pressure also changes according to the hydrostatic head for fluids at rest. Therefore, compositional grading with depth due to variation in these two variables should be well expected especially in long columns with long geological residence times due to the significant variations in fugacity due to variations in pressure and temperature.

A petroleum mixture exhibiting a compositional gradient is expected to get richer in heavier components and poorer in light components with depth. The saturation pressures as well as other PVT properties in this hydrocarbon mixture are

expected to vary with depth due to these variations in compositions and PT conditions. The oil saturation pressure generally decreases with decreasing methane content for black oil, while it increases with increasing plus fraction for gas condensates. The reservoir petroleum fluid remains as a single phase as long as the saturation pressure is below the reservoir pressure. Once the saturation pressure equals the reservoir pressure, this will result in two-phase system and in a two phase accumulation, the point where the saturation pressure is equal to reservoir pressure is the gas oil contact. The petroleum fluid behaves oil-like and gas-like below and above the gas oil contact in the hydrocarbon column respectively. There are cases where undersaturated gas oil contacts exists where there is a continuous gradient of composition along the hydrocarbon column, and so the liquid phase gradually and continuously changes to a gas phase across the gas oil contact (Hoier & Whitson, 2001) (see Figure 7-11).

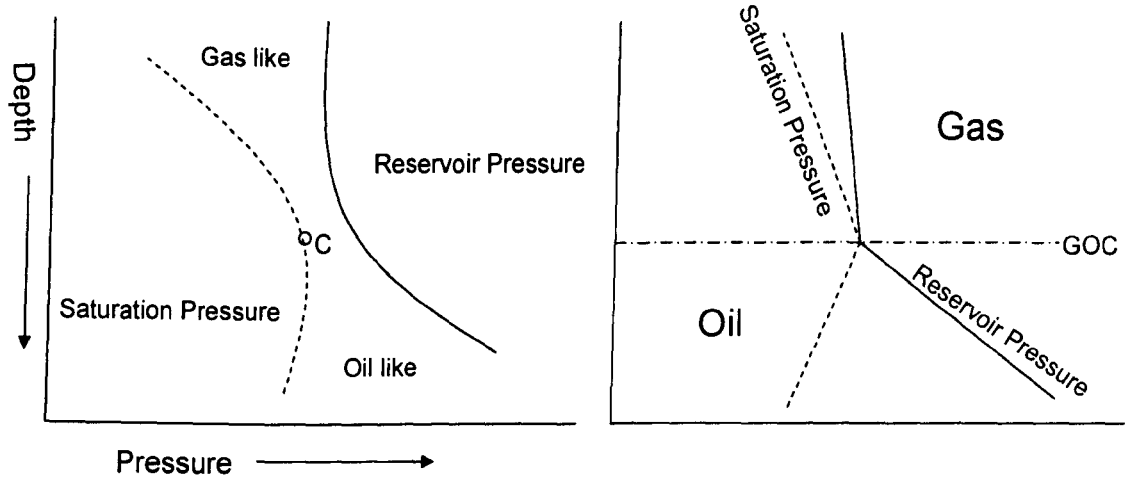

Figure 7-11: variations of saturation pressure petroleum fluids with depth and reservoir pressure. The Saturation pressure never meets the reservoir pressure in the left hand side diagram as the fluid is characterised by under saturated gas-oil contact because it is at near a critical state, while the gas oil contact is well defined in normal oils with the saturation pressure equalling the reservoir pressure at the gas oil contact.

The two main models of compositional grading in reservoirs that receive much interest and research were 1D models of isothermal gravity induced compositional gradients and non-isothermal gravity induced compositional gradients e.g. (Hoier & Whitson, 2001). Both models assume zero mass flux such that all components are existing in a stationary state in the absence of convection i.e. the chemical energy is balanced by gravity and thermal diffusion (Hoier & Whitson, 2001). The best-known model is Isothermal gravity induced compositional gradient model or abbreviated as

GCE (Gravity/chemical equilibrium) and many case histories of compositional gradients are attributed to gravity effect (Bath et al., 1980; Riemens et al., 1985; Schulte, 1980). This model was first given by Gibbs and he satisfies the equilibrium condition in the oil column by defining the difference in chemical potential of each component is balanced by the difference in force caused by gravity with respect to a reference depth as shown below

$\mu_i (p^o, z^o, T) = \mu_i (p,z,T) + M_i g(h-h^o)$ $i = 1,2.....N$ ----------Equation 7-2

μ_i is the chemical potential of component i,
z^o is a homogeneous single phase mixture at pressure p^o at a reference depth h^o.
p is the pressure and z is the mixture composition at depth h. M is the mass of the component i, g is the gravity acceleration. The entire system is at constant temperature.

A simple solution of the above equation based on a simplified equation of state (ideal mixing) was introduced by Muskat, 1994 . However, this oversimplified equation of state (EOS) leads to a misleading conclusion that gravity has a negligible effect on compositional variations within the reservoir. A more realistic EOS model was introduced by (Sage & Lacey, 1938)to solve equation 1 assuming ideal gas behaviour. They showed examples of gradients exhibiting significant variations of compositions with depth. They noticed that the systems at critical conditions should be expected to show significant compositional variations. Forty two years later, Schulte (1980) was the first to solve equation 1 using cubic equations of state, Soave and Ping-Robinson. Significant compositional gradients were identified using the isothermal grading model introduced by Schulte in various parts of the world (Whitson & Belery, 1994) such as Brent field exhibits a methane gradient of -0.033 mol% per m, while the saturation pressure decreases with depth at about 0.82 bar/m (Schulte, 1980). Other improvements have been introduced to this GCE (Gravity/chemical equilibrium) of (Schulte, 1980) through investigation of using different EOS and the effect of particular chemical components such as aromatics as well as thermodynamic conditions on this gradient.

Schulte (1980) proposed that the Gibbs equation can be solved using a cubic equation of state, Soave and Ping Robinson. He examined the effect of aromatic content on the GCE compositional gradients based on Cubic EOS. Aromatic content

increases with depth at a rate greater than for paraffins as shown in Figure 7-12. Higher aromatic contents can result in higher gradients of bubble point pressure and average molecular weight. He also observed that similar gradients are predicted by the Soave and Peng Robinson EOS but completely different gradient (lower) is predicted by Soave equation with the binary interaction coefficients (Soave-1). He also concluded that the reservoir pressure is very sensitive to segregation process when the fluid is near saturation.

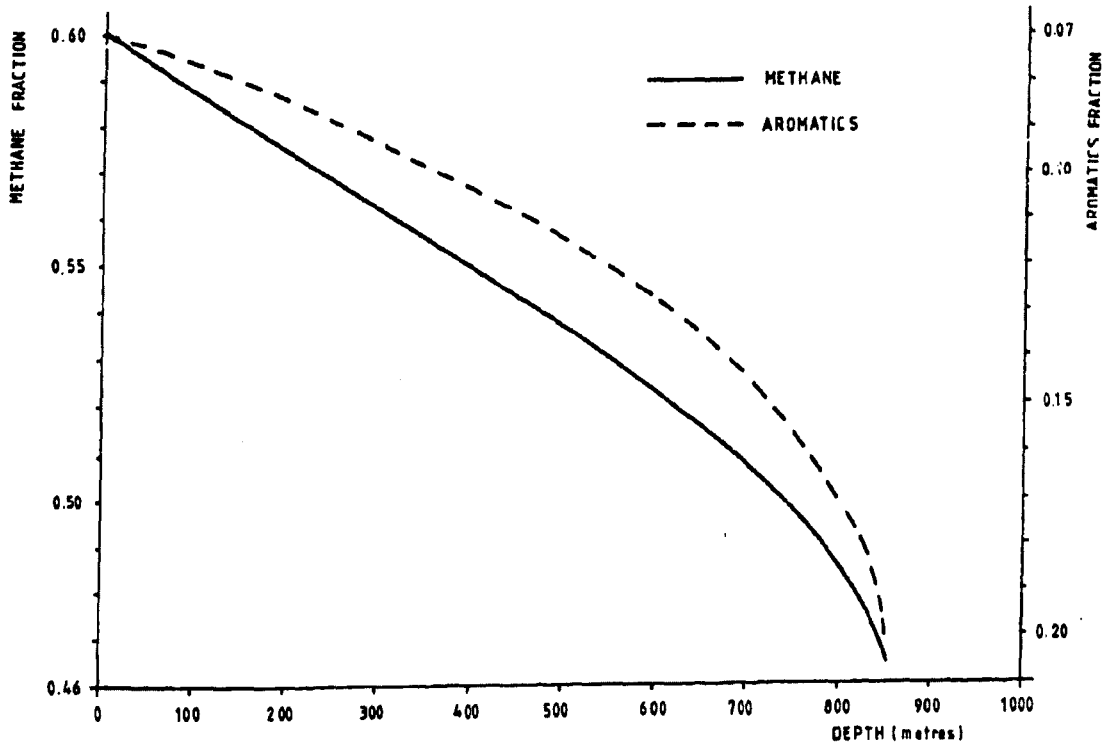

Figure 7-12: variations of methane fraction and aromatic fraction with depth (Schulte, 1980)

Gravity/Chemical equilibrium model (GCE) is characterised by increasing C_{7+} mole fraction and dew point temperature with depth, while C_1 mole fraction, GOR and bubble point pressure decrease with depth e.g. (Whitson & Belery, 1994). Dew points are very sensitive to the amount and properties of C_{7+} while bubble points are very sensitive to the amount of methane e.g. (Whitson & Belery, 1994). For saturated systems, the low GOR oils have a lean gas cap (high GOR), and for more volatile oils, the gas cap contains a richer mixture. Compositions and most phase properties are nearly linear with depth unless the reservoir fluids are near critical (GORs range from 500 to 800 Sm^3/Sm^3). Compositional gradients predicted by an isothermal GCE

model can be particularly large if the partial derivative of chemical potential with respect to compositions is small such as near critical conditions and/or the gravity gradient is very high such as when significant amount of asphaltenes are present, (Hirschberg, 1984). Compositional gradients decrease with increasing degrees of unsaturation, i.e. saturated or nearly saturated fluids should have larger compositional gradients (Whitson & Belery, 1994).

Riemens et al. (1985) identified a strong compositional grading in the Birba Field, Oman (studied area) based on isothermal grading model (Figure 7-30). They confirmed this gradient by Interference pressure tests to prove field communication (Riemens et al., 1985). This GCE model (gravity/chemical equilibrium) will be discussed in more details later in this report in section 7.3.2.

Another important evolution to the vertical compositional grading models is inclusion of thermal diffusion in these models. Thermal diffusion or the Soret effect is the tendency for a mixture to separate under a temperature gradient in the absence of convection (Kempers, 1989). This is very important, as any long reservoir should have at least the normal thermal gradient, i.e. temperature increasing with depth. Therefore, it is not accurate to ignore the temperature effect. Those compositional gradients that result from coupling temperature and gravity are called non-isothermal gradients or GCT gradient (Gravity/chemical/thermal) models.

Holt et al., (1983) presented a calculation for gravity induced compositional gradients for only simple binary system but they also included the effect of thermal diffusion in their formulation and focused on the distribution of methane. There are three methods to estimate thermal diffusion effect and incorporate it in the compositional gradient models, thermodynamic or viscosity based method such as Haase and Kempers models, activation energy based models (Belery-da Silva), and Shukla-Firozabadi models which require an empirical term relating the relative energies of vaporization and viscous flow, (Hoier & Whitson, 2001, and references therein).

Belery and da Silva, (1990) presented a model that couple gravity and thermal diffusion in compositional grading for petroleum columns for a system of zero net

mass flux. They modified the (Dougherty & Drickamer, 1955)'s method for thermal diffusion to extend it to multi-component systems. They used Ekofisk Field in North Sea as a case history to illustrate their model. However, their model shows inaccurate comparison between the measured PVT properties and calculated data by the model.

Thermal diffusion may enhance, reduce, balance, or completely reverse the compositional gradients calculated by a GCE model (Hoier & Whitson, 2001; Whitson & Belery, 1994). The compositional gradients are consistently reduced when compared with the isothermal model for both thermal diffusion models based on thermodynamic expressions (Haase and Kempers) while models based on activation energy (Belery da silva) always give larger gradient than both isothermal and thermal models. These models are described represented by the following equations below. Figure 7-13 shows the predicted methane and plus fraction variations in Ekofisk field using isothermal model and all thermal models.

$$F_{Ti} = \frac{1}{M_m} \cdot (M_i H_m - M_m H_i) \quad \text{(Haase)}$$

$$F_{Ti} = \frac{1}{V_m} \cdot (V_i H_m - V_m H_i) \quad \text{(Kempers)}$$

$$F_{Ti} = -\frac{1}{2\bar{V}} \cdot (V_i \Delta U_m^* - V_m \Delta U_i^*) \quad \text{(Belery-da Silva)}$$

Where:

F_{Ti} = term including model for thermal diffusion, component i, J/kmol
H_i = partial molar enthalpy, component i, J/kmol
H_m = mixture enthalpy, J/kmol
M_i = molecular weight, component i, kg/kmol
M_m = mixture molecular weight, kg/kmol
V_i = partial molar volume, component i, m^3/kmol
V_m = mixture molar volume, m^3/kmol
ΔU_i^* = partial molar activation energy, component i, J/kmol
ΔU_m^* = viscosity-to-density ratio dependent term used to calculate ΔU_i^*, J/kmol

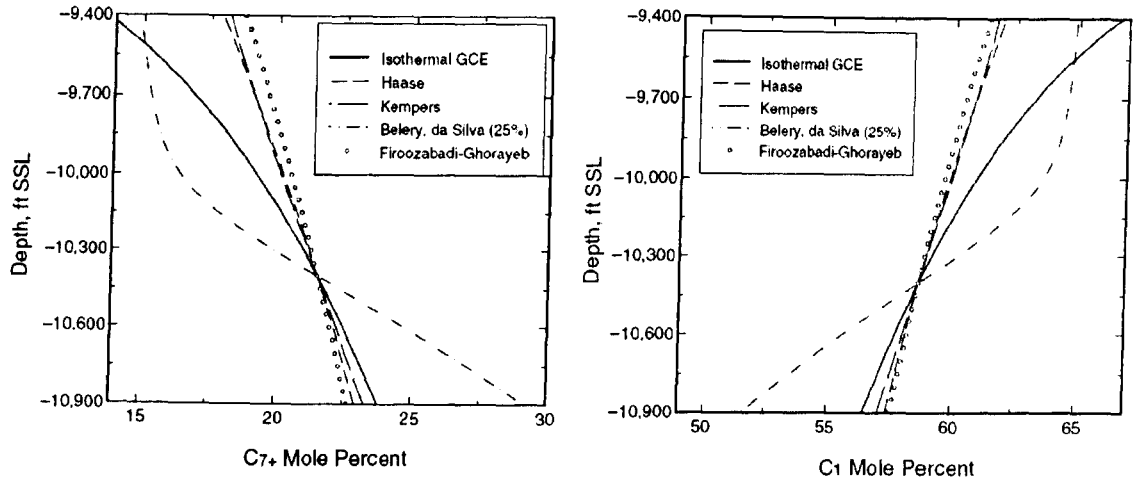

Figure 7-13: Predicted variations in methane and plus fraction in Ekofisk (North Sea) using isothermal model and other thermal models.

In near critical condition, the Belery da silva model generally counteracts gravity and might result in constant composition throughout the column until the fluid become away from the critical condition deeper in the reservoir, below which the Belery-da Silva model gives exaggerated gradients for C_{7+} and CH_4 (Whitson & Belery, 1994). Thermal diffusion effects might become larger than the gravity segregation effect in near critical systems and this may result in mechanically unstable conditions that would naturally induce convection (Hoier & Whitson, 2001). This may results in mixed system with more or less constant composition with depth.

(Whitson & Belery, 1994) presented comparison results between four different types of fluids in terms of compositional (CH_4 and C_{7+}) and PVT properties eg GOR, saturation pressure and density gradients based on both GCE and thermal/GCE models. They compared black oils, volatile oils, slightly volatile oils and near critical fluids. Their results show that the saturation pressure gradients for petroleum vary with different types of fluids and the largest gradient is observed in near critical fluid systems (about 1bar/m). The volatile systems show large non-linear saturation pressure gradients. They also show that under-saturation can reduce significantly the compositional grading for both gradient models.

Several case histories on compositional gradients were presented at SPE technical conferences in 1984 and 1985 and a special session of the 1985 SPE annual technical conference and exhibition was dedicated to this subject (Creek & Schrader,

1985; Metcalfe *et al.*, 1985; Montel & Gouel, 1984; Montel & Gouel, 1985). In some cases, the models predict strong compositional gradients while the measured data show constant compositions with depth sometimes over thousands of feet. Other reservoirs exhibit compositional gradients, which are larger than predicted by the isothermal model. These might result for many reasons that cannot be modelled readily with any quantitative uncertainty.

The mismatch between some of the physical properties gradients such as saturation pressures and GORs is observed despite the good match in composition, e.g. (Creek & Schrader, 1985). These authors concluded that their studied area exhibits varying degrees of compositional grading. Compositional gradients are not just controlled by thermodynamic properties; other controls might result in these variations as mentioned before. Wheaton, (1991) discussed the influence of the capillary pressure in the calculation of GCE predicted compositional gradients. His results suggested that neglecting compositional variations in a gas condensate reservoir might result in potentially large errors in the initial hydrocarbons in place. (Whitson & Belery, 1994) attributed these errors to neglecting the compositional variation due GCE and they thought that this can happen in both oil and condensate reservoirs. (de Oliveira Padua, 1997) studied a compositional gradient in large deep-water field and related PVT properties. He identified that besides temperature and gravity effect, there are other controls that cause these variations such as biodegradation, source maturity and secondary migration. Other factors such as permeability, porosity, and capillary pressure could also affect the gradients. Montel (2003) provided a mathematical model for dynamic reservoir fluid systems that involve gas diffusion due to biodegradation at the oil water contact. They found out that stripping is the main process behind the difference between the Oligocene and Miocene reservoirs.

Stainforth, 2004 suggests that many vertical gradients do not represent true isothermal or non-isothermal gradients, but they formed due to charge composition variation during filling. He proposed new models for reservoir filling and mixing by attributing the observed vertical compositional and properties variations throughout hydrocarbon columns to filling downwards from maturing source rocks. New charge advances to the top of the column and replaces old oil charge by pushing them down

due to the difference in density, which decreases with maturity. This model is opposing the well-known and widely accepted hypothesis of incomplete mixing and segregation after complete mixing (main controls of reservoir fluids heterogeneities) by proposing that equilibrium is attained by complete mixing starting with an initial heterogeneous state due to filling. According to Stainforth (2004)'s model, API gravity variations are controlled by maturity change of the source rocks and the shape of API-depth trends controlled by the interaction between the source rocks geometry and the trap geometry (volume versus depth). The GOR variations according to this model are explained by the interaction between the geometry of the trap as well as the PT conditions during trap filling. Several combinations for the API and GOR can be expected due to the difference between the trap and kitchen evolving history over geological ages.

Thompson, (2004) proposed the slope factor concept and gave explanation to some of the important charging related phenomena. Slope factors define the rates of exponential decrease in concentration of light n-alkanes (C3-C5) and liquid pseudo-components (P10+) with increasing carbon number. These two should increase with maturity and should be well correlated. However, the admixture of allochthonous gas or gas condensates frequently destroys this correlation. He also proposed that secondary gas enrichment is requisite for the formation of gas condensates by evaporative fractionation when the lower slope factor should exceed 1.69.

7.1.3 PVT samples

PVT reports

Eight PVT data reports were retrieved from PDO database for eight wells in the Greater Birba area as shown in Figure 7-14. However, these PVT analysis reports were done by different companies and at different times. The sample can be collected either as a single petroleum phase at the bottom hole, when the pressure is still above the saturation pressure value, or at the surface. The bottom hole samples are usually collected during formation testing prior to production. Surface sampling is conducted on producing wells either at the wellhead as the sample representing the producing mixture stream, or as a separated gas and liquid samples out of the separators. These

analysis were done on 3 bore hole samples and 5 recombined surface (separator) samples from the eight wells. Reservoir fluid samples should be sampled as early as possible during the production life of a reservoir to avoid samples taken after the reservoir pressure drops below saturation pressure. Most of the samples were taken some time after production. In that sense, they are not very representative of the original fluids. However, they can be representative of the present reservoir fluids and therefore they can be useful for geochemical purposes.

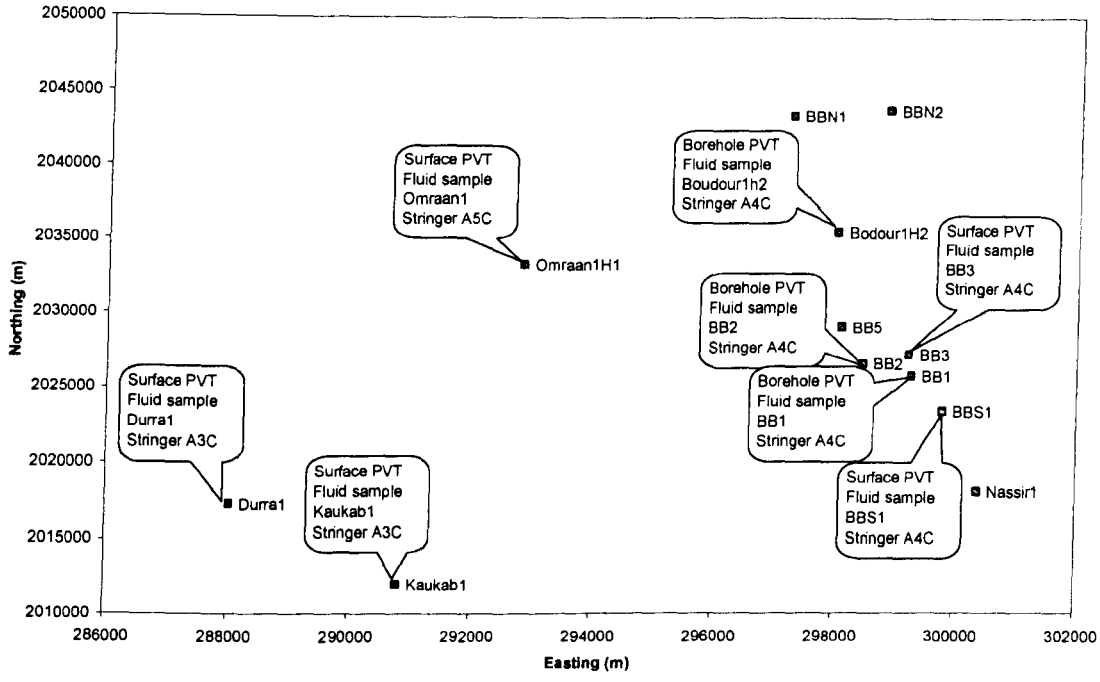

Figure 7-14: the distribution of the wells in the Greater Birba area with sample ids and reservoir units they were sampled from. Oil samples start with O and reservoir units start with A.

When the reservoir fluid is saturated and the compositional grading (composition systematically varies with depth) within the reservoir is minimal, the pressure-temperature at the gas oil contact identifies the saturation point as illustrated in Figure 7-11. Hence, the measured saturation pressure of the recombined fluid should be compared with the field data (measured during sampling). When there is a match between the two values for recombined samples, this indicates representative samples. When the oil bubble point is known with confidence, it is recommended to adjust the recombination ratio (gas oil ratio) to achieve it instead of relying on the field gas oil ratio (calculated from numerically combining the separator oil and gas flows) (Danesh, 1998). This might be more difficult in gas condensates and very often, there is big difference between field gas oil ratio (measured gas oil ratio at field) and

predicted gas oil ratio using dew point pressure (Danesh, 1998). The dew point pressure might increase or decrease when increasing gas condensate ratio, depending on the sample (Danesh, 1998). All the PVT data available for this study are listed in Table 7-1.

Table 7-1: The real PVT data for all studied samples.

	Components mole%	BB1	BB2	BBS1 Expro	BBS1 KSPL	BB3	Budour 1H2	Durra 1	Omraan 1	Kaukab 1
Nitrogen	N2	0.59	0.71	0.32	0.86	0.48	0.95	0.63	0.41	0.38
Carbon Dioxide	CO2	3.39	3.84	2.84	3.89	3.65	3.68	4.99	6.03	3.97
Hydrogen Sulfide	H2S	2.29	1.17	0.9	0.58	2.72	0.93	2.39	3.83	2.91
Methane	C1	59.33	59.49	73.52	74.66	53.58	78.85	65.92	53.9	50.68
Ethane	C2	5.04	5.55	6.38	5.5	5.11	5.96	4.95	4.71	4.44
Propane	C3	3.66	4.06	3.07	3.46	4.14	3.16	3.53	3.69	3.72
iso-Butane	i-C4	0.47	1.13	0.37	0.43	0.56	0.35	0.47	0.54	0.52
n-Butane	n-C4	1.67	1.93	1.38	1.51	2.2	1.29	1.57	1.68	1.94
iso-Pentane	i-C5	1.02	0.49	0.31	0.39	0.58	0.33	0.47	0.47	0.64
n-Pentane	n-C5	1.19	1.09	0.9	0.89	1.36	0.69	0.98	0.87	1.37
pseudo Hexane	C6	1.45	1.27	1.32	1.21	1.76	0.79	1.2	1.44	1.82
pseudo Heptane	C7	1.06	1.38	1.22	0.76	1.82	0.66	12.9	22.43	27.61
pseudo Octane	C8	1.52	1.6	1.02	0.87	2.03	0.52			
pseudo Nonane	C9	1.51	1.23	0.87	0.72	1.66	0.36			
pseudo Decane	C10	1.37	1.17	5.58	0.62	1.5	0.28			
pseudo Undecane	C11	1.38	1.01		0.49	1.29	0.22			
pseudo C12H26	C12	0.95	0.86		0.38	1.1	0.17			
pseudo C13H28	C13	0.95	0.85		0.37	1.1	0.15			
pseudo C14H30	C14	0.93	0.77		0.31	0.99	0.12			
pseudo C15H32	C15	0.74	0.71		0.25	0.9	0.09			
pseudo C16H34	C16	0.92	0.64		0.21	0.75	0.07			
pseudo C17H36	C17	0.72	0.56		0.21	0.69	0.06			
pseudo C18H38	C18	0.56	0.51		0.18	0.66	0.05			
pseudo C19H40	C19	0.56	0.48		0.16	0.51	0.04			
heavy end	C20	6.73	7.5		1.07	8.87	0.21			
molecular weight of plus fraction	Mol Wt Cn+	266	297.4	181		539.5	334.7	272.2	531.6	288.1
density of the plus fraction	Density Cn+ (kg/m3)	0.873		0.827	0.8031	0.943	0.889		0.88	0.883
True vertical depth of sampling or producing interval	Depth TVD m	2511	2556	2321.2	2321.2	2618		2666.4	2608	2525
Reservoir pressure bar		528.5	531.1	520.4	520.4	418	418	566.9	536.1	548.2
Reservoir temperature °C		73.9	70	68.33	68.33	70	75.6	76	71.1	71
Bubble/Dew point pressure bar		460.2	474.7	482.4	473.8	380.4	368.5	576.1	359.5	309.4
GOR Sm^3/Sm^3		282.3	260.9	1076.5	1103	135.2	344.2	483.6	189	168
density (at surface conditions) kg/m^3		0.862	0.8661	0.8	0.7899		0.788	0.863	0.869	0.881
Reservoir unit		A4C	A4C	A4C	A4C	A4C	A3C	A3C	A5C	A3C
Type of samples		BHS	BHS	SS	SS	SS	BHS	SS	SS	SS
sampling date or report date		1978	1979	1981	1982	2001	2002	1984	1981	1984

* Each column represents the compositions and PVT properties for a PVT sample from each well.

** BBS1 was samples twice by Expro in 1981 and by Shell (RKTR) in 1982. ***BHS bore hole sample, SS surface sample.

Evaluation of samples

To evaluate those samples, I have compared between measured bubble point pressures and predicted saturation pressures and between measured gas oil ratios and predicted GOR using saturation pressure with the aid of PVTsim and the data are shown in Table 7-2 and illustrated in Figure 7-15. The predictions were done using Soave-Redlich-Kwong (SRK) equation of state (Soave, 1972) with Peneloux volume correction (Peneloux et al., 1982) using PVTsim 14. Clearly, the bore-hole samples (BH) show close measured and predicted bubble point pressures including those which are thought to have strong compositional grading (BB1 and BB2, Riemns *et al*, 1985). Most of the separator samples show good match between measured and predicted bubble point pressures. However, Birba south 1 (BBS1) shows large difference between measured and predicted bubble point pressures. There is a slight difference in BB3 (BB3) and Omraan1 separator fluid samples. The predicted gas oil ratios by recombination using saturation pressures and measured separator gas oil ratios are good indicators of quality of separator samples. The prediction again is based on the same equation of state above. Four out of five samples show good agreement suggesting good representation of the reservoir fluids. BBS1 fluid shows significant difference between the two values especially the later. However, it must be emphasized that this agreement between the measured and predicted bubble point pressures and gas oil ratios does not prove by any means the reliability of the surface PVT samples. This is because if there is error in determining the amount of gas or liquid from the separator, there will be definite error in determining the gas oil ratio. Therefore, the surface samples must be treated with caution.

Table 7-2: comparison between measured bubble point pressures and predicted bubble point pressures and comparison between measured GOR at field and predicted GOR by PVTsim.

Wells	Unit	TVD m	sampling date	P bar reservoir	T °C reservoir	Pb bar	Pb Predicted bar	GOR Sm^3/Sm^3	GOR predicted Sm3/Sm3
BB1	A4C	2533.1	Apr-79	528.5	73.9	460.2	441.8	282.3	BH
BB2	A4C	2554.8	Nov-79	531.1	71	474.7	482.3	260.9	BH
BB3	A4C	2661.8	Aug-01	418.0	70	380.5	360.1	135.2	155.2
BBS1	A4C	2343.4	Mar-81	520.3	68.3	482.4	344.4	1076.5	2387.6
Budour 1H2	A4C	2963.7	Aug-02	418.0	75.6	368.5	377.2	3442.6	BH
Kaukab 1	A3C	2504.1	Oct-83	548.2	72	309.4	311.1	150.5	144.4
Omraan 1	A3C	2608.9	May-81	536.0	71.1	359.5	381.1	171.7	188.7
Durra 1	A3C	2666.4	Feb-83	567.9	76	563.6	540.1	404.4	396.4

TVD: True vertical depth, P: pressure, P_b: Bubble point pressure for oils and dew point pressure for condensates (BBS1 and Bud our 1h2). GOR: gas/oil ratio.

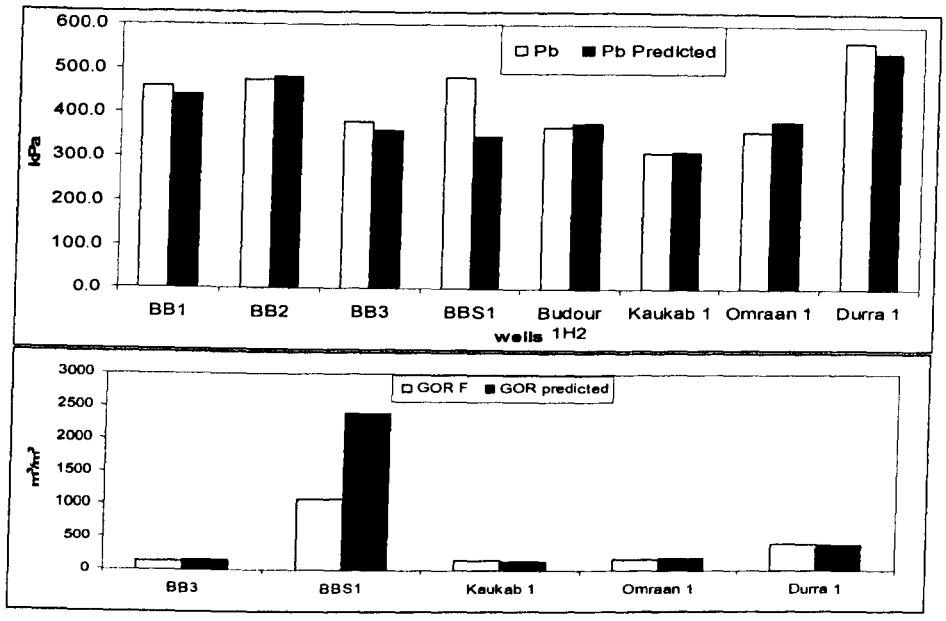

Figure 7-15: Histograms showing the comparison between measured values for bubble point pressures (top) and gas oil ratios GOR (bottom). The prediction was performed with the aid of the PVT sim package version 14 developed by Calsep. No tuning or regression was performed on these data.

7.2 PVT modelling of different fluid samples

7.2.1 Cubic Equations of state

The classical method of modelling phase equilibria of reservoir fluids is to use a cubic equation of state. Equation 7-3 shows one of these equations that are frequently used to predict PVT behaviour of petroleum fluids. These type of equation are sophisticated versions of the original equation of state that was designed for ideal gases (PV=RT) by considering compressibility factor (mutual interaction of individual molecules with each other) in the real gases. All petroleum fluids in the Greater Birba area are modelled using the above cubic equation of state (Soave-Redlich-Kwong (SRK) equation of state (Soave, 1972) with Peneloux volume correction (Peneloux et al., 1982)) using PVTsim 14. It was found empirically that this equation is the most suitable equation for the study fluids.

Equation 7-3: Soave-Redlich-Kwong equation (Soave, 1972) with Peneloux volume correction (Peneloux et al., 1982).

$$P = \frac{RT}{V-b} - \frac{a}{(V+c)(V+b+2c)}$$

P Pressure, T temperature, V Peneloux molar volume, R universal gas constant, a, b and c are equation of state constants for each component in the petroleum fluid and these are calculated based on critical conditions.

In order to simulate fluid behaviour in a complex 3D model of reservoirs, the composition of the fluid generally is simplified in a few pseudo-components. Normally the defined components consist of methane through normal hexane, the main non-hydrocarbon gases (e.g. CO_2, H_2S, & N_2) and the heavier than C_7 components expressed as single carbon number fractions. Dependent upon the analytical techniques used to determine the composition, the molecular weights of the single carbon number fractions and the plus fraction (the heavy components e.g. C_{7+} or C_{10+}, explained next section) can influence the overall composition. Using these input data as well as density of the plus fraction, the cubic equation of state can predict fluid properties like saturation pressure, formation volume factor, density, viscosity and gas oil ratio. Each PVT sample should be measured for some of these properties as will be mentioned later (section 7.2.3), which makes it easier to choose which equation of state will give the best model for this fluid.

7.2.2 Plus fraction Characterization

PVT samples in this study were collected and supplied by various companies (different labs) and each lab has its own standards. As clear in Table 7-1, different fluids show different plus fractions or heavy ends (it is called C_{7+} fraction by PVT sim); some oils have C_{7+} (e.g. Omraan1 in Table 7-1), some have C_{10+} and some others have C_{21+} (e.g. BB1 in Table 7-1). Therefore, for the best results, all samples were re-characterized by 12 C_{7+} fractions as clear in Table 7-3. This characterization was chosen to avoid the effect of lumping on the modelled fluids; we tried to lump some of these fluids to one or more C_{7+} and the models were well away from the real data (e.g. there is no match at all between measured bubble point pressure and predicted values, data are not shown here). This characterization resulted in less

tuning was performed on most of the fluids. The 12 C_{7+} fractions are C_7, C_8, C_9, C_{10}, C_{11}, (C_{12}-C_{13}), C_{14}, C_{15}, (C_{16}-C_{17}), (C_{18}-C_{20}), (C_{21}-C_{24}), and (C_{25}-C_{80}) (Table 7-3). However, comparison of the results was by back lumping these fractions to C_{7+} to be able to compare the row data with the modelled values because the compositions of most of the fluids were measured to this plus fraction.

Table 7-3: The characterization of the petroleum fluids in the Greater Birba area using Soave-Redlich-Kwong (SRK) equation of state (Soave, 1972) with Peneloux volume correction (Peneloux et al., 1982)) using PVTsim 14.1. Compared with the raw data in Table 7-1.

Component mol%	BB1	BB2	BB3	BBS1 EXPRO	Budour1h2	Kaukab1	Durra1	Omraan1
N2	0.594	0.71	0.482	0.322	0.95	0.375	0.631	0.4
CO2	3.411	3.84	3.664	2.854	3.681	3.915	4.995	5.883
H2S	2.304	1.17	2.73	0.905	0.93	2.869	2.392	3.737
C1	59.695	59.49	53.782	73.895	78.863	49.973	65.984	52.589
C2	5.071	5.55	5.129	6.413	5.961	4.378	4.955	4.595
C3	3.683	4.06	4.156	3.086	3.161	3.668	3.533	3.6
iC4	0.473	1.13	0.562	0.372	0.35	0.513	0.47	0.527
nC4	1.68	1.93	2.208	1.387	1.29	1.913	1.572	1.639
iC5	1.026	0.49	0.582	0.312	0.33	0.631	0.47	0.459
nC5	1.197	1.09	1.365	0.905	0.69	1.351	0.981	0.849
C6	1.459	1.27	1.767	1.327	0.79	1.795	1.201	1.405
C7	1.067	1.38	1.415	1.226	0.66	2.021	0.909	1.621
C8	1.529	1.6	1.331	1.025	0.52	1.879	0.845	1.514
C9	1.519	1.23	1.252	0.874	0.36	1.747	0.785	1.414
C10	1.378	1.17	1.178	0.911	0.28	1.624	0.73	1.32
C11	1.388	1.01	1.108	0.748	0.22	1.51	0.678	1.233
C12-C13	1.912	1.71	2.022	1.119	0.32	2.709	1.216	2.225
C14	0.936	0.77	0.922	0.415	0.12	1.213	0.544	1.003
C15	0.745	0.71	0.867	0.34	0.09	1.128	0.506	0.937
C16-C17	1.65	1.2	1.583	0.509	0.13	2.024	0.907	1.692
C18-C20	1.318	1.41	2.039	0.471	0.134	2.533	1.135	2.14
C21-C24	0.721	1.146	2.197	0.319	0.102	2.621	1.172	2.248
C25-C80	5.244	5.934	7.658	0.266	0.067	7.611	3.387	6.969
Bubble/dew point pressure bar	457.6	475.9	380.4	480.8	369.0	309.4	564.0	369.0
Gas oil ratio (GOR) Sm3/Sm3	265.3	256.9	195.5	1111.6	3617.6	168.3	468.5	198.8
API gravity	30.2	31.3	30.3	47.4	45.2	32.8	33.6	35.7

7.2.3 Regression of the fluid models

It is extremely important to tune the equation of state (EOS) for all PVT samples and is recommended that one EOS should be used for all samples used in the study for reliable and comparable results (Whitson and Belery, 1994). It is not important what EOS to use as long as the measured data are well fitted in the model. The EOS tuning accounts for critical properties, acentric factors, and binary interaction coefficients (de Oliveira Padua, 1997). The petroleum fluids are normally characterized with one (C_{7+}) or four (C_{10+}) or six (C_{12+}) C7+ fractions (Whitson and Belery, 1994).

The EOS models chosen for each fluid are listed in Table 7-3. Most of the fluid models give good prediction of PVT properties with small deviation from the measured values as shown before (Figure 7-15 & Table 7-2) and as will be also shown here in this section. Therefore, little slight tuning will be done on those fluids. BBS1 and BB3 need a lot of tuning because they show a large departure from the measured values (see Figure 7-15).

There are several PVT experiments routinely performed on PVT samples, to enable us modelling the PVT fluid samples as accurate as possible. These experiments include in addition to the measurements of viscosity and bubble point pressure:

- Constant mass expansion: during this experiment, the reservoir fluid is kept in a cell at reservoir conditions and the pressure is reduced in steps at constant temperature and the change in volume is measured. The saturation point volume is used as a reference value and the results presented are relative volumes, i.e., the volumes divided by saturation point (bubble point for oil and dew point for condensates) pressure volume.
- Constant volume depletion: This experiment is performed for gas condensates and volatile oils. The reservoir fluid is kept in a cell at reservoir temperature and saturation point pressure. The pressure is reduced in steps, and at each level so much gas is removed that the volume of the remaining gas and oil mixture equals the saturation point volume. The main output used in this study from this experiment is the amount of liquid remaining (% of volume at saturation point).
- Differential depletion: This experiment is only carried out for oil mixtures. The reservoir fluid is kept in a cell at the reservoir temperature and then the pressure is reduced in steps and all the liberated gas is displaced and flashed to standard conditions, i.e. 1 atm and 15 °C. This procedure is repeated 6-10 times. The final pressure is usually 1 atm. At the end the temperature of the cell is lowered to 15 °C. The main output used in this study from this experiment is the oil

density increase of the remaining fluid with successive liberation of gas during stepwise pressure reduction.

- Separator experiments: A separator experiment is started at the saturation pressure at the reservoir temperature and the volume and the density are recorded. Subsequently a series of PT flash separations is performed. The gas phase from each separator stage is flashed to standard conditions (1 atm and 15 °C). The liquid phase is let to a new separator in which a new PT flash separation takes place, and so on. The last separator is at atmospheric conditions. The main output from this experiment is series of GOR with stepwise pressure reduction.

Not all of these data might be available in each and these data can help us to tune equation of state used to predict fluid models in Table 7-3, to give the best prediction of the fluid behaviour at reservoir and surface conditions. The main tuning parameters are critical temperatures and pressures and the acentric factors of the single carbon number fraction and the plus fraction. These parameters are derived from various correlations based upon the molecular weight and density (Danesh, 1998).

7.2.3.1 The PVT fluid sample from reservoir A4C of Well Birba 1 (Oil)

This sample is a borehole sample that was taken from A4C reservoir. The SRK-P predicted saturation pressure is about 4% less than the measured bubble point pressure, which is a good match (Table 7-2 & Figure 7-15). However, minor tuning was done to match the relative volume increase with releasing pressure from constant mass expansion experiment and that was predicted by equation of state (Figure 7-16). The model shows a good match between the oil density decrease with increasing pressure from differential depletion experiment and the oil density decrease predicted by equation of state chosen to model this petroleum fluid (Figure 7-16).

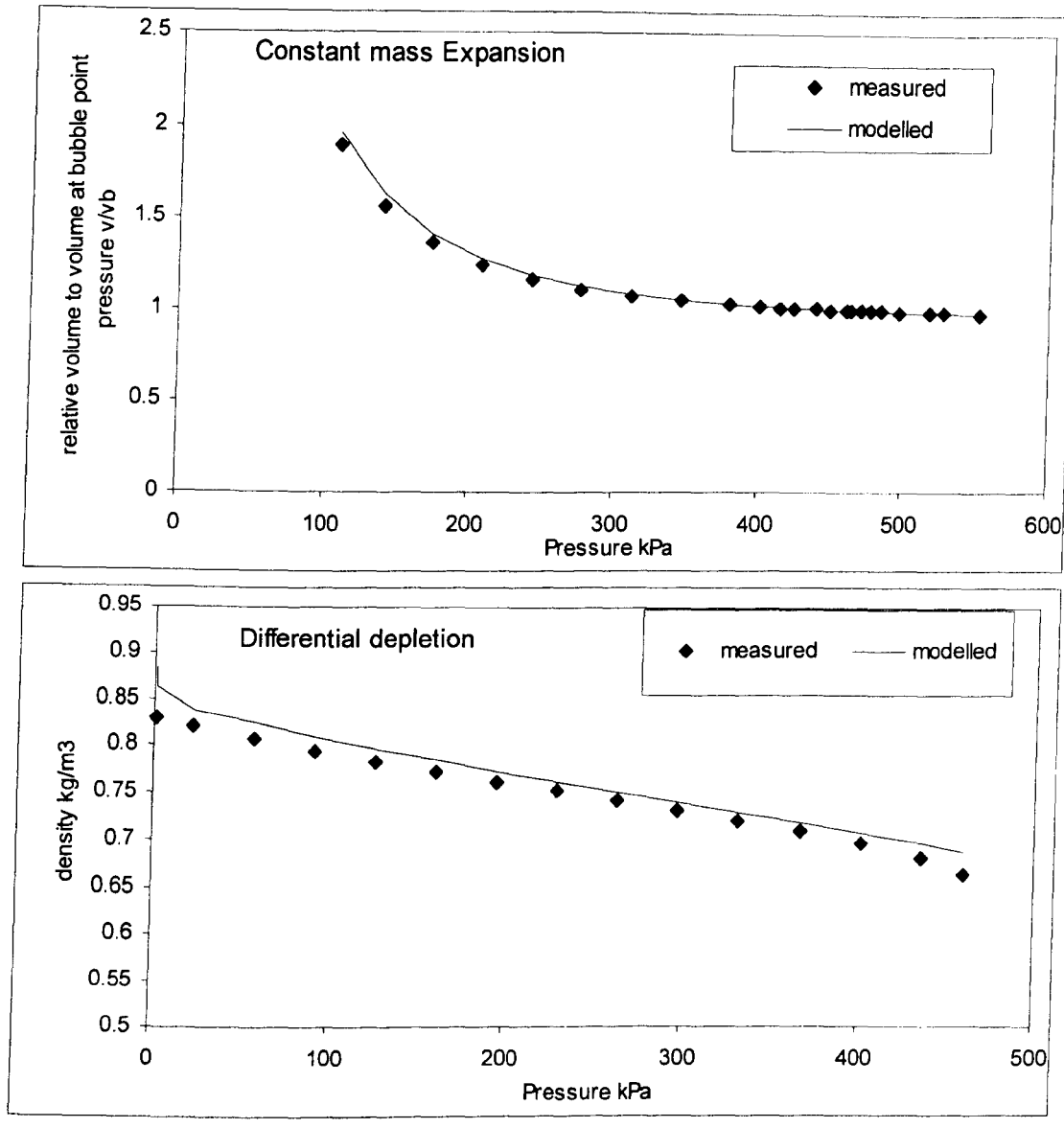

Figure 7-16: Correlation between PVT experimental data and predicted data by the cubic equation of state used to model this petroleum fluid (oil); constant mass depletion (top) and differential depletion (bottom).

7.2.3.2 The PVT fluid sample from reservoir A4C of Well Birba 2 (Oil)

No PVT experimental data are available for this fluid except separator data and saturation pressure. It was regressed against those data and produce a model with a very close predicted properties to those measured. This is not quite accurate though due to limited measured data. If there is an error in the measurement of these data, this will lead to a wrong model. However, this is assumed to be the right model.

Table 7-4: comparison between separator measured gas oil ratios (GOR) and predicted GOR by equation of state at two different PT conditions. Std is standard deviation of the two different GOR (measured and predicted) and CV is coefficient of variation (std/average) to measure the departure of predicted GOR from the measured GOR.

Pressure kPa	Temperature °C	GOR measured	GOR predicted	std	average	CV
26.96	22.78	228.5	230.1	1.13	229.3	0.005
1.01	22.78	32.4	26.8	3.96	29.6	0.134

7.2.3.3 The PVT fluid sample from reservoir A4C of Well Birba 3 (Oil)

This fluid is difficult to tune as there is no data to regress against except saturation pressure. Apparently the fluid is behaving well and shows a good match between measured saturation pressure and predicted value (Figure 7-15). Furthermore, when recombining the separator fluids to get the monophasic fluid using cubic equations of state adjusted to saturation pressure, the gas oil ratio predicted is very close to the separator measured value (Figure 7-15).

7.2.3.4 The PVT fluid samples from reservoir A4C of Well Birba South 1 (BBS1) and Budour1H2 (Gas condensates)

There are two PVT fluid samples from A4C of Birba South1. Each PVT sample was measured by different lab, KSPL (Shell) and EXPRO. The former only provide composition and bubble point pressure (Table 7-1) with a separator test data. The later provides a full package of all measurements needed to tune a model. Therefore, the full report provided by EXPRO was used to model the gas condensate in BBS1. This gas condensate is difficult to be tuned because it is gas and is near its critical point. I tried to regress it carefully possible, however the final tuned model failed to find a critical point for the fluid (Figure 7-17).

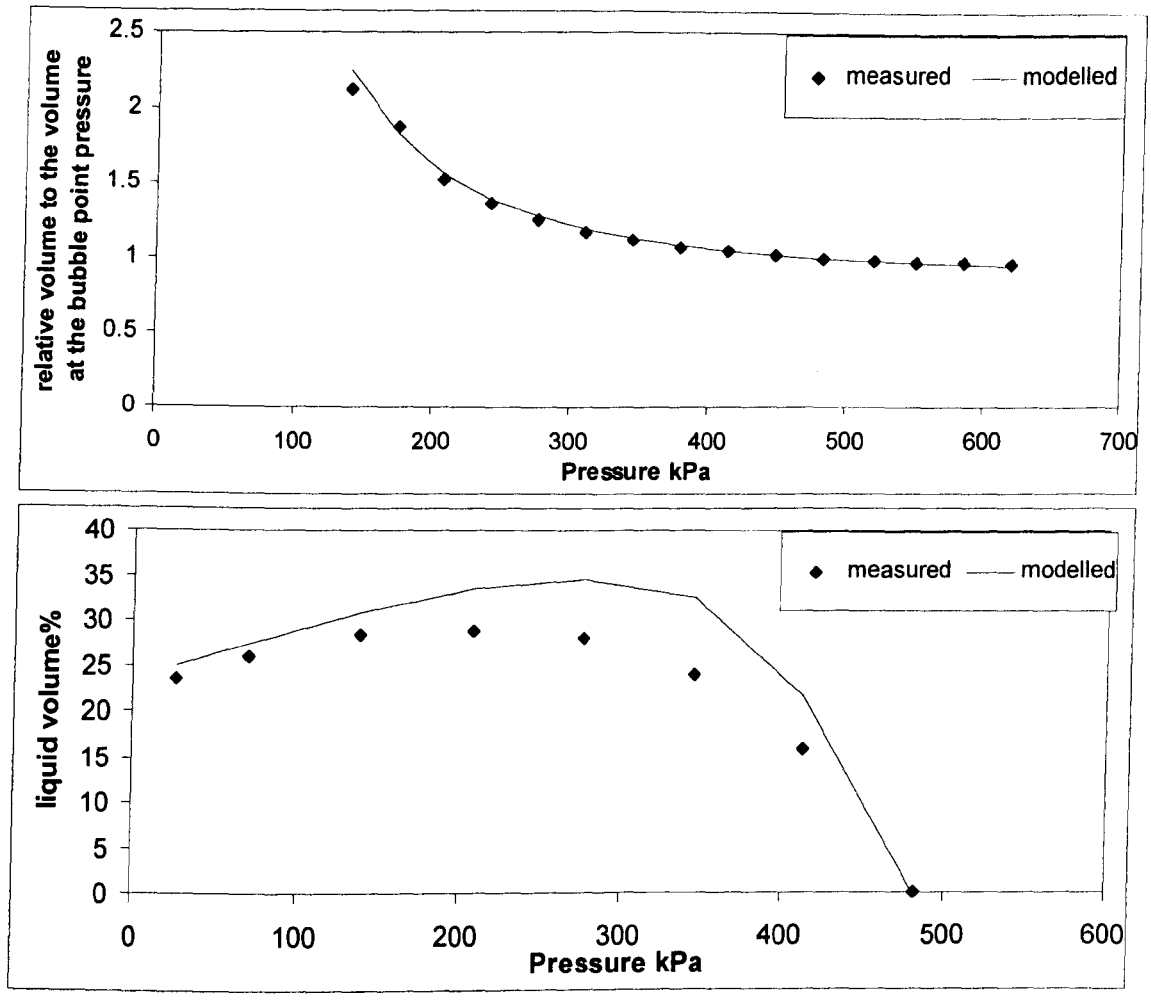

Figure 7-17: Constant mass expansion (Top) and constant volume depletion (Bottom) experimental data for Birba South1 PVT Condensate sample.

Budour1 has a full PVT report and enough data to be tuned to (Figure 7-18) but the same problem exist as no critical point was found by the SRK modelling of this fluid. Apparently, this is more likely to be the case, I presume, with gas condensates. Critical properties calculations are based on specific gravity, boiling point and/or molecular weight of single carbon groups. The first two can be used to calculate the critical temperature and pressure of the fluid (Danesh, 1998). Therefore, incorrect measurement of these two properties might result in an unrealistic critical point or an absence of a critical point in a model run.

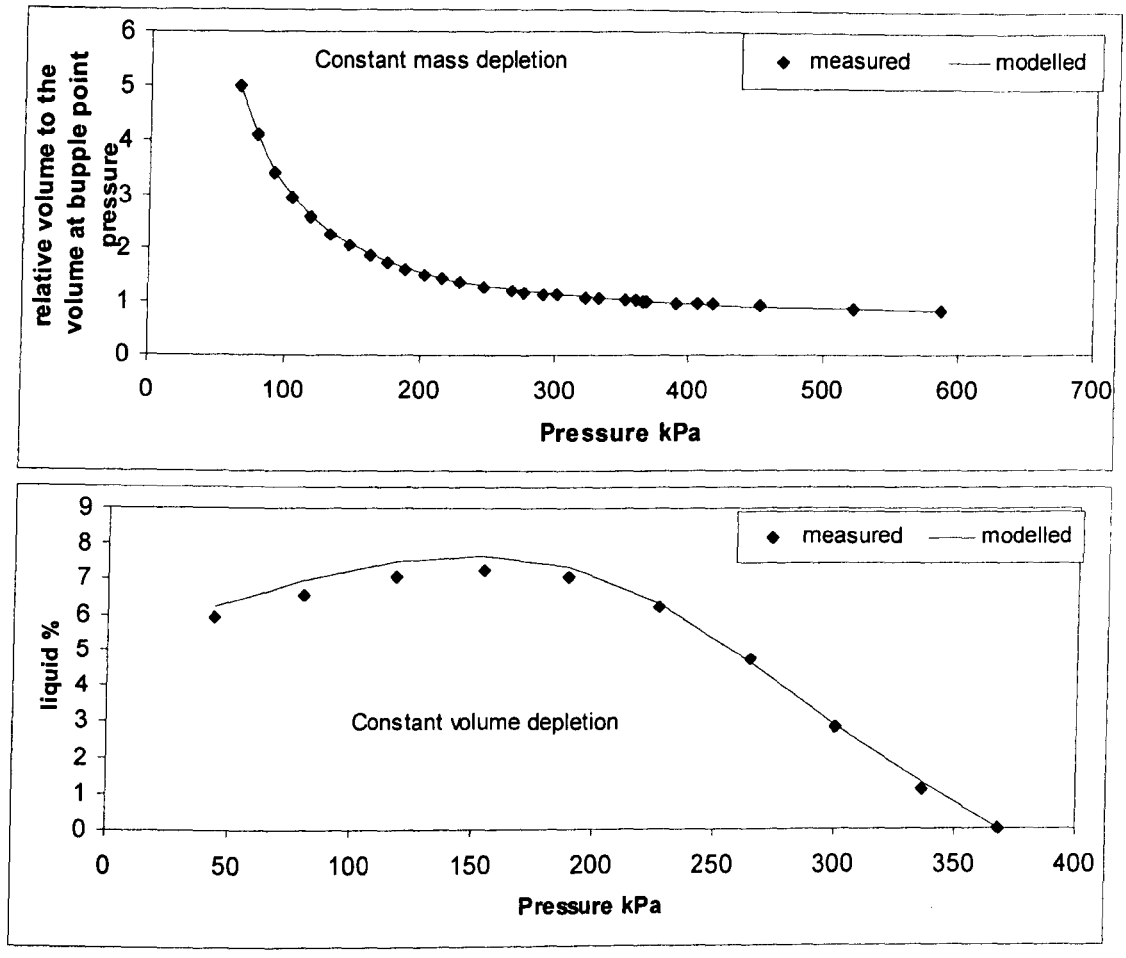

Figure 7-18: Constant mass expansion (Top) and constant volume depletion (Bottom) experimental data for Budour1H2 PVT Condensate sample.

7.2.3.5 The PVT fluid samples from reservoir A3C of Well Kaukab1, and Durra1 and a PVT sample from A5C of well Omraan1 (Oils)

These three petroleum fluids have all necessary data to regress their models. The first two are well-behaved fluids and show a good match between the model and PVT data without any tuning (Figure 7-19 and Figure 7-20).

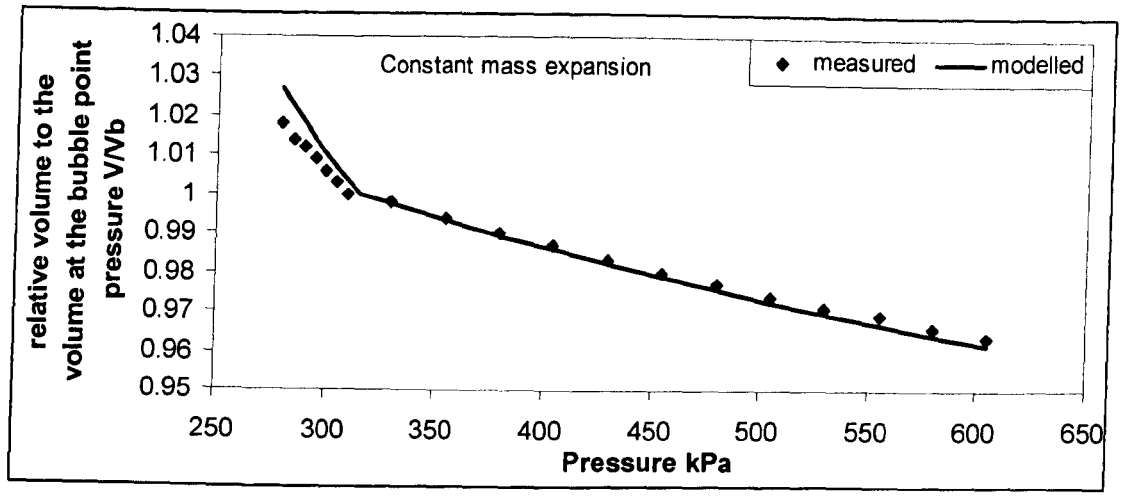

Figure 7-19: Constant mass expansion of the Kaukab PVT sample by lab experiment (measured values) and predicted values (modelled values) by Soave-Redlich-Kwong (SRK) equation of state (Soave, 1972) with Peneloux volume correction (Peneloux et al., 1982) using PVTsim 14.1.

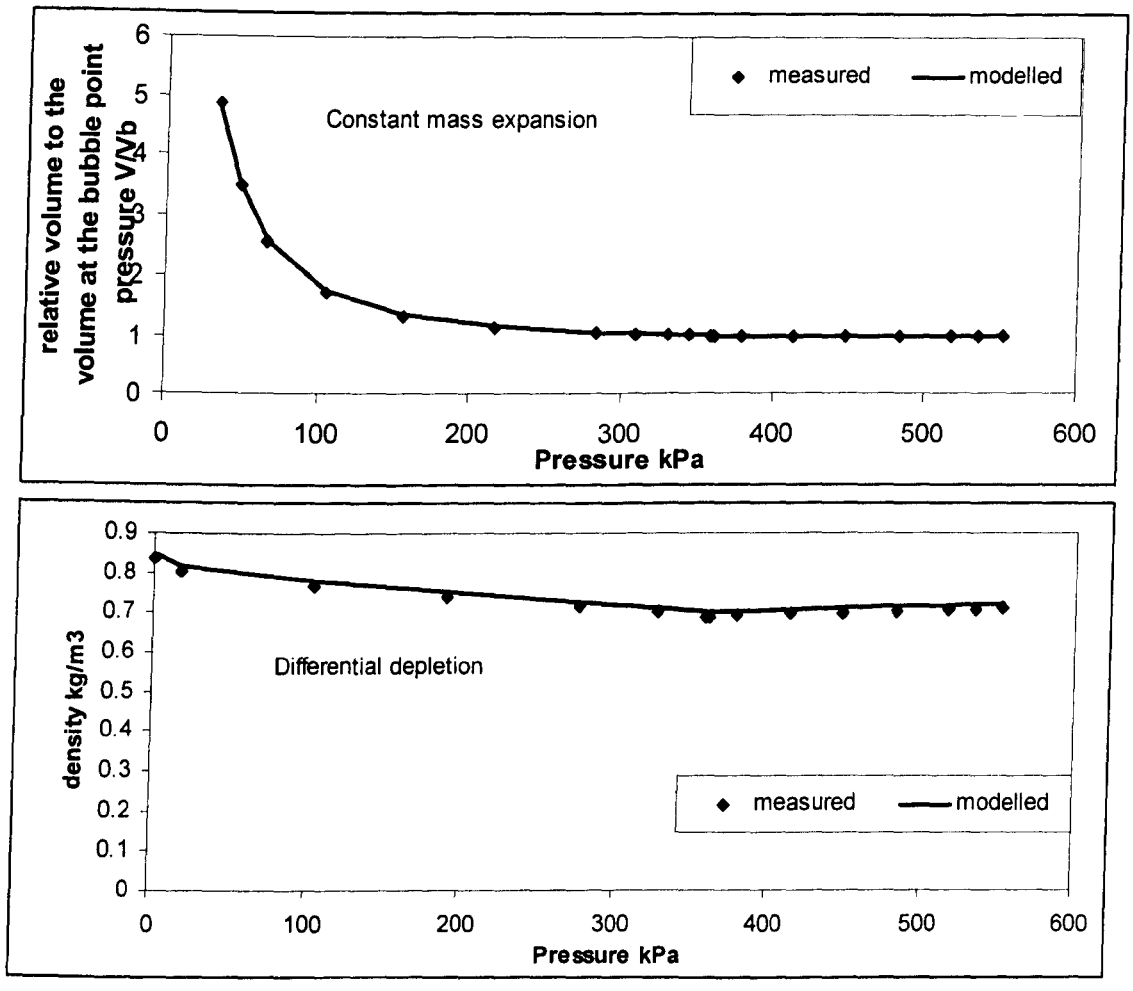

Figure 7-20: Constant mass expansion and differential depletion experimental data for Omraan1 PVT sample. (Oil)

The Durra1 fluid shows near critical behaviour and so it was regressed rigorously to get the best model of the fluid using constant mass expansion and differential depletion experimental data. Figure 7-21shows a good match between the measured data and the predicted values by the final tuned model.

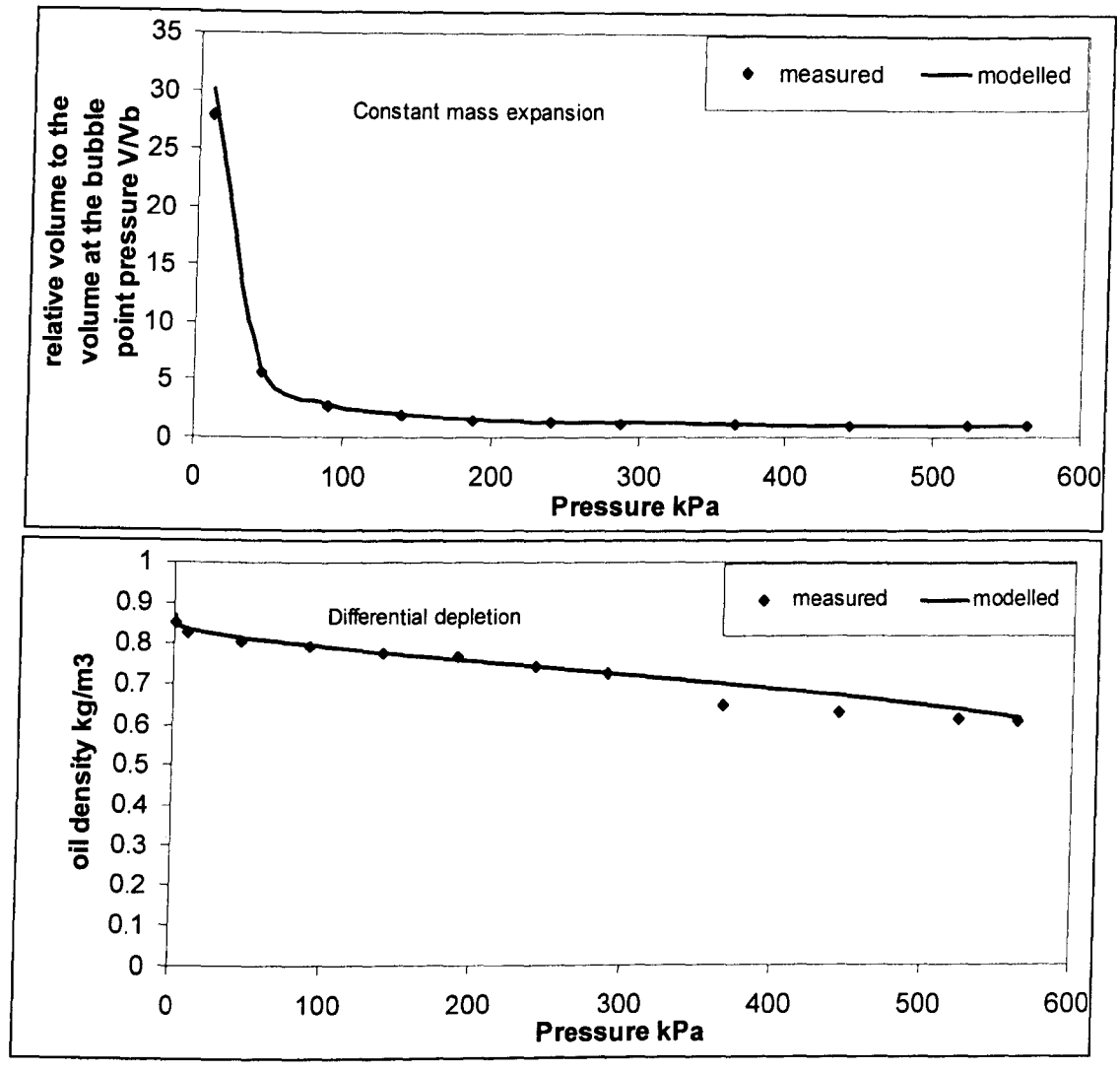

Figure 7-21: constant mass expansion and differential depletion experimental data for Durra1 PVT sample. (Oil)

7.3 Discussion

7.3.1 The phase relationship between Greater Birba area petroleum fluids

The phase behaviour of a petroleum fluid is usually described by a pressure vs. temperature envelope or diagram but it can also be described by means of specific physical properties such as saturation pressure or gas oil ratio. In this work, both methods are used to explore the phase relationship between petroleum fluids in the Greater Birba area. The phase envelope consists of a region where a fluid occurs in a single-phase state and a region where it exists as two separate phases. The two-phase region is enclosed by a bubble point curve and a dew point curve as shown previously in Figure 7-5. The bubble point curve marks the PT conditions where separation of a gas phase from a supercritical liquid phase takes place, while the dew point curve marks the PT conditions where separation of a liquid phase from a supercritical gas phase occurs. The 'critical point', located where bubble point and dew point curves meet, characterises fluid conditions intermediate between those of a liquid and a vapour phase. The software 'PVTsim 14' is used to predict the phase envelopes of the petroleum fluids using SRK equations of state with Peneloux volume correction. Those equations of state however can only be tuned to reservoir conditions and the rest of the phase envelope is totally predicted rather than measured and model accuracy is difficult to assess because measurements are not commonly made at these pressures and temperatures (Di Primio et al., 1998). The phase envelope shape depends strongly on the composition of the fluid analysed. The strongest compositional control on phase behaviour of a fluid is the quantity of light hydrocarbons (gas) dissolved in the liquid phase (oil), described as the gas-oil ratio (GOR). The GOR used in this work is defined as the gas oil ratio measured at surface conditions (1Bar, 15°C) and reported in original PVT reports. The concentration, density and molecular weight of individual compounds or compound classes of petroleum also have strong effects on the phase behaviour of petroleum systems. Therefore, those properties are extremely important to accurately characterise a petroleum fluid (Danesh, 1998; Di Primio et al., 1998). A detailed literature review is presented in the Introduction chapter of this thesis.

The GOR of petroleum is reported to increase systematically with increasing source maturity e.g. (Dueppenbecker & Horsfield, 1990; Hughes *et al.*, 1985). The

molecular weight and density of petroleum is also known to change regularly with maturity e.g. (Baskin & Peters, 1992; di Primio & Horsfield, 1996; Tissot & Welte, 1984). However, those properties can also be altered by facies variations (di Primio, 2002) and other secondary processes such as uplift (di Primio, 2002), phase fractionation (Thompson, 2004), oil mixing (Di Primio et al., 1998) and biodegradation (Larter *et al.*, 2000a). It has been shown previously that the studied oils from the Greater Birba area are mainly derived from similar source facies with only minor facies variations, and that they are probably at similar maturity. Figure 7-22 shows a cross-plot of GOR and saturation pressure of the modelled petroleum fluids of the Greater Birba area versus the maturity parameter vitrinite reflectance equivalent (based on methylphenanthrene index (MPI-1)). High GOR oils are generally characterised by high bubble point pressures, while petroleum fluids with high proportions of high molecular weight material (C7+ fraction) are characterised by high dew point temperatures.

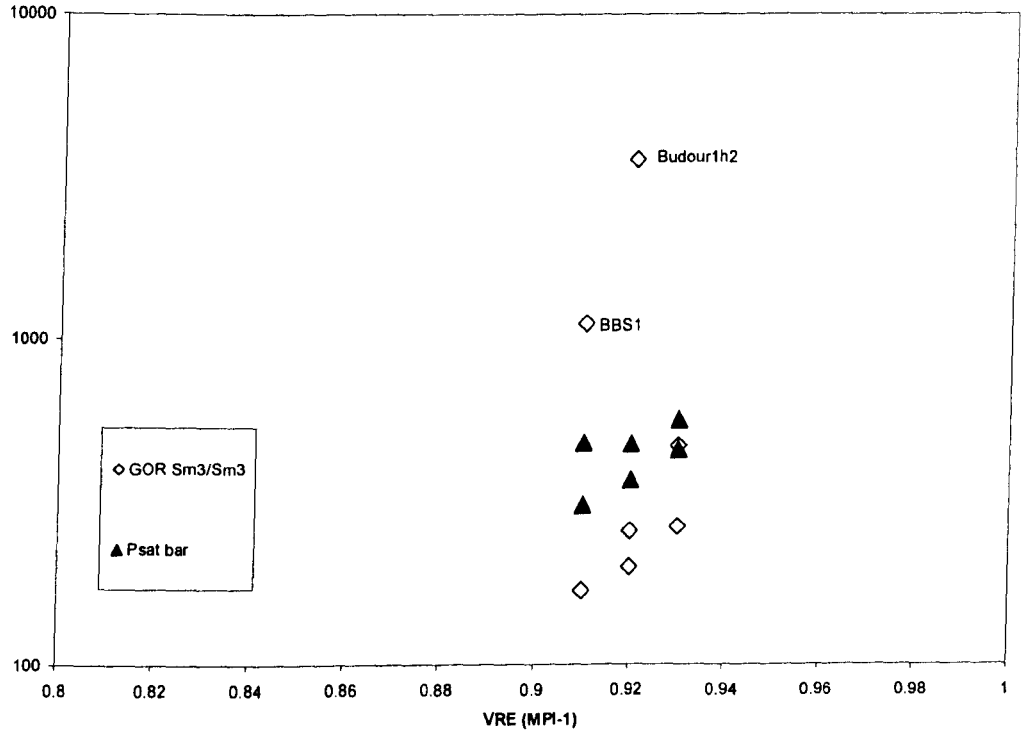

Figure 7-22: Cross-plot of gas oil ratios Y axis (GOR Sm^3/Sm^3) and saturation pressure (Psat bar) versus vitrinite reflectance equivalent based on methylphenanthrene index (MPI-1).

The phase envelopes and critical points of the petroleum fluids in the Greater Birba area, shown in Figure 7-23, reveal two main groups (comprising black oils) in addition to gas condensates. The petroleum fluid from well Durral (A3C) shows a

completely different envelope and critical point, and forms a different group to the rest. There is an increase in dew point temperature and bubble point pressure from well Kaukab1 (A3C) through well Omraan1 (A5C), well BB3 (A4C) and finally to well BB2 (A4C) and well BB1 (A4C). The critical point, however, remains similar. This is a typical mixing sequence (di Primio, 2002) and will be tested further when I look at the origin of the Birba 3 and Durra1 fluids later in this section. Evidence has been presented elsewhere in this thesis to suggest that the original petroleum fluids in the Greater Birba area have been subjected to condensate mixing to various extents. It will be shown later in this section, that the BB3 fluid (main Birba field, 100 m below BB1) may result from mixing of BB1/Kaukab1 oils, and that the Durra1 oil (from the A3C reservoir unit, SW of the Birba field) can also be predicted by mixing Kaukab1 oil with a Budour condensate. This is significant, as it supports the condensate-oil mixing theory proposed for the distribution of the petroleum fluids in the Greater Birba area, and supported by various data.

The gas condensates from well BBS1 and well Budour1H2 show different phase-envelopes with much lower dew point temperatures due to the low amount of the C7+ fraction and the high amount of methane. No critical points were found for the gas condensates from well BBS1 (A4C) and well Budour1H2 (A4C) gas condensates, i.e. there is no bubble point curve for these condensates. The well BBS1 condensate shows a similar saturation pressure to the associated black oils from well BB1 and well BB2; this indicates (as previously mentioned) that these two phases are in equilibrium as is also inferred by the interference pressure response, according to (Riemens et al., 1985). Riemens et al. (1985) proved that there is continuous column in the A4C unit between well BB2 and well BBS1 (3 km apart) which exhibits a strong compositional gradient (i.e. there are systematic variations in composition and PVT properties with depth). This model will be presented in the next section and tested using the Calsep PVT simulation package version 14. It is possible that the Budour1H2 condensate is associated down dip with black oil similar to Omraan1 black oil as there is a good match in terms of saturation pressure with well Budour gas condensate. Obviously, this oil cannot be Omraan1 oil as there is a large pressure difference between the two accumulations and they are from two different stratigraphic units).

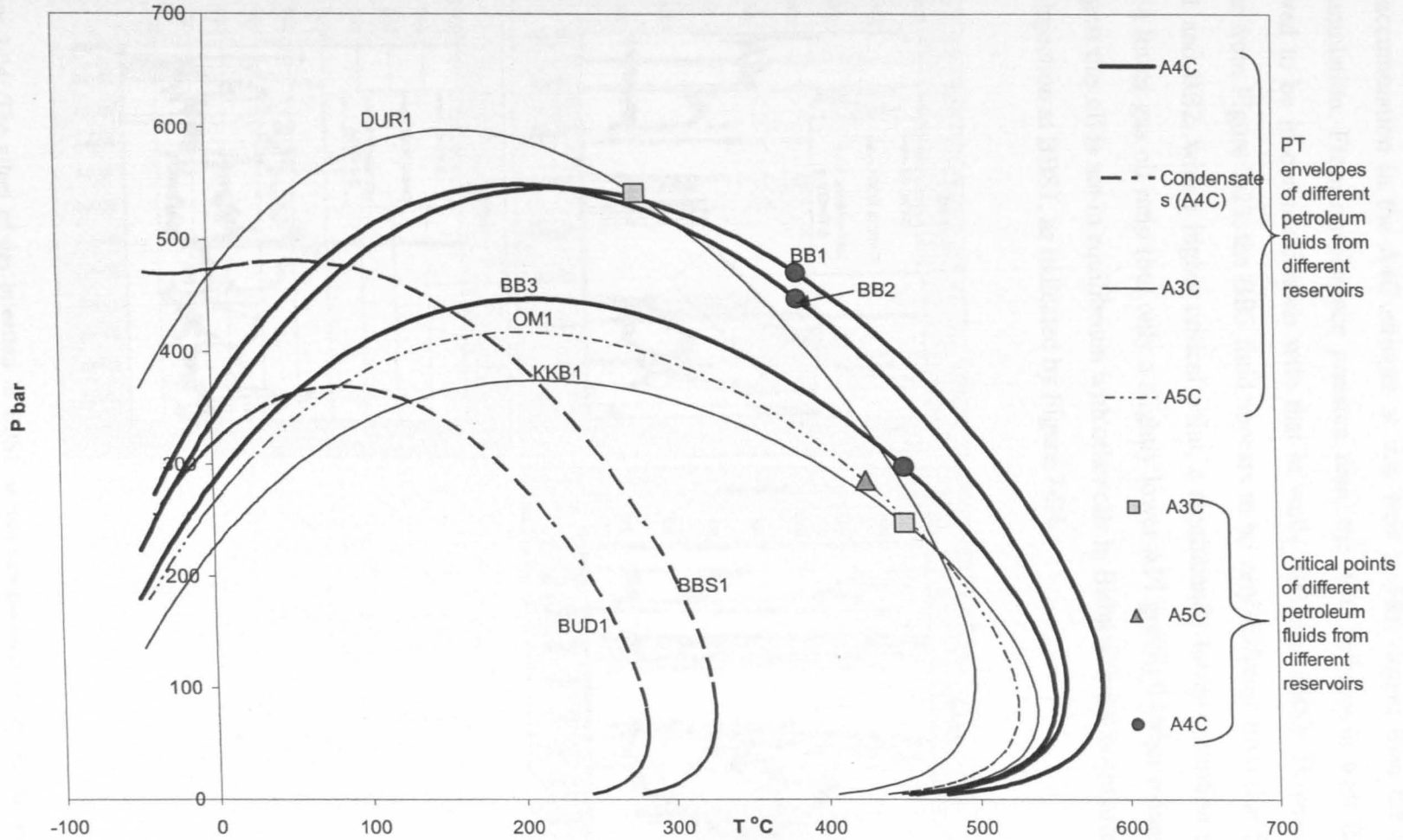

Figure 7-23: The phase envelopes of petroleum fluids from the Greater Birba area with their critical points classified by reservoir units. Each envelope also carries the name of the corresponding well. KKB1 is well Kaukab1, OM1 is well Omraan1, BUD1 is well Budour1H2, DUR1 is well Durra1.

Figure 7-23 suggests that BB3 oil might have originated from mixing of a Kaukab1-like oil and a Birba1-like oil. Well BB3 is 1.3km north of well BB1 and the oil accumulation in the A4C stringer at this well is 44m deeper than the BB1 oil accumulation. From interference pressure data, the A4C stringer in well BB3 was proved to be in communication with that in wells BB1 and BBS1. However, as is clear from Figure 7-23, the BB3 fluid appears to be very different from that found in BB1 and BB2, with a higher critical point, a significantly lower saturation pressure and a lower gas oil ratio (but only a slightly lower API gravity). Other evidence that suggest this oil is not in equilibrium with other oils in Birba is that it is not affected by gas injection at BBS1, as indicated by Figure 7-24.

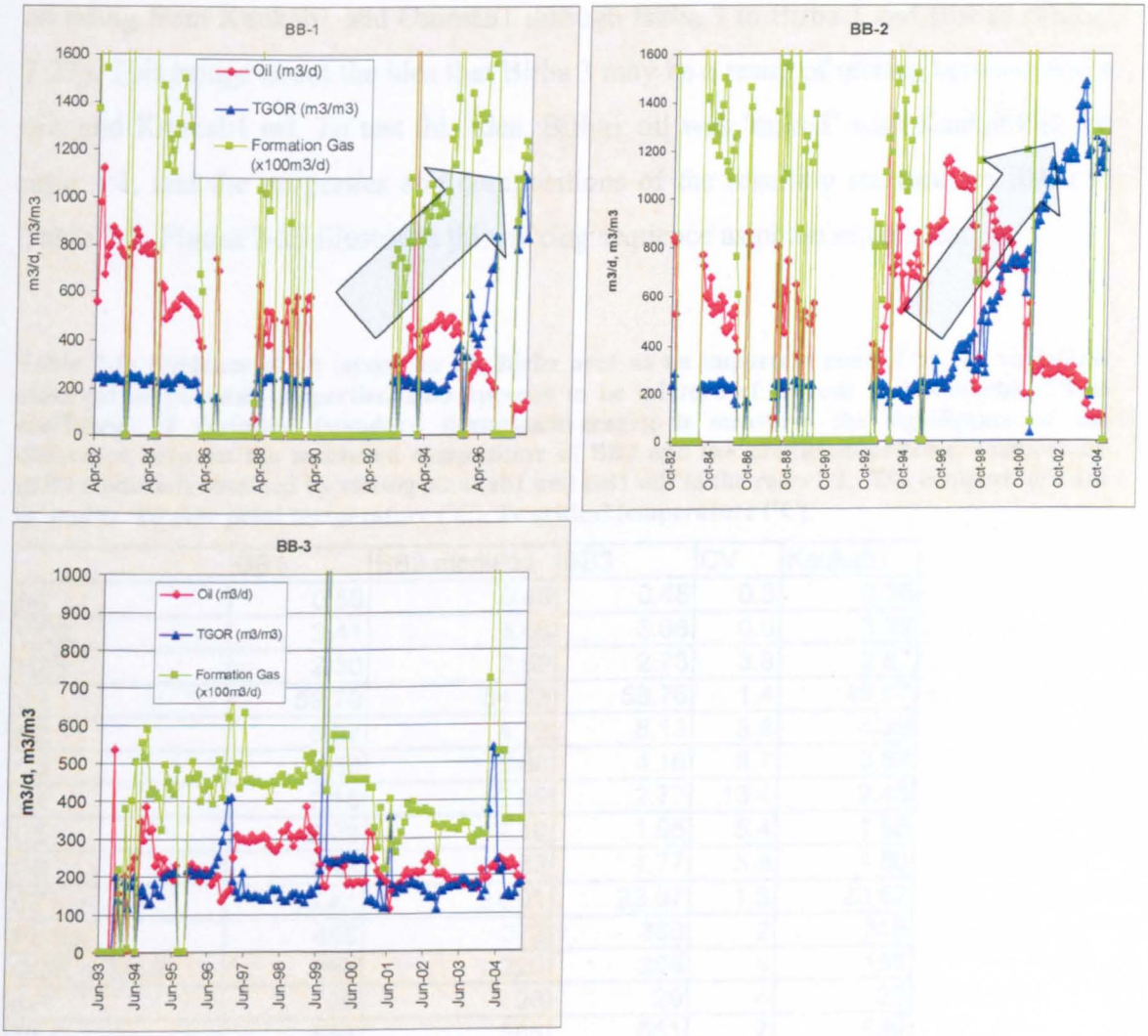

Figure 7-24: The effect of gas injection in BBS1 on the composition of the fluids that are in pressure communication with it. The gas injection in BBS1 was set up in 1993 to enhance production from well BB1 and BB2. Since then, the GOR in BB1 and BB2 has increased, as is obvious from the charts. There is, however, no change in BB3, which might be taken as evidence that there is restriction of flow (i.e. a barrier) between BB3 and the other Birba wells.

Unfortunately, no geochemical data are available for the BB3 oil which can be used for correlation with the other oils in the area. Although this oil is expected to have similar geochemistry to other Birba oils (e.g. BB1), the phase envelope and the PVT properties suggest that it is more similar to the A3C/A5C oils, as indicated by Figure 7-23 (Note that in previous chapters it was concluded that there are two end-members of a mixing sequence namely, A3C/A5C oils and condensates, and that the Birba oils are mixtures of these). Moreover, a compositional grading model of the Birba field failed to predict the composition and properties of this oil down the column. On the basis of PVT modelling alone, Birba 3 oil was found to originate from Kukab1 oil mixed with oil from Birba. A comparison of the phase envelopes of the petroleum fluids of the Greater Birba area, indicates that the envelope becomes wider on going from Kaukab1 and Omraan1 through Birba 3 to Birba 1 and Birba2 (Figure 7-23). This brings about the idea that Birba 3 may be a result of mixing between Birba oils and Kaukab1 oil. To test this idea, Birba1 oil was 'mixed' with Kaukab1 in the ratio 1:1, and the properties and compositions of the resulting mixture are listed in Table 7-5. Figure 7-25 illustrates this mixing sequence as phase envelopes.

Table 7-5: Evidence of oil mixing in the Birba area as an important control on the variations observed in physical properties. BB3 appears to be mixture of BB oils and Kaukab1. CV is coefficient of variation (standard deviation/average); it measures the significance of the difference between the measured composition of BB3 and the predicted/modelled composition (BB3 modelled) obtained by mixing Kaukab1 and BB1 oils in the ratio 1:1. The compositions are in mol%. Td dew point temperature (°C), Tc critical temperature (°C).

	BB1	BB3 modeled	BB3	CV	Kaukab1
N2	0.59	0.48	0.48	0.3	0.38
CO2	3.41	3.66	3.66	0.0	3.92
H2S	2.30	2.59	2.73	3.8	2.87
C1	59.70	54.83	53.78	1.4	49.97
C2	5.07	4.73	5.13	5.8	4.38
C3	3.68	3.68	4.16	8.7	3.67
C4	2.15	2.29	2.77	13.4	2.43
C5	2.22	2.10	1.95	5.4	1.98
C6	1.46	1.63	1.77	5.8	1.80
C7+	19.41	24.01	23.57	1.3	28.62
Pb bar	458	372	380	2	315
GOR m3/m3	265	220	208	4	168
API	30	28	29	4	33
Td C	583	566	551	2	539
Tc C	385	432	453	3	452
Pc bar	471	336	298	9	247

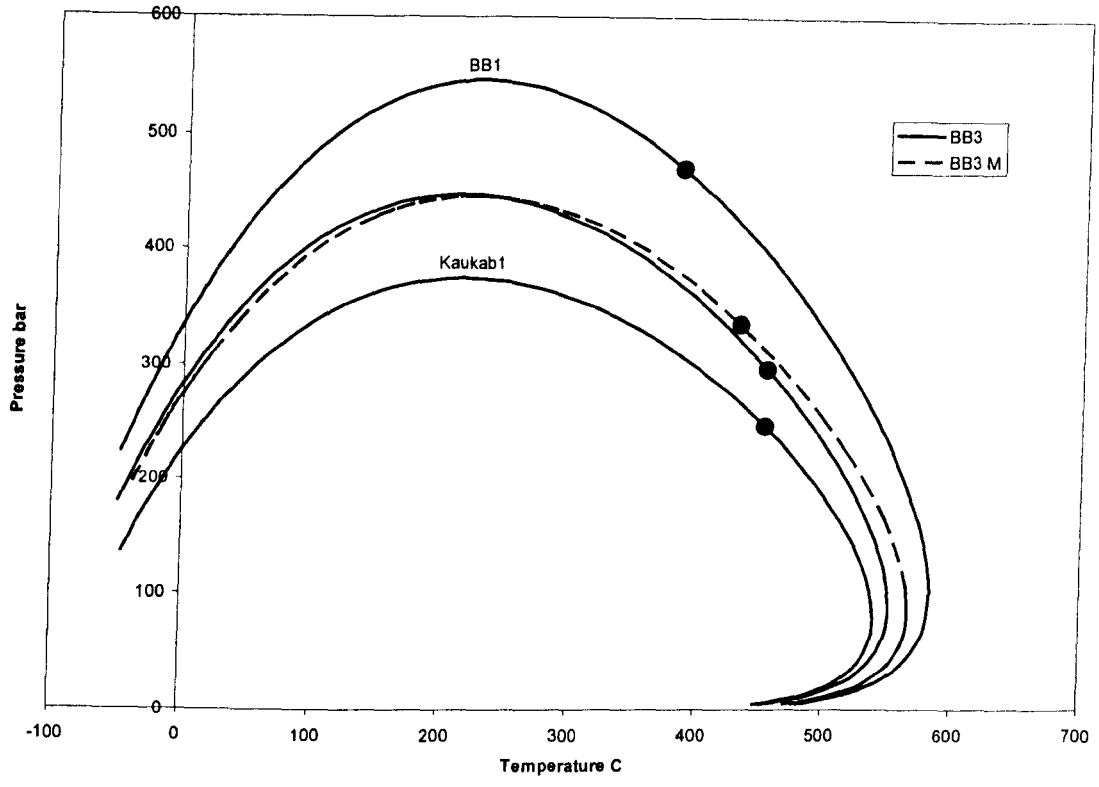

Figure 7-25: The phase envelopes of different petroleum fluids (Kaukab1 and BB1) used in the mixing model to obtain the BB3 petroleum fluid.

In summary, it is very clear from the results (Table 7-5 and Figure 7-25) that BB3 is likely to be a mixing product of Kaukab1 and Birba1 oils. Although well BB3 is in close proximity to wells BB1 and BB2 and the oils are from the same reservoir unit, BB3 does not appear to lie within a compositional gradient, assuming that such a gradient exists in the main Birba Field. The BB3 oil is undersaturated and shows a different critical point to the Birba oils; furthermore, compositional grading models failed to predict its composition using Birba 1 oil as a datum. However, the mixing model, using parameters for the Kaukab1 and Birba1 oils, shows good agreement in most of the properties, as shown in Table 7-5 and Figure 7-25 above.

The oil from well Durra1 shows a phase envelope typical of higher maturity (see Figure 7-23). Geochemical data, however, indicate that this accumulation contains petroleum of maturity similar to oils from the geographically close to well Kaukab1 (well Durra1 is represented by oil sample O14, while well Kaukab1 is represented by oil sample O11), Similarly the geochemical data show no big maturity and facies differences between the Durra1 oil and the Omraan1 oil (equivalent to oil

sample O12) and others (chapter 4). Therefore, there must be another factor causing the formation of this oil with such high saturation pressure and near saturation conditions, and it is suggested that mixing with both gas condensate with a very low C7+ fraction (heavy end) and probably a dry gas is involved. Inappropriate sampling of the Durra1 fluid might also have caused this behaviour. This is mainly down to determination of GOR; the measured GOR of the Durra1 oil is very high and it is possible that the true value is a lot lower.

As previously mentioned, the Durra1 oil accumulation was proved geochemically to be not very different from the rest of the accumulation in the Greater Birba area, with minor differences suggested to be due to facies variation. One of the main conclusions of the geochemical work is that the mixing of oils with a condensate charge is the main control on physical properties. So far, this agrees with the phase relationships found using PVT data. The Durra1 oil accumulation shows a very different phase envelope, with the highest saturation pressure and the lowest dew point temperature of all the oils (but not lower than the gas condensates). The quality of the data was assessed in Section 7.1.3, where it was mentioned there that surface PVT samples could have been subjected to serious error in determining the gas oil ratio. The composition of the combined fluid relies largely on the determined gas oil ratio. Therefore, one possibility behind the different behaviour of the Durra1 oil is that there was an error in determining the gas oil ratio. This is supported by geochemical observations made on the oil samples (O14 and O17) taken from this reservoir.

Assuming that the Durra1 PVT fluid sample is representative of the actual fluid in this accumulation and using purely PVT modelling, this oil may result from mixing either with a dry gas or with gas condensates with a very low content of the C7+ fraction. The former (dry gas) is supported by the presence of heavier methane in gas mixtures in these accumulations (no gas sampled from Durra1) and the latter is supported by the random distribution of gas condensates throughout the A4C reservoir unit. This is assuming that there was no error in sampling or measurement of gas oil ratios. Kaukab1 was assumed to be the modal fluid and Durra1 should be a mixture of this fluid, which was previously filling the A4C structure in Durra1, and a

gas condensate and a dried gas with some inorganic components. The mixing modelling procedure was as follows:

- Kaukab1 oil was first mixed using PVTsim mixing rules with Budour gas condensate in the molar ratio 1:1.
- The resulting mixed fluid was then mixed with a gas composed mainly of methane (but also containing hydrogen sulphide and carbon dioxide) in the ratio 1:0.1.

The compositions and PVT properties of the fluids involved in the mixing model are listed in Table 7-6, which also compares the main physical properties of the Durra1 fluid and the modelled mixture. Notice that coefficient of variations are within the measurement error for most of the properties. Figure 7-26 shows the modelled Durra composition as a phase envelope compared to the other fluids involved in the mixing. However, as previously mentioned, the PVT fluid sample of Durra1 may be questionable and therefore caution is needed when drawing any implications from the model.

Table 7-6: Comparison between modelled and measured composition for Durra oil. KKB1 is Kaukab1 fluid sample, Bud1 is Budour1H2 fluid sample, Durra 1 modelled resulting fluid generated by mixing Kaukab1 oil, Budour1H2 gas condensate and dry gas. CV is the coefficient of variation between the modelled composition of Dura1 and the actual composition of the Durra1 accumulation. The compositions are in mol%.

mol%	KKB1	Bud1	GAS	Durra 1 modelled	Dur1	CV
N2	0.375	0.95		0.602	0.63	3
CO2	3.915	3.681	15	4.816	5	3
H2S	2.869	0.93	7	2.363	2.39	1
C1	49.973	78.863	78	65.653	66	0
C2	4.378	5.961		4.7	4.96	4
C3	3.668	3.161		3.104	3.53	9
C4	2.426	1.64		1.848	2.04	7
C5	1.982	1.02		1.365	1.45	4
C6	1.795	0.79		1.175	1.2	2
C7+	28.62	3.003		14.374	12.8	8
Pb bar	314.9	369.04		557.11	564	1
GOR m3/m3	168.3	3617.6		465.1	469	1
API	32.812	45.2		34	33.6	1
Td C	539.46	282		504.46	497	1
Tc C	452.25	nf		298.18	281	4
Pc bar	247.4	nf		525.63	542	2

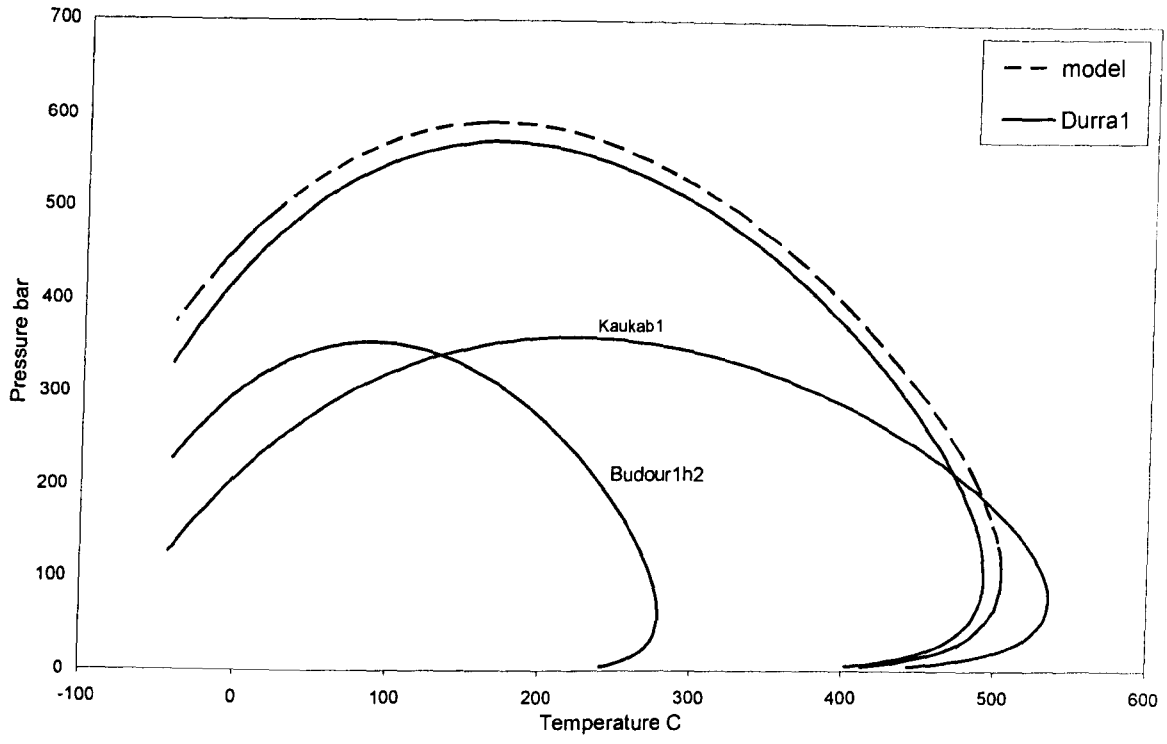

Figure 7-26: Phase envelopes of different petroleum fluids involved in the mixing model of Durra and of the actual Durra 1 fluid.

7.3.2 Compositional grading

7.3.2.1 The Riemens et al 1985 model

Riemens *et al* (1985), using an isothermal model-based equation of state, claimed that there was a strong compositional gradient in the A4C reservoir in the Birba Field. They set up a compositional grading model focusing on variations in composition and saturation points (dew and bubble), and used a phase equilibria package based on the Soave cubic equation of state to calculate fluid properties (dew point and bubble point pressures). They used petroleum fluid from the A4C reservoir unit in well Birba2 as a starting point and a datum, which is 255m deeper than well Birba south. They checked the connectivity of four wells in the Birba field (BB1, BB2, BB3, BBS1, Figure 7-27) by interference pressure tests. During these tests, BB1 was produced for two periods: at low rates for 20 days and at maximum rate (1225 m^3/d) for 32 days. The response of the production in well BB1 was monitored in wells BB2, BB3, and BBS1 by downhole recording gauges. There was a small retardation in response in these wells and Riemens *et al* (1985) suggested that this is due to some

flow restriction between the two wells despite them being in communication. The main conclusion from this test was that BBS1 is in excellent communication with BB2 and BB3.

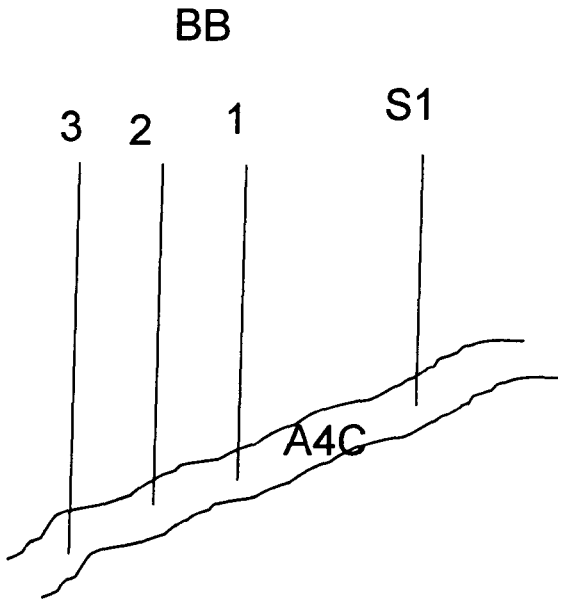

Figure 7-27: Schematic diagram showing the relative locations of the different Birba wells (BB1, BB2, BB3, and BBS1) along the A4C reservoir unit.

To recap, it has already been mentioned that there are two PVT samples for well BBS1; one was obtained by Shell (KSPL) and the other was obtained by EXPRO. The BBS1 data shown in Figure 7-23 is for the PVT sample obtained by EXPRO as this was the only sample with sufficient data for modelling work. Riemens et al (1985) compared data from KSPL samples with the predicted composition by an isothermal gravity induced model. Table 7-7 shows the calculations done by Riemens et al (1985). Figure 7-28 shows a comparison between the composition of their modelled oil BBS1 M and the real compositions measured using the BBS1 PVT oil samples by Shell (BBS1 KSPL) and by Expro (BBS1 EXPRO). Clearly, the modelled composition of the BBS1 condensate (BBS1 M) is in good agreement with the measured compositions of the actual PVT sample by Shell (BBS1 KSPL).

Table 7-7: Riemens et al (1985) model. BBS1 (M) is the Riemens *et al* model predicted using BB2 as a datum, while BBS1 KSPL (obtained by Shell) and BBS1 Expro obtained by EXPRO are the measured composition of the real petroleum fluid in well BBS1. Notice that the BBS1 model shows good agreement with BBS1 KSPL (the measured PVT oil sample from BBS1 analysed by Shell).

mole%	BB2	BBS1 M	BBS1 KSPL	BBS1 Expro
C1	59.49	73.82	74.66	73.52
C2	5.55	5.5	5.5	6.38
C3	4.06	3.69	3.46	3.07
iC4	1.13	0.98	0.43	0.37
nC4	1.39	1.6	1.51	1.38
iC5	0.49	0.39	0.39	0.31
nC5	1.09	0.84	0.89	0.9
C6	1.27	0.91	1.23	1.32
CO2	3.84	4.19	3.89	2.84
N2	0.71	0.97	0.86	0.32
H2S	1.17	1.15	0.58	0.9
C7+	19.27	5.96	6.6	8.69
P_R bar	532.2	518.6	520.3	520.3
P_b bar	474.7	502.5	473.8	482.4
GOR m3/m3	260	?	1103	1076
API	32	?	48	45

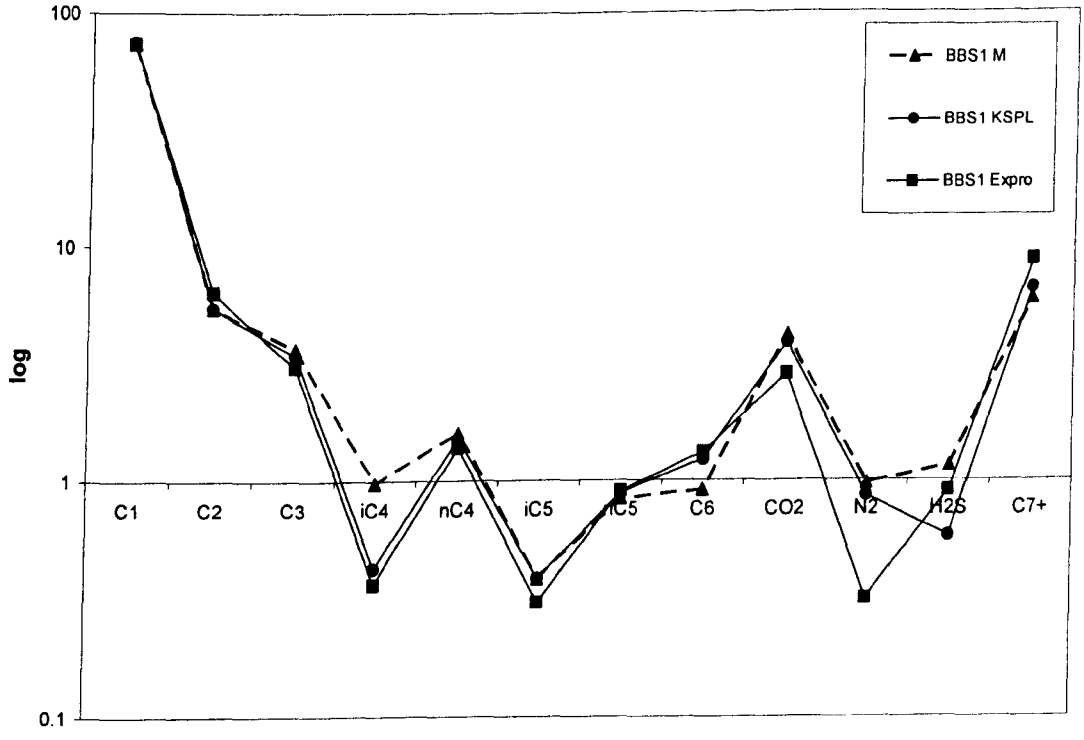

Figure 7-28: Comparison between Riemens *et al.* (1985) model (BBS1 M) and the real compositions for BBS1 PVT oil sample obtained by Shell (BBS1 KSPL) and EXPRO (BBS1 Expro). Y-axis is log of mol% of each component.

Riemens *et al* (1985) used the composition and PVT properties (GOR, saturation pressure, reservoir pressure) of the petroleum fluid from well BB2 as a starting point (depth 0). Then, they used an isothermal gravity model to calculate the compositional variation from this datum along the hydrocarbon column. They found that the composition predicted at similar depth (true vertical depth (TVD) = 265m above BB2) to where the actual BBS1 petroleum fluid is situated (TVD interval = 255-292 m) and the measured composition of the PVT sample from BBS1 provided by Shell (KSPL) are in a satisfactory agreement (Figure 7-28). This is supposed to be equivalent to the BBS1 fluid in the depth interval of 255-292 m above datum (well BB2). Figure 7-29 shows the variation in methane and plus fraction (C_{7+}) with depth as predicted by the Riemens *et al* (1985) model.

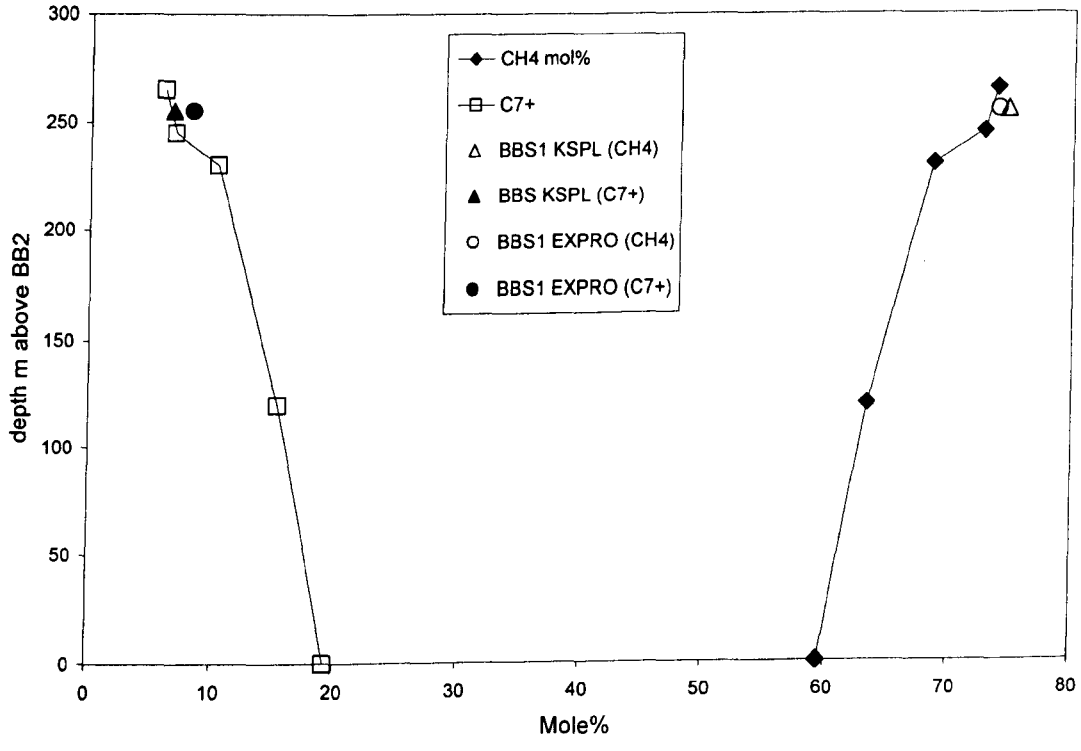

Figure 7-29: Variation in methane (CH_4) and heavy end (C_{7+}) contents with depth predicted by the isothermal gravity model formulated by Riemens *et al* (1985). The graph also shows the real data from the BBS1 PVT sample provided by SHELL (KSPL) (triangles) and the PVT sample provided by EXPRO (circles).

Riemens *et al* (1985) calculated an estimated GOC at a depth of 235m above BB2. According to their model, the reservoir pressure at the gas oil contact is equal to the saturation pressure of the petroleum fluids in this reservoir (A4C between BB2 to BBS1, Figure 7-30). The authors claimed that there may be a tarmat present within the column which formed as the result of the same gravitational segregation process that formed the compositional gradient between well BB2 and well BBS1. The authors suggested that as the oil column in BB2 grades upwards to lighter oil and eventually to gas), it might be expected that there is also a grading downward to heavier oil and eventually to tarmat. There are some issues about this model: firstly, the origin of the BB2 fluid which was used is questionable as the A3C reservoir in this well was open when sampling was done from A4C (personal contact with Harweel Team, PDO); this might have resulted in a co-mingled bore sample. Secondly, Riemens *et al* (1985) did not compare measured and predicted values for GOR and density even though these two properties can be easily influenced by other factors. Thirdly, the authors do not present the phase envelope of this fluid and this is important if we are to know the critical state of the fluid

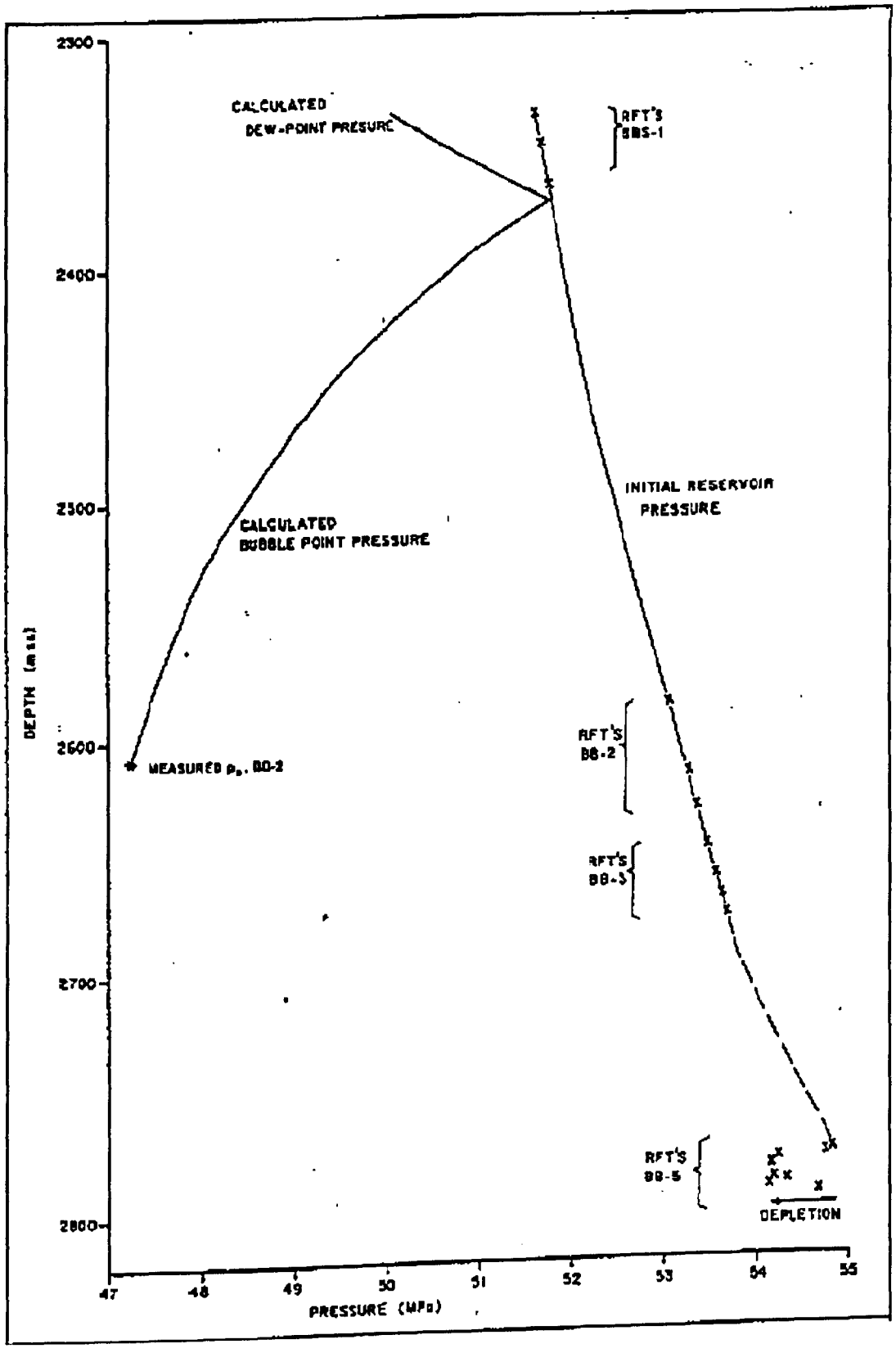

Figure 7-30: Saturation pressure and reservoir pressure versus depth FOR WHAT ?? (Riemens *et al.*, 1985).

The authors tried to model this gradient using different C7 plus fraction characterizations. All fluids were tuned against available experimental data but the BB2 fluid (A4C) was only tuned against saturation pressure and separator data as there were no other data available for this sample (section 7.2.3.2), which is another problem in using this fluid as a datum. Starting with BB2 as a datum, PVTsim 14 predicted the compositional variations with depth on going away from this well along the A4C hydrocarbon column and towards BBS1. Isothermal compositional grading model using BB2 fluid as a datum, generated using the Calsep PVTsim 14 software. The depths listed are relative to the datum (BB2). The (-) sign means the datum is deeper. The compositions of the real PVT fluid samples from BB1, BB3, and BBS1 are shown on the right hand side of the table. Table 7-8 shows a model (depth: 257.9m above datum) that predicts an isothermal compositional gradient using BB2 as a datum.

Table 7-8: Isothermal compositional grading model using BB2 fluid as a datum, generated using the Calsep PVTsim 14 software. The depths listed are relative to the datum (BB2). The (-) sign means the datum is deeper. The compositions of the real PVT fluid samples from BB1, BB3, and BBS1 are shown on the right hand side of the table. Compositions (mol%), Pressure (bar), GOR (Sm^3/Sm^3), Temperature (°C). Sat point = saturation point pressure (bar), Depth (m)

Depth m	-257.9	-246.6	-63.6	-63.6	-53.7	0	48.5		BBS1 Expro	BBS1 KSPL	BB1H1	BB3H1
N2	1.10	1.10	0.92	0.80	0.76	0.70	0.67		0.32	0.86	0.59	0.48
CO2	3.88	3.89	3.93	3.88	3.85	3.81	3.78		2.85	3.89	3.41	3.66
H2S	0.86	0.87	1.00	1.09	1.12	1.16	1.19		0.91	0.58	2.30	2.73
C1	74.15	73.99	67.80	63.24	61.72	59.03	57.32		73.90	74.74	59.70	53.78
C2	5.56	5.57	5.67	5.63	5.59	5.51	5.44		6.41	5.51	5.07	5.13
C3	3.64	3.65	3.95	4.04	4.04	4.03	4.00		3.09	3.46	3.68	4.16
iC4	0.97	0.98	1.09	1.12	1.12	1.12	1.11		0.37	0.43	0.47	0.56
nC4	1.55	1.56	1.79	1.88	1.90	1.92	1.92		1.39	1.51	1.68	2.21
iC5	0.37	0.38	0.45	0.48	0.48	0.49	0.49		0.31	0.39	1.03	0.58
nC5	0.80	0.81	0.98	1.05	1.07	1.08	1.09		0.91	0.89	1.20	1.37
C6	0.88	0.89	1.12	1.22	1.24	1.26	1.27		1.33	1.21	1.46	1.77
C7+	6.22	6.34	11.32	15.59	17.11	19.90	21.71		8.22	6.52	19.41	23.57
Pressure	517.89	518.38	526.89	526.89	527.51	531.10	534.36		520.34	520.34	528.1	418
Phase	Gas	Gas	Gas	Oil	Oil	Oil	Oil		gas	gas	oil	oil
Sat Point	469.0	471.2	526.9	526.9	519.3	498.1	484.9		482.43	473.79	460.2	380.45
GOR	1652.7	1612.6	700.1	418.2	357.1	274.4	242.7		1076.5	1103.4	282	135
API	44.9	44.7	37.8	33.0	31.5	29.5	28.9		45.4	47.6	30	31.7

Figure 7-31 shows the predicted variations in the bubble point pressures and dew point pressures of the BB2 petroleum fluid with depth along the A4C hydrocarbon column. This should resemble the compositional gradient produced by Riemens *et al* (1985) and shown in Figure 7-30. The gas oil contact (GOC) is predicted by this model to occur at a depth of 63.6 m above the BB2 petroleum fluid.

This is a lot deeper than the GOC predicted by the Riemens *et al* (1985) model (which was at depth of 235m above BB2) and is closer to the real GOC in the BBS1 accumulation. Both models predicted saturated gas oil contacts i.e. the saturation pressure at the gas oil contact equals the reservoir pressure at GOC depth.

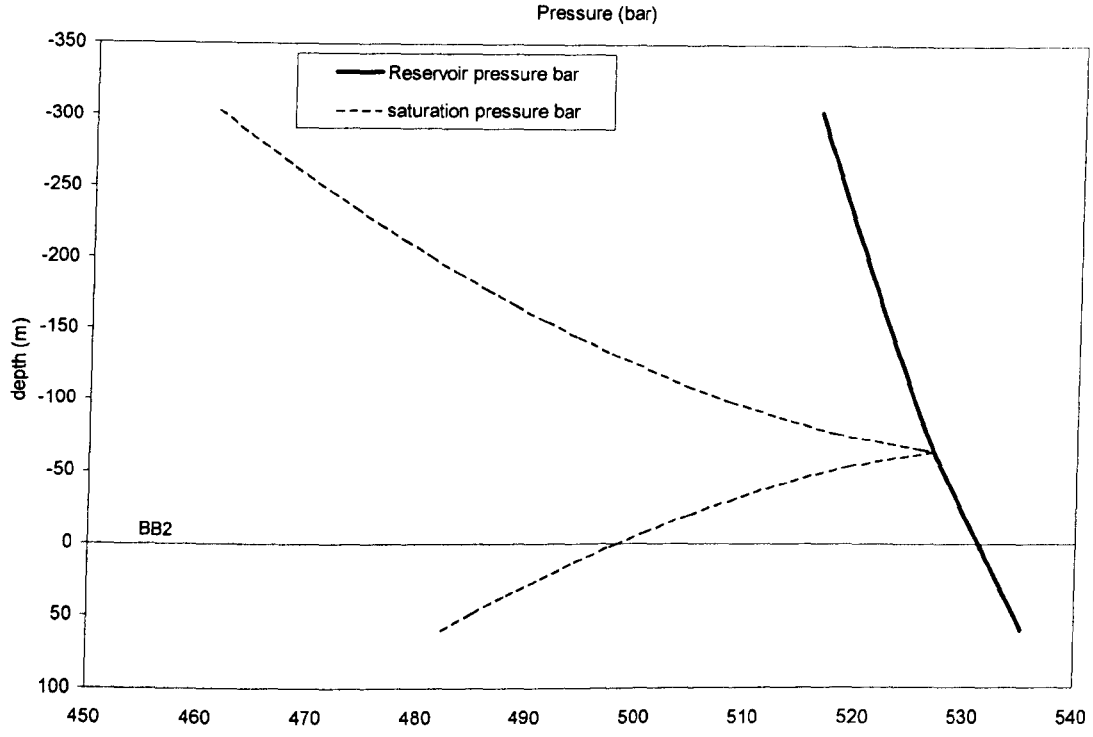

Figure 7-31: Saturation pressures (broken line) and reservoir pressures (solid line) versus depth predicted from A4C oil at well BB2 by an isothermal gravity induced gradient model using PVT SIM package version 14.

The testing model (testing the Riemens et al (1985) model using the Calsep PVTsim 14 software) shows a good match between the predicted BBS1 oil and the real BBS1 fluid measured by Shell (BBS1 KSPL) for most of the important properties e.g. CH_4 (-0.78% from the real value), C_{7+} (-4.6% from the real value) as shown in Figure 7-32 and saturation pressure (-1% from the real value). There is also a moderate match for API gravity (-5.6% from the real value). However, there is a big difference (50%) between GORs of the BBS1 gas condensate and the predicted condensate. It is not possible to compare these results to Riemens et al's (1985) work because they only show the composition and saturation pressure, which agree well with the presented model and show a close match between BBS1 measured by KSPL and the predicted gas cap at the same depth. This model can also be used to predict the properties of BB1 and BB3 fluids, as these wells are in pressure communication

(Riemens et al, 1985). The BB1 predicted fluid at a depth of 53.7m above datum shows a poor to moderate match with the real Birba 1 fluid analysed by Corelab (Table 7-8) in some of the properties e.g. CH_4 (3.39% deviation from the real value), C_{7+} (-11.9%), saturation pressure (12.8%) and API gravity (5.1%) and GOR (27%). Although BB3 is quite similar to the model in terms of CH_4 and C_{7+} content , as shown in Figure 7-32, a poor match is observed between the model and BB3 fluid in most of the other properties, such as saturation pressure (27.5% from the real value), API gravity (-9% from the real value) and GOR (80% from the actual value). Although there might be a compositional gradient in the Birba Field, it is probably not a simple isothermal gradient as suggested by Riemens *et al* because of the poor agreement between some of the important predicted properties and the values obtained by laboratory analysis, such as API gravity, saturation pressure and gas oil ratio. Without knowing the actual C_{7+} composition used in the Riemens *et al* (1995) model, a comparison is not possible. The author chose to use the default characterisation done by PVT Sim and tuned it using critical properties of the C_{7+} fraction. In the next section, I will attempt to predict compositional grading using BB1 as a fluid datum, because this fluid is better tuned and reliable.

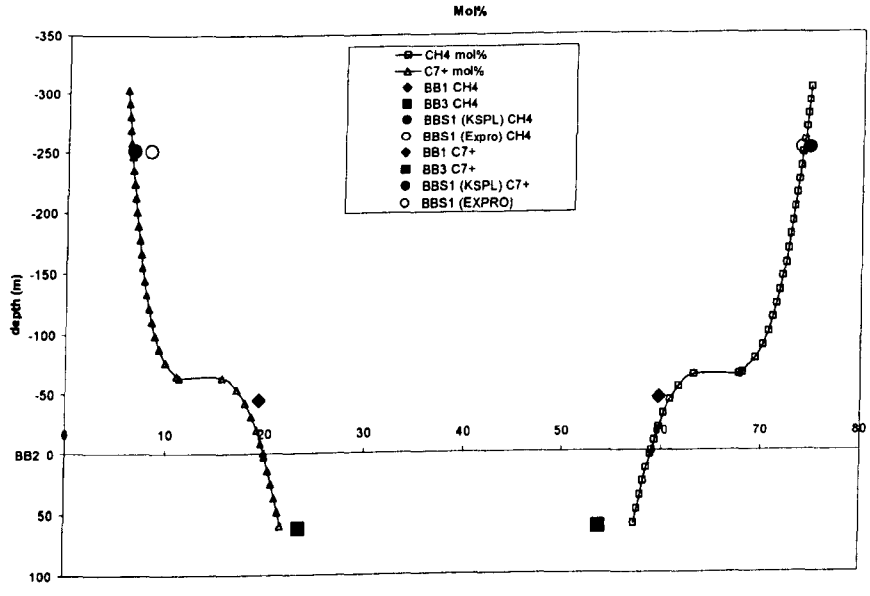

Figure 7-32: Variations in methane and heavy end (C7+) content with depth as predicted by the proposed isothermal gravity induced compositional gradient model using PVTsim 14 and with BB2 as a datum (y=0).

To summarise this section, the aim of the whole chapter is to use PVT modelling to test the hypothesis presented throughout this thesis that the gas

condensates in the Greater Birba area were formed by admixture of a separate condensate charge to the original oils. Riemens et al (1985) proposed a different model to account for the origin of these condensates, advocating that the condensate in BBS1 formed by gravitational segregation of the oil in main Birba field. Their isothermal gravity induced compositional grading (GCE) model is presented here in Table 7-7, Figure 7-28, Figure 7-29 and Figure 7-30. Riemens et al's work does not include some of the important properties of the petroleum fluids such as API gravity and gas oil ratio. In this section I have attempted to reproduce the Rieman et al (1985) model using the very recent PVTsim version 14 software but employing the same gravitational-compositional-equilibrium concepts. Although the model achieved good agreement between the modelled BBS1 and real fluid encountered in well BBS1 in terms of saturation pressure and compositions (CH_4 and C_{7+}), the API gravities and gas oil ratio values predicted for BBS1 (and also for BB1) were significantly different from the real values (Table 7-8).

7.3.3 Birba 1-(Birba 2-BB3)-Birba South 1 oil column

After showing that the Riemens *et al* model was not able to predict some important PVT properties (API gravity and GOR), the Calsep PVTsim Package 14 was used to model the compositional grading proposed by Riemens *et al* (1985) using different boundary conditions (e.g. different datum) and different models (isothermal versus non-isothermal gravity induced compositional gradient models). This is meant to be an investigation of a possible compositional gradient in Birba field. The locations of the wells in the Birba field are shown in Figure 7-1 and Figure 7-14. The initial conditions and properties of the BB1 fluid used in this model are presented in Table 7-9. There is an apparent difference in the temperature of the reservoirs for different wells. It can be seen that the temperature at well BB1 is 73.9°C, which is 4-6°C higher than other wells. The temperature measured for this reservoir is 71.1°C, which is in good agreement with other Birba wells. These two temperatures are included in our models.

Table 7-9: The initial composition and the properties of the petroleum fluids from the Birba field referenced to a datum at the BB1 sample. These are the original data without any tuning. They are also listed in Table 7-1 but there are slight differences in the heavy end. For comparison purposes they are all aggregated to comprise the C7+ fraction.

wells	BBS1 Expro	BBS1 KSPL	BB1	BB2	BB3
Depth m	-206.5	-206.5	0	44.5	107
N2 mol%	0.32	0.86	0.59	0.70	0.48
CO2 mol%	2.85	3.89	3.41	3.81	3.66
H2S mol%	0.91	0.58	2.30	1.16	2.73
C1 mol%	73.90	74.74	59.70	59.03	53.78
C2 mol%	6.41	5.51	5.07	5.51	5.13
C3 mol%	3.09	3.46	3.68	4.03	4.16
iC4 mol%	0.37	0.43	0.47	1.12	0.56
nC4 mol%	1.39	1.51	1.68	1.92	2.21
iC5 mol%	0.31	0.39	1.03	0.49	0.58
nC5 mol%	0.91	0.89	1.20	1.08	1.37
C6 mol%	1.33	1.21	1.46	1.26	1.77
C7+ mol%	8.22	6.52	19.41	19.90	23.57
Pressure bar	520.34	520.34	528.1	531.10	418
Temperature °C	67.60	67.60	73.90	70.00	70.00
Phase	gas	gas	oil	Oil	oil
Saturation Pressure (bar)	482.43	473.79	460.2	498.1	380.45
GOR Sm3/Sm3	1076.5	1103.4	282	274.4	135
API °	45.4	47.6	30	29.5	31.7

There is a clear increase in GOR with depth but this trend is not apparent in density and saturation pressures for Birba1 and Birba2, as shown in Figure 7-33. One possible reason for the lack of a trend is that the Birba 2 sample is probably contaminated with a small amount of oil from the A3C unit, as the A3C stringer valve was open when sampling from A4C was performed (personnel communication with Qasim Al-Riyami, Harweel Team, PDO). The fluids models were tuned thoroughly using the data given in Section 7.2.3 in order to have the best possible representative model of the real fluid. BB1 was used as a datum to predict the composition of the gas cap and down the column due to the limited data available for BB2. Two models will be presented, the isothermal gravitational grading model and the thermal-gravitational grading model, and the results are compared.

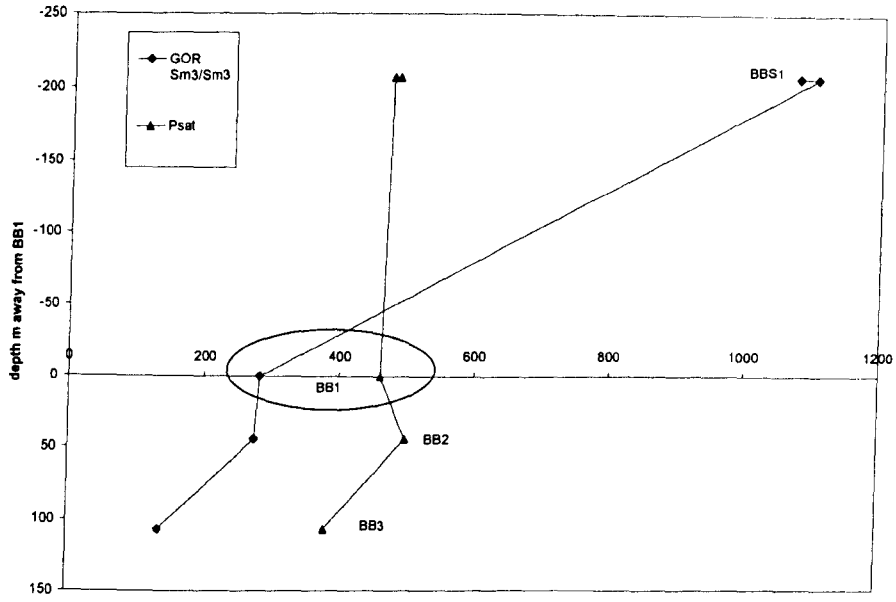

Figure 7-33: A cross-plot showing variation in measured GOR and saturation pressures of different Birba petroleum fluids with depth.

7.3.3.1 Isothermal gravitational gradient in the main Birba Field

In this model, the petroleum column is assumed to be in thermodynamic equilibrium. The temperature is assumed to be constant throughout the column and the only control on composition is gravity. The model was initialised using the tuned compositional model of BB1 (Table 7-9) and the results from this model are compared with the tuned model of BBS1. Since different temperatures were reported for well BB1, it was decided to initialise the model with two possible temperatures, namely 73.9 °C as reported by EXPRO and 71.1 °C as reported in another PVT report; and the latter temperature is preferred by the Harweel Team (PDO). Table 7-10 shows the results for the Expro reported initial temperature (73.9°C) while Table 7-11shows the results for the other initial temperature (71.1°C).

Table 7-10: Compositional grading variations calculated by the isothermal gravity induced model using BB1 as a datum and a reservoir temperature of 71.1°C. BBS1 is at a depth of -206.5m, BB2 is at a depth of 44.5m, BB3 is at a depth of 107m from the datum. Compositions (mol%), Pressure (bar), GOR (Sm^3/Sm^3), Temperature (°C). Sat point = saturation point pressure (bar), Depth (m).

Depth	-211.5	-197.7	-170.1	-156.3	0	36.8	50.6	105.7	119.5		BBS1 Expro	BBS1 KSPL	BB2H1	BB3H1
N2	0.80	0.78	0.73	0.71	0.59	0.58	0.58	0.57	0.56		0.32	0.86	0.71	0.48
CO2	3.48	3.48	3.47	3.46	3.41	3.41	3.41	3.40	3.40		2.85	3.89	3.84	3.66
H2S	1.93	1.96	2.04	2.09	2.30	2.33	2.33	2.36	2.36		0.91	0.58	1.17	2.73
C1	70.16	69.43	67.26	65.91	59.70	58.97	58.73	57.82	57.62		73.90	74.70	59.50	53.80
C2	5.21	5.22	5.22	5.21	5.07	5.05	5.04	5.00	4.99		6.41	5.51	5.55	5.13
C3	3.55	3.57	3.63	3.66	3.68	3.68	3.67	3.66	3.65		3.09	3.46	4.06	4.16
iC4	0.45	0.45	0.46	0.47	0.47	0.47	0.47	0.47	0.47		0.37	0.43	1.13	0.56
nC4	1.52	1.54	1.59	1.62	1.68	1.68	1.68	1.68	1.68		1.39	1.51	1.93	2.21
iC5	0.90	0.92	0.96	0.98	1.03	1.03	1.03	1.03	1.03		0.31	0.39	0.49	0.58
nC5	1.03	1.05	1.10	1.13	1.20	1.20	1.20	1.20	1.20		0.91	0.89	1.09	1.37
C6	1.22	1.25	1.32	1.36	1.46	1.46	1.46	1.47	1.47		1.33	1.21	1.27	1.77
C7	9.74	10.34	12.20	13.41	19.41	20.15	20.41	21.34	21.56		8.22	6.52	19.27	23.57
Pressure bar	515.03	515.73	517.21	517.99	528.10	530.63	531.59	535.48	536.46		520.34	520.34	528.10	418.00
Phase	Gas	Gas	Gas	Oil	Oil	Oil	Oil	Oil	Oil		gas	gas	oil	oil
Sat Pressure bar	481.24	484.81	490.24	489.69	454.04	447.25	444.84	435.74	433.60		482.43	473.79	460.20	380.45
GOR m3/m3	885.70	807.10	619.10	528.20	272.90	254.40	248.50	228.20	223.90		1077	1103	282	135
API (density)	40	39	37	36	32	31	31	30	30		45	48	32	30

Table 7-11: Compositional grading variations calculated by the isothermal gravity induced model using BB1 as a datum and at reservoir temperature 73.9°C. BBS1 is at a depth of -206.5m, BB2 is at a depth of 44.5m, BB3 is at a depth of 107m from the datum. Compositions (mol%), Pressure (bar), GOR (Sm^3/Sm^3), Temperature (°C), Sat point = saturation point pressure (bar), Depth (m).

Depth	-211.5	-197.7	-170.1	-156.3	0.0	36.8	50.6	105.7	119.5		BBS1 Expro	BBS1 KSPL	BB2	BB3
N2	0.81	0.80	0.75	0.72	0.59	0.58	0.58	0.57	0.56		0.32	0.86	0.71	0.48
CO2	3.49	3.49	3.49	3.48	3.41	3.41	3.40	3.40	3.40		2.85	3.89	3.84	3.66
H2S	1.91	1.94	2.01	2.07	2.30	2.33	2.33	2.36	2.36		0.91	0.58	1.17	2.73
C1	70.6	70.0	68.1	66.7	59.7	59.0	58.7	57.8	57.6		73.90	74.70	59.50	53.80
C2	5.21	5.22	5.22	5.22	5.07	5.05	5.04	5.00	4.99		6.41	5.51	5.55	5.13
C3	3.53	3.55	3.61	3.65	3.68	3.67	3.67	3.66	3.65		3.09	3.46	4.06	4.16
iC4	0.44	0.45	0.46	0.46	0.47	0.47	0.47	0.47	0.47		0.37	0.43	1.13	0.56
nC4	1.51	1.53	1.57	1.61	1.68	1.68	1.68	1.68	1.68		1.39	1.51	1.93	2.21
iC5	0.89	0.91	0.94	0.97	1.03	1.03	1.03	1.03	1.03		0.31	0.39	0.49	0.58
nC5	1.02	1.04	1.08	1.11	1.20	1.20	1.20	1.20	1.20		0.91	0.89	1.09	1.37
C6	1.20	1.23	1.30	1.34	1.46	1.46	1.47	1.47	1.47		1.33	1.21	1.27	1.77
C7	9.36	9.88	11.47	12.73	19.41	20.17	20.43	21.38	21.60		8.22	6.52	0.00	23.57
Pressure	515.18	515.87	517.31	518.07	528.10	530.63	531.58	535.46	536.44		520.34	520.34	528.10	418.00
Phase	Gas	Gas	Gas	Oil	Oil	Oil	Oil	Oil	Oil		gas	gas	oil	oil
Sat Pressure	481.25	484.97	492.14	493.58	457.57	450.64	448.17	438.93	436.75		482.43	473.79	460.20	380.45
GOR	941	867	685	577	273	254	248	228	223		1077	1103	282	135
API	40	39	38	37	32	31	31	30	30		45	48	32	30

Both models give similar results as is obvious from Figure 7-34 and Figure 7-35. The model predicts unsaturated continuous gas oil contact for both initial temperatures (i.e. the saturation pressure never intersects the reservoir pressure profile). The unsaturated gas oil contact (GOC) is located at a depth of 160-180m above BB2. There is good agreement between the predicted and measured values for saturation pressure for the BBS1 fluid, as illustrated in Figure 7-34, The API gravity

differs from the real value by 11% (BBS1 EXPRO) to 16% (BBS1 KSPL), while GORs are under-predicted by 12-17% (BBS1 EXPRO) and 14-19% (BBS1 EXPRO). As indicated in Figure 7-34 and Figure 7-35, these models could not predict the fluid properties for either BB2 or BB3; the real data for both fluids departure significantly from modelled values. The two most important properties that control both petroleum density and saturation pressure are the relative amount of methane and the C7plus fraction. The model under-predicts the amount of methane and over-predicts the C7plus fraction of BBS1 (compare BBS1 KSPL and BBS1 EXPRO between depth 206m). This results in under-prediction of API gravity and GOR of the gas cap. Figure 7-38 shows the variation in different PVT properties predicted by the models incorporated in this study, including these two models in this section; the real data for different petroleum fluids of Birba field are also plotted in this diagram for comparison. Again, neither model gives a good match with the real data. Therefore, using BB1 as a datum does not prove the occurrence of an isothermal gravity induced compositional gradient in the Birba Field.

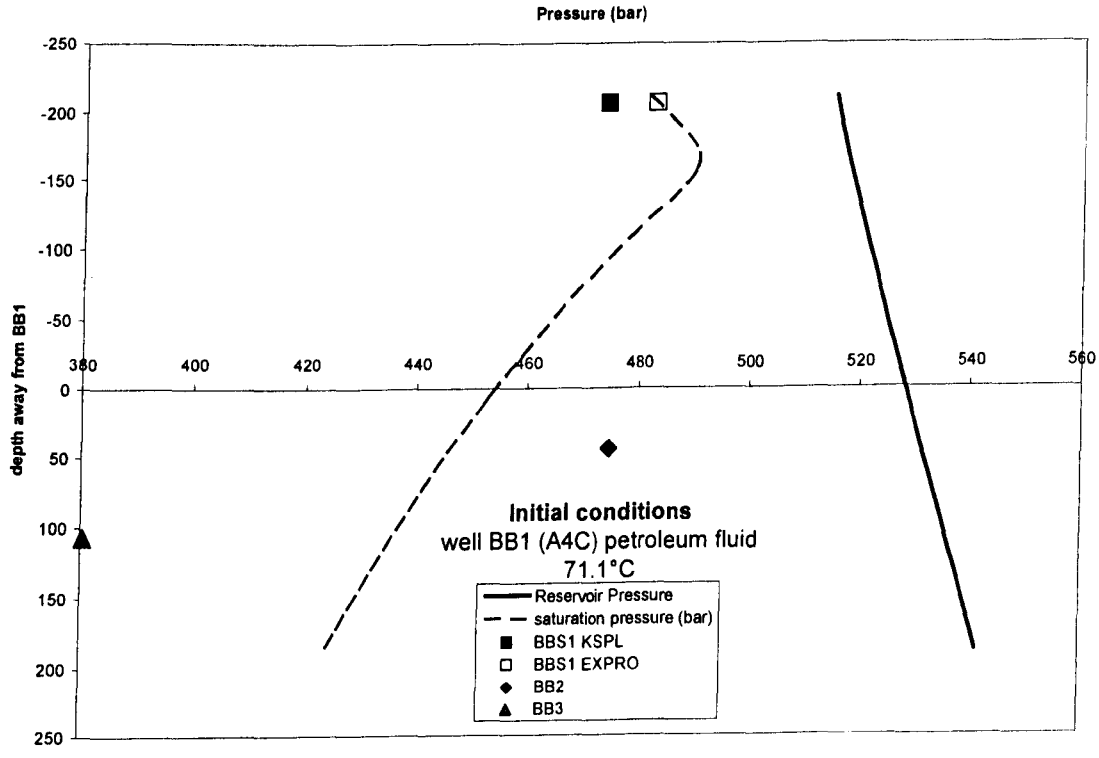

Figure 7-34: Variation in saturation pressure and reservoir pressure with depth as predicted by isothermal gravity induced compositional gradient model using BB1 properties as initial conditions and a temperature of 71.1°C.

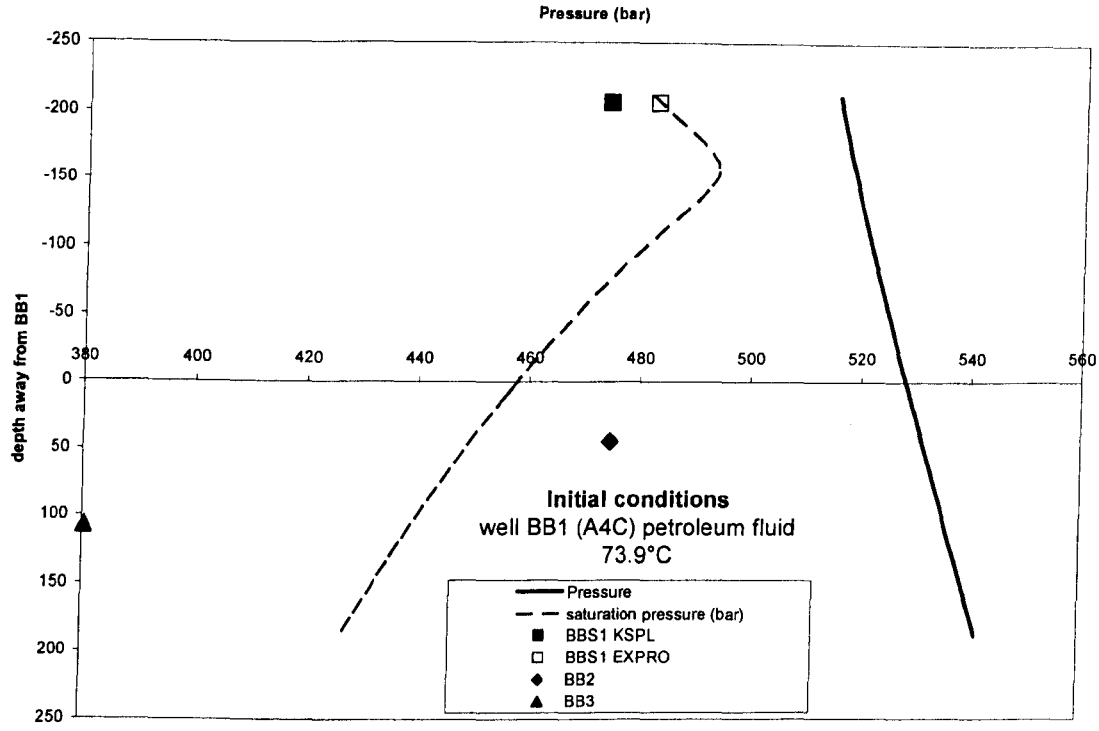

Figure 7-35: Variation in saturation pressure and reservoir pressure with depth as predicted by isothermal gravity induced compositional gradient model using BB1 properties as initial conditions and a temperature of 73.9°C.

7.3.3.2 Thermal gravity induced compositional grading

The two models described above were improved by including thermal gradients. The first model was initialised at a temperature of 73.9°C and coupled with a thermal gradient of 0.03°C/m ((temperature of BBS1 - temperature of BB1)/difference in depth between BBS1 and BB1)) in order to predict the variations in composition and PVT properties of petroleum fluids in A4C reservoir unit of the Birba field away from BB1. The results were given in Figure 7-12 and illustrated in Figure 7-36 and Figure 7-38.

Table 7-12: The compositional variations calculated by thermo-gravity induced compositional grading model using a thermal gradient of 0.03°C/m and initial temperature of 73.9°C for BB1 petroleum fluid (the initial conditions). BBS1 is at a depth of -206.5m, BB2 is at a depth of 44.5m, BB3 is at a depth of 107m from the datum. Compositions (mol%), Pressure (bar), GOR (Sm^3/Sm^3), Temperature (°C). Sat point = saturation point pressure (bar), Depth (m)

Depth	-211.50	-197.70	-87.40	-73.60	0.00	36.80	50.60	105.70	119.50	BBS1 Expro	BBS1 KSPL	BB2H1	BB3H1
N2	0.90	0.89	0.77	0.72	0.59	0.57	0.56	0.54	0.53	0.32	0.86	0.71	0.48
CO2	3.58	3.58	3.56	3.54	3.41	3.36	3.35	3.29	3.27	2.85	3.89	3.84	3.66
H2S	1.74	1.75	1.99	2.06	2.30	2.35	2.36	2.40	2.41	0.91	0.58	1.17	2.73
C1	74.2	73.8	68.5	66.6	59.7	58.1	57.6	55.9	55.5	73.90	74.70	59.50	53.80
C2	5.24	5.24	5.26	5.25	5.07	4.99	4.96	4.86	4.83	6.41	5.51	5.55	5.13
C3	3.42	3.44	3.64	3.68	3.68	3.65	3.63	3.57	3.55	3.09	3.46	4.06	4.16
iC4	0.43	0.43	0.46	0.47	0.47	0.47	0.46	0.45	0.45	0.37	0.43	1.13	0.56
nC4	1.44	1.45	1.60	1.63	1.68	1.67	1.66	1.63	1.62	1.39	1.51	1.93	2.21
iC5	0.80	0.81	0.94	0.97	1.03	1.03	1.03	1.02	1.02	0.31	0.39	0.49	0.58
nC5	0.90	0.92	1.08	1.12	1.20	1.20	1.20	1.19	1.19	0.91	0.89	1.09	1.37
C6	1.02	1.04	1.28	1.33	1.46	1.47	1.47	1.47	1.47	1.33	1.21	1.27	1.77
C7	6.36	6.62	10.99	12.65	19.41	21.17	21.75	23.72	24.16	8.22	6.52	19.27	23.57
Pressure	516.77	517.37	522.63	523.39	528.10	530.66	531.64	535.64	536.66	520.34	520.34	528.10	418.00
Phase	68.0	68.2	69.8	70.0	71.1	71.6	71.8	72.6	72.9	68.3	68.3	71.0	70.0
	Gas	Gas	Gas	Oil	Oil	Oil	Oil	Oil	Oil	gas	gas	oil	oil
Sat Point	420.58	425.64	476.86	481.55	454.04	440.51	435.91	419.43	415.69	482.43	473.79	460.20	380.45
GOR	1654	1567	739	587	273	231	219	185	178	1077	1103	282	135
API	44	43	39	37	32	30	30	29	29	45	48	32	30

Figure 7-36 shows that when coupling thermal effects to gravity gradient models there seems to be an increase in the undersaturation of the gas oil contact (GOC is under saturated by about 40 bars). Apparently, the undersaturated gas oil contact in the Birba Field given by thermo-gravity gradient models is deeper than that predicted by isothermal gravity compositional grading models. Table 7-12 shows a good match between some of the measured and predicted compositions of BBS1 (KSPL) using this model, for example the measured and predicted values of API gravity are very similar, as illustrated in Figure 7-38. The methane and C_{7+} fraction show modelled values of 74.2 mol% and 6.36 mol%, respectively, which are in good agreement with the actual reported values of 73.9-74.7mol% and 6.52-8.22 mol%. This suggests that coupling thermal effects with gravity effects can give a better compositional gradient model. However, the model under-predicts other important properties like density and saturation pressure and gives very high predicted GORs for both thermal gradients (49-53% higher than the real value for BBS1 KSPL and BBS1 EXPRO, respectively) as illustrated in Figure 7-38.

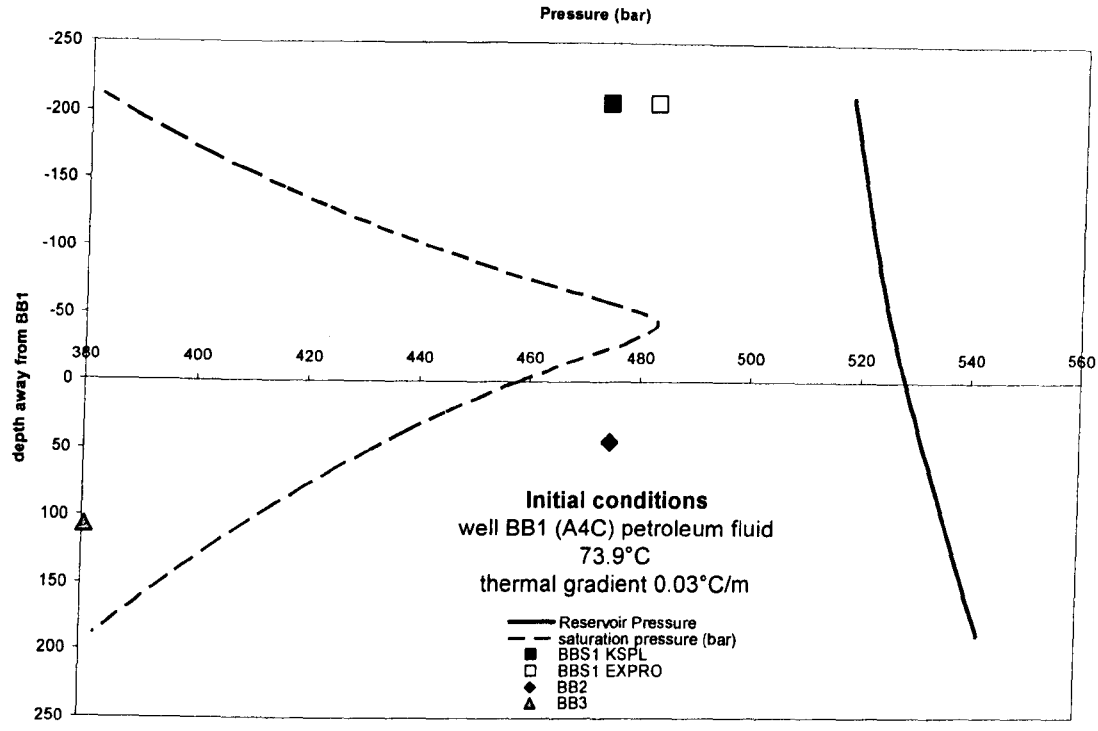

Figure 7-36: Variation in saturation pressure and reservoir pressure with depth as predicted by non-isothermal gravity induced compositional gradient model using BB1 properties as initial conditions and a temperature of 73.9°C with a thermal gradient of 0.03°C/m.

The second isothermal gradient model presented in the previous section was initialised at a temperature of 71.1°C and coupled with a thermal gradient of 0.015°C/m ((temperature of BBS1 - temperature of BB1)/difference in depth between BBS1 and BB1)). The results are listed in Table 7-13.

Table 7-13: The compositional variations calculated by thermo-gravity induced compositional grading model using thermal gradient of 0.015°C/m. BBS1 is at a depth of -206.5m, BB2 is at a depth of 44.5m, BB3 is at a depth of 107m from the datum. Units: Compositions (mol%), Pressure (bar), GOR (Sm^3/Sm^3), Temperature (°C). Sat point = saturation point pressure (bar), Depth (m)

Depth	-211.5	-197.7	-59.8	-46	0	36.8	50.6	105.7	119.5		BBS1 Expro	BBS1 KSPL	BB2H1	BB3H1
N2	0.94	0.933	0.781	0.724	0.594	0.556	0.546	0.515	0.509		0.32	0.86	0.71	0.48
CO2	3.649	3.647	3.587	3.557	3.411	3.323	3.292	3.179	3.153		2.85	3.89	3.84	3.66
H2S	1.647	1.663	1.964	2.067	2.304	2.366	2.38	2.418	2.424		0.91	0.58	1.17	2.73
C1	75.86	75.555	69.111	66.54	59.695	57.31	56.615	54.377	53.907		73.90	74.70	59.50	53.80
C2	5.27	5.271	5.278	5.261	5.071	4.94	4.894	4.727	4.687		6.41	5.51	5.55	5.13
C3	3.365	3.379	3.625	3.684	3.683	3.615	3.588	3.479	3.452		3.09	3.46	4.06	4.16
iC4	0.423	0.425	0.463	0.473	0.473	0.461	0.456	0.438	0.433		0.37	0.43	1.13	0.56
nC4	1.415	1.423	1.588	1.639	1.68	1.649	1.635	1.574	1.558		1.39	1.51	1.93	2.21
iC5	0.734	0.745	0.924	0.969	1.026	1.024	1.022	1.007	1.002		0.31	0.39	0.49	0.58
nC5	0.832	0.845	1.06	1.117	1.197	1.198	1.195	1.178	1.173		0.91	0.89	1.09	1.37
C6	0.898	0.918	1.247	1.332	1.459	1.471	1.472	1.465	1.462		1.33	1.21	1.27	1.77
C7	4.97	5.20	10.37	12.64	19.41	22.09	22.90	25.64	26.24		8.22	6.52	19.27	23.57
Pressure	517.6	518.2	524.4	525.2	528.1	530.7	531.7	535.8	536.8		520.34	520.34	528.10	418.00
Temperature	67.8	68.2	72.2	72.6	73.9	75.0	75.4	77.0	77.4		68.3	68.3	71.0	70.0
Phase	Gas	Gas	Gas	Oil	Oil	Oil	Oil	Oil	Oil		gas	gas	oil	oil
Sat Point	382	387.95	473.46	482.78	457.57	437.66	431.2	408.93	404.04		482.43	473.79	460.20	380.45
GOR	2308	2178.6	812	589.3	272.9	212.5	197.8	157.9	150.7		1077	1103	282	135
API	45	45	39	37	32	30	30	29	28		45	48	32	30

Figure 7-37 shows the variations in saturation pressure and reservoir pressure with depth (m). As with the previously described thermo-gravity model, there is no sharp gas oil contact found by this modified model; instead, there is a continuous unsaturated gas oil contact. A comparison of some of the PVT properties predicted by this model and by the previous models with the measured data for the petroleum fluids in the Greater Birba area is given in Figure 7-38.

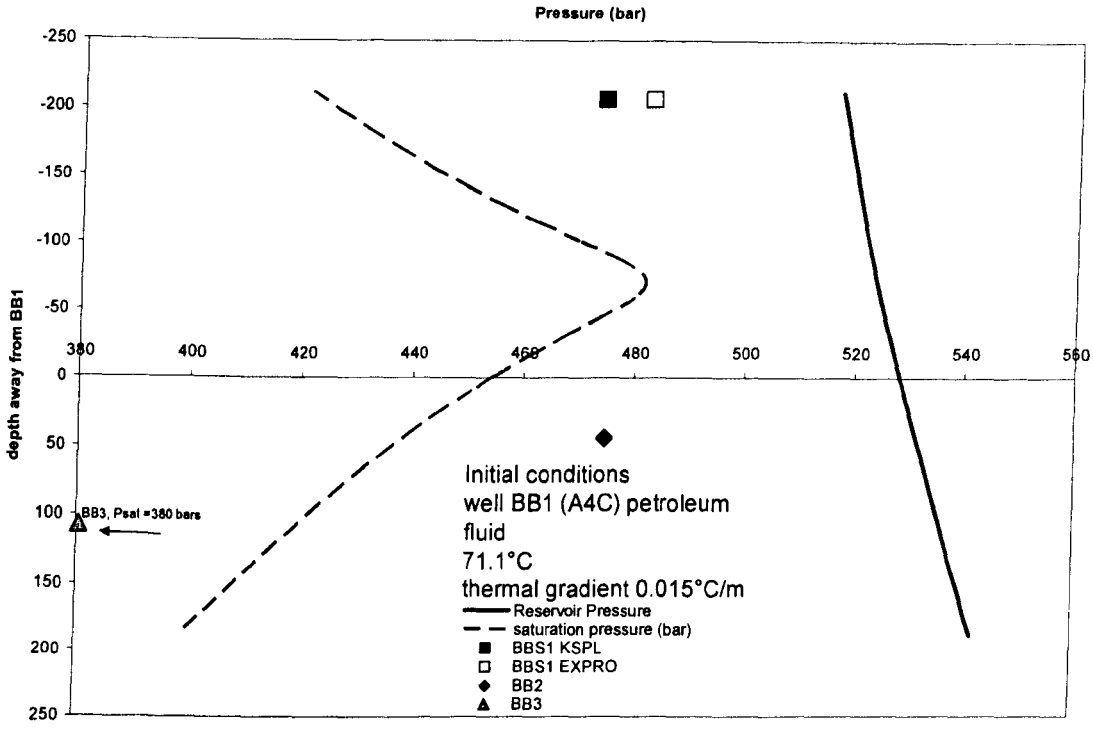

Figure 7-37: Variation in saturation pressure and reservoir pressure with depth as predicted by the non-isothermal gravity induced compositional gradient model using BB1 properties as initial conditions and a temperature of 71.1°C and thermal gradient of 0.015°C/m

7.3.3.3 Is there a compositional gradient in the Birba Field?

All models are plotted in Figure 7-38. As stated previously, these models are based on the assumption that that the measured PVT data are accurate. The quality of the data is assessed in Section 7.1.3. All models, whether isothermal or non-isothermal, predict a gas oil contact at or below the BBS1 interval. Some models were able to quite accurately predict some fluid properties, as shown above, but there is no single model that could accurately predict the gas oil ratio, which is a very important property. Any uncertainty in this ratio affects directly the composition of the fluid and

its properties (Danesh, 1998). As far as the author is aware, very few modelling studies have included the prediction of physical properties other than saturation pressure and composition. Figure 7-38 shows a comparison between different modelled compositional gradients using the BB1 fluid as the starting mixture datum and the measured data. The gradients cross each other and the x axis at the BB1 fluid (datum), the red triangles below the datum are for BB2 and BB3, respectively, and the triangles above the datum are for the BBS1 fluid (KSPL and Expro). The differences between predicted and real compositional gradients are reduced when gravity effects are coupled with thermal diffusion effects (Hoier & Whitson, 2001), as is clear from Figure 7-38. The main two compositional properties, CH_4 and the C7plus fraction, show a good match with the non-isothermal compositional gradients. However, this match is not observed in the other properties, suggesting that they are controlled by other factors. These properties are closely related thermodynamically. Figure 7-38 shows that the measured properties are not well related; saturation pressure and GOR are well predicted by the isothermal models whereas API gravity and compositions are best predicted by the non-isothermal model. The plot in the right bottom corner of Figure 7-35 shows that API gravity of the fluids and saturation pressures are not well correlated with the values calculated by the SRK equation of state. This suggests that the apparent compositional grading in the Birba Field is not a simple thermodynamically driven compositional grading, although this effect might occur, and that other controls such as gas/condensate admixture, charge history and reservoir geological evolution are probably more effective in the field.

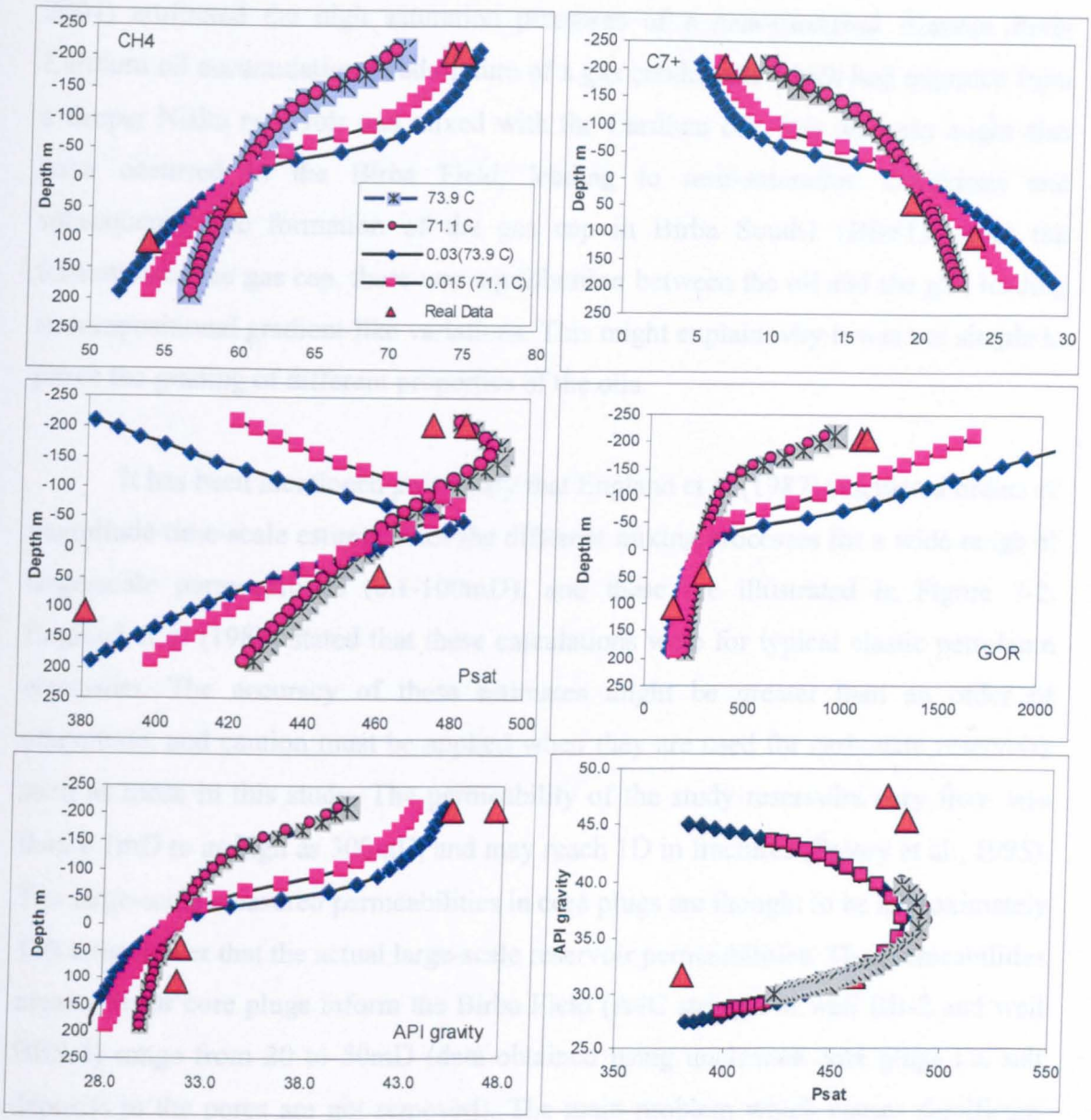

Figure 7-38: The variation in different PVT properties with depth using BB1 as a datum for the model and comparison with measured data of BB2, BB3 and BBS (KSPL+Expro). The legend is shown in the upper left chart.

It is important to include other properties in the prediction of compositional grading as well as compositions, yet many researchers avoid including them in their models. (Stainforth, 2004) stated that the current thermodynamic theories of compositional equilibrium under both gravity and temperature do not adequately explain the large compositional gradients observed, as will be discussed later, and (Hoier & Whitson, 2001)doubted that most petroleum fields satisfy the fundamental assumptions in most of the present compositional grading models. Therefore, there might be another explanation for the grading observed in the Birba Field. (Thompson,

2004) attributed the high saturation pressures of a near-saturated Brazeau River Cardium oil accumulation to admixture of a gas condensate which had migrated from a deeper Nisku reservoir and mixed with the Cardium oil. This scenario might also have occurred in the Birba Field, leading to near-saturation conditions and subsequently the formation of the gas cap in Birba South1 (BBS1). After the formation of the gas cap, there was equilibration between the oil and the gas, leading to compositional gradient-like variations. This might explain why it was not simple to prove the grading of different properties of the oils.

It has been mentioned previously that England et al (1987) calculated orders of magnitude time-scale estimates for the different mixing processes for a wide range of large-scale permeabilities (0.1-100mD), and these are illustrated in Figure 7-2. England et al (1987) stated that these calculations were for typical clastic petroleum reservoirs. The accuracy of these estimates might be greater than an order of magnitude, and caution must be applied when they are used for carbonate reservoirs such as those in this study. The permeability of the study reservoirs vary from less than 0.1mD to as high as 300mD, and may reach 1D in fractures (Protoy et al., 1995). The large-scale measured permeabilities in core plugs are thought to be approximately 100 times lower that the actual large-scale reservoir permeabilities. The permeabilities measured for core plugs inform the Birba Field (A4C stringer at well BB-2 and well BBS-1) range from 20 to 50mD (data obtained using uncleaned core plugs i.e. salt deposits in the pores are not removed). The main problem which causes significant degradation of reservoir quality carbonate stringers is the salt/anhydrite plugs, which can decrease the permeability by more than three orders of magnitudes, as shown in Chapter 2., The main Birba Field therefore probably has large-scale permeabilities in the range 0.2-0.5mD, since the large-scale permeability may be ca.100 times smaller than the core plug permeability.

Molecular diffusion and density-driven mixing are the two main processes that are responsible for mass transfer within the petroleum reservoir. Diffusion is the transfer of mass within a petroleum reservoir by the random motion of molecules and results in the mitigation of the chemical potential gradients (England et al., 1987). The time necessary for vertical diffusion to achieve equilibrium within a reservoir (i.e. to eliminate the chemical potential gradient) can be calculated using the equation below:

Equation 7-4: Order of magnitude time scale for vertical diffusion (seconds)

$$\frac{0.1 H^2 \theta_v^2}{D}$$

While the time necessary to achieve equilibrium horizontally by molecular diffusion is calculated using the following;

Equation 7-5: Order of magnitude time scale for horizontal diffusion (seconds)

$$\frac{0.1 L^2 \theta_h^2}{D}$$

Where:

- H is the height of the petroleum reservoir (m)
- L is the length of the reservoir (m)
- D is the diffusion coefficient and is estimated for pure C_{12} component 1.7 x 10^{-10} m^2/s (England et al., 1987)
- θ_v is the vertical tortuosity due to shales etc. (assumed to vary between 1 and 10, inversely related to permeability) (England et al., 1987)
- θ_h is the horizontal tortuosity (assumed to be 1.0) (England et al., 1987)

In the main Birba field, the modelled compositionally graded hydrocarbon column (from well BB-2 to well BBS-1) has a length of 3310m and a height of 260m, approximately. Therefore, the time necessary for vertical diffusion to achieve equilibrium is 1.3 Ma and 126.2 Ma for tortuosities of 1 and 10, respectively, while horizontal diffusion needs about 204Ma (assuming $\theta = 1$) to eliminate the chemical potential gradient.

Density-driven mixing is a mechanical equilibration mass transfer process that tends to eliminate density differences. England et al (1987) combined Darcy's Law with lateral density gradients estimated from GOR data and calculated an order of magnitude time-scale for this mechanical equilibration process. This time-scale can be calculated using the equation below:

Equation 7-6: Order of magnitude time-scale for density-driven mixing (seconds). The best values for these parameters that are relevant to the main Birba field are given in parentheses.

$$\frac{\phi L^2 \mu}{S\langle k\rangle g \Delta\rho H}$$

Where:

- Φ = porosity (0.1)
- μ = viscosity (10^{-2} Pa s)
- $\Delta\rho$ = density difference between the two oil charges (120 Kg/m^3) since oil-condensate mixing is proposed in this study.
- S = 0.95
- ‹k› the reservoir wide permeability (0.2mD = 1.93 * 10^{-13} m^2)

The time-scale for this mixing process was calculated for the main Birba field using the data above (in parenthesis); it is found to be fast, due to the large contrast between the densities of the oil and condensate involved in mixing (using density of 0.8810 and 0.760 kg/m^3 for an oil and a condensate, respectively). Using this calculation, it was found that only 6.1Ma was needed for density-driven mixing to eliminate the density gradient in the whole petroleum reservoir.

Unfortunately, no reliable basin modelling study has been performed for the Greater Birba area. The most relevant basin modelling study is that reported by Toth (2000), and this has a fundamental problem in that it was based on the assumption of a low heat rate. This model predicted that the main oil charge to the carbonate stringers occurred between the early Palaeozoic (500-400Ma) and early Mesozoic and the present day (250-0Ma). From these conclusions and taking Toth's model as the only model available, there has been enough time for the Birba Field to develop gravitational compositional gradients and there is therefore a strong possibility that the gravity or thermal gravity gradients are present.

Stainforth (2004) hypothesized a theory that explains the compositional gradient patterns observed in many basins all over the world, as alternative to the most widely accepted "insufficient mixing" theory proposed by England *et al.* The main difference between the Stainforth (2004) model and the England *et al* model, is in the filling pattern. Stainforth (2004) proposed that new charges to a reservoir

should advance to the top of the structure and progressively displace the earlier charges. This should produce a strong compositional gradient controlled by the maturity of the different charges arriving at the reservoir. According to England et al, this gradient is a result of mixing driven by density and molecular diffusion and reworked by gravity segregation. Stainforth (2004) agreed with England et al that the key factor in trap filling is the general "inadequacy of diffusive mixing". This is related, as mentioned above, to aspects such as the dimensions and quality of the reservoir and the complex composition of the petroleum (for simplicity, diffusive mixing is calculated assuming that the diffusion coefficient of the petroleum is similar to that for C_{12} = 1.7 x 10^{-10} m^2/s). According to the Stainforth (2004) model, the compositional gradient produced by filling will move gradually towards equilibrium, eliminating the chemical potential driven by gravity and temperature fields. Therefore, in most common cases where diffusive mixing is limited, the API gravity gradient mainly reflects the charge-filling history (i.e. the changes in charge composition during trap filling) rather than gravitational or Soret (temperature-gravity gradient) effects, i.e. the high API gravity of petroleum at the top of the structure reflects the highest maturity charge that advanced to the top of the reservoir. Applying this model to the Greater Birba study, the gas condensate in the top of the structure should have arrived late in the filling history and should be of higher maturity than the initially emplaced oil, which it displaced down the column, and there has been insufficient time for complete mixing in the column. Since the reservoir may attain equilibrium in less than 200Ma (as calculated above), it may be suggested here that the condensate charge came only recently. In the absence of a reliable basin modelling study, either filling model could be applicable. However, neither model can explain the geochemical features observed in this project.

7.4 Summary and conclusions:

The aim of this chapter was to confirm the conclusions from previous chapters, in which it was proposed that oil-condensate mixing is a more plausible explanation for the observed variation in physical properties of the oils in the Greater Birba area. The intention was also to discuss and test Riemens *et al* (1985)'s isothermal gravity induced compositional gradient; to examine the phase relationships of the study fluids;

and to investigate whether various compositional gradient models could explain the apparent compositional gradient in the Birba field.

The phase relationship between the petroleum fluids in the Greater Birba area show characteristics typical of mixed oils and might suggest that the control on the observed variations in geochemistry and bulk properties is the mixing of oil with light gas condensates and gas charges. Only oils from wells BB31 and Durra1 were examined to prove this relationship. Mixing models were hypothesized for each of these fluids and good matches were obtained using both models. Although these models confirm that mixing is a plausible explanation for the distribution of the fluids in the Greater Birba area, caution must be applied due to the unreliability resulting from inappropriate sampling.

A simple thermodynamic model cannot adequately model the compositional grading observed in Birba field, and it is suggested that a model which involves a combination of thermodynamic grading and admixture of gas condensates is more appropriate. The distribution of PVT properties present in the oils from the Birba field was found to reflect neither incomplete mixing, as proposed by England et al (1987), nor the reservoir charge/ filling history, as proposed by Stainforth (2004).

Chapter 8 Conclusions and future work

8.1 Overall conclusions

8.1.1 Introduction

This research work is a geochemical study of petroleum fluids from the Greater Birba area in the South Oman Salt Basin in South Oman; part of an on-going project run by Shell and PDO to understand the distribution and the origin of petroleum fluids in carbonate stringers which are fractured and floating in salt. The main aim of this work is to improve understanding of the distribution of petroleum fluids in the Greater Birba area using both Geochemistry and PVT modelling. Towards this aim, a number of objectives were considered:

- Geochemical characterization of petroleum fluids in the studied area was done on oil, condensate and gas to understand the nature of the source facies for these oils and their level of maturity as well as any other secondary processes they were affected by.
- To perform oil-oil and oil-condensate correlations using conventional parameters as well as statistical evaluation such as principal component analysis.
- To contribute to the understanding of the controls on the variations on acidity and sulphur in the studied oils.

This chapter presents the conclusions drawn from this work as well as their significance and any future work needed to elucidate the whole picture.

The petroleum reservoirs in the study area are 4 carbonate stringers, A1C, A3C, A4C and A5C (Upper Huqf supergroup) of Infracambrian age. Twenty two oils and 20 reservoir core rock samples were collected from these carbonate reservoirs from 11 wells distributed in an area of 250 km^2. The reservoir core rock samples were collected from A4C reservoir unit from 4 different wells in the main Birba area.

8.1.2 Characterization of petroleum fluids in the Greater Birba area

Most of the oils in the Greater Birba area are probably derived from organic rich carbonate facies source rocks deposited in hypersaline and highly reducing environment. Some geochemical characteristics suggested a Precambrian-Cambrian (Infracambrian) age of the source of these oils. Only two exceptions were observed, oil O15, which is sampled from A1C reservoir unit (in contact with middle Huqf sediments) from well Kaukab1 and oil O5 (A3C, well BBN1). Oil O15 shows geochemical features of low sulphur carbonate source rocks, while oil O5 might be contaminated sample with a younger oil.

A number of maturity parameters based on biomarkers and aromatic hydrocarbons suggested that most of the studied oils are of similar thermal maturity and in most cases the condensates also show similar maturity as oils, based on these maturity parameters. However, the light hydrocarbon composition differentiates between gas condensates, A4C oils and A3C/A5C oils in terms of maturity as A4C oils show higher maturity characteristics than A3C/A5C oils, and both types of oils are probably of lower maturity than the condensates. It is concluded that this difference in maturity is due to mixing with a higher maturity condensate charge. The estimated thermal maturity varies depending on the hydrocarbon range; most of the studied oils show vitrinite reflectance equivalence in the range of 0.8 to 0.9 based on methylphenanthrene index (MPI1), while a lower estimated thermal maturity of 0.3 R_c% (R_c = calculated vitrinite reflectance equivalence) was suggested by gas analysis. Some of the maturity ratios of light hydrocarbons (e.g. V = C_7 paraffins (acyclic alkanes)/naphthenes) suggested anomalously high over mature values (4-6 R_c%). It is considered that in addition to maturity effect, this is a consequence of a combination of minor facies variations between those oils and phase fractionation effect.

Biodegradation, water washing and bacterial/thermochemical sulphate reduction processes have not been found to have a significant effect on the studied oils. Only oil O13, which is from A4C reservoir unit of well Nassir1 south-south-east of the greater Birba area, may show a noticeable effect of water washing in the light hydrocarbons fraction suggested by low benzene and toluene contents and is isotopically heavier toluene in this oil relative to the other oils, but no evidence

supporting the effect of water washing in oil O13 was found in the other analyses. In contrary, the relative abundances of alkyl phenanthrene and alkylnaphthalene suggests against this effect. Therefore, these geochemical features in this oil might be possibly related to facies variations.

There is no apparent spatial trend on the data from the analysis of the C_0-C_2 alkyl carbazoles and C_0-C_2 alkyl phenols could be related to migration. Birba oils show higher values of shilded/exposed isomers ratios of alkylcarbazoles and alkylphenols than other oils, suggesting longer migration distance. However, since the carrier beds are mostly carbonate and the migration pathway was most probably vertical faults, longer migration distance for only birba oils may be unlikely. The higher values of shilded/exposed isomers ratios of alkylcarbazoles and alkylphenols may possibly be related to the proposed mixing of the original oils with the condensate charge. This is further supported by the high values of these parameters in condensates as well.

It is proposed that the oils in the Greater Birba area were subjected to mixing with a single or multiple condensate charge, and that the variations in physical and chemical properties of these fluids are related to this mixing. Several evidences were presented throughout the thesis supporting this proposal including biomarkers and aromatic concentrations, statistical evaluation, light hydrocarbons, sulphur distribution, alkylcarbazoles distribution, and finally PVT modelling. Statistical evaluation of biomarker concentrations allowed me to distinguish between two main groups of oils except the condensates, which otherwise look similar using conventional parameters. These are the Birba oils (O4 from well BB1 and O1 from well BB2) and Birba North oil (O7 from well BBN2) in one group and the rest of the surrounding oils in another group. The first group of oils are all associated with condensates up dip. This was used as indication that these oils were mixed with a condensate charge-rich in *n*-alkanes followed by formation of liquid rich gas phase. The other oils were also mixed with condensates but to a less extent. The light hydrocarbons analysis distinguished clearly between A4C oils and A3C/A5C oils and suggested that A4C oils are mixtures of A3C/A5C oil and condensates. The light hydrocarbons analysis suggested that the condensates are probably of high maturity

and A4C oils show higher maturity characteristics due to the mixing with these condensates. Alkylcarbazoles and the distribution of sulphur and sulphur isotopes also support the hypothesis that the oils were mixed with condensates. PVT modelling allowed the testing of this hypothesis; a good match between the models and the real data for two oils by mixing an oil having the same composition to the oil from well Kaukab1 (A3C) (assuming this oil is the original) and a condensate having the same composition to the condensate from Budour1H2 (A4C) and further mixed with a heavy dry gas component.

Two types of mixing curves were suggested and both might have occurred. There might be mixing between the original oils which are similar to the A3C oil (e.g. O11) from well Kaukab1 with condensates, suggested by biomarkers, aromatic hydrocarbons, and light hydrocarbons, and there might also be mixing between the original oils which are similar to oil O15 (A1C, well Kaukab1) with condensates, suggested by sulphur contents and isotopes distributions, and the minor facies variations observed in various parameters in chapter 4 and chapter 5, both have the condensates as an end member. There is no enough evidence for the second type of mixing sequence, but it may suggest that prior mixing of the original oils with condensate charge, the original oils were mixtures of two slightly different oils similar to O15 as one end member and A3C oils as the other end member.

From PVT modelling, it is concluded that the compositional gradient claimed by Riemens *et al* (1988), could not be proved by the available PVT simulation package. However, there was a form of compositional gradient found between BB1 and BBS1. The principals of compositional grading in most of the PVT simulation packages were based on the gravity and/or thermal effect during residence time in reservoirs. However, the studied oils show signs of mixing with a condensate charge(s) and gas charge(s) and therefore the gradient formed as a result of an increase in the gas content of the system.

The core extracts show noticible differences with the studeid oils using number of parameters suggesting different oil charges. The core extracts are probably of higher maturity than the produced oils. This indicates that the fresh new charges of oil that flooded the Birba Field were from another source of lower maturity. There

were no big variations among maturity parameters identified in produced oils and so the filling direction of these new charges cannot be predicted. It is possible that the oils in the carbonate stringers at present day reflects new charge different to that present in the bitumen. It is also important to note that the oils extracted from condensate zones are similar to other oils but different to the condensates. This suggests that the oil was there before the arrival of condensate charge that displace oil downwards. It is also concluded here that the latest oil charge did not reach A4C in BB4 suggesting that the sealing fault that separate the BB4 block was there before this charge.

The analysis of five gas samples from the study area revealed that these gases have been subjected to secondary alteration. Most of the gas samples are characterised by heavier methane relative to ethane. It was suggested that there was a probably an isotopically heavier higher maturity dry gas charge that mixed with the original normal maturity gases in reservoir. This may have contributed in raising the saturation pressure of the studied oils and led to formation of two phases, which is coherent with proposed theory and PVT modelling. The other possibility for the heavy methane is leakage through the cap rock, which is anhydrite in our case. However, the possibility of some selective biogenic alteration of these gases remains; the bacteria might have utilised ethane selectively, as possibly suggested by the large variation observed in carbon isotopic ratios of ethane and methane, while the rest of the light hydrocarbons show high similarity.

8.1.3 The origin of gas condensates

The distribution of the condensates in the Greater Birba area (they are confined to only one reservoir A4C, at least in the study area), suggested indirectly that these were probably phase fractionation products from the original oil that should look like similar as in A3C/A5C reservoirs. However, this was proved not accurate based largely on the basis of the analysis done on light hydrocarbons and supported by other data from biomarkers, aromatic hydrocarbons and others. The distribution of light hydrocarbons and various light hydrocarbons parameters suggested that the original oils in A4C were mixed with a condensate charge of probably higher maturity

than the original oils. Only very minor facies variations were discerned using light hydrocarbons analysis. However, it is suggested that these condensates had been sourced from slightly different facies (of probably higher sulphur content) and this is supported by mainly facies related mixing sequence (condensates-Birba oils/Birba North-surrounding oils) suggested by biomarkers and aromatic hydrocarbons.

I think that the condensate charge came as a separate charge and mixed with the originally unsaturated oil in place, which raised the saturation pressure of the mixture. Another dry gas charge flooded the reservoirs and pushed the saturation pressure even higher till it led to the formation of the gas phase. Phase fractionation effect occurred due to the subsequent equilibration between the two phases. This is one of several scenarios might be possible but all of them have one common conclusion which is that the condensates formed due to the arrival of a separate condensate charge and gas charge and mixed with original oil in place.

8.1.4 Phase fractionation effect

Phase fractionation/separation effect is proposed to have a significant impact on the study oils; this is inferred by the distribution of condensates in the study area. It was proposed that the mixing of the original oils with a separate condensate charge led to formation of two phase systems, which is usually accompanied by phase fractionation effect as suggested by Larter & Mills, (1992) and Thompson, (2004). It was not an easy task to distinguish between the two processes, mixing and phase fractionation. The effect of phase fractionation in the study oils was suggested by a number of phenomena: the distribution and concentration of alkylphenols, and light hydrocarbons as well as the distribution of the total acid number. These show a distributions similar to that expected by phase fractionations; i.e. the condensates are expected to have high contents of alkylphenols and light hydrocarbons and lower total acid numbers, while those "fractionated" oils should contain lower concentration of alkylphenols and light hydrocarbons and higher total acid numbers. The "unfractionated" oils are expected to have middle values of these parameters between condensates and oils. Obviously, this is opposite to the mixing theory. However, it is thought that the concentrations of light compounds were probably more sensitive to

phase separation, while the ratios are more sensitive to oil-condensate mixing. A separate study is needed to distinguish between these two processes especially in this case study. API gravity is found to have a good relationship with concentrations of the light hydrocarbons as illustrated in Figure 8-1. This is opposite to what is expected from oil-condensate mixing; assuming that the measured API gravities are accurate, this might be related to the phase separation resulting from oil-condensate mixing.

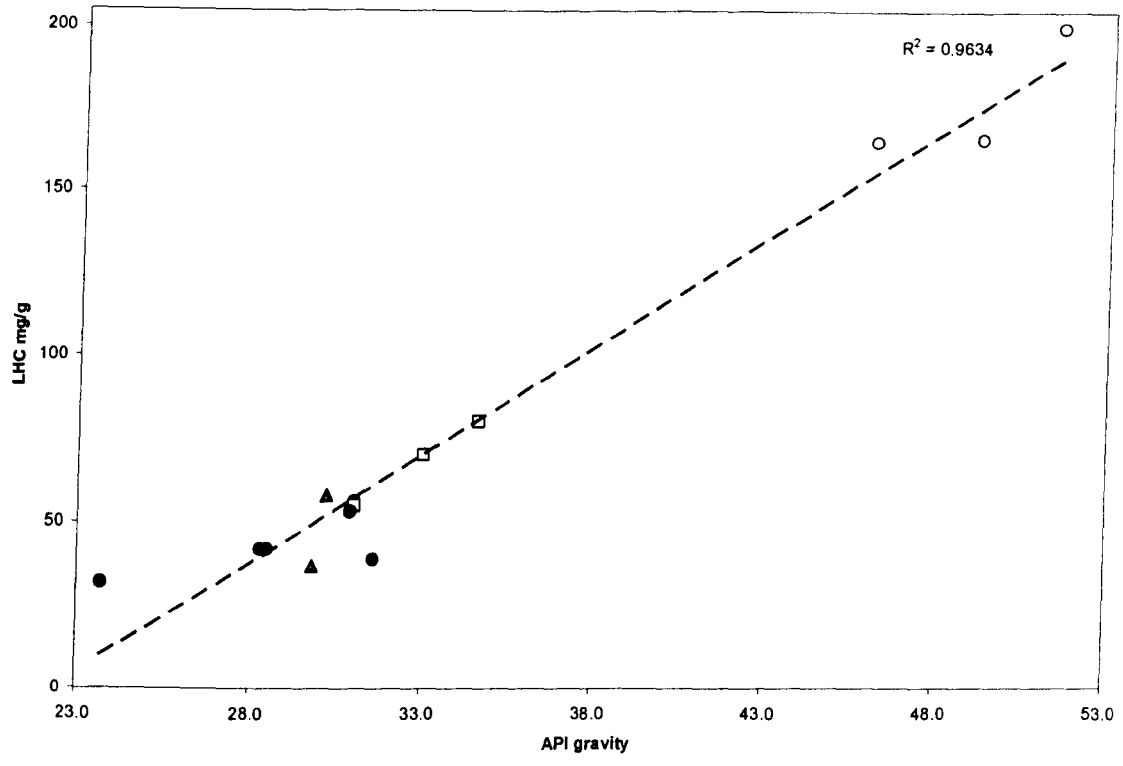

Figure 8-1: cross plot of API gravity versus Total amount of LHC (*n*-C_3-*n*-C_8, mg/g).

8.1.4.1 Controls on acidity and sulphur distribution

The studied oils are characterised by high TAN (Total Acid Number) values (mostly>0.5mg KOH/g oil). However, acidity needs further work as there were virtually no acids found in the studied oils using the chromatographic method developed by Aitken (2004). It was suggested though that the large variations in TAN were probably controlled by the phase fractionation/separation as mentioned above, due to the good relationship found between TAN and C_{15+} NSO compounds. Therefore, there should be a good relationship expected between API gravity and

TAN because they share the same control. Indeed, their cross-plot in Figure 8-2 reveals such a relationship confirming the statement above.

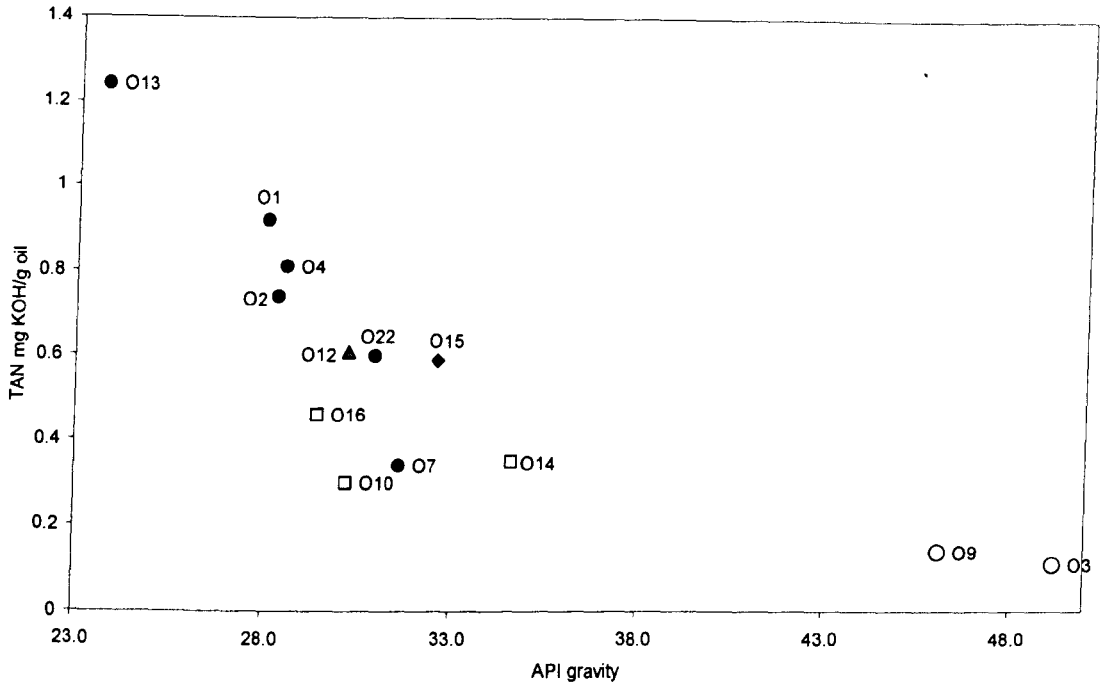

Figure 8-2: Cross plot of TAN versus API gravity.

Sulphur distribution might also be controlled by reactions with hydrogen sulphide which probably migrated from down dip. The sulphur addition mechanism was probably radiogenic alteration of hydrocarbons to olefins, which were readily attacked by hydrogen sulphide. Most of the sulphur was found in the aromatic fraction. The aromatic fractions analysed by FPD revealed that there are probably large numbers of different sulphur compounds as suggested by the presence of hump in the FPD chromatograms.

8.1.5 Filling model

Source facies variations, bacterial/thermal sulphate reduction, water washing and biodegradation processes are believed not to have had any significant impact in the distribution of the oils in the Greater Birba area. Phase fractionation and mixing with condensate (probably of higher maturity) were considered to be the major controls on the variations observed in the light hydrocarbons and also on the composition of oil and gas in the area. The filling scenario in the Greater Birba area is difficult to define accurately in the absence of accurate and reliable basin modelling studies. However, a model is suggested here based on the available evidence from this study:

- Similarity in most of the geochemical features in C_{15+} fraction suggests that the oils were either sourced from the same source rock or similar facies or sourced from different facies but it had time to homogenize.
- There is no systematic trend in chemical and physical properties, thus, filling direction cannot be predicted. It is thought that several migration pathways existed during charging of reservoir units, and probably the migration was mainly vertical (chapter 6).
- A condensate charge of possibly higher maturity and sourced from high sulphur source.
- Another isotopically heavy dry gas charge of higher maturity was added to the system. (chapter 4)
- Different types of fluids with widely different densities increased the free energy and degree of heterogeneity as well as saturation pressure of the system. This led to the formation of a gas cap, which equilibrated with the oil leg and form compositional grading column as illustrated in Figure 8-3.
- The isothermal gravitational compositional-grading model proposed by Riemens *et al* (1988) is not adequate to explain the geochemical features observed in both light and higher molecular weight hydrocarbons as discussed in chapter 7.

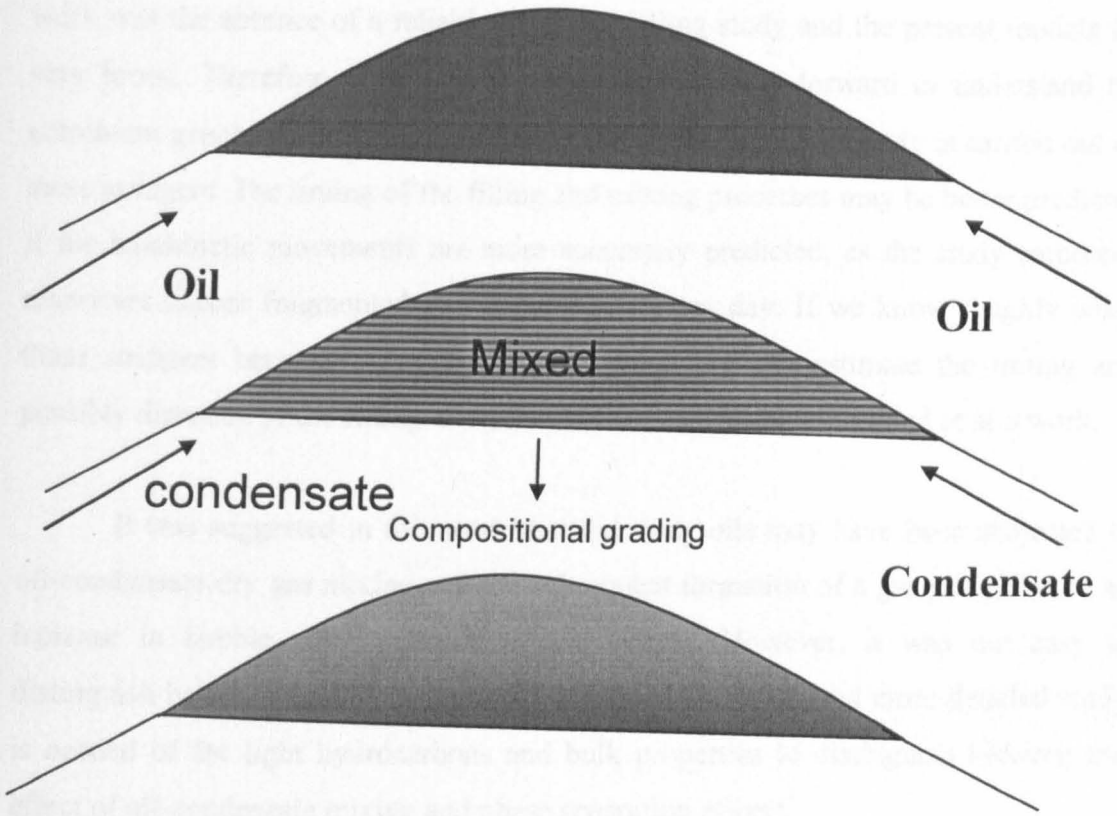

Figure 8-3: The proposed model for the filling of A4C reservoir based on the observation of light hydrocarbons.

8.1.6 Future work

It was a wonderful and challenging project to work with. However, there were gaps which could not be filled because of the lack of enough data and time allowed for the project. Some future works are suggested here which should provide a better understanding of the distribution of the petroleum fluids in the Greater Birba area.

More reservoir core rock samples should be acquired, and studied in details to understand the vertical and spatial variations in geochemical properties as well as some of the bulk properties. Although one of the implications of this study is that a self charge model is not adequate to explain the geochemical variations observed in the studied carbonate stringers, one of the important future studies could and should be done on the reservoir core rock samples are pyrolysis-GC/GC-MS and GC-IRMS to test further this self charge model. More integration is needed between geology, geophysics and geochemistry. I also recommend a separate study focusing on microscopy of the source facies. One of the potential difficulties during my research

work was the absence of a reliable basin modelling study and the present models are very broad. Therefore, it will be a very important step forward to understand the petroleum geochemistry of these stringers if a basin modelling study is carried out on these stringers. The timing of the filling and mixing processes may be better predicted if the halokinetic movements are more accurately predicted, as the study carbonate reservoirs appear fragmented and isolated at present day. If we know roughly when these stringers became fragmented and isolated, we can estimate the timing and possibly direction of the filling as well as mixing scales using England et al's work.

It was suggested in this work that the study oils may have been subjected to oil-condensate-dry gas mixing and the subsequent formation of a gas phase due to an increase in bubble point pressure of the system. However, it was not easy to distinguish between the two processes. Therefore, a separate and more detailed study is needed of the light hydrocarbons and bulk properties to distinguish between the effect of oil-condensate mixing and phase separation effects.

This study was aimed at exploring the controls on the main bulk properties that impact directly on the quality and economic value of the oil accumulation. However, it was not possible to arrive at a clear cut conclusion about what controls these properties. A high TAN but virtually no acids content was found in the study oils. Therefore, the relationship between sulphur content and acidity needs to be explored using detailed organic geochemical methods. It is also suggested that the methodologies of measuring acidity and/or TAN may need to be re-evaluated especially for high sulphur non degraded oils. The distribution of sulphur compounds and total sulphur content also need to be explored further.

The sulphur distributions in the studied crude oils also need to be studied further. Although it was concluded from this work that bacterial/thermochemical sulphate reduction are not occurring in the study reservoirs, a basin modelling study and more geochemical analysis such as hydrogen sulphide sulphur isotopic ratio, was needed to confirm this. One of the important data was needed to confirm these two processes were the sulphur isotopic signatures of the hydrogen sulphide in these reservoirs.

Fresh oils samples from the study area are needed in order to investigate alkylphenols, as the distribution of these species were anomalous and very different what has been reported so far; most of the study oils show anomalously high trimethylphenols contents and specifically 2,4,6 and 2,3,5 TMP. One suggestion here is that we need revaluation of response factors for these alkylphenols, specifically for the study oils.

Chapter 9 Reference

Ahmed, M.M., (2004) Application of GC-MS-MS to Biomarker Fingerprinting in Petroleum Geochemistry. In: *Civil Engineering and Geosciences, MSc*, pp. 75. University of Newcastle upon Tyne, Newcastle upon Tyne.

Ahsan, A., Karlsen, D.A., Patience, R., (1997) Petroleum biodegradation in the Tertiary reservoirs of the North Sea. *Marine and Petrol. Geol.*, 14, 55-63.

Aitken, C., (2004) Identification of non-hydrocarbon metabolites of deep subsurface anaerobic petroleum hydrocarbon biodegradation In: *Civil Engineering and Geosciences, PhD*, pp. 216. University of Newcastle upon Tyne, Newcastle upon tyne

Al-Barwani, B., (2003) Tectonic evolution of the South Oman salt basin. , pp. 450. Royal Holloway University of London

Al-Marjeby, A., Nash, D., (1986) A Summary of the Geology and Oil Habitat of the Eastern Flank Hydrocarbon Province of South Oman. *Marine and Petrol. Geol.*, 3, 306-314.

Al-Riyami, Q., (2005) Birba Field, A4C reservoir. *Field Strategy note* EMH05/154/PE, 30pp.

Al-Siyabi, H., (2005) Exploration history of the Ara intrasalt carbonate stringers in the South Oman Salt Basin. *GeoArabia*, 10, 39-68.

Alsharhan, A.S., Nairn, A.E.M., (1997) *Sedimentary Basins and petroleum geology of the Middle East*. Elsvier, Amsterdam.

Amthor, J., Grotzinger, J., Schrooder, S., Bowring, S., Ramezani, J., Martin, M., Matter, A., (2003) Extinction of Cloudina and Namacalathus at the Precambrian-Cambrian boundry in Oman G. *Geology*, 31, 431-434.

Amthor, J., Ramseyer, K., Faulkner, T., Lucas, P.T., (2005) Stratigraphy and sedimentology of a chert reservoir at the Precambrian-Cambrian Boundary: the Al Shomou Silicilyte, South Oman Salt Basin. *GeoArabia*, 10, 89-122.

Anderson, T.F., Pratt, L.M., (1995) Isotopic evidence for the origin of organic sulfur and elemental sulfur in marine sediments In: M.A. Vairavamurthy, M.A. Schoonen (Eds.), *Geochemical transformation of sedimentary sulfur, ACS Symposium series 612* (Ed. by M.A. Vairavamurthy, M.A. Schoonen), pp. 378-396. American Chemical Society, Washington DC.

Anissimov, L., Bylinkin, G., (2003) Washing processes and fluid variations: phase equilibria to petroleum geochemistry. *Oil & Gas Journal*, 101(1), 32-38.

Aplin, A.C., Coleman, M.L., (1995) Sour gas and water chemistry of the Bridport Sands reservoir, Wytch Farm, UK. In: W.A. England, J. Cubitt (Eds.), *The Geochemistry of Reservoirs., 86, Geological Society Special Publication* (Ed. by W.A. England, J. Cubitt), pp. 303-314. The Geological Society, London.

Aquino Neto, F.R., Trendel, J.M., Restle, A., Connan, J., Albrecht, P.A., (1983) Occurrence and formation of tricyclic and tetracyclic terpanes in sediments and petroleum. In: M. Bjor'y, et al. (Eds.), *Advances in Organic Geochemistry 1981* (Ed. by M. Bjor'y, et al.), pp. 659-667. Wiley, Chichester.

Bailey, N.J.L., Krouse, H.R., Evans, C.R., Rogers, M.A., (1973) Alteration of crude oil by waters and bacteria - evidence from geochemical and isotopic studies. *AAPG*, 57, 1276-1290.

Bakr, M.M.Y., Wilkes, H., (2002) The influence of facies and depositional environment on the occurrence and distribution of carbazoles and benzocarbazoles in crude oils: a case study from the Gulf of Suez, Egypt. *Organic Geochemistry*, 33(5), 561-580.

Barakat, A.O., Rullkoetter, J., (1995) Extractable and bound fatty acids in core sediments from the Nordlinger Ries, southern Germany. *Fuel*, 74, 416-425.

Baskin, D.K., Peters, K.E., (1992) Early generation characteristics of a sulfur-rich Monterey kerogen. *AAPG Bull.*, 76(1), 1-13.

Bastow, T.P., van Aarssen, B.G.K., Herman, R., Alexander, R., Kagi, R.I., (2003) The effect of oxidation on the distribution of alkylphenols in crude oils. *Organic Geochemistry*, 34(8), 1103-1111.

Bath, P.G.H., Fowler, W.N., Russell, M.P.M., (1980) The Brent Field, a reservoir engineering review. In: *The 1980 SPE European offshore petroleum conference and exhibition, paper EUR 164*, pp. 21-24.

Beach, F., Peakman, T.M., Abbott, G.D., Sleeman, R., Maxwell, J.R., (1989) Laboratory thermal alteration of triaromatic steroid hydrocarbons. *Org. Geochem.*, 14, 109-111.

Béchennec, F., Le Métour, J., Platel, J.-P., Roger, J., (1994) Drowning and down-warping of the Arabian Platform in Oman in relation to Eoalpine tectonics. In: M.I. Al-Husseini (Ed.), *GEO'94 Middle East Petroleum Geosciences, 1* (Ed. by M.I. Al-Husseini), pp. 167-178.

Belery, P., da Silva, F.V., (1990) Gavity and thermal diffusion in hydrocarbon reservoirs. In: *paper presented at the Third Chalk Research Program*, pp. 11-12, Copenhagen.

BeMent, W.O., Levey, R.A., Mango, F.D., (1994) The Temperature of Oil Generation as Defined with a C7 Chemistry Maturity Parameter (2,4-DMP/2,3-DMP Ratio). In: *Geologic Aspects of Petroleum Systems*, Mexico City, Mexico.

BeMent, W.O., Levey, R.A., Mango, F.D., (1995) The temperature of oil generation as defined with C_7 chemistry maturity parameter. In: J.O. Grimalt, C. Dorronsoro (Eds.), *Org. Geochem.: Developments and Applications to Energy, Climate, Environment and Human History - Selected papers from the 17th International Meeting on Org. Geochem.* (Ed. by J.O. Grimalt, C. Dorronsoro), pp. 505-507. AIGOA, San Sebastian.

Bennett, B., Bowler, B., Larter, S., (1996) Determination of C0-C3 Alkylphenols in Crude oils and waters. *Analytical Chemistry*, 68(20), 3697-3702.

Bennett, B., Chen, M., Brincat, D., Gelin, F.J.P., Larter, S.R., (2002) Fractionation of benzocarbazoles between source rocks and petroleums. *Organic Geochemistry*, 33(5), 545-559.

Bennett, B., Larter, S., (2000) Quantitative Separation of Aliphatic and Aromatic Hydrocarbons Using Silver Ion-Silica Solid-phase Extraction. *Analytical Chemistry*, 72, 1039-1044.

Bennett, B., Larter, S.R., (1997) Partition behaviour of alkylphenols in crude oil/brine systems under subsurface conditions. *Geochim. Cosmochim. Acta*, 61, 4393-4402.

Berner, U., Faber, E., (1988) Maturity related mixing model for methane, ethane and propane, based on carbon isotopes. *Org. Geochem.*, 13, 67-72.

Bigge, M.A., Farrimond, P., (1998) Biodegradation of oils in the Wessex Basin: a complication of correlation. In: J.R. Underhill (Ed.), *Development, Evolution and Petroleum Geology of the Wessex Basin, 133, Geological Society of London, Special Publication* (Ed. by J.R. Underhill), pp. 373-386.

Brocks, J.J., Logan, G.A., Buick, R., Summons, R.E., (1999) Archean molecular fossils and the rearly rise of eukaryotes. *Science*, 285, 1033-1036.

Brooks, P.W., (1986) Unusual biological marker geochemistry of oils and possible source rocks, offshore Beaufort-Mackenzie Delta, Canada. In: D. Leythaeuser,

J. Rullk.tter (Eds.), *Advances in Organic Geochemistry 1985, Org. Geochem., 10* (Ed. by D. Leythaeuser, J. Rullk.tter), pp. 401-406. Pergamon.

Cai, C., Worden, R.H., Wang, Q., Xiang, T., Zhu, J., Chu, X., (2002) Chemical and isotopic evidence for secondary alteration of natural gases in the Hetianhe Field, Bachu Uplift of the Tarim Basin. *Organic Geochemistry*, 33(12), 1415-1427.

Carnipa-Morales, N.K., Galan-Vidal, C.A., Guzman, M., Jarvie, D., (2003) Effect of evaporation on C7 light hydrocarbon parameters. *Organic Geochemistry*, 34, 813-826.

Carpentier, B., Ungerer, P., Kowalewski, I., Magnier, C., Courcy, J.P., Huc, A.Y., (1996) Molecular and isotopic fractionation of light hydrocarbons between oil and gas phases. *Org. Geochem.*, 24, 1115-1139.

Chen, J., Deng, C., Liang, D., Wang, X., Zhong, N., Song, F., Shi, X., Jin, T., Xiang, S., (2003) Mixed oils derived from multiple source rocks in the Cainan oilfield, Junggar Basin, Northwest China. Part II: artificial mixing experiments on typical crude oils and quantitative oil-source correlation. *Organic Geochemistry*, 34(7), 911-930.

Chung, H., Walters, C., Buck, S., Brinham, G., (1998) Mixed signals of the source and thermal maturity for petroleum accumulations from light hydrocarbons: an example of the Beryl field. *Org. Geochem.*, 29(1-3), 381-396.

Clark, J.P., Philp, R.P., (1989) Geochemical characterization of evaporite and carbonate depositional environments and correlation of associated crude oils in the Black Creek Basin, Alberta. *Canadian Petroleum Geologists Bulletin*, 37, 401-416.

Claypool, G.E., (1974) Anoxic diagenesis and bacterial methane production in deep sea sediments. University of California, Los Angeles.

Clayton, J.L., Rice, D.D., Michael, G.E., (1991) Oil-generating coals of the San Juan basin, New Mexico and Colorado, U.S.A. *Org. Geochem.*, 17, 735-742.

Clegg, H., Wilkes, H., Horsfield, B., (1997) Carbazole distributions in carbonate and clastic source rocks. *Geochim. Cosmochim. Acta*, 61, 5335-5345.

Clegg, H., Wilkes, H., Oldenburg, T., Santamaria-Orozco, D., Horsfield, B., (1998) Influence of maturity on carbazole and benzocarbazole distributions in crude oils and source rocks from the Sonda de Campeche, Gulf of Mexico. *Org. Geochem.*, 29(1-3), 183-194.

Connan, J., (1984) Biodegradation of crude oils in reservoirs. In: J. Brooks, D.H. Welte (Eds.), *Advances in Petroleum Geochemistry, 1* (Ed. by J. Brooks, D.H. Welte), pp. 299-335. Academic Press, London.

Connan, J., Bouroullec, J., Dessort, D., Albrecht, P., (1986) The microbial input in carbonate-anhydrite facies of a sabkha palaeoenvironment from Guatemala: A molecular approach. *Org. Geochem.*, 10, 29-50.

Connan, J., Dessort, D., (1987a) Novel family of hexacyclic hopanoid alkanes (C_{32}-C_{35}) occurring in sediments and oils from anoxic palaeoenvironments. *Org. Geochem.*, 11, 103-113.

Connan, J., Dessort, D., (1987b) Novel family of hexacyclic hopanoid alkanes (C_{32}-C_{35}) occurring in sediments and oils from anoxic paleoenvironments. *Org. Geochem.*, 11, 103-113.

Cosentino, L., (2001) *Integrated reservoir studies*. Edition Technip, Paris.

Coveney, R.M.J., Goebel, E.D., Zeller, E.J., Dreschhoff, G.A.M., Angino, E.E., (1987) Serpentinization and the origin of hydrogen gas in Kansas. *AAPG Bull.*, 71, 39-48.

Creek, J.L., Schrader, M.L., (1985) Eeast Painter Reservoir: an example of a compositional gradient from a gravitational field. In: *Paper SPE 14411 presented at the 1985 SPE Annual Technical Conference and Exhibition*, pp. 22-25, Las Vegas.

Cross, M.M., (1999) Rates and mechanisms of thermochemical sulphate reduction. In: *Department of Earth Sciences, PhD.* University of Manchester Manchester

Cumbers, K.M., Alexander, R., Kagi, R.I., (1987) Methylbiphenyl, ethylbiphenyl and dimethylbiphenyl isomer distributions in some sediments and crude oils. *Geochemica et Cosmochemica Acta*, 51, 3105-3111.

Curiale, J., Frolov, E., (1998) Occurrence and origin of olefins in crude oils. A critical review. *Org. Geochem.*, 29(1-3), 397-408.

Curiale, J.A., Bromley, B.W., (1995) Migration-induced compositional changes in oils/condensates of a single field. In: J.O. Grimalt, C. Dorronsoro (Eds.), *Org. Geochem.: Developments and Applications to Energy, Climate, Environment and Human History - Selected papers from the 17th International Meeting on Org. Geochem.* (Ed. by J.O. Grimalt, C. Dorronsoro), pp. 327-328. AIGOA, San Sebastian.

Curiale, J.A., Bromley, B.W., (1996) Migration induced compositional changes in oils and condensates of a single field. *Org. Geochem.*, 24, 1097-1114.

Curiale, J.A., Cameron, D., Davis, D.V., (1985) Biological marker distribution and significance in oils and rocks of the Monterey Formation, California. *Geochim. Cosmochim. Acta*, 49, 271-288.

Dai, J., (1992) Identification and distinction of various alkane gases. *Science in China*, 35, 1246-1257.

Danesh, A., (1998) *PVT and Phase Behaviour of Petroleum Reservoir Fluids.* Elsevier.

de Oliveira Padua, K.G., (1997) Non-Isothermal Gravitational Composition Variation in a Large Deep Water Field , Paper No. 38854. *SPE.*

di Primio, R., (2002) Unraveling secondary migration effects through the regional evaluation of PVT data: a case study from Quadrant 25, NOCS. *Organic Geochemistry*, 33(6), 643-653.

Di Primio, R., Diekkmann, V., Mills, N., (1998) PVT and phase behaviour analysis in petroleum exploration. *Organic Geochemistry*, 29, 207-222.

di Primio, R., Horsfield, B., (1996) Predicting the generation of heavy oils in carbonate/ evaporitic environments using pyrolysis methods. *Org. Geochem.*, 24, 999-.

Dougherty, E.L., Drickamer, H.G., (1955) Thermal diffusion and molecular motion in liquids. *Journal of Physical chemistry*, 59, 443.

Droste, H.H.J., (1997) Stratigraphy of the Lower Paleozoic Haima Supergroup of Oman. *GeoArabia*, 2, 419-492.

Dueppenbecker, S., Horsfield, B., (1990) Compositional information for kinetic modelling and petroleum type prediction. In: B. Durand, F. Béhar (Eds.), *Advances in Organic Geochemistry 1989* (Ed. by B. Durand, F. Béhar), pp. 250-266. Pergamon Journals, Oxford.

Dzou, L.I.P., Hughes, W.B., (1993) Geochemistry of oils and condensates, K field, offshore Taiwan: a case study in migration fractionation. *Org. Geochem.*, 20(4), 437-462.

Ekweozor, C.M., Strausz, O.P., (1983) Tricyclic terpanes in the Athabasca oil sands: Their geochemistry. In: M. Bjor´y, et al. (Eds.), *Advances in Organic*

Geochemistry 1981 (Ed. by M. Bjor'y, et al.), pp. 746-766. J. Wiley & Sons, New York.

Eneogwe, C.I., (2004) The invariance ratio in isoheptanes: a powerful tool for oil-oil correlation in the Tertiary Niger Delta, Nigeria. *Organic Geochemistry*, 35, 989-oo2.

England, W.A., (1990) The organic geochemistry of petroleum reservoirs. In: B. Durand, F. Behar (Eds.), *Advances in Organic Geochemistry 1989, Org. Geochem.*, *16* (Ed. by B. Durand, F. Behar), pp. 415-425.

England, W.A., Mackenzie, A.S., (1989) Some aspects of the organic geochemistry of petroleum fluids. *Geologische Rundschau*, 78, 291-303.

England, W.A., Mackenzie, A.S., Mann, D.M., Quigley, T.M., (1987) The movement and entrapment of petroleum fluids in the subsurface. *Journal of the geological society*, 144, 327-347.

Farrimond, P., Taylor, A., Telnaes, N., (1998) Biomarker maturity parameters: the role of generation and thermal degradation. *Org. Geochem.*, 29(5-7), 1181-1198.

Fowler, M.G., Douglas, A.G., (1984) Distribution and structure of hydrocarbons in four organic-rich Ordovician rocks. *Org. Geochem.*, 6, 105-114.

Fowler, M.G., Douglas, A.G., (1987) Saturated biomarkers in oils of Late Precambrian age from Eastern Siberia. *Org. Geochem.*, 11, 201-213.

Frewin, N.L., Indrelid, S., Kowalewski, I., Carpentier, B., Huc, A., Gelin, F., Albercht, P., (2000) *Accurate charge risking of unconventional source rock/reservoir in South Oman.* GeoArabia.

Fu, J., Guoying, S., Pingan, P., Brassell, S.C., Eglinton, G., Jigang, J., (1986) Peculiarities of salt lake sediments as potential source rocks in China. *Org. Geochem.*, 10, 119-126.

Gabrielsen, R.H., Ulvoen, S., Elvsborg, A., Fredrik, O., (1985) The geological history and geochemical evaluation of Block 2/2 offshore Norway. In: B.M. Thomas (Ed.), *Geochemistry in Exploration of the Norwegian Shelf* (Ed. by B.M. Thomas), pp. 165-178. Graham and Trotman, London.

Gaffney, J.S., Premuzic, E.T., Manowitz, B., (1980) On the usefulness of sulphur isotope ratios in crude oil correlations. *Geochim. Cosmochim. Acta*, 44, 135-139.

Galimov, E.M., Posyagin, V.I., Porkhorov, V.S., (1972) Carbon isotope fractionation as a function of temperature in the CH4-C2H6-C3H8-C4H10 system. *Geokhimiya*, 8, 977-987.

George, S.C., Boreham, C.J., Minifie, S.A., Teerman, S.C., (2002) The effect of minor to moderate biodegradation on C5 to C9 hydrocarbons in crude oils. *Organic Geochemistry*, 33(12), 1293-1317.

Goldhaber, M.B., Orr, W.L., (1995) Kinetic controls on thermochemical sulfate reduction as a source of sedimentary H_2S. In: M.A. Vairavamurthy, M.A. Schoonen (Eds.), *Geochemical transformation of sedimentary sulfur, ACS Symposium series 612* (Ed. by M.A. Vairavamurthy, M.A. Schoonen), pp. 412-425. American Chemical Society, Washington DC.

Gorin, G.E., Racz, L.G., Walter, M.R., (1982) Late Precambrian -Cambrian sediments of the Huqf Group, Sultanate of Oman. *AAPG Bulletin*, 66, 2609-2627.

Gransch, J.A., Posthuma, J., (1974) On the origin of sulfur in crudes. In: B. Tissot, F. Bienner (Eds.), *Advances in Organic Geochemistry 1973* (Ed. by B. Tissot, F. Bienner), pp. 727-739. Editions Technip, Paris.

Grantham, P.J., lijmbach, G.W.M., Posthuma, J., (1990) Geochemistry of crude oils in Oman. In: S.T. Brookes (Ed.), *Clastic petroleum provinces, 50, Geological Society Special Publication* (Ed. by S.T. Brookes), pp. 317-328. Geological Society, London

Grantham, P.J., Lijmbach, G.W.M., Posthuma, J., Hughes Clarke, M.W., Willink, R.J., (1988) Origin of crude oils in Oman. *J. Petrol. Geol.*, 11(1), 61-80.

Grantham, P.J., Posthuma, J., De Groot, K., (1981) Variation and significance of the C27 and C28 triterpane content of a North sea core and various North Sea crude oils. In: A.G. Dougals, J.R. Maxwell (Eds.), *Advances in organic Geochemistry 1979* (Ed. by A.G. Dougals, J.R. Maxwell), pp. 29-38. Pergamon Press.

Grantham, P.J., Wakefield, L.L., (1988) Variations in the sterane carbon number distributions of marine source rock derived crude oils through geological time. *Org. Geochem.*, 12, 61-73.

Green, F.W., Graham, G.M., (1983) A reservoir geological model of the Birba Field, South Oman. *PDO Exploration Library* BO1902, 25p.

Halpern, H.I., (1995) Development and Applications of Light-Hydrocarbon-Based Star Diagrams. *AAPG Bull.*, 79(6), 801-815.

Hase, A., Hites, R.A., (1976) On the origin of the polycyclic aromatic hydrocarbons in recent sediments: biosynthesis by anaerobic bacteria. *Geochimica et Cosmochimca Acta*, 40, 1141-1143.

Heum, O.R., Dalland, A., Meisingset, K.K., (1986) Habitat of hydrocarbons at Haltenbanken (PVT-modelling as a predictive tool in hydrocarbon exploration). In: A.M. Spencer (Ed.), *Habitat of hydrocarbons at the Norwegian continental shelf* (Ed. by A.M. Spencer), pp. 259-274. Graham and Trotman, London.

Heward, A.P., (1990) Salt removal and sedimentation in Southern Oman. In: A.H.F. Robertson, M.P. Searle, A.C. Ries (Eds.), *The Geology and Tectonics of the Oman Region, 49, Geological Society Special Publication* (Ed. by A.H.F. Robertson, M.P. Searle, A.C. Ries), pp. 637-651.

Hirschberg, A., (1984) The role of asphaltenes in compositional grading of a reservoir's fluid column. *Society of Petroleum Engineers of the American Institute of Mining and Metallurgical Engineers, SPE paper No. 13171.*

Ho, T.Y., Rogers, M.A., Drushel, H.V., Koons, C.B., (1974) Evolution of sulfur compounds in crude oils *AAPG Bull*, 58, 2338-2348.

Hoier, L., Whitson, C.H., (2001) Compositional Grading - Theory and Practice. *SPE Reservoir Engineering.*

Hold, I.M., Schouten, S., Jellema, J., Sinninghe Damsté, J.S., (1999) Origin of free and bound mid-chain methyl alkanes in oils, bitumens and kerogens of the marine, Infra-Cambrian Huqf Formation (Oman). *Org. Geochem.*, 30, 1411-1429.

Hollis, C.E., Amthor, J., Grotzinger, J., Johnson, I.G., Lamers, E., (2002) Pore-system analysis of the Ara Group carbonates, South Oman Salt Basin. *Geo2004 Abstracts*, 7, 248.

Holt, T., Lindeberg, E., Ratkje, S.K., (1983) The effect of gravity and temperature gradients on methane distributions in oil reservoirs. *SPE*, 11761.

Horsfield, B., Clegg, H., Wilkes, H., Santamaria-Orozco, D., (1998) Maturity control of carbazole distributions in petroleum systems Naturwissenschaften. 85, 233-237.

Huang, H., Bowler, B.F.J., Zhang, Z., Oldenburg, T.B.P., Larter, S.R., (2003a) Influence of biodegradation on carbazole and benzocarbazole distributions in oil columns from the Liaohe basin, NE China. *Organic Geochemistry*, 34(7), 951-969.

Huang, H., Pearson, M.J., (1999) Source rock palaeoenvironments and controls on the distribution of dibenzothiophenes in Lacustrine crude oils, Bohai Bay Basin, eastern China. *Organic geochemistry*, 30, 1455-1470.

Huang, H.P., Jin, G., Lin, C., Zheng, Y., (2003b) Origin of unusual heavy oil from the Baiyinchagan depression, Erlian basin, northern China. *Marine and Petroleum Geology*, 20, 1-12.

Hughes-Clarke, M.W., (1988) Stratigraphy and rock unit nomenclature in the oil-producing area of Interior Oman. *Journal of Petroleum Geology*, 11, 5-60.

Hughes, W.B., Holba, A.G., Dzou, L.I.P., (1995) The ratios of dibenzothiophene to phenanthrene and pristane to phytane as indicators of depositional environment and lithology of petroleum source rocks. *Geochim. Cosmochim. Acta*, 59(17), 3581-3598.

Hughes, W.B., Holba, A.G., Mueller, D.E., Richardson, J.S., (1985) Geochemistry of greater Ekofisk crude oils. In: B.M. Thomas (Ed.), *Geochemistry in Exploration of the Norwegian Shelf* (Ed. by B.M. Thomas), pp. 75-92. Graham and Trotman.

Hunt, J.M., (1995) *Petroleum Geochemistry and Geology*. W. H. Freeman and Company, San Francisco.

Hunt, J.M., Huc, A.Y., Whelan, J.K., (1980) Generation of light hydrocarbons in sedimentary rocks. In: *Nature*, *288*, pp. 688-690.

Husseini, M.I., (1988) The Arabian Infracambrian extensional system. *Tectonophysics*, 148, 93-103.

Husseini, M.I., (1991) Tectonic and depositional model of the Arabian and adjoining plates during the Silurian-Devonian. *AAPG Bulletin*, 75, 108-120.

Hussler, G., Chappe, B., Wehrung, P., Albrecht, P., (1981) C_{27}-C_{29} ring A monoaromatic steroids in Cretaceous black shales. *Nature*, 294, 556-558.

Immerz, P., Oterdoom, W.H., El-Tonbary, M., (2000) The Huqf/Haima hydrocarbon system of Oman and the terminal phase of the Pan-African Orogeny: evaporite deposition in a compressive setting (Abstract). In: *Proceedings of GEO'2000; GeoArabia 5 (1)*, pp. 113-114, Bahrain.

Intertek-Caleb-Brett, (2006) *ASTM Testing Methods*. Intertek Group PLC.

Ioppolo-Armanios, M., Alexander, R., Kagi, R.I., (1994) Identification and origins of isopropylmethylphenols in crude oils. *Org. Geochem.*, 22, 815-824.

Ioppolo, M., Alexander, R., Kagi, R.I., (1992) Identification of C_0-C_3 phenols in some Australian crude oils. *Organic Geochemsitry*, 18, 603-609.

Ivelv, A.A., Pankina, R., Gal'peri, G.D., (1973) Thermodynamics of reactions of sulfurization of oil. *Petroleum Geology*, 11, 70-74.

Jarvie, D., Lundell, L., (2001) Kerogen type and thermal transformation of organic matter in the Miocene Monterey Formation. In: C.M. Issacs, J. Rullkoetter (Eds.), *The Monterey Formation: From rocks to moelcules* (Ed. by C.M. Issacs, J. Rullkoetter), pp. 268-295. Columbia University Press, New York.

Jenden, P.D., J., D.D., Kaplan, I.R., (1993) Mixing of thermogenic natural gases in Northern Appalachian Basin. *AAPG Bull.*, 77, 980-998.

Jenden, P.D., Kaplan, I.R., (1989) Origin of natural gas in Sacramento basin, California, *AAPG Bull.*, *73*, pp. 431-453.

Ji-Zhou Dong, Vorkink, W.P., Lee, M.L., (1993) Origin of long-chain alkylcyclohexanes and alkylbenzenes in a coal-bed wax. *Geochimica et Cosmochimica Acta*, 57(4), 837-849.

Jiang, C., Li, M., (2002) Bakken/Madison petroleum systems in the Canadian Williston Basin. Part 3: geochemical evidence for significant Bakken-derived oils in Madison Group reservoirs. *Organic Geochemistry*, 33(7), 761-787.

Johns, R.B., (1986) *Biological Markers in the Sedimentary Record.* Elsevier, New York.

Jones, D.M., Watson, J.S., Meridith, W., Chen, M., Bennett, B., (2001) Determination of Naphthenic acids in crude oils using nonaqueous ion exchange solid-phase Extraction. *Anal. Chem.*, 73, 703-707.

Karlsen, D.A., Larter, S.R., (1991) Analysis of petroleum fractions by TLC-FID: applications to petroleum reservoir description. *Org. Geochem.*, 17, 603-617.

Katz, B.J., Elrod, L.W., (1983) Organic geochemistry of DSDP Site 467, offshore California, Middle Miocene to Lower Pliocene strata. *Geochim. Cosmochim. Acta*, 47, 389-386.

Kempers, L.J., (1989) A thermodynamic theroy of the soret effect in a multicomponent liquid. *J. Chem. Phys.*, 90, 6541-6548.

Khavari-Khorasani, G., C. Dolson, J., Michelsen, J.K., (1998) The factors controlling the abundance and migration of heavy versus light oils, as constrained by data from the Gulf of Suez. Part I. The effect of expelled petroleum composition, PVT properties and petroleum system geometry. *Organic Geochemistry*, 29(1-3), 255-282.

Killops, S.D., Killops, V.J., (1993) *An Introduction to Organic Geochemistry.* Wiley, New York.

Killops, S.D., Killops, V.J., (2005) *Introduction to Organic Geochemistry.* Blackwell, New York.

Kissin, Y.V., (1987) Catagenesis and composition of petroleum: Origin of n-alkanes and isoalkanes in petroleum crudes. *Geochim. Cosmochim. Acta*, 51, 2445-2457.

Klomp, U.C., (1986) The chemical structure of a pronounced series of iso-alkanes in south Oman crudes. *Org. Geochem.*, 10, 807-814.

Kohnen, M., (1991) Sulphurised lipids in sediments: The key to reconstruct palaeobiochemicals and their origin, *PhD*, pp. 248. Door het College van Dekanen.

Kohnen, M.E.L., Sinninghe Damsté, J.S., ten Haven, H.L., de Leeuw, J.W., (1989) Early incorporation of polysulphides in sedimentary organic matter. *Nature*, 341, 640-641.

Krooss, B.M., Littke, R., Muller, B., Frielingsdorf, J., Schwochau, K., Idiz, E.F., (1995) Generation of nitrogen and methane from sedimentary organic matter: implications on the dynamics of natural gas accumulations. *Chem. Geol.*, 126, 291-318.

Krouse, H.R., Viau, C.A., Eliuk, L.S., Ueda, A., Halas, S., (1988) Chemical and isotopic evidence of thermochemical sulphate reduction by light hydrocarbon gases in deep carbonate reservoirs. *Nature*, 333, 415-419.

Kruge, M.A., Hubert, J.F., Bensley, D.F., Crelling, J.C., Akes, R.J., (1990) Organic geochemistry of a Lower Jurassic synrift lacustrine sequence, Hartford Basin, Connecticut, U.S.A. *Org. Geochem.*, 16, 689-701.

Kvalheim, O.M., (1987) Oil-source correlation by the combined use of principal component analysis modelling, analysis of variance and a coefficient of congruence. *Chemometrics and Intelligent labaratory systems*, 2, 127-136.

Lafargue, E., Le Thiez, P., (1996) Effect of waterwashing on light ends compositional heterogeneity. *Org. Geochem.*, 24, 1141-1150.

Larter, S., (1989) Chemical-Models of Vitrinite Reflectance Evolution. *Geologische Rundschau*, 78(1), 349-359.

Larter, S., Aplin, A., Wilhelms, A., Telnaes, N., Di Primio, R., Horstad, I., Olsen, S., (2000a) Biodegradation induced PVT changes in oil-rimmed gas accumulations. *Abstracts of Papers of the American Chemical Society*, 219, 50-GEOC.

Larter, S., Mills, N., (1991) Phase-controlled molecular fractionations in migrating petroleum charges. In: W.A. England, A.J. Fleet (Eds.), *Petroleum migration: Geological Society Special Publication No. 59* (Ed. by W.A. England, A.J. Fleet), pp. 137-147. Geological Society.

Larter, S., Mills, N., (1992) Phase-controlled molecular fractionations in migrating petroleum charges. In: W.A. England, A.J. Fleet (Eds.), *Petroleum migration, 59, Geological Society, Special Publication* (Ed. by W.A. England, A.J. Fleet).

Larter, S.R., Aplin, A.C., (1995) Reservoir geochemistry: methods, applications and opportunities. In: W.A. England, J. Cubitt (Eds.), *The Geochemistry of Reservoirs, 86, Geological Society Special Publication* (Ed. by W.A. England, J. Cubitt), pp. 5-32. The Geological Society, London.

Larter, S.R., Bowler, B., Clarke, E., Wilson, C., Moffat, B., Bennett, B., Yardley, G., Garruthers, D., (2000b) An experimental invistigation of geochromatographyduring secondary migration of petroleum performed under subsurfaces conditions with a real rock *Geochemical Transactions* 9.

Larter, S.R., Bowler, B.F.J., Li, M., Chen, M., Brincat, D., Bennett, B., Noke, K., Donohoe, P., Simmons, D., Kohnen, M., Allan, J., Telnaes, N., Horstad, I., (1996) Molecular Indicators of Secondary Oil Migration Distances. *Nature*, 383, 593-597.

Leythaeuser, D., Schaefer, R.G., Weiner, B., (1979) Generation of low molecular weight hydrocarbons from organic matter in source beds as a function of temperature and facies. *Chemical Geology*, 25, 95-108.

Li, M., Fowler, M.G., Obermajer, M., Stasiuk, L.D., Snowdon, L.R., (1999) Geochemical characterisation of Middle Devonian oils in northwestern Alberta: Possible source and maturity effect on pyrrolic nitrogen compounds. *Org. Geochem.*, in press.

Li, M., Larter, S.R., Stoddart, D., Bjoroy, M., (1992) Practical liquid chromatographic separation schemes for pyrrolic and pyridinic nitrogen aromatic heterocycle fractions from crude oils suitable for rapid characterisation of geochemical samples. *Analytical Chemistry*, 64, 1337-1344.

Li, M., Larter, S.R., Stoddart, D., Bjoroy, M., (1995) Fractionation of pyrrolic nitrogen compounds in petroleum during migration - Derivation of migration-related geochemical parameters. In: W.A. England, J. Cubitt (Eds.), *The Geochemistry of Reservoirs., 86, Geological Society Special Publication* (Ed. by W.A. England, J. Cubitt), pp. 103-123. The Geological Society, London.

Li, M., Yao, H., Stasiuk, L.D., Fowler, M.G., Larter, S.R., (1997) Effect of maturity and petroleum expulsion on pyrrolic nitrogen compound yields and distributions in Duvernay Formation petroleum source rock in Central Alberta, Canada. *Org. Geochem.*, 26, 731-744.

Loosveld, R., Bell, A., Terken, J., (1996) The tectonic evolution of interior Oman. *GeoArabia*, 1, 28-51.

Lucach, S.O., Bowler, B.F.J., Frewin, N., Larter, S.R., (2002) Variation in alkylphenol distributions in a homogenous oil suite from the Dhahaban petroleum system of Oman. *Organic Geochemistry*, 33(5), 581-594.

Machel, H.G., (2001) Bacterial and thermochemical sulfate reduction in daigenetic settings - Old and new insights. *Sedimentary Geol.*, 140, 143-175.

Machel, H.G., Krouse, H.R., Sassen, R., (1995) Products and distinguishing criteria of bacterial and thermochemical sulfate reduction. *Applied Geochem.*, 10, 373-389.

Mackenzie, A.S., (1984) Application of biological markers in petroleum chemistry. In: J. Brooks, D.H. Welte (Eds.), *Advances in Petroleum Geochemistry* (Ed. by J. Brooks, D.H. Welte), pp. 115-214. Academic Press, London.

Mackenzie, A.S., Brassell, S.C., Eglinton, G., Maxwell, J.R., (1982) Chemical fossils: the geological fate of steroids. *Science*, 217, 491-504.

Mackenzie, A.S., Patience, R.L., Maxwell, J.R., Vandenbroucke, M., Durand, B., (1980) Molecular parameters of maturation in the Toarcian shales, Paris Basin, France-I. Changes in the configuration of acyclic isoprenoid alkanes, steranes, and triterpanes. *Geochimica Cosmochimica Acta*, 44, 1709-1721.

Macleod, G., Petch, G.S., Larter, S.R., Aplin, A.C., (1993) Investigations on the composition of hydrocarbon fluid inclusions. *Abstract-205th American Chemical Society Meeting, Denver.*

Mango, F., (2005) The case for catalytic gas. *Geochimica Et Cosmochimica Acta*, 69(10), A556-A556.

Mango, F.D., (1987) An invariance in the isoheptanes of petroleum. *Science*, 237, 514-517.

Mango, F.D., (1990a) The origin of light cycloalkanes in petroleum. *Geochim. Cosmochim. Acta*, 54, 23-27.

Mango, F.D., (1990b) The origin of light hydrocarbon in petroleum: A kinetic test of the steady state catalytic hypothesis. *Geochim. Cosmochim. Acta*, 54, 1315-1323.

Mango, F.D., (1992) Transition metal catalysis in the generation of petroleum and natural gas. *Geochim. Cosmochim. Acta*, 56, 553-555.

Mango, F.D., (1994) The origin of light hydrocarbons in petroleum: Ring preference in the closure of carbocyclic rings. *Geochim. Cosmochim. Acta*, 58(2), 895-901.

Mango, F.D., (1996) Transition metal catalysis in the generation of natural gas. *Org. Geochem.*, 24, 977-984.

Mango, F.D., (1997) The light hydrocarbons in petroleum: a critical review. *Organic Geochemistry*, 26, 417-440.

Mango, F.D., (2000) The origin of light hydrocarbons. *Geochim. Cosmochim. Acta*, 64, 1265-1277.

Mango, F.D., (2001) Methane concentrations in natural gas: the genetic implications. *Organic Geochemistry*, 32(10), 1283-1287.

Mango, F.D., Elrod, L.W., (1999) The carbon isotopic composition of catalytic gas: a comparative analysis with natural gas. *Geochim. Cosmochim. Acta*, 63, 1097-1106.

Manzano, B.K., Fowler, M.G., Machel, H.G., (1997) The influence of thermochemical sulphate reduction on hydrocarbon composition in Nisku reservoirs, Brazeau river area, Alberta, Canada. *Org. Geochem.*, 27, 507-521.

Masterson, W.D., Dzou, Leon I. P., Holba, A.G., Fincannon, A.L., Ellis, L., (2001) Evidence for biodegradation and evaporative fractionation in West Sak, Kuparuk and Prudhoe Bay field areas, North Slope, Alaska. *Organic Geochemistry*, 32(3), 411-441.

Mattes, B.W., Conway Morris, S., (1990) Carbonate/evaporite deposition in the Late Pre-cambrian- Early Cambrian Ara Formation of Southern Oman. In: A.H.F. Robertson, M.P. Searle, A.C. Ries (Eds.), *The Geology and Tectonics of the Oman Region, 49, Geological Society Special Publication* (Ed. by A.H.F. Robertson, M.P. Searle, A.C. Ries), pp. 617-636.

McKirdy, D.M., Aldridge, A.K., Ypma, P.J.M., (1983) A geochemical comparison of some crude oils from pre-Ordovician carbonate rocks. In: M. Bjor˙y, et al. (Eds.), *Advances in Organic Geochemistry 1981* (Ed. by M. Bjor˙y, et al.), pp. 99-107. J. Wiley & Sons, New York.

Mello, M.R., Maxwell., J.R., (1990) Organic Geochemical and Biological marker Characterization of Source Rocks and Oils Derived from Lacustrine Environments in the Brazilian Continental Margin. In: B.J. Katz (Ed.), *Lacustrine basin exploration : case studies and modern analogs: AAPG memoir 50* (Ed. by B.J. Katz), pp. 77. AAPG, Tulsa.

Mello, M.R., Telnaes, N., Gaglianone, P.C., Chicarelli, M.I., Brassel, S.C., Maxwell, J.R., (1988) Organic geochemical characterization of depositional paleoenvironments in Brazilian marginal basins. *Org. Geochem.*, 14, 529-542.

Meredith, W., Kelland, S.-J., Jones, D.M., (2000) Influence of biodegradation on crude oil acidity and carboxylic acid composition. *Org. Geochem.*, 31, 1059-1073.

Metcalfe, R.S., Vogel, J.L., Morris, R.W., (1985) Compositional gradients in the Anschutz Ranch East field. In: *Paper SPE 14412 presented at the 1985 SPE Annual Technical Conference and Exhibition*, pp. 22-25, Las Vegas.

Meulbroek, P., Cathles, L., Whelan, J., (1998) Phase fractionation of south Eugene Island Block 330. *Org. Geochem.*, 29(1-3), 223-240.

Meulbroek, P., MacLeod, G., (2002) PVT properties in exploration. *Organic Geochemistry*, 33(6), 611-612.

Millson, J.A., Mercadier, C.G.L., Livera, S.E., Peters, J.M., (1996) The Lower Paleozoic of Oman and its context in the evolution of a Gondwana continental margin. *Journal of the Geological Society*, 153, 213-230.

Moldowan, J.M., Fago, F.J., (1986) Structure and significance of a novel rearranged monoaromatic steroid hydrocarbon in petroleum. *Geochim. Cosmochim. Acta*, 50, 343-351.

Moldowan, J.M., Lee, C.Y., Sundararaman, P., Salvatori, R., Alajbeg, A., Gjukic, B., Demaison, G.J., Slougui, N.E., Watt, D.S., (1992) Source correlation and maturity assessment of select oils and rocks from the Central Adriatic basin (Italy and Yugoslavia). In: J.M. Moldowan, P. Albrecht, R.P. Philp (Eds.), *Biological Markers in Sediments and Petroleum* (Ed. by J.M. Moldowan, P. Albrecht, R.P. Philp), pp. 370-401. Prentice Hall, Englewood Cliffs, New Jersey.

Moldowan, J.M., Seifert, W.K., Arnold, E., Clardy, J., (1984) Structure proof and significance of stereoisomeric 28,30-bisnorhopanes in petroleum and petroleum source rocks. *Geochim. Cosmochim. Acta*, 48(8), 1651-1661.

Moldowan, J.M., Seifert, W.K., Gallegos, E.G., (1983) Identification of an extended series of tricyclic terpanes in petroleum. *Geochimica Cosmochimica Acta*, 47, 1531-1534.

Moldowan, J.M., Seifert, W.K., Gallegos, E.J., (1985) Relationship between petroleum composition and depositional environment of petroleum source rocks. *AAPG Bull.*, 69, 1255-1268.

Moldowan, J.M., Sundararaman, P., Schoell, M., (1986) Sensitivity of biomarker properties to depositional environment and/or source input in the lower Toarcian of SW-Germany. In: D. Leythaeuser, J. Rullkötter (Eds.), *Advances in Organic Geochemistry 1985, Org. Geochem., 10* (Ed. by D. Leythaeuser, J. Rullkötter), pp. 915-926, Pergamon.

Montel, F., Bickert, J., Hy-Billiot, J., Royer, M., (2003) Pressure and compositional gradients in reservoirs. *SPE 85668*, 1-7.

Montel, F., Gouel, P.L., (1984) A new lumping scheme of Analytical data fro compositional studeis. In: *Paper SPE 13119 presented at the 1984 SPE Annual Technical Conference and Exhibition*, pp. 16-19, Houston.

Montel, F., Gouel, P.L., (1985) Prediction of compositional grading in a reservoir fluid column. In: *Paper SPE 14410 presented at the 1985 SPE Annual Technical Conference and Exhibition, SPE 14410*, pp. 22-25.

Muskat, M., (1994) Distribution of Non-Reacting Fluids in the Gravitational Field. *Physical Review*, 35, 1348-1393.

Norgate, C., Boreham, C., Wilkins, A.J., (1999) Changes in hydrocarbon maturity indices with coal rank and type, Buller Coalfield, New Zealand *Organic Geochemistry*, 30, 985-1010

Obermajer, M., Osadetz, K.G., Fowler, M.G., Snowdon, L.R., (2000) Light hydrocarbon (gasoline range) parameter refinement of biomarker-based oil-oil correlation studies: an example from Williston Basin. *Org. Geochem.*, 31, 959-976.

Odden, W., Patience, R., Graas, G., (1998) Application of light hydrocarbons (C4-C13) to oil/source rock correlations: a study of the light hydrocarbon compositions of source rocks and test fluids from offshore Mid-Norway. *Org. Geochem.*, 28(12), 823-848.

Orr, W.L., (1974) Changes in sulfur content and isotopic ratios of sulfur during petroleum maturation-Study of Big Horn Paleozoic oils. *AAPG Bull.*, 58, 2295-2318.

Orr, W.L., (1977) Geologic and geochemical controls on the distribution of hydrogen sulfide in natural gas. In: R. Campos, J. Goni (Eds.), *Advances in Organic Geochemistry 1975* (Ed. by R. Campos, J. Goni), pp. 571-597. Empressa nacional adaro de investigaciones mineras, Madrid.

Orr, W.L., (1986) Kerogen/asphaltene/sulphur relationships in sulfur-rich Monterey oils. In: D. Leythaeuser, J. Rullk.tter (Eds.), *Advances in Organic Geochemistry 1985, Org. Geochem., 10* (Ed. by D. Leythaeuser, J. Rullk.tter), pp. 499-516. Pergamon.

Orr, W.L., Sinninghe Damsté, J.S., (1990) Geochemistry of sulfur in petroleum systems. In: W.L. Orr, C.M. White (Eds.), *Geochemistry of Sulfur in Fossil Fuels, ACS Symposium Series* (Ed. by W.L. Orr, C.M. White), pp. 2-29. American Chemical Society, Washington, D. C.

Ourisson, G., Albrecht, P., Rohmer, M., (1979) The hopanoids. Palaeochemistry and biochemistry of a group of natural products. *Pure Appl. Chem.*, 51, 709-729.

Ourisson, G., Albrecht, P., Rohmer, M., (1982) Predictive microbial biochemistry-from molecular fossils to procaryotic membranes. *Trends in Biological Sciences*, 7, 236-239.

Palacas, J.G., Anders, D.E., King, J.D., (1984) South Florida Basin—A prime example of carbonate source rocks in petroleum. In: J.G. Palacas (Ed.), *Petroleum Geochemistry and Source Rock Potential of Carbonate Rocks, 18* (Ed. by J.G. Palacas), pp. 71-96. AAPG, Studies in Geology No. 18.

Pallasser, R.J., (2000) Recognizing biodegradation in gas/oil accumulations through the d13C compositions of gas components. *Org. Geochem.*, 31, 1363-1373.

Parfitt, M., Farrimond, P., (1998) The Mupe Bay Oil Seep: a detailed organic geochemical study of a controversial outcrop. In: J.R. Underhill (Ed.), *Development, Evolution and Petroleum Geology of the Wessex Basin, 133, Geological Society of London, Special Publication* (Ed. by J.R. Underhill), pp. 387-397.

Pasadakis, N., Obermajer, M., Osadetz, K.G., (2004) Definition and characterization of petroleum compositional families in Williston Basin, North America using principal component analysis. *Organic Geochemistry*, 35(4), 453-468.

Peneloux, A., Rauzy, E., Freze, R., (1982) A consistent correlation for Redlich-Kwong-Soave volumes. *Fluid Phase Equilibria*, 8, 7-23.

Pepper, A.S., Dodd, T.A., (1995) Simple kinetic models of petroleum formation. Part II: oil-gas cracking. *Marine and Petrol. Geol.*, 12, 321-340.

Peters, K.E., Clifford, C.W., Moldowan, J.M., (2005) *The Biomarker Guide: Biomarkers and isotopes in petroleum exploration and earth history.* Cambridge University Press, Cambridge.

Peters, K.E., Moldowan, J.M., (1991) Effects of source, thermal maturity and biodegradation on the distribution and isomerization of homohopanes in petroleum. *Org. Geochem.*, 17(1), 47-61.

Peters, K.E., Moldowan, J.M., (1993) *The Biomarker Guide, Interpreting molecular fossils in petroleum and ancient sediments.* Prentice Hall.

Philippi, G.T., (1981) correlation of crude oils with their oil source formations, using high resolution GLC C6-C7 component analysis. *Geochemica et Cosmochemica Acta*, 45, 1495-1513.

Prinzhofer, A.A., Huc, A.Y., (1995) Genetic and post-genetic molecular and isotopic fracionations in natural gases. *Chem. Geol.*, 126, 281-290.

Protoy, A., MacDonald, C., Borgomano, J., (1995) Prospectivity Evaluation of the Greater Birba Area. *PDO Exploration Report NR. 349*, 150.

Radke, M., (1987) Organic geochemistry of aromatic hydrocarbons. In: J. Brooks, D. Welte (Eds.), *Advances in Petroleum Geochemistry* (Ed. by J. Brooks, D. Welte), pp. 141-207. Academic Press, New York.

Radke, M., Welte, D.H., (1983) The methylphenanthrene index (MPI). A maturity parameter based on aromatic hydrocarbons. In: M. Bjor˙y, et al. (Eds.), *Advances in Organic Geochemistry 1981* (Ed. by M. Bjor˙y, et al.), pp. 504-512. J. Wiley & Sons, New York.

Radke, M., Welte, D.H., Willsch, H., (1982a) Geochemical study on a well in the Western Canada Basin: Relation of the aromatic distribution pattern to maturity of organic matter. *Geochim. Cosmochim. Acta*, 46, 1-10.

Radke, M., Welte, D.H., Willsch, H., (1986) Maturity parameters based on aromatic hydrocarbons: Influence of the organic matter type. *Org. Geochem.*, 10, 51-63.

Radke, M., Willsch, H., Leythaeuser, D., Teichmuller, M., (1982b) Aromatic components of coal: relation of distribution pattern to rank. *Geochim. Cosmochim. Acta*, 46, 1833-1848.

Rice, D.D., Claypool, G.E., (1981) Generation, accumulation, and resource potential of biogenic gas. *AAPG Bull.*, 65, 5-25.

Riemens, W.G., A. M. Schulte, and L. N. J. de Jong, (1988) Birba Field PVT variations along the hydrocarbon column and confirmatory field tests. *Journal of Petroleum Technology*, 83-88.

Riemens, W.G., Schulte, A.M., De Jong, L.N.J., (1985) Birba field PVT variations along the hydrocarbon column and confirmatory field tests. *Paper SPE 13719.*

Riolo, J., Hussler, G., Albrecht, P., Connan, J., (1986) Distribution of aromatic steroids in geological samples: Their evaluation as geochemical parameters. *Org. Geochem.*, 10, 981-990.

Rooney, M.A., (1995) Carbon isotope ratios of light hydrocarbons as indicators of thermochemical sulfate reduction. In: J.O. Grimalt, C. Dorronsoro (Eds.), *Org. Geochem.: Developments and Applications to Energy, Climate, Environment and Human History - Selected papers from the 17th International Meeting on Org. Geochem.* (Ed. by J.O. Grimalt, C. Dorronsoro), pp. 523-525. AIGOA, San Sebastian.

Rooney, M.A., Vuletich, A.K., Griffith, C.E., (1998) Compound-Specific isotope analysis as a tool for characterizing mixed oils: an example from the West of Shetlands area. *Org. Geochem.*, 29(1-3), 241-254.

Rubintsein, I., Sieskind, O., Albrecht, P., (1975) Rearranged steranes in a shale: Occurence and simulated formation. *J. of Chemical Society, Perkin Transaction I*, 1833-1836.

Sage, B.H., Lacey, W.N., (1938) Gravitational Concentration Gradients in Static columns of Hydrocarbon Fluids. *AIME*, 132, 120-131.

Sassen, R., (1988) Geochemical and carbon isotopic studies of crude oil destruction, bitumen precipitation, and sulfate reduction in the deep Smackover Formation. *Org. Geochem.*, 12, 351-361.

Schaefer, R.G., Littke, R., (1988) Maturity-related compositional changes in the low-molecular-weight hydrocarbon fraction of Toarcian shales. In: L. Mattavelli, L. Novelli (Eds.), *Organic Geochemistry, Advances in Organic Geochemistry 1987, 3* (Ed. by L. Mattavelli, L. Novelli), pp. 887-892.

Schoell, M., (1980) The hydrogen and carbon isotopic composition of methane from natural gases of various origins. *Geochim. Cosmochim. Acta*, 44, 649-661.

Schouten, S., Eglington, T.I., Sinninghe Damasté, J., Leeuw, J.W.d., (1995) Influence of sulphur cross-linking on the molecular size distribution of sulphur-rich Macromolecules in Bitumen. In: M.A. Vairavamurthy, M.A. Schoonen (Eds.), *Geochemical transformation of sedimentary sulfur, ACS Symposium series 612* (Ed. by M.A. Vairavamurthy, M.A. Schoonen), pp. 80-92. American Chemical Society, Washington DC.

Schrooder, S., (2000) Reservoir quality prediction in Ara Group carbonates of the South Carbonate Platform, South Oman Salt Basin. In: *Geologisches Institut*, pp. 232. Universitat Bern, Bern.

Schulte, A.M., (1980) Compositional variations within a hydrocarbon column due to gravity. *SPE Paper No. 9235.*

Seifert, W.K., Carlson, R.M.K., Moldowan, J.M., (1983) Geomimetic synthesis, structure assignment, and geochemical correlation application of monoaromatized petroleum steranes. In: M. Bjor˙y, et al. (Eds.), *Advances in Organic Geochemistry 1981* (Ed. by M. Bjor˙y, et al.), pp. 710-724. J. Wiley & Sons, New York.

Senftle, J.T., Larter, S.R., Bromley, B.W., Brown, J.H., (1986) Quantitative chemical characterization of vitrinite concentrates using pyrolysis-gas chromatography. Rank variation of pyrolysis products. *Org. Geochem.*, 9, 345-350.

Sieskind, O., Joly, G., Albrecht, P., (1979) Simulation of the geochemical transformation of sterols: Superacid effects of clay minerals. *Geochim. Cosmochim. Acta*, 43, 1675-1679.

Silverman, S., (1965) Migration and segregation of oil and gas. In: A. Young, G. Galley (Eds.), *Fluids in Subsurface Environments, 4, AAPG Memoir* (Ed. by A. Young, G. Galley), pp. 53-65.

Sinninghe Damasté, J., De Las Heras, F.X.C., Van Bergen, F., de Leeuw, J.W., (1993) Characterization of Tertiary Catalan Lacustrine oil shales: Discovery of extremely organic sulphur-rich type I kerogens. *Geochemica et Cosmochemica Acta*, 57, 389-415.

Sinninghe Damsté, J.S., de Leeuw, J.W., (1992) Organically bound sulphur in coal: A molecular approach. *Fuel Processing Technology*, 30, 109-178.

Sinninghe Damsté, J.S., de Leeuw, J.W., Dalen, A.C.K., Zeeuw, M.A.d., DeLange, F., Rukstra, I.C., Schenck, P.A., (1987) The occurrence and identification of series of organic sulfur compounds in oils and sediment extracts. I. A study of Rozel Point oil (U.S.A.). *Geochim. Cosmochim. Acta*, 51, 2369-2391.

Sinninghe Damsté, J.S., Eglinton, T.I., Rijpstra, W.I.C., de Leeuw, J.W., (1990) Characterization of organically bound sulfur in high-molecular-weight, sedimentary organic matter using flash pyrolysis and Raney Ni desulfurization. In: W.L. Orr, C.M. White (Eds.), *Geochemistry of Sulfur in Fossil Fuels, ACS Symposium Series* (Ed. by W.L. Orr, C.M. White), pp. 486-528. American Chemical Society, Washington, D. C.

Sinninghe Damsté, J.S., Kenig, F., Koopmans, M.P., Koster, J., Schouten, S., Hayes, J.M., de Leeuw, J.W., (1995) Evidence for gammacerane as an indicator of water column stratification. *Geochim. Cosmochim. Acta*, 59(9), 1895-1900.

Sinninghe Damsté, J.S., Rijpstra, W.I.C., de Leeuw, J.W., Schenck, P.A., (1988) Origin of organic sulphur compounds and sulfur-containing high molecular weight substances in sediments and immature crude oils. In: L. Novelli, L. Mattavelli (Eds.), *Advances in Organic Geochemistry 1987, Org. Geochem., 10* (Ed. by L. Novelli, L. Mattavelli), pp. 593-606.

Soave, G., (1972) Equilibrium constants from a modified Redlich -Kwong Equation of State. *chem. Eng. Sci.* , 27, 1197.

Stahl, W., et al., (1977) Carbon isotopes in oil and gas exploration. In: *Internat. Symposium on Nuclear Technology in Exploration, Extraction, and Processing of Mineral Resources*, pp. 73-82. Vienna, Internat. Atomic Energy Agency, Vienna.

Stahl, W.J., (1977) Carbon and nitrogen isotopes in hydrocarbon research and exploration. *Chem. Geol.*, 20, 121-149.

Stainforth, J.G., (2004) New insights into reservoir filling and mixing processes. In: J.M. Cubbit, W.A. England, S.R. Larter (Eds.), *Understanding petroleum reservoirs: towards an integrated engineering and geochemical approach, 237, Geological Society Special Publications* (Ed. by J.M. Cubbit, W.A. England, S.R. Larter), pp. 115-132. The Geological Society, London.

Staudt, W.J., Schoonen, A.A., (1995) Sulfate incorporation into sedimentary carbonates. In: M.A. Vairavamurthy, M.A. Schoonen (Eds.), *Geochemical transformation of sedimentary sulfur, ACS Symposium series 612* (Ed. by M.A. Vairavamurthy, M.A. Schoonen), pp. 332-345. American Chemical Society, Washington DC.

Summons, R.E., (1987) Branched alkanes from ancient and modern sediments: Isomer discrimination by GC/MS with multiple reaction monitoring. *Org. Geochem.*, 11(4), 281-289.

Taylor, P., Idiz, E., Kommeren, C., Buiskool Toxopeus, J.M.A., Farrimond, P., (2003) oil and source rock geochemistry of the South Oman Salt Basin. *SIEP report*, EP-2003-6010, 179pp.

Taylor, P., Larter, S., Jones, M., Dale, J., Horstad, I., (1997) The effect of oil-water-rock partitioning on the occurrence of alkylphenols in petroleum systems. *Geochim. Cosmochim. Acta*, 61, 1899-1910.

Taylor, P.N., (1994) Controls on the occurrence of phenols in petroleums and waters. University of Newcastle.

ten Haven, H.L., (1996) Applications and limitations of Mango's light hydrocarbon parameters in petroleum correlation studies. *Org. Geochem.*, 24, 957-976.

ten Haven, H.L., de Leeuw, J.W., Schenck, P.A., (1985) Organic geochemical studies of a Messinian evaporitic basin, northern Apennines (Italy) I: Hydrocarbon biological markers for a hypersaline environment. *Geochim. Cosmochim. Acta*, 49, 2181-2191.

Terken, J., Frew, N., Indrelid, S., (2001) Petroleum systems of Oman: Charge timing and risks *AAPG*, 85, 1817-1845.

Terken, J.M.J., Frewin, N.L., (2000) The Dhahaban petroleum system of Oman. *AAPG Bull.*, 84(4), 523-544.

Thode, H.G., (1981) Sulfur Isotope Ratios in Petroleum Research and Exploration: Williston Basin. 1526-1535.

Thode, H.G., Monster, J., (1965) Sulfur-Isotope Geochemistry of Petroleum, Evaporites, and Ancient Seas. In: A. Young, J. Galley (Eds.), *Fluids in Subsurface Environments: AAPG Memoir No. 4* (Ed. by A. Young, J. Galley), pp. 367. AAPG, Tulsa.

Thompson, K.F.M., (1979) Light hydrocarbons in subsurface sediments. *Geochemica et Cosmochemica Acta*, 43, 657-672.

Thompson, K.F.M., (1983) Classification and thermal history of petroleum based on light hydrocarbons. *Geochim. Cosmochim. Acta*, 47, 303-316.

Thompson, K.F.M., (1987) Fractionated aromatic petroleums and the generation of gas condensates. *Organic Geochemistry*, 11, 573-590.

Thompson, K.F.M., (1988) Gas-condensate migration and oil fractionation in deltaic systems. *Marine and Petrol. Geol.*, 5, 237-246.

Thompson, K.F.M., (2000a) Slope of the exponential distribution of normal alkanes in petroleum. I: index of maturity in unaltered oils, indicator of alteration in U.S. Gulf Coast oils. *Geochim. Cosmochim. Acta, submitted for publication.*

Thompson, K.F.M., (2000b) Slope of the exponential distribution of normal alkanes in petroleum. II: indicator of the pressure and temperature of gas-condensate equilibrium. *Geochim. Cosmochim. Acta, submitted for publication.*

Thompson, K.F.M., (2004) Interpretation of charging phenomena based on reservoir fluid (PVT) data. In: J.M. Cubbit, W.A. England, S.R. Larter (Eds.), *Understanding Petroleum Reservoirs: towards an Integrated Reservoir Engineering and Geochemical Approach, 237, Special Publications* (Ed. by J.M. Cubbit, W.A. England, S.R. Larter), pp. 7-26. The Geological Society of London 2004, London.

Thorn, K., Aiken, G., (1998) Biodegradation of crude oils into nonvolatile organic acids in a contaminated aquifer near Bemidji, Minnesota. *Org. Geochem.*, 29(4), 909-932.

Tissot, B., Welte, D.H., (1984) *Petroleum Formation and Occurence*. Springer-Verlag, New York.

Toth, J., (2001) South Oman Salt Basin: A regional thermal and charge model. SIEP Report EP 2001-5401.

Trudinger, P.A., Chambers, L.A., Smith Jr, W.O., (1985) low temperature sulphate reduction: biological versus abiological. *Canadian Journal of Earth Sciences*, 22, 1910-1918.

Tyson, R.V., (1994) *Sedimentary Organic Matter- Organic Facies and Palynofacies*. Kluwer Academic Publishers, Dordrecht.

Vairavamurthy, M.A., Orr, W.l., Manowitz, B., (1995) Geochemical transformation of sedimentary sulfur: An Introduction In: M.A. Vairavamurthy, M.A. Schoonen (Eds.), *Geochemical transformation of sedimentary sulfur, ACS Symposium series 612* (Ed. by M.A. Vairavamurthy, M.A. Schoonen). American Chemical Society, Washington DC.

Vairavamurthy, M.A., Zhou, W., (1995) characterization of a transient +2 sulfur oxidation state intermediate from the oxidation of aqueous sulfide. In: M.A. Vairavamurthy, M.A. Schoonen (Eds.), *Geochemical transformation of sedimentary sulfur, ACS Symposium series 612* (Ed. by M.A. Vairavamurthy, M.A. Schoonen), pp. 280-291. American Chemical Society, Washington DC.

Van Duin, A.C.T., Larter, S.R., (1997) Unraveling Mango's mysteries: a kinetic scheme describing the diagenetic fate of C7-alkanes in petroleum systems. *Organic Geochemistry*, 27, 597-599.

van Graas, G.W., (1990) Biomarker maturity parameters for high maturities: Calibration of working range up to the oil-condensate threshold. *Org. Geochem.*, 16, 1025-1032.

van Graas, G.W., Elin Gilje, A., Isom, T.P., Aase Tau, L., (2000) The effects of phase fractionation on the composition of oils, condensates and gases. *Org. Geochem.*, 31, 1419-1439.

van Graas, G.W., Gilje, A.E., Isom, T.P., Tau, L.A., (1999) The effects of phase separation on the composition of oils condensates and gases. *19th International Meeting on Org. Geochem., 6-10 September 1999, Istanbul, Turkey*, Abstracts Part I, 85-86.

Venkatesan, M.I., Ohta, K., Stout, S.A., Steinberg, S., Oudin, J.L., (1993) Diagenetic trends of lignin phenols in Mahakam Delta coals: correlation between laboratory thermal maturation and natural samples. *Organic Geochemistry*, 20, 463-473.

Visser, W., (1991) Burial and thermal history of Proterozoic source rocks in Oman. *Precambrian Research*, 54, 15-36.

Volkman, J.K., (1986) A review of sterol markers for marine and terrigenous organic matter. *Org. Geochem.*, 9(2), 83-99.

Volkman, J.K., Alexander, R., Kagi, R.I., Woodhouse, G.W., (1983) Demethylated hopanes in crude oils and their applications in petroleum geochemistry. *Geochim. Cosmochim. Acta*, 47, 785-794.

Volkman, J.K., Allen, D.I., Stevenson, P.L., Burton, H.R., (1986) Bacterial and algal hydrocarbons in sediments from a saline Antarctic lake, Ace Lake. In: D. Leythaeuser, J. Rullk.tter (Eds.), *Advances in Organic Geochemistry 1985, Org. Geochem., 10* (Ed. by D. Leythaeuser, J. Rullk.tter), pp. 671-681. Pergamon.

Volkman, J.K., Gillan, F.T., Johns, R.B., Eglinton, G., (1981) Sources of neutral lipids in a temperate intertidal sediment. *Geochim. Cosmochim. Acta*, 45, 1817-1828.

Wang, T.G., Li, S.-M., S.-C., Z., (2004) Oil migration in the Lunn region, Tarim Basin, China based on the pyrrolic nitrogen compound distribution. *Journal of Petroleum Science and Engineering* 41, 123-134.

Wardroper, A.M.K., Hoffmann, C.F., Maxwell, J.R., Barwise, A.J.G., Goodwin, N.S., Park, P.J.D., (1984) Crude oil biodegradation under simulated and natural conditions-II. Aromatic steroid hydrocarbons. *Org. Geochem.*, 6, 605-617.

Weinlich, F.H., (1991) Genesis and Distribution of Free Gases in the Stassfurt Carbonate of the Lausitz : Pt.2 : the Distribution Principles of Free Gases (Genese Und Verteilung Der Freien Gase Im Stassfurtkarbonate (Ca 2) Der Lausitz : Teil 2 : Die Verteilungsprinzipien Der Freien Gase). *Z Angew Geol*, 37(2), 52-58.

Welte, D.H., Kratochvil, H., Rullkotter, J., Ladwein, H., Schaefer, G., (1982) Organic geochemistry of crude oils from the Vienna Basin and an assessment of their origin. *Chem. Geol.*, 35, 33-68.

Welte, D.H., Schaefer, R.G., Stoessinger, W., Radke, M., (1984) Gas generation and migration in the Deep basin of western Canada. *AAPG Memoir*, 38, 35-47.

Wheaton, R.J., (1991) Treatment of variations of composition with depth in gas-condensate reservoirs. *SPE Res. Eng.*, May, 239-244.

Whiticar, J.J., Snowdon, L., (1999) Geochemical characterization of selected Western Canada oils by C5-C8 Compound Specific Isotope Correlation (CSIC). *Organic Geochemistry*, 30, 1127-1161.

Whiticar, M.J., (1994) Correlation of natural gases with their sources. In: L.B. Magoon, W.G. Dow (Eds.), *The Petroleum System, From Source to Trap, Memoir 60* (Ed. by L.B. Magoon, W.G. Dow), pp. 261-283. AAPG.

Whitson, C.H., Belery, P., (1994) Compositional gradients in petroleum reservoirs. *SPE Paper No. 2800.*

Wilhelms, A., (1992) An investigation into the factors influencing tar mat formation in petroleum reservoirs. University of Oslo, Norway.

Williams, J.A., (1974) Characterization of Oil Types in Williston Basin. *AAPG Bull.*, 58(7), 1243-1252.

Williams, L.A., (1984) Subtidal stromatolites in Monterey Formation and other organic-rich rocks as suggested source contributors to petroleum formation. *AAPG Bull.*, 68, 1879-1893.

Wingert, W.S., Pomerantz, M., (1986) Structure and significances of some twenty-one and twenty-two carbon petroleum steranes. *Geochim. Cosmochim. Acta*, 50, 2763-2769.

Worden, R.H., Smalley, P.C., (1996) H_2S-producing reactions in deep carbonate gas reservoirs: Khuff Formation, Abu Dhabi. *Chem. Geol.*, 133, 157-172.

Worden, R.H., Smalley, P.C., Oxtoby, N.H., (1995) Gas Souring by ThermoChemical Sulfate Reduction at 140° C. *AAPG Bull.*, 79(6), 854-863.

Wright, V.P., Ries, A.C., Munn, S.G., (1990) Intraplatformal basin-fill deposits from the Infracambrian Huqf Group, east central Oman. In: A.H.F. Robertson, M.P. Searle, A.C. Ries (Eds.), *The Geology and Tectonics of the Oman Region, 49, Geological Society Special Publication* (Ed. by A.H.F. Robertson, M.P. Searle, A.C. Ries), pp. 601-616. Geological Society.

Yao, W., Millero, F.H., (1995) Oxidation of hydrogen sulfide by Mn (IV) and Fe (III) (Hydr) oxides in seawater. In: M.A. Vairavamurthy, M.A. Schoonen (Eds.),

Geochemical transformation of sedimentary sulfur 612, ACS Symposium series (Ed. by M.A. Vairavamurthy, M.A. Schoonen). American Chemical Society, Washington DC.

Younes, M.A., El-Ghamri, M.A., (2006) Source rock depositional environment and maturation assessment dependent C7 light hydrocarbons from crude oils in the Gulf of Suez, Egypt. *Petroleum Science and Technology*, 24(5), 563-585.

Zou, Y.R., Zhao, C.Y., Wang, Y.P., Zhao, W.Z., Peng, P.A., Shuai, Y., (2006) Characteristics and origin of natural gases in the Kuqa Depression of Tarim Basin, NW China. *Organic Geochemistry*, 37(3), 280-290.

Zumberge, J.E., (1984) Source rocks of the La Luna (Upper Cretaceous) in the Middle Magdalena Valley, Colombia. In: J.G. Palacas (Ed.), *Geochemistry and Source Rock Potential of Carbonate Rocks, 18* (Ed. by J.G. Palacas), pp. 127-133. AAPG, Studies in Geology No. 18.

Chapter 10 Appendices

10.1 The Chapter 4 Appendices

Appendix 4. 1: Full compound names of the different biomarkers employed in the study.

Name used in the study	Compound name	Molecular formula	m/z
Steranes			
C_{21} pregnane	5α sterane	$C_{21}H_{36}$	217
C_{22} pregnane	5α sterane	$C_{22}H_{38}$	217
C_{27} ααα S sterane	5α(H), 14α(H), 17α(H), 20(S)-Cholestane	$C_{27}H_{48}$	217
C_{27} αββ R sterane	5α(H), 14β (H), 17β (H), 20(R)-Cholestane	$C_{27}H_{48}$	217
C_{27} αββ S sterane	5α(H), 14β (H), 17β (H), 20(S)-Cholestane	$C_{27}H_{48}$	217
C_{27} ααα R sterane	5α(H), 14α(H), 17α(H), 20(R)-Cholestane	$C_{27}H_{48}$	217
C_{28} ααα S sterane	24-methyl-5α(H), 14α(H), 17α(H), 20(S)-Cholestane	$C_{28}H_{50}$	217
C_{28} αββ R sterane	24-methyl-5α(H), 14 β (H), 17 β (H), 20(R)-Cholestane	$C_{28}H_{50}$	217
C_{28} αββ S sterane	24-methyl-5α(H), 14 β (H), 17 β (H), 20(S)-Cholestane	$C_{28}H_{50}$	217
C_{28} ααα R sterane	24-methyl-5α(H), 14α(H), 17α(H), 20(R)-Cholestane	$C_{28}H_{50}$	217
C_{29} ααα S sterane	24-ethyl-5α(H), 14α(H), 17α(H), 20(S)-Cholestane	$C_{29}H_{52}$	217
C_{29} αββ R sterane	24-ethyl-5α(H), 14 β (H), 17 β (H), 20(R)-Cholestane	$C_{29}H_{52}$	217
C_{29} αββ S sterane	24-ethyl-5α(H), 14 β (H), 17 β (H), 20(S)-Cholestane	$C_{29}H_{52}$	217
C_{29} ααα R sterane	24-ethyl-5α(H), 14α(H), 17α(H), 20(R)-Cholestane	$C_{29}H_{52}$	217
Isoprenoids			
Pristane	2,6,10,14-Tetramethylpentadecane	$C_{19}H_{40}$	GC
Phytane	2,6,10,14-Tetramethylhexadecane	$C_{20}H_{42}$	GC
Triterpanes			
C_{20} βα Tricyclic terpane	13β (H), 14α (H)-C_{20} Tricyclic terpane	$C_{20}H_{36}$	191
C_{21} βα Tricyclic terpane	13β (H), 14α (H)-C_{21} Tricyclic terpane	$C_{21}H_{38}$	191
C_{22} βα Tricyclic terpane	13β (H), 14α (H)-C_{22} Tricyclic terpane	$C_{22}H_{40}$	191
C_{22} αα Tricyclic terpane	13α (H), 14α (H)-C_{22} Tricyclic terpane	$C_{22}H_{40}$	191
C_{23} βα Tricyclic terpane	13β (H), 14α (H)-C_{23} Tricyclic terpane	$C_{23}H_{42}$	191
C_{24} βα Tricyclic terpane	13β (H), 14α (H)-C_{24} Tricyclic terpane	$C_{24}H_{44}$	191
C_{25} βα Tricyclic terpane	13β (H), 14α (H)-C_{25} Tricyclic terpane	$C_{25}H_{46}$	191
C_{24} Tetracyclic terpane	C_{24} Tetracyclic terpane	$C_{24}H_{42}$	191
C_{26} βα Tricyclic terpane	13β (H), 14α (H)-C_{26} (24S)Tricyclic terpane	$C_{26}H_{48}$	191
C_{26} βα Tricyclic terpane	13β (H), 14α (H)-C_{26} (24R) Tricyclic terpane	$C_{26}H_{48}$	191
C_{28} βα Tricyclic terpane	13β (H), 14α (H)-C_{28} (24S) Tricyclic terpane	$C_{28}H_{52}$	191
C_{28} βα Tricyclic terpane	13β (H), 14α (H)-C_{28} (24R) Tricyclic terpane	$C_{28}H_{52}$	191
C_{29} βα Tricyclic terpane	13β (H), 14α (H)-C_{29} (24S) Tricyclic terpane	$C_{29}H_{54}$	191
C_{29} βα Tricyclic terpane	13β (H), 14α (H)-C_{29} (24R) Tricyclic terpane	$C_{29}H_{54}$	191
C_{30} βα Tricyclic terpane	13β (H), 14α (H)-C_{30} (24S) Tricyclic terpane	$C_{30}H_{54}$	191
C_{30} βα Tricyclic terpane	13β (H), 14α (H)-C_{30} (24R) Tricyclic terpane	$C_{30}H_{54}$	191
Ts	18α(H)-22,29,30-trisnorneohopane	$C_{27}H_{46}$	191
Tm	17α(H)-22,29,30-trisnorhopane	$C_{27}H_{46}$	191
C_{28} BNH	17α(H), 18α (H), 21β (H)-28,30-Bisnorhopane	$C_{28}H_{48}$	191
C_{29}αβ hopane	17α(H), 21β (H)-norhopane	$C_{29}H_{50}$	191
C_{30}αβ hopane	17α(H), 21β (H)-hopane	$C_{30}H_{52}$	191
C_{31}αβ hopane	17α(H), 21β (H), 22(S)-homohopane	$C_{31}H_{54}$	191
C_{31}αβ hopane	17α(H), 21β (H), 22(R)-homohopane	$C_{31}H_{54}$	191
C_{32}αβ hopane	17α(H), 21β (H), 22(S)-Bishomohopane	$C_{32}H_{56}$	191
C_{32}αβ hopane	17α(H), 21β (H), 22(R)-Bishomohopane	$C_{32}H_{56}$	191
C_{33}αβ hopane	17α(H), 21β (H), 22(S)-Trishomohopane	$C_{33}H_{58}$	191
C_{33}αβ hopane	17α(H), 21β (H), 22(R)-Trishomohopane	$C_{33}H_{58}$	191
C_{34}αβ hopane	17α(H), 21β (H), 22(S)-Tetrakishomohopane	$C_{34}H_{60}$	191
C_{34}αβ hopane	17α(H), 21β (H), 22(R)-Tetrakishomohopane	$C_{34}H_{60}$	191
C_{35}αβ hopane	17α(H), 21β (H), 22(S)-Pentakishomohopane	$C_{35}H_{62}$	191
C_{35}αβ hopane	17α(H), 21β (H), 22(R)-Pentakishomohopane	$C_{35}H_{62}$	191

Name used in the study	Compound name	m/z
C-ring Monoaromatic steroids		
C_{21} Monoaromatic steroid	C_{21} Monoaromatic steroid	253
C_{22} Monoaromatic steroid	C_{22} Monoaromatic steroid	253
$C_{27}\beta S$ Monoaromatic steroid	5β(H), 20(S)-C_{27} Monoaromatic steroid	253
$C_{27}\beta R$ Monoaromatic steroid	5β(H), 20(R)-C_{27} Monoaromatic steroid	253
$C_{28}\beta S$ Monoaromatic steroid	5β(H), 20(S)-C_{28} Monoaromatic steroid	253
$C_{28}\alpha S$ Monoaromatic steroid	5α(H), 20(S)-C_{28} Monoaromatic steroid	253
$C_{28}\alpha R$ Monoaromatic steroid	5α(H), 20(R)-C_{28} Monoaromatic steroid	253
$C_{29}\beta S$ Monoaromatic steroid	5β(H), 20(S)-C_{29} Monoaromatic steroid	253
$C_{29}\alpha S$ Monoaromatic steroid	5α(H), 20(S)-C_{29} Monoaromatic steroid	253
$C_{29}\beta R$ Monoaromatic steroid	5β(H), 20(R)-C_{29} Monoaromatic steroid	253
$C_{29}\alpha R$ Monoaromatic steroid	5α(H), 20(R)-C_{29} Monoaromatic steroid	253
ABC-ring Triaromatic steroids		
C_{20} Triaromatic steroid	C_{20} Triaromatic steroid	231
C_{21} Triaromatic steroid	C_{21} Triaromatic steroid	231
$C_{26}S$ Triaromatic steroid	20(S)-C_{26} Triaromatic steroid	231
$C_{26}R$ Triaromatic steroid	20(R)-C_{26} Triaromatic steroid	231
$C_{27}S$ Triaromatic steroid	20(S)-C_{27} Triaromatic steroid	231
$C_{27}R$ Triaromatic steroid	20(R)-C_{27} Triaromatic steroid	231
$C_{28}S$ Triaromatic steroid	20(S)-C_{28} Triaromatic steroid	231
$C_{28}R$ Triaromatic steroid	20(R)-C_{28} Triaromatic steroid	231

Appendix 4. 2: The description of the molecular parameters used in this study.

Parameter	Description	m/z	Reference	Use
Tricyclics				
C23/C21 tri	C23βα/C21βα (Tricyclics)	191	(Ekweozor & Strausz, 1983)	Maturity
C23/C24 tri	C23βα/C24βα (Tricyclics)	191	(Peters *et al.*, 2005)	Maturity
(C20+21)/(C23+24) tri	(C20βα+C21βα)/ (C23βα+C24βα) (Tricyclics)	191	(Peters *et al.*, 2005)	Maturity
C26 Tri(S+R)/C25 Tri(S+R)	C26βα(S+R)/ C25βα(S+R) (Tricyclics)	191	(Peters *et al.*, 2005)	Environment
C_{24}tetra/C_{30}αβ H	C_{24}tetra /C_{30}αβ Hopane			
C24tetra/C23tri	C24tetracyclic/C23βα tricyclics	191	(Aquino Neto *et al.*, 1983)	Environment
Tricyclics-Hopanes				
C23tri/ C30αβ H	C23βα (Tricyclics)/ C30αβ hopane	191	(Aquino Neto *et al.*, 1983)	Maturity
C28+29tri/C29-33 H	Sum C28+29 (Tricyclics)/sum C29-33ab hopanes	191	(Peters & Moldowan, 1993)	Maturity
Tri/Hop	C19-30tris/ sum C27-35αβ hopanes	191	(van Graas, 1990)	Maturity
Hopanes				
% 22S	C31αβ 22S/(22S+22R) % Hopanes C32αβ 22S/(22S+22R) % Hopanes	191	(Peters & Moldowan, 1993)	Maturity
% Ts	Ts/(Ts+Tm)%	191	(Farrimond *et al.*, 1998)	Maturity
Ts/C_{30}αβH	Ts/(C_{30}αβ Hopane)	191	(Volkman *et al.*, 1983)	Maturity
Homohopane Index	C35αβ (S+R)/sum C31-35αβ (S+R) %	191	(Peters & Moldowan, 1991)	Environment
Hopane distribution	Line diagram of % of each carbon number from C31 to C35αβ hopanes	191	(Peters & Moldowan, 1991)	Environment
C29/C30 αβ	C29αβ/C30αβ hopanes	191	(Peters & Moldowan, 1993)	Environment
BNH/hops	BNH/C29αβ+C30αβhopanes	191	(Moldowan *et al.*, 1984)	Environment
Gammacerane Index	Gammacerane/C30αβ hopane	191	(Peters & Moldowan, 1993)	Environment
Hopanes-Steranes				
Hopane/sterane	Total hopanes/total steranes C29-35αβ (S+R)/C27-29ααα(S+R)+ αββ(S+R)	217 & 191	(Peters & Moldowan, 1993)	Maturity
Steranes				
%20S	C29ααα (20S)/(20S+20R) %	217	(Mackenzie *et al.*, 1980)	Maturity
%αββ	C29αββ(20S+20R)/(C29αββ (20S+20R)+ C29ααα(20S+20R))	217	(Mackenzie *et al.*, 1980)	Maturity
C27:C28:C29	C27ααα (20R):C28ααα (20R):C29ααα (20R)	217	(Peters & Moldowan, 1993)	Environment

C27/C29	C27ααα (20R)/C29ααα (20R)	217	(Volkman, 1986)	Environment
C28/C29	C28ααα (20R)/C29ααα (20R)	217	(Grantham & Wakefield, 1988)	Age
Aromatic hydrocarbons				
MNR	2-MN/1-MN	142	(Radke *et al.*, 1982b)	
DNR1	(2,6-DMN+2,7-DMN)/1,5-DMN DMN=Dimethyl naphthalene	156	(Radke *et al.*, 1982b)	Maturity
DNRx	2,6+2,7-DMN/1,6-DMN	156		
TNR1	2,3,6-TMN/(1,3,5-TMN+1,4,6-TMN) TMN=Trimethyl naphthalene	170	(Radke, 1987)*	Maturity
ENR	2-EN/1-EN	170	(Radke *et al.*, 1982b)	Maturity
TMNR1	1,3,5-TMN/1,2,5-TMN	170	**	
MPI1	1.5(2-MP+3-MP)/(P+1-MP+9-MP) Methyl phenanthrene	192 & 178	(Radke *et al.*, 1982a)	Maturity
MPI2	3(2-MP+3-MP)/(P+1-MP+9-MP)	192 &178	(Radke *et al.*, 1982a)	Maturity
MPI3	(2-MP+3-MP)/(1-MP+9-MP)	192	(Radke, 1987)*	Maturity
VRE	(0.60*MPI1)+0.40 for %Rm (measured reflectance)<1.35		(Radke & Welte, 1983)	Maturity
MPR	2-MP/1-MP Methyl phenanthrene	192	(Radke *et al.*, 1982b)	Maturity
MPR1	3-MP/P	192	(Radke *et al.*, 1982a)	Maturity
MPR9	9-MP/P	192	(Radke *et al.*, 1982a)	Maturity
F1	(3-MP+2-MP)/(3-MP+2-MP+1-MP+9-MP) Methyl phenanthrene	192	PDO internal report (Bennett et al)	Maturity
F2	2-MP/(3-MP+2-MP+1-MP+9-MP) Methyl phenanthrene	192	PDO internal report (Bennett et al)	Maturity
MDR1	(1-MDBT)/DBT DBT=Dibenzothiophene) MDBT=Methyl dibenzothiophene	198/184	(Radke *et al.*, 1982a)	Maturity
MDR4	4-MDBT/DBT	198/184	(Radke *et al.*, 1982a)	Maturity
MDR2,3	(2-MDBT+3-MDBT)/DBT	198/184	(Radke *et al.*, 1982a)	Maturity
MDR	4-MDBT.1-MDBT	198	(Radke *et al.*, 1986)	Maturity
2+3MDBT/1-MDBT	(2-MDBT+3-MDBT)/1-MDBT	198	**	Maturity
C/F	C2-benzothiophens	162	**	

3+4/6	C3-Benzothiophenes	176	**	
BDR	Total sulfur in benzothiphenes/total sulfur in dibenzothiophenes	134&148 162&176 184&198	(Radke, 1987)*	Maturity
$C_{20}TA$ ($/C_{20}+C_{28}$)	$C_{20}TAS/(C_{20}TAS+C_{28}(S)TAS+C_{28}(R)TA)$ % TAS=Triaromatic steroids	231	(Beach *et al.*, 1989)	Maturity
MA/(MA+TA)	sum monoaromatic steroids (MA)/sum MA+sum Triaromatic steroids (TA)	253&231	(Peters & Moldowan, 1993)	Maturity
MAI/I+II	∑C20-C22MAS/∑C27-C29MAS	253	(Peters & Moldowan, 1993)	Maturity
TA C_{26} 20S/C_{28} 20S	C_{26}20STAS/C_{28}20STAS	231	(Peters *et al.*, 2005)	Environment
TA C_{27}20R/C_{28} 20R	C_{27}20RTAS/C_{28}20RTAS	231	(Peters *et al.*, 2005)	Environment
MA C27/ (C28+C29)	C27 (S+R)MAS/C28 (S+R)MAS+C29 (S+R)MAS	231	(Peters *et al.*, 2005)	Environment
TAI/(I+II)	∑C20+C21 TAS/∑C26-C28 (S+R) TAS	231	(Peters & Moldowan, 1993)	Maturity
F/∑MF	Fluorene/sum of methylfourenes	166/180	**	
MBpR1	2methylBiphenyl/3methylBiphenyl	154/168	**	
4MBp/3MBp	4MethylBiphenyl/3MethylBiphenyl	168	**	
4MBp/Bp	4MethylBiphenyl/Biphenyl	154/168	**	
DBF/Bp	Dibenzofurane/Biphenyl	154/168	**	
DBT/P	DBT/P	184/178	(Hughes *et al.*, 1995)	Environment

* The original reference is therein **suggested by the author as correlation parameters.

Appendix 4. 3: GC-Ms chromatograms of some aromatic hydrocarbons

1) Naphthalenes, alkylnaphthalenes, phenathrenes, and alkylphenathrenes

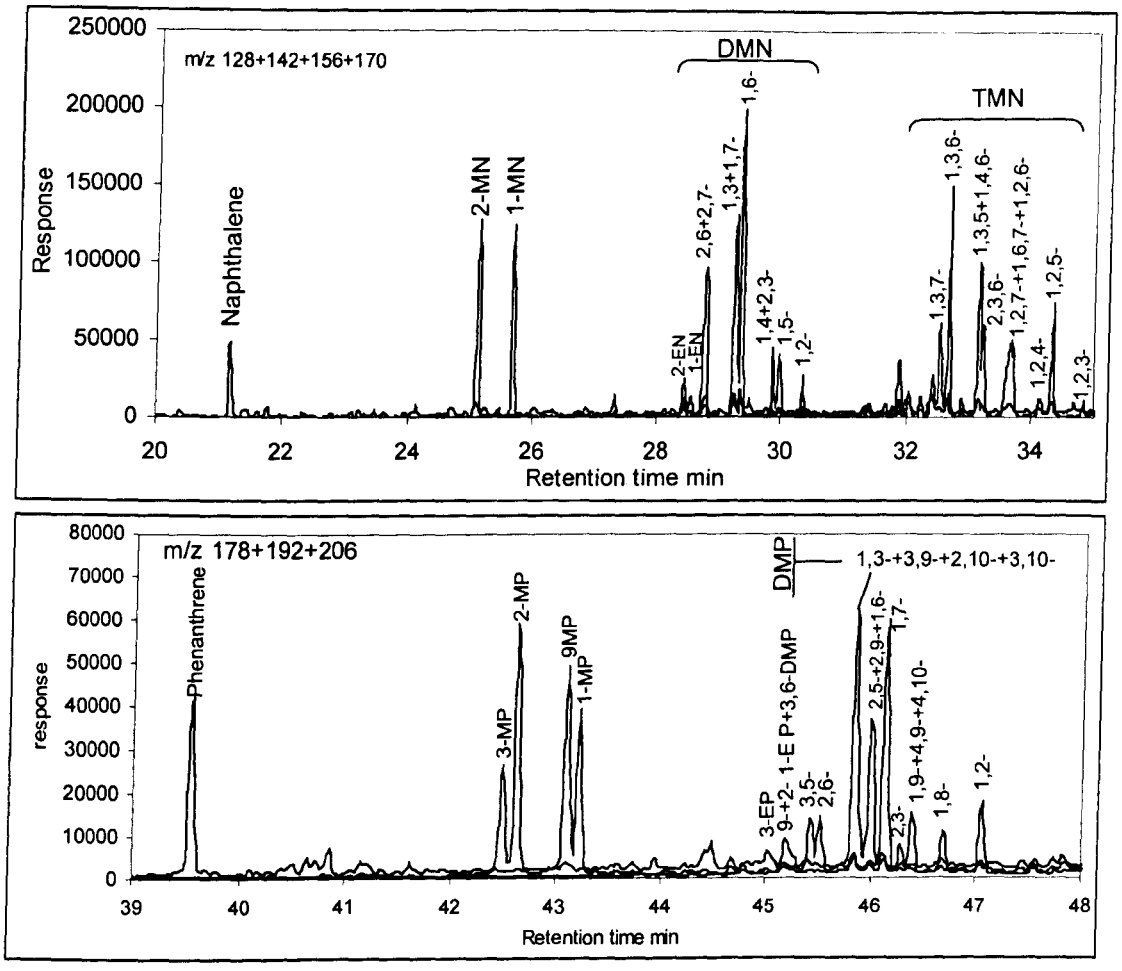

MN=Methylnaphthalene
DMN=Dimethylnaphthalene
EN=Ethylnaphthalene
TMN=Trimethylnaphthalene
MP=Methylphenanthrene
DMP=Dimethylphenanthrene
EP=Ethylphenanthrene

2) Biphenyl, methylbiphenyls, Fluorene and methylfluorenes

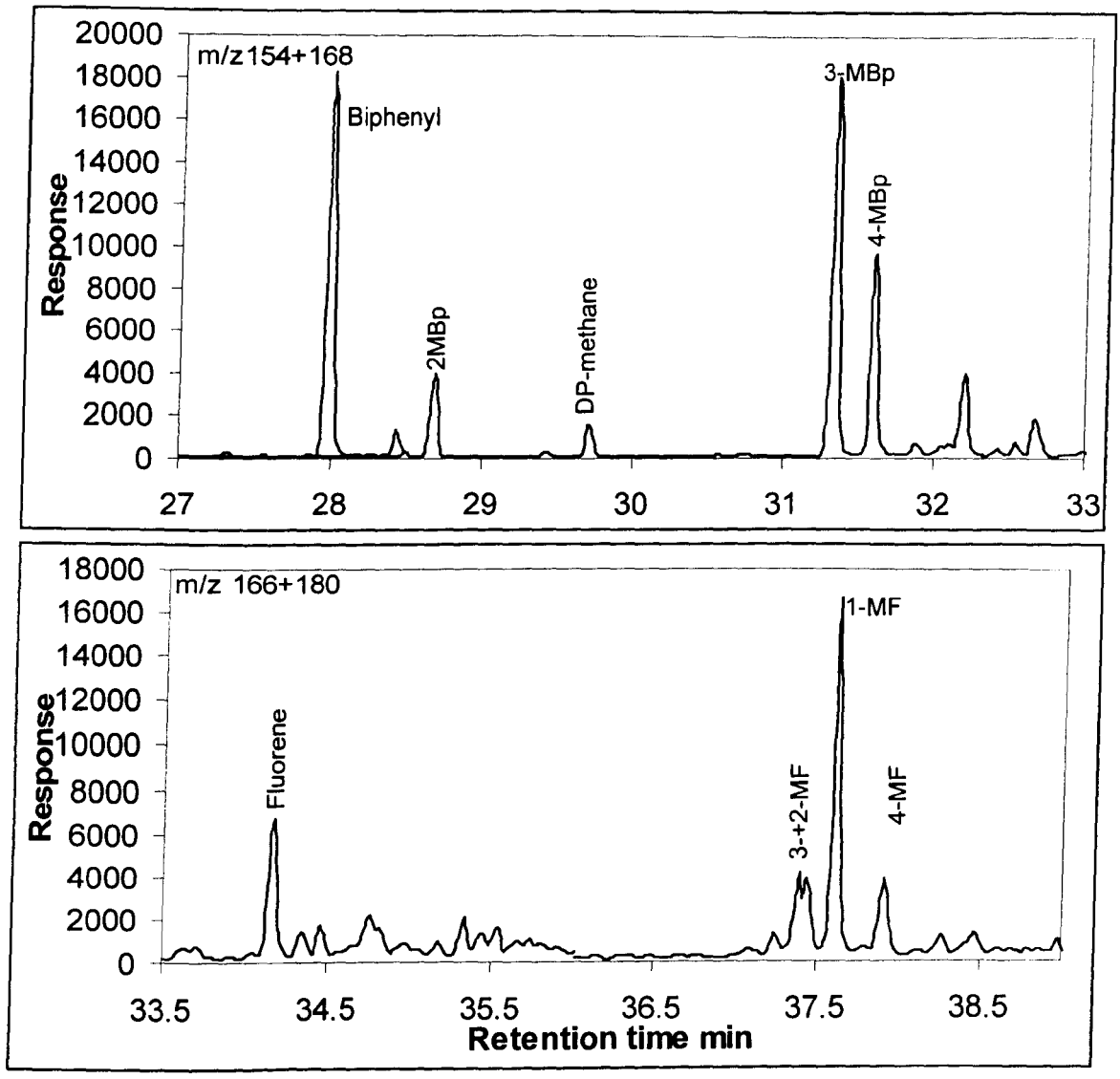

MBp=methylbiphenyl
MF=MethylFluorene

Appendix 4. 4: The concentrations (ppm) of various compounds incorporated in this study for oils.

1) Tricyclics:

sample ID	C20TRI	C21Tr	C22Tr	C22Tr(αα)	C23Tr	C24Tr	C24Tr(αα)	C25Tr	C25Tr(αα)	C24Tet	C26Tr	C26Tr(L)	C28Tr	C28Tr(L)
O1	25.30	32.22	16.06	10.09	98.55	43.97	6.57	34.72	6.27	16.42	20.68	19.78	15.04	14.82
O2	27.43	36.11	17.49	10.82	107.23	45.36	7.51	37.13	7.56	17.07	23.22	18.13	15.89	17.34
O3	18.57	23.30	11.02	7.58	63.47	27.03	4.14	20.75	4.32	8.58	11.52	10.75	7.44	9.57
O4	22.43	27.46	13.69	9.25	86.28	36.40	6.19	30.89	5.68	13.67	17.92	15.29	13.89	14.82
O5	1.97	3.08	1.39	1.00	4.35	3.97	0.23	4.09	0.15	3.99	1.44	1.79	1.57	1.66
O6	22.79	28.37	14.10	8.69	86.76	36.18	5.77	31.37	6.42	13.87	19.54	17.08	13.43	14.65
O7	19.53	25.99	12.24	8.13	72.62	31.54	5.09	25.33	5.45	13.80	14.15	12.22	10.61	11.87
O8	23.23	29.83	15.05	8.73	91.99	40.29	6.46	32.77	6.37	13.84	20.43	15.84	12.94	15.12
O9	18.76	22.44	10.60	7.45	67.43	28.10	4.42	22.52	4.75	4.75	12.93	12.20	9.27	9.16
O10	32.23	40.35	21.46	3.87	127.85	56.05	7.96	46.41	8.40	21.02	25.85	24.58	20.34	22.07
O12	35.06	42.41	21.36	3.92	124.40	59.50	7.38	48.92	8.99	23.83	25.93	24.66	20.33	19.92
O13	29.37	40.36	21.56	12.07	134.87	54.95	8.49	44.86	8.63	20.03	27.33	24.43	19.94	19.60
O14	28.53	35.78	18.46	3.50	113.72	49.21	6.57	40.42	7.30	19.10	21.85	4.26	16.62	17.14
O15	2.57	4.42	2.04	0.43	10.33	5.62	0.78	4.96	0.64	2.97	2.37	2.33	1.96	2.04
O16	27.50	34.77	17.97	10.32	110.83	49.70	7.19	41.37	8.04	19.17	23.68	18.64	15.92	17.53
O18	29.07	36.09	17.67	3.10	110.58	49.76	6.51	39.51	7.87	19.48	23.48	18.15	16.45	16.59
O19	30.05	38.16	19.06	11.50	118.31	54.88	7.00	45.28	8.80	22.79	26.66	22.68	19.30	19.49
O20	14.59	17.08	7.00	2.32	44.02	18.59	3.19	13.65	3.43	4.57	8.24	8.19	5.57	6.22
O21	27.82	34.41	17.36	3.44	104.13	47.71	6.39	39.60	0.70	19.94	21.42	20.23	16.86	16.95
O22	28.64	34.96	17.01	2.97	106.50	45.19	6.14	38.77	6.82	19.01	22.08	21.30	17.54	18.20

2) Hopanes:

sample ID	Ts	Tm	C28bis	C29αβ	C29βα	C30αβ	C31(22S)	C31(22R)	Gamma	C32(22S)	C32(22R)	C33(22S)	C33(22R)	C34(22S)	C34(22R)
O1	5.22	43.33	24.35	104.00	8.41	83.78	43.66	41.48	24.32	31.35	22.01	24.79	12.76	13.42	8.23
O2	7.09	48.56	26.59	115.68	8.65	95.22	52.20	49.53	28.37	37.49	24.16	28.97	13.57	16.34	9.30
O3	2.31	16.34	6.61	44.78	3.57	30.44	15.02	7.30	7.30	9.73	7.16	7.20	4.15	3.95	2.49
O4	5.36	40.02	22.04	97.35	7.57	78.44	42.08	39.30	22.31	31.02	21.76	25.08	11.80	14.54	8.06
O5	12.38	13.34	10.96	54.81	6.41	108.49	52.25	38.04	2.25	35.98	26.40	32.30	19.53	19.91	12.53
O6	5.29	38.87	23.47	102.99	7.62	81.90	43.79	41.29	23.01	33.17	22.85	25.20	13.03	14.53	8.89
O7	4.27	36.25	14.20	100.97	7.37	66.94	34.26	36.03	21.54	25.98	17.31	19.79	9.67	9.79	6.10
O8	4.91	36.99	23.34	88.77	6.29	71.55	38.14	31.32	21.10	24.26	17.77	17.77	8.82	10.03	5.82
O9	2.43	19.25	11.06	49.29	3.72	40.33	20.45	19.37	9.85	15.41	9.76	12.46	5.45	6.31	10.71
O10	9.47	74.47	41.13	205.05	14.34	163.41	92.08	82.93	52.34	69.40	46.03	52.98	26.28	33.20	19.71
O12	8.88	70.93	42.61	199.28	13.28	153.61	85.59	79.53	48.74	62.63	42.99	49.04	24.60	30.27	17.20
O13	6.32	66.71	38.52	170.06	11.81	149.76	81.94	74.52	46.36	61.47	42.16	46.51	24.02	28.50	17.10
O14	9.52	61.56	34.30	177.06	11.29	136.10	77.00	70.25	41.70	57.79	38.97	43.37	22.60	28.39	16.47
O15	3.89	5.64	1.57	18.53	1.61	19.36	10.85	8.99	4.31	8.84	6.71	5.70	3.07	3.58	2.50
O16	7.69	62.93	39.82	173.88	11.58	142.51	79.83	73.36	46.46	61.95	43.13	45.47	23.07	28.17	16.93
O18	9.36	57.43	33.59	164.22	11.33	123.65	69.92	65.11	38.69	51.30	33.26	39.22	19.02	24.78	14.63
O19	7.87	69.57	40.39	200.08	14.29	154.58	86.65	80.13	47.03	64.40	44.66	49.73	25.75	28.44	18.12
O20	2.65	8.43	4.95	19.54	1.65	14.48	7.08	6.81	3.86	5.51	3.86	5.97	1.57	1.65	1.46
O21	9.92	60.79	36.48	172.23	13.10	132.70	74.24	67.66	43.47	53.53	36.75	41.72	20.99	25.92	15.25
O22	7.50	57.45	30.84	159.15	11.18	120.23	66.69	61.31	37.88	48.86	32.78	37.83	19.50	23.49	13.98

3) Steranes:

sample ID	C21preg	C22preg	C27ααα(20S)	C27αββ(20R)	C27αββ(20S)	C27ααα(20R)	C28ααα(20S)	C28αββ(20R)	C28αββ(20S)	C28ααα(20R)	C29ααα(20S)	C29αββ(20R)	C29ββ(20S)	C29ααα(20R)
O1	26.83	14.86	10.71	13.76	12.70	9.96	5.41	13.22	15.89	10.37	40.22	60.78	50.08	40.09
O2	27.10	15.52	12.78	15.05	14.16	11.35	10.62	13.56	16.46	8.89	45.71	74.97	51.52	44.49
O3	16.34	7.61	4.04	5.21	4.77	3.40	3.03	5.13	6.16	3.06	15.18	23.45	15.85	12.98
O4	21.08	12.75	11.44	13.10	13.39	12.43	5.19	11.56	14.84	10.19	37.89	59.28	45.93	36.66
O5	7.66	4.64	19.86	21.56	11.56	10.20	9.29	12.96	9.75	8.01	13.21	15.18	9.82	16.88
O6	21.15	13.24	11.26	13.99	14.59	13.36	6.16	11.24	13.42	7.36	39.34	64.05	43.43	37.85
O7	19.90	10.28	7.08	8.80	8.71	6.85	4.16	9.79	10.43	8.03	27.44	43.39	31.28	27.29
O8	23.72	12.97	9.54	12.59	12.59	9.91	4.40	12.65	14.55	9.82	40.28	64.21	46.67	38.81
O9	14.34	8.27	8.31	8.32	9.00	7.28	2.74	6.87	8.80	4.60	21.57	33.40	26.95	20.22
O10	28.41	17.07	14.35	18.76	17.24	12.79	7.07	20.70	20.70	40.49	61.79	96.20	73.89	60.23
O12	33.52	19.41	15.52	19.49	19.28	19.16	12.64	17.41	20.46	11.86	61.25	95.91	75.85	62.67
O13	29.01	17.03	14.47	18.67	15.99	12.82	12.79	17.59	20.95	11.24	59.86	91.84	75.49	61.23
O14	26.88	15.39	15.87	18.77	18.50	19.86	12.05	17.65	17.23	13.04	52.20	83.82	62.64	54.21
O15	3.38	2.19	2.92	5.31	2.93	2.52	0.99	3.69	3.18	2.03	10.07	15.16	10.07	9.84
O16	24.16	15.10	14.50	18.23	18.74	17.89	12.99	15.67	17.41	10.04	55.71	91.89	60.75	58.08
O18	28.56	15.48	13.91	16.37	16.96	17.39	10.87	14.45	16.63	9.59	50.65	78.53	59.29	51.68
O19	31.01	17.25	15.34	19.73	18.52	21.33	12.07	19.18	21.53	15.05	58.70	93.12	73.10	60.67
O20	14.13	1.30	5.30	4.27	4.57	3.00	2.89	3.40	5.11	3.35	11.19	17.08	13.40	9.76
O21	26.19	15.27	14.11	16.55	17.09	18.68	12.24	14.40	15.13	9.87	50.37	83.67	63.84	52.70
O22	25.09	14.96	14.73	18.24	17.87	17.28	11.50	14.22	15.48	8.79	49.77	80.73	56.56	49.83

Aromatic biomarkers:

	Triaromatic steroids								Monoaroamtic steroids									
sample ID	$C_{20}TA$	$C_{21}TA$	$C_{26}S$	$C_{26}R+C_{27}S$	$C_{28}S$	$C_{27}R$	$C_{28}R$	sum TA	$C_{21}MAS$	$C_{22}MAS$	$C_{27}\beta S$	$C_{27}\beta R$	$C_{28}\beta S$	$C_{29}\beta S+C_{28}\alpha S$	$C_{29}\alpha S$	$C_{29}\beta R+C_{28}\alpha R$	$C_{29}\alpha R$	sum MA
O1	18	17	3	8	21	5	14	86	35	35	17	14	14	57	15	30	11	228
O2	17	16	2	6	16	4	11	73	38	35	16	14	14	53	14	28	11	223
O3	9	7	0	1	5	1	3	26	26	21	7	5	5	19	5	9	3	100
O4	18	17	2	7	18	4	12	79	35	40	17	13	14	54	14	28	11	226
O5	30	26	24	80	48	43	37	287	6	3	4	18	40	62	5	23	3	165
O6	17	16	2	6	15	3	10	69	37	38	16	13	13	49	13	26	9	213
O7	35	26	1	5	20	4	13	104	41	39	8	7	7	28	7	15	6	160
O8	18	17	3	7	19	5	13	81	35	37	17	14	14	55	15	29	11	227
O9	7	7	1	2	5	1	3	27	28	28	10	8	8	31	8	15	5	143
O10	30	26	3	11	32	7	21	131	38	50	20	16	20	73	19	38	14	289
O11	30	28	3	12	35	9	24	140	41	49	21	17	22	77	20	41	15	303
O12	34	30	2	9	30	7	21	133	33	39	14	11	12	49	13	26	9	206
O13	18	17	2	7	18	4	11	78	30	38	13	11	13	49	12	25	9	200
O14	27	24	2	9	28	6	18	114	44	43	22	17	19	73	18	38	14	287
O15	26	27	4	16	54	11	39	176	15	14	5	7	9	52	9	29	6	147
O16	29	27	3	11	31	8	22	132	28	28	15	12	16	56	14	30	10	210
O17	30	27	3	12	37	8	26	144	44	49	24	20	22	87	23	46	17	330
O18	33	29	2	9	31	7	22	134	38	34	14	12	13	49	13	27	11	210
O19	39	35	2	12	40	9	29	165	37	46	15	13	13	54	15	30	11	233
O20	3	2	0	1	1	0	1	9	15	15	7	5	5	5	5	8	3	67
O21	33	28	1	8	24	6	16	117	42	47	13	11	11	43	12	24	8	210
O22	29	25	2	7	24	5	17	109	35	35	12	10	10	41	11	21	8	183

Phenanthrene and alkylphenanthrene

sample ID	Phenanthrene	3-MP	2-MP	9-MP	1-MP	3-Ep	9, 2, +1-Ep+3,6DMP	3,5+2,6-DMP	1,3+3,9+2,10+3,10-DMP	2,5+2,9+1,6-DMP	1,7-DMP	2,3-DMP	1,9+4,9+4,10-DMP	1,8-DMP	1,2-DMP	sum Phen
O1	95	48	107	99	76	5	27	47	127	67	91	12	24	17	26	868
O2	90	49	109	101	77	6	26	42	126	67	87	11	25	17	25	859
O3	56	30	60	70	49	3	17	25	85	47	52	6	17	10	15	542
O4	89	48	108	99	75	6	27	43	128	69	90	11	25	17	26	861
O5	396	161	163	305	227	17	73	54	17	185	98	75	30	58	30	1887
O6	87	52	111	105	77	5	28	44	133	69	94	12	26	17	27	887
O7	154	83	171	200	138	8	44	68	251	139	162	19	49	32	52	1569
O8	91	50	108	103	74	5	27	43	126	66	88	11	25	17	25	860
O9	49	26	53	52	38	3	14	20	67	34	44	6	12	8	11	438
O10	139	69	149	137	106	7	33	61	164	94	131	14	32	22	41	1199
O11	135	69	151	138	104	6	33	63	166	90	130	14	31	23	39	1191
O12	181	86	196	178	134	9	42	78	209	121	167	19	41	29	47	1536
O13	182	66	120	135	89	5	28	44	132	67	90	12	25	16	26	1036
O14	151	79	163	147	113	7	37	71	175	95	129	15	33	23	39	1276
O15	147	59	98	166	123	7	43	46	172	90	111	14	47	29	25	1175
O16	159	82	177	154	117	8	38	73	183	102	146	16	34	25	40	1354
O17	141	72	161	142	111	6	36	66	170	95	134	15	33	23	42	1248
O18	154	87	182	173	126	9	41	76	206	114	157	17	40	28	47	1457
O19	175	89	202	189	145	7	44	84	234	134	179	20	45	32	53	1632
O20	28	16	31	30	23	3	10	14	38	20	24	3	7	5	6	259
O21	157	73	165	173	131	7	38	63	203	112	142	16	41	27	41	1389
O22	149	81	168	165	122	6	39	72	189	105	150	15	38	26	46	1372

Naphthalene and alkyl naphthalene

sample ID	Napthalene	2-MN	1-MN	2-EN	1-EN	2,6+2,7-DMN	1,3+1,7-DMN	1,6-DMN	1,4- (1,4+2,3)-DMN	1,5-DMN	1,2-DMN	1,3,7-TMN	1,3,6-TMN	1,3,5+1,4,6-TMN	2,3,6-TMN	1,2,7+1,6,7-TMN	1,2,6-TMN	1,2,4-TMN	1,2,5-TMN	1,2,3-TMN	sum Naph
O1	199	404	372	65	33	341	370	479	118	106	79	154	342	243	146	155	118	29	162	25	3939
O2	226	441	414	70	38	375	400	526	127	124	86	176	371	299	132	204	96	34	179	27	4345
O3	43	263	272	59	33	391	397	507	126	129	78	204	416	348	154	205	118	37	166	28	3972
O4	204	405	377	65	35	349	369	497	120	114	86	161	346	274	119	188	92	31	167	26	4027
O5	372	917	956	164	113	656	1107	823	414	242	217	447	584	564	296	526	206	83	372	73	9133
O6	446	467	441	72	39	393	405	527	133	127	88	172	368	289	135	193	107	34	177	28	4638
O7	418	733	740	110	55	682	756	826	262	204	148	329	689	528	294	290	210	57	276	43	7650
O8	985	555	503	76	40	401	421	533	136	129	88	172	362	278	133	185	103	32	168	27	5326
O9	194	371	340	58	31	324	341	437	103	100	69	150	319	252	108	166	76	25	138	20	3621
O10	388	657	637	107	49	524	532	683	182	148	129	203	451	351	154	191	162	41	210	33	5834
O11	389	703	673	110	55	558	574	719	194	155	136	211	493	335	209	342	364	42	219	35	6516
O12	425	779	754	131	58	625	721	771	236	169	147	240	559	392	226	242	172	47	258	37	6989
O13	702	1196	1194	150	72	744	887	904	314	308	224	248	513	417	202	274	149	54	255	39	8846
O14	489	839	810	141	66	671	706	841	238	188	161	266	588	409	248	254	187	51	248	41	7446
O15	331	509	639	89	60	365	489	620	185	168	110	206	485	358	148	232	153	44	208	33	5432
O16	469	810	735	129	59	624	611	837	213	178	151	230	539	372	198	262	145	46	252	37	6898
O17	446	769	752	132	61	605	629	767	212	166	144	229	536	366	223	225	171	47	233	38	6750
O18	383	698	701	125	58	599	640	799	218	175	141	245	564	439	182	224	187	45	253	37	6713
O19	385	750	746	132	57	654	662	880	223	190	148	252	612	464	193	234	202	51	264	38	7136
O20	72	168	151	28	17	184	216	245	57	58	36	109	217	171	88	129	46	17	87	15	2111
O21	426	806	832	134	67	700	728	1018	236	211	161	274	679	437	276	246	212	53	294	40	7831
O22	366	659	639	116	54	546	572	727	199	158	130	220	511	397	170	210	175	42	233	36	6162

Benzothiophenes and alkylbenzothiophenes

	Benzothiophenes&methylbenzothiophenes					C2-benzothiophenes						C3-benzothiophenes							
sample ID	BT	2MBT	7MBT	6/5MBT	4/3MBT	A	B	C	D	E	F	1	2	3	4	5	6	7	sum BT
O1	228	76	7	20	19	50	17	62	63	19	115	10	47	30	84	57	176	196	1275
O2	274	89	8	22	21	56	18	66	67	19	125	11	50	33	92	63	194	220	1428
O3	87	335	9	12	15	55	9	73	57	29	161	13	45	39	104	70	297	343	1751
O4	241	76	8	20	19	51	17	62	63	17	115	10	48	31	85	58	180	205	1307
O5	160	37	6	8	10	13	2	15	10	7	18	2	8	8	17	6	32	22	381
O6	252	82	8	22	21	54	18	69	71	22	130	11	51	33	90	62	192	220	1408
O7	341	218	11	42	52	101	15	176	159	75	234	18	53	78	183	108	486	498	2847
O8	276	81	9	21	22	52	16	65	65	19	125	10	49	32	88	60	186	208	1383
O9	350	107	11	20	15	46	15	44	52	12	109	9	43	25	75	51	160	185	1329
O10	253	56	9	54	59	84	31	148	142	50	174	15	67	60	153	109	289	304	2057
O11	271	60	9	56	63	88	33	160	151	53	189	16	72	64	163	110	309	322	2188
O12	300	235	9	42	48	75	21	130	120	50	175	15	54	54	139	105	289	314	2176
O13	351	62	18	49	71	78	38	141	171	42	241	13	75	59	165	102	307	296	2279
O14	327	76	10	45	50	85	26	145	138	49	194	18	68	68	161	105	317	327	2209
O15	200	47	8	4	7	5	3	3	3	3	24	1	6	2	7	5	29	31	390
O16	289	67	10	52	53	66	44	120	148	36	181	12	76	50	152	104	267	300	2026
O17	317	71	9	43	49	83	25	138	129	44	179	18	64	64	152	97	302	310	2094
O18	279	116	8	30	32	70	17	109	114	36	175	14	55	51	133	90	286	316	1931
O19	284	78	9	30	33	69	14	116	110	40	172	15	47	54	130	88	298	313	1900
O20	315	157	16	12	13	23	3	19	6	12	65	7	22	9	33	20	112	100	945
O21	348	88	10	30	35	72	13	120	113	38	185	16	47	58	139	97	321	339	2069
O22	280	137	8	30	31	64	18	101	107	34	165	13	55	49	127	85	269	298	1871

Dibenzothiophene and alkyldibenzothiphenes

sample ID	DBT	4-MeDBT	3+2-MeDBT	1-MeDBT	4EDBT	4,6 DMDBT	2,4 DMDBT	2,6+3,6DMDBT	2,7+2,8+3,7DMDBT	1,4+1,6DMDBT	1,8DMDBT	1,3 DMDBT	1,7+1,9+3,4DMDBT	sum DBT
O1	98	145	104	63	21	102	36	231	14	61	77	46	19	1019
O2	97	152	103	64	21	103	36	233	13	61	82	45	20	1029
O3	76	116	93	44	14	77	27	150	9	50	56	36	16	764
O4	99	152	109	66	20	103	35	208	13	62	83	47	21	1018
O5	71	96	53	57	15	40	27	31	5	9	57	18	9	489
O6	101	159	111	68	23	107	36	241	12	65	85	46	21	1075
O7	144	261	195	99	35	192	67	437	29	144	153	102	45	1904
O8	104	156	110	68	21	104	35	233	12	62	84	46	21	1058
O9	60	90	62	38	13	60	20	127	7	32	44	23	11	586
O10	113	186	130	81	24	127	44	309	28	86	113	70	31	1342
O11	113	191	130	84	25	130	42	313	25	86	117	72	29	1357
O12	153	242	178	95	28	152	55	386	32	107	129	86	36	1680
O13	324	277	185	132	26	120	44	255	19	67	110	56	26	1641
O14	128	212	149	89	30	147	51	331	23	103	119	75	32	1490
O15	77	116	61	50	20	78	25	173	6	28	68	28	15	745
O16	148	218	148	97	29	126	51	334	27	87	121	55	32	1474
O17	120	196	141	82	27	138	45	327	29	91	107	67	28	1397
O18	142	230	168	93	31	154	54	373	28	103	126	79	33	1611
O19	145	242	174	98	32	168	55	417	22	121	138	91	40	1745
O20	41	59	44	23	9	40	14	69	3	21	29	15	7	375
O21	125	220	143	91	27	155	48	318	25	90	124	70	29	1465
O22	137	213	162	90	29	148	51	357	26	100	121	75	33	1542

Flourne, alkylfluorenes, biphenyl and alkylbiphenyls

	BiPhenyl&Alkylbiphenyls							Fluorene&Methylfluorenes					
sample ID	BiPhenyl	2-MBp	DP-M	3-MBp	4-MBp	DBF	sum Bp	Fluorene	3-MeFl	2-MeFl	1-MeFl	4-MeFl	sum F
O1	49	9	4	45	23	10	130	18	8	6	34	9	75
O2	53	10	4	50	25	10	142	20	8	7	36	10	80
O3	44	9	5	48	25	14	132	13	6	4	30	10	64
O4	50	9	4	47	24	10	134	18	10	5	35	9	76
O5	64	43	23	138	47	71	315	98	38	38	117	29	320
O6	56	10	5	51	26	11	148	21	10	5	36	10	82
O7	74	13	9	86	43	21	226	41	20	15	69	19	164
O8	64	11	5	53	26	12	159	21	9	5	36	10	81
O9	52	11	4	47	24	9	138	15	6	3	26	8	58
O10	62	10	5	57	28	14	161	31	13	11	50	14	120
O11	64	11	5	59	29	14	168	31	14	10	52	15	122
O12	78	12	6	74	36	23	206	38	17	12	61	16	144
O13	138	27	14	99	54	40	331	78	21	13	68	17	197
O14	77	14	7	76	36	19	211	38	17	12	60	17	144
O15	92	34	5	71	34	7	236	16	7	4	24	5	56
O16	73	12	5	69	32	16	191	43	22	11	59	17	152
O17	68	11	5	64	32	16	181	25	10	8	42	8	94
O18	86	12	6	71	35	16	211	32	18	8	56	15	130
O19	80	13	6	77	37	16	212	37	18	14	62	17	147
O20	41	11	4	41	22	6	118	10	4	3	18	6	41
O21	92	14	6	81	37	18	231	37	20	10	62	18	146
O22	66	11	5	64	31	16	177	4	6	3	21	3	37

Appendix 4. 5: The molecular ratios used and unused in this study

	Hopanes Parameters										
Sample ID	**Ts/(Tm+Ts) %**	**Ts/(Ts+30αβ) %**	Ts/C30αβ	**C31 22S/(22R**	**C32 22S/(22R**	**22S/22S+ 22R(C32-**	**Homohopane Index**	**Gammacerane Index**	**HOEP**	C31αβ(S+R)/C31+C33αβ(S+R)	∑Hopanes
O1	10.75	5.86	0.06	51.28	58.75	59.78	18.30	0.29	1.18	0.69	511.07
O2	12.74	6.93	0.07	51.31	60.81	62.78	16.63	0.30	1.15	0.71	579.54
O3	12.39	7.06	0.08	67.28	57.61	56.80	17.96	0.24	1.10	0.66	173.54
O4	11.81	6.40	0.07	51.71	58.77	61.71	17.82	0.28	1.14	0.69	486.41
O5	48.13	10.24	0.11	57.87	57.68	60.03	10.52	0.02	1.13	0.64	471.17
O6	11.98	6.07	0.06	51.47	59.21	61.80	16.82	0.28	1.12	0.69	503.91
O7	10.54	6.00	0.06	48.74	60.01	59.77	19.14	0.32	1.20	0.70	426.56
O8	11.72	6.42	0.07	54.91	57.72	60.61	15.17	0.29	1.11	0.72	413.27
O9	11.22	5.69	0.06	51.35	61.21	57.95	14.80	0.24	0.98	0.69	243.35
O10	11.28	5.48	0.06	52.62	60.12	61.17	20.62	0.32	1.13	0.69	1040.26
O12	11.13	5.46	0.06	51.83	59.30	60.89	18.92	0.32	1.14	0.69	971.84
O13	8.65	4.05	0.04	52.37	59.32	61.40	19.13	0.31	1.12	0.69	908.41
O14	13.40	6.54	0.07	52.29	59.72	61.35	20.05	0.31	1.12	0.69	873.68
O15	40.80	16.73	0.20	54.68	56.87	59.24	15.41	0.22	0.94	0.69	109.98
O16	10.88	5.12	0.05	52.11	58.96	60.36	20.14	0.33	1.10	0.69	904.09
O18	14.01	7.03	0.08	51.78	60.67	61.31	19.12	0.31	1.13	0.70	791.82
O19	10.16	4.84	0.05	51.95	59.05	60.31	19.52	0.30	1.15	0.69	981.15
O20	23.90	15.46	0.18	50.97	58.79	65.08	8.79	0.27	1.25	0.65	88.88
O21	14.03	6.96	0.07	52.32	59.30	60.06	19.78	0.33	1.14	0.69	844.18
O22	11.55	5.87	0.06	52.10	59.84	60.60	19.26	0.32	1.14	0.69	763.41

	Tricyclics Parameters							Hopanes-Tricyclics Parameters					
Sample ID	C20+C21Tr/ C23+C24Tr	C28/C29(Tri)	C23/C21 Triβα	C23/C24 Triβα	C26Tri(S+R)/ C25Tri(S+R)	C24Tetra/C23 Triβα	∑TRI	Tri/hop	C28+C 29Tr(S	C28+C29Tr(S+R) /[C29+C30αβ+C2	C28+C29Tri/C29-33hop	C24Tetr/C3 0ab	TriC23βα/ho pC30αβ
O1	0.40	0.94	3.06	2.24	0.99	0.17	375.78	0.74	0.33	0.25	0.17	0.20	1.18
O2	0.42	0.84	2.97	2.36	0.93	0.16	410.85	0.71	0.35	0.26	0.17	0.18	1.13
O3	0.46	1.13	2.72	2.35	0.89	0.14	234.54	1.35	0.43	0.30	0.26	0.28	2.09
O4	0.41	0.96	3.14	2.37	0.91	0.16	330.04	0.68	0.33	0.25	0.17	0.17	1.10
O5	0.61	0.53	1.41	1.09	0.76	0.92	32.80	0.07	0.06	0.05	0.03	0.04	0.04
O6	0.42	0.91	3.06	2.40	0.97	0.16	335.83	0.67	0.32	0.24	0.16	0.17	1.06
O7	0.44	0.95	2.79	2.30	0.86	0.19	278.54	0.65	0.28	0.22	0.15	0.21	1.08
O8	0.40	0.96	3.08	2.28	0.93	0.15	348.30	0.84	0.36	0.26	0.19	0.19	1.29
O9	0.43	0.96	3.00	2.40	0.92	0.07	249.25	1.02	0.42	0.30	0.22	0.12	1.67
O10	0.39	0.91	3.17	2.28	0.92	0.16	483.87	0.47	0.24	0.19	0.12	0.13	0.78
O12	0.42	0.82	2.93	2.09	0.87	0.19	491.88	0.51	0.25	0.20	0.13	0.16	0.81
O13	0.37	0.90	3.34	2.45	0.97	0.15	490.29	0.54	0.26	0.21	0.13	0.13	0.90
O14	0.39	0.83	3.18	2.31	0.55	0.17	403.85	0.46	0.24	0.19	0.12	0.14	0.84
O15	0.44	0.78	2.34	1.84	0.84	0.29	45.58	0.41	0.24	0.19	0.11	0.15	0.53
O16	0.39	0.82	3.19	2.23	0.86	0.17	424.21	0.47	0.23	0.19	0.12	0.13	0.78
O18	0.41	0.77	3.06	2.22	0.88	0.18	417.80	0.53	0.26	0.21	0.13	0.16	0.89
O19	0.39	0.86	3.10	2.16	0.91	0.19	466.19	0.48	0.24	0.19	0.12	0.15	0.77
O20	0.51	1.11	2.58	2.37	0.96	0.10	162.71	1.83	0.66	0.40	0.35	0.32	3.04
O21	0.41	0.86	3.03	2.18	1.03	0.19	396.22	0.47	0.24	0.19	0.12	0.15	0.78
O22	0.42	0.91	3.05	2.36	0.95	0.18	405.59	0.53	0.27	0.21	0.14	0.16	0.89

	Steranes Parameters															
Sample ID	C27Steranes %	C28Steranes %	C29Steranes %	Pregnanes/ Steranes	C27/C29	C28/C29	C27/C28	C29% αββ/ααα	C29% 20S/(20S+20R)	C27ααα R/C29 ααα R%	C27αββ/C29αββ (S+R)	C28αββ/C29αββ(S+R)	∑Steranes	C29αβ/C29αββ	Hopanes/ steranes
O1	16.64	15.85	67.51	0.22	0.29	0.21	1.82	58.0	50.1	35.29	0.27	0.23	324.87	0.54	1.57
O2	16.69	15.50	67.81	0.20	0.25	0.23	1.24	58.4	50.7	25.51	0.23	0.24	362.18	0.53	1.60
O3	17.04	17.00	65.96	0.36	0.26	0.26	1.22	58.3	53.9	26.18	0.25	0.29	126.21	0.66	1.37
O4	18.52	15.36	66.12	0.19	0.28	0.23	1.55	58.5	50.8	33.91	0.25	0.25	305.72	0.54	1.59
O5	39.92	25.28	34.81	0.22	1.15	0.73	1.74	45.4	43.9	60.41	1.32	0.91	170.59	0.99	2.76
O6	19.27	13.83	66.90	0.19	0.29	0.21	1.82	58.2	51.0	35.29	0.27	0.23	310.43	0.56	1.62
O7	16.27	16.77	66.96	0.23	0.24	0.25	1.14	57.7	50.1	25.09	0.23	0.27	223.42	0.78	1.91
O8	16.17	15.01	68.82	0.19	0.23	0.22	1.37	58.4	50.9	25.53	0.23	0.25	312.72	0.47	1.32
O9	20.82	14.56	64.62	0.22	0.32	0.23	2.12	59.1	51.6	35.99	0.29	0.26	180.69	0.48	1.35
O10	14.22	20.03	65.76	0.16	0.22	0.30	0.57	58.2	50.6	21.24	0.21	0.24	489.71	0.70	2.12
O12	17.02	14.46	68.52	0.18	0.25	0.21	1.42	58.1	49.4	30.57	0.23	0.22	484.44	0.67	2.01
O13	15.00	15.15	69.85	0.16	0.21	0.22	1.14	58.0	49.4	20.95	0.21	0.23	458.98	0.59	1.98
O14	18.92	15.54	65.54	0.17	0.29	0.24	1.42	57.9	49.1	36.64	0.25	0.24	428.10	0.70	2.04
O15	19.92	14.40	65.68	0.12	0.30	0.22	1.80	55.9	50.6	25.64	0.33	0.27	74.29	0.41	1.48
O16	17.70	14.32	67.99	0.15	0.26	0.21	1.41	57.3	49.0	30.80	0.24	0.22	431.17	0.65	2.10
O18	18.14	14.46	67.40	0.18	0.27	0.21	1.53	57.4	49.5	33.66	0.24	0.23	400.37	0.68	1.98
O19	17.49	15.84	66.67	0.17	0.26	0.24	1.35	58.2	49.2	35.15	0.23	0.24	476.63	0.70	2.06
O20	20.56	17.71	61.73	0.30	0.33	0.29	1.33	59.3	53.4	30.75	0.29	0.28	98.74	0.38	0.90
O21	18.02	14.01	67.97	0.17	0.27	0.21	1.48	58.9	48.9	35.45	0.23	0.20	410.10	0.69	2.06
O22	19.19	14.08	66.73	0.17	0.29	0.21	1.58	58.0	50.0	34.67	0.26	0.22	395.03	0.67	1.93

	Triaromatic and monoaromatic steroids ratios							Phenanthrenes ratios								
Sample code	TAC20/C20+C28	TA C26 20S/C28 20S	TA C27 20RC28 20R	MA C27/C28+C29	MA/MA+TA	MAI/MAI+II	TAI/I+II	MPI-1	VRE(MPI-1)	MPR	MPR-1	MPI-2	MPI-3	MPR-9	F1	F2
O1	0.33	0.13	0.35	0.24	0.73	0.31	0.40	0.86	0.92	1.41	0.80	1.12	0.51	1.04	0.47	0.32
O2	0.39	0.14	0.38	0.25	0.75	0.33	0.45	0.88	0.93	1.41	0.85	1.20	0.54	1.12	0.47	0.32
O3	0.56	0.07	0.33	0.29	0.79	0.47	0.62	0.77	0.86	1.21	0.89	1.07	0.54	1.26	0.43	0.29
O4	0.37	0.12	0.34	0.25	0.74	0.33	0.44	0.89	0.93	1.44	0.85	1.22	0.54	1.12	0.47	0.33
O5	0.26	0.51	1.16	0.16	0.36	0.05	0.20	0.52	0.71	0.72	0.57	0.41	0.41	0.77	0.38	0.19
O6	0.41	0.13	0.36	0.26	0.76	0.35	0.48	0.91	0.94	1.45	0.88	1.27	0.59	1.20	0.47	0.32
O7	0.52	0.06	0.31	0.24	0.61	0.51	0.59	0.77	0.86	1.24	0.89	1.11	0.54	1.30	0.43	0.29
O8	0.35	0.13	0.34	0.25	0.74	0.32	0.42	0.88	0.93	1.46	0.81	1.18	0.54	1.13	0.47	0.32
O9	0.45	0.13	0.36	0.27	0.84	0.39	0.51	0.85	0.91	1.39	0.78	1.08	0.53	1.07	0.47	0.31
O10	0.36	0.09	0.34	0.22	0.69	0.31	0.43	0.86	0.91	1.41	0.76	1.07	0.50	0.98	0.47	0.32
O11	0.34	0.09	0.37	0.22	0.68	0.30	0.41	0.87	0.92	1.45	0.77	1.12	0.51	1.02	0.48	0.33
O12	0.40	0.07	0.32	0.23	0.61	0.35	0.48	0.86	0.92	1.47	0.74	1.08	0.48	0.98	0.48	0.33
O13	0.38	0.13	0.36	0.21	0.72	0.34	0.45	0.69	0.81	1.35	0.49	0.66	0.36	0.74	0.45	0.29
O14	0.37	0.09	0.33	0.24	0.72	0.30	0.45	0.88	0.93	1.44	0.75	1.08	0.52	0.98	0.48	0.32
O15	0.22	0.07	0.30	0.12	0.46	0.20	0.30	0.54	0.72	0.79	0.84	0.67	0.40	1.12	0.35	0.22
O16	0.35	0.10	0.35	0.22	0.61	0.27	0.43	0.90	0.94	1.51	0.73	1.11	0.51	0.97	0.49	0.33
O17	0.32	0.09	0.32	0.23	0.70	0.28	0.40	0.89	0.93	1.45	0.79	1.14	0.51	1.01	0.48	0.33
O18	0.38	0.07	0.31	0.23	0.61	0.34	0.47	0.89	0.93	1.44	0.82	1.18	0.56	1.12	0.47	0.32
O19	0.36	0.06	0.30	0.23	0.59	0.35	0.44	0.86	0.91	1.39	0.83	1.16	0.51	1.08	0.47	0.32
O20	0.56	0.16	0.38	0.47	0.88	0.45	0.60	0.86	0.92	1.34	0.81	1.08	0.57	1.07	0.47	0.31
O21	0.45	0.05	0.36	0.25	0.64	0.42	0.52	0.85	0.91	1.35	0.83	1.05	0.46	1.10	0.44	0.30
O22	0.41	0.07	0.32	0.24	0.63	0.38	0.49	0.86	0.91	1.37	0.82	1.13	0.55	1.11	0.46	0.31

	Naphthalenes				Dibenzothiophenes							Biphenyls			Fluorene	benzothiophenes	
Sample code	MNR	DNR-1	TNR1	ENR	MDR1	MDR4	MDR2,3	MDR	DBT/P	MDBT/Mphen	(2+3-MDBT)/1-MDBT	4MBp/2MBp	4MBp/3MB	4MBp/Bp	F/∑MF	C/F	3+4/6
O1	1.09	3.22	0.60	1.98	0.64	1.48	1.06	2.32	1.03	0.95	1.66	2.65	0.51	0.48	0.24	0.54	0.65
O2	1.07	3.02	0.44	1.86	0.66	1.58	1.07	2.38	1.07	0.95	1.62	2.41	0.50	0.47	0.25	0.53	0.64
O3	0.97	3.02	0.44	1.80	0.58	1.53	1.24	2.64	1.36	1.21	2.13	2.65	0.52	0.57	0.21	0.45	0.48
O4	1.07	3.06	0.43	1.87	0.66	1.54	1.11	2.32	1.11	0.99	1.67	2.59	0.51	0.47	0.24	0.54	0.64
O5	0.96	2.71	0.53	1.45	0.80	1.35	0.75	1.68	0.18	0.24	0.94	1.08	0.34	0.72	0.31	0.82	0.78
O6	1.06	3.08	0.47	1.86	0.67	1.57	1.10	2.33	1.15	0.98	1.63	2.44	0.50	0.45	0.25	0.54	0.64
O7	0.99	3.35	0.56	1.98	0.69	1.82	1.36	2.63	0.93	0.94	1.97	3.26	0.50	0.58	0.25	0.75	0.54
O8	1.10	3.10	0.48	1.91	0.65	1.49	1.05	2.29	1.14	1.00	1.62	2.37	0.49	0.40	0.26	0.52	0.64
O9	1.09	3.24	0.43	1.87	0.64	1.50	1.03	2.35	1.22	1.12	1.61	2.24	0.51	0.46	0.27	0.40	0.63
O10	1.03	3.54	0.44	2.18	0.72	1.64	1.14	2.29	0.82	0.86	1.59	2.85	0.49	0.46	0.26	0.85	0.74
O11	1.04	3.60	0.62	2.00	0.74	1.68	1.15	2.28	0.84	0.88	1.56	2.71	0.49	0.45	0.26	0.85	0.73
O12	1.03	3.69	0.58	2.25	0.62	1.58	1.16	2.55	0.84	0.87	1.87	3.07	0.49	0.47	0.27	0.74	0.67
O13	1.00	2.41	0.48	2.08	0.41	0.86	0.57	2.10	1.78	1.45	1.40	1.97	0.54	0.39	0.39	0.59	0.73
O14	1.04	3.57	0.61	2.13	0.70	1.66	1.17	2.37	0.85	0.90	1.67	2.61	0.48	0.47	0.26	0.75	0.72
O15	0.80	2.18	0.41	1.48	0.65	1.51	0.80	2.32	0.52	0.51	1.23	1.01	0.48	0.37	0.28	0.14	0.30
O16	1.10	3.51	0.53	2.18	0.65	1.47	1.00	2.25	0.93	0.87	1.53	2.74	0.47	0.44	0.29	0.66	0.76
O17	1.02	3.64	0.61	2.16	0.68	1.63	1.18	2.40	0.85	0.86	1.73	2.76	0.49	0.46	0.27	0.77	0.72
O18	1.00	3.42	0.41	2.15	0.66	1.62	1.18	2.46	0.92	0.87	1.80	2.89	0.48	0.40	0.25	0.62	0.65
O19	1.01	3.44	0.42	2.33	0.68	1.67	1.20	2.47	0.83	0.82	1.77	2.96	0.48	0.47	0.25	0.67	0.62
O20	1.12	3.16	0.52	1.70	0.56	1.41	1.05	2.51	1.47	1.26	1.87	2.04	0.54	0.54	0.24	0.30	0.37
O21	0.97	3.31	0.63	2.00	0.73	1.76	1.15	2.42	0.79	0.84	1.57	2.62	0.46	0.40	0.25	0.65	0.61
O22	1.03	3.46	0.43	2.15	0.66	1.55	1.18	2.36	0.93	0.87	1.79	2.80	0.48	0.46	0.11	0.61	0.66

Appendix 4. 6: the compounds used to perform Principal component analysis; the left contains aromatic hydrocarbons and the right aliphatic HCs.

A1	Phenanthrene	A27	3-MBp
A2	3-Methyl Phenanthrene (MP)	A28	4-MBp
A3	2-MP	A29	Dibenzofurane (DBF)
A4	9-MP	A30	Fluorene
A5	1-MP	A31	3-MeFl (methyl Flourene)
A6	1,3+3,9+2,10+3,10 DMP (Dimethyl phenanthrene)	A32	2-MeFl
A7	1,3+3,9+2,10+3,10 DMP	A33	1-MeFl
A8	C20 Triaromatic steroids (TAS)	A34	4-MeFl
A9	C21TAS	A35	C2-Benzothiphene1
A10	C26S TAS	A36	C2-Benzothiphene2
A11	C26R+C27S TAS	A37	C2-Benzothiphene3
A12	C28S TAS	A38	C2-Benzothiphene4
A13	C27R TAS	A39	C2-Benzothiphene5
A14	C28R TAS	A40	C2-Benzothiphene6
A15	C21 Monoaromatic steroids (MAS)	A41	C2-Benzothiphene7
A16	C22 MAS	A42	C3-BenzthiopheneA
A17	C27βS MAS	A43	C3-BenzthiopheneB
A18	C27βR MAS	A44	C3-BenzthiopheneC
A19	C28βS MAS	A45	C3-BenzthiopheneD
A20	C29βS+C28αS MAS	A46	C3-BenzthiopheneE
A21	C29αS MAS	A47	C3-BenzthiopheneF
A22	C29βR+C28αR MAS	A48	Dibenzothiphene (DBT)
A23	C29αR MAS	A49	4-MeDBT (methyl DBT)
A24	Biphenyls	A50	3+2-MeDBT
A25	2-Methyl Biphenyls (MBp)	A51	1-MeDBT
A26	DP-M		

V1	C20 βαTricyclics (TRI)	V25	Gammacerane
V2	C21TRI	V26	C32 22S HH
V3	C22TRI	V27	C32 22R HH
V4	C22ααTRI	V28	C33 22S HH
V5	C23TRI	V29	C33 22R HH
V6	C24TRI	V30	C34 22S HH
V7	C24ααTRI	V31	C34 22R HH
V8	C25TRI	V32	C35 22S HH
V9	C25ααTRI	V33	C35 22R HH
V10	C24Tetracyclics	V34	C21pregnane
V11	C26STRI	V35	C22 homopregnane
V12	C26RTRI	V36	C27 ααα 20S steranes (St)
V13	C28STRI	V37	C27 αββ 20R St
V14	C28RTRI	V38	C27 αββ 20S St
V15	C29STRI	V39	C27 ααα 20R St
V16	C29RTRI	V40	C28 ααα 20S St
V17	Ts	V41	C28 αββ20R St
V18	Tm	V42	C28 αββ 20S St
V19	C28 bisnorhopane	V43	C28 ααα 20R St
V20	C29 αβ norhopane	V44	C29 ααα 20S St
V21	C29 βα moretane	V45	C29 αββ 20R St
V22	C30αβ hopane	V46	C29 αββ 20S St
V23	C31 22S homohopane (HH)	V47	C29 ααα 20R St
V24	C31 22R HH		

10.2 The Chapter 5 Appendices

Appendix 5. 1: The full name of light hydrocarbons abbreviated in the text.

short	full name	short	full name
n-C_1	Methane	33DMP	3,3-dimethylpentane
n-C_2	ethane	11DMCP	1,1-dimethylcyclopentane
n-C_3	propane	2MH	2-methylhexane
IC_4	isobutane	23DMP	2,3-dimethylpentane
n-C_4	butane	1C3DMCP	1-*cis*-3-dimethylcyclopentane
IC_5	isopentane	3MH	3-methylhexane
n-C_5	pentane	1T3DMCP	1-*trans*-3-dimethylcyclopentane
22DMB	2,2-dimethylbutane	1T2DMCP	1-*trans*-2-dimethylcyclopentane
CP	cyclopentane	3EP	3-ethylpentane
23DMB	2,3-dimethylbutane	n-C_7	heptane
2MP	2-methylpentane	1C2DMCP	1-cis-2-dimethylcyclopentane
3MP	3-methylpentane	MCH	methylcyclohexane
n-C_6	hexane	113TMCP	1,1,3-trimethylcyclopentane
MCP	methylcyclopentane	22DMH	2,2-dimethylhexane
22DMP	2,2-dimethylpentane	ECP	ethylcyclopentane
BENZ	benzene	25DMH	2,5-dimethylhexane
24DMP	2,4-dimethylpentane	223TMP	2,2,3-trimethylpentane
223TMB	2,2,3-trimethylbutane	1T2C4TCP	1-trans-2-cis-4-trimethylcyclopentane
CH	cyclohexane	TOL	Toluene

Appendix 5. 2: Definitions of the Parents and daughters of the Mango kinetic scheme

P1	n-C_7
P2	2MH+3MH
P3	3EP+23DMP+22DMP+33DMP+233TMB
N^5_1	ECP + 1*c*2-DMCP + 1*t*2-DMCP
N^5_2	1,1-DMCP + c-l,3-DMCP + t-1,3-DMCP
N^6_1	MCH+Tol